

2

RD-92.17

ad Development Service
CC 20591

AD-A257 157



PROCEEDINGS

Unified Airport Pavement Design
and Analysis Concepts Workshops

July 16-17, 1991

Volpe National Transportation
Systems Center

DTIC
ELECTE
NOV 6 1992
S C D

Sponsored by the
Federal Aviation Administration

This document is available to the public through the
National Technical Information Service, Springfield,
Virginia 22161.

340170

92-28972



57988

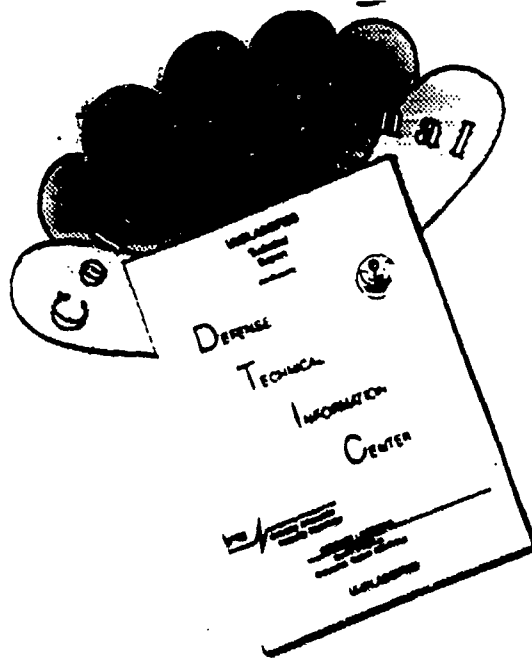


U.S. Department
of Transportation
Federal Aviation
Administration

82 1 1 0 4

This document is disseminated under the sponsorship of the U.S. Department of Transportation in the interest of information exchange. The United States Government assumes no liability for its contents or use thereof.

DISCLAIMER NOTICE



THIS DOCUMENT IS BEST QUALITY AVAILABLE. THE COPY FURNISHED TO DTIC CONTAINED A SIGNIFICANT NUMBER OF COLOR PAGES WHICH DO NOT REPRODUCE LEGIBLY ON BLACK AND WHITE MICROFICHE.

1. Report No. DOT/FAA/RD-92/17	2. Government Accession No.	3. Recipient's Catalog No.	
4. Title and Subtitle Unified Airport Pavement Design and Analysis Concepts Workshop		5. Report Date July 1992	
		6. Performing Organization Code DTS-77	
7. Author(s) Industry, Institutes, Academia		8. Performing Organization Report No.	
9. Performing Organization Name and Address Volpe National Transportation Systems Center, U.S.DOT		10. Work Unit No. (TRAIS)	
		11. Contract or Grant No. GWA 89-EA	
12. Sponsoring Agency Name and Address U.S. Department of Transportation Federal Aviation Administration 800 Independence Avenue Washington, DC 20591		13. Type of Report and Period Covered Proceedings	
		14. Sponsoring Agency Code ARD-200	
15. Supplementary Notes			
16. Abstract <p>This publication outlines the proceedings of a workshop held in July 1991 at Cambridge, MA. The workshop provided a forum for leading pavement engineers, researchers and materials scientists to present concepts for the formulation of a unified mechanistic methodology for the analysis and design of pavements serving civil aircraft. The need developed from industry's requests for adequate methods to design, analyze and predict performance of pavements serving more demanding aircraft. The publication contains essential elements of papers and reports presented at the workshop.</p> <p>The general agreement was that, given the prevailing state of the art in computer capability, the requirements for increased capacity through more frequent passes and heavier aircraft, and the development of new man-made construction materials, a more realistic and cost-beneficial approach to pavement analysis and design could be accomplished through the use of discrete material elements, faithful representation of actual material behavior and geometry, and dynamic interaction with rates of loading from any gear configuration. The belief was that computer programs capable to perform the task already exist in other areas of engineering (continued)</p>			
17. Key Words Pavement discrete model formulation, Heavy aircraft multigear gear compatibility, Micro-mechanical behavior, Stress analysis Advanced airport pavement design systems.		18. Distribution Statement Document is available to the public through the National Technical Information Service, Springfield, Virginia 22161.	
19. Security Classif. (of this report) Unclassified	20. Security Classif. (of this page) Unclassified	21. No. of Pages 570	22. Price

(Abstract continued)

mechanics and that they could be tailored for pavement applications. The papers presented would substitute current methods based on empirical data and broad theoretical assumptions with a generally applicable mechanistic approach. The suggested approach would obviate anomalies that result when current methods are applied to certain cross-section configurations. The recommended approaches would provide the comprehensive vehicle necessary for the analysis of stresses and strains, displacements, and pavement damage under virtually all operating conditions and material types, as well as, provide a foundation for nondestructive testing of airport pavements.

This publication presents customary constitutive relationships in common engineering notation and offers plans for the treatment of failure surfaces for many different classes of pavement materials. The authors point to the need for improved laboratory testing and materials characterization for input into any practical formulation. They also repeat the need for accurate and pertinent field data to verify the adequacy and reliability of computations derived from the use of an advanced theoretical model.

DTIC QUALITY INSPECTED 4

Accession For	
NTIS GRAB	<input checked="checked" type="checkbox"/>
DTIC TAB	<input type="checkbox"/>
Unannounced	<input type="checkbox"/>
Justification	
By	
Distribution/	
Availability Codes	
Dist	Avail and/or Special
A-1	

ACKNOWLEDGEMENTS

This work was initiated in response to a request from the Office of Airport Safety and Standards, Federal Aviation Administration (FAA), to address developing and projected needs of the aviation industry. A General Working Agreement between the FAA and the Research and Special Programs Administration (RSPA) facilitated the performance of this effort.

In-house work as well as contract administration and contractor supervision was conducted or supervised by Messrs. Andrew Sluz, Michael Silver, and Dr. Frederick Rutyna at the Transportation Systems Center in Cambridge, MA. The FAA technical officer was Dr. Aston McLaughlin.

List of Attendees

S. K. Reddy
Pennsylvania State University

Jacob Uzan
Texas Transportation Institute

Thomas D. White
Purdue University

John zaniwski
Arizona State University

Lynn Seaman
SRI International

Terry W. Sherman
U.S. Army Corps of Engineers

Donald A. shockey
SRI International

Mike Silver
U.S. Department of Transportation

Jeff Simons
SRI International

Andy Sluz
U.S. Department of Transportation

Harold Smetana
Federal Aviation Administration

Hisao Tomita
Federal Aviation Administration

Prem Pradhan
Foster Miller, Inc.

Stephen J. Kokkins,
Foster Miller Inc.

Gopal Samavedam
Foster Miller Inc.

A. Robert Raab
SHRP, National Research Council

Raymond Rawe
Burns & McDonnell, Inc.

Carl Monismith
University of California at Berkeley

Frank Noonan
Edwards & Kelcey, Inc.

Emmanuel B. Owusu-Antwi
ERES Consultants, Inc.

Robert G. Packard
Portland Cement Assoc.

John Pietrak
U. S. Department of Transportation

Robert Lytton
Texas Transportation Institute

Fred Koletty
Port Authority Tech. Center

Alice Krol
Transport Canada

Victor Lung
FAA - N.E. Region

Sudan Lutwak
Infrasense, Inc.

Kamran Majidzadeh
Ohio State University

Farah Majidzadeh
Resource International, Inc.

B. Frank McCullough
University of Texas

Paul McDonough
Howard, Needles, Tammen & Bergendoff

Jim W. Hall, Jr.,
U. S. Corps of Engineers

Peter Hilton
A. D. Little, Inc.

Anastasios I. Ioannides
University of Illinois

Michael P. Jones
Naval Facilities Engineering Command

Leonore Katz Rhoads
U. S. Department of Transportation

James C. Kennedy
Battelle Memorial Institute

Maureen Kestler
USA CRREL

Starr D. Kohn
Pavement Services, Inc

Michael I. Darter
University of Illinois

William C. Dass
Applied Research Associates, Inc.

Chandra S. Desai
University of Arizona

Bob H. Dodds, Jr.
University of Illinois

Tom Forte
Battelle Memorial Inst.

Karen J. Frink
Hoyle, Tanner & Assoc. Inc.

Edward L. Gervais
Boeing Corp.

Jeff Hadden
Battelle Memorial

S. N. Atluri
Georgia Institute of Technology

Moussa Bagate,
City of Rochester

Cemal Basaran
Cygnus Group

Philip Becker
CH2M Hill

Richard Berg
USA CRREL

Andre Bisailon
Sirem Inc.

R. Frank Carmichael, III
ARE Inc.

Ken Crow
Espey-Houston and Associates

Raymond Rawe
Burns & McDonnell

D. V. Reddy
Florida Atlantic University

Fred Rutyna
U. S. Dept. of Transportation

Gajan Sabnis
Howard University

John McGuiggin
U. S. Dept. of Transportation,

Aston McLaughlin
Federal Aviation Administration

Table of Contents

State of the Art of Airport Pavement Analysis and Design.....	1
Development of User Guidelines for a Three-Dimensional Finite Element Pavement Model.....	53
Micro Mechanical Behavior of Pavements.....	87
Thermoviscoelastic Analysis of Pavements.....	125
FAA Unified Pavement Analysis 3-D Finite Element Method.....	169
Federal Aviation Administration Pavement Modeling.....	233
State of the Art Review of Rutting and Cracking in Pavements.....	315
Development of a Unified Airport Pavement Analysis and Design System	393
Unified Airport Pavement Design Procedure	447
Three-Dimensional Stress Analysis of Multilayered Airport Pavements: Integral Transform Approach.....	539

State of the Art of Airport Pavement Analysis and Design

J. Zarlewski

**Department of Civil Engineering
Arizona State University**

1. Background

Air transportation is a vital component of interregional, interstate and international commerce and recreation of the United States. In the past two decades there has been a tremendous growth in air traffic. The construction of airport facilities during this time, however, has been virtually stagnant. As a result, the airport system has been stretched near its limits of capacity. Closure of a pavement, especially a runway at a major airport, can affect the operations of the entire airport system. Pavement reliability, therefore, is critical to air transportation convenience and dependability.

The need for reliable pavement design has long been recognized as integral to the smooth functioning of airports. However, the airport pavements that serve their original design life without extensive maintenance are the exception rather than the rule. One of the most prevalent problems in airport pavement design has been underestimating the rate of air traffic growth and hence the underdesign of the pavements.

Pavements are one of the most difficult design problems faced by civil engineers. Pavements are constructed with low-cost materials whose properties are highly variable and dependent on environmental and load conditions. Traffic loadings are difficult to forecast as air traffic growth frequently exceeds expectations and as new aircraft are introduced. Environmental conditions can be evaluated on a probabilistic basis from historical trends; however, the specific environment at a particular point in time can have a dramatic effect on the performance of the pavement.

Due to the difficulty of the airport pavement analysis process, design methods have evolved in an empirical manner. While these methods produced workable designs, they have several shortcomings. There have been significant developments in the areas of engineering mechanics and materials evaluation that can provide the foundation for the development of improved airport pavement design procedures. The purpose of this report is to summarize the state of the art in airport pavement analysis models. This task does not have a clear boundary. There are models that have been used for many years for pavement design. There are also models that are applied only by engineers that are on the leading edge of technology for the design of pavement structures. Other models have been proposed by researchers but have not been used extensively for airport pavement analysis. Finally, there are models that have been developed in other engineering fields that can be applied to the analysis of airport pavements.

1.1 Design Models

The Federal Aviation Administration (FAA) pavement design procedure presents methods for the design of flexible and rigid pavements for light and heavy aircraft. Only the procedure for heavy aircraft, weighing more than 30,000 pounds is reviewed here. The flexible pavement design procedure is based on the California Bearing Ratio (CBR) test. The rigid pavement design procedure is based on the Westergaard stress equation for joint edge stress.

1.1.1 FAA Flexible Pavement Design

The essence of the CBR design procedure is the protection of the subgrade from overstressing by using layers of successively weaker materials with depth. Separate design curves are available for single, dual, and dual-tandem gears and for each of the wide body aircraft.

In this procedure, it is assumed the asphalt concrete will meet specified criteria in terms of mix design and construction quality. There is no method for adjusting the thicknesses based on the quality of the surface material. It is assumed the base will be a granular material with a CBR of 80.

Required layer thickness is determined by the following sequence of functional relationships:

$$T_p = f(SG_{CBR}, W_D, N_E)$$

$$T_s = \text{Specified on the design charts} \quad (2)$$

$$T_{sbb} = f(SB_{CBR}, T_p, W_D, N_E) \quad (3)$$

$$T_{Bmin} = f(SB_{CBR}, T_p) \quad (4)$$

$$T_B = \max(T_{Bmin}, T_{sbb}) \quad (5)$$

$$T_{SB} = T_p - T_s - T_B \quad (6)$$

Design charts are used to quantify equations 1, 3, and 4. In some cases, the thickness requirement for the subbase is adjusted if the upper portion of the subgrade has a thin layer of material near the surface.

The thickness of the surface is 5 inches for wide-bodied aircraft, 4 inches for all other aircraft in the critical areas, and 1 inch less for all other areas. The thickness of the surface is determined based on whether or not there are wide-bodied aircraft and not on the design aircraft.

Stabilized bases are required for all airports serving jet aircraft weighing more than 100,000 pounds, unless there is a history of satisfactory performance of the locally available granular materials. Stabilized bases and subbases can also be used if there is an economic advantage in using these materials. A reduction in the thickness of the pavement is allowed for stabilized materials through the use of material equivalency factors. However, the design manual only provides ranges for the adjustment factors based on the type of the material. Selection of a specific material equivalency factor is left to the experience of the designer.

The design curves are limited to 25,000 applications. For a greater number of departures, the design is increased on a simple extrapolation. For high-traffic volumes, the total pavement thickness is increased by a multiplier and the surface thickness is increased by 1 inch.

1.1.2 FAA Rigid Pavement Design

The slab thickness for a concrete pavement is determined from design charts based on the flexural strength of the concrete, the modulus of subgrade reaction, weight of the design aircraft, and equivalent number of applications. Subbase is required to be a minimum of 4 inches of granular material. If the airport serves aircraft with weights in excess of 100,000 pounds, then a stabilized base is required. The strength of the stabilized base can be used to increase the modulus of subgrade reaction and thereby reduces the thickness of the slab.

As with flexible pavements, the design curves are limited to 25,000 load applications and extrapolated; multiplying factors are used to increase the thickness of the slab. These factors are relatively insensitive to the number of applications. Increasing the number of applications from 25,000 to 50,000 only increases the thickness of the slab by 4 percent.

1.2 Asphalt Institute

The pavement design charts for the Asphalt Institute design procedure for full-depth asphalt concrete pavements were developed based on elastic layer theory analysis and two distress types, fatigue and permanent deformation. The fatigue criteria are based on limiting the horizontal tensile strain at the bottom of the surface layer. The permanent deformation criteria is based on limiting the vertical compressive stress at the top of the subgrade. All aircraft classes are converted to the "standard aircraft;" the DC-8-63F was "arbitrarily" selected to be the standard. Taxiways are considered to be the critical portion of the airfield pavement. The design process is summarized in Figure 1-1.

The inputs to the design process are the mean annual air temperature, the design subgrade modulus, and the expected number of repetitions of each aircraft type. The design subgrade modulus requires performing a series of soils tests and selecting the 85 percentile value, e.g., only 15 percent of the subgrade tests have a lower value than the design value. The manual recommends laboratory evaluation of the modulus using the triaxial test procedure specified in the manual. Approximations are available for estimating the modulus from the CBR test, plate bearing test and the FAA Soil Classification. The manual provides specifications for the asphalt concrete but the properties of the asphalt concrete are not a direct input to the design process.

The procedure requires the development of curves for the allowable number of applications and the estimation of equivalent applications for both fatigue and plastic deformation. Design charts are used for selecting the allowable number of applications as a function of the subgrade modulus and the mean annual temperature. For a given subgrade modulus and temperature, the required thickness is determined for several different assumed traffic loadings and the results are plotted on a design graph for both the fatigue and plastic analysis. This establishes the allowable traffic curve.

The traffic equivalency curves are then used to convert the number of aircraft loadings into equivalent loadings. Equivalencies are determined for four wheel paths and four different pavement thicknesses. For each assumed thickness, critical wheel path is determined as the one with the greatest number of total equivalencies. The number of equivalencies and corresponding thicknesses are plotted on the design graph to establish the predicted traffic curve.

The intersection of the predicted and allowable traffic curves defines the required pavement thickness for each of the design modes. The final pavement thickness is the greater of the thicknesses required for either the fatigue or plastic deformation load.

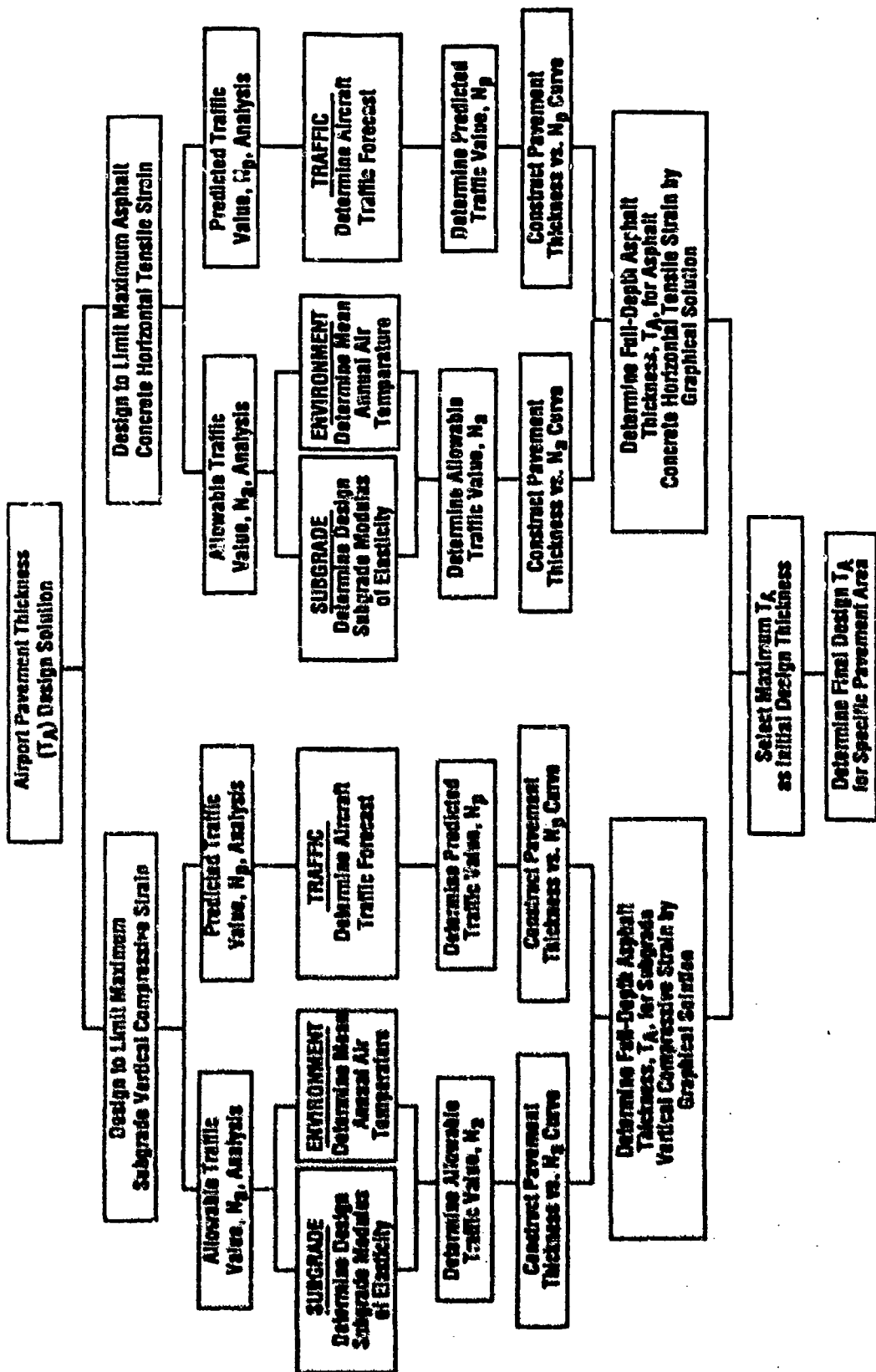


Figure 1-1. Flow of Asphalt Institute Design Procedures

That equivalency factors for each of the aircraft types is a function of the pavement thickness is a major difference between the Asphalt Institute method and the FAA procedure. Theory would favor the Asphalt Institute method since the relative damage caused by an aircraft is a function of the stiffness of the pavement and, therefore, the equivalency factors should consider the thickness of the pavements.

1.3 Portland Cement Association

The Portland Cement Association design manual for rigid pavements presents two design methods: one based on the critical aircraft that will use the facility and the other based on the fatigue life of the pavement. Both methods use the Westergaard theories for determining the stresses in the pavement structure.

The steps in the critical aircraft design method are:

1. Determine the K value of subgrade support with plate bearing tests or correlation to subgrade soil test data.
2. Select a safety factor based on the estimated operating and load conditions. The safety factor is the ratio of the design modulus of rupture of the concrete to the working stress that will be used for design. The safety factor ranges from 1.7 to 2.0 for the critical areas, and 1.4 to 1.7 for noncritical areas. The critical areas are aprons, taxiways, hard stands, runway ends and hangar floors. The noncritical areas are the central portion of the runway and some high-speed exit taxiways. The selection of a specific safety factor for an aircraft depends on the expected number of loadings.
3. The working stress for the design is determined by dividing the modulus of rupture of the concrete by the chosen safety factor.
4. The required pavement thickness is determined from the design charts as a function of the working stress, gear load, and K value.
5. The process is repeated for other aircraft that can have critical loads. The safety factor is adjusted for each of the types of critical aircraft.

The PCA states that the fatigue method of design applies to:

1. Design for specific volumes of mixed traffic:

2. Evaluation of future traffic capacity of existing pavements or of an existing pavement's capacity to carry a limited number of overloads;
3. Evaluation of the fatigue effects of future aircraft with complex gear arrangements; and
4. More precise definition of the comparative thicknesses of runways, taxiways, and other pavement areas depending on the operational characteristics.

The fatigue method introduces three additional design parameters:

1. Traffic width for taxiways, runways and ramps;
2. Variability of concrete strength; and
3. Downgrading of service life where a good subbase support is not provided.

The basic steps in the fatigue analysis method are:

1. Estimate the number of operations of each type of aircraft.
2. Use influence charts or the PCA computer program to estimate the stress each aircraft will cause in the pavement. For design, this requires assuming a thickness.
3. Estimate the design modulus or rupture (DMR) for the concrete as a function of the variability of the concrete:

$$DMR = MR_{90}(1-V/100)M \quad (7)$$

where

MR_{90} = average modulus of rupture at 90 days

V = Coefficient of variation of modulus of rupture in percent (range 10 to 18 percent)

M = factor for the average modulus of rupture during design life, recognizing that concrete strength increases with age (typically 1.10).

4. Compute the stress ratio of the estimated stress for each aircraft to the design modulus of rupture.
5. Determine the load repetition factor (LRF) for each aircraft. LRF is determined from stresses, the fatigue 1 , curve and the probability distribution of aircraft wander. The design manual provides tabular values for LRF.
6. Determine the number of fatigue repetitions for each aircraft by multiplying the expected number of departures by the LRF.

7. Determine the number of allowable repetitions for each aircraft as a function of the stress ratio and the fatigue curve.
8. Determine the percent of structural capacity used by each aircraft as the ratio of the fatigue repetitions to the allowable repetitions. Sum the percent of structural capacity used by all of the aircraft. Adjust the percent of fatigue life used when the K value is less than 200 pci. This adjustment ranges from 8 for a K value of 50 to 1 for a K value of 200 pci. The adjusted percent of fatigue life should be close to but not exceed 100 percent.

The PCA manual addresses the design of continuously reinforced concrete pavements, but recommends that the thickness design be the same as for plain concrete pavements. This manual states that reducing the thickness can increase deflection and promote spalling of the joints.

1.4 Department of Defense Pavement Design Methods

The Army and Air Force share a common procedure for the design of rigid pavements, while the Navy has a separate design procedure for a triservice manual used for the design of flexible pavements for all services. In addition, the Army and Air Force have a manual for the design of flexible pavements using elastic layer theory.

Each of the pavement design manuals requires designing different pavement sections based on the airfield class and traffic areas. For example, the Air Force defines four pavement area types ranging from highly channelized traffic such as on primary taxiways, type A, to low-volume and low-weight traffic areas, type D. In addition, each airfield is designated as a light, medium and modified-heavy, heavy load, or short-field facility. The traffic area types for each facility are shown in Figures 1-2 through 1-4. The aircraft design loads and number of applications for Air Force pavement design are given in Table 1-1. The Army and Navy use a similar concept with different terminology for the airfield designations and traffic areas.

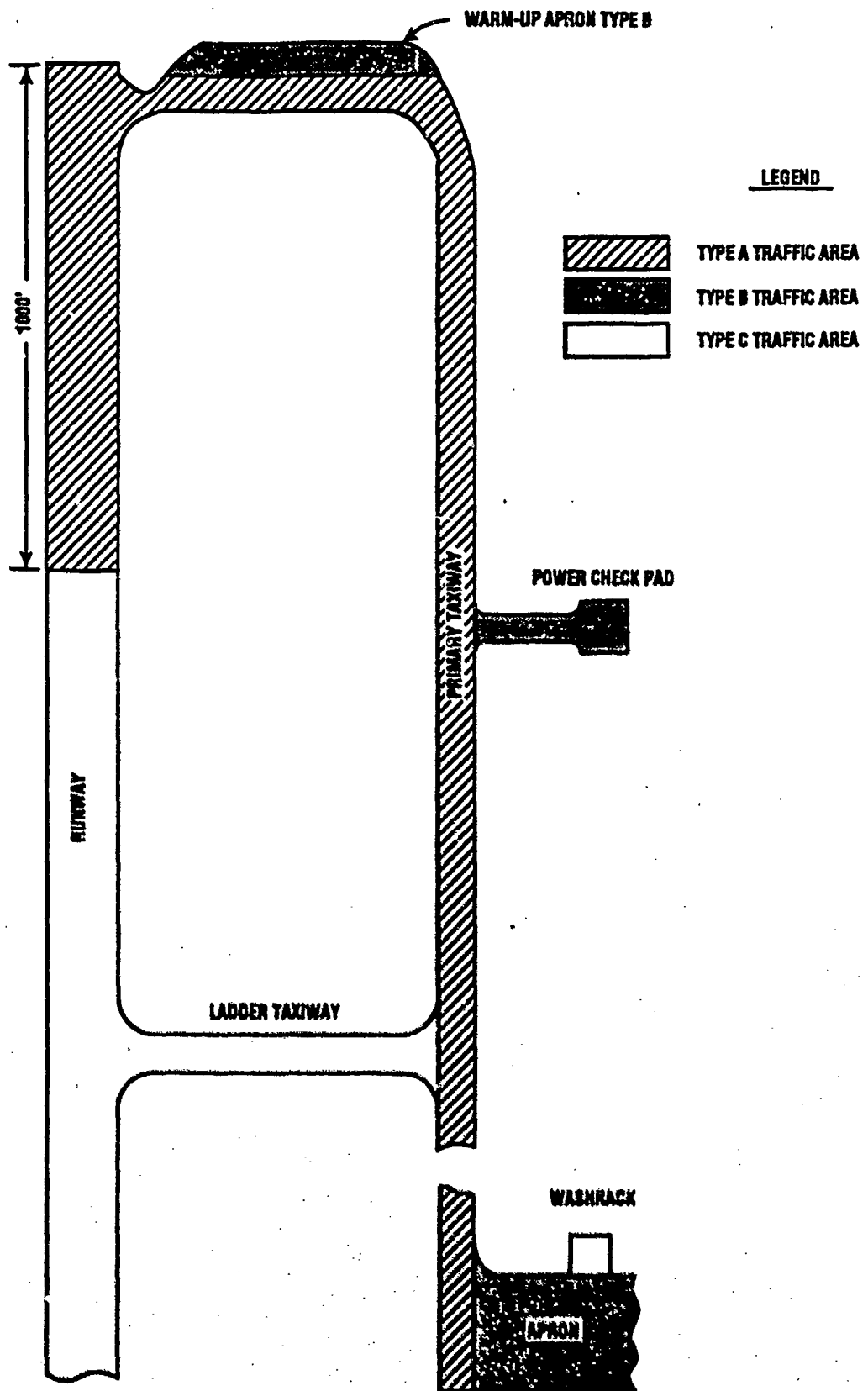


Figure 1-2. Air Force Traffic Areas, Light Load Airfields

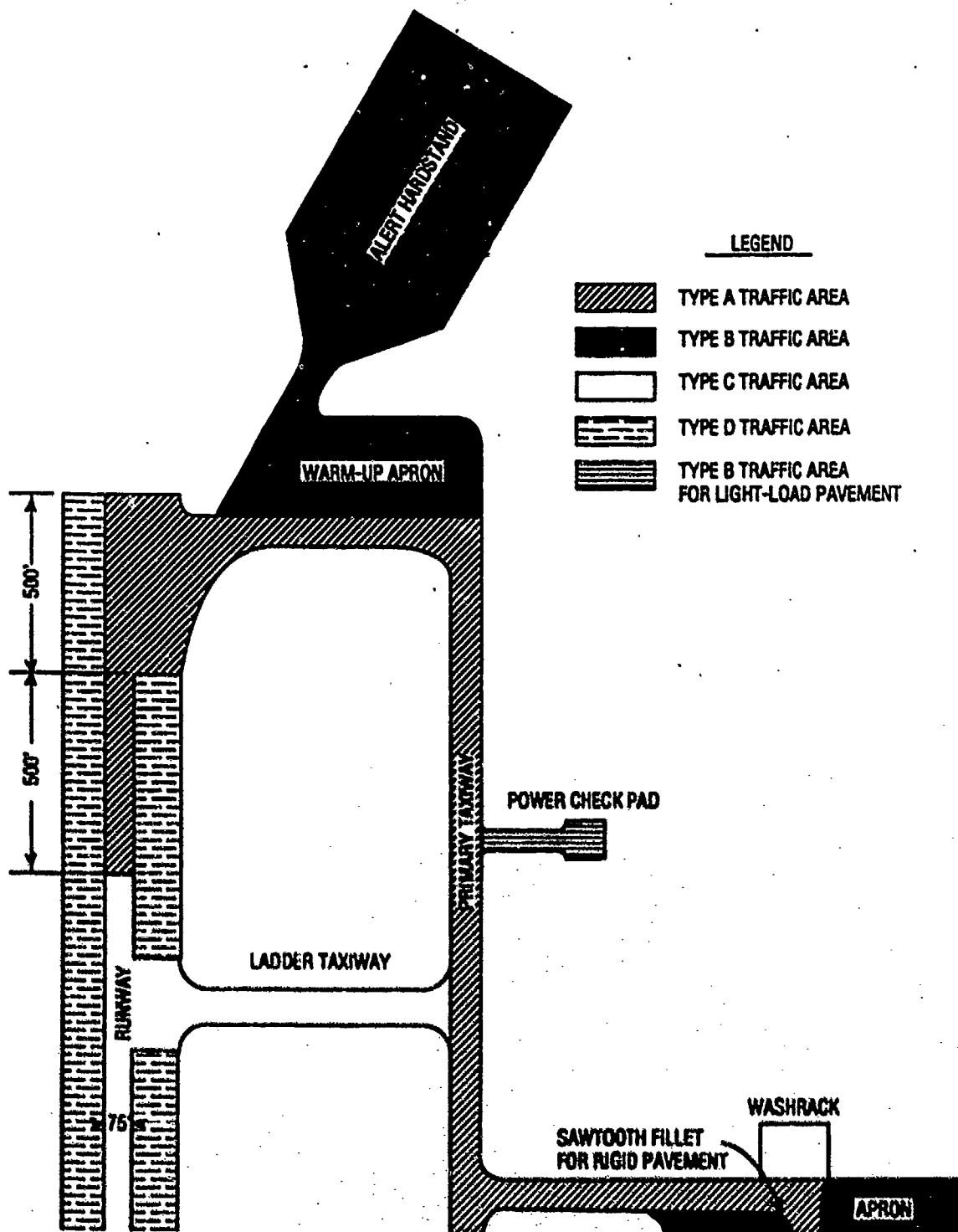


Figure 1-3. Air Force Traffic Areas, Medium and Modified-Heavy Load Airfields

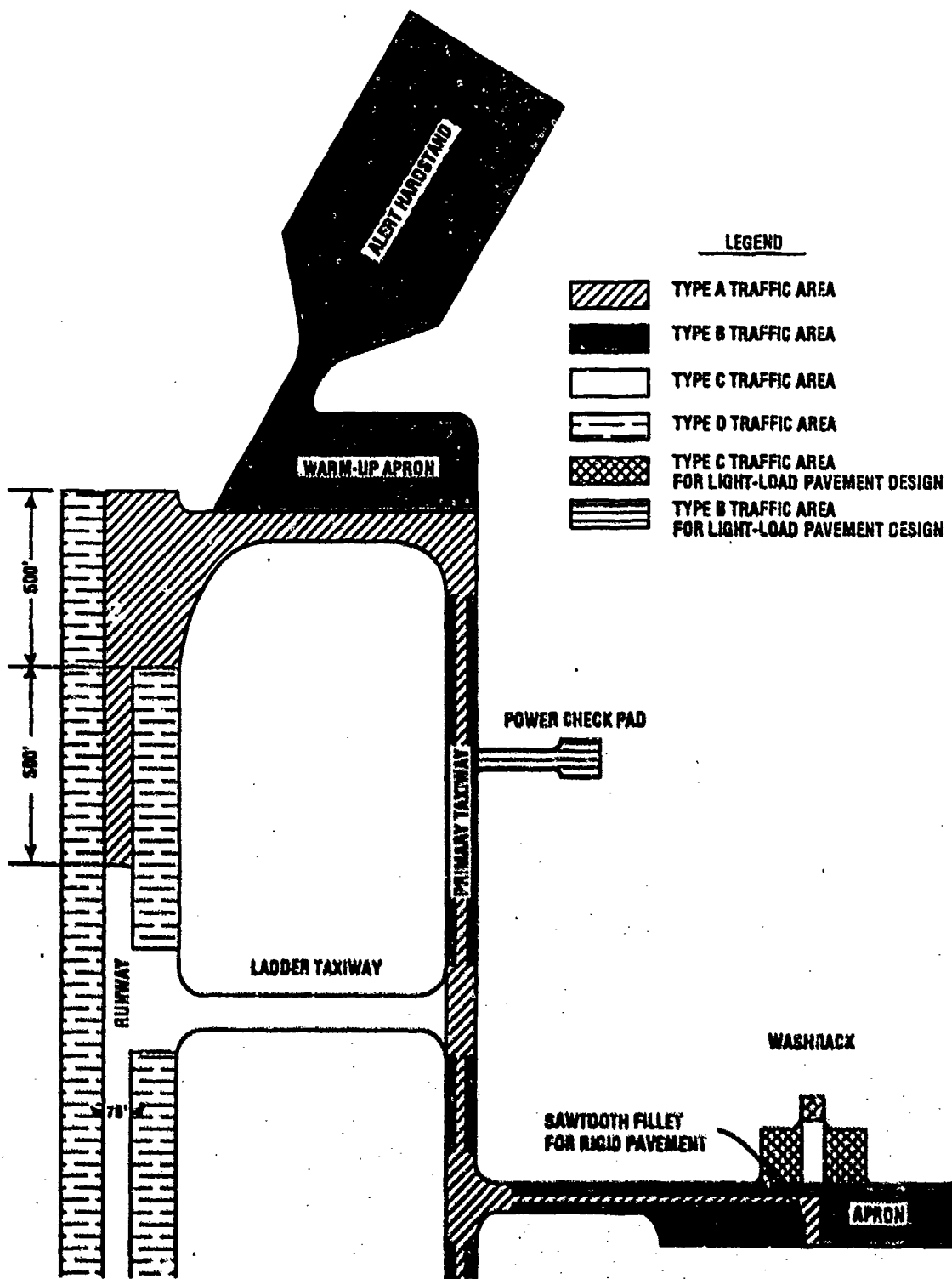


Figure 1-4. Air Force Traffic Areas, Heavy Load Airfields

Table 1-1. Design Weights and Pass Levels for Airfield Pavements, Air Force
(Weights in 1000 pounds)

Aircraft Type	Design Aircraft	A Traffic Area			B Traffic Area			C Traffic Area			D Traffic Area			Overruns		
		Weight	Passes	Area	Weight	Passes	Area	Weight	Passes	Area	Weight	Passes	Area	Weight	Passes	Area
Light	F-15 C/D	68	100000		68	100000		51	100000		NA			51	1000	
	C-141	345	100		345	100		258.75	100					258.75	1	
Medium	F-15 E	81	25000		81	25000		60.75	25000		60.75	250		60.75	250	
	C-141	345	100000		345	100000		258.75	100000		258.75	1000		258.75	1000	
	B-52**	400	100		400	100		360	10		300	1		300	1	
Heavy	F-15 E	81	25000		81	25000		60.75	25000		60.75	250		60.75	250	
	C-141	345	50000		345	50000		258.75	50000		258.75	500		258.75	500	
	B-52	480	30000		480	30000		360	30000		360	300		360	300	
Modified Heavy	F-15 E	81	25000		81	25000		60.75	25000		60.75	250		60.75	250	
	C-141	345	50000		345	50000		258.75	50000		258.75	500		258.75	500	
	B-1	480	30000		480	30000		360	30000		360	300		360	300	
Short-Field	C-130	175	50000		NA	NA		NA	NA		NA	NA		175	50000	
			PER SQUADRON												PER SQUADRON	

**B-52 will not be included in the mixed traffic design of medium load airfields with less than 200 foot wide runways
Shoulders are designed to support 5,000 coverages of a 10,000 pound single wheel load having a tire pressure of 100 psi

1.4.1 Triservice Manual for Flexible Pavement Design

The design of conventional flexible pavements and flexible pavements with stabilized bases and/or subbases are covered in reference. The design process uses the CBR procedure for the distribution of stresses through the layered pavement section. Design of full-depth bituminous concrete pavements is beyond the scope of this report. The design sequence is:

1. Determine design CBR of the subgrade, depending on the variability of the subgrade. (Either distinct pavement design areas can be used, or the 85 percentile of the subgrade tests can be used.
2. Determine the total pavement thickness required based on the type of facility, subgrade CBR, gross aircraft weight and number of passes.
3. Determine the design CBR of the subbase.
4. Determine the thickness of surface and base required by entering the design curves with the subbase CBR.
5. Determine the minimum thickness of the surface from the appropriate table. Minimum base thicknesses are given for base materials with CBR values of 80 and 100 percent. There is no incentive in the design procedure for using a surface thickness greater than the minimum, so practical design would use the minimum surface thickness. The thickness of the base is the maximum of either the minimum required base thickness or the difference between the total pavement thickness and the minimum surface thickness.
6. The thickness of the subbase is equal to the difference between the total required thickness and the combined thickness of the surface and the base. If this produces a subbase thickness less than 6 inches, consideration should be given to increasing the thickness of the base and eliminating the subbase.

Design of pavements with stabilized base and subbases requires the design of a conventional pavement and then a reduction of the required thicknesses based on equivalency factors. There are a variety of rules that address the appropriate application of stabilization materials.

1.4.2 Army-Air Force Rigid Pavement Design

The Army-Air Force rigid pavement design manual presents procedures for the design of plain, jointed-reinforced, steel-fibrous, continuously reinforced and prestressed concrete pavements.

1.4.2.1 Plain Concrete Airfield Pavements

The edge stresses are reduced by 25 percent to account for load transfer afforded by the joint designs required. The flexural modulus of elasticity of the concrete is assumed to be 4,000,000 psi and Poisson's ratio is assumed to be 0.15. The design curves are available for light, medium, heavy and modified-heavy load pavements. Select pavement thickness is a function of the flexural strength of the concrete, modulus of subgrade reaction, and type of traffic area. The design curve for short-field pavements uses the gross weight of the aircraft and number of aircraft passes instead of the type of traffic area. The design thickness is rounded to the nearest half inch.

When the base or subgrade is stabilized, or the base is lean or existing concrete, the pavement slab is designed as an overlay using the equation:

$$h_o = ((h_d)^{1.4} - ((E_b/E_c)^{1/3}(h_b))^{1.4})^{1/1.4} \quad (8)$$

where

h_o = required thickness of the plain concrete slab on a stabilized subgrade

h_d = thickness of plain slab that would be required if the slab was placed directly on the subgrade

E_b = modulus of elasticity of the base

E_c = modulus of elasticity of the concrete

h_b = thickness of stabilized layer or lean concrete base

1.4.2.2 Reinforced Concrete Pavements

Thickness design for both continuously and jointed reinforced concrete pavements is the same. Different procedures are used for designing the amount of steel. Design of a reinforced concrete pavement requires first selecting the thickness for a plain concrete pavement. A nomograph is then used for the selection of the reduced thickness of the reinforced pavement based

on the thickness of slab required for a plain concrete pavement, the area of steel reinforcement, the percent of steel reinforcement and the length of the slab.

There is an interdependence between the amount of steel required, the size of the slab and the thickness. Designing the pavement requires assuming either a percent steel or reduced slab thickness and solving for the other value.

1.4.2.3 Fibrous Concrete Pavements

The design of fibrous concrete pavements is based on limiting the ratio of the flexural strength and maximum tensile stress at the joint, with the load either parallel or normal to the pavement edge. The limiting criteria for the stress ratio is based on field experiments. These experiments were performed with steel fibers which limit the application of the design method. In addition, the design procedure limits the vertical deflection to prevent potential pumping, densification and/or shear failures of the subgrade.

Design curves are presented for each of the classes and types of Army and Air Force airfields. The Army design curves consider: flexural strength of the fibrous concrete; modulus of subgrade reaction; aircraft gross weight; number of passes; and type of traffic area.

The Air Force design curves consider: flexural strength of the fibrous concrete, modulus of subgrade reaction; and type of traffic area.

In the Air Force procedure, the aircraft weight and number of 4-inch passes are defined by the traffic area, as shown in Table 1-1.

1.4.2.4 Prestressed Pavement Design

The design of prestressed concrete pavements requires balancing the level of prestressing with the thickness of the slab to obtain an economical design. The design equation is:

$$d_s = (6PNB/(w(h_p)^2 - R + r_s + t_s) \quad (9)$$

where

d_s = design prestress required in the concrete

P = aircraft gear load

N = load repetition factor

- B = load moment factor
- w = ratio of multiple wheel gear load to single wheel gear load
- h_p = design thickness of prestressed concrete
- R = design flexural strength of concrete
- r_s = foundation restraint stress
- t_s = temperature warping stress

The design manual presents curves and equations for quantifying each of the design factors except for the design prestress and the thickness of the slab. The manual suggests the design prestress should be in the range of 100 to 400 psi and the minimum thickness of the slab is 6 inches.

1.4.3 Navy Rigid Pavement Design

The Navy design manual for rigid pavements is similar to the Portland Cement Association procedures. Westergaard's theory is used for computing the maximum stress in the pavement. The thickness is selected to keep the computed stress less than the working stress. The working stress is the flexural strength divided by a safety factor of 1.4 and 1.2 for primary and secondary traffic areas respectively. Design charts are presented for single, dual and dual-tandem gear types. The manual endorses the use of the PCA pavement design computer program when designing for other gear types. The design curves are limited to modulus of subgrade reactions of 100 and 500 pci and interpolation is used for other K values.

1.4.4 Army-Air Force Flexible Pavement Design - Elastic Layer Theory Method

The Corps of Engineers has developed a mechanistic design procedure for flexible pavements. The analysis is performed with either CHEV5L or BISAR. As described in Chapter 4, two design criteria are used for the selection of the pavement thickness, fatigue of the asphalt surface or stabilized base layer, and subgrade strain criteria. The pavement designs are performed for the critical aircraft at the airfield rather than for a mix of aircraft.

The design procedure considers three design situations:

1. granular base and subbase;
2. stabilized base and granular subbase; and
3. stabilized base and subbase.

Several steps are required for the design process, as shown in Figures 1-5, 1-6, and 1-7. The variables used in these figures are defined as:

E_{BC} = modulus of the base course

ϵ_{ALL} = allowable strain, may be for either the subgrade strain criteria or the fatigue criteria depending on the step in the flow chart

ϵ_h = horizontal tensile strain at the bottom of the surface layer or stabilized base or subbase

ϵ_v = vertical compressive strain at the top of the subgrade

n_i = expected number of strain repetitions of traffic for the fatigue or subgrade strain analysis

N_i = allowable number of strain repetitions estimated from either the fatigue or subgrade strain criteria

As demonstrated with the design procedure flow charts, many steps are required for designing a flexible pavement with this procedure. However, the procedure can be summarized in five steps.

1. Determine material properties.
2. Determine a trial pavement section.
3. Computation of the critical strains
4. Determine expected number of applied strain repetitions.
5. Computation of damage factors and the cumulative damage.

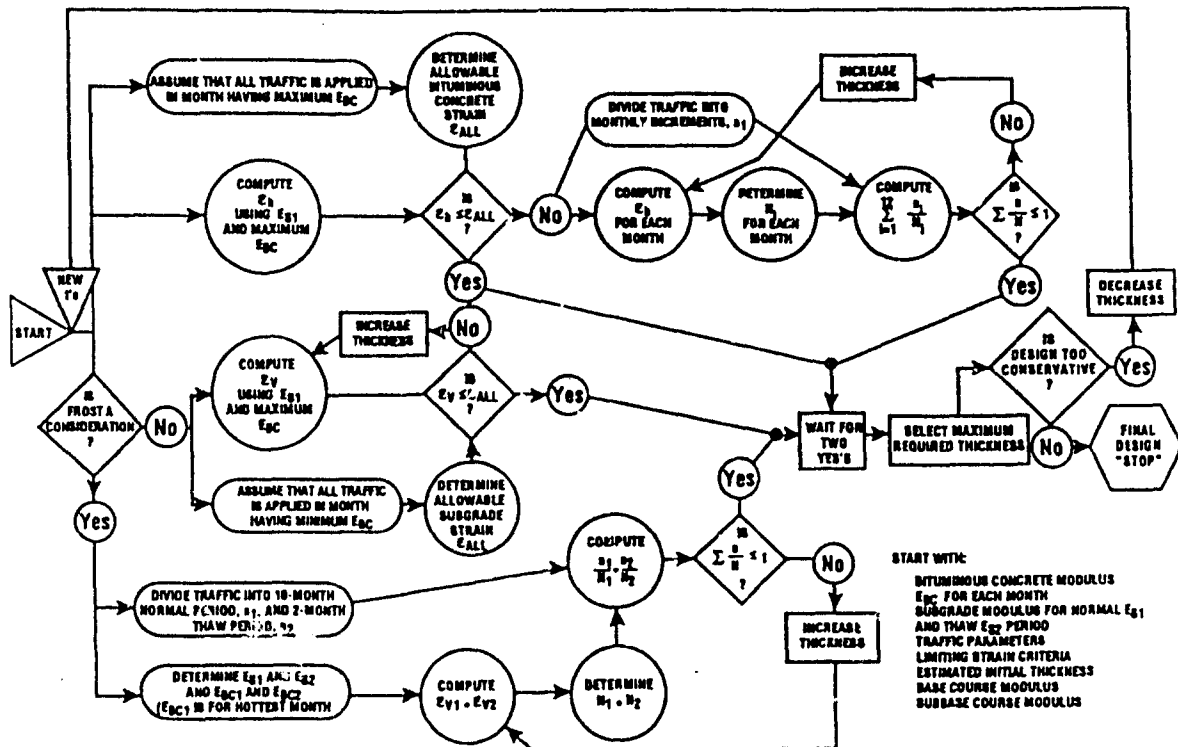


Figure 1-5. Elastic Layer Theory Design Method, Conventional Pavements

START WITH:

SITUMINOUS CONCRETE MODULUS FOR EACH MONTH
 SUBGRADE MODULUS FOR NORMAL AND THAW PERIODS
 TRAFFIC PARAMETERS
 LIMITING STRAIN CRITERIA
 ESTIMATED INITIAL THICKNESS
 BASE COURSE MODULUS DETERMINED IN FLEXURE E_{Bf}
 BASE COURSE MODULUS DETERMINED FROM EQUIVALENT CRACKED SECTION E_{Bc}
 SUBBASE MODULUS

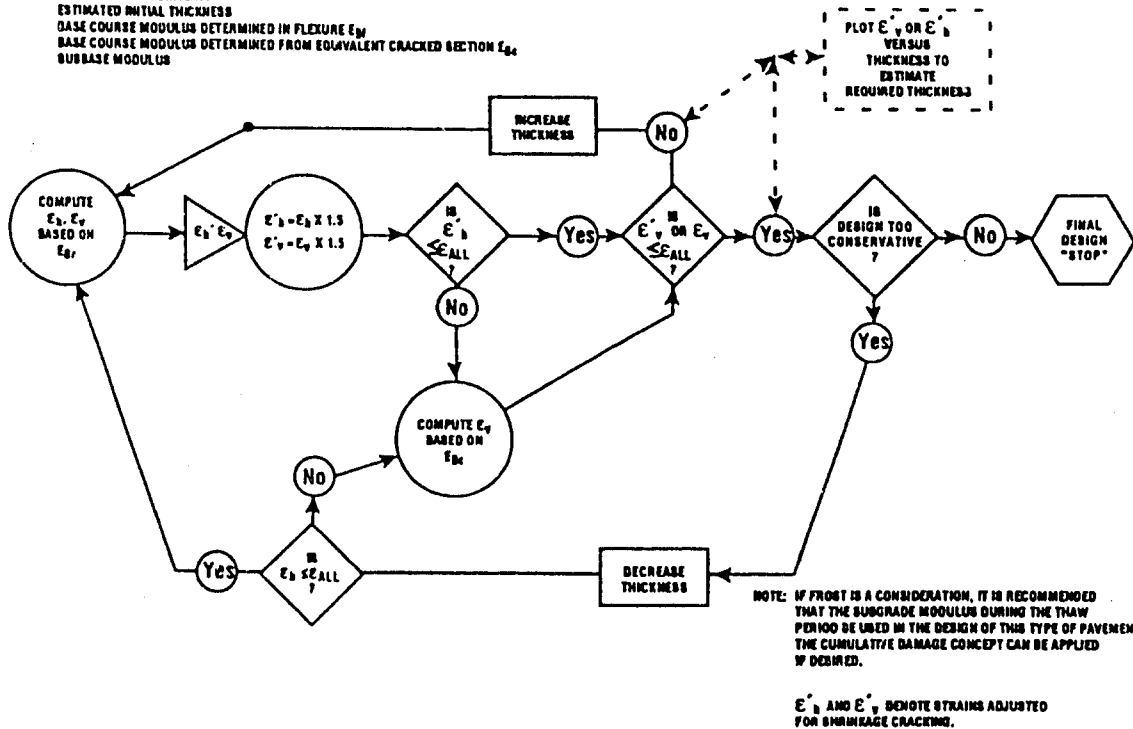


Figure 1-6. Elastic Layer Theory Design Method, Pavements with Stabilized Bases

START WITH:

BITUMINOUS CONCRETE MODULUS FOR EACH MONTH
SUBGRADE MODULUS FOR NORMAL AND THAW PERIODS
TRAFFIC PARAMETERS
LIMITING STRAIN CRITERIA
ESTIMATED INITIAL THICKNESS

BASE COURSE MODULUS DETERMINED IN FLEXURE E_{Bf}
BASE COURSE MODULUS DETERMINED FROM EQUIVALENT CRACKED SECTION E_{Bc}
SUBBASE COURSE MODULUS DETERMINED IN FLEXURE E_{SBf}
SUBBASE COURSE MODULUS DETERMINED FROM EQUIVALENT CRACKED SECTION E_{SBc}

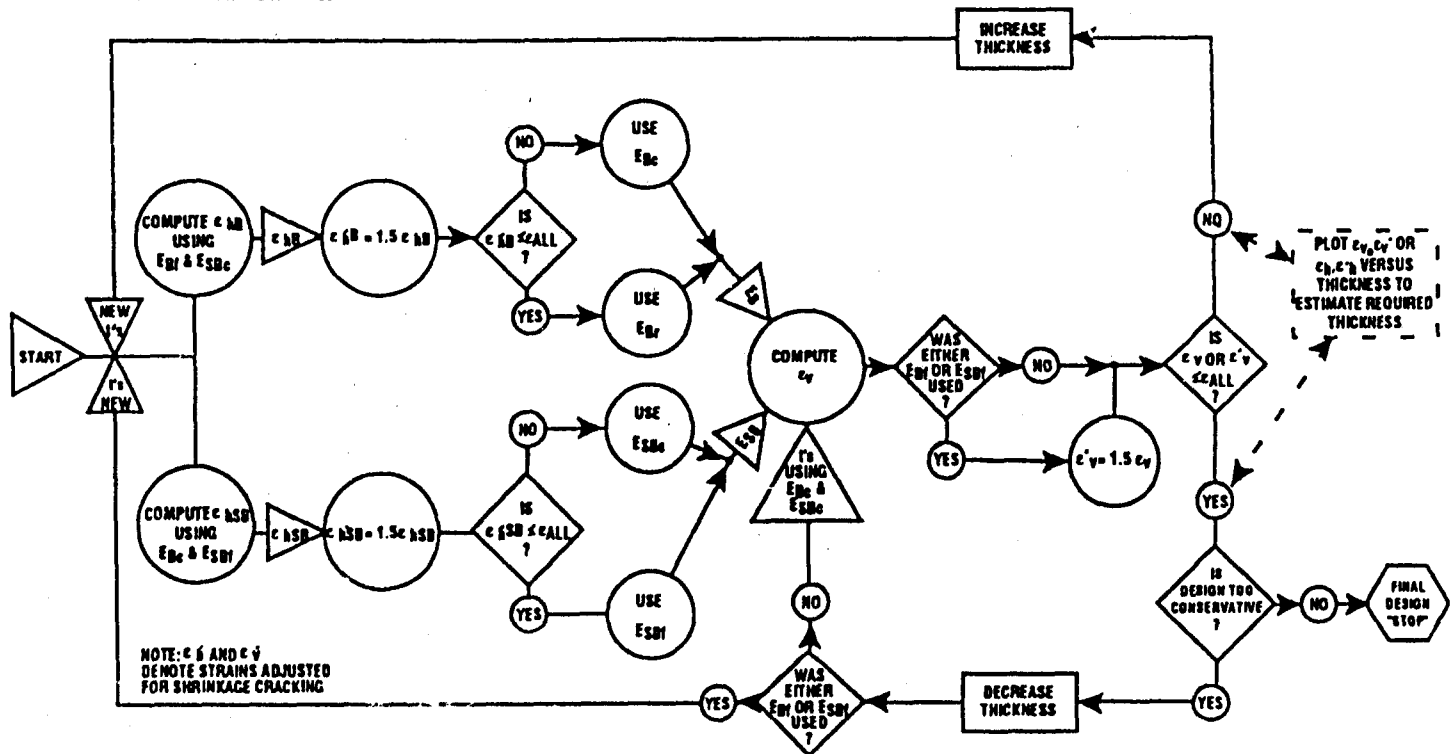


Figure 1-7. Elastic Layer Theory Design Method, Pavements with Stabilized Subbases

Material characterization requires measurement of the modulus of elasticity for each layer in the pavement. In general, dynamic testing of the materials is required with the exception of granular materials where the manual states "an empirical-based procedure was judged a better approach for obtaining usable material parameters." The subgrade modulus is determined with respect to the anticipated deviator stress on the subgrade. The modulus of the asphalt concrete must be determined for a variety of temperatures. In the design process, two temperatures are used for determining the asphalt concrete modulus for each month. For the fatigue analysis, a modulus is selected corresponding to the average daily maximum temperature. For the subgrade strain analysis, the average of the average daily mean temperature and the average daily maximum temperature is used to select the asphalt concrete modules. These air temperatures are corrected to a design temperature of the pavement. If the temperature variations between months are relatively small, months can be grouped to reduce the calculation requirements.

To determine trial pavement design for analysis the procedure in TM 5-825-2/AFM 88-6, Chapter 2 [4] should be used. The mechanistic analysis procedure is then used to check the design of a thicker and thinner pavement structure to determine the optimum pavement design.

Strains in the pavement structure due to the design aircraft wheel loading are computed with an elastic layer theory program. These strains are input to the criteria equations for fatigue and subgrade strain to determine the allowable number of strain repetitions.

The expected number of passes on the pavement for the design aircraft is then reduced to the number of strain repetitions based on the configuration of the landing gear, tire imprint area and wander of the aircraft, and the thickness of the pavement. Design curves are presented for determining the percent of passes of an aircraft that produce strain repetitions based on the aircraft type and the thickness of the pavement. For aircraft with tandem tires, the number of strain repetitions can actually exceed the number of operations.

The final step in the design process is to compute the cumulative damage. Since only critical aircraft are considered in the design, the computation is required to account for the different strains resulting from changes in temperature.

As a final note, it should be emphasized that the design of conventional flexible pavements only considers the subgrade strain criteria. Fatigue criteria are not considered in the design. The stated reason for this limitation is:

Conventional pavements consist of relatively thick aggregate layers with a thin (3 to 5 inch) wearing course of bituminous concrete. In this type of pavement the bituminous concrete structure is a minor structural element of the pavement and the temperature effects on the stiffness properties of the bituminous concrete may be neglected. Also, it must be assumed that if the minimum thickness of bituminous concrete is used as specified in TM 5-825-2/AFM 88-6, Chapter 2, then the fatigue cracking will not be considered. Thus, for a conventional pavement, the design problem is one of determining the thickness of pavement required to protect the subgrade.

2. Pavement Analysis Models

2.1 Elastic Layer Theory - Static Loads

Burmister's solution of the elastic two-layer problem laid the foundation for the extension of the theory to multiple layers. The equations for the two-layer case are relatively simple and can be solved on a pocket calculator. However, the extension of the theory to multiple layers greatly complicates the problem and practical application of the theory requires computer analysis. Fortunately, there are several computer programs available for performing this analysis.

The general concept of elastic layer theory (ELT) is shown in Figure 2-1. Yoder and Witczak state that the assumptions used for model development are:

1. homogeneous material properties;
2. finite layer thickness except for the bottom layer which is assumed to be infinite;
3. isotropic material properties;
4. full friction between the layers;
5. no shear stresses at the surface; and
6. materials are linear-elastic and obey Hooke's law, i.e., the constitutive behavior of the material is defined by the elastic modulus and Poisson's ratio.

In addition, the load is assumed to be uniformly distributed over a circular area and static. Some of these assumptions have been relaxed with the development of various elastic layer theory computer codes.

Strictly speaking, elastic layer theory is not always an accurate model of a pavement structure. Comparison of the material characteristics, pavement geometry, and traffic loading conditions described in Chapter 1 indicates that real pavement structures do not conform with the assumptions specified for the theory development. When the theory was introduced, engineers recognized the potential of the model, if properly applied, to improve the state of the art in pavement design. Numerous researchers investigated the effects of the differences between the theory and reality on the utility of elastic layer theory for pavement analysis.

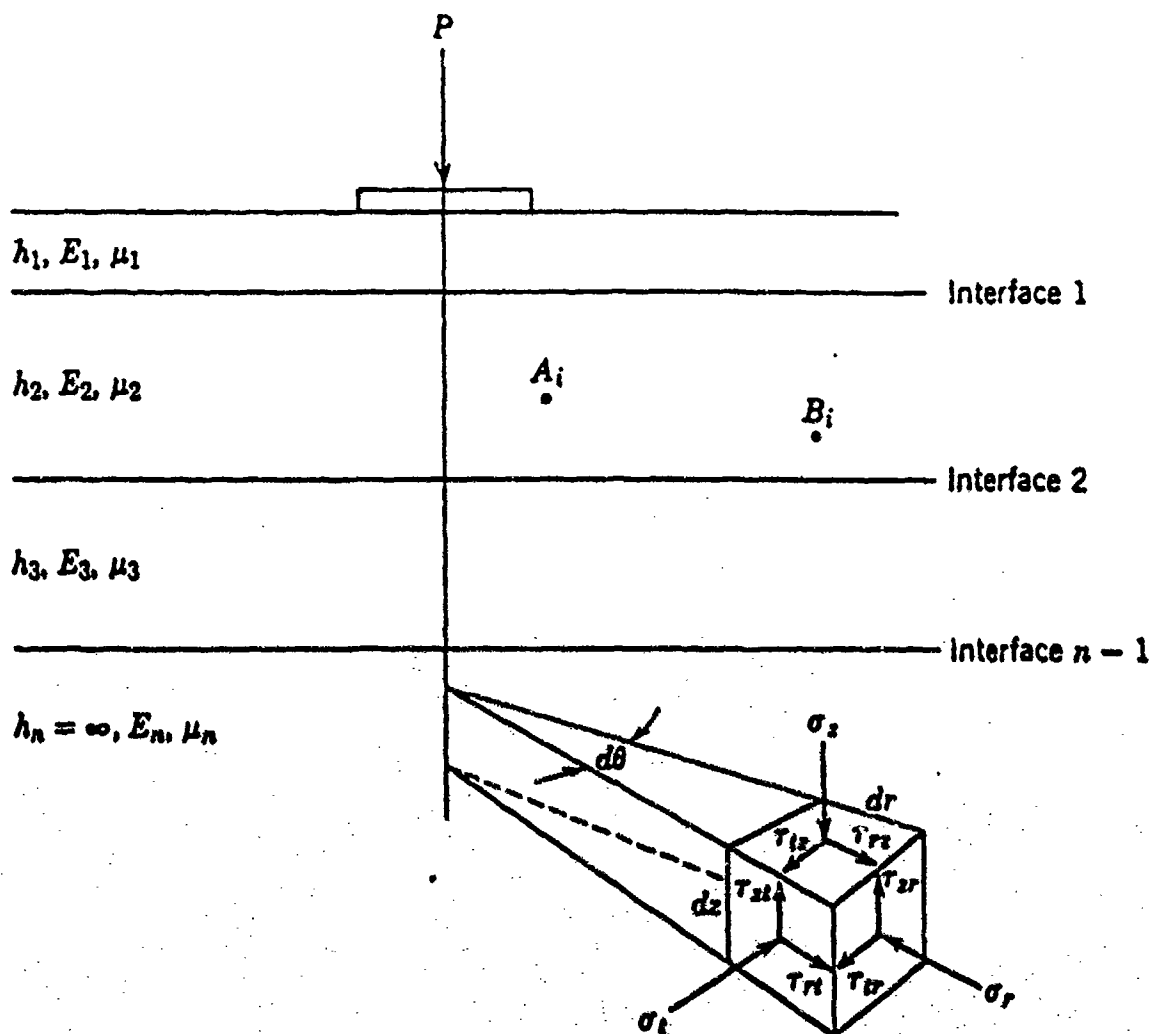


**Figure 2-1. Generalized Multilayer Elastic System
(Yoder and Witczak)**

Avramesco concluded from a theoretical study that for elastic materials, if the speed of the load is a fraction of the Rayleigh wave velocity of the subgrade, the distribution of stresses and strains is equal to the static case. Comparison stresses and strains for a static load to values corresponding to vehicles with a speed of 270 mph resulted in a difference of less than 10 percent. Other studies reported at the Second International Conference on the Structural Design of Asphalt Pavement show that as the speed of the load increases, strains and deflections decrease and stresses increase. This is attributed to an increase in the modulus of asphalt concrete with decreasing load duration and stress relaxation with time. These studies suggest the assumption of static load can be compensated for by characterizing the properties of the asphalt concrete at a load duration equal to the field conditions.

Lister and Jones studied the effect of nonuniform, noncircular loads and concluded that the net effect of these two assumptions resulted in an error of less than two percent under a whole range of realistic tire and load conditions. Gross overloading of a tire results in an error of about seven percent. Saraf et al. concluded elastic layer theory overestimates the tensile strain at the bottom of the asphalt layer compared to a finite element analysis.

The principle of superposition is commonly used for the analysis of structures. Ahlvin et al. presented experimental data supporting the use of this theory for pavement analysis.

McCullough and Brown and Pell concluded the assumption of continuity across the interface of the layers is valid for pavement analysis.

The assumption of infinite horizontal dimensions of the layers is a major drawback to the use of the model for pavement structures. Edges, joints and cracks in pavements increase the stresses generated by wheel loads. Since the interior loading condition is a more realistic assumption for flexible pavements than for concrete pavements, ELT has been more widely applied to flexible pavements.

Several investigators have demonstrated that the stresses and strains in a pavement are sensitive to the thickness of the subgrade. While determining the thickness of the subgrade is a concern, it is not a limitation of the model as a rigid layer can be simulated by using high modulus values to simulate the presence of a bed rock layer.

The material assumptions used in ELT are vastly different from the behavior of the material characteristics, especially for asphalt pavement. Therefore, there has been considerable research into the effects of these assumptions on the reliability of the ELT analysis. Engineers that employ

ELT for pavement analysis rely on measuring the material properties under simulated field conditions. Different test procedures will produce different measures of the material properties. This will result in different primary responses estimated by ELT and, therefore, when the primary responses are used in the limiting response functions, the prediction of distress may be in error due to the formulation of the analysis problem.

There are several computer codes for the solution of elastic layer theory equations. Three widely used programs in the United States are:

1. CHEV5L or LAYER developed by California Research Company, a division of Chevron Oil;
2. BISAR developed by Shell Oil Co.40; and
3. ELSYM5 developed by Ahlborn at the University of California.

The CHEVRON program is capable of analyzing five layers and a single load. Input and output are in the radial coordinate system which complicates the interpretation of the data. The ELSYM5 program uses the same basic algorithm as CHEV5L for the solution of layer theory equations. However, an input and output processor are used to allow the use of rectangular coordinates. In addition to being more convenient to the user, the rectangular coordinate system permits the use of superposition to permit the analysis of multiple loads. ELSYM5 can analyze up to ten identical loads. As with CHEV5, ELSYM5 can analyze up to five layers. In addition, ELSYM5 permits the definition of a rigid layer under the five conventional layers. The interface at the rigid layer can be full friction or full slip.

The accuracy of these programs has been tested by several researchers with the conclusion that the programs faithfully perform the required calculations in most cases. However, there are some problems near the pavement surface directly under the load. With respect to ELSYM5 Ahlborn states that the program uses a truncated series for the integration process that leads to some approximations for the results at and near the surface and at some points out at some distance from the load.

The CHEV5L and ELSYM5 programs are widely available and are in the public domain. The Federal Highway Administration sponsored the modification of the program to operate on a microcomputer with a full-screen editor for inputting the data. This program is available from the McTRANS Center at the University of Florida.

BISAR is the most powerful of the ELT programs. It can handle up to 10 layers and 10 different loads. Burmister's theory has been modified in this program to permit the analysis of shear loads at the pavement surface and varying interface continuity between the pavement layers ranging from full continuity to full slip. The mathematical techniques used in the BISAR programs are reported to be more sophisticated than the CHEV5L program. Shahin, Krichner, and Blackmon demonstrated the application of the capability of the BISAR program for the analysis of slip between an overlay and the original pavement surface. Parker et al. selected the BISAR program for use in a pavement design procedure developed by the Corps of Engineers. Reasons for this selection included the mathematical sophistication of the solution process and the ability to analyze varying interface conditions.

The capabilities of the CHEV5L program have been expanded by several researchers. Shahin developed an iteration method for introducing stress sensitivity into the elastic layer theory analysis. Other modifications permit the analysis of up to 15 layers.

The Kausel and Peek program computes displacements. This program was modified by Sebaaly to include the calculation of stresses and strains.

2.2 Thin Plate Theory

As opposed to flexible pavements which distribute the load gradually through the pavement structure, rigid pavement slabs act as a structural element (a plate) resting on an elastic foundation. Since the deflection of rigid pavements is small relative to their thickness, they can be analyzed as thin plates. The following approximations are required for the development of thin plate models:

1. There is no deformation in the middle plane of the slab; this plane remains neutral.
2. The planes in the slab initially normal to the middle plane of the slab remain normal after bending.
3. The normal stresses in the direction transverse to the plane of the slab can be ignored.

Sargious reports that the differential equation describing the deflected surface of a slab subjected to a uniform load was developed by LaGrange in 1811. This report identifies Westergaard as the first to develop a theoretical solution for rigid pavement design. Sargious identifies the assumptions used in the development of the Westergaard equations as:

1. The concrete slab acts as a homogeneous elastic solid in equilibrium.

2. The reaction of the subgrade is solely vertical, and proportional to the deflection of the slab.
3. The reaction of the subgrade per unit area at any given point is equal to a constant, X (modulus of subgrade reaction), multiplied by the deflection at that point.
4. The thickness of the slab is uniform.
5. The load at the interior and at the corner of the slab is distributed uniformly over a circular contact area; for the corner loading the circumference of this circular area is tangential to the edge of the slab.
6. The load at the interior edge of the slab is distributed uniformly over a semicircular contact area, the diameter of the semicircle being along the edge of the slab.

Although not commonly stated, it should be noted that Westergaard also assumed a static load condition. Based on these assumptions, Westergaard developed equations for computing the stresses in the slab for the following cases:

1. Maximum tensile stress at the bottom of the slab due to central loading.
2. Maximum tensile stress at the bottom of the slab for an interior edge loading in a direction parallel to the edge.
3. Maximum tensile stress at the top of the slab in a direction parallel to the bisector of the corner angle for corner loading.

Subsequently, Westergaard modified the equations specifically for the analysis of airport pavements assuming elliptical load areas and load transfer across the joint or edge of the pavement. In 1951, Pickett presented equations for "protected" and "unprotected" corners. The Westergaard equations are widely used for the design of concrete pavements. Pickett and Ray developed influence charts for the solution of these equations and Packard incorporated them into a generalized program for the sign of portland cement concrete pavements.

3. Distress Models

The mechanistic models described in the preceding chapter compute the response of the pavement to traffic and environmental loads. Relationships are now needed for using these responses to estimate the life of the pavement. Since pavements are designed for multiple applications of repeated loads, the distress models should capture the accumulated damage to the pavement materials. However, damage is a vague term. Pavements display many types of distress and, in general, damage functions must be developed for the prediction of specific distress types. In the related literature, there is a preponderance of information on two primary distress types:

1. fracture of the pavement surface due to repeated axle load applications, fatigue; and
2. distortion of the surface to repeated accumulation of plastic or viscous strains in the wheel path (rutting).

Several other distress types have also been examined in the literature including reflection cracking of asphalt overlays of jointed pavements and stripping of asphalt concrete.

3.1 Fatigue

Fatigue is generally considered to be the fracture of the pavement surface due to the repeated application of traffic loads. Both asphalt and concrete pavements are subject to fatigue failure. Two basic approaches have been taken to the modeling of fatigue behavior: phenomenological and power law. In the phenomenological approach, the number of applications a pavement can carry prior to failure is estimated directly as a function of the stress or strain levels generated by the traffic loadings. The power law approach uses concepts developed in fracture mechanics to estimate the growth of a crack through the pavement layer.

The phenomenological approach has been widely applied in the analysis of pavement fatigue life. Although both asphalt and concrete pavements will fail in fatigue, the behavior of these materials with respect to repeated loads is very different in that concrete appears to have a "fatigue limit." It is generally assumed that concrete will not fail in fatigue if the stresses in the slab are kept below 50 percent of the modulus of rupture, as measured with the flexural test.

Conversely, asphalt concrete does not appear to have a fatigue limit. In other words, repeated application of even the smallest level of strain will eventually result in fatigue failure.

3.1.1 Phenomenological Model

In the phenomenological approach, the fatigue life of the asphalt is generally related to the strain in the pavement as:

$$N = a(1/\epsilon)^b \quad (10)$$

where

N = the number of applications to failure

a, b = fatigue-life coefficients

ϵ = strain in the asphalt concrete

Some authors have modified this equation to include the stiffness of the asphalt and others substitute stress for the strain term. Laboratory tests have demonstrated that a and b coefficients are sensitive to mix design parameters, such as asphalt content, air voids, aggregate gradation, etc., and to the mode of testing. Attempts to compare the results of laboratory testing with field performance have demonstrated poor correlation. Generally, pavements last longer than laboratory fatigue testing and analysis predict. The difference between field performance and laboratory estimates are expressed in terms of a shift factor. This shift factor is frequently in the range of 20 to 25, but factors as large as 1000 have been reported.

In addition to the problem of the correlation of laboratory and field testing, the variability of fatigue testing should be considered in the development of a design procedure based on the phenomenological approach. Navarro and Kennedy reported the coefficient of variation of laboratory fatigue testing ranges from 53 to 73 percent.

There are many examples of the use of the phenomenological approach for the prediction of the fatigue life of highway pavements. However, there are relatively few examples of the use of this approach for the design and analysis of airport pavements. Kelly and Thompson used the ILLIPAVE program and a fatigue equation for the analysis of airfield pavements for F15 aircraft. Strain at the bottom of the asphalt concrete surface was computed with ILLIPAVE and the fatigue life was computed with the equation:

$$N = 259(1/\epsilon)^{3.16} (1/E)^{1.4} \quad (11)$$

where

N = number of estimated applications of strain

ϵ = strain at the bottom of the asphalt concrete layer

E = modulus of the asphalt concrete.

This equation was developed through an ILLIPAVE analysis of the AASHTO Road Test.

The Waterways Experiment Station has developed an elastic layer theory method for the design of flexible pavements that uses the phenomenological approach for estimating the fatigue life of airfield pavements. This design procedure uses the equation:

$$N = 479(1/\epsilon)^5(1/E)^{2.665} \quad (12)$$

This equation was developed from an analysis of experimental pavement sections designed and tested to simulate airfield pavements.

While the WES and the Kelly-Thompson equations have the same form, the coefficients are considerably different. For a strain of 0.0005 in/in and a modulus of 500,000 psi, the WES equation estimates approximately 10,000 repetitions can be applied to the pavement while the Kelly-Thomas equation estimates in excess of 73,000 applications. This demonstrates the problem with the phenomenological approach to fatigue analysis. Prediction models developed by different researchers appear to be more a function of the analysis procedure used in the development than determined from the basic properties of the materials.

3.2 Deformations

Plastic and viscous deformations of the pavement materials result in permanent deformations of the surface. Channelized traffic generates an accumulation of deformations in the wheel paths of the vehicle or rutting. Three approaches have been defined for relating the primary response of pavements to rutting:

1. limiting the magnitude of the maximum vertical strain in the subgrade;
2. relating permanent strains to stresses or strains computed with elastic theories; and
3. direct estimates of permanent strains with viscoelastic models.

The limiting strain approach was first presented by Dorman in 1962 and Klomp and Dorman in 1964. It is currently used in the Asphalt Institute airfield pavement design method and the Joint Department of Army and Air Force elastic layer theory method for the design of flexible pavements. The basic hypothesis of this approach is that if the maximum compressive strain at the surface of the subgrade is less than a critical value, then excessive rutting will not occur for a specified number of repetitions. These relationships were developed based on analysis of the Corps of Engineers pavement design procedures.

The Army and Air Force elastic layer theory procedure for the design of flexible pavements uses limiting subgrade criteria for estimating the number of applications a pavement can withstand before excessive permanent deformation occurs. The criteria are specified by the equation:

$$N = 10,000(A/S_s)^B \quad (13)$$

where

N = number of applications the pavement can sustain at a given strain level

S_s = vertical compressive strain at the top of the subgrade

A = $0.000274 + 0.000245 \log M_R$

M_R = Modulus of the subgrade

B = $0.0658(M_R)^{0.559}$

All pavement designs are based on a 20-year design life and the traffic volume is expressed in terms of the annual number of departures. All departures are assumed to be at 95 percent of the maximum aircraft weight. The design curves are based on the number of coverages of aircraft based on the statistical distribution of aircraft wander across the pavement rather than the actual number of departures. This modification to the number of applications is transparent to the designer and is documented in an Appendix.

The traffic analysis procedure is common to the design of both flexible and rigid pavements. All classes of aircraft that will use the facility are reduced to the number of equivalent annual departures of a design aircraft. The design aircraft is defined as the aircraft that would require the greatest pavement thickness if it were the only aircraft using the facility. Since the pavement design charts consider both the number of applications and the aircraft weight, the design

aircraft will not necessarily be the heaviest aircraft. In essence, determining the equivalent annual applications requires:

1. Converting all aircraft types to the gear type of the design aircraft by multiplying the number of annual applications for each aircraft type by equivalency factors.
2. Converting the number of adjusted annual applications to the equivalent number of design aircraft applications by using the equation:

$$\log(R_1) = (w_2/w_1)^{1/2} \log(R_2) \quad (14)$$

where

- R_1 = equivalent number of annual departures for the design aircraft
 - R_2 = annual departures expressed in design aircraft landing gear
 - w_1 = wheel load of design aircraft
 - w_2 = wheel load of the aircraft being analyzed (the wheel load for wide-bodied aircraft is computed on the basis of 300,000 lbs maximum aircraft weight rather than the actual gross maximum weight)
3. The number of equivalent departures is summed to determine the total number of departures for use in design.

4. References

1. Shahin, M.Y., and Kohn, S.D., (1981) "Pavement Management System for Roads and Parking Lots," Technical Report M-294, U.S. Army Corps of Engineers Construction Engineering Research Laboratory, Champaign, IL.
2. Yoder, E.J., and Witczak, M.W. (1975) Principles of Pavement Design, John Wiley & Sons, New York
3. Sargious, M., (1975) Pavements and Surfacing for Highway and Airports, John Wiley and Sons, New York
4. Chou, Y.T. (1977) "Engineering Behavior of Pavement Materials: State of the Art," Federal Aviation Administration Report No. FAA-RD-77-37, Washington, DC
5. Westmann, R.A., (1971) "Fundamentals of Material Characterization," Structural Design of Asphalt Concrete Pavement Systems, Highway Research Board Special Report 126, Washington, DC
6. Sentler, L., (1987) "A Strength Theory for Viscoelastic Materials," Document D9:1987, Swedish Council for Building Research, Stockholm
7. Derucher, K.N., and Korfiatis, G.P. (1988) Materials for Civil and Highway Engineers, Prentice Hall, New Jersey
8. Cordon, W.A. (1979) Properties, Evaluation and Control of Engineering Materials, McGraw-Hill, Inc., New York
9. Mazaras, J., and Pijandier-Cabot, G. (1989) Continuum Damage Theory - Application to Concrete, Journal of Engineering Mechanics, Vol. 115(2) ASCE
10. Monismith, C., Epps, J.A., and Finn, F.N. (1985) "Improved Asphalt Concrete Mix Design," American Association of Asphalt Paving Technologists, Proceedings, Volume 54
11. Deacon, J.A. (1971) "Material Characterization - Experimental Behavior," Structural Design of Asphalt Concrete Pavement Systems, Highway Research Board Special Report 126, Washington, DC
12. Mamlouk, M., and Sarofim, R.T. (1988) "Modulus of Asphalt Mixtures - An Unresolved Dilemma," Transportation Research Board, Research Record 1171, p. 193, Washington, DC

13. Cedergren, H.R. (1988) "Why All Important Pavements Should Be Well Drained," Transportation Research Board, Research Record 1188, p. 56, Washington, DC
14. Hicks, R.G., (1970) Factors Influencing the Resilient Properties of Granular Materials, Dissertation Series, University of California, Berkeley
15. Kohn, S.D., and Bentsen, R.A. (1987) "Performance of Flexible Airfield Pavements Subjected to High Traffic Volumes," p. 638 Proceedings, The Sixth International Conference Structural Design of Asphalt Pavements, Ann Arbor, Michigan
16. Saraf, C., Marshak, K., Chen, H., and Hudson, W.R., (1987) "The Effect of Truck Tire Contact Pressure Distribution on the Design of Flexible Pavements," Proceedings, The Sixth International Conference Structural Design of Asphalt Pavements, Ann Arbor, Michigan
17. Bonaquist, R., Surdahl, R., and Mogawer, W. (1989) "Effect of Tire Pressure on Flexible Pavement Response and Performance," Transportation Research Board, Research Record 1227, p. 97, Washington, DC
18. Huhatla, M., Pihlajamaki, J., and Pieninaki, M. (1989), "Effect of Tires and Tire Pressures on Road Pavements," Transportation Research Board, Research Record 1227, p. 107, Washington, DC
19. Sebaaly, P., and Tabatabaee, N. (1989), "Effect of Tire Pressure and Type on the Response of Flexible Pavements," Transportation Research Board, Research Record 1227, p. 115, Washington, DC
20. Wignot, J.E., Durup, P.C., Wittlin, G., Scott, R.B., and Gamom, M.A. (1970) "Aircraft Dynamic Wheel Load Effects on Airport Pavements," Federal Aviation Administration, Report No. FAA-RD-70-19, Washington, DC
21. Hightner, W.H., and Harr, M.E. (1973) "Application of Energy Concepts to the Performance of Airfield Pavements," Air Force Weapons Laboratory, Technical Report Number AFWL-TR-72-225, Kirtland Air Force Base, New Mexico
22. HoSang, V.A. (1975) "Field Survey and Analysis of Aircraft Distribution on Airport Pavements," Federal Aviation Administration, Report FAA-RD-74-36, Washington, DC
23. HoSang, V.A. (1978) "Field Survey and Analysis of Aircraft Distribution on Airport Pavements," Transportation Research Board, Special Report 175, Washington, DC

24. Ledbetter, R.H. (1978) "Effects of Dynamic Loads on Airport Pavements," Transportation Research Board, Special Report 175, Washington, DC
25. Himeno, K., Watanabe, T., and Maruyama, T. (1987) "Estimation of Fatigue Life of Asphalt Pavement," p. 272, Proceedings, The Sixth International Conference Structural Design of Asphalt Pavements, Ann Arbor, Michigan
26. Haas, R.C.G., and Hudson, W.R. (1978) Pavement Management Systems, McGraw-Hill, Inc., New York
27. Hudson, W.R., and McCullough, B.F., (1973) "Flexible Pavement Design and Management: Systems Formulation," National Cooperative Highway Research Program Report 139
28. Gomez-Achecar, M. and Thompson, M.R. (1986) "ILLI-PAVE-Based Response Algorithms for Full-Depth Asphalt Concrete Flexible Pavements," p. 11, Transportation Research Board, Transportation Research Record 1095, Washington, DC
29. Sentler, L., (1987) "A Strength Theory for Viscoelastic Materials," Report D9:1987, Swedish Council for Building Research, Stockholm, Sweden
30. Nair, K. (1971), "Solutions and Solution Techniques for Boundary Value Problems," p. 103, Structural Design of Asphalt Concrete Pavement Systems, Highway Research Board, Special Report 126, Washington, DC
31. Burmister, D.M. (1945) "The General Theory of Stresses and Displacements in Layered Systems," Journal of Applied Physics, Vol. 16(2) p. 89, Vol. 16(3) p. 126, Vol. 16(5), p. 296
32. Westergaard, H.M. (1927), "Theory of Concrete Pavement Design," Proceedings, Highway Research Board
33. Avramesco, A., (1967) "Dynamic Phenomena in Pavements Considered as Elastic Layered Structures," Proceedings, The Second International Conference on the Structural Design of Asphalt Pavements, Ann Arbor, Michigan
34. Lister, N.W., and Jones, R. (1967), "The Behavior of Flexible Pavements Under Moving Wheel Loads," Proceedings, The Second International Conference on the Structural Design of Asphalt Pavements, Ann Arbor, Michigan

35. Saraf, C., Marshak, K., Chen, H., and Hudson, W.R., (1987) "The Effect of Truck Tire Contact Pressure Distribution on the Design of Flexible Pavements," Proceedings, The Sixth International Conference Structural Design of Asphalt Pavements, Ann Arbor, Michigan
36. Ahlvin, R.G., Chou, Y.T., and Hutchinson, R.L. (1973), "The Principle of Superposition in Pavement Analysis," Highway Research Board, Highway Research Record 466, p. 153, Washington, DC
37. McCullough, B.F. (1969) A Pavement Overlay Design System Considering Wheel Loads, Temperature Changes and Performance, Doctoral Dissertation, University of California, Berkeley
38. Brown, S.F., and Pell, P.S. (1967), "An Experimental Investigation of the Stresses, Strains and Deflections in a Layered Pavement Subjected to Dynamic Loads," Proceedings, The Second International Conference on the Structural Design of Asphalt Pavements, Ann Arbor, Michigan
39. Chevron Oil Company, (1963) development of the elastic layer theory program
40. De Jong, D.L., Peutz, M.G.F., and Korswagen, (1973) "Computer Program BISAR," External Report Koninklijke/Shell Laboratorium, Amsterdam, Holland
41. Ahlborn, G., (1972) "Elastic Layer System with Normal Loads," Institute for Transportation and Traffic Engineering, University of California, Berkeley
42. McTrans, The Center for Microcomputers in Transportation, The University of Florida, 512 Weil Hall, Gainesville, FL, 32611, (904) 392-0373
43. Shahin, M.Y., Kirchner, K., and Blackmon, E. (1987), "Analysis of Asphalt Concrete Layer Slippage and Its Effect on Pavement Performance," p. 958, Proceedings, Sixth International Conference on the Structural Design of Asphalt Concrete Pavements, Ann Arbor, Michigan
44. Parker, F., Barker, W.R., Gunkel, R.C., and Odum E.C. (1979) "Development of a Structural Design Procedure for Rigid Airport Pavements," Federal Aviation Administration Report No. FAA-RD-77-81, Washington, DC

45. Shahin, M.Y., (1971), "A Computer Program for an Iterative Method of Pavement Structural Analysis," Unpublished technical memorandum, Center for Highway Research, University of Texas, Austin
46. Zaniwski, J.P., (1978) Design Procedure for Asphalt Concrete Overlays of Flexible Pavements, Doctoral Dissertation, University of Texas, Austin
47. Aston, J.E., and Moavenzadeh, F. (1967), "Analysis of Stresses and Displacements in a Three-Layered Viscoelastic System," p. 149, Proceedings, Second International Conference on the Structural Design of Asphalt Concrete Pavements, Ann Arbor, Michigan
48. Lee, E.H. (1961), "Stress Analysis in Viscoelastic Materials," Journal of Applied Physics, Vol. 13(2) p. 183
49. Pister, K.S. (1961), "Viscoelastic Plates on Viscoelastic Foundations," Journal of the Engineering Mechanics Division, ASCE, p. 43
50. Pister, K.S., and Westman, R.A. (1962), "Analysis of Viscoelastic Pavements," p. 20, Proceedings, International Conference on the Structural Design of Asphalt Pavements, Ann Arbor, Michigan
51. Ishihara, K., (1962), "The General Theory of Stresses and Displacements in Two-Layer Viscoelastic Systems," The Japanese Society of Soil Mechanics and Foundations Engineering, Soils and Foundations, Vol. 2(2), Tokyo, Japan
52. Lee, E.H. and Rogers, T.G. (1961) "Solution of Viscoelastic Stress Analysis Problems Using Measured Creep or Relaxation Functions," Division of Applied Mathematics, Brown University
53. Hopkins, I.L. and Hamming, R.W. (1957), "On Creep and Relaxation," p. 906, Journal of Applied Physics, Vol. 28
54. Moavenzadeh, F., and Elliot, J.F. (1972), "A Stochastic Approach to Analysis and Design of Highway Pavements," Proceedings, Third International Conference on the Structural Design of Asphalt Pavements, London, England
55. Rauhut, J.B., et al. (1975), Sensitivity Analysis of VESYS, Austin Research Engineers, Final Report to the Federal Highway Administration

56. Hufferd, W.L. and Lai, J.S. (1978) "Analysis of N-Layered Viscoelastic Pavement Systems," Federal Highway Administration Report No. FHWA-RD-78-22, Washington, DC
57. Khosla, N.P. (1987), "A Field Verification of VESYS IIIA Structural Subsystems," p. 486, Proceedings, Sixth International Conference Structural Design of Asphalt Pavements, Ann Arbor, Michigan
58. Beckedahl, H., Gerlach, A., L_cke, H., and Schwaderer, W. (1987), "On Improvements of the Existing VESYS Concepts," p. 677, Proceedings, Sixth International Conference Structural Design of Asphalt Pavements, Ann Arbor, Michigan
59. Lattes, R., Lions, J.L., and Bonitzer, J. (1962), "Use of Galerkin's Method for the Study of Static and Dynamic Behavior of Road Structures," p. 238, Proceedings, International Conference on the Structural Design of Asphalt Pavements, Ann Arbor, Michigan
60. Bastiani, A. (1962), "The Explicit Solution of the Equations of the Elastic Deformations for a Stratified Road Under Given Stresses in the Dynamic Case," p. 351, Proceedings, International Conference on the Structural Design of Asphalt Pavements, Ann Arbor, Michigan
61. Ishihara, K., and Kimura, T. (1967), "The Theory of Viscoelastic Two-Layer Systems and Conception of Its Application to the Pavement Design," p. 189, Second International Conference on the Structural Design of Asphalt Concrete Pavements, Ann Arbor, Michigan
62. Perloff, W.H., and Moavenzadeh, F. (1967), "Deflection of Viscoelastic Medium Due to a Moving Load," p. 212, Second International Conference on the Structural Design of Asphalt Concrete Pavements, Ann Arbor, Michigan
63. Mamlouk, M.S. (1987), "Dynamic Analysis of Multilayered Pavement Structures - Theory, Significance and Verification," p. 466, Proceedings, Sixth International Conference on the Structural Design of Asphalt Concrete Pavements, Ann Arbor, Michigan
64. Weiss, R.A. (1977), "Subgrade Elastic Moduli Determined from Vibratory Testing of Pavements," U.S. Army Engineer, Waterways Experiment Station, Vicksburg, Miss.
65. Weiss, R.A. (1979), "Pavement Evaluation and Overlay Design: Method that Combines Layered-Elastic Theory and Vibratory Nondestructive Testing," Transportation Research Board, Research Record 700, p. 20, Washington, DC

66. Szendrei, M.E. and Freeme, C.R. (1967), "The Computation of Road Deflections Under Impulsive Loads from the Results of Vibration Measurements," p. 89, International Conference on the Structural Design of Asphalt Concrete Pavements, Ann Arbor, Michigan
67. Eringen, A.C. and Suhubi, E.S. (1975), Elastodynamics, Vol. 2. Linear Theory, Academic Press, New York
68. Kausel, E. and Peek, R. (1982) "Dynamic Loads in the Interior of a Layered Stratum: An Explicit Solution," p. 1459, Bulletin of the Seismological Society of America, Vol. 72(5)
69. Sebaaly, B.E. (1987), Dynamic Models for Pavement Analysis, " Doctoral Dissertation, Arizona State University, Tempe
70. Westergaard, H.M., (1927) "Theory of Concrete Pavement Design," Proceedings, Highway Research Board
71. Westergaard, H.M., (1948) "New Formulae for Stresses in Concrete Pavements of Airfields," Transactions, ASCE
72. Pickett, G., and Ray, G.K. (1951), "Influence Charts for Concrete Pavements," Transactions, ASCE
73. Packard, R.G., "Computer Program for Airport Pavement Design," Portland Cement Association, Skokie, IL.
74. Packard, R.G., (1973) "Design of Concrete Airport Pavement," Portland Cement Association, Skokie, IL.
75. Stelzer, C.F., and Hudson, W.R. (1967), "A Direct Computer Solution for Plates and Pavement Slabs," Research Report 569, Center for Highway Research, University of Texas, Austin
76. Burnet, D. (1987), Finite Element Analysis from Concepts to Applications, Addison-Wesley Publishing Co., Mass
77. Ioannides, A.M. (1987) "Axisymmetric Slabs of Finite Extent Solid," American Society of Civil Engineers, Journal of Transportation Engineering, Vol. 113, pp. 277-290
78. Duncan, J.M., Monismith, C.L., and Wilson, E.L. (1968), "Finite Element Analysis of Pavements," Highway Research Board, Highway Research Record 228, Washington, DC

79. Pichumani, R. (1972), "Application of Computer Codes to the Analysis of Flexible Pavement," Proceedings, Third International Conference on the Structural Design of Asphalt Pavements, London, England
80. Raad, L., and Figueroa, J.L. (1980), "Load Response of Transportation Support Systems," p. 111, Transportation Engineering Journal, ASCE, Vol. 106, No. TE1
81. Baladi, G. (1989), "Fatigue Life and Permanent Deformation Characteristics of Asphalt Concrete Mixes," p. 75, Transportation Research Board, Transportation Research Record 1227, Washington, DC
82. Smith, R.B., and Yandell, W.O. (1987), "Predicted and Field Performance of a Then Full-Depth Asphalt Pavement Placed Over a Weak Subgrade," p. 443, Proceedings, Sixth International Conference on the Structural Design of Asphalt Concrete Pavements, Ann Arbor, Michigan
83. Lim, P.N., and Yandell, W.O. (1988) "Reevaluation of Shell Life by Mechano-Lattice Analysis," ASCE Journal of Transportation Engineering, Vol. 114, pp. 435-449
84. Wang, S.K., Sargious, M.A., and Cheung, Y.K., (1972) "Advanced Analysis of Rigid Pavements," ASCE, Transportation Engineering Journal
85. Chou, Y.T., (1981) "Structural Analysis Computer Programs for Rigid Multicomponent Pavement Structures with Discontinuities, WESLIQID and WESLAYER," U.S. Army Engineering Waterways Experiment Station, Technical Report, GL-81-6, Vicksburg, Mississippi
86. Chou, Y.T., (1983) "Subgrade Contact Pressures Under Rigid Pavements," ASCE Journal of Transportation Engineering, Vol. 109, pp. 363-379
87. Tabatabaie, A.M., and Barenberg, E.J. (1980), "Structural Analysis of Concrete Pavement Systems," p. 493, Transportation Engineering Journal, ASCE, Vol. 106, No. TE5
88. Tia, M., Arnaghani, J.M., Wu, C.L., Lei, S., and Toye, K.L. (1987), "FEACONS III Computer Program for an Analysis of Jointed Concrete Pavements," p. 12, Transportation Research Board, Transportation Research Record 1136, Washington, DC

89. Triado-Crovetti, M.R., Darter M.I., Jayawickrama, P.W., Smith, R.E., and Lytton, R.L. (1988), "ODE Computer Program: Mechanistic-Empirical Asphalt Concrete Overlay Design," p. 30, Transportation Research Board, Research Record 1207, Washington, DC
90. Majidzadeh, K., Abdulshafi, A., Iives, G.J., and McLaughlin, A. (1987), "A Mechanistic Approach for Thermally Induced Reflection Cracking of Portland Cement Concrete Pavement with Reinforced Asphalt Overlay," p. 83, Transportation Research Board, Transportation Research Record 1117, Washington, DC
91. McCullough, B.F., Abou-Ayash, A., Hudson, W.R., and Randall, J.P. (1975), "Design of Continuously Reinforced Concrete Pavements for Highways," Final Report, NCHRP Project 1-15
92. Bradburu, R.D., (1938) "Reinforced Concrete Pavement," Wire Reinforced Institute
93. Ioannides, A.M., and Salsilli-Murua, R.A. (1989), "Temperature Curling in Rigid Pavements: An Application of Dimensional Analysis," p. 1, Transportation Research Board, Transportation Research Record 1227, Washington, DC
94. Navarro, D., and Kennedy, T.W. (1975), "Fatigue and Repeated Load Elastic Characteristics of Inservice Asphalt-Treated Materials," Center for Highway Research, University of Texas, Austin
95. Kelly, H.F., and Thompson, M.R. (1988) "Mechanistic Design Concepts for Heavyweight F15 Aircraft on Flexible Pavements," ASCE, Journal of Transportation Engineering, Vol. 114, pp. 323-340
96. "The AASHO Road Test: Report 5 - Pavement Research," Highway Research Board, Special Report 61E, 1962
97. "Flexible Pavement Design Method for Airfields (Elastic Layer Method)," Joint Departments of the Army and Air Force, U.S.A., Report No. TM 5-825-2-11, AFM 88-6, Ch. 2, 1989
98. "Comparative Performance of Structural Layers in Pavement Systems, Vol. II, Analysis of Test Section Data and Presentation of Design and Construction Procedures," Federal Aviation Administration Report No. FAA-RD-73-198II, 1977

99. Majidzadeh, K., and Kauffmann, E.M. (1971) "Analysis of Fatigue and Fracture of Bituminous Pavement Mixtures," Final Report, Phases I and II, Project RF 2845, Ohio Research Foundation
100. Majidzadeh, K., Kauffmann, E.M., and Chang, C.W. (1973) "Verification of Fracture Mechanics Concepts to Predict Cracking of Flexible Pavement," FHWA Final Report No. FHWA-RD-73-91
101. Majidzadeh, K., Kauffmann, E.M., and Ramsamooj, D.J. (1971) "Application of Fracture Mechanics in the Analysis of Pavement Fatigue," Association of Asphalt Paving Technologist, Vol. 40
102. Ramsamooj, D.V. (1970) The Design and Analysis of Flexible Pavements, PHD Dissertation, Ohio State University
103. Jayawickrama, P.W., and Lytton, R.L. (1987), "Method for Predicting Asphalt Concrete Overlay Life Against Reflection Cracking," p. 913, Proceedings, Sixth International Conference Structural Design of Asphalt Concrete Pavements, Ann Arbor, Michigan
104. Schapery, R.A. (1975), "A Theory of Crack Initiation and Growth in Viscoelastic Media, II Approximate Methods of Analysis," p. 369, International Journal of Fracture, Netherlands
105. George, K.P. (1970) "Theory of Brittle Fracture Applied to Soil Cement," p. 991, Journal of Soil Mechanics and Foundation Engineering, ASCE Vol. 96(3)
106. Crockford, W.W., and Little, D.N. (1987), "Tensile Fracture and Fatigue of Cement-Stabilized Soil," p. 520, Journal of Transportation Engineering, ASCE, Vol. 113(5)
107. Majidzadeh, K., Abdulshafi, A., Ilves, G.J., and McLaughlin, A. (1987), "A Mechanistic Approach for Thermally Induced Reflection Cracking of Portland Cement Concrete Pavement with Reinforced Asphalt Overlay," p. 83, Transportation Research Board, Transportation Research Record 1117, Washington, DC
108. Dormon, G.M. (1962) "The Extension to Practice of a Fundamental Procedure for the Design of Flexible Pavements," International Conference on the Structural Design of Asphalt Pavements, University of Michigan, Ann Arbor
109. Klomp, A.J.G., and Dormon, G.M. (1964) "Stress Distributions and Dynamic Testing in Relation to Road Design," Australian Road Research Board

110. Asphalt Institute, (1973) "Full-Depth Asphalt Pavements for Air Carrier Airports," The Asphalt Institute, Manual Series No. 11
111. Khosla, N.P. (1987), "A Field Verification of VESYS IIIA Structural Subsystems," p. 486, Proceedings, Sixth International Conference Structural Design of Asphalt Pavements, Ann Arbor, Michigan
112. Sneddon, R.V. (1986) "Evaluation and Verification of the VESYS IIIA Structural Design System for Two Test Sites in Nebraska," p. 18, Transportation Research Board, Transportation Research Record 1095, Washington, DC
113. Federal Aviation Administration, (1978) "Airport Pavement Design and Evaluation," AC 150/5320-6C, with change 1.
114. General Provisions for Airfield Pavement Design, Department of Defense, TM 5-824-1/AFM 88-1, Ch. 1 (1987)
115. Flexible Pavement Design for Airfields (1978), Triservice manual, Navy DM 21.3, Army TM 5-825.2, Air Force AFM 88-6, Ch. 2
116. Rigid Pavements for Airfields (1988) Army TM 5-825-3, Air Force AFM 88-6, Ch. 3
117. Airfield Pavements, (1973) NAVFAC DM-21, with changes 1 and 2

List of Symbols

a, b, n, A, k = constants

C_1, C_2 = relative stiffness coefficients

C/S = design prestress in concrete

DMR = design modulus of rupture

D_j = creep compliance function

E = modulus of the asphalt concrete

E_R = resilient modulus

E^* = complex modulus

f = average subgrade coefficient

f'_e = ultimate strength of concrete

$G(t)$ = relaxation function for a constant strain test

G_i = coefficient of the Dirichlet series

h_i = thickness of the i^{th} layer

$J(t)$ = creep function under constant stress

$J_v(t)$ = volumetric creep function

k = stress intensity factor

L = length

M_i = mass of i

MR = modulus of rupture

MR_{90} = 90 day average modulus of rupture

N = load repetition factor; number of applications to failure

N_E = number of equivalent departures of design aircraft

P = vertical point load or aircraft gear load

v = (as subscript) radial direction

r_s = foundation restraint stress

R = design flexural strength of concrete

R_1 = equivalent number of annual departures for the design aircraft

R_2 = annual departures expressed in design aircraft landing gear

S = stiffness of cohesionless soils

$S_{mix}(t,T)$ = volumetric creep function

S_s = vertical compressive strain at the top of subgrade

SB_{CBR} = subbase vertical compressive strain at the top of subgrade

SB_{CBR} = subgrade California Bearing Ratio (CBR)

t = time, (as subscript) time, tangential or transverse

T_p, T_B, T_S, T_{SB} = thickness of, respectively, pavement, base, surface, and subbase. Total pavement thickness $T_p = T_S + T_B + T_{SB}$

μ_i = i th component of the displacement vector in Cartesian coordinates

w = ratio of multiple wheel gear load to single wheel gear load

w_i = wheel load of the i^{th} wheel

W, W_D = weight, weight of design aircraft

α = coefficient of thermal expansion

δ_i = exponent of the Dirichlet series

ϵ = strain

ϵ_c = longitudinal strain

ϵ_0 = initial and constant strains

$\epsilon(t)$ = strain as a function of time

λ = Lame's constant

μ = Poisson's ratio, Lame's constant

ϕ = phase difference between stress and strain

ρ = mass density

σ = stress

σ_c = "frictional" stress

σ_o = hydrostatic stress

σ_3 = transverse principal stress

τ = shear stress

ω = angular frequency

CBR = California Bearing Ratio

T_{BM} = thickness of base

T_{sbb} = thickness of stabilized base

V = coefficient of variation of modulus of rupture, percent

M = factor for the average modulus of rupture during design life

E_b = modulus of elasticity of the base

E_c = modulus of elasticity of the concrete

h_o = required thickness of the plain concrete slab on a stabilized subgrade

h_d = thickness of plain slab that would be required if the slab was placed directly on the
subgrade

h_b = thickness of stabilized layer or lean concrete base

d_s = design prestress required in the concrete

B = load moment factor

h_p = design thickness of prestressed concrete

t_s = temperature warping stress

E_{BC} = modulus of the base course

ϵ_{ALL} = allowable strain

ϵ_h = horizontal tensile strain

ϵ_v = vertical compressive strain

n_i = expected number of strain repetitions of traffic

N_i = allowable number of strain repetitions

a, b = fatigue-life coefficients

Development of User Guidelines for a Three-Dimensional Finite Element Pavement Model

A. M. Ioannides

University of Illinois

J. P. Donnelly

Wiss, Janney, and Elstner Associates

Acknowledgements

The investigations for this paper were supported by Grant No. AFOSR-82-0143 from the Air Force Office of Scientific Research, Air Force Systems Command, Bolling Air Force Base, Washington, D.C. The Project Manager was Lt. Col. L. D. Kokanson. Professors M. R. Thompson and E. J. Barenberg were the Project Supervisors. Their advice and comments on the manuscript are greatly appreciated. The authors also acknowledge the cooperation of M. W. Salmon, formerly graduate research assistant at the University of Illinois.

Disclaimer

The contents of this paper reflect the views of the authors who are responsible for the facts and the accuracy of the data presented herein. Statements made do not necessarily reflect the official views or policies of the U.S. Air Force. This paper does not constitute a standard, specification, or regulation.

1. Introduction

A multi-component project, sponsored by the U.S. Air Force Office of Scientific Research (AFOSR), has recently examined current computerized analysis techniques for slabs-on-grade [1; 2]. The final stage of those investigations involved the use of an existing three-dimensional finite element model, which was adapted to provide a more realistic representation of a pavement system [3; 2]. One of the conclusions of that study was that a three-dimensional finite element program will be "indispensible in future efforts to establish the elusive 'unified' approach (to pavement design) and to develop a generalized mechanistic design procedure." The Federal Aviation Administration (FAA) initiative for the development of a "Unified Pavement Theory" has provided new impetus for considering the three-dimensional finite element approach and has renewed interest in studies for the development of user guidelines for this sophisticated technique.

This paper reports in detail the results of more than 100 three-dimensional finite element runs conducted to develop such user guidelines during the aforementioned AFOSR study. Research reported of the slab-on-grade problem. Findings presented provide an essential guide for the effective utilization of the three-dimensional finite element approach, and are described herein to facilitate development efforts under the FAA initiative, and perhaps eliminate the need for conducting such preliminary and time-consuming studies again.

2. Three-Dimensional Finite Element Computer Program Choice

The following features were considered necessary in selecting a three-dimensional finite element model for the analysis of a slab on an elastic solid foundation:

- a. Ease of data preparation and application;
- b. Output that is meaningful and easy to interpret;
- c. Flexibility in modeling a variety of pavement systems and loading conditions;
- d. Subgrade stress dependence; and
- e. Effective machine implementation with respect to memory storage and duration of execution.

Two programs with three-dimensional analysis capabilities are currently available at the University of Illinois: FINITE [5] and GEOSYS [4]. Both are multipurpose programs, i.e., they

include libraries of one-, two- and three-dimensional elements. FINITE is primarily designed as a tool for the structural engineer, while GEOSYS is geared more toward geotechnical problems. Unfortunately, due to their general nature, neither program is practical for routine analysis of pavement systems. The major problems are:

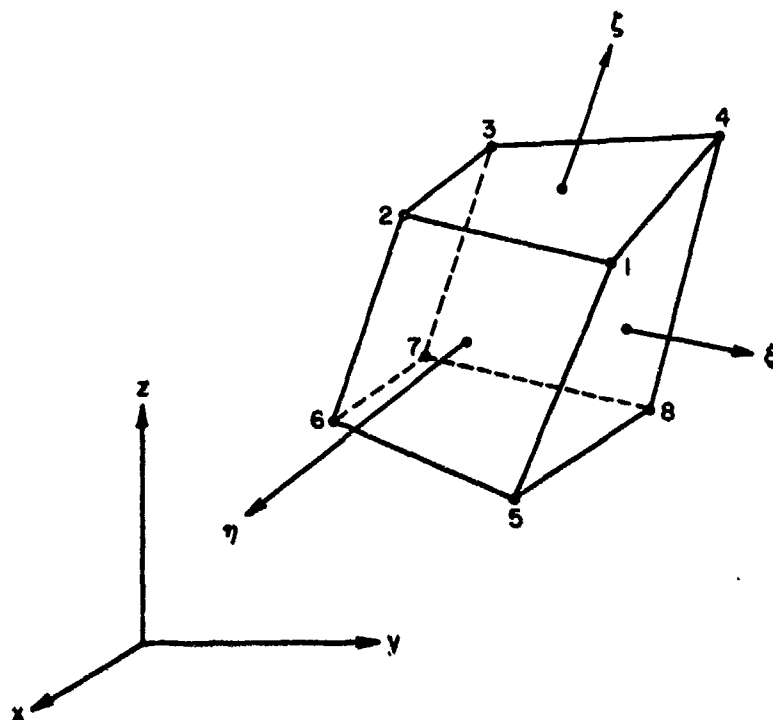
- a. A tremendous quantity of input data is required, even for the simplest slab-on-grade three-dimensional analysis; and
- b. Execution times are prolonged. This translates to prohibitive costs when the programs are implemented on a mainframe system.

For the purpose of this study, the GEOSYS finite element program was selected, primarily because its shorter code was freely accessible. This allowed its installation on a MARRIS 800-2 computer, on which a total of 48 Mbytes of virtual memory are available. Furthermore, the GEOSYS source code was modified to suit the needs of the present investigation. Thus, both of the deficiencies mentioned above could be addressed in a satisfactory manner.

3. GEOSYS

GEOSYS was developed in the early 1970s by a group of engineers, members of the technical staff of Agbabian Associates, El Segundo, California [4]. This program applies to general two- and three-dimensional problems and can accommodate time-dependent loading, gravity loading, and staged excavation or construction, using a wide variety of material characteristics. Multibuffering techniques allow accessing peripheral storage units, thereby reducing computer runtime for large, out-of-core problems. The element library contains several element types, including beam, rod, plane quad, brick and shell elements.

For the purpose of this study, the linear, isoparametric, three-dimensional hexahedral brick element was retained. This has eight nodes with three degrees-of-freedom per node (the displacements in each of the x, y and z directions). The assumed displacement approximations for this element are shown in Figure 1. The first eight are the standard compatible interpolation



Assumed displacement approximations:

$$u_x = \sum_{i=1}^8 h_i u_{xi} + h_9 a_{x1} + h_{10} a_{x2} + h_{11} a_{x3}$$

$$u_y = \sum_{i=1}^8 h_i u_{yi} + h_9 a_{y1} + h_{10} a_{y2} + h_{11} a_{y3}$$

$$u_z = \sum_{i=1}^8 h_i u_{zi} + h_9 a_{z1} + h_{10} a_{z2} + h_{11} a_{z3}$$

where:

$$h_1 = 1/8 (1+\xi) (1+\eta) (1+\zeta)$$

$$h_2 = 1/8 (1-\xi) (1+\eta) (1+\zeta)$$

$$h_3 = 1/8 (1-\xi) (1-\eta) (1+\zeta)$$

$$h_4 = 1/8 (1+\xi) (1-\eta) (1+\zeta)$$

$$h_5 = 1/8 (1+\xi) (1+\eta) (1-\zeta)$$

$$h_6 = 1/8 (1-\xi) (1+\eta) (1-\zeta)$$

$$h_7 = 1/8 (1-\xi) (1-\eta) (1-\zeta)$$

$$h_8 = 1/8 (1+\xi) (1-\eta) (1-\zeta)$$

$$h_9 = (1-\xi^2)$$

$$h_{10} = (1-\eta^2)$$

$$h_{11} = (1-\zeta^2)$$

Figure 1. Linear, Three-Dimensional, Isoparametric Brick Element

functions. The other three are incompatible and are associated with linear shear and normal strains. The nine incompatible modes are eliminated at the element stiffness level by static condensation.

A typical input file for GEOSYS consists of several hundred lines, each formatted according to a strict pattern. Since data for different slab-on-grade analysis runs are generally similar in structure, a preprocessor called GEZIN (GEOSYS Easy INput) was coded early in this study. This automatically prepares the data in the required format. Input for GEZIN includes fewer than 10 data cards, the format of which is similar to the one used for ILLI-SLAB [1]. The latter is a two-dimensional finite element rigid pavement analysis program, extensively used at the University of Illinois and elsewhere. Thus, data preparation is reduced to an almost trivial task and the probability of errors during this stage is practically eliminated.

Several post-processing programs were also coded during this investigation, to assist interpretation of computer results. These post-processors are used in conjunction with an iterative scheme introduced to account for the stress-dependent behavior of typical fine grained soils [2; 3].

4. Scope of Studies

The problem of a slab-on-grade may be investigated in three dimensions using a finite element mesh similar to the one shown in Figure 2. The slab rests on a cube of soil, carved out of the Boussinesq half-space and maintained intact by the assumption of boundary conditions on the four vertical sides and on the base. The implication is that if arbitrarily introduced boundaries are far enough from the critical locations of response, they will have no effect on the behavior of the system. It is, therefore, necessary to determine the required lateral and vertical extents of the subgrade, dictated by each of the available boundary condition choices.

The effect of mesh fineness must also be considered, as is the selection of a method for extrapolating finite element stress results. Investigations for both interior and edge loading conditions have been conducted [2]. Only the former are discussed in this paper, however, since they have been found to be adequately representative.

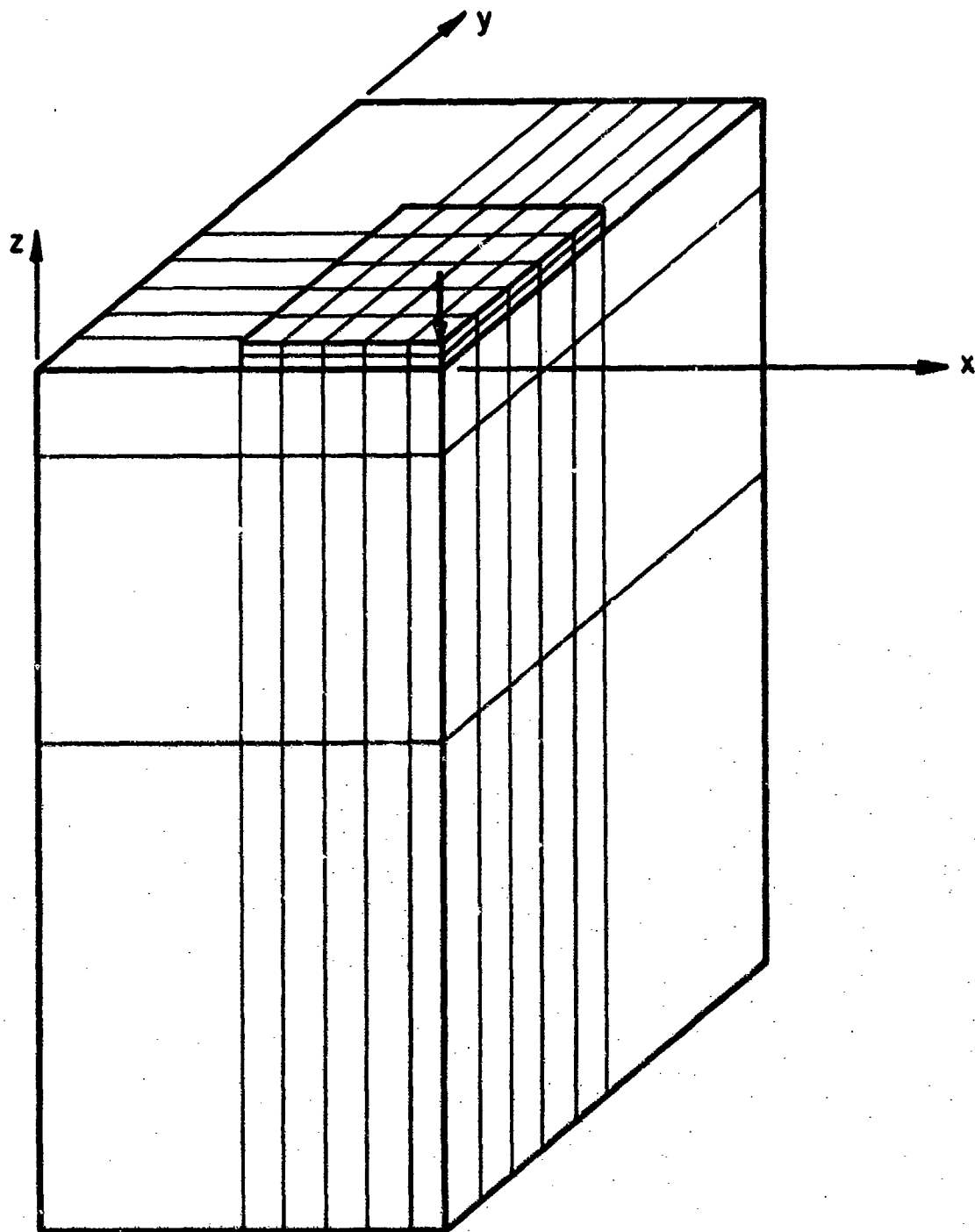


Figure 2. Three-Dimensional Finite Element Mesh for Run 5

5. Selection of Stress Extrapolation Method

For the linear solid (brick) element (see Figure 1), displacements are calculated at each of the eight nodal points, but stresses (and strains) are determined only at the centroid of the element ($\xi = \eta = \zeta = 0$). This location can be shown to be the optimal stress point for the brick element at which "stresses may be almost as accurate as nodal displacements" [6]. It is, therefore, often necessary to extrapolate from calculated values to obtain the required stresses at the critical locations.

Consider, for example, the case of a slab loaded by a point load at its interior. This problem will be the test-case for most of the analyses in this paper. Taking advantage of symmetry, only one-quarter of the slab needs to be modeled. Thus, although the point load is applied at the central node, the closest estimate of the maximum bending stress (developing under this node) will be that for the centroid of the element on which the load is applied. Extrapolation is needed to obtain the stress under the load. Table 1 shows a comparison between values of the maximum interior bending stress under the load σ_i , determined by three different extrapolation schemes using results from five GEOSYS runs. Figure 3 is a schematic illustration of the three methods compared in Table 1. The mesh for one of the runs performed (Run 5) is shown in Figure 2.

Theoretically, σ_i tends to infinity as the size of the applied loaded area tends to zero [7]. Application of the closed-form equation, however, indicates that even for a very small, but finite, loaded area the increase in σ_i is much less drastic. Nonetheless, it can be concluded that the orthogonal linear extrapolation method gives best results for this example. This procedure involves more computations, but takes into account a larger number of computer results.

Unless otherwise indicated, orthogonal linear extrapolation will be used in analyzing bending stress results in the remainder of this paper. This method may also be used with subgrade stress data. When the stress state is known to be axisymmetric, however, diagonal linear or quadratic extrapolations are more appropriate. An example is the subgrade stress due to an interior load. In such cases, diagonal linear extrapolation is used below.

Table 1. Comparison of Three Extrapolation Methods

Run	Slab Mesh	Max. Bending Stress, σ_1 (psi)		
		Diagonal	Orthogonal	Quadratic
2	2x2	17.17	13.83	-
3	3x3	24.79	19.45	22.82
4	4x4	29.99	23.85	27.42
5	5x5	33.80	27.23	30.77
6	6x6	36.96	29.94	33.43

Notes:

Slab : 15 ft x 15 ft x 1 ft

Soil : 30 ft x 30 ft x 30 ft

$E = 4 \times 10^6$ psi; $\mu = 0.15$

$E_s = 1 \times 10^4$ psi; $\mu_s = 0.45$

$l_c = 45.5$ in.

Load, $P = 3600$ lbs (interior, point load)

Mesh : See Figure 2 (Run 5)

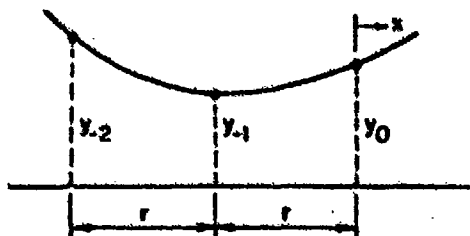
Equations Used:

Orthogonal, Diagonal:

$$y = y_0 + (y_0 - y_{-1}) x/r$$

Quadratic:

$$y = y_0 + (y_{-2} - 4y_{-1} + 3y_0) x/2r + (y_{-2} - 2y_{-1} + y_0) x^2/2r^2$$



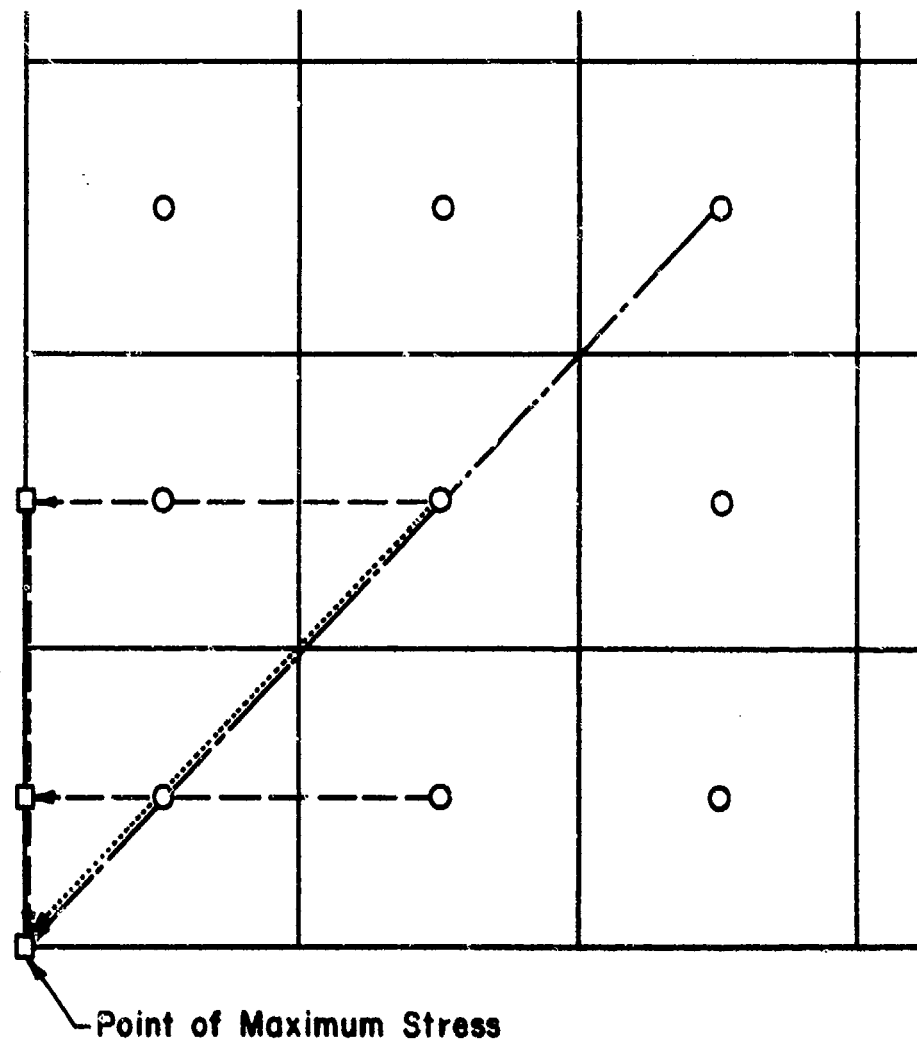


Figure 3. Schematic Illustration of Extrapolation Methods Considered

6. Vertical Subgrade Extent

Two series of runs were performed to provide some guidelines for determining the depth to which the subgrade should be modeled, so that bottom effects are eliminated and computer storage required remains within the available limits. Series A comprised seven runs, results from which are tabulated in Table 2. It is observed that both maximum bending and subgrade stresses (σ_i and q_i) converge to a constant value fairly quickly. Increasing the subgrade depth, Z , beyond 20 to 25 ft (or 5 to 7 times the radius of relative stiffness, l_e) will have no effect on these stresses.

The behavior of deflection, however, requires more attention. Maximum deflection, δ_i , increases with subgrade depth as expected, but does not converge to a constant value, even for a depth of 35 ft ($9 l_e$). An additional 0.044 mils of deflection is accumulated for every additional 5 ft of subgrade beyond 20 ft. This is due to the presence of lateral boundaries at a finite distance, X , from the slab edges, which in this case was 7.5 ft ($2 l_e$). As a result, vertical strains in the subgrade reach a level where they remain constant, rather than decrease as in a truly semi-infinite elastic solid, since they are not allowed to be distributed beyond the model boundaries.

To investigate this phenomenon further, Series B, consisting of seven additional runs was conducted. The lateral subgrade extent, X , beyond the slab edges was increased to 35 ft ($9 l_e$). A plot of maximum responses obtained is shown in Figure 4. Comparison with Series A indicates that the depth at which vertical strain decreases to a constant value, as well as this value itself, are both influenced by the lateral extent of the subgrade. Therefore, for a given lateral subgrade extent, the finite element model will overestimate vertical deformation, if the subgrade extends vertically beyond the constant vertical strain depth, z_{cvs} .

Although this is influenced by the lateral extent of the subgrade, a subgrade depth of about 40 ft ($10 l_e$) may be used as a typical value.

Table 2. Effect of Subgrade Vertical Extent - Series A

Run	Subgrade Depth, Z (ft)	δ_i		q_i		σ_i	
		mls	%	psi	%	psi	%
7	5	1.334	69.05	(0.3012)	(105.28)	32.73	96.67
8	10	1.643	85.04	0.2840	99.27	33.79	99.79
9	15	1.750	90.58	0.2864	100.10	33.85	99.97
10	20	1.799	93.12	0.2861	100.00	33.86	100.00
11	25	1.844	95.45	0.2864	100.10	33.86	100.00
12	30	1.888	97.72	0.2861	100.00	33.86	100.00
13	35	1.932	100	0.2861	100	33.86	100

Notes:

- See Table 1 for problem specifications.
- Subgrade is divided into 5-ft thick layers.
- Maximum deflection, δ_i , under interior point load, at top of slab.
- Maximum subgrade stress, q_i , under interior point load, at top of subgrade, by diagonal linear extrapolation (except for Run 7, q_i at $z = 2.5$ ft).
- Maximum bending stress, σ_i , under interior point load, at bottom of slab, by orthogonal linear extrapolation.
- Responses expressed as a percentage of the values for Run 13.

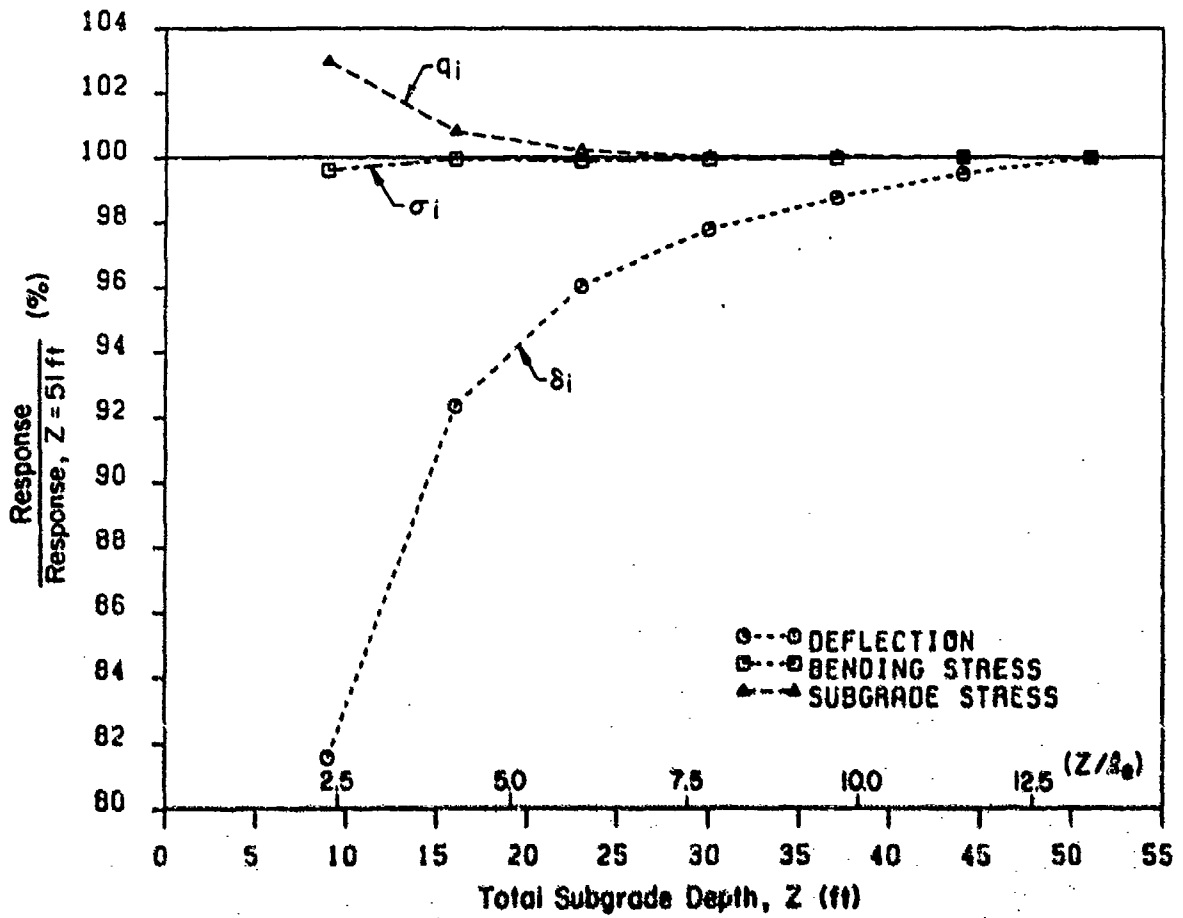


Figure 4. Effect of Subgrade Vertical Extent - Series B

7. Lateral Subgrade Extent

The effect of the size of the soil model cube in the horizontal direction was examined more closely by another set of seven runs, results from which are plotted in a normalized fashion in Figure 5. Maximum bending and subgrade stresses (σ_i and q_i) are not significantly affected by lateral subgrade extent, but deflection, δ_i , can be grossly underestimated if lateral boundaries are too close to the slab edges. The trends in Figure 5 confirm the observations made in the previous section that the depth at which vertical strain decreases to a constant value, as well as this value itself, are both influenced by the lateral extent of the subgrade. Since the total depth of the subgrade, Z , is kept constant at 30 ft ($8 l_c$) in these runs, the effect of increasing the subgrade lateral extent, X , is to increase the depth at which vertical strain becomes a constant, z_{CVS} , and to decrease the value of this constant vertical strain itself. Major improvement in the value of δ_i is achieved even when X is only 24 ft ($6 l_c$). Therefore, a lateral extent between 25 and 35 ft (or 7-10 l_c) should be used.

8. Boundary Conditions

Several different boundary condition options exist for the problem examined in this study. The primary consideration in selecting one from among these, is the simple observation that at an infinite distance from the load, a subgrade boundary will experience neither displacements nor stresses. This suggests that any boundary condition (e.g., fixed, free, or on rollers) will be adequate if the soil extends to infinity. As the boundaries move closer to the load, either or both the stress-free and displacement-free conditions will inevitably be violated, introducing an error into the solution [8].

If lateral displacements in the horizontal lower boundary are restrained, the model will be too stiff compared to the semi-infinite elastic half-space. On the other hand, a horizontal lower boundary that is free to move laterally allows the elements to distribute their load by deforming. Therefore, a smooth base should be assumed. For the vertical lateral boundaries, vertical displacements should be permitted, being similar to the lateral displacements on the horizontal base. Both free and roller-type boundaries would allow such displacements.

In order to examine the behavior of these two types of lateral boundaries (i.e., free, or on rollers), results from four runs are compared in Figure 6. These confirm that maximum responses are more sensitive to the boundary conditions used when the lateral boundaries are closer to the

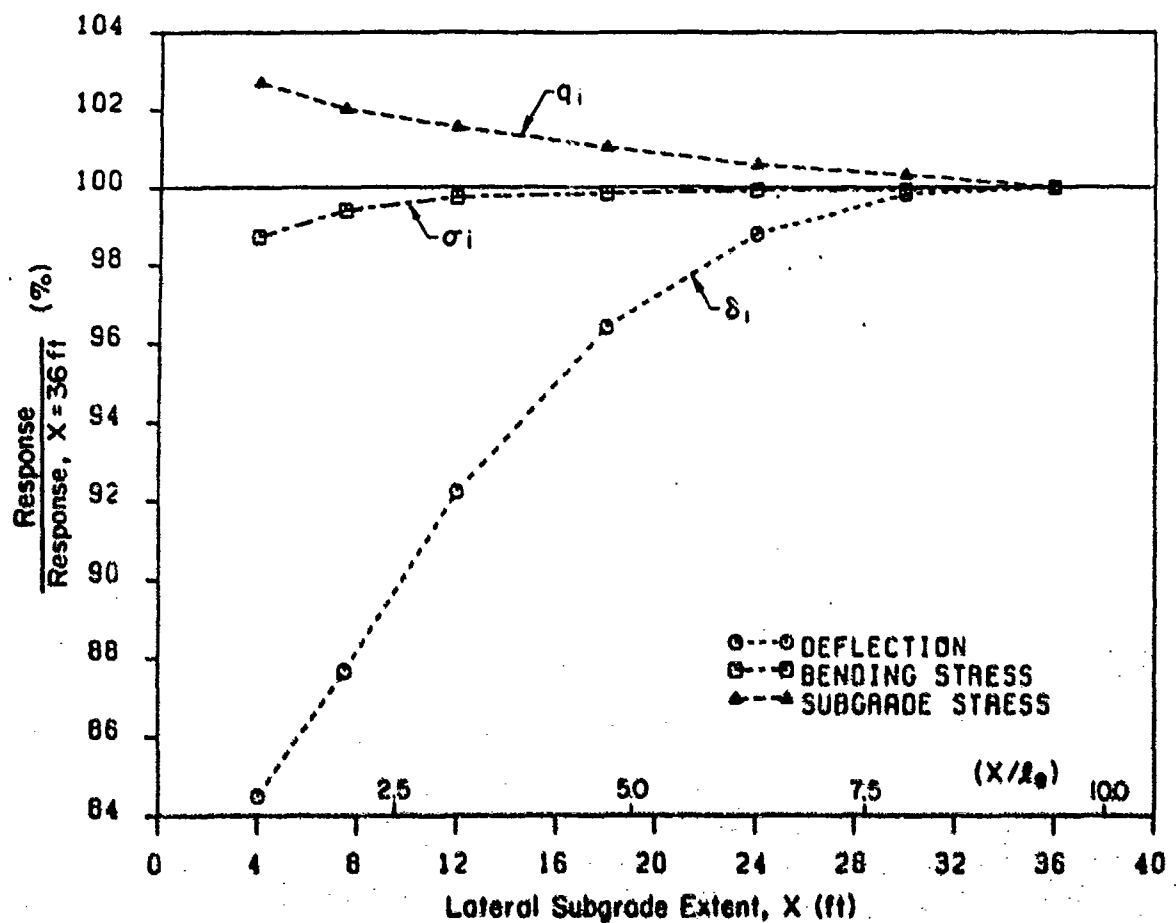


Figure 5. Effect of Subgrade Lateral Extent Beyond Slab Edges

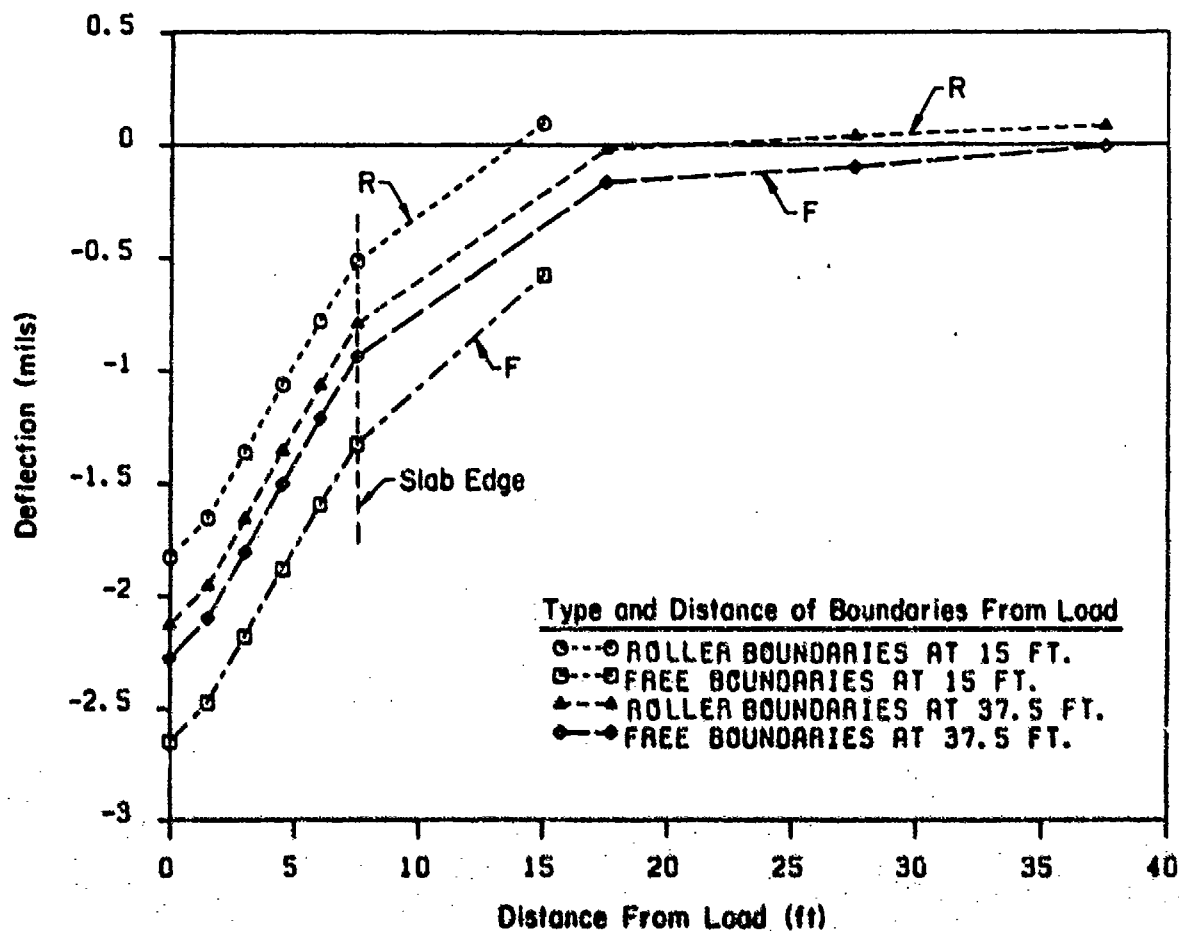


Figure 6. Effect of Boundary Conditions on Subgrade Surface Deflection Profiles

load. Furthermore, maximum deflection, δ_1 , is once again affected much more significantly than the other two responses. As expected, a stiffer response (lower deflection) is obtained with the roller-type, compared to the free boundaries. The two curves for boundaries at 37.5 ft (10 l_c) from the load are fairly close to each other. They may be assumed to provide a better approximation to the elastic half-space response than the curves for boundaries at 15 ft (4 l_c) from the load. When the lateral boundaries are this close, however, neither boundary condition appears to have an advantage over the other.

Figure 7 presents the variation of radial strain in the surface subgrade layer. Of the two curves for boundaries at 15 ft (4 l_c) from the load, the one with the roller-type boundary condition is closer to the curves for boundaries at 37.5 ft (10 l_c) from the load. For these reasons, roller-type lateral boundaries are adopted in this study.

9. Number of Slab Layers

Figure 8 is a graphical presentation of results from five runs, employing an increasing number of slab layers, normalized with respect to the responses obtained using the greatest number of slab layers (NLAYER = 6). It is observed that although there is a slight improvement in the results as the number of layers increases, maximum responses can be determined fairly accurately even using only two layers. Note that, according to the extrapolation method adopted, only values from the lower two slab layers are used in calculating the maximum bending stress. This probably explains the good performance of the two-layer slab, which is the only case involving a calculated stress point above the neutral axis. As a result, the two-layer slab gives results very close to those obtained using five or six layers, which makes it a very attractive option.

10. Vertical Division of Subgrade

In most of the preceding runs, the soil cube has been divided into three layers, by horizontal nodal planes located at depth, z , values of 0, -3, -13 and -30 ft. This follows from an arbitrary but intuitive assumption, that the total depth of the subgrade may be divided into an upper, a middle and a lower portion. Any number of layers may be ascribed to each of these three portions. In the runs above, one layer per portion was used for simplicity. In this section the

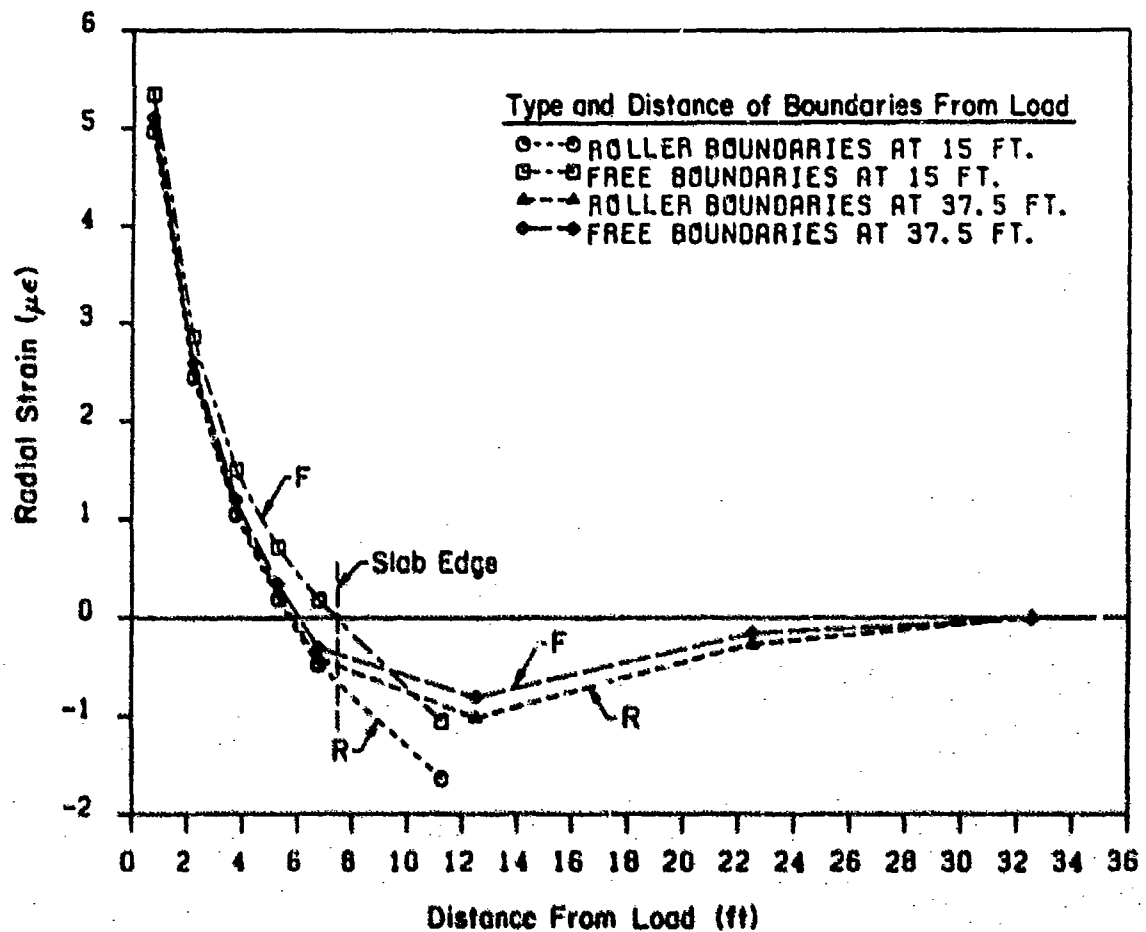


Figure 7. Radial Strain, E_{yy} Distributions Along Slab y-Axis of Symmetry at 1.5 Feet Below Subgrade Surface: Effect of Boundary Conditions

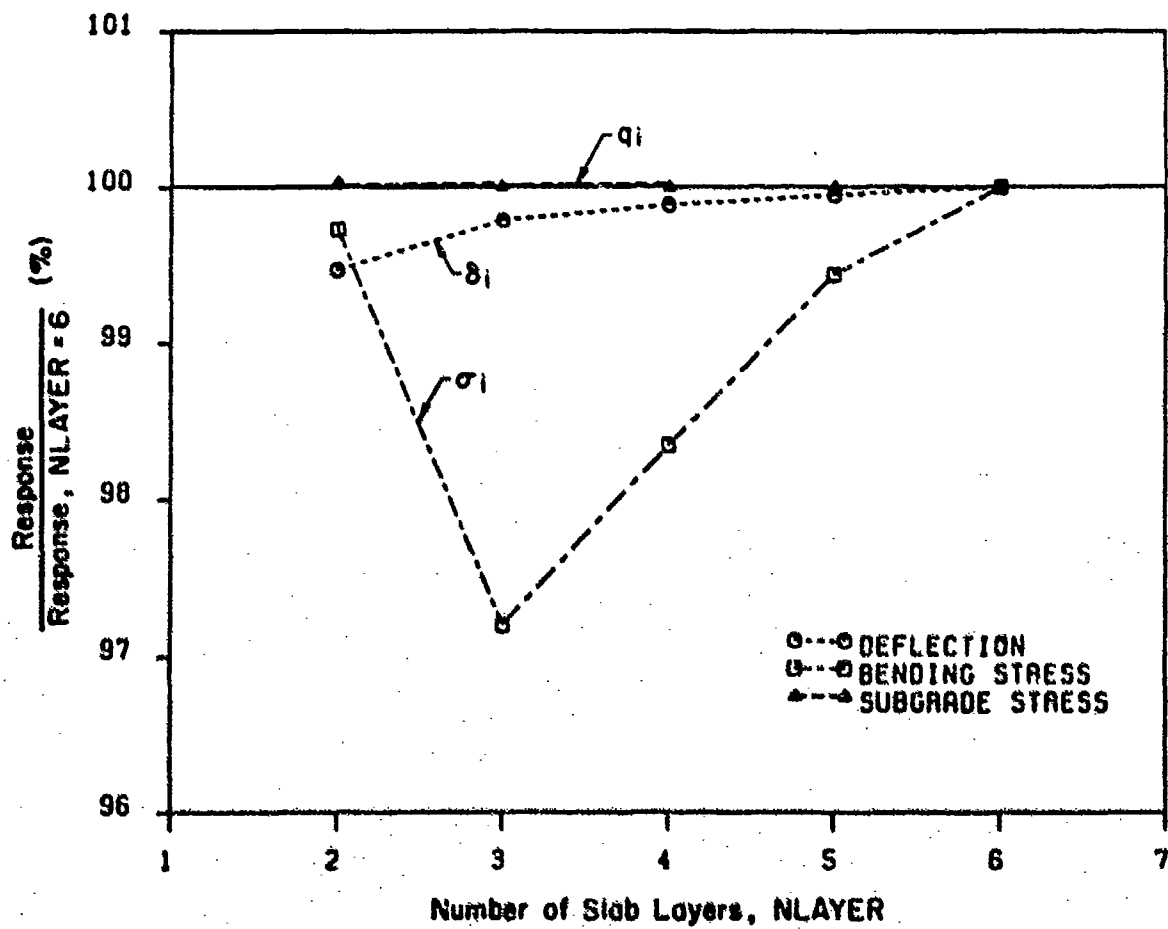


Figure 8. Effect of Number of Slab Layers

effect of the number of layers used in the subgrade will be examined, with a view of developing some user guidelines for later runs.

Several series of runs were conducted to determine both the extent and the required fineness of the three arbitrary portions of the subgrade. These confirmed the overriding importance of the upper subgrade portion fineness, which is illustrated in Figure 9. Here, this portion is assumed to consist of the top 8 ft of the subgrade, whose total depth is 30 ft. Maximum deflection and bending stress are only slightly sensitive to this effect. The subgrade stress, however, is significantly improved as the upper portion is divided into more layers. This is to be expected since the stress points, from which maximum subgrade stress is extrapolated, move closer to the surface (as the upper layers become thinner). The accuracy of the extrapolation is thereby improved. In fact, Figure 9 suggests that further improvement is possible using a still finer upper portion. An alternative interpretation is that the assumed thickness of the upper portion (8 ft or $2 \lambda_c$) was too large.

In a second series, the upper portion was considered to be only 4 ft thick, and results indicated the choice of a shallower upper portion and correspondingly thinner upper layers is warranted. In addition, the thickness of the upper layers should be between 1 and 2 ft (0.25 to $0.5 \lambda_c$) for better accuracy.

The sensitivity of the results to lower portion fineness appears to be limited, provided the lower portion begins at a considerable depth, preferably below half the constant vertical strain depth, z_{cvs} . The sensitivity of the results to the fineness of the middle portion is less than for the upper portion, but greater than for the lower portion (Figure 10). Although one middle portion layer would be adequate for maximum response determination under these conditions, it is recommended that at least two layers be used when considering distribution of stresses and displacements with depth.

The preceding analyses have led to the following conclusions which can be used as guidelines in future runs. The subgrade may be divided into three portions in the vertical direction. The upper portion should extend from 0 to 4 ft (0 to $1 \lambda_c$) and should consist of layers not more than 1 to 2 ft thick (0.25 to $0.5 \lambda_c$). The middle portion should extend from 4 to 15 ft (1 to $4 \lambda_c$), or half the constant vertical strain depth, z_{cvs} , if known, and should be divided into at least two layers. Finally, the lower portion should cover the remainder of the soil cube, and may be divided into one or more layers.

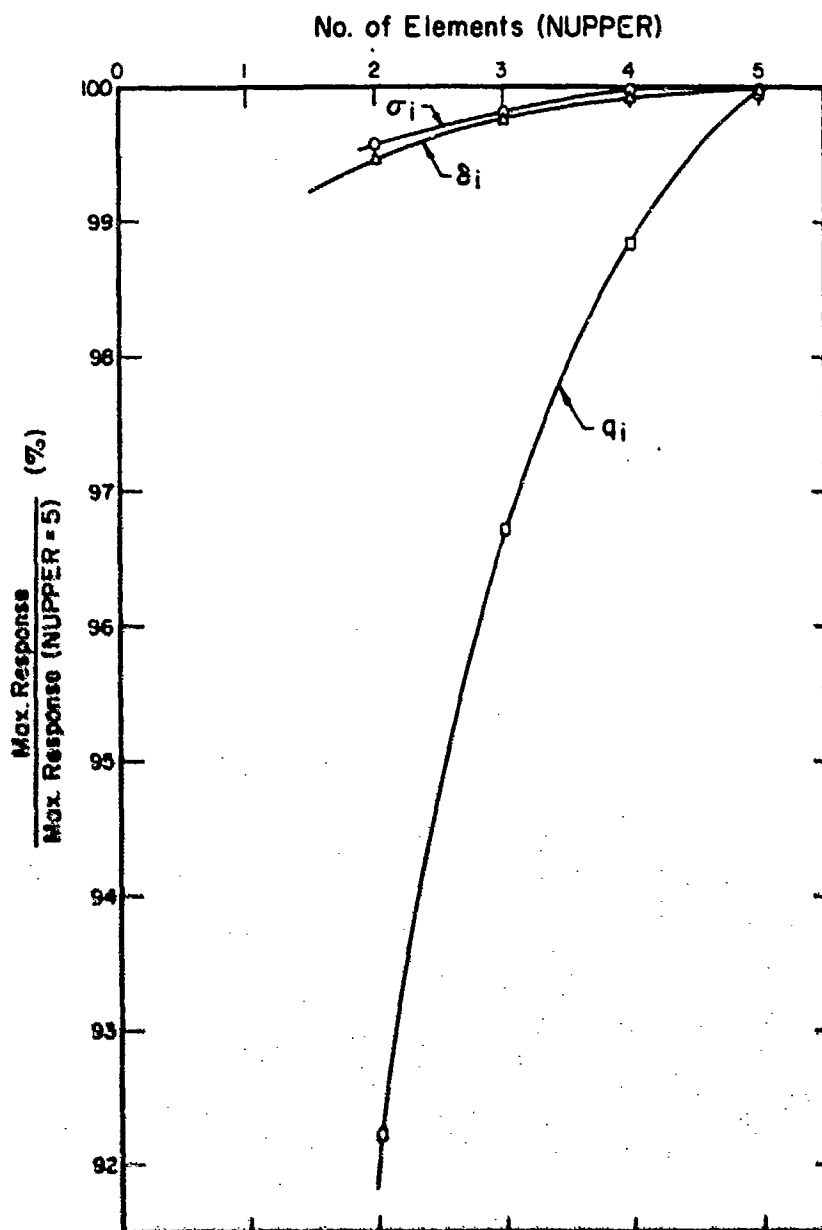


Figure 9. Effect of Subgrade Upper Portion Fineness - Series A

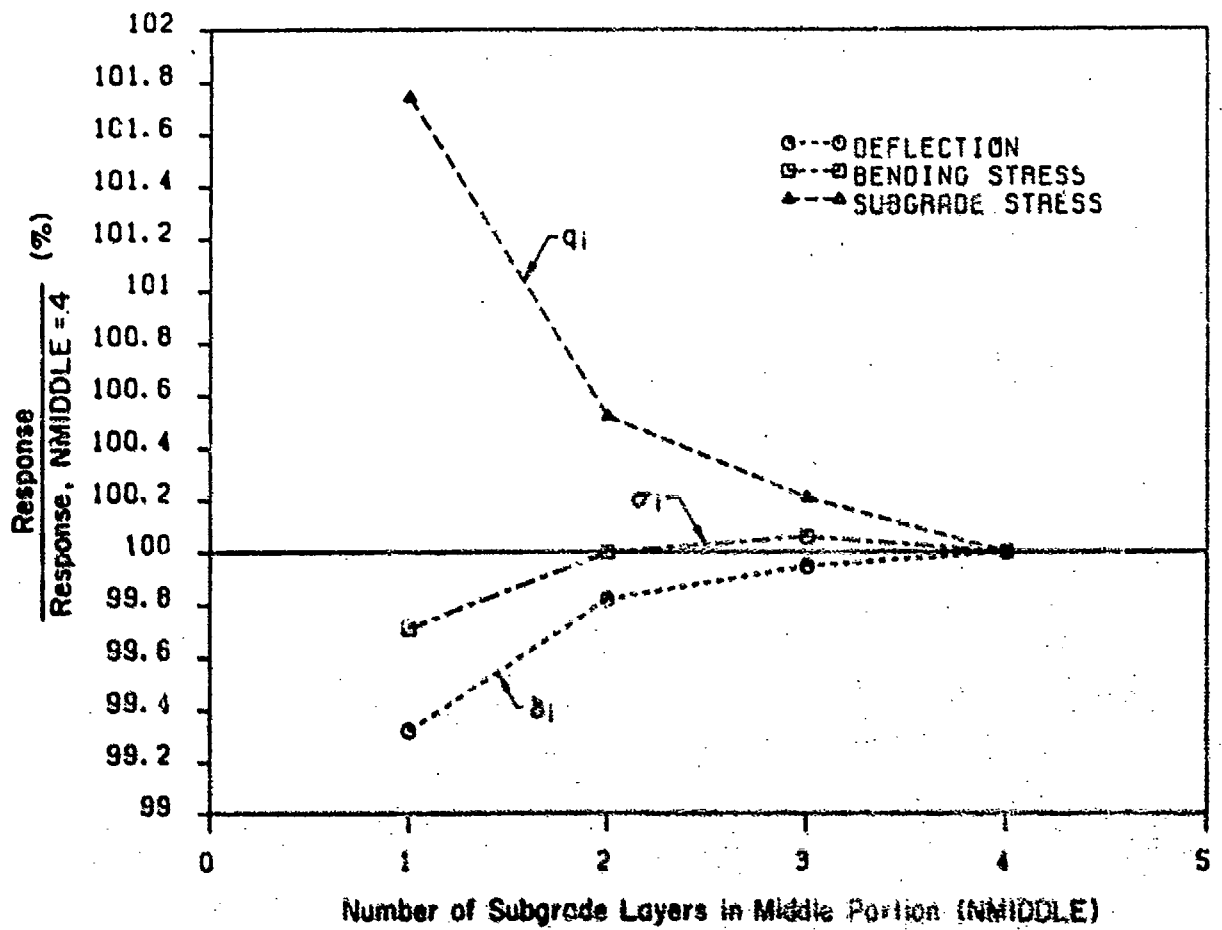


Figure 10. Effect of Subgrade Middle Portion Fineness - Series E

11. Horizontal Subgrade Mesh Fineness

Mesh fineness in the horizontal plane has been identified as one of the most important factors influencing the accuracy of finite element results in earlier two-dimensional studies conducted at the University of Illinois [1; 9] and elsewhere. The investigation of this effect for the three-dimensional case was conducted in two stages. The horizontal mesh fineness in the region of the model beyond the slab edges to the vertical lateral boundaries is considered first.

Maximum responses from several runs are shown in a normalized form in Figure 11. All three responses converge from below, and bending stress is not sensitive to this mesh fineness effect. For accurate subgrade stress and deflection values, however, a relatively fine mesh is needed. Naturally, this will be more demanding on computer storage requirements.

An alternative was sought in the use of elements of unequal size. The effect of the load applied on the slab diminishes with distance from the slab edges. Therefore, in modeling the subgrade, smaller elements are appropriate near the slab, while the mesh can become coarser closer to the vertical lateral boundaries. Based on the results obtained, it is recommended that X be divided into two elements, one 4 ft in size near the slab ($1 l_0$), and another 26 ft for the remainder ($7 l_0$).

12. Horizontal Slab Mesh Fineness and Element Aspect Ratio

Three series of GEOSYS runs were conducted to examine the influence of horizontal slab mesh fineness on the response of the three-dimensional slab-on-grade. The trends observed in Figure 12 are similar to those noted in earlier two-dimensional finite element studies [1; 9], inasmuch as all three maximum responses converge from below. Deflection and subgrade stress appear to be less sensitive to horizontal mesh fineness, and adequate accuracy may be expected as the mesh fineness ratio, $(2a/h)$, of the (short) side length of the finite element (plan view) to the slab thickness, approaches the value of 0.8. This is similar to the value determined from the two-dimensional studies [1; 9]. Bending stress appears to be more sensitive to this effect, requiring values of $(2a/h)$ less than 0.8 for convergence.

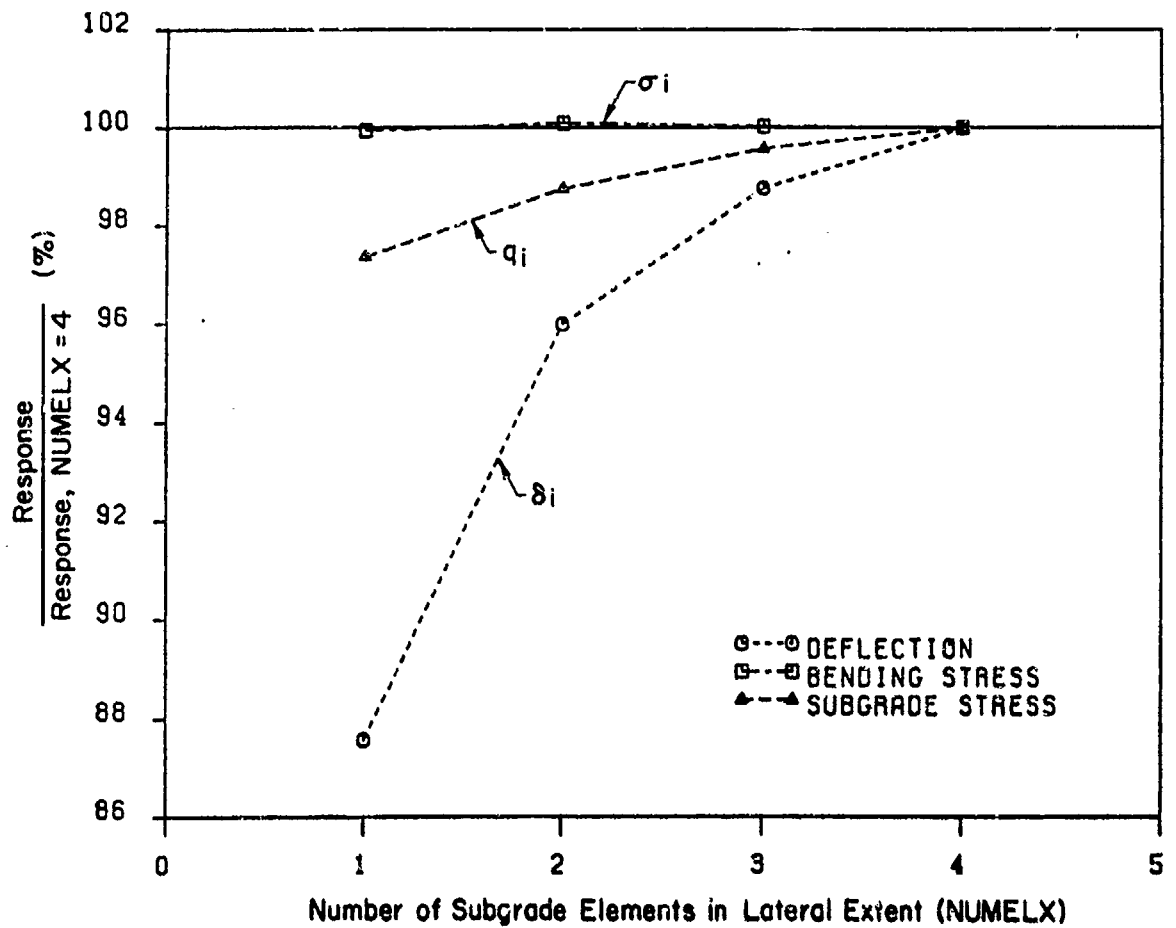


Figure 11. Effect of Horizontal Subgrade Mesh Fineness

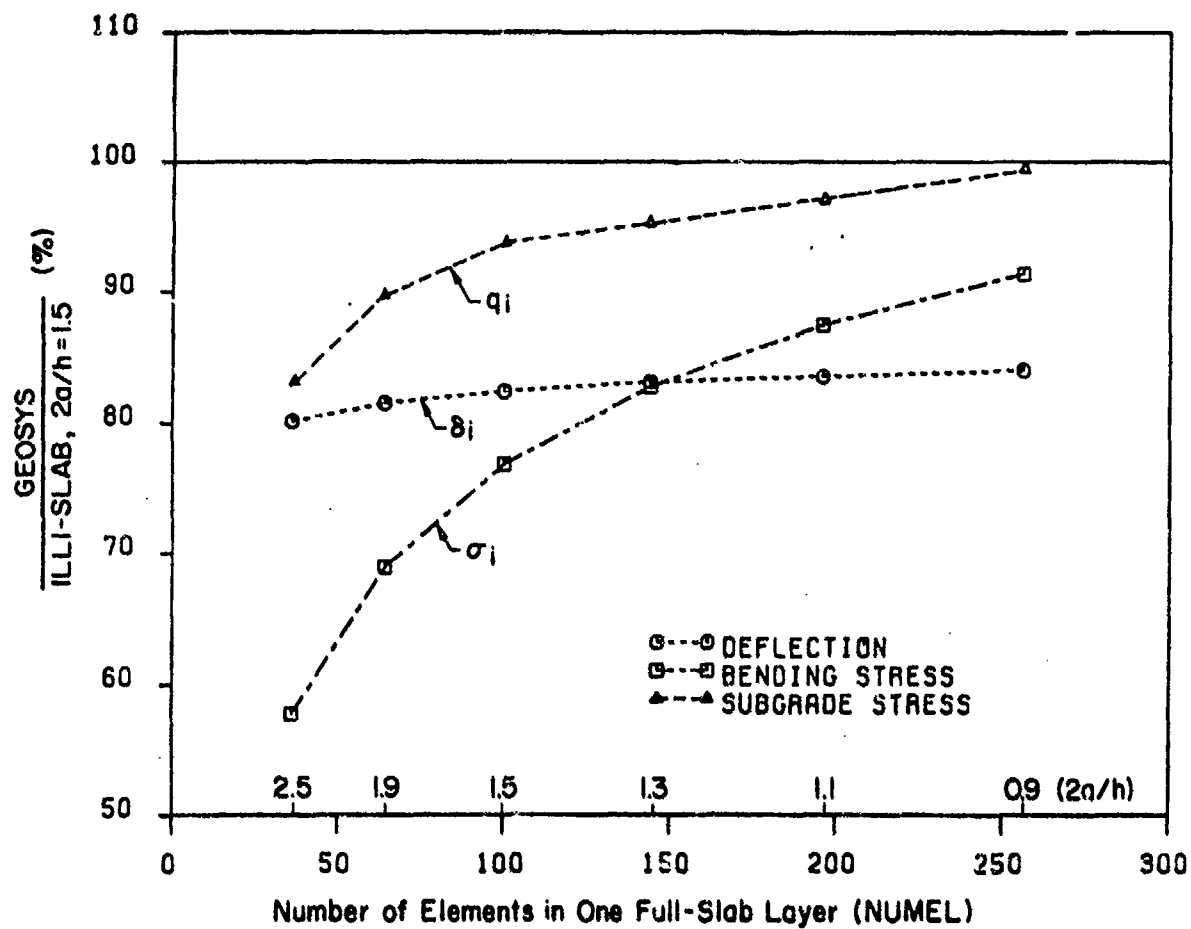


Figure 12. Effect of Horizontal Slab Mesh Fineness (Interior Loading)

It was also found that although the solution deteriorates as the maximum slab element aspect ratio, α_{\max} , increases, the impact of this factor is limited, especially if α_{\max} is kept below 4. Element aspect ratio (in plan view) is defined as the quotient of the long side, $2b$, of the finite element divided by the short side, $2a$. This recommendation is somewhat less stringent than the one developed using the two-dimensional ILLI-SLAB model [1; 9].

13. Discussion - Conclusions

The main focus of investigations discussed herein has been the application of the three-dimensional finite element program GEOSYS [4] to the solution of the slab-on-grade problem. The program uses an elastic solid foundation. Naturally, three-dimensional analysis presents several problems, such as: prolonged execution times (especially when an iterative scheme is used to introduce subgrade stress dependence [2; 3]); the use of relatively coarse meshes; the need for stress extrapolation to determine critical responses, etc. Nonetheless, considerable progress has been made in establishing user guidelines for the application of this finite element slab-on-grade model.

Investigations conducted during this study have shown that several important decisions must be made with respect to the design of the finite element mesh used for three-dimensional slab-on-grade analysis. To provide the database for establishing some user guidelines for this purpose, 108 GEOSYS runs have been conducted. Despite the tremendous amount of information accumulated from these results, the present study cannot be considered exhaustive. It does represent, however, a substantial effort to provide adequate answers to very complex questions.

For example, the loading assumed for the mesh investigation runs was almost always a point load. This is simple and easy to apply at a node, compared to a uniformly distributed load covering, in general, only part of an element. The latter must be converted into work equivalent nodal load components. The point load, however, conceals a mesh fineness effect related to the size of the loaded area [10].

The overriding importance of mesh fineness was first identified and quantified in previous University of Illinois studies, using two-dimensional models [1; 9]. A major conclusion reached was that a more stringent mesh fineness criterion is required under the loaded area, than elsewhere in the finite element mesh [11]. This counterbalances the approximation involved in discretizing applied distributed loads. A corollary of this, which has serious implications with respect to recent

efforts to model nonuniform pressure distributions [12; 13], may be stated as follows: In view of the conversion of external distributed loads into nodal components (which inevitably leads to at least some approximation, especially in the case of partially loaded elements), refinement of the applied pressure distribution, for the purpose of simulating observed deviations from simplistic uniformity, without due consideration and reciprocal improvement of mesh fineness, will be self-defeating, leading only to an illusion of improved accuracy.

14. References

1. Ioannides, A.M., "Analysis of Slabs-On-Grade for a Variety of Loading and Support Conditions," thesis presented to the University of Illinois, at Urbana, Il., in partial fulfillment of the requirements for the degree of Doctor of Philosophy, 1984. Also published by U.S. Air Force Office of Scientific Research, Report No. TR-85-0083, Air Force Systems Command, USAF, Bolling AFB, D.C. 20332, September 1984.
2. Ioannides, A.M., Donnelly, J.P., Thompson, M.R., and Barenberg, E.J., "Three-Dimensional Finite Element Analysis of a Slab on Stress Dependent Elastic Solid Foundation," U.S. Air Force Office of Scientific Research, Report No. TR-86-0143, Air Force Systems Command, USAF, Bolling AFB, D.C. 20332, October 1986.
3. Ioannides, A.M., "Three-Dimensional Analysis of Slab on Stress Dependent Foundation," Transportation Research Record 1196, Transportation Research Board, National Research Council, Washington, D.C., 1988.
4. Agbabian Associates, "Analytic Modeling of Rock-Structure Interaction," Volumes 1-3, prepared for Advanced Research Projects Agency of U.S. Department of Defense, and U.S. Bureau of Mines, Report No. AD-761-648; 649; 650, April 1973.
5. Lopez, L.A., "FINITE: An Approach to Structural Mechanics Systems," International Journal for Numerical Methods in Engineering, Vol. 11, 1977.
6. Cook, R.D., "Concepts and Applications of Finite Element Analysis," Second Edition, John Wiley and Sons, New York, N.Y., 1981.
7. Losberg, A., "Structurally Reinforced Concrete Pavements Doktorsavhandlingar Vid Chalmers Tekniska Hogskola, Goteborg, Sweden, 1960.
8. Carrier, W.D. and Christian, J.T., "Rigid Circular Plate Resting on a Non-Homogeneous Elastic Half-Space," Geotechnique, Vol. 23, No. 1, 1973.
9. Ioannides, A.M., Thompson, M.R., and Barenberg, E.J., "Finite Element Analysis of Slabs-on-Grade Using a Variety of Support Models Proceedings, 3rd International Conference on Concrete Pavement Design and Rehabilitation, Purdue University, West Lafayette, Ind., April 1985.

10. Ioannides, A.M., Thompson, M.R., and Barenberg, E.J., "Westergaard Solutions Reconsidered," Transportation Research Record 1043, Transportation Research Board, National Research Council, Washington, D.C., 1985.
11. Ioannides, A.M., "Axisymmetric Slabs of Finite Extent on Elastic Solid," Journal of Transportation Engineering, ASCE, Vol. 113, No. 3, May 1987.
12. Marshek, K.M., Chen, H.H., Connell, R.B., and Saraf, C.L., "Effect of Truck Tire Inflation Pressure and Axle Load on Flexible and Rigid Pavement Performance," Transportation Research Record 1070, Transportation Research Board, National Research Council, Washington, D.C., 1986.
13. Chen, H.H., Marshek, K.M., and Saraf, C.L., "The Effects of Truck Tire Contact Pressure Distribution on the Design of Flexible Pavements - A 3D Finite Element Approach," presented at the 65th Annual Meeting of the Transportation Research Board, Washington, D.C., January 1986.

15. List of Symbols

2a	=	short side of finite element (plan view)
2b	=	long side of finite element (plan view)
E	=	Young's modulus of slab
E _s	=	Young's modulus of elastic solid foundation
h	=	slab thickness
h _i	=	shape function for brick element
l	=	dummy index
l _e	=	radius of relative stiffness for elastic solid foundation [$= \sqrt[3]{Eh^3(1-\mu_s^2)/6(1-\mu^2)E_s}$]
NLAYER	=	number of slab layers
NMIDDLE	=	number of layers in middle subgrade portion
NUMEL	=	number of slab elements (plan view)
NUMELX	=	number of subgrade element columns (plan view)
NUPPER	=	number of layers in upper subgrade portion
NLOWER	=	number of layers in lower subgrade portion
P	=	applied load (force)
q	=	(maximum value of) vertical subgrade pressure
r	=	radial distance
u	=	generalized nodal displacement for brick element
u _x , u _y , u _z	=	displacements in x, y, z directions, respectively

X	=	subgrade lateral extent beyond slab edges
x	=	horizontal Cartesian coordinate
y	=	horizontal Cartesian coordinate
Z	=	total subgrade depth assumed in finite element model
z	=	vertical Cartesian coordinate
z_{cvs}	=	constant vertical strain depth
α	=	finite element aspect ratio (plan view) [=2b/2a]
α_{ni}	=	coefficients of incompatible displacement functions
δ	=	(maximum value of) vertical deflection
δ_i	=	maximum deflection under interior load
q_i	=	maximum subgrade stress
σ_i	=	maximum bending stress
ϵ	=	strain
ζ	=	local orthogonal coordinate
η	=	local orthogonal coordinate
μ	=	Poisson's ratio for slab
μ_s	=	Poisson's ratio for elastic solid
ξ	=	local orthogonal coordinate
σ	=	(maximum value of) slab bending stress
za/n	=	mesh fineness ratio

Subscripts

i = pertaining to interior loading

max = maximum value of

Micro Mechanical Behavior of Pavements

R. Lytton

Texas Transportation Institute

1. Introduction

The design of an airport pavement must be based upon an analysis of its ability to withstand different forms of distress while being subjected to the rigors of aircraft traffic and weather. Of major importance are the structural integrity of the pavement and the formation of fragments which create a potential for Foreign Object Damage (FOD) to both propeller and jet-driven aircraft.

In considering new materials for use in airport pavements, some means of predicting the rate of appearance of distress and FOD potential must be devised. Prediction means being able to test a material to determine relevant material properties, and to use these properties to analyze the anticipated effects of traffic and weather on the distress rate. Maximum use should be made of the discipline of mechanics because of its proven efficiency in summarizing and extrapolating data.

In considering new aircraft, mechanics should be used to analyze and anticipate the effects of landing gear, tire, and tire contact pressure configurations on the distress and FOD potential rates on both existing and planned airport pavements.

In considering alternative rehabilitation methods, mechanics once more will prove useful in being able to predict the effects of existing or future aircraft on the distress and FOD potential rates that are to be expected.

Mechanics requires material properties in order to make its predictions. Material properties are characteristics of a material that appear in constitutive relations. They do not include, nor are they dependent upon, the geometry or thickness of pavement layers.

This paper presents a brief summary of the types of distress, the types of material properties and which types of material properties are needed to describe each type of distress in each pavement layer are tabulated. Constitutive equations that are appropriate for these material properties are listed in increasing order of complexity, with the simpler ones being preferred for microcomputer applications.

Illustrations of materials characterizations are presented covering a simple way of representing the damage done to a material by microcracking, the formulation of elastic dilatancy, and the determination of material properties for a hypoelastic base course material. These illustrations demonstrate the kind of materials characterization that will be required to permit accurate predictions of the rate of appearance of pavement distress and FOD potential. It is envisioned that all of these materials characterizations will be implemented in a three-dimensional

(3-D) finite element (FE) program and thus the materials properties must have two principal attributes: 1) they must be capable of being determined from laboratory tests, and 2) they must be capable of being represented in a finite element program and lead to stable convergence in an iterative computational scheme.

2. Types of Pavement Distress

Tables 1 and 2 indicate the principal types of distress which occur with flexible pavements (Table 1) and concrete pavements (Table 2), with each table listing those types of distress which produce fragments which can cause FOD potential. It is particularly important to be able to predict mechanistically each of these types of distress. This capability will make it possible to make laboratory determinations of the properties of new materials which enhance or inhibit the formation of distress, and thus to screen efficiently and inexpensively the promising materials from those that are less so.

3. Categories of Material Properties

As shown in Table 3, there are four broad categories of material properties which must be known for each material in a pavement to be analyzed: resilient, dilatancy, plasticity, and fracture. Each of these is altered by interaction with the surrounding elements (oxygen, water, water vapor, salt solutions) and the action of the elements of the weather.

Resilient properties have to do with the stiffness of each material under conditions of repeated loading and unloading.

Dilatancy properties are of two types: elastic and plastic. Elastic dilatancy is a volume change that occurs during loading and unloading in which the net elastic work is zero. Plastic dilatancy occurs when the material has reached its yielding state and irreversible volume change occurs.

Table 1. Flexible Pavement Distress

- Rutting
- Fatigue Cracking (FOD Potential)
- Thermal Cracking
 - Low temperature
 - Thermal fatigue
- Spalling (FOD Potential)
- Stripping
- Weather and Raveling (FOD Potential)
- Block Cracking
- Corrugations
- Pumping

Table 2. Concrete Pavement Distress

- Fatigue Cracking (FOD Potential)
- Faulting
- Spalling (FOD Potential)
- Thermal Cracking
- Shrinkage Cracking
- Debonding of Reinforcing
- Pumping

Table 3. Categories of Material Properties

- Resilient
- Dilatancy
 - Elastic
 - Plastic
- Plasticity
 - Work-hardening (isotropic, kinematic)
 - Work-softening (shear banding)
- Fracture
 - Microfracture process
 - Crack propagation

A special case which has characteristics similar to both resilient and plastic dilatancy is that of hypoelasticity, in which the stress-strain curve of a material is stress-path dependent. Thus, the stress-strain curve on loading may be curved while the unloading curve follows a straight line, and permanent deformation results from each loading and unloading cycle. This is typical of many materials of which pavements are constructed.

Plasticity properties include the yield surface, the plastic potential, and the work-hardening rule. The hardening rule may be either for isotropic hardening which is used for monotonic loading or kinematic hardening which is used with cyclic loading. Mixed hardening provides for a combination of both isotropic and kinematic hardening. For many materials of which pavements are constructed, work-softening occurs, producing narrow shear bands of plastically deformed material.

Fracture properties govern the rate of growth of cracks in a material. Cracking is generally divided into the growth and coalescence of distributed microcracks and the subsequent growth of the visible crack. The first phase is commonly termed crack initiation and the second is crack propagation. The growth of cracks is governed by the same material properties regardless of the size of the cracks. However, representing the effects of microcracking in FE analysis poses a different problem than with the propagating crack.

Fracture properties are defined in the discipline of fracture mechanics in which an energy budget is used to account for the strain energy that is released as the cracks grow, or is dissipated with each load cycle, or is stored on the surface of the newly created cracks. The paving materials which are fractured are nonlinear, viscoelastic, and disordered materials in which scale effects become important in governing the rate of microcrack growth and of crack propagation.

Table 9-4 shows which of these material properties are needed to predict the various kinds of *flexible* pavement distress previously mentioned in each of the pavement layers. Table 5 shows the different material properties that are needed to predict *concrete* pavement distress in each of the pavement layers.

Table 4. Properties Relevant to Pavement Distress

FLEXIBLE PAVEMENTS						
	Resilient	Dilatancy (Elastic)	Dilatancy (Plastic)	Plasticity (Hardening)	Fracture (Micro)	Fracture (Propagation)
Rutting	All	All	All	All	S	S
Fatigue Cracking (F.O.D.)	All	All	S	S,B	S	S
Thermal Cracking	S	-	-	-	S	S
Low Temperature	S	-	-	-	S	S
Thermal Fatigue	S	-	-	-	S	S
Spalling (F.O.D.)	S	-	All	All	S	S
Stripping	S	S	-	-	S	S
Weathering & Raveling (F.O.D.)	S	-	-	-	S	S
Block Cracking	S	-	-	-	S	S
Corrugations	All	All	All	All	-	-
Pumping	S,B	S,B	S,B	S,B	-	-

Relevant Layer: Surface (S), Base (B), Subbase (SB), Subgrade (SG)

Table 5. Properties Relevant to Pavement Distress

CONCRETE PAVEMENTS							
	Resilient	Dilatancy (Elastic)	Dilatancy (Plastic)	Plasticity (Hardening)	Plasticity (Softening)	Fracture (Micro)	Fracture (Propagation)
Fatigue Cracking (F.O.D.)	All	-	SB,SG	SB,SG	S	S	S
Faulting	All	SB,SG	SB,SG	SB,SG	-	-	-
Spalling (F.O.D.)	S,SB	-	-	-	S	S	S
Thermal Cracking	S	-	-	-	-	S	S
Shrinkage Cracking	S	-	-	-	-	S	S
Debonding of Reinforcing	S	-	-	-	S	S	S
Pumping	S,SB	SB,SG	SB,SG	SB,SG	-	-	-

Relevant Layer: Surface (S), Subbase (SB), Subgrade (SG)

4. Implementation of Material Properties Models

Some of the material properties described above have been included in existing 3-D FE programs and others have not. In order to develop the ability to analyze, predict, and thus to design airport pavements in the future, all of these properties must be introduced into a single program and the convergence and stability characteristics of each must be experimented with before settling upon those ways of describing material properties mathematically. The material properties must possess these threefold capabilities:

1. To represent the material response accurately,
2. To be able to be represented conveniently and realistically in a numerical integration method, and
3. To converge rapidly with iterations while remaining stable.

Such experimentation as is needed is best undertaken in a systematic way, introducing each new desired characteristic, and determining its accuracy, numerical compatibility, and convergence and stability capabilities before advancing to include still more desirable characteristics.

Table 6 shows a schematic phase development for introducing resilient and elastic dilatant properties into a numerical model. The column marked "Now" shows the capabilities that are included in commercially-available 3-D FE codes at present.

Some of these properties are self-explanatory and others are not. The hyperelastic formulation preserves stress-path independence and generates no elastic work on loading and unloading, while introducing several additional material properties. For example, the Cauchy second-order elastic model requires six material properties and the Green second-order elastic model requires five material properties. Both of these models are capable of representing the elastic dilatancy of a material.

Elastic dilatant materials are derived in a more phenomenological way than the Cauchy or Green hyperelastic material models. While requiring that the secant modulus of a stress-strain curve is dependent upon the stress state of the material, it also meets the requirements of stress-path independence and zero elastic work on loading and unloading. An example of such a formulation is presented later in this paper.

Hypoelastic models are stress-path dependent and are hysteretic on loading and unloading. As such, they are typical of many of the kinds of materials of which pavements are constructed.

The zero-order hypoelastic model requires two material constants which are the familiar elastic constants. The first -order model requires seven material parameters.

The material properties required for each of the models in Table 6 can be found from simple laboratory tests but ones in which all components of stress and strain are known or measured.

Table 6. Present and Future Material Properties in 3-D FE Response Models

	Phase of Development		
	Now	I	II
• Resilient Properties			
- Linear	██████████		
- Non-linear			
• J_1 dependent		██████████	
• J_1, J_2' dependent		██████████	
- Hyperelastic		██████████	
• Elastic Dilatant			
• J_1, J_2' dependent		██████████	
• Hypoelastic			
• Order 0	██████████		
• Order 1		██████████	

Table 7 lists some typically plasticity properties that need to be incorporated into existing 3-D FE models in order to properly represent pavement materials. As with Table 6, the column marked "Now" indicates those properties which can be found in commercially-available 3-D FE programs.

The Tresca, von Mises, and Mohr-Coulomb yield functions have been incorporated into a number of FE programs along with associated flow rules. More appropriate for many pavement materials are the Vermeer [1;2] and Lade [3;4;5] which use non-associated flow rules and a more realistic yield function.

The work-hardening and work-softening formulations are for the most part in developmental stages at present. Only the linear work-hardening characteristics are found in commercially-available FE programs.

Table 8 shows the present and future fracture properties to be included in 3-D FE models. Fracturing presents a problem to represent in a continuum finite element program because it breaks up the continuum.

One way to present the *effect* of a crack is to reduce the moduli in the elements where the crack exists. To be realistic, however, the amount of modulus reduction that occurs should be controlled by an energy budget which keeps up with the amount of energy dissipated or redistributed as the crack grows. Those changes should be reflected in the stiffness matrix of each element. An example of this is presented later in the paper; first with respect to a single crack and then with respect to microcracking.

Reduced modulus formulations treat the presence of cracking or microcracking as damage which may be dependent upon the maximum strain the material has experienced in its history, the current strain level, and the number of load repetitions. The quasi-elastic representation is due to Schapery [6; 7] who has developed an extended correspondence principle to permit the application of the same methods to viscoelasticity.

Strain energy release rate methods are presently in use in FE programs to determine the stress intensity factors and J-Integral values as a function of crack length for various loading conditions. Used in this way, the computed results assist in the interpretation of laboratory test results when the tests are run on elastic and viscoelastic materials. Various methods of representing the presence and the effects of a microcrack process zone surrounding and in advance

Table 7. Present and Future Plasticity Properties in 3-D FE Response Models

	Phase of Development			
	Now	I	II	III
• Plasticity Properties				
- Yield function				
• Tresca				
• Von Mises				
• Mohr-Coulomb				
• Vermeer				
• Lade				
- Plastic potential				
• Associative				
• Non-associative				
- Work hardening				
• Linear				
- Isotropic				
- Kinematic				
- Mixed				
• Non-linear				
- Isotropic				
- Kinematic				
- Mixed				
• Soil models				
- Work softening				
• Shear banding				

Table 8. Present and Future Properties in 3-D FE Response Models

	Phase of Development			
	Now	I	II	III
• Fracture Properties				
- Reduced modulus				
• Strain-dependent	██████			
• Repeated load dependent		██████		
• Quasi-elastic		██████		
- Strain energy release				
• Elastic			██████	
• Viscoelastic				██████
• Microcrack process				██████

of a propagating crack are also in use. Principal among these is to treat the microcrack process zone as a "damaged" zone with altered stress-strain curve characteristics.

Whether it is necessary or even desirable to adapt these methods to the prediction of pavement distress remains to be seen. Although it can be done, it will result in longer computer running times in which the finite element mesh must be restructured each time the cracks take on an increment of growth. The decision whether to remain with the reduced modulus methods or to change to the strain energy release rate methods must be made on the basis of their threefold capabilities of accuracy, numerical compatibility, and convergence and stability.

In the following sections, several of the ideas mentioned above will be illustrated. Specifically, these will include:

1. resilient elastic dilatancy,
2. hypoelastic formulation, and
3. reduced modulus to represent microcracking damage.

Example No. 1: Resilient Elastic Dilatancy

Path dependence upon loading and unloading requires that the contour integral in Figure 1, representing the elastic work done in the process, be zero. The bulk modulus, K , and the shear modulus, G , are equal to:

$$\begin{aligned} K &= \frac{E}{3(1-2\nu)} \\ G &= \frac{E}{2(1+\nu)} \end{aligned} \quad (1)$$

in terms of Young's modulus and Poisson's ratio. Substituting these expressions for K and G into the integral and requiring the kernel to be zero produces a partial differential equation in terms of $\ln E$ and ν as follows:

$$0 = -\frac{2}{3} \frac{\partial \nu}{\partial J_2'} + \frac{1}{J_1} \frac{\partial \nu}{\partial J_1'} + \frac{1-2\nu}{3} \frac{\partial(\ln E)}{\partial J_2'} - \frac{1+\nu}{J_1} \frac{\partial(\ln E)}{\partial J_1'} \quad (2)$$

where

E = resilient modulus

ν = resilient Poisson's ratio

A phenomenological expression of the resilient modulus as a function of stress state which has proven to be very accurate in representing laboratory and field results [8]:

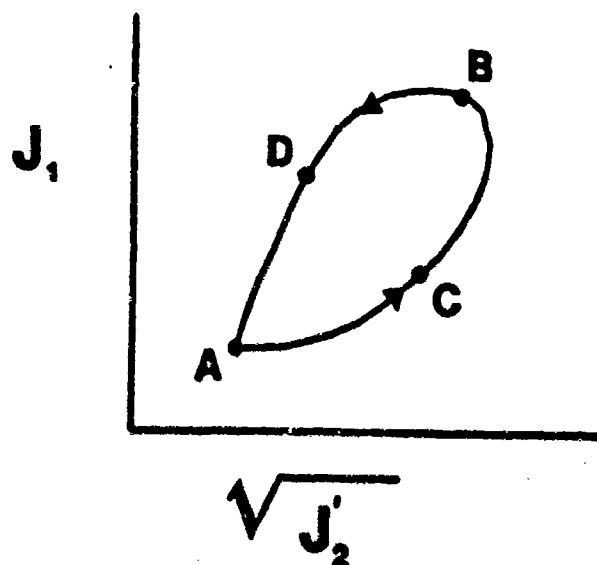
$$E = k_1 (J_1)^{k_2} (J_2')^{k_3} \quad (3)$$

which means that

$$\ln E = \ln k_1 + k_2 \ln J_1 + k_3 \ln J_2' \quad (4)$$

substituting this expression into the partial equation for path independence wherever $\ln E$ appears results in the following differential equation in terms of Poisson's ratio, ν , the stress state (J_1, J_2') and the material coefficients (k_1, k_2, k_3) .

$$0 = -\frac{2}{3} \frac{\partial \nu}{\partial J_2'} + \frac{1}{J_1} \frac{\partial \nu}{\partial J_1'} - \nu \left(\frac{2}{3} \frac{k_3}{J_2'} + \frac{k_2}{J_1^2} \right) - \left(-\frac{1}{3} \frac{k_3}{J_2'} + \frac{k_2}{J_1^2} \right) \quad (5)$$



$$\text{ELASTIC WORK} = \int_{ACBDA} \left(\frac{J_1 dJ_1}{9K} + \frac{dJ_2'}{2G} \right)$$

Figure 1. The Condition for Resilient Elastic Dilatancy

The solution to this equation is

$$u_2 = k_4 u_1^{k_3} \quad (6)$$

where

$$u_1 = 3J_2' - J_1^2 \quad (7)$$

$$u_2 = \frac{\nu}{J_1^{k_3} J_2^{k_3}} - \frac{3k_3}{2(J_1^2 - 3J_2')} \times \left[-k_2 B\left(\frac{k_2}{2} + k_3, -k_3 + 1\right) + k_3 B\left(\frac{k_2}{2} + k_3, -k_3\right) \right] \quad (8)$$

$B(x, y)$ = the incomplete *Beta Function*

As an illustration of the accuracy of representation of material properties of which this formulation is capable, the resilient modulus data measured by Allen [9] is presented in Figures 2 and 3. In addition to the usual accuracy of representing the laboratory test in which both the vertical and lateral strains were measured, is the fact that there was an increase of volume under load which resulted in values of Poisson's ratio greater than 0.5.

Implementing this property resilient elastic dilatancy in a finite element program requires a certain amount of manipulation of the element stiffness matrices and load vectors, and an iterative process to converge on the final values of stress state, secant modulus, and Poisson's ratio in each element.

The following formulation has been developed and programmed into a two-dimensional finite element program in cylindrical coordinates. It makes use of an initial strain formulation to account for the effects of Poisson's ratio being greater than 0.5. The formulation is as follows. The secant modulus relation between stress and strain is written as:

$$\begin{bmatrix} \epsilon_r \\ \epsilon_z \\ \gamma_{rz} \\ \epsilon_\theta \end{bmatrix} = \frac{1}{E} \begin{bmatrix} 1 & -\nu & 0 & -\nu \\ -\nu & 1 & 0 & -\nu \\ 0 & 0 & 2(1+\nu) & 0 \\ -\nu & -\nu & 0 & 1 \end{bmatrix} \begin{bmatrix} \sigma_r \\ \sigma_z \\ \tau_{rz} \\ \sigma_\theta \end{bmatrix} \quad (9)$$

when

$$\begin{aligned} \nu &> 0.5, \text{ let} \\ \nu &= \mu + \alpha(\sigma) \\ \mu &< 0.5 \end{aligned}$$

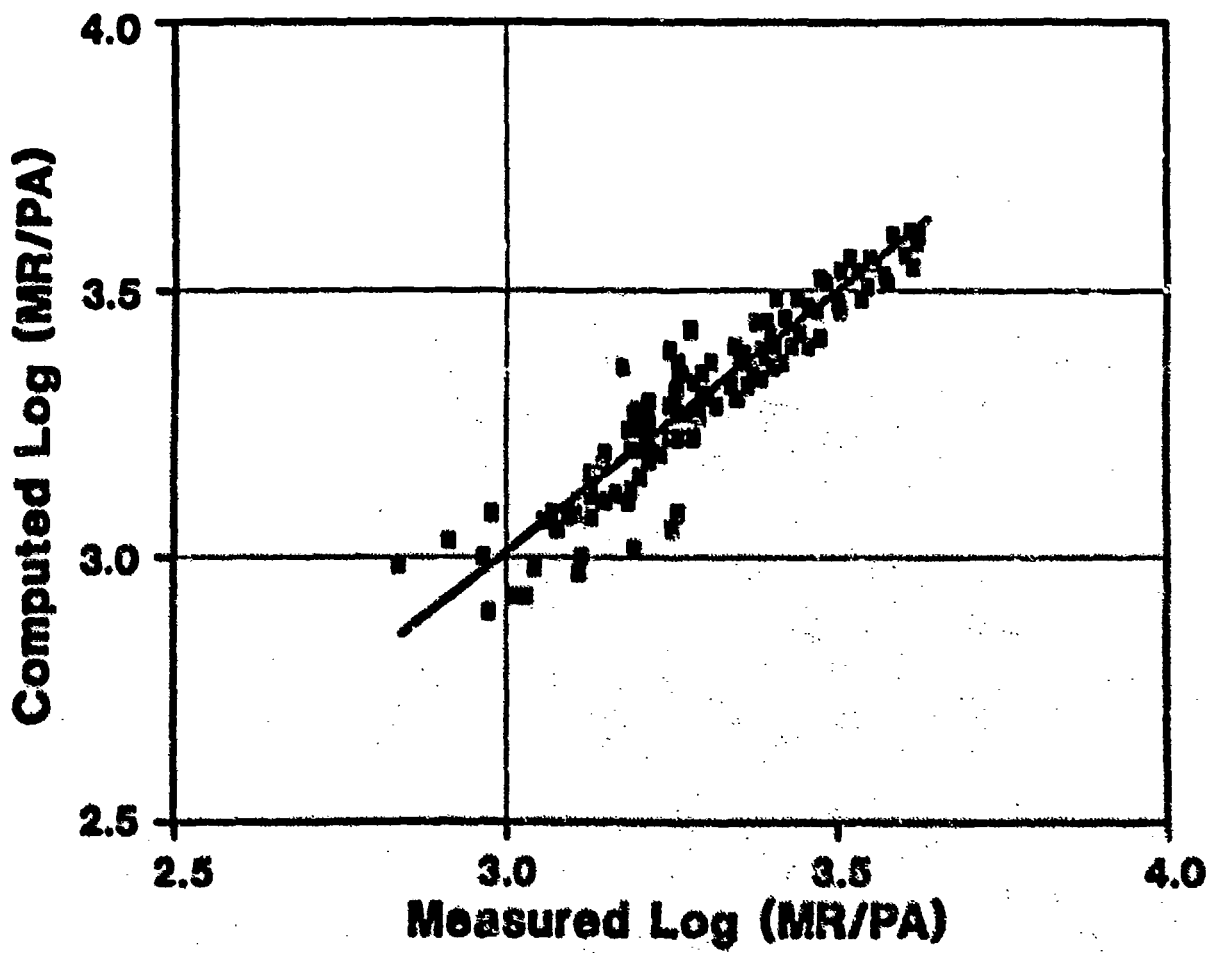


Figure 2. Measured vs. Computed Resilient Modulus

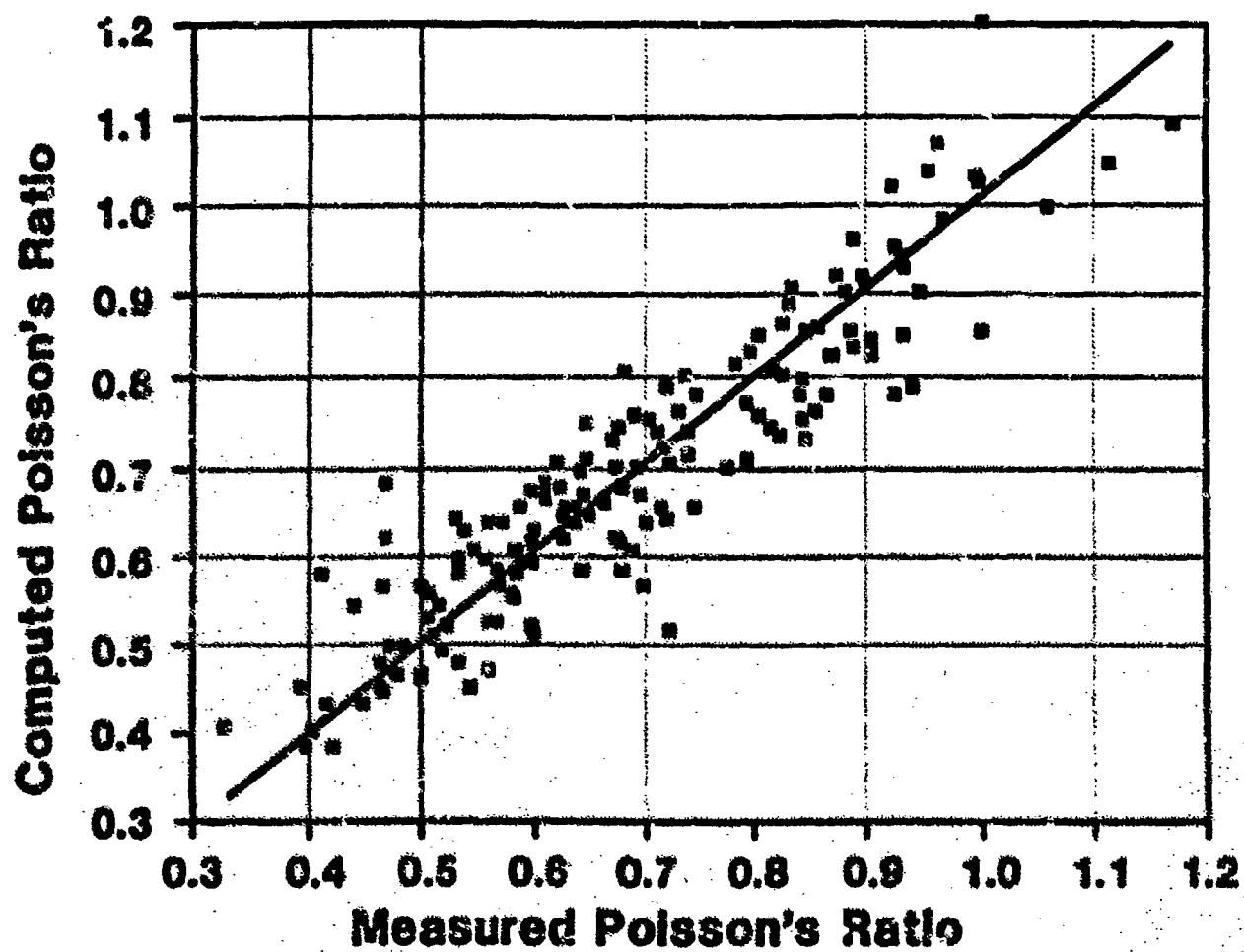


Figure 3. Measured vs. Computed Poisson's Ratio

This produces two matrices as follows:

$$\{\varepsilon\} = \frac{1}{E} \begin{bmatrix} 1 & -\mu & 0 & -\mu \\ -\mu & 1 & 0 & -\mu \\ 0 & 0 & 2(1+\mu) & 0 \\ -\mu & -\mu & 0 & 1 \end{bmatrix} \{\alpha\} + \begin{bmatrix} 1 & -\alpha & 0 & -\alpha \\ -\alpha & 1 & 0 & -\alpha \\ 0 & 0 & 2\alpha & 0 \\ -\alpha & -\alpha & 0 & 1 \end{bmatrix} \sigma \quad (10)$$

or in matrix notation

$$\underline{\underline{\varepsilon}} = C^\mu \underline{\underline{\sigma}} + C^\alpha \underline{\underline{\sigma}} = \underline{\underline{\varepsilon}}^\mu + \underline{\underline{\varepsilon}}^\alpha \quad (11)$$

but since

$$\underline{\underline{\sigma}} = [C^\mu]^{-1} \underline{\underline{\varepsilon}}^\mu \quad (12)$$

then

$$\underline{\underline{\sigma}} = D^\mu [\underline{\underline{\varepsilon}} - \underline{\underline{\varepsilon}}^\alpha] \quad (13)$$

where

$$D^\mu = [C^\mu]^{-1} \quad (14)$$

and

$$\underline{\underline{\varepsilon}}^\mu = \underline{\underline{\varepsilon}} - \underline{\underline{\varepsilon}}^\alpha \quad (15)$$

This is substituted into the equation for element equilibrium, the iterative equation is the result. The steps in the derivations are as follows:

The equation for element equilibrium is:

$$\int_V [B]^T \underline{\underline{\sigma}} dV - \underline{\underline{f}} = 0 \quad (16)$$

Internal
Forces

External
Forces

A series of substitutions from the deviations given above produces the following:

$$\int_V B^T D^u [\underline{\underline{\epsilon}} - \underline{\underline{\epsilon}}^\alpha] dV - \underline{\underline{f}} = 0$$

$$\int_V B^T D^u \underline{\underline{\epsilon}} dV - \int_V B^T D^u \underline{\underline{\epsilon}}^\alpha dV - \underline{\underline{f}} = 0 \quad (17)$$

or

$$\int_V B^T D^u \underline{\underline{u}} dV - \underline{\underline{f}}(\underline{\underline{\epsilon}}^\alpha) - \underline{\underline{f}} = 0$$

The last equation requires iteration and convergence to reach a solution. Convergence requires the residual vector in the following equation to be reduced to zero within tolerances.

$$K^n \underline{\underline{u}}^n - \underline{\underline{f}}(\underline{\underline{\epsilon}}^\alpha) - \underline{\underline{f}} = \underline{\underline{r}} \quad (18)$$

_____ Residual Vector

when

$$\underline{\underline{r}} = \underline{\underline{0}} \quad (19)$$

then the iterations have converged to the desired solution.

This formulation is different than the Cauchy and Green formulations, but shares the stress-path independence of the material properties and the fact that no elastic energy is generated on loading and unloading with them. It has the advantage of using the material coefficients (k_1, k_2, k_3) with which soils and pavement engineers are familiar and have broad experience.

Example No. 2: Hypo Elastic Formulation

One of the problems with a resilient, elastic dilatancy, or hyperelastic secant modulus formulation when used with plasticity to represent permanent deformation or rutting is that when granular materials are represented with friction angles above 30 degrees, instability is found in the convergence process.

In order to overcome this difficulty, a hypoelastic formulation may be used to allow for both resilient and inelastic or plastic behavior. The seven material constants for a Grade One hypoelastic model may all be found using conventional triaxial tests. The stiffness matrix used in a finite element program is non-symmetric and this results in relatively higher computational efforts.

Using data from several tests by Allen [9], the graphs in Figures 4, 5 and 6 were developed to illustrate how accurately a Grade One hypoelastic formulation represents the material response as compared with the $k_1 - k_5$ resilient, elastic dilatancy method. Although the resilient, elastic dilatancy model appears to fit the data somewhat better, the hypoelastic has advantages in the stable convergence of numerical computations. In making a decision between the two approaches, the better convergence capability of the hypoelastic formulation will very likely prove to be the determining factor.

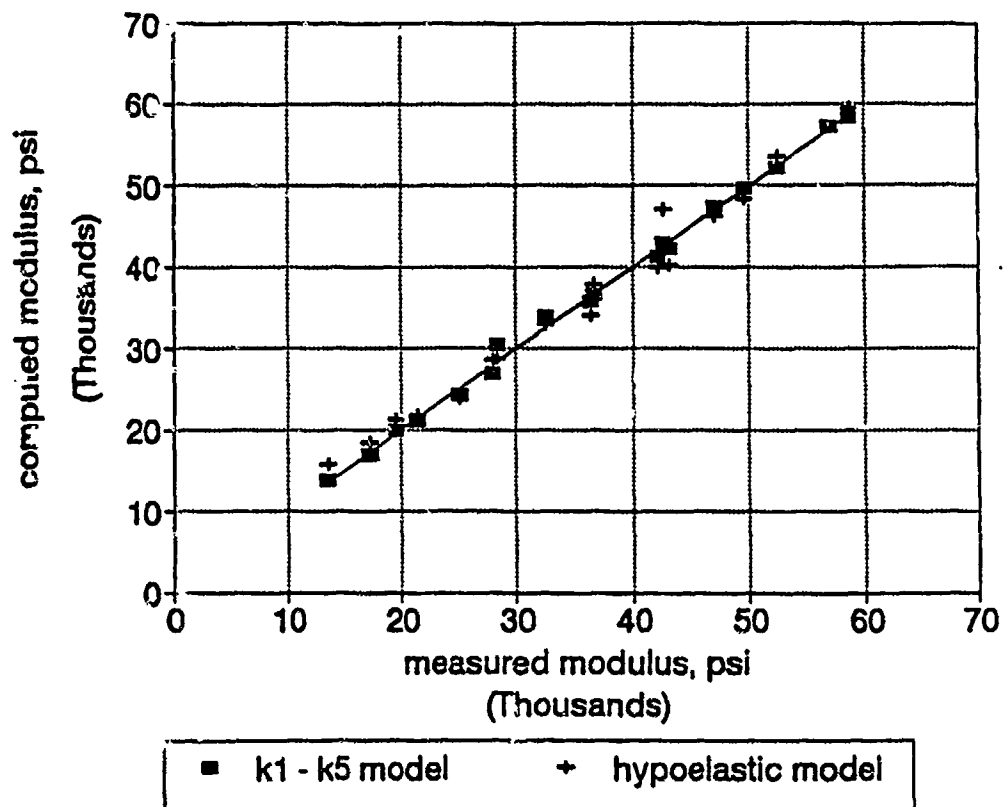


Figure 4a. Comparison of Moduli for the Resilient Elastic Dilatancy Model and the Hypoelastic Model

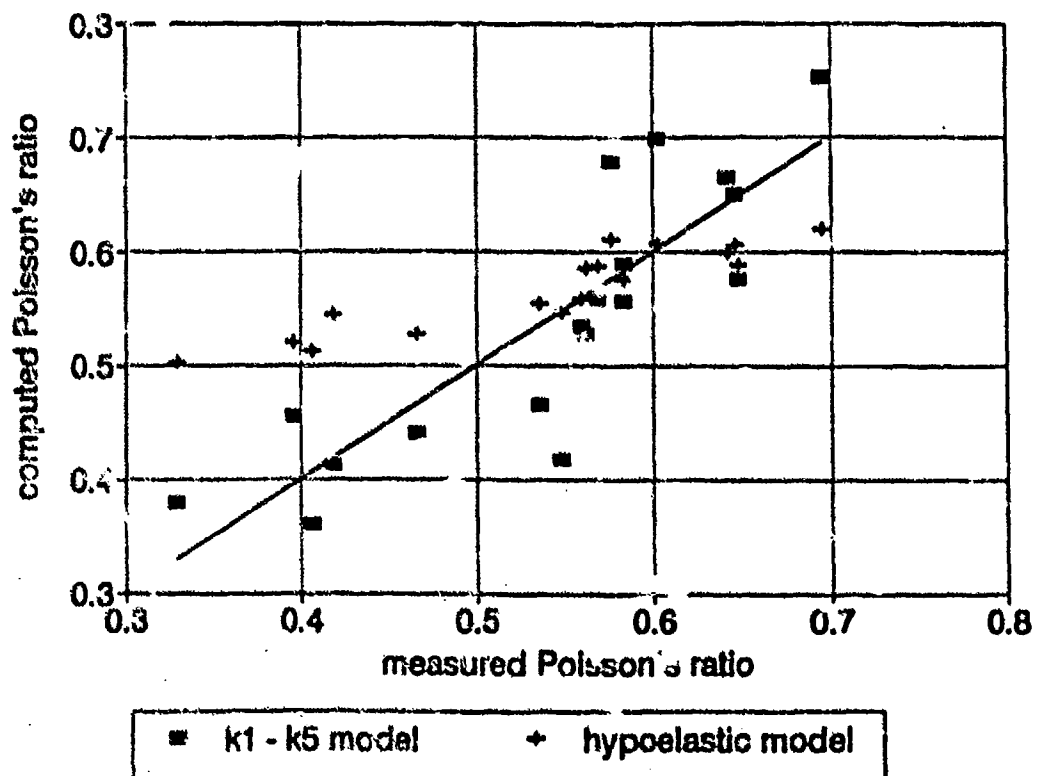


Figure 4b. Comparison of Poisson's Ratio for the Resilient Elastic Dilatancy Model and the Hypoelastic Model

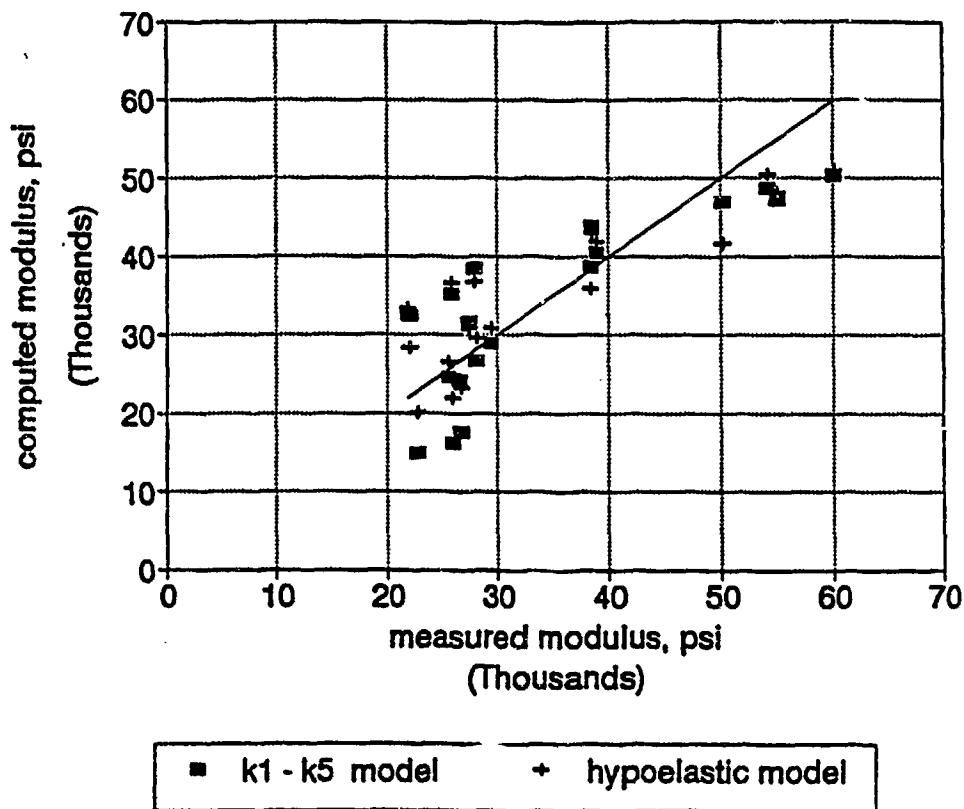


Figure 5a. Comparison of Modulus for the Resilient Elastic Dilatancy Model and the Hypoelastic Model

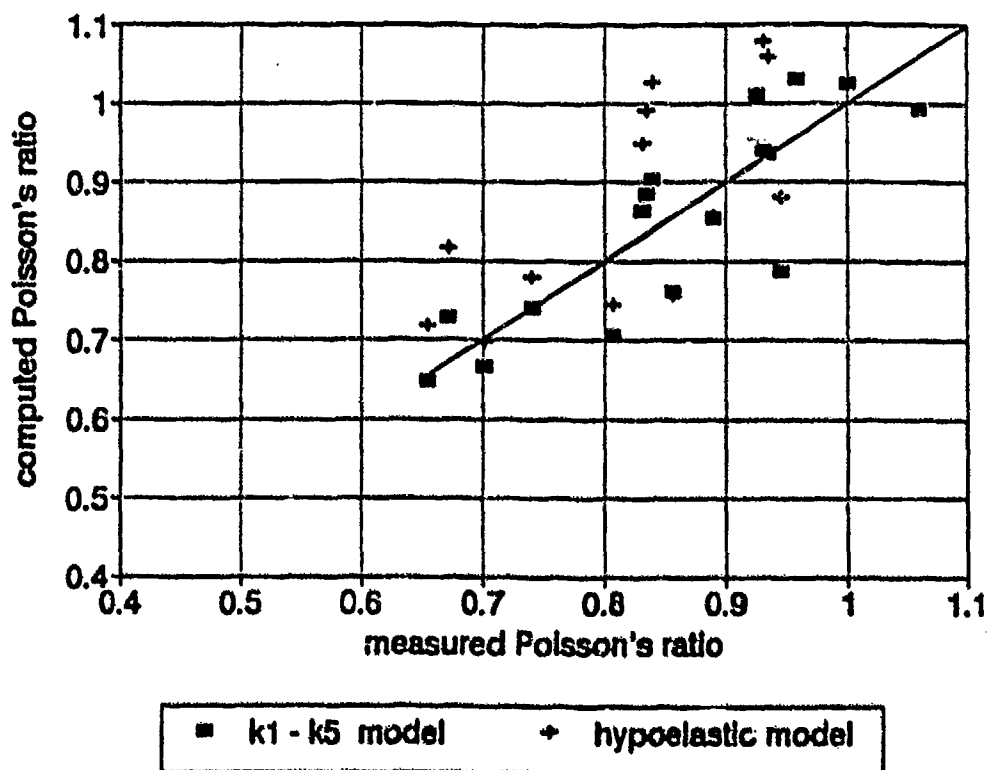


Figure 5b. Comparison of Poisson's Ratio for the Resilient Elastic Dilatancy Model and the Hypoelastic Model

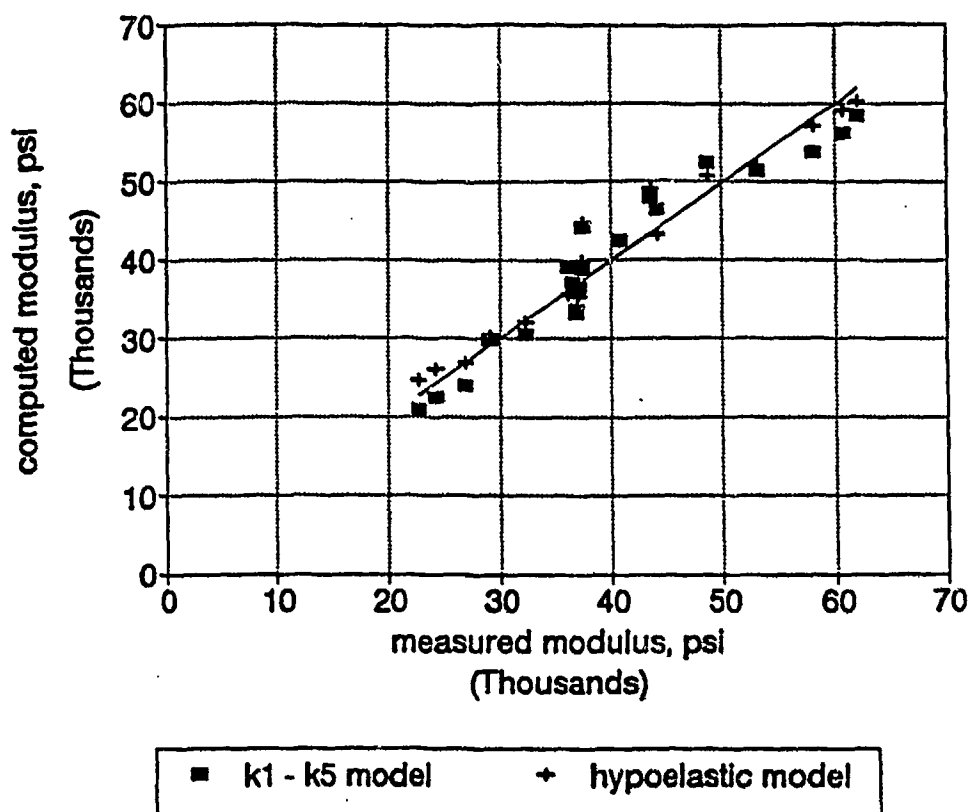


Figure 6a. Comparison of Moduli for the Resilient Elastic Dilatancy Model and the Hypoelastic Model

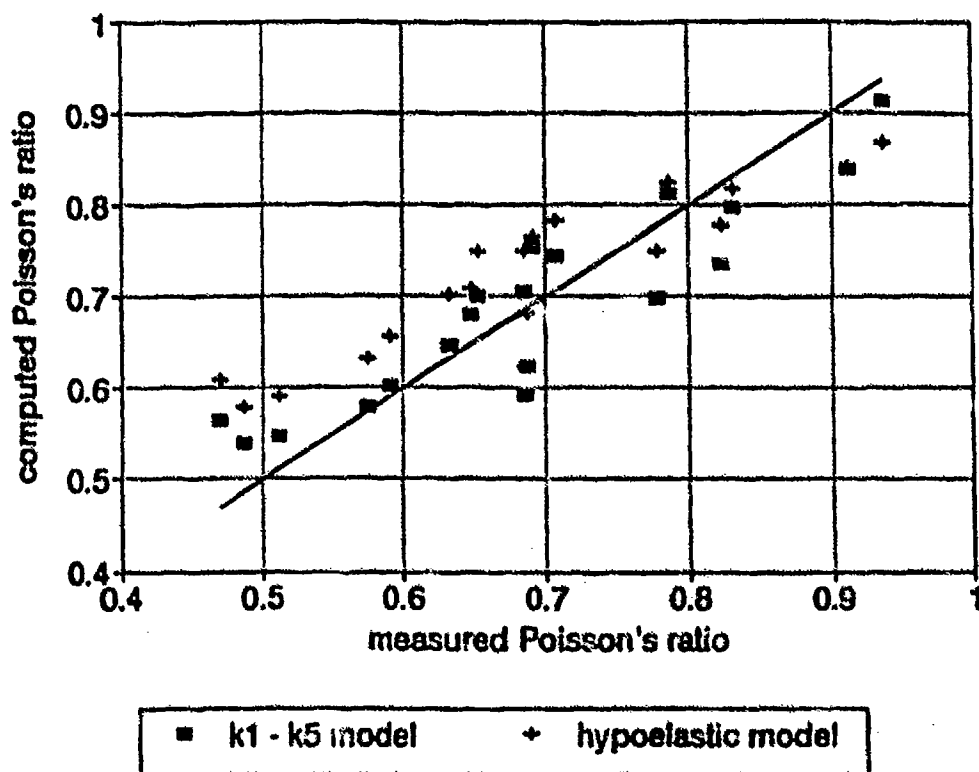


Figure 6b. Comparison of Poisson's Ratio for the Resilient Elastic Dilatancy Model and the Hypoelastic Model

Example No. 3: Reduced Modulus Due to Microcracking

The third and final example is the formulation of a materials model which is compatible with a finite element continuum formulation and, at the same time, satisfies the requirements of accurately representing the material response. In the reduced modulus approach, two straps, Nos. 1 and 2 (illustrated in Figure 7) are arranged to store the same strain energy.

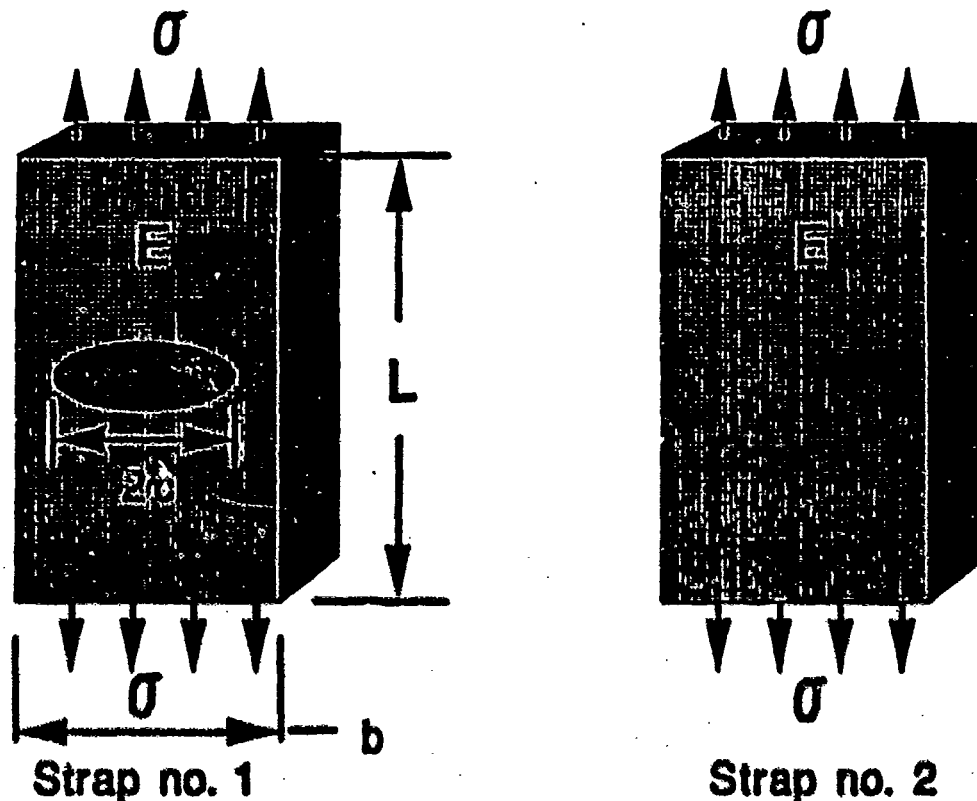


Figure 7. Reduced Modulus Due to Microcracking

Strap No. 1 has a modulus of E and a crack in it of length, $2c$, whereas Strap No. 2 has an equivalent modulus of E' and no crack. The strain energy, U , Strap No. 1 is redistributed as a result of the formation of the crack.

$$U = \underbrace{\frac{1}{2} \frac{\sigma^2}{E} b L t}_{\text{Strain Energy}} - \underbrace{2\pi c^2 \cdot \frac{\sigma^2}{E} \cdot t}_{\text{Released}} + \underbrace{4 \int c t}_{\text{Stored}} \quad (20)$$

where

t = thickness of the strap

Γ = surface energy storage density.

The strain energy in Strap No. 2 is

$$u = \frac{1}{2} \frac{\sigma_2}{E'} b l t \quad (21)$$

where

E' = the reduced modulus

Using the fact that $\pi J_{1c} = 2 \Gamma$ and J_{1c} is the critical J-Integral value above which the crack propagates in an unstable manner, some algebra results in the following expression for one crack

$$E' = E \left\{ \frac{1}{1 + 2\pi \left(\frac{1}{b l}\right) c \left[\frac{2J_{1c}}{E \epsilon^2} \right] - c} \right\} \quad (22)$$

If, instead of one crack, there are n microcracks within the area of the strap, and n_i is the number of cracks of length, c_i , then the ratio, n_i/n is the probability of having a crack of length, c_i ,

$$\frac{n_i}{n} = p(c_i) \quad (23)$$

The reduced modulus in this case becomes

$$E' = E \left\{ \frac{1}{1 + 2\pi \left(\frac{1}{b l}\right) \sum_{i=1}^k p(c_i) c_i \left[\frac{2J_{1c}}{E \epsilon^2} - c_i \right]} \right\} \quad (24)$$

Damage Function

where

$\left(\frac{n}{b l}\right)$ = the microcrack density

$p_i(C)$ = the probability of having a crack of length between $c_i - \frac{DC}{2}$ and $c_i + \frac{DC}{2}$

k = the number of crack length increments

J_{lc} = the critical J-Integral of the material.

The microcrack density will be a function of the maximum strain experienced by the material within the strap (or finite element) and be of the form

$$\frac{n}{b\Delta} = a (\epsilon_{\max} - \epsilon_0)^q \quad (25)$$

where q is greater than 2. The shape of this function is illustrated in Figure 8. The term ϵ_0 is a threshold strain below which no microcracks form and no damage is done to the material.

Microcracks will be of various sizes, resulting in $p(c_i)$ being a probability density function which changes as the cracks grow with repeated loads. This is illustrated in Figure 9.

If the crack length distribution follows a Weibull distribution with parameters λ and γ so that the probability density function is

$$p(c) = \lambda \gamma (\lambda c)^{\gamma-1} \exp [- (\lambda c)^\gamma] \quad (26)$$

then the J-Integral for the mean crack length, \bar{c} , when the microcracks range in size between 0 and c_{\max} is

$$J_1(\bar{c}) = \pi E \epsilon^2 \int_0^{c_{\max}} c p(c) dc \quad (27)$$

Here the J-Integral is defined as

$$\frac{\frac{d}{dN} (\text{Dissipated Energy per Load Cycle})}{t \frac{d\bar{c}}{dN}} = J_1(\bar{c}) \quad (28)$$

The dissipated energy per load cycle is the area enclosed by the load-displacement curve with each load cycle; t is the thickness of the test sample; and \bar{c} is the mean microcrack length. When the expression for $J_1(\bar{c})$ is integrated it gives

$$\bar{c} = \frac{1}{\lambda} \left[\left(1 + \frac{1}{\lambda}\right) I_1 + \frac{1}{\gamma} [\lambda(c_{\max})^\gamma] \right] \quad (29)$$

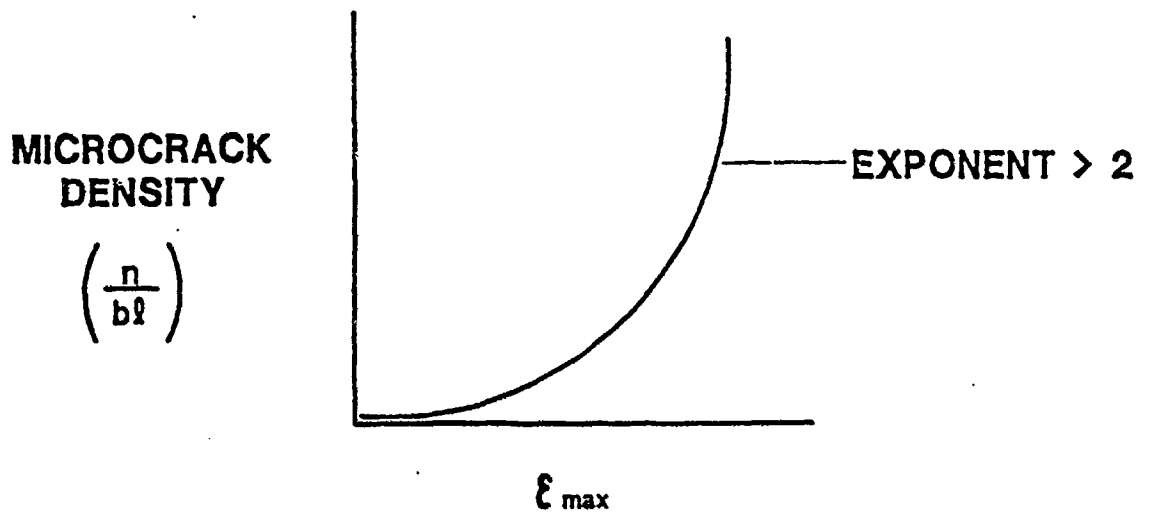


Figure 8. Relation of Microcrack Density to Maximum Strain, ϵ_{\max}

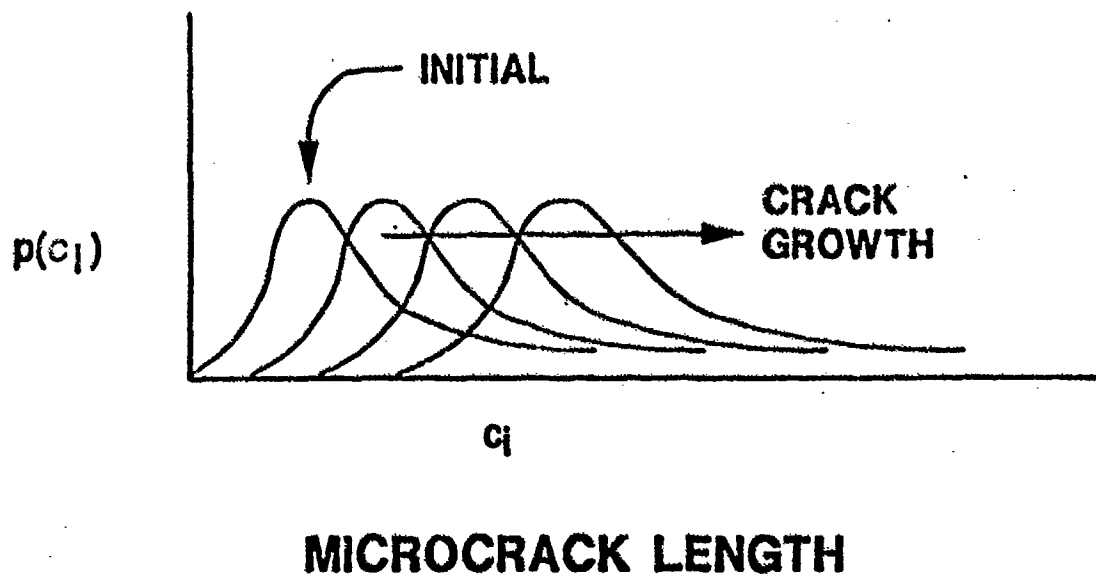


Figure 9. Change of Probability Density Function as Crack Lengths Grow

$$\text{and } J_1(\bar{c}) = p E \bar{c}^2$$

where

$$\Gamma\left(1 + \frac{1}{\gamma}\right) = \text{the Gamma function with argument } 1 + \frac{1}{\gamma}$$

$$I_{1 + \frac{1}{\gamma}}[(\lambda c_m)^\gamma] = \text{the incomplete Gamma function of order } \left(1 + \frac{1}{\gamma}\right) \\ \text{and with argument } \lambda(c_{\max})^\gamma$$

If the rate of change of dissipated energy per load cycle is a constant, β , and if a visible crack begins to propagate when the maximum microcrack length reaches c_0 , then the number of load cycles required to start crack propagation is N_i and is equal to

$$N_i = t \frac{J_1(\bar{c}_0)}{\beta} c_0 \quad (30)$$

where

$$J_1(\bar{c}_0) = \pi E \bar{c}_0^2$$

\bar{c}_0 = the mean microcrack length when the maximum microcrack length is c_0 .

$$\bar{c}_0 = \frac{\Gamma\left(1 + \frac{1}{\gamma}\right)}{\lambda} I_{1 + \frac{1}{\gamma}}[(\lambda c_0)^\gamma] \quad (31)$$

The equations given above establish the fact that the number of load cycles to "crack initiation" is dependent on the J-Integral of the mean microcrack length. The damage function by which the reduced modulus E' is related to the modulus of the intact material, E , also depends upon the J-Integral of the individual microcracks, and ultimately upon the length of the cracks and the number of load repetitions. The damage function for the reduced modulus is:

$$\frac{E'}{E} = f_{xx} = \frac{1}{1 + D_{xx}} \quad (32)$$

where

$$D_{xx} = 2\pi \left(\frac{n}{b\theta}\right) \int_0^{c_{\max}} p(c) c \left[\frac{2J_k}{E \bar{c}^2}(\bar{c}) - \bar{c}^2 \right]$$

Integration of the equation for D_{xx} gives:

$$D_{xx} + 2\pi \left(\frac{n}{b\ell} \right) \int_0^{c_{\max}} \left[\frac{2J_{Ic}}{E \epsilon^2} (\bar{c}) - \bar{c}^2 \right] d\bar{c} \quad (33)$$

The equation for the mean microcrack length has been given previously whereas the equation for the expected value of the square of the microcrack length is:

$$(\bar{c}^2) = \frac{1}{\lambda^2} \left[\left(1 + \frac{2}{\lambda} \right) I_{1+\frac{2}{\lambda}} [\lambda (c_{\max})^\gamma] \right] \quad (34)$$

The symbols for the Gamma function, $\Gamma(\cdot)$, and the incomplete Gamma function, $I_\gamma(\cdot)$, have been defined previously.

Making use of the Paris-Erdogan law [10] for the growth of the mean crack length gives:

$$(\bar{c}) = \left[\frac{2-n}{2} \pi_2^{\frac{n}{2}} A (E \epsilon)^n \right]^{\frac{2}{2-n}} N_2^{\frac{2}{2-n}} \quad (35)$$

where

A, n = the fracture properties of the material in which the crack grows

This, together with an expression for (\bar{c}^2) , may be substituted into the equation for D_{xx} to give the damage function in terms of the microcrack density $\left(\frac{n}{b\ell} \right)$ the fracture properties of the medium, A, n , and J_{Ic} and the number of load cycles, N . The term (\bar{c}^2) may be expressed as a function of A, n, E, ϵ , and N by first determining the ratio of (\bar{c}^2) to (\bar{c})

$$\text{Ratio} = \frac{\bar{c}^2}{\bar{c}} = \frac{1}{\lambda} \frac{I_{1+\frac{2}{\lambda}} [\lambda (c_{\max})^\gamma] \left(1 + \frac{2}{\lambda} \right)^{\frac{1}{\gamma}}}{I_{1+\frac{1}{\lambda}} [\lambda (c_{\max})^\gamma] \left(1 + \frac{1}{\lambda} \right)^{\frac{1}{\gamma}}} \quad (36)$$

Then the ratio may be multiplied by the expression for \bar{c} to give the desired equation for (\bar{c}^2) . The variance of the microcrack length is $\text{var}(c) = (\bar{c}^2) - (\bar{c})^2$

MICROCRACK DAMAGE FUNCTION

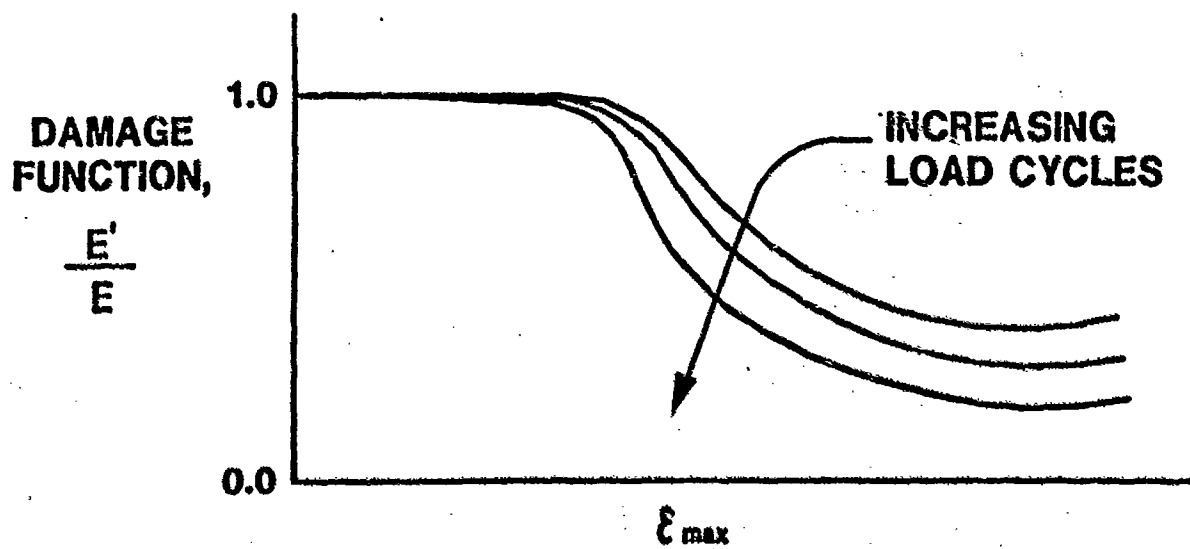


Figure 10. Schematic Illustration of a Microcrack Damage Function

The resulting damage function appears as shown in Figure 10. A non-linear search technique applied to the laboratory records of deflection and dissipated records per load cycle in a fatigue test can be used to determine the Weibull coefficients, λ and γ , as well as the fracture properties A , n , and J_{Ic} , and the microcrack density and the maximum microcrack length, c_{max} . Only the latter will vary with the number of load repetitions, while the microcrack density will vary with location within the test sample.

Applying the reduced modulus model of microcrack damage to finite elements is a simple matter once the fracture properties A , n , and J_{Ic} , and the intact modulus of the material, E , are input. As the number of load repetitions increase, the damage will also increase and the modulus for each finite element will be reduced accordingly.

The shear modulus is also reduced by the presence of the same crack as illustrated in Figure 7. Following the same procedure as before, a reduction in shear modulus, G , is determined to:

$$\frac{G'}{G} = f_{xy} \frac{1}{1 + 2\pi \left(\frac{n}{b} \right) c \left[\frac{2 J_{Ic}}{G \gamma^2} - c \right]} \quad (37)$$

for one crack and the same formulation holds for a distribution of microcracks with the exception of the following substitutions.

J_{Ic} = critical shearing mode J-Integral

G = intact shear modulus

γ = shear strain

The same expressions as before for the mean and expected value of the square of the microcrack length also hold for the shear modulus damage function. The altered Poisson's ratio of the damaged material may be determined from:

$$\nu' = \frac{E}{2G} \left(\frac{t_{xx}}{t_{yy}} \right) - 1 \quad (38)$$

The element elasticity matrix is for a plane strain condition and is written as:

$$\frac{E' (1 - \nu')}{(1 + \nu') (1 + 2\nu')} \begin{bmatrix} 1 & \frac{\nu'}{1 - \nu'} & 0 \\ \frac{\nu'}{1 - \nu'} & f_{yy} & 0 \\ 0 & 0 & \frac{1 - 2\nu'}{2(1 - \nu')} \end{bmatrix} \quad (39)$$

using the reduced modulus and altered Poisson's ratio. The net effect of distributed, oriented microcracks on the properties of a finite element are to reduce the modulus with load repetitions and strain level, and to induce anisotropy. The modulus in the direction parallel to the crack will remain unaltered so that the modulus reduction term, f_{xx} , is in fact, the reciprocal of f_{xy} .

5. Conclusion

The constitutive representation of material properties for modern airport pavement analysis and design must be chosen astutely to meet several criteria:

- a. Accuracy in describing the material response;
- b. Compatibility with a selected numerical computational scheme;
- c. Favorable convergence and stability characteristics; and
- d. Ability to extract the needed material property parameters from consistent and repeatable tests.

The material properties needed are the resilient, dilatant, elastic, and fracture properties. Examples are given to illustrate the way that a resilient, elastic dilatant material can be represented in an iterative FE method, and also how accurately the actual material response can be predicted. An alternative formulation using a Grade One hypoelastic model was presented as an alternative to demonstrate the kind of decisions that must be made in developing constitutive models of pavement materials. Advantages and disadvantages of each constitutive relation were compared to illustrate the kind of criteria that must be used in arriving at a decision. Another example shows how microcracking damage may be represented in a finite element program and, at the same time, permit an interpretation of laboratory test data to produce the needed material properties. The damage function was shown to be dependent upon the strain level, the maximum strain level experienced,

the fracture properties of the material, the Young's and Shear modulus of the material, the Weibull distribution parameters, and the range of sizes of microcracks. Oriented microcracks induce anisotropy in the material. This approach to microcracking damage is based on making an accounting of all of the energy stored or dissipated during the growth of the microcracks. The approach makes it possible to estimate the number of load cycles to reach "crack initiation."

All of this adds up a need to carefully compose and select the material property constitutive relationships that are used in pavement analysis and design. The principles of mechanics will need to be relied on even more in the future than they have been in the past. The speed and power of present and future microcomputers, and the incredible efficiency available in using mechanistic relations to extrapolate from known data to other cases in which little is known make it too important to do otherwise.

6. References

1. Vermeer, P.A., "A Five-Constant Model Unifying Well Established Concepts," International Workshop on Constitutive Relations for Soils, Grenoble, 6-8 Sept. 1982, pp. 175-197, 1982.
2. Vermeer, P.A. and R. de Brost, "Non-associated Plasticity for Soils, Concrete and Rock," HERON Journal, Delft University of Technology, Delft, The Netherlands, Vol. 29, No. 3, pp. 1-64, 1984.
3. Lade, P.V., "Elasto-Plastic Stress-Strain Theory for Cohesionless Soil with Curved Yield Surfaces," Int'l Journal of Solids Structures, Vol. 13, pp. 1019-1035, 1977.
4. Kim, M.K. and P.V. Lade, "Single Hardening Constitutive Model for Frictional Materials, I. Plastic Potential Function," Computers and Geotechnics 5, Elsevier Science Publishers Ltd., England, pp. 307-324, 1988.
5. Lade, P.V., "Single Hardening Model with Application to NC Clay," Journal of Geotechnical Engineering, ASCE, Vol. 116, No. 3, pp. 394-414, 1990.
6. Schapery, R.A., "Correspondence Principles and a Generalized J-Integral for Large Deformation and Fracture Analysis of Viscoelastic Media," International Journal of Fracture, Vol. 25, pp. 195-223, 1984.
7. Schapery, R.A., "Models for Damage Growth and Fracture in Nonlinear Viscoelastic Particulate Composites," Proceedings, Ninth U.S. National Congress of Applied Mechanics, American Society of Mechanical Engineers, pp. 237-245, 1982.
8. Uzan, J., "Granular Material Characterization," Transportation Research Record 1022, Transportation Research Board, Washington DC, pp. 52-59, 1985.
9. Allen, John J., "The Effect of Non-constant Lateral Pressures on the Resilient Response of Granular Materials," Ph.D. Thesis, University of Illinois, Urbana, 1973.
10. Paris, P.C., and F. Erdogan "A Critical Analysis of Crack Propagation Laws," Transactions of the ASME, Journal of Basic Engineering, Series D, Vol. 85, No. 3, 1963.

7. List of Symbols

S	=	surface
B	=	base
SB	=	subbase
SG	=	subgrade
K	=	bulk modulus
G	=	shear modulus
E	=	Young's modulus
ν	=	Poisson's ration
J_1	=	first stress invariant
J_2'	=	second deviatoric stress invariant
k_1, k_2, k_3, k_4, k_5	=	constants, material coefficients
u_1, u_2	=	functions of J_1, J_2, k 's
$B()$	=	the incomplete Beta function
ϵ_r, σ_r	=	radial normal strain and stress respectively
ϵ_z, σ_z	=	vertical strain and stress respectively
$\epsilon_\theta, \sigma_z$	=	tangential normal strain and stress respectively
γ_z, τ_z	=	shear strain and stress respectively
$\alpha(\sigma)$	=	function of stress
K^n	=	stiffness matrix time step n

n = time step

\tilde{u}^n = displacement vector, time step n

\tilde{f} = external force vector

\tilde{r} = residual vector

V = volume

B = interpolation functions for strains

$\tilde{\sigma}$ = stress vector

$\tilde{\varepsilon}$ = strain vector

D^{μ}, C^{μ} = material constitutive matrices

μ = dilatancy parameter

c = crack length

E' = equivalent modulus

U = strain energy

b, l, t = specimen width, length, thickness, respectively

Γ = surface energy storage density

J_{1c} = critical J-integral value

n = number of microcracks

$p_i(C)$ = probability mass function

k = number of crack length increments

q = constant

\bar{c} = mean crack length

c_{\max} = maximum crack length

λ, γ = Weibull distribution parameters

β = rate of change of dissipated energy per load cycle

A, n = fracture properties

$\Gamma()$ = Gamma function

$I_r()$ = incomplete Gamma function, order r

$\text{var}()$ = variance

$E()$ = expected value

G' = reduced shear modulus

J_{IIc} = critical shearing mode J-integral

γ = shear strain

f_{xx}, D_{xx} = reduction and damage function, mode I

f_{xy}, D_{xy} = reduction and damage function, mode II

Thermoviscoelastic Analysis of Pavements

S. K. Reddy

M. G. Sharma

Pennsylvania State University

1. Thermoviscoelastic Analysis of Pavements

1.1 Introduction

In design and rehabilitation of pavements, it is necessary to evaluate damage due to traffic loading and environmental conditions. Damage in multilayered asphalt pavements could be of various types, namely transverse and longitudinal cracking, delamination, rutting and degradation of material properties. Computation of stresses and strains is essential for the evaluation of damage. In the present work, analysis of stresses due to the effect of temperature has been considered.

The stresses in the surface layer could be severe, as it is subjected to a wider range of temperatures compared to the underlying layers. Also, since the asphaltic top layer is a rheological material, the stresses are functions of both loading and time. These stresses could cause damage due to cracking, especially at low temperatures during winter or due to thermal fatigue as the pavement is subjected to cyclic variation of temperature. Also, delamination can occur due to the multilayered nature of pavements and the resulting mismatch in thermal properties of adjacent layers.

Since pavements are layered systems, the temperature variations give rise to complex stresses in the system which can be evaluated only through numerical methods such as finite element analysis. Although a three-dimensional analysis is desirable, it is complex and time consuming. Hence, as a primary step, two-dimensional analyses with and without temperature gradients have been performed in this investigation. In addition, the effect of physical hardening of asphalt layer on thermal stress has been evaluated in this investigation.

2. Analytical Model

2.1 Review

The pavement is modeled as a single layered slab of linear viscoelastic material resting on a rigid base (Figure 2-1). The slab is 6 inches thick and extends to infinity in transverse and longitudinal directions. The material is assumed to be homogeneous and isotropic in nature.

In order to compute the stresses as a function of time, it is required to have a knowledge of the appropriate constitutive equations governing the behavior of the material. For any given thermal history, stresses could be computed with the knowledge of these properties along with the thermal conductivity and thermal expansion properties of the material.

The computation of thermal stresses is accomplished in two steps, namely calculation of transient temperature distribution and subsequent computation of thermal stresses for the given boundary constraints.

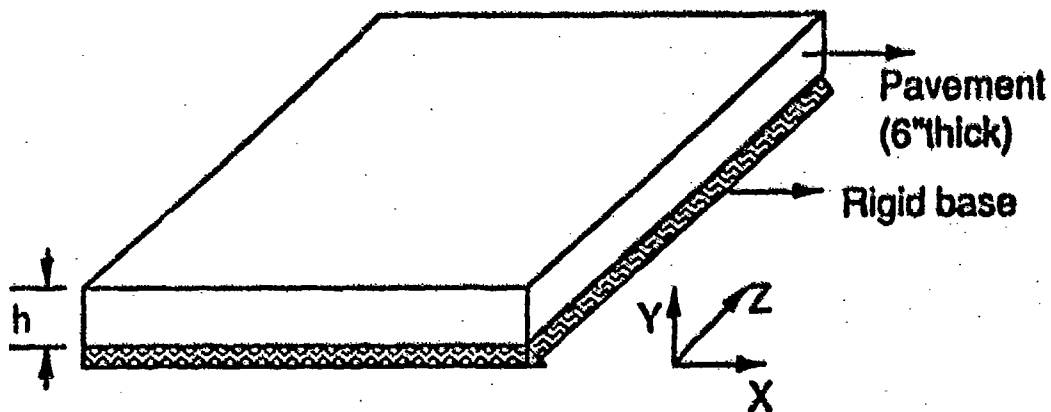


Figure 2-1. Analytical Model

2.2 Computation of Temperature Distribution

The computation of the temperature distribution is achieved by solving the transient thermal conductivity equation.

$$\nabla^2 T(x_k, t) = \frac{1}{\kappa} \frac{\partial T}{\partial t} \quad (1)$$

where

κ	=	thermal diffusivity
k	=	thermal conductivity
T	=	temperature
t	=	time
x_k	=	position coordinate

However, if it is assumed that temperature does not vary with depth, which is possible when the rate of change of temperature at the surface is very low, the above equation need not be applied.

2.3 Computation of Thermal Stresses

For simple problems, the stresses could be evaluated in closed form. However, for complex problems numerical methods have to be adopted.

3. Constitutive Equations

3.1 Review

For a general three dimensional linear viscoelastic material in isothermal conditions, the constitutive relations are given by Equations (2) and (3) [1].

a. Shear

$$S_{ij}(x_k, t) = 2 \int_0^t G(t-t') \frac{\partial e_{ij}(x_k, t')}{\partial t'} dt' \quad (2)$$

where

- S_{ij} = deviatoric stress
- G = shear relaxation modulus
- e_{ij} = deviatoric strain
- x_k = position coordinate

b. Dilation

$$s_{ii}(x_k, t) = 3K e_{ii}(x_k, t) \quad (3)$$

where

- s_{ii} = hydrostatic stress
- e_{ii} = hydrostatic strain
- K = bulk modulus (assumed to be non-relaxing)

For a case where temperature changes are involved, the above equations are modified as shown below [1]:

c. Shear

$$S_{ij}(x_k, x) = 2 \int_0^x G(x-x') \frac{\partial e_{ij}(x_k, x')}{\partial x'} dx' \quad (4)$$

d. Dilation

$$s_{ij}(x_k, x) = 3K \left[e_{ij}(x_k, x) - 3 \int_{T_0}^T a(T') dT' \right]$$

or

$$s_{ij}(x_k, x) = 3K \left[e_{ij}(x_k, x) - 3a_0(T^* - T_0) \right] \quad (5)$$

where

$$T^*(x_k, t) \text{ is pseudo temperature} = \frac{1}{a_0} \int_{T_0}^T a(T') dT'$$

- a = temperature dependent coefficient of thermal expansion
- T_0 = reference temperature for computing thermal strains
- a_0 = coefficient of thermal expansion at T_0

If a is independent of temperature, which is the case in present investigation, Equation (5) can be written as

$$s_{ij}(x_k, x) = 3K \left[e_{ij}(x_k, x) - 3a(T - T_0) \right] \quad (6)$$

The variable x is the reduced time, related to the shift factor by the following integral.

$$x = \int_0^t \frac{dt'}{a_T(x_k, T(t'))} \quad (7)$$

The shift factor is assumed to be of the form shown below [2]:

$$\ln a_T = \frac{H}{R} \left(\frac{1}{T} - \frac{1}{T_0} \right) \quad (8)$$

where

- H = activation energy of the viscoelastic process
- R = universal gas constant

In the form shown above, the shift factor is assumed to be a function of temperature alone. This assumption is valid when the material is in liquid state or glassy state. However, materials like asphalt have a transition region and exhibit structural relaxation (physical hardening). Hence, the above assumption is no longer valid and shift factor has to be a function of structural relaxation also. This is explained in detail in Appendix A.

When the physical hardening is taken into consideration, the shift factor is written as

$$\ln a_T = \frac{H_g}{R} \left(\frac{1}{T_0} - \frac{1}{T} \right) + \frac{H_s}{R} \left(\frac{1}{T_0} - \frac{1}{T_f} \right) \quad (9)$$

where

H_g = activation energy governing the glassy change

H_s = activation energy governing the structural change.

Also, $H = H_g + H_s$

where H is total activation energy.

4. Analysis and Results

4.1 Review

For the present problem, the viscoelastic material is represented by a generalized Maxwell model (Figure 4-1). The relaxation modulus for such a model is represented by a Prony series. The data points and the curve fitted using a Prony series of nine elements is shown in Figure 4-2. The plot for shift factor is shown in Figure 4-3. While considering physical hardening, it is assumed that the activation energy is equally divided between glassy and structural changes.

A variety of models that have been considered are explained below.

4.2 Uniaxial Restrained Bar

The foremost and the simplest model considered is a uniaxial bar, which is restrained in the axial direction. This is considered in order to get a basic understanding of the response of the viscoelastic material to thermal loadings.

The stress-strain relation for the uniaxial case can be written as

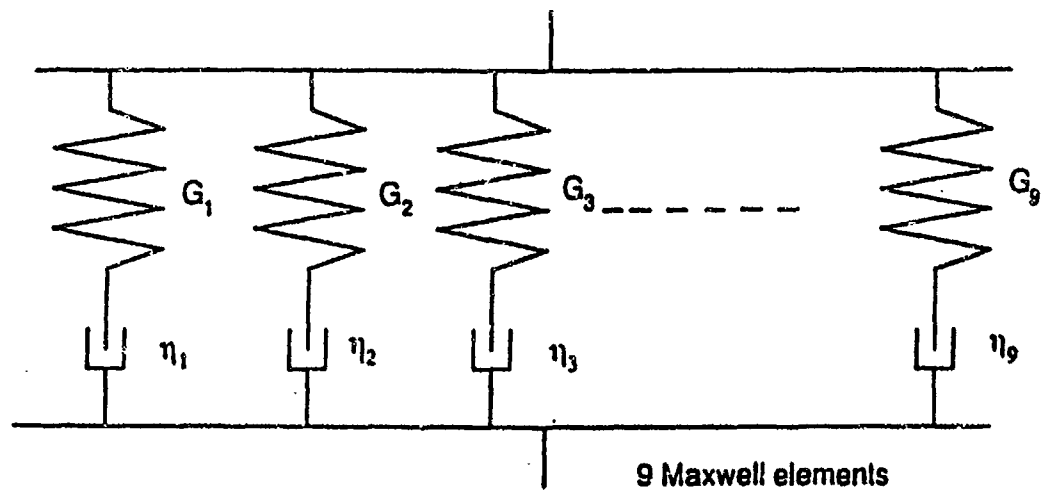
$$s(x) = \int_0^x E(x-x') \frac{\partial(e - e^{th})}{\partial x'} dx' \quad (10)$$

where

E = tensile relaxation modulus and

e^{th} = thermal strain = $a(T - T_0)$

Since the bar is assumed to be completely restrained, e is zero. Hence, with the knowledge of the thermal history and the shift factor, the above equation allows us to compute the thermal stress by using a simple numerical integration scheme [4]. The reference temperature for thermal strain and stress calculations is arbitrarily chosen to be 44 °F.



$$G(t) = \sum_{i=1}^N G_i \exp(-t / \tau_i) \quad \text{where } \tau_i = \frac{\eta_i}{G_i}$$

Figure 4-1. Generalized Maxwell Model

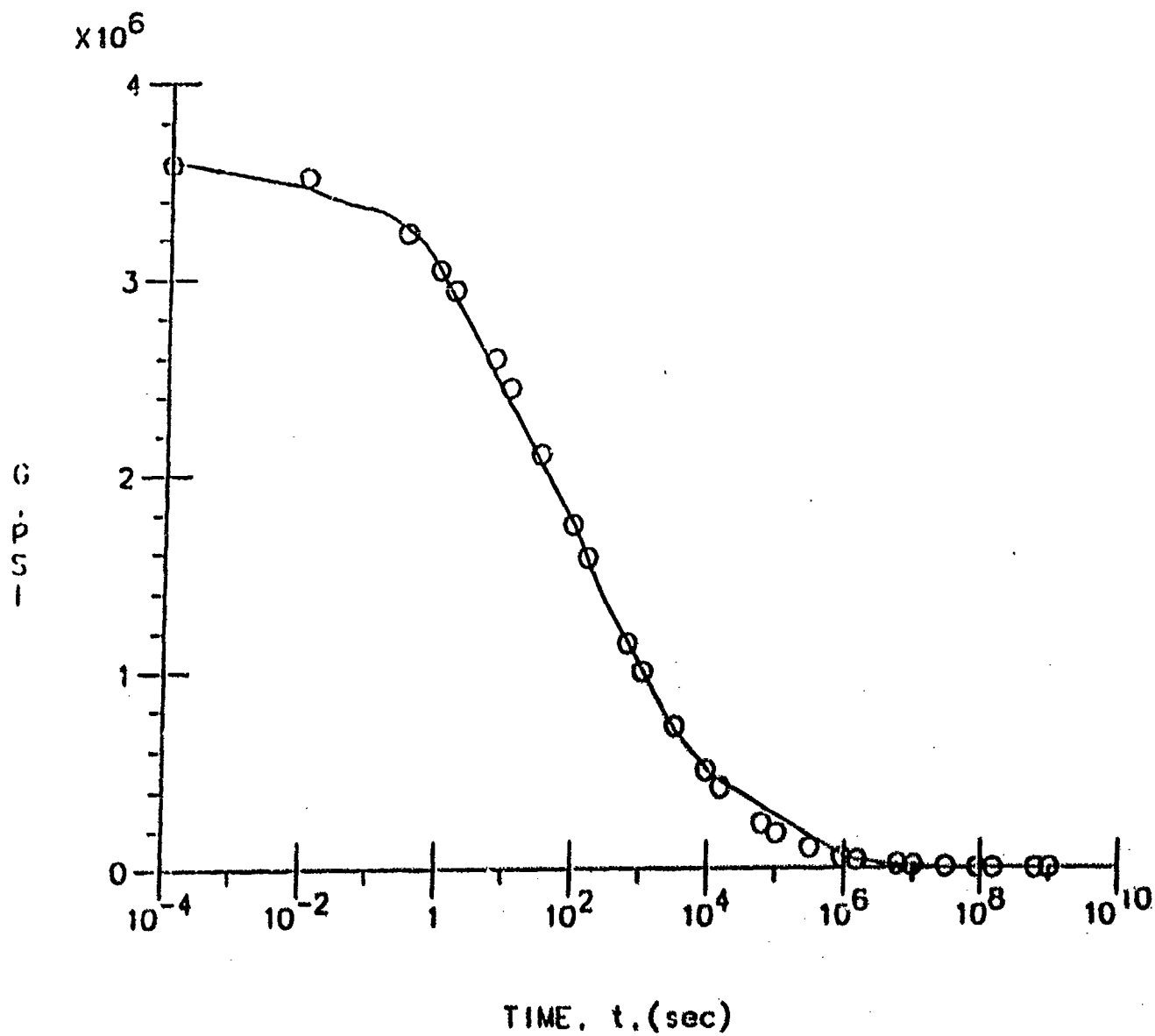


Figure 4-2. Shear Relaxation Modulus

SHIFT FACTOR

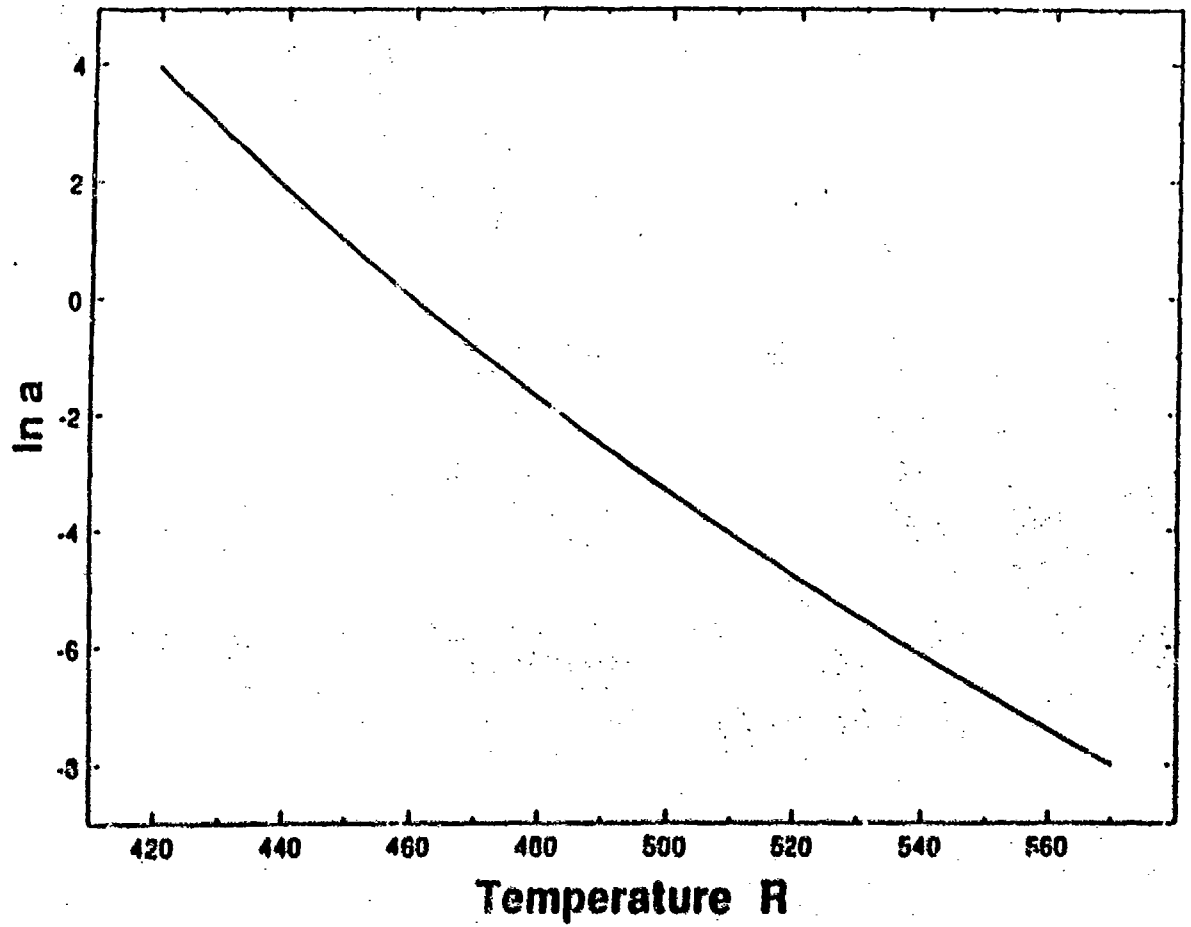


Figure 4-3. Shift Factor

- a. Response to a single thermal cycle: The temperature of the bar is dropped from 44 °F to 26 °F at the rate of 1 °F and then increased back to 44 °F at the same rate (Figure 4-4). The stress response of the bar to this thermal load is shown in Figure 4-5. As the temperature is dropped, a tensile stress is developed in the bar. As temperature is increased, a compressive stress develops and at 44 °F we have some compressive stress left in the bar. This relaxes slowly to zero as time passes, as shown in the figure.
- b. Effect of rate of cooling: A comparison of responses is made to different rates of cooling. In one case, the bar is cooled at the rate of 1 °F (solid line in Figure 4-6) and in the other case at the rate of 2 °F (dotted line in Figure 4-6). The responses are shown in Figure 4-7. As it can be seen, higher the rate of cooling, higher the stress developed. Hence, rate of change of temperature could be a significant factor in producing stresses.
- c. Cyclic variation of temperature: The model is subjected to a cyclic variation of temperature, with a constant amplitude (Figure 4-9) The stress response is shown in Figure 10. During the first cycle, a high tensile stress and a low compressive stress are observed. But, as number of cycles increases, the tensile stress decreases to a lower value.

4.3 Slab

The other problem considered is that of a linearly viscoelastic slab resting on a rigid base. The slab is analyzed both with and without temperature gradient along depth. It is assumed that there is no thermal gradient present in the horizontal plane.

The problem without temperature gradient would take less time for analysis, compared to the case with temperature gradient since the former is the simpler of the two and does not involve application of conductivity equation. Also in the former case computation of stresses at different depths need not be computed. This could be useful to get an understanding of the long-term response and for damage calculations. However, it is more realistic to assume thermal gradients since the presence of gradients could increase the stresses due to the viscoelastic nature of the pavement.

Also, the above mentioned model is analyzed by including the effect of physical hardening.

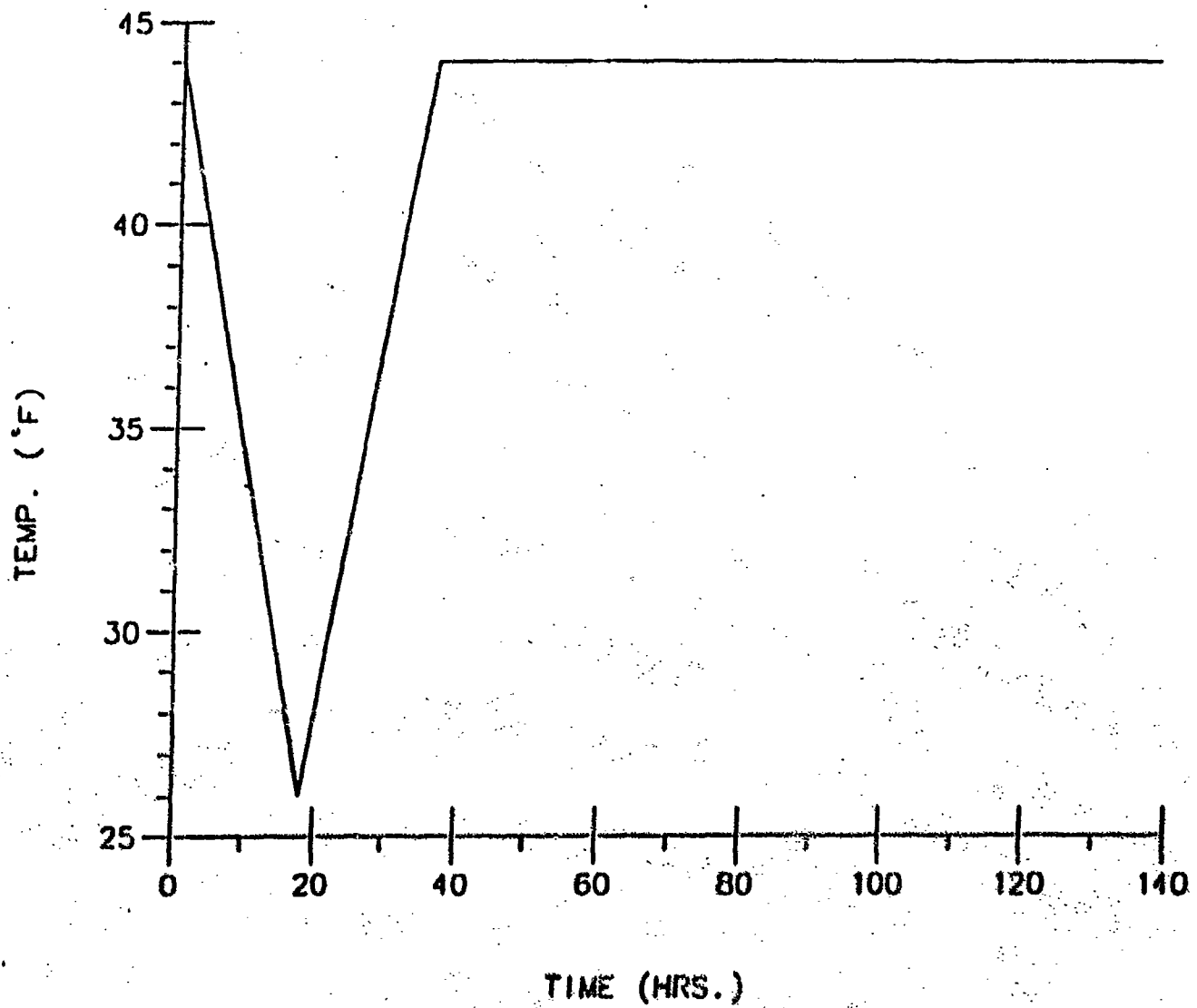


Figure 4-4. Temperature History (Restrained Bar)

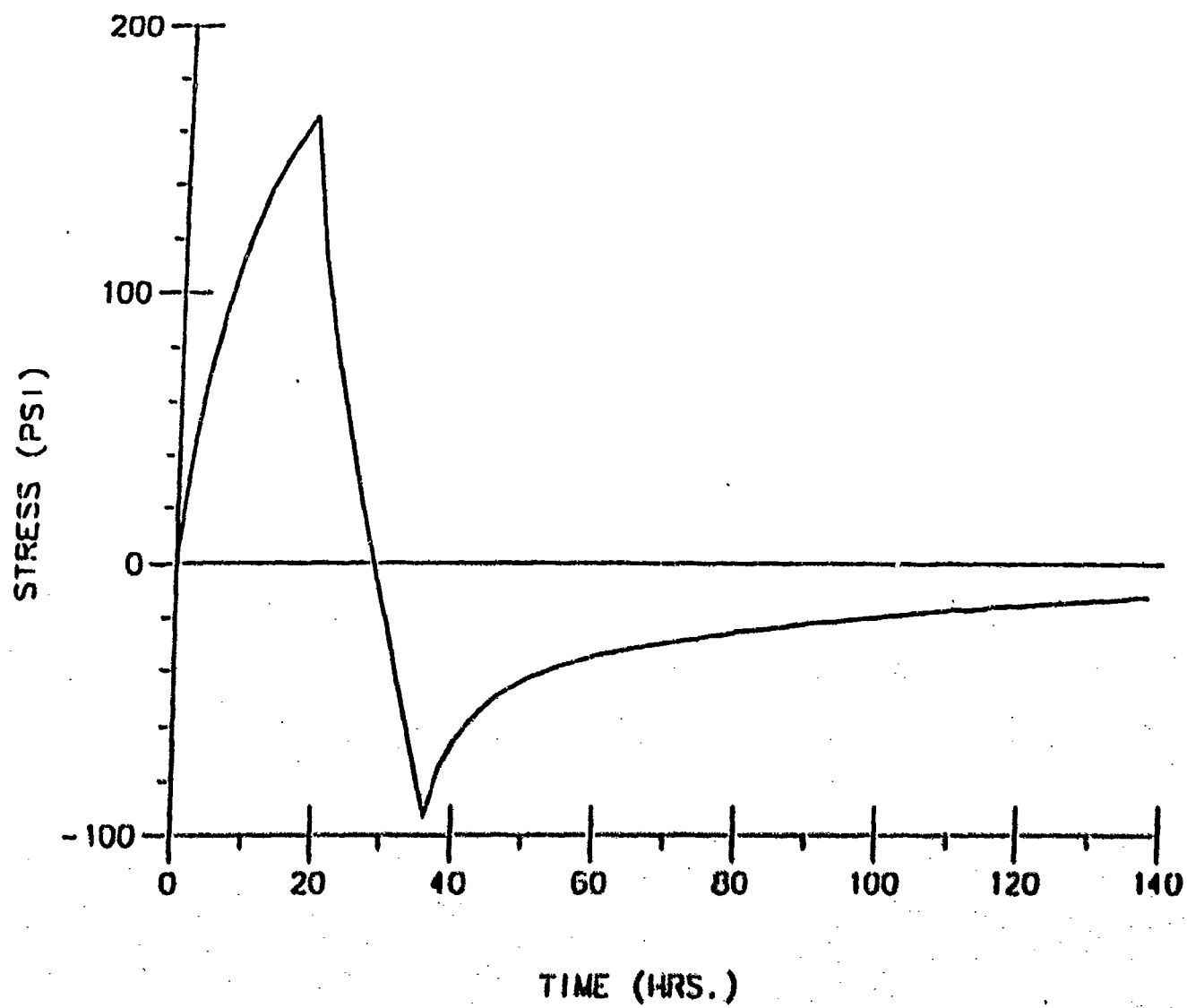


Figure 4-5. Stress History (Restrained Bar)

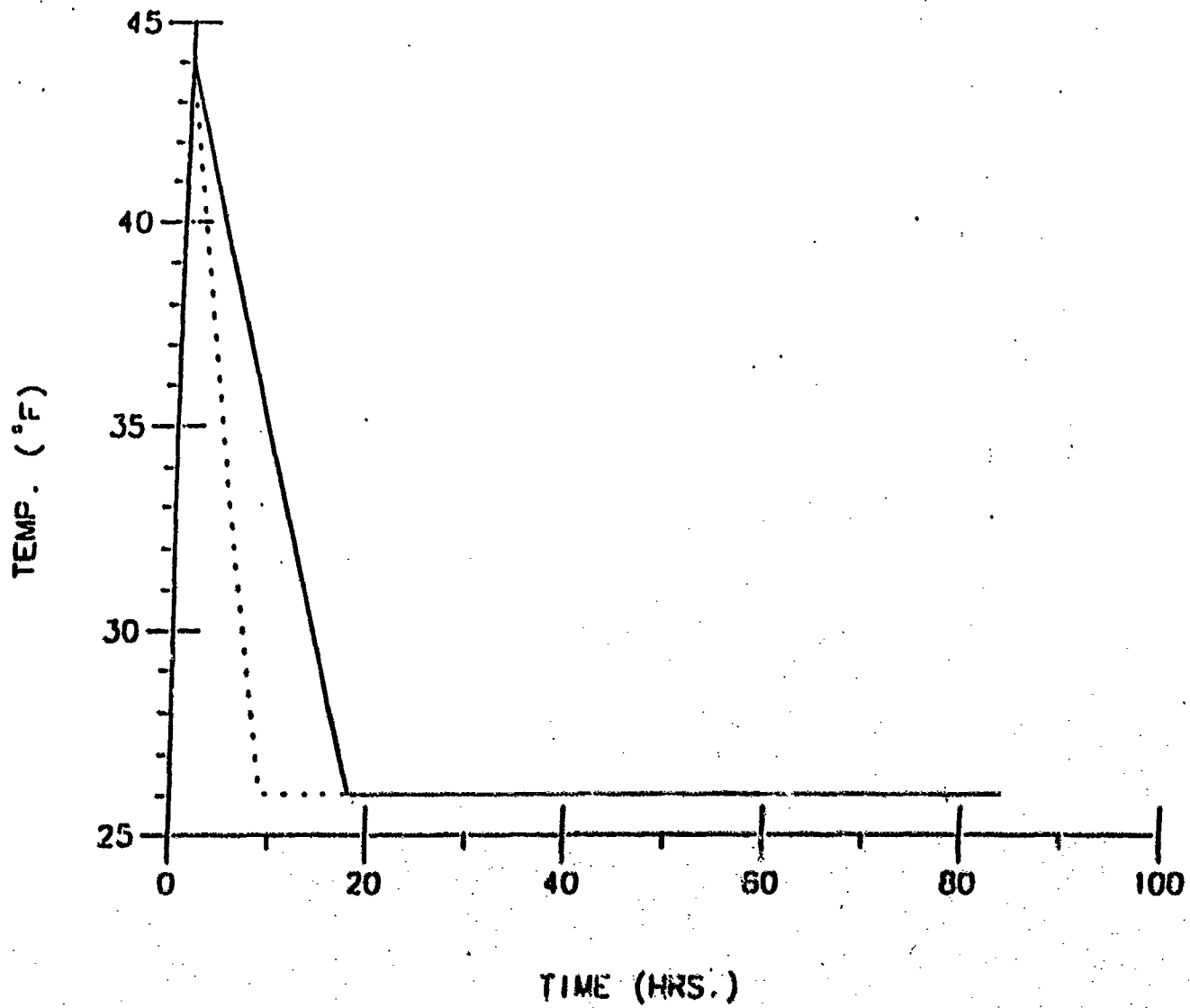


Figure 4-6. Temperature History (Restrained Bar)

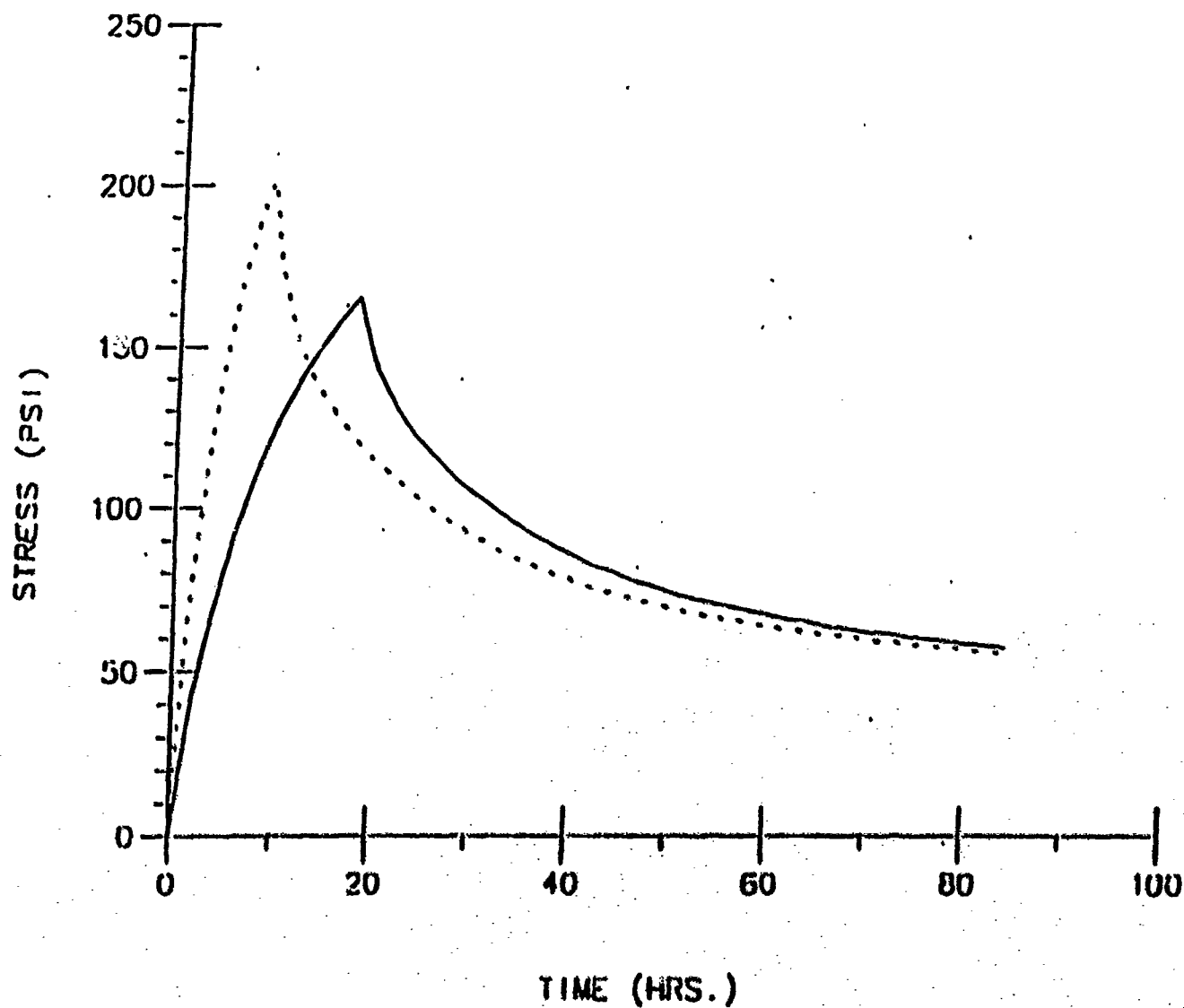


Figure 4-7. Stress History (Restrained Bar)

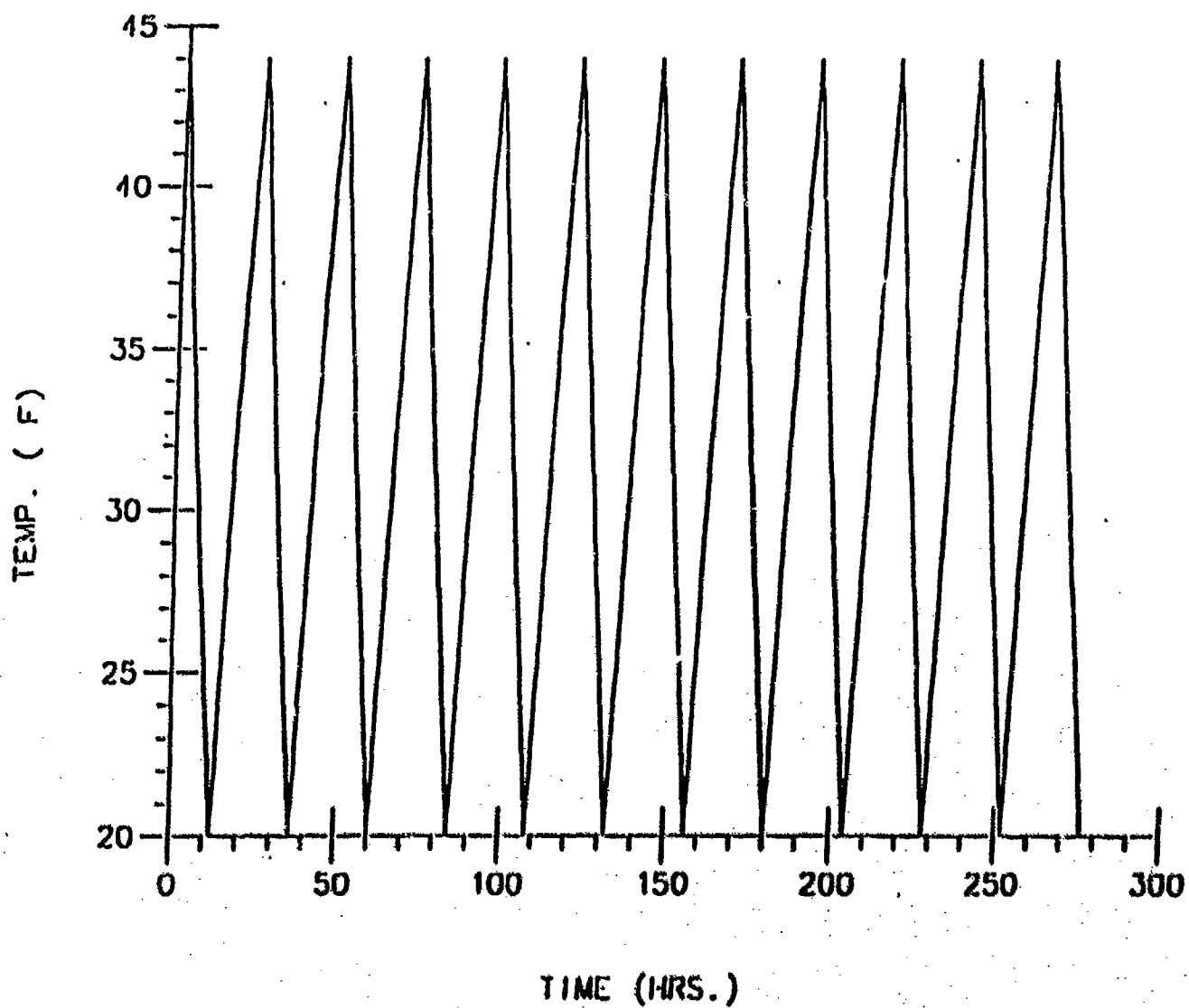


Figure 4-8. Temperature History (Restrained Bar)

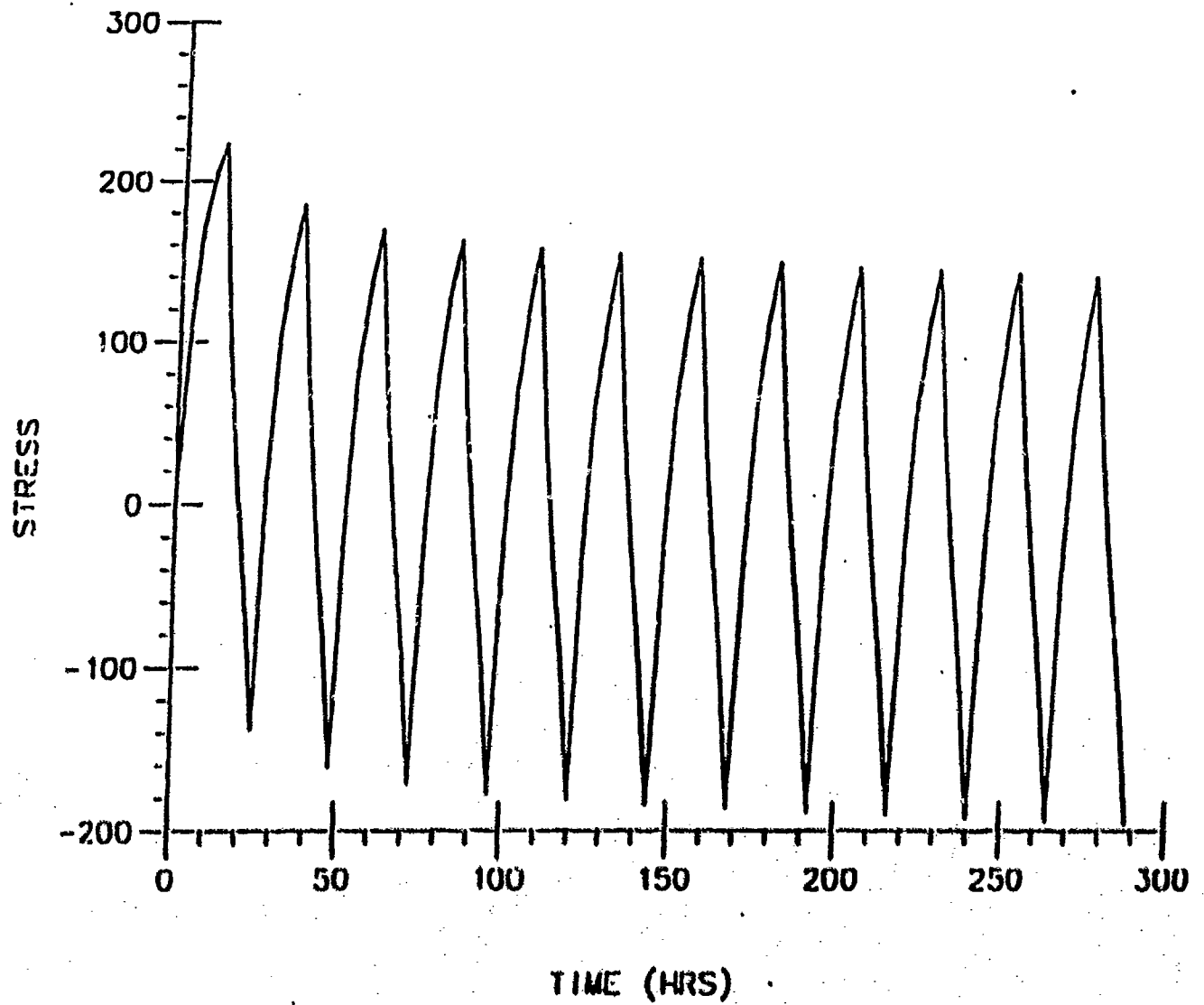


Figure 4-9. Stress History (Restrained Bar)

The finite element package ANSYS has been used for this purpose [5, 6]. A 2-dimensional 4-node isoparametric viscoelastic element (Stif 88) is used. The problem is considered to be of plane strain type, and deflection in horizontal direction is constrained.

- a. Response to a single thermal cycle: The same cycle used in the case of restrained bar (Figure 4-4) is applied on slab, neglecting the thermal gradient. The response is shown by dotted line in Figure 4-10. The stress in this case is clearly higher than the one developed in the bar. Also, the solid line shows the response when the physical hardening is taken into account.
- b. Response to measured daily temperatures: The actual temperature history measured in the field at Washington, D.C. during a typical winter season is applied on the slab (Figure 4-11). These were the temperatures measured during the period Jan. 16 to Jan. 27. The solid line shows the temperatures measured on the surface and the dashed line shows the temperatures at a depth of 3 inches. For the case where temperature gradient is neglected, it is assumed that the whole pavement is at the temperature measured at the surface. Figure 4-12 shows the response of the pavement when there is no gradient. Figure 4-13 shows the stress response of a pavement at surface when gradient along depth is considered. Figure 4-14 shows the stress response at a depth of 3 inches. In addition, the stress history with physical aging included is shown in Figure 4-15 (at surface) and Figure 4-16 at a depth of 3 inches.

It can be noticed that stresses are the highest when the physical hardening is considered on a pavement with thermal gradient along depth.

- c. Response for a complete year: For the case of no temperature gradient, the analysis is carried out for a temperature history spanning a whole year, starting from June 21. The reference temperature is chosen to be 70 °F, which is also the starting temperature. The temperature plots and the corresponding stress responses for a few months are shown in Figures 4-17 and 4-24.

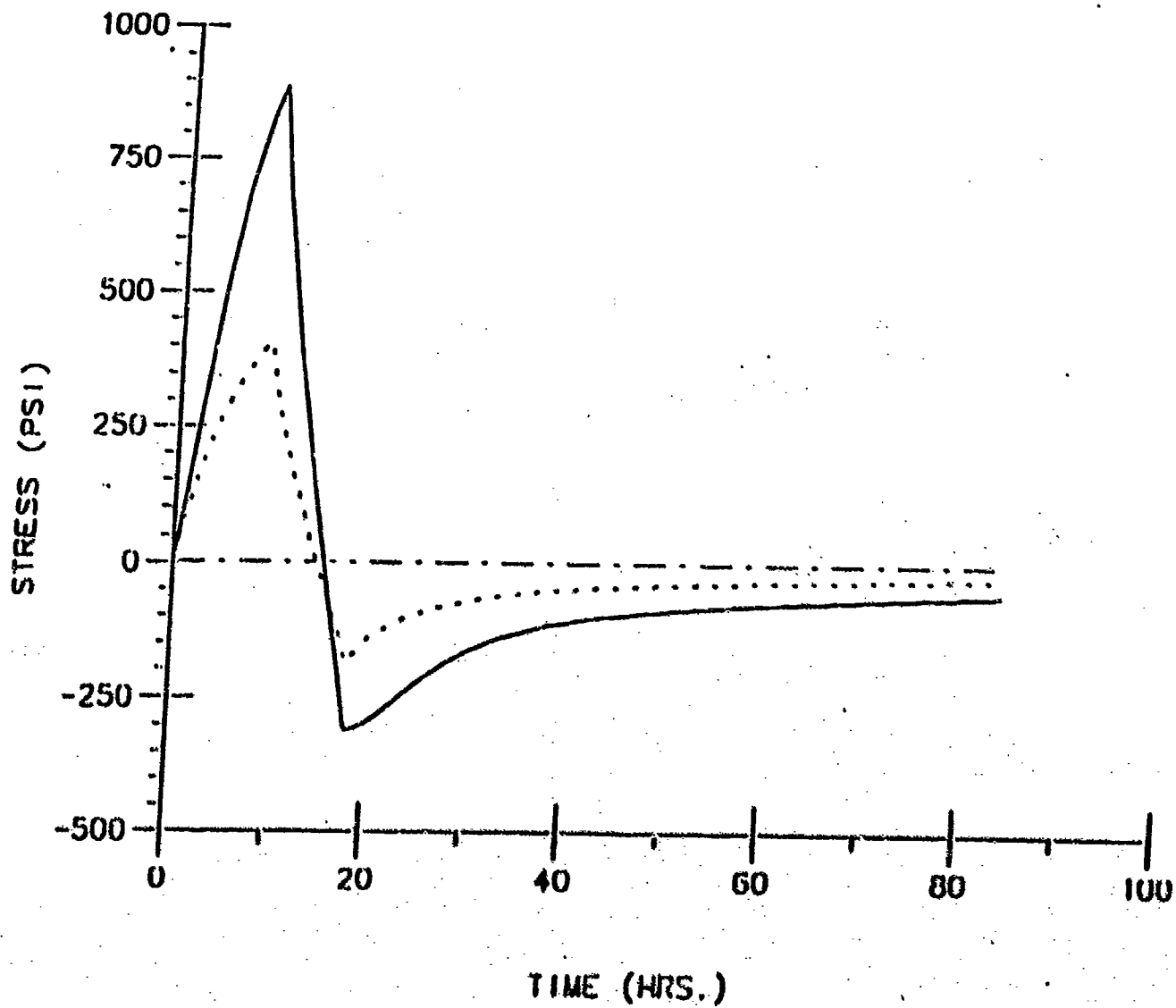


Figure 4-10. Stress History (Slab w/o Temp. Gradient)

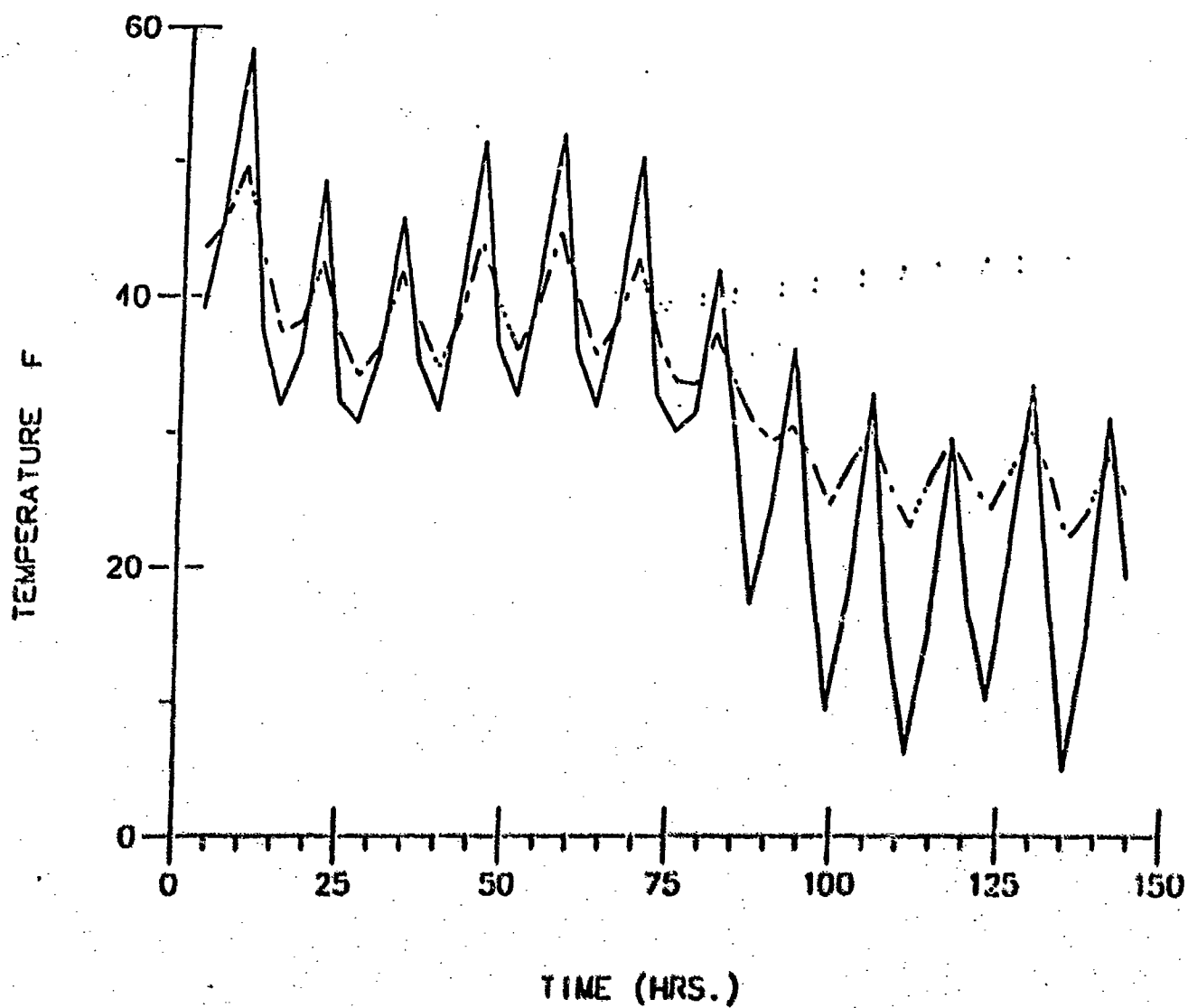


Figure 4-11. Temperature History

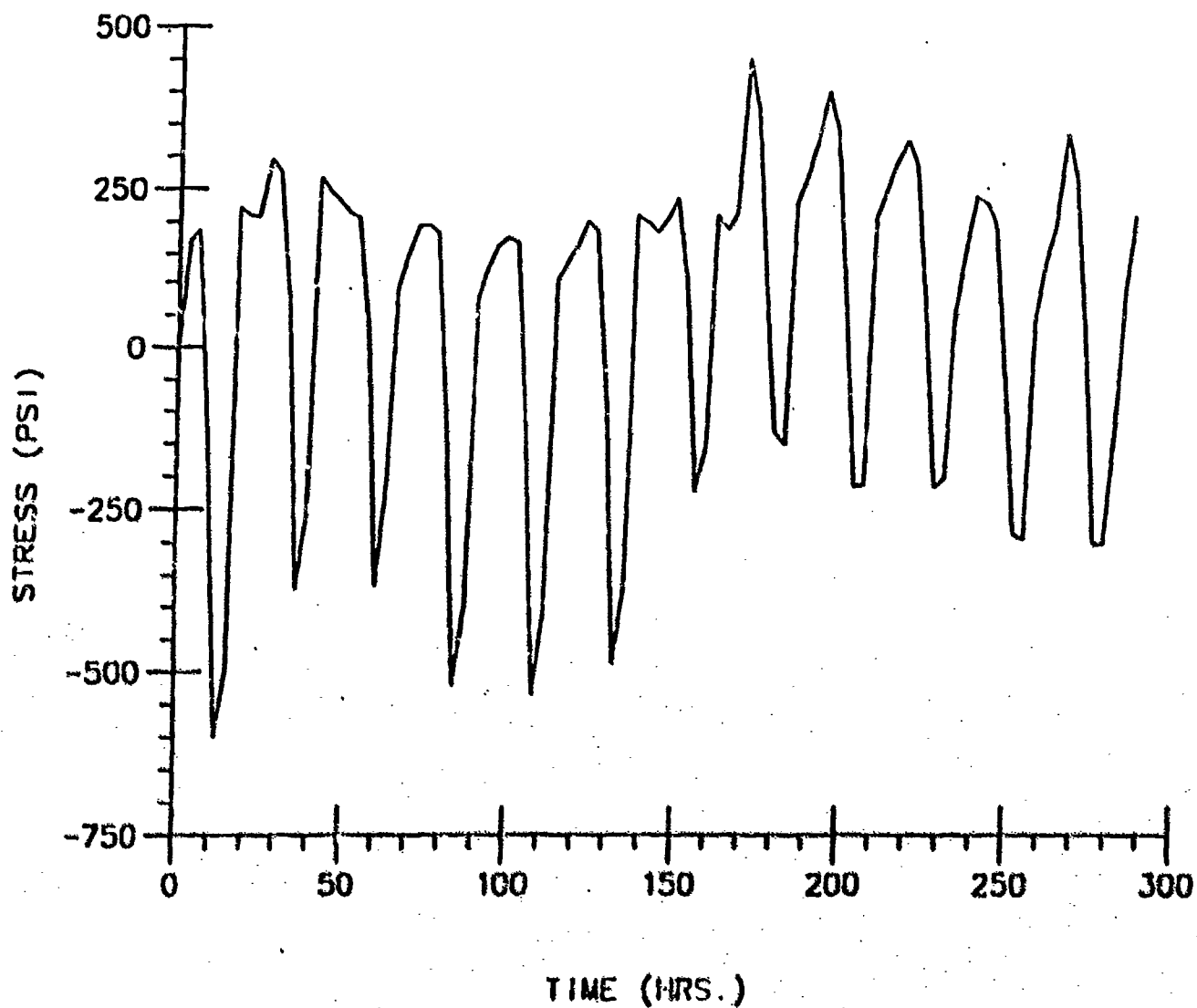


Figure 4-12. Stress History (Slab w/o Temp. Gradient)

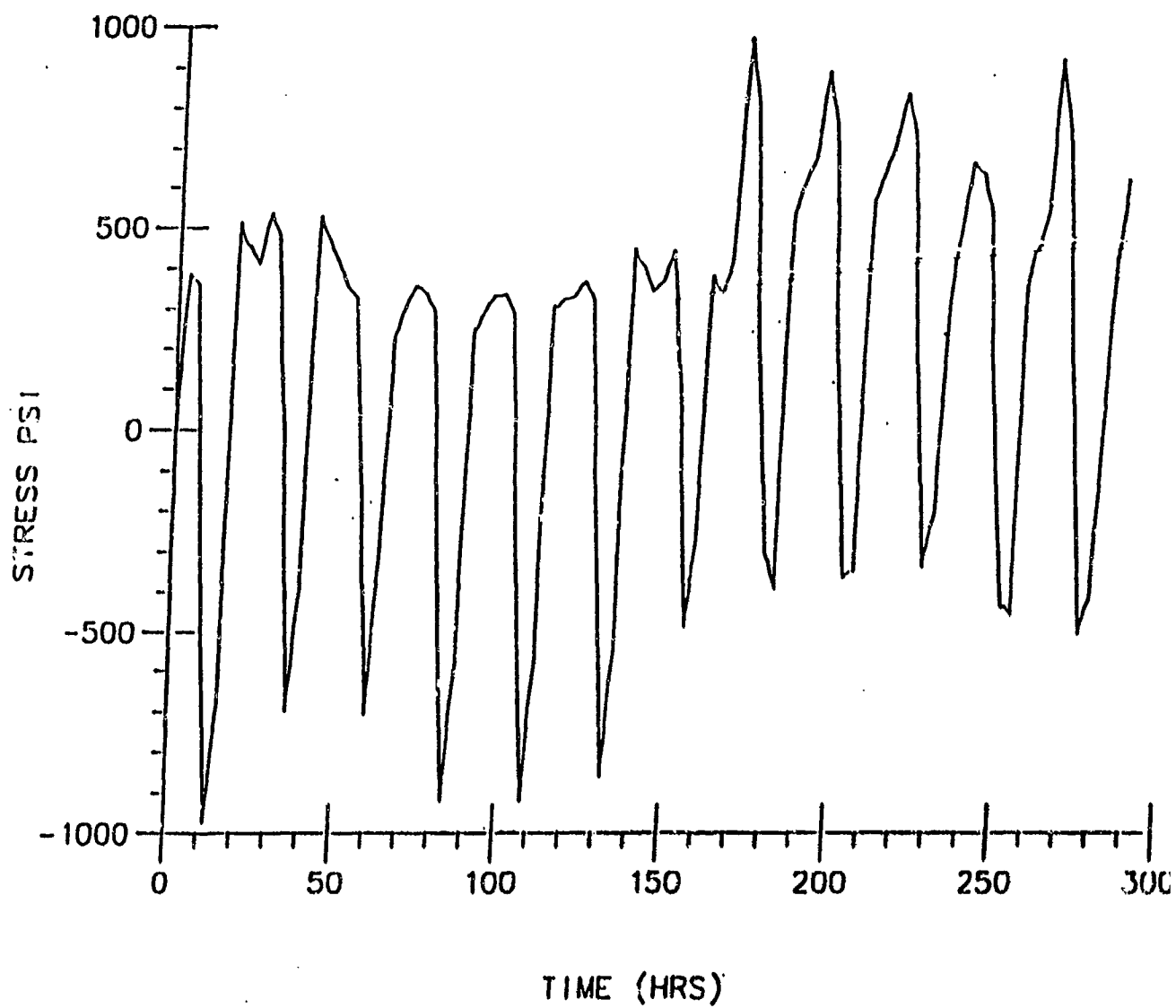


Figure 4-13. Stress at Surface (Slab with Temp. Gradient)

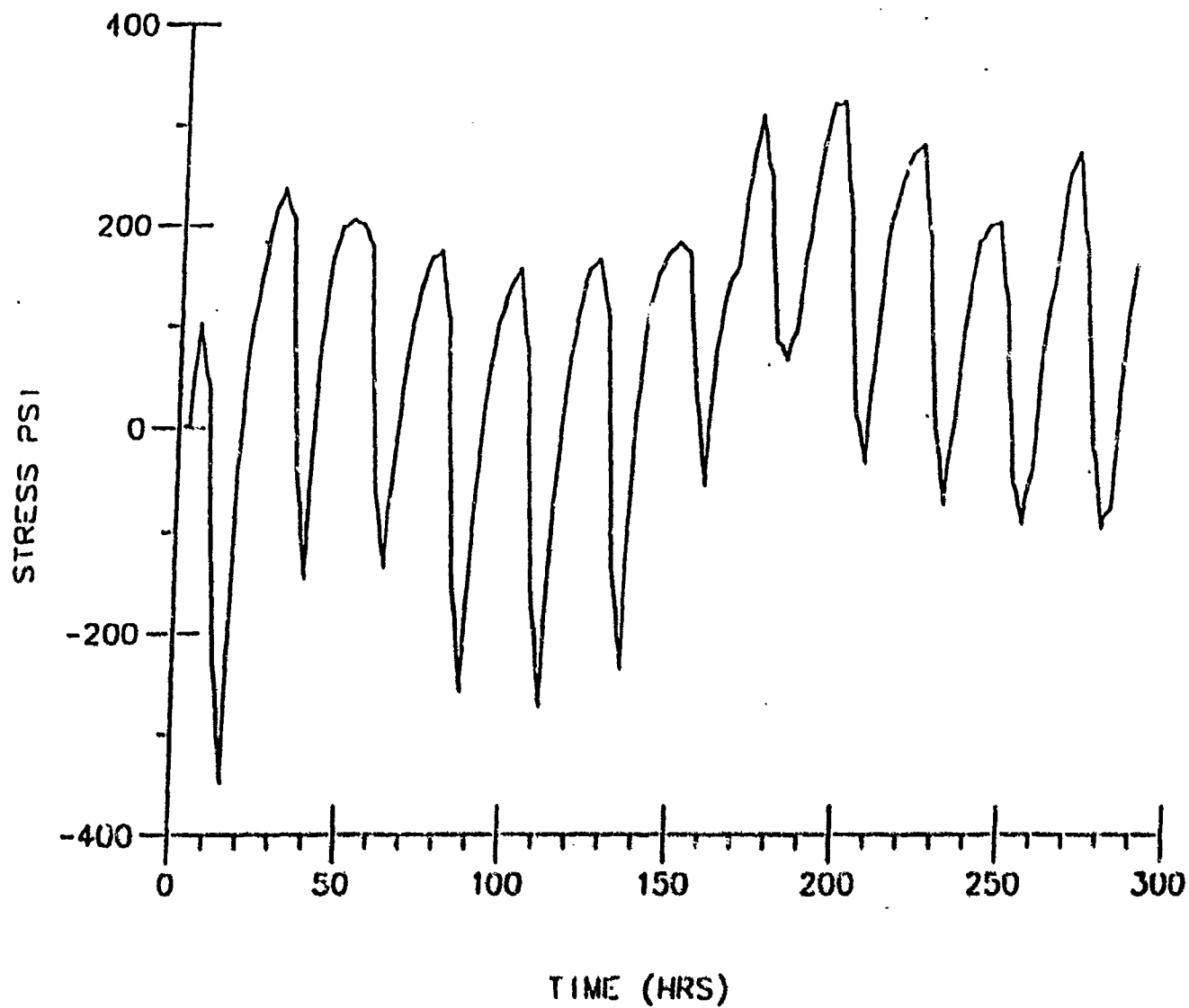


Figure 4-14. Stress at H=3" (Slab with Temp. Gradient)

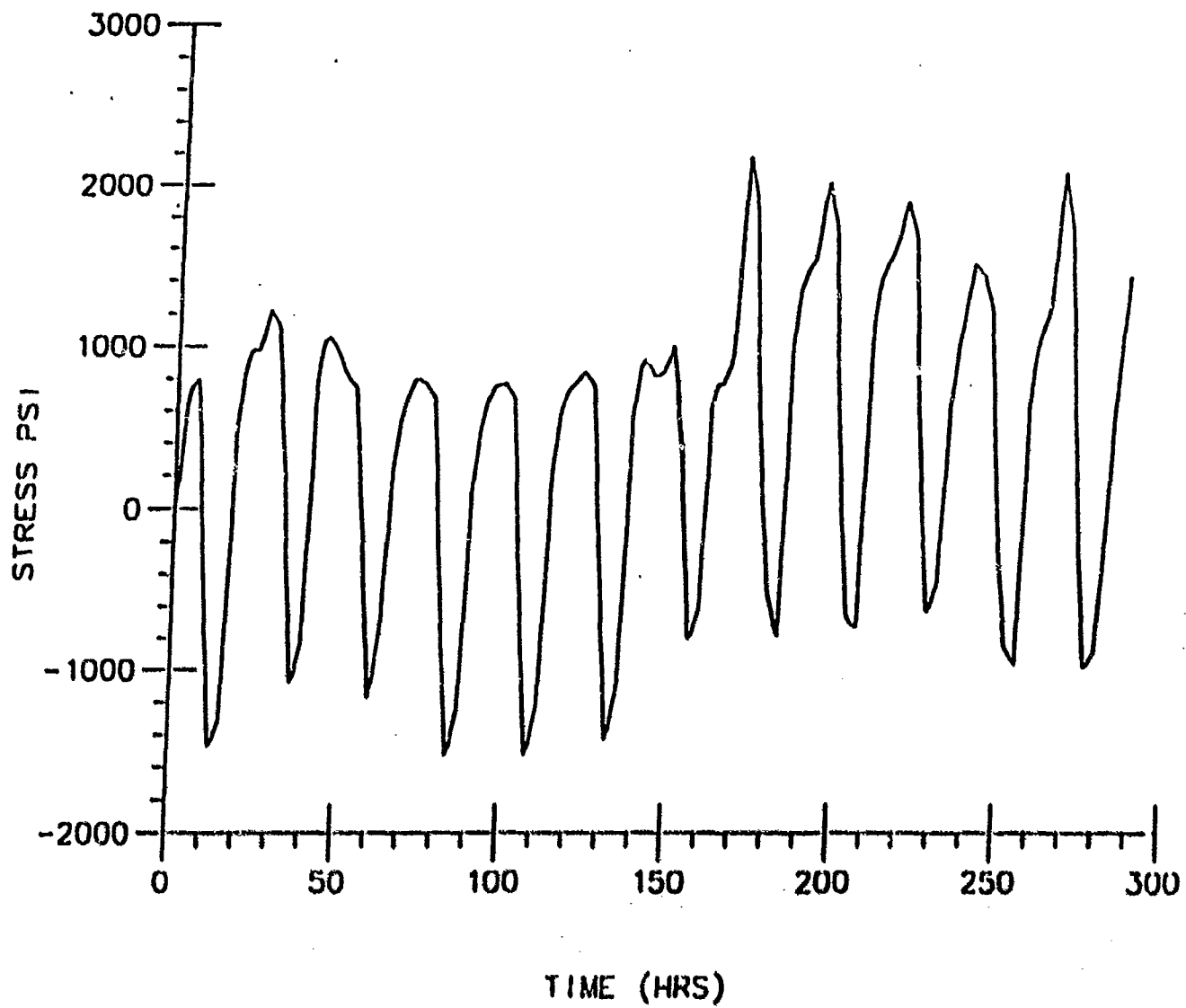


Figure 4-15. Stress at Surface (with Physical Aging)

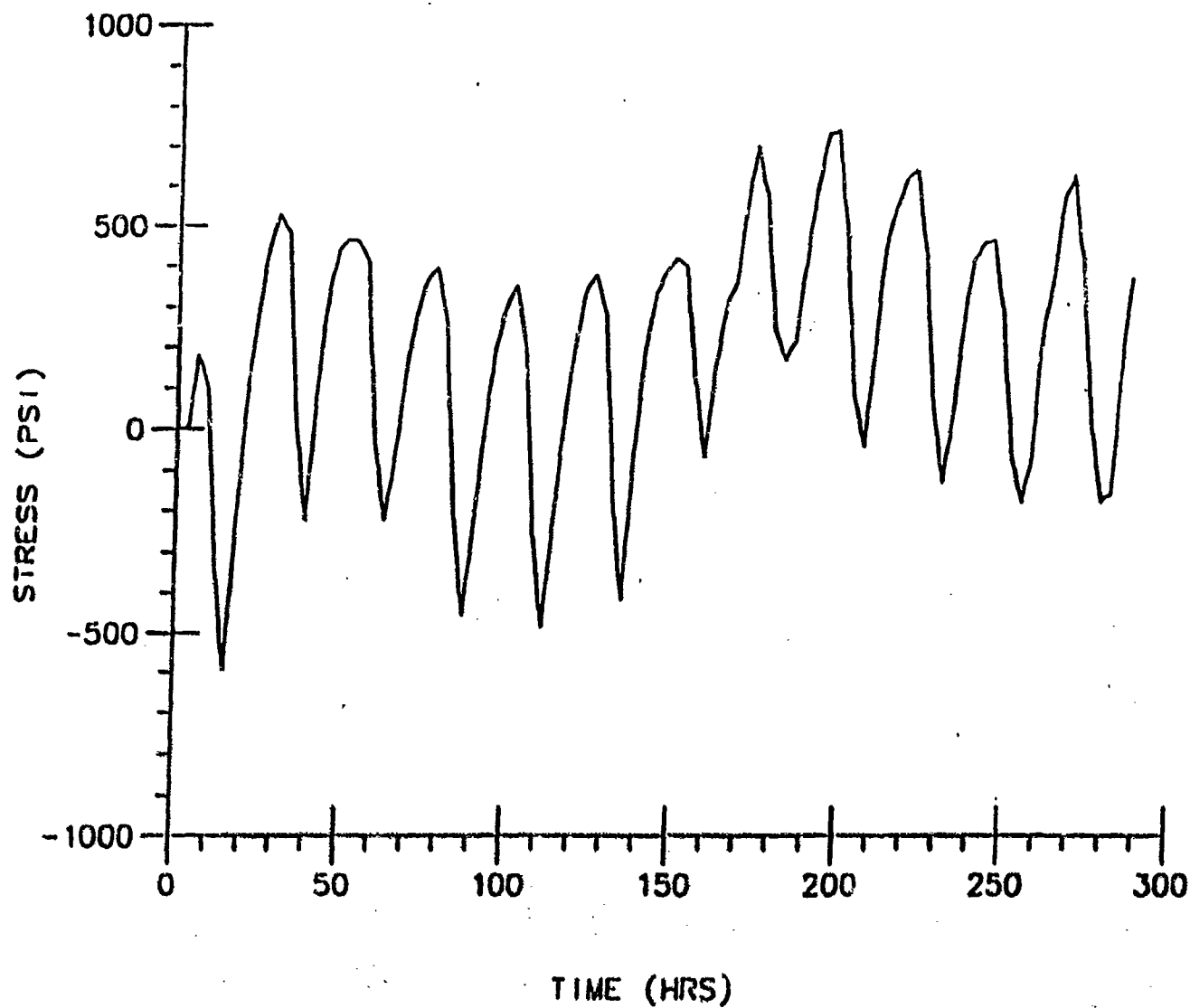


Figure 4-16. Stress at H=3" (with Physical Aging)

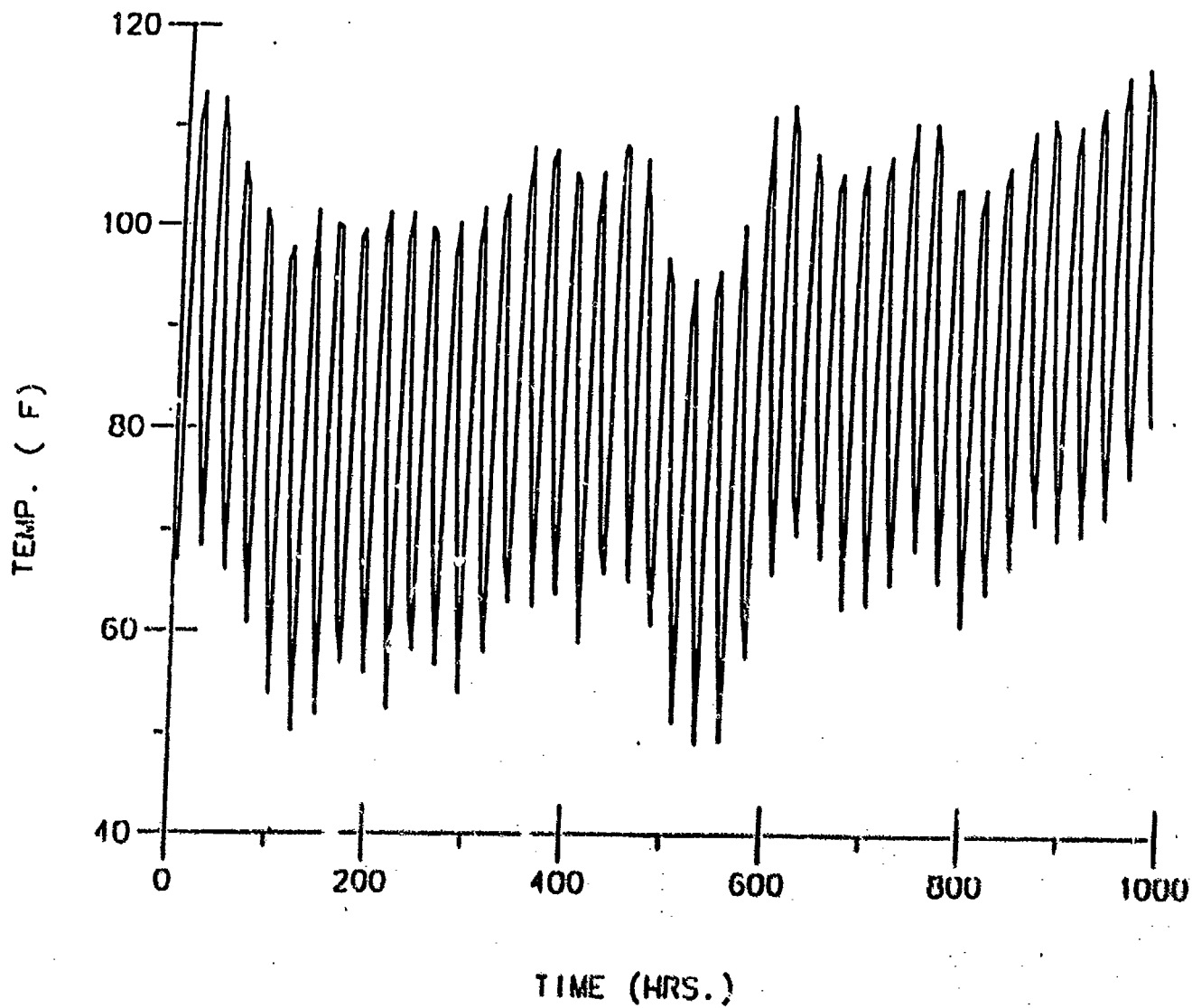


Figure 4-17. Temperature History (Jun 21 - Jul 31)

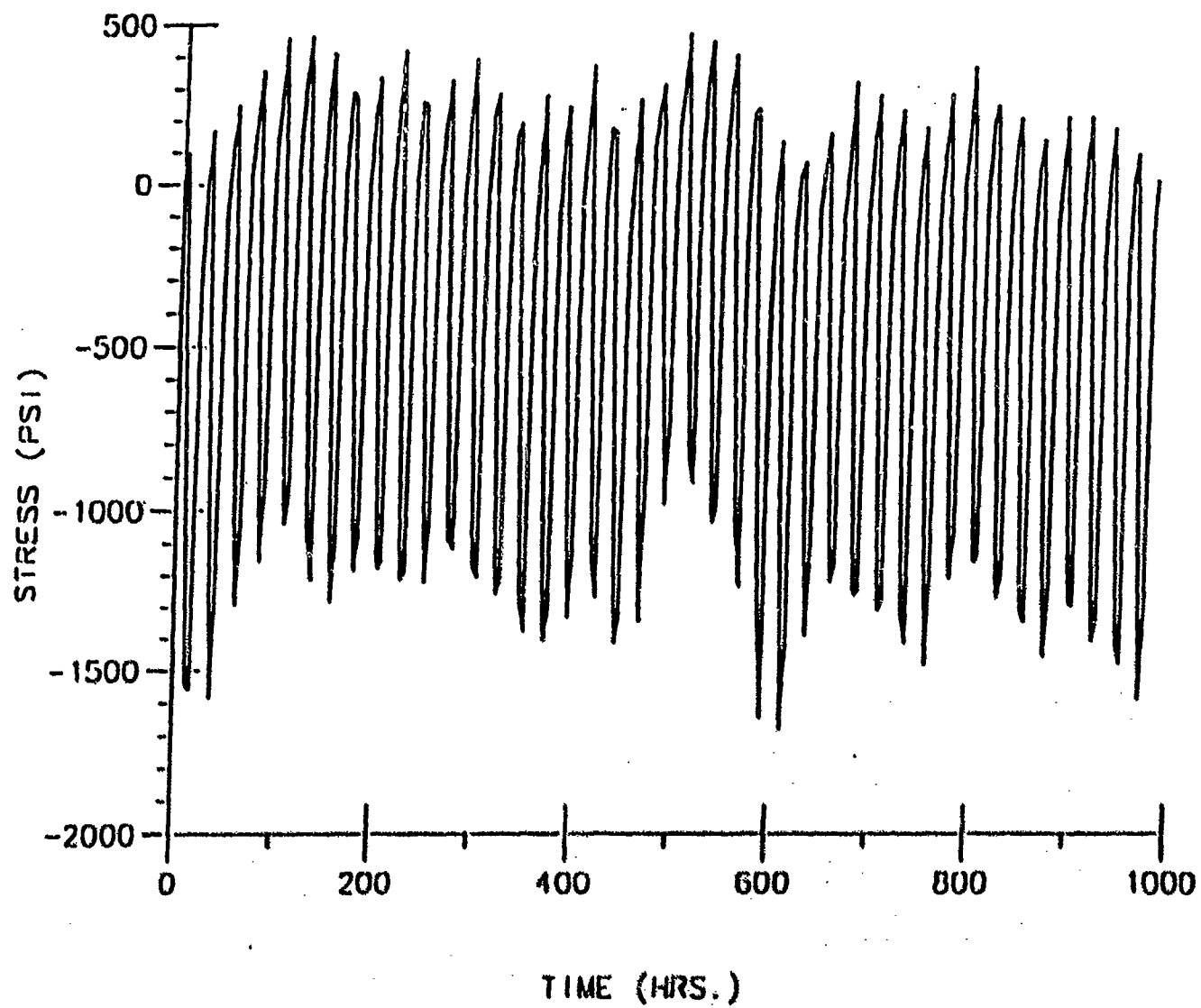


Figure 4-18. Stress History (Jun 21 - Jul 31)

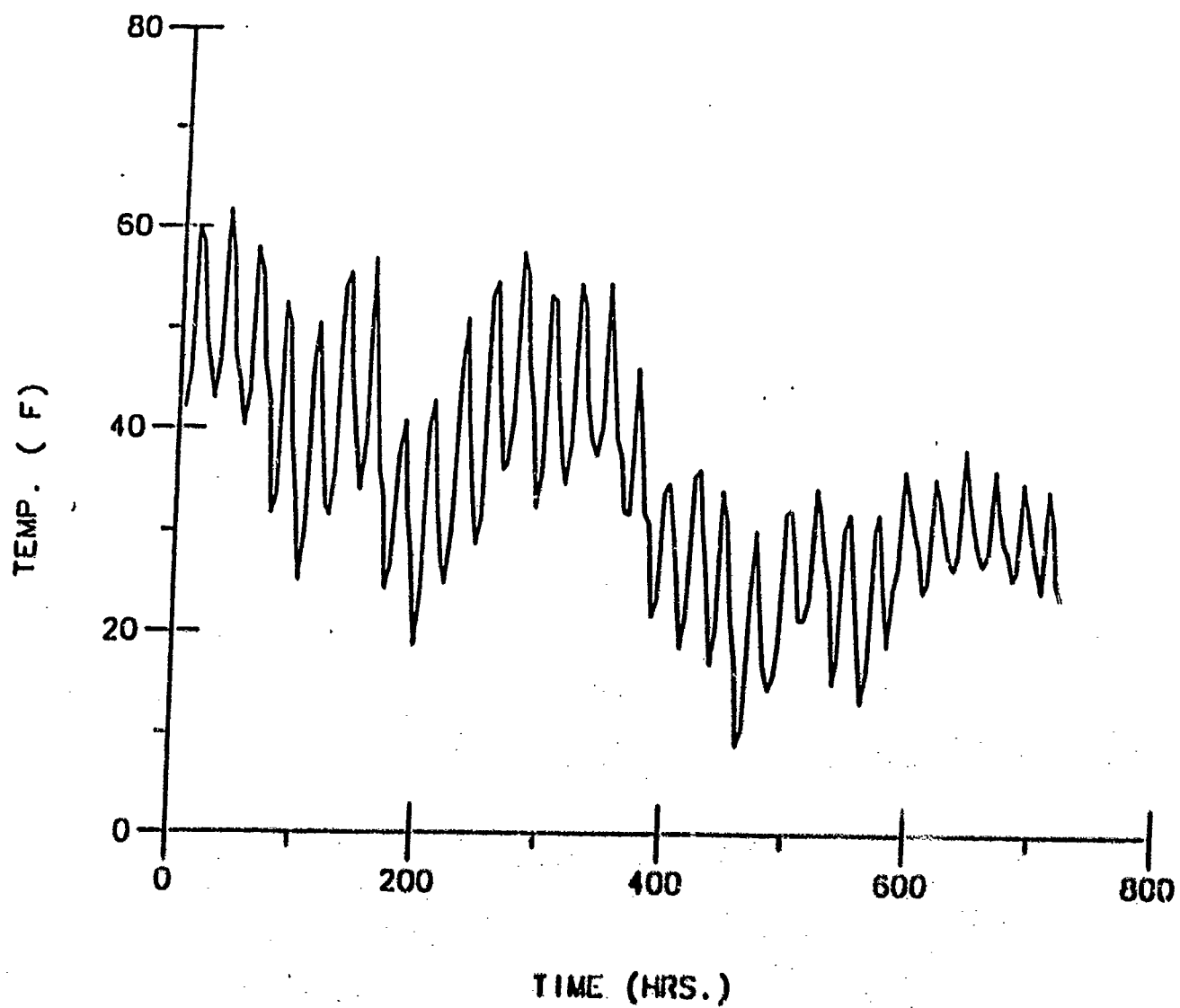


Figure 4-19. Temperature History (Nov 1 - Nov 30)

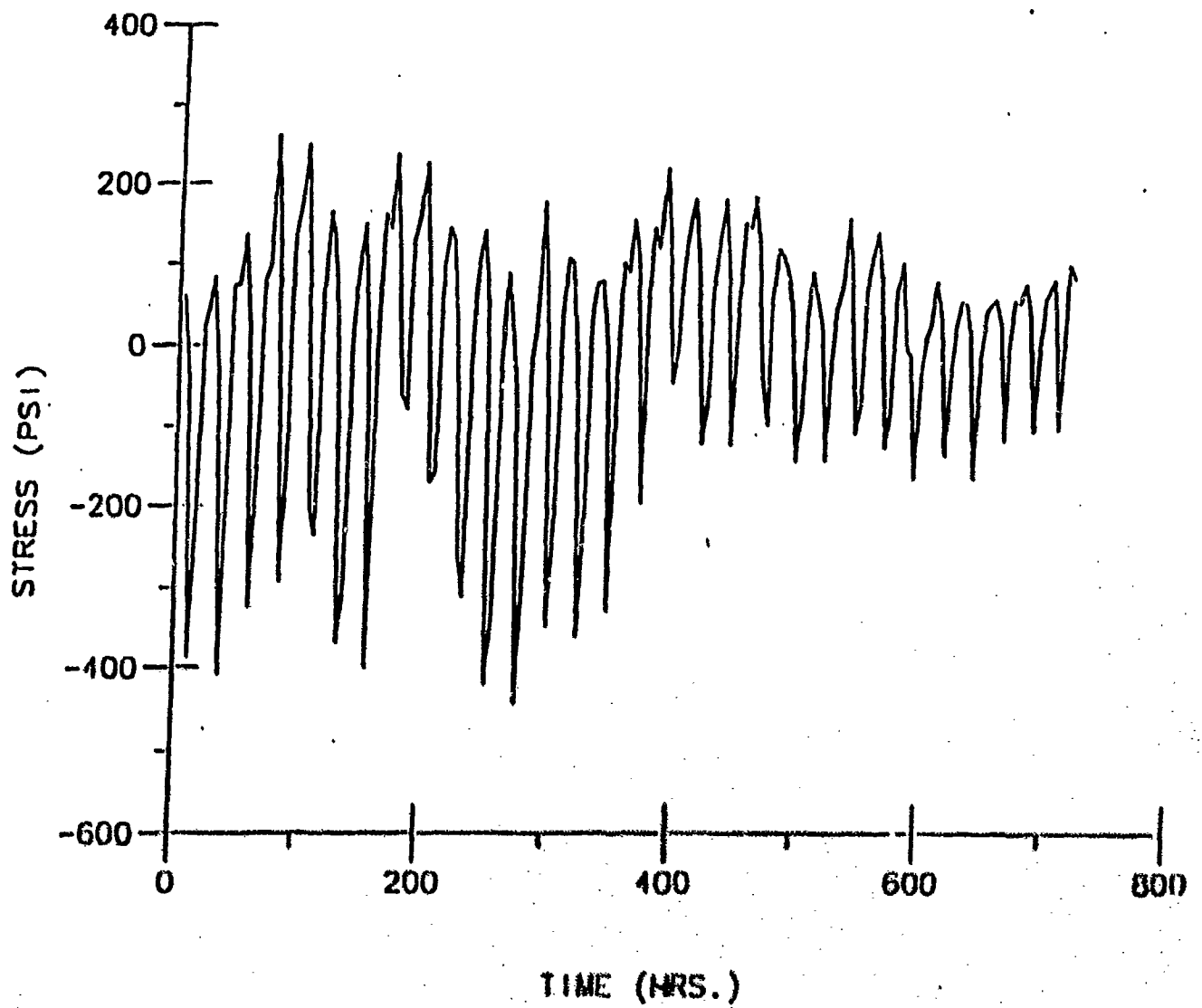


Figure 4-20. Stress History (Nov 1 - Nov 30)

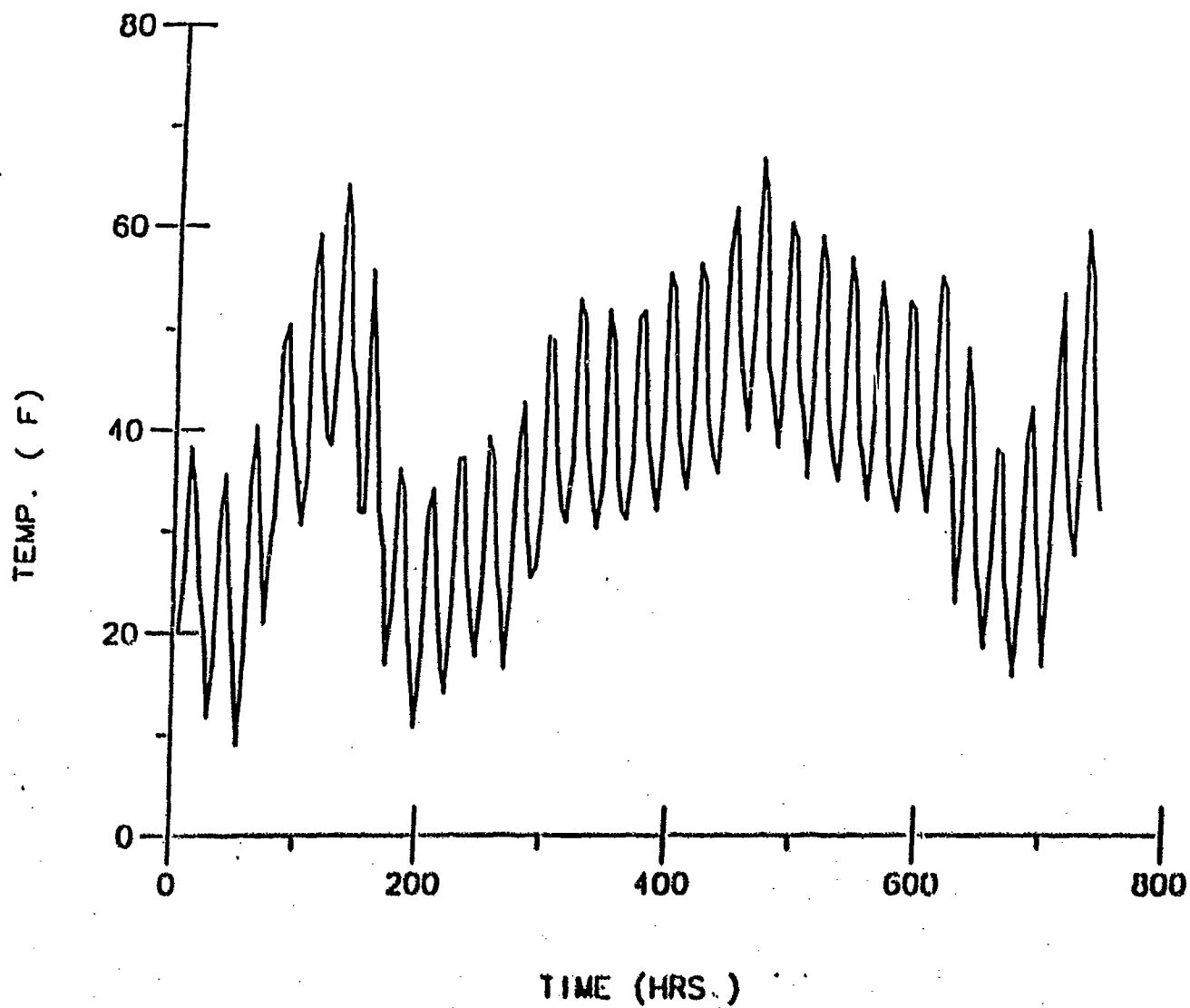


Figure 4-21. Temperature History (Mar 1 - Mar 31)

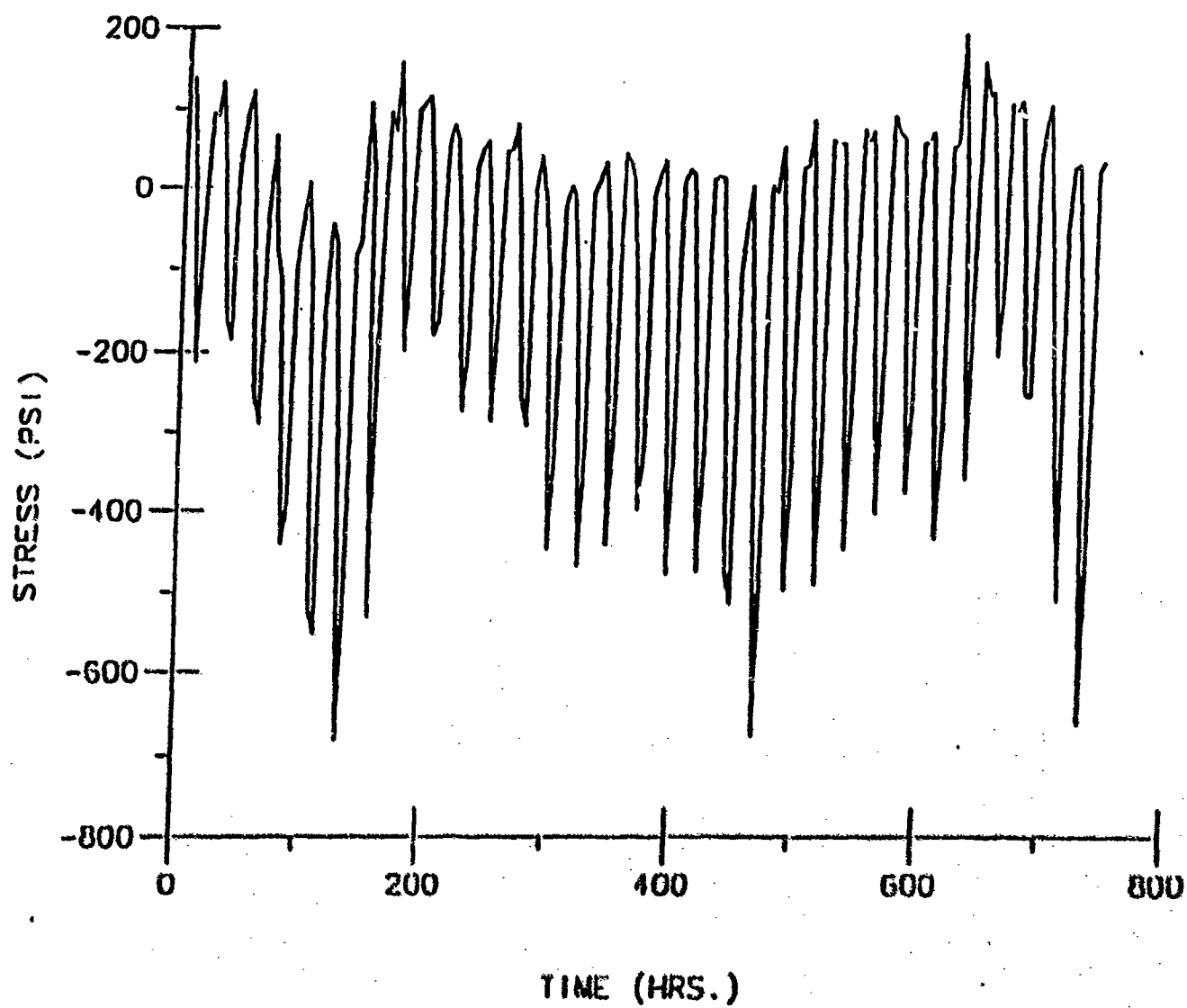


Figure 4-22. Stress History (Mar 1 - Mar 30)

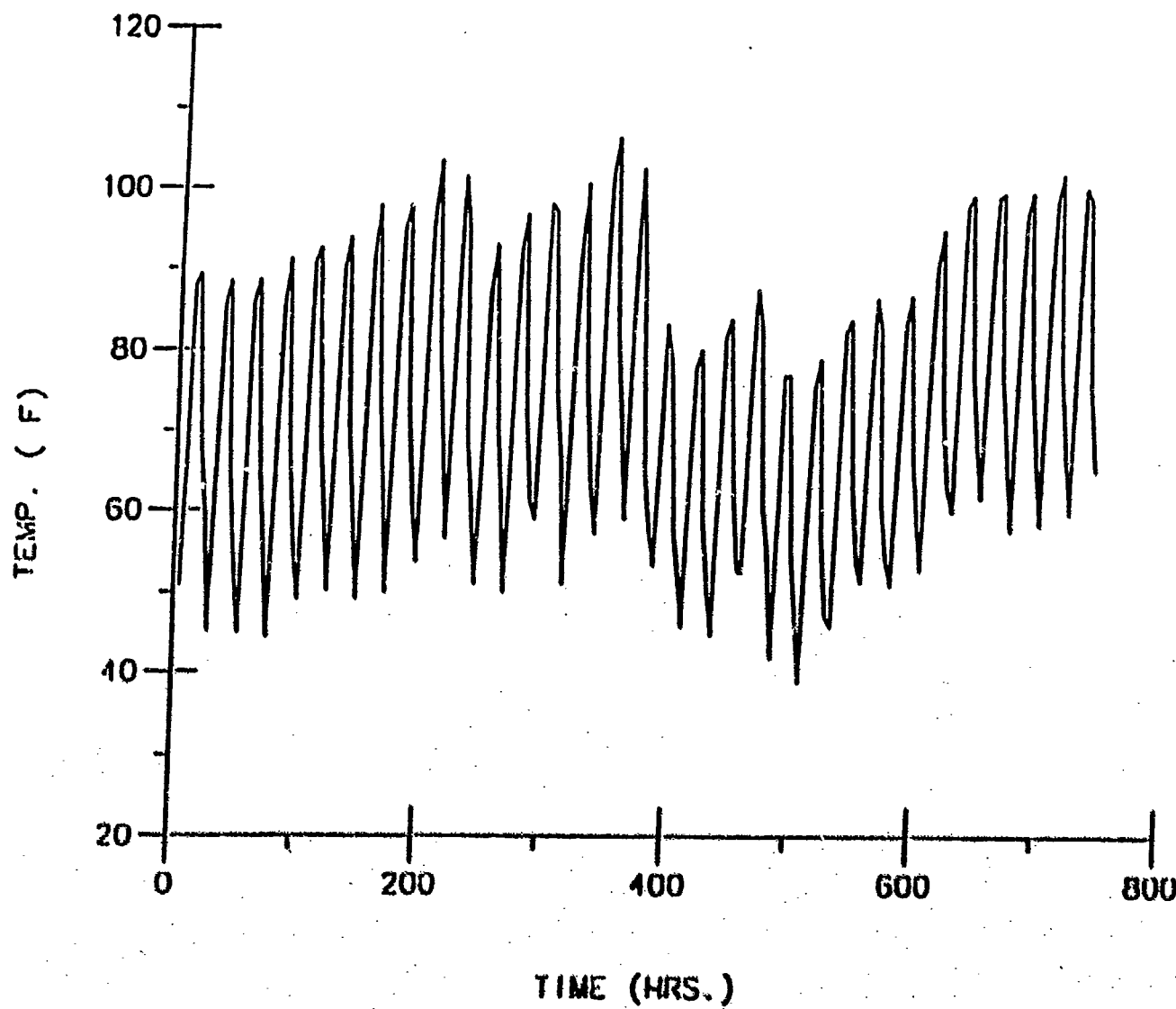


Figure 4-23. Temperature History (May 1 - May 31)

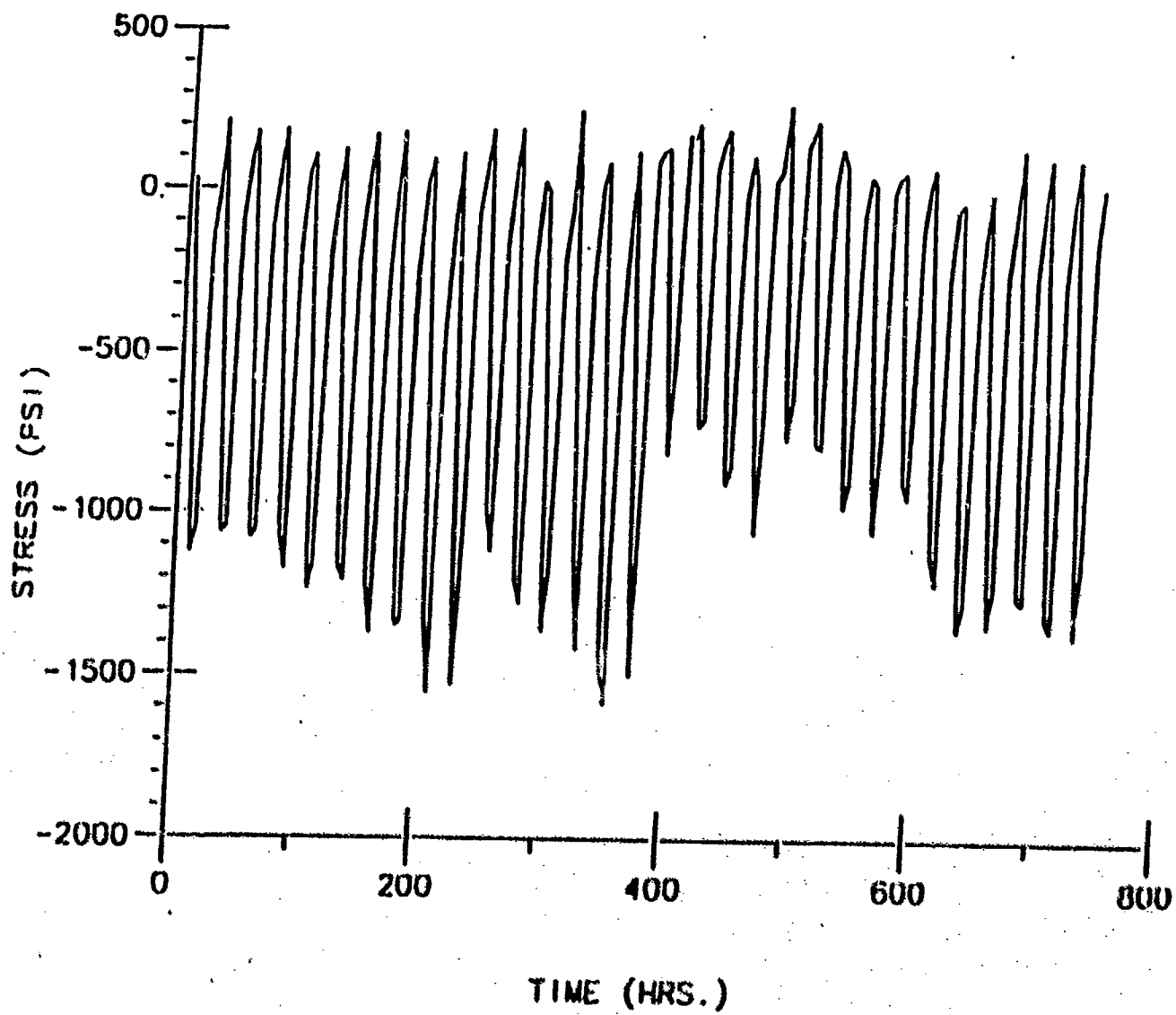


Figure 4-24. Stress History (May 1 - May 30)

4.4 Conclusions

The stresses are considerably higher when the temperature gradient is taken into account. This could be due to the bending stresses induced due to temperature gradient. Also, while cooling the surface would be stiffer compared to the interior region. Hence there would be a gradient in the modulus. This could be another reason for higher stresses on the surface. Also, physical hardening contributes considerably to the stress response.

5. References

1. R. M. Christensen, "Theory of Viscoelasticity, An Introduction," Second Edition, Academic Press, New York, (1982)
2. Arthur Q. Tool, "Relation Between Inelastic Deformability and Thermal Expansion of Glass in its Annealing Range," *Journal of The American Ceramic Society*, 29 [9], 240-253, (1946).
3. O. S. Narayanaswamy, "A Model of Structural Relaxation in Glass," *Journal of The American Ceramic Society*, 54 [10], 491-498, (1971).
4. Thomas F. Soules, Robert F. Busbey, Simon M. Rekhson, and Alex Markovsky, "Finite-Element Calculation of Stresses in Glass Parts Undergoing Viscous Relaxation," *Journal of The American Ceramic Society*, 70 [2], 90-95, (1987).
5. ANSYS User's Manual.
6. Revision 4.4A Changes to the ANSYS Program.

6. Appendix A

When the temperature of a material is changed in the liquid state, it attains equilibrium structure almost instantaneously. When it is in glassy state, the relaxation is so slow that it takes infinite time to reach equilibrium state. Hence, it can be assumed that in the glassy and the liquid states, the structural changes are functions of temperature only and for all practical purposes are independent of time. However, in the transition region the structural changes are functions of both temperature and time. In the transition region, the volume $V(t)$ relaxes towards equilibrium value in finite time.

The normalized response of volume change, $M_v(t)$ to a step change in temperature from T_1 to T_2 could be written as [3]

$$M_v(t) = \frac{(V(t) - V_{2,\bullet})}{(V_{2,0} - V_{2,\bullet})} = \frac{T_f(t) - T_2}{T_1 - T_2} \quad (A.1)$$

Here, the subscripts 0 and \bullet denote the instantaneous and the long-time volumes upon changing the temperature. M_v is normalized to 1 at $t = 0$, and 0 when $t = \infty$. Here, the fictive temperature T_f , introduced by Tool [2], defines the structural state that exists in the material at any time. Tool defined fictive temperature as the actual temperature of an equilibrium state that corresponds to the given nonequilibrium state. It is obtained by adding the change of temperature remembered by the material to the actual temperature.

Applying Boltzmann's superposition principle, the volume at any time due to an arbitrary change in temperature is given by the following equation [3].

$$V(t) - V(0) = V(0)a_l(T - T_0) - V(0)a_s \int_0^x M_v[x(t) - x(t')] \frac{dT}{dx'} dx' \quad (A.2)$$

a_l is the coefficient of thermal expansion in liquid state.

The coefficient a_l may be considered as the sum of two coefficients, one due to change in temperature (a_g) and the other due to change in structure (a_s).

$$a_l = a_g + a_s \quad (A.3)$$

However, in liquid state since structural changes are very rapid, only a_l can be measured. This is given by the slope of the line AB in Figure A-1. In glassy state, there is no structural change. Hence, $a_s = 0$. a_g is given by the slope of the line CD.

Defining the fictive temperature T_f by the following memory integral [3].

$$T_f(x) = T - \int_{x(T)}^{x(T_0)} M_v [x(t) - x(t')] \frac{dT}{dx'} dx' \quad (A.4)$$

and substituting Equations (9) and (10) in Equation (8) gives

$$V(t) - V(0) = V(0) [a_l (T_f - T_0) + a_g (T - T_f)] \quad (A.5)$$

In liquid state, relaxation is very rapid and the fictive temperature is always equal to the actual temperature. In this region, $M_v = 0$. If the material is quenched from an initial temperature T_0 to a final temperature T below transition range, $M_v = 1$ and $T_f = T_0$.

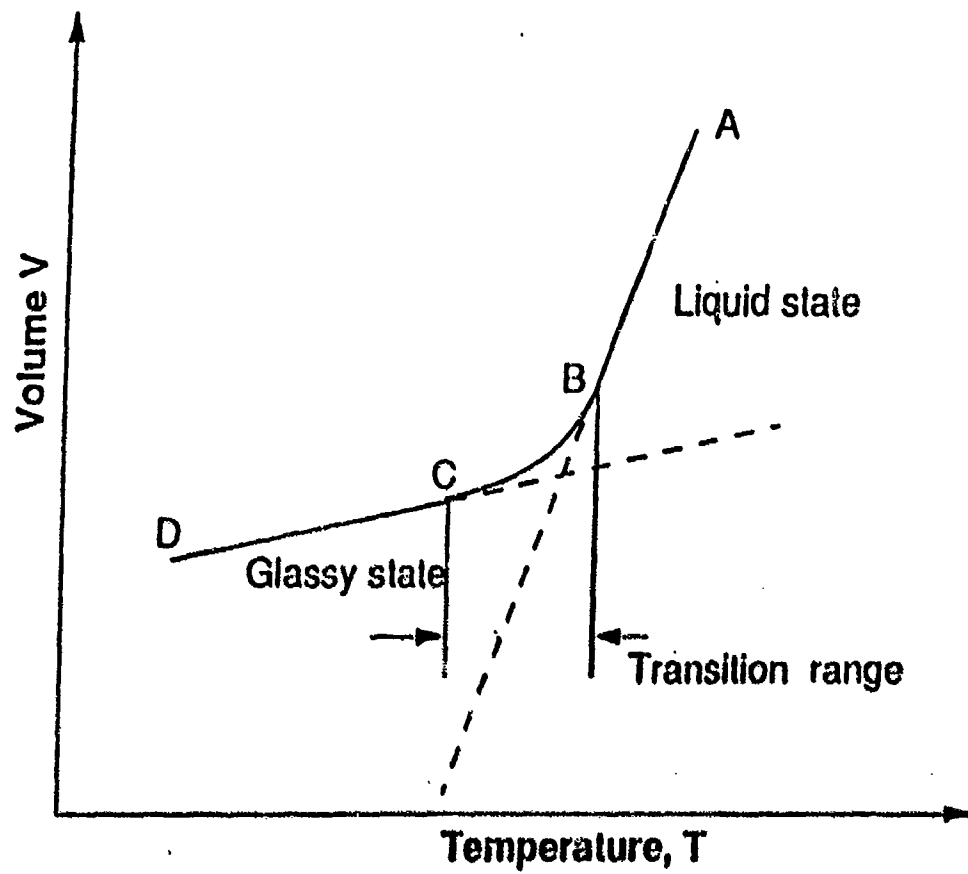


Figure A-1. Structural Changes (Liquid State)

7. List of Symbols

κ	=	thermal diffusivity
h	=	thickness
k	=	thermal conductivity
K	=	bulk modulus (assumed to be non-relaxing)
T	=	temperature
T_i	=	temperature at step i
t	=	time
x_k	=	position coordinate
S_{ij}	=	deviatoric stress
G	=	shear relaxation modulus
e_{ij}	=	deviatoric strain
x_k	=	position coordinate
σ_{ii}	=	hydrostatic stress
ϵ_{ii}	=	hydrostatic strain
α	=	temperature dependent coefficient of thermal expansion
T_0	=	reference temperature for computing thermal strains
α_0	=	coefficient of thermal expansion at T_0
α_l	=	coefficient of thermal expansion in liquid state
α_g	=	coefficient of thermal expansion due to change in temperature

- α_s = coefficient of thermal expansion due to change in structure
 H = activation energy of the viscoelastic process
 R = universal gas constant
 H_g = activation energy governing the glassy change
 H_s = activation energy governing the structural change
 E = tensile relaxation modulus and
 ϵ^{th} = thermal strain = $\alpha (T - T_0)$
 v = volume
 M_v = normalized response of volume change
 T_f = fictive temperature
 ξ = reduced time

FAA Unified Pavement Analysis 3-D Finite Element Method

S. J. Kokkins, P. E.

Foster-Miller, Inc.

1. Introduction

1.1 Background

The airport system of the United States is a cornerstone of our transportation network. Every year, system demands exceed capacity in many areas. The capability of our airports to continually accommodate more operations for larger and heavier aircraft is certainly one of the crucial ingredients in meeting these demands.

At the same time, in common with all other elements of our transportation infrastructure, the airport system must function at levels of safety and cost-effective operation not envisioned decades ago. The design and maintenance of the airport pavements, which are the central elements of any airport, must take full advantage of our technical ability to produce long-lived pavement systems providing maximum benefit - dollar and non-dollar - to the airport network. This is the central function of the unified pavement design and analysis method being proposed.

Existing theories and methods used for the analysis and design of pavement structures have several limitations related to the characterization of material properties, the variability of material properties with time and use, and the underlying assumptions of the load transfer and deformation functions.

The limitations of the existing pavement analysis and design methods do not yet provide a model capable of accurately predicting the useful life of airport pavements. This includes the prediction of pavement performance in terms of distress as a function of traffic and environmental loadings, and their mutual interaction. The eventual model must be sensitive to the initial material properties and must respond to the daily, seasonal, and aging variations in these properties.

Primarily, the unified theory must provide the theoretical foundation for the prediction of pavement displacement and deflection basin profile under different types of aircraft as well as under different types of nondestructive testing devices. The pavement evaluation methodology should include the ability to determine pavement properties from the results of nondestructive testing.

Important contributions towards improving the state of the art in this area can be made from several directions:

- a. Better analytical modeling of pavement systems from a structural point of view;
- b. Improved and realistic representation of material properties for all pavement system elements, interrelated with the structural approaches above;
- c. Systemization of the vast amounts of analytical, statistical and test data that are now, and will be available in the future, in order to substantiate the relationships between pavement design and observed response, including durability and failure modes; and
- d. Use of alternative (i.e., nonmechanistic) analogs of pavement systems to achieve insight into important response or failure modes.

This program approaches the need for a unified method by demonstrating the feasibility of unified analysis built around the use of modern 3-D finite-element structural modeling. These techniques will be used in conjunction with a highly automated system of pre- and post- processing programs specifically designed for airport pavement configurations and integrating essential parameters governing material behavior. Equally important is that this approach can be used as a continuing framework for including the advances in structural analysis, material science and construction methods that are sure to occur over the duration of this project.

The value of using a 3-D approach should be emphasized, since many of the essential characteristics which determine usability and durability of pavement systems are not well represented otherwise. Adequate representation of the complex moving loads from large aircraft landing gear, the pavement response near joints or failure zones, including local areas of base/subbase voids, and the following of cracks and related failure in lateral as well as vertical directions are only a few strengths of a 3-D approach. Previously, the complexity and computer solution time required for representative 3-D problems discouraged many researchers, but today the ability to efficiently model the layered system, and to develop a highly automated solution procedure to eliminate much of the tedious and repetitive effort makes this a potentially very productive and flexible method. This is especially true when the great increases in computational speed on the new generations of workstations now in development are considered.

The development of any unified pavement analysis method must from the beginning consider the ongoing, intensive efforts in the research and design community to improve our knowledge of material behavior. The wide range of materials used in airport pavement systems and the complex relationships being evaluated for their structural performance, failure and deterioration govern to a large degree the development process of such a method.

1.2 Program Accomplishments

We have demonstrated in this program to date that 3-D finite element (FE) structural modeling is an effective and practical method for evaluating the response of airport pavement systems, and that it can form the basis of the unified pavement analysis method. Although the work so far has used existing analytical tools, similar methods tailored to the needs of airport pavements, together with appropriate constitutive material relationships and modern computer graphics can be integrated into a unified pavement analysis system using 3-D FE modeling.

Accomplishments, described in this report, include:

- a. Demonstration and verification of the solution of classical pavement problems using 3-D FE analysis;
- b. Formulation and solution of a range of practical aircraft load and airport pavement configurations, showing the capabilities of these methods;
- c. Visualization of the results using 3-D color graphics;
- d. Evaluation of two forms of nonlinear soil response; and
- e. Developments in the constitutive material modeling relationships for pavement materials, suitable for inclusion in FE solution procedures.

This program phase, then, shows the potential and direction that continuing work will take in the actual development of the unified pavement response model, constitutive material properties and lab validation.

2. Objectives

2.1 General Objectives

A primary objective of the overall program will be to develop a response oriented structural model suitable for a wide range of airport pavement system types. The structural model will be a complete system of programs capable of rapid, efficient modeling of individual pavement systems including loads and material constitutive relations. This will form a common analytical framework to be used for all pavement configurations, and will include a complete range of materials now in use and proposed for the future. It will be capable of incorporating general aircraft tire loading configurations to suit existing and future aircraft, which are anticipated to increase in size and severity. The method will also be capable of incorporating both existing construction configurations, repair or overlay configurations and also be suitable for investigators to develop new configurations possibly incorporating new materials such as fiber concrete, etc.

An important part of the development of the unified pavement analysis method will be the incorporation of the constitutive material properties needed for each element of the pavement system. Besides the primary structural elements of reinforced and unreinforced Portland cement and asphalt concretes, there will be included the families of base, subbase and subgrade materials used in airport construction. In the new procedures, appropriate failure mechanisms will be incorporated which can be integrated with the constitutive properties above so that long-term pavement behavior may be predicted.

The overall response, therefore, will include not only the immediate structural response in terms of stresses, strains and deflections but will be reflected in the various failure modes for the airport pavements including permanent settlements, fatigue damage, rutting, pumping at joints and other important failure modes.

2.2 Specific Objectives for this Program Phase

A primary objective here is to present examples of our 3-D finite element approach and demonstrate its potential for meeting the requirements of the Unified Pavement Analysis System. So far, we have demonstrated the principle via the use of an existing commercial code, to

demonstrate the potential that the 3-D finite element approach has to form the basis of the Unified Analysis Method.

2.3 Work Accomplished

This report describes work completed to date in the use of 3-D FE methods which first demonstrate the applicability to classic pavement problems, and then which apply the method to analysis of multi-wheel gear loadings on a three-layer pavement system. Also, the application of 3-D FE methods in verifying earlier 3-D work is shown, which included comparisons with present day 2-D and other simplified methods for typical pavement problems. In this section is shown, as well, the ability of modern 3-D FE analysis to incorporate some nonlinear material properties for subsurface layers in the analysis. These include plasticity and resulting permanent settlements.

A study was also conducted comparing the response effects of various constitutive plasticity models, including a single-surface continuous hardening model.

Separate work was also performed in this phase of the contract at Texas Transportation Institute by Dr. Robert Lytton to relate pavement failure modes to the constitutive material properties that will be compatible with the operational modes of the FE analysis technique.

Finally, recommendations will be made for implementation of the methods proposed here into the development of user friendly software for advanced pavement analysis.

3. Background

3.1 The Advantages of the 3-D Finite Element Method

In the 3-D FE method the problem is formulated directly. The physical configuration, the material properties (in simplified form), and the loading pattern are all represented realistically. Naturally, full advantage is taken of common techniques such as symmetry to minimize the size of the model, but no major simplifying structural assumptions need be made. The pavement slab need not be modeled as a plate. The subbase atop soil layers need not be modeled by springs or liquids. The loading and the physical configuration need not be axisymmetric. All of these features allow a realistic representation of the airport pavement loading problem.

An important issue to be addressed in the 3-D FE method, as it is applied to the needs of the pavement problem, will be its capability to handle complex material constitutive relations and to incorporate the appropriate failure mechanisms. We anticipate that standard solution techniques which have been used for complex problems involving plasticity and visco-plasticity will be used, but with constitutive material behavior appropriate for the geo-technical materials.

3.2 Traditional Concerns with 3-D Finite Element Analysis

There are several key issues involving the use of 3-D FE analysis which should be addressed early:

- a. In the past, computational labor required for the detailed formulation 3-D problems made early applications of this method impractical. Today, however, the use of automatic mesh generation software and predetermined mesh layouts that are appropriate for the range of pavement problems make the effort on the input phase of the analysis very manageable.
- b. The large amounts of output data that are produced by 3-D FE analysis in the past have made the interpretation of the results tedious and difficult. Further, much of the response escaped evaluation due to the sheer volume of data. However, modern data editing and plotting techniques, specifically the automatic production of color graphics in isometric 3-D views, are an extremely valuable tool allowing the engineer to have a rapid look at the results of a particular analysis without laborious manual reading of

individual data. Of course, these data can also be manipulated by other special post-processors to highlight local stresses and deflections where appropriate.

- c. The long solution times which characterized early 3-D analysis are rapidly being reduced. We can show that the better workstations and PC-based desktop computers are now capable of producing results for representative problems in a very manageable time. Furthermore, the speed of PCs and workstations continues to rapidly increase, doubling every two or three years, for the same or lower costs.
- d. Memory size and instruction storage capability of new workstations is likewise increasing.
- e. In the past, the complex organization of the problem which involved manually drawing, plotting and creating FE meshes, making the various computer runs involved, organizing and presenting the data, etc., can now be done by an overall expert system incorporating FE analysis techniques. The unified pavement method should be as simple a design tool as possible. The objective here is that the essential elements of the solution process will all be contained internally in a complete program system so that the formulation by the engineer and the interpretation of the response can be performed as efficiently as possible.

A summary of these key issues is shown in Table 3-1.

Table 3-1. Key Issues In 3-D FE Application

Issue	Solution
1. Computational Labor	Automatic Mesh Generation Software
2. Post Processing Output Data	Automatic Color Graphics in Isometric Views
3. Computer Time	Modern High-Speed Processors and Integrated Chips
4. Availability of Machines	Powerful PC/Workstations Becoming Routinely Available
5. Simplicity as Design Tool	Can be an Expert System

4. Structural Response Model Method

4.1 Demonstrating the Application of 3-D FE Analysis

In the work completed we have exploited the range of available experience for applying the 3-D FE method efficiently to the airport problem. These included, as well, mesh optimization studies and some simplified representation for pavement materials.

The Foster-Miller work has used the PC/workstation environment as a baseline for the FE method. PCs are accessible and economical for the end user, which is the airport design and evaluation community. Also, a wide range of FE modules available now and in development are designed for use in PCs and workstations. Many of these are also available in mainframe or supercomputer versions if warranted.

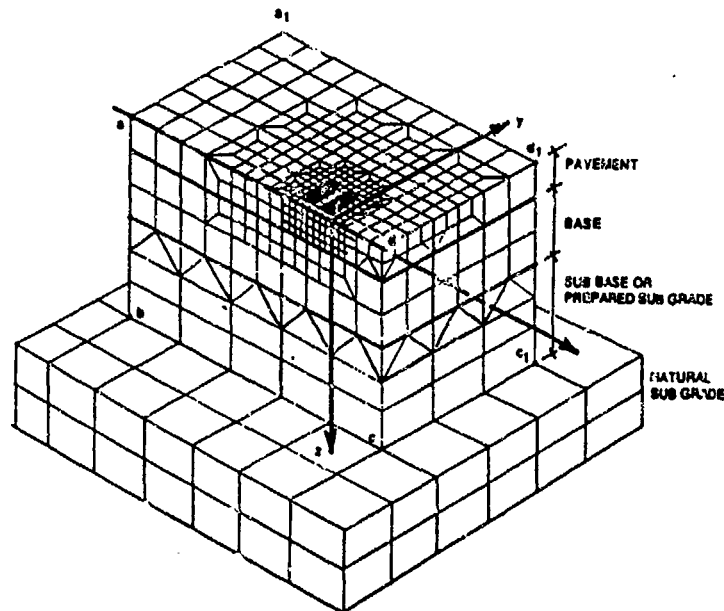
This demonstration of the 3-D FE approach for airport pavements builds on previous studies using earlier FE tools. An example is the United States Air Forces/Ioannides solution for some typical military aircraft pavement problems within the last five years [1]. Also, there are several classical pavement problems which we will analyze by the 3-D finite element method and compare with classical solutions.

One key element in making the 3-D FE analysis practical for the airport problem is the incorporation of labor-saving features that drastically reduce the repetitive preparation of input and evaluation of output. In particular, 3-D FE analysis will produce vast amounts of raw data which must be edited and presented in a form which is most useful to the end user. For demonstration analyses we incorporated the following:

- a. Automated mesh generation, which is important to reduce the complexity of input labor.
- b. The use of symmetry and symmetric boundary conditions to reduce the mathematical size of the model, thereby reducing solution time and preparation complexity.
- c. Use of a coarser model mesh away from the region of maximum loads and deflections, which results in a model which uses a smaller mathematical formulation but sacrifices little in the way of accuracy. It is important here to recognize the need for first obtaining overall accurate structural response, followed if necessary by substructuring in the immediate area of interest for a detailed picture of stresses or deflections. The use of a progressively coarser model away from the region of maximum loads and

deflections eventually eliminates areas of the model that are for all practical purposes unaffected by the loads.

We can depict schematically a typical 3-D FE structural model for airport pavements, referring to Figure 4-1.



abcd = Plane of Symmetry W/Symmetric Boundary Conditions
yz PLANE = Joint Plane (if app.) in Pavement Level
add₁a₁ = Surface (Loading) Plane - 1/2 Dual Tandem Gear Shown
Other Vertical Planes = Model Boundary Conditions

Figure 4-1. Schematic Representation of Typical Finite Element Model

4.2 Layout of FE Structural Response Models

As an example, we have indicated a typical dual-tandem gear load such as that for Boeing 707 adjacent to a longitudinal joint in Figure 4-2. The area of interest, which represents the primary response region of the model, will be the area in which maximum stresses and deflections are anticipated. Local, more detailed failure models will also focus on portions of this area. At the periphery of the model, away from the area of interest, the model is terminated using linear boundary conditions. This region can be determined by the use of dimensional parameters referred

to in earlier work by Dr. A. Ioannides for the U.S. Air Force [1]. Here, a single axis of symmetry perpendicular to the pavement joint and to the direction of travel for the gear is shown, and the resulting model area is indicated by the crosshatch.

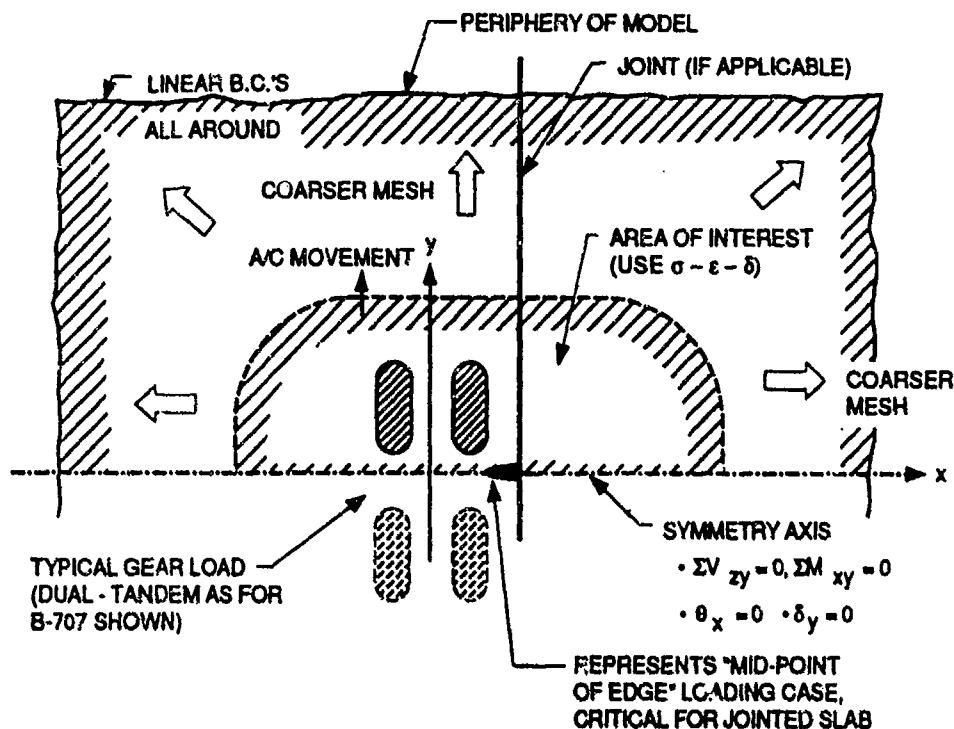


Figure 4-2. Typical Model Layout Showing Lateral Symmetry with Longitudinal Joint

An even greater reduction in model mathematical size can be used with bilateral symmetry, as shown in Figure 4-3, in which a plan view of a typical model layout for a so-called interior or an unjointed pavement case is shown. Here the same dual-tandem gear load is shown. Two axes, or planes, of symmetry are indicated passing through the center of the gear truck. The area of interest near the gear, contained within a larger, coarser area is also indicated.

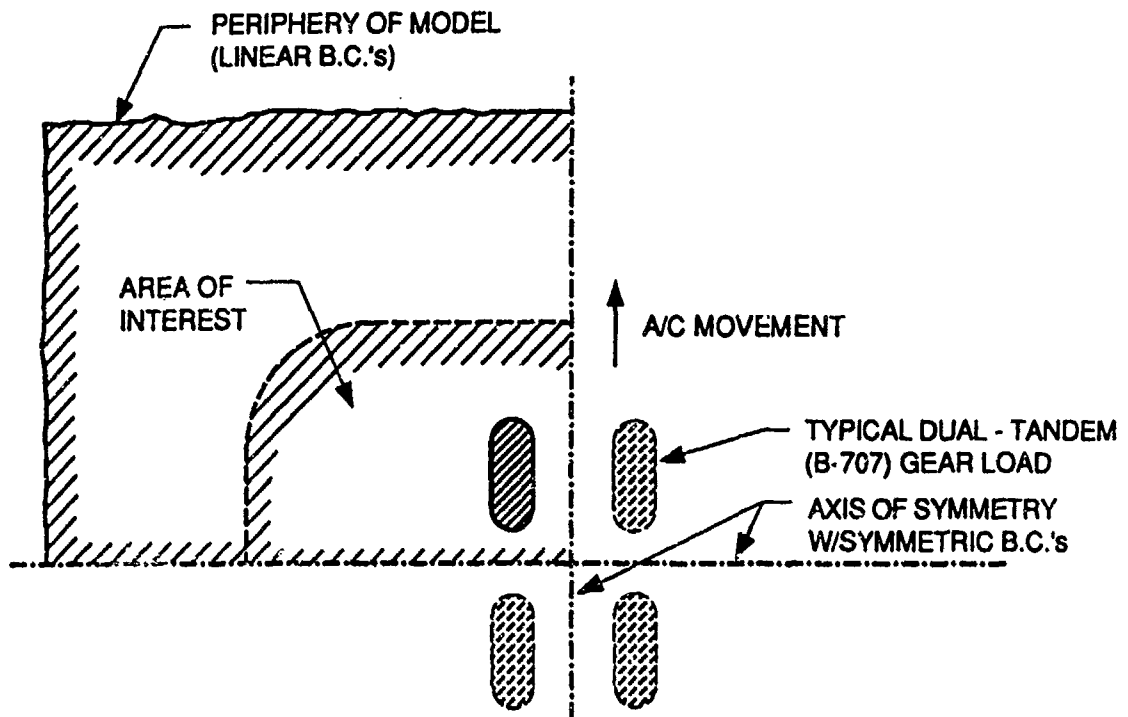


Figure 4-3. Typical Model Layout Showing Bilateral Symmetry

4.3 Finite Element Program for Demonstration of 3-D Analysis

For demonstration purposes, in this program phase we have used an advanced commercial finite element code, NISA 90.0, which contains many key capabilities needed for 3-D pavement analysis. However, we should note that the eventual goal of the Unified Pavement Program is to assemble the best available modules for the complete unified pavement analysis process. This will include customized writing of key solution modules and material constitutive modules, which will be combined with the pavement mesh generation pre-processors and plotting type post processors referred to earlier.

With this demonstration program, we can formulate the solution of typical linear and non-linear material problems, with a selection of material failure laws (including Von Mises, Drucker-Prager, Mohr-Coulomb, and other similar formulations) which indicate at least a general applicability to the type of materials encountered in airport pavements.

This program system also has excellent graphics and data preparation features that reflect the features needed in the final 3-D analysis method. Extensive use of color graphics enables the user to rapidly assess the response of a given model. These color graphics can be produced on a multicolor laser printer integrated with the workstation so the graphical output is available immediately upon solution of the problem. This capability includes not only multicolored isometric plots of stresses and displacements throughout solid objects, but also the wide capability for slicing through the model in various directions to highlight certain zones for stress, deflection, strain and various forms of principal stress.

4.4 Benchmark 3-D FE Analyses for Classical Pavement Problems

The 3-D FE techniques described above were first applied here to several benchmark problems. In the past, these simple, idealized cases have been formulated with a closed-form solution, and in some cases, also with earlier 2-D axisymmetric programs such as ILLI-SLAB, ILLI-PAVE, Chevron, etc.

4.4.1 Westergaard Plate Problem

The first benchmark analysis using our 3-D FE approach was a check of the classic [6] Westergaard solution for an elastic slab with an interior load supported on a dense liquid foundation. This solution was in the form later updated by Losberg for a square interior load. The general characteristics of this sample case are shown in Figure 4-4.

In this model, a thin concrete slab 6 in. thick is supported on an elastic subgrade with a bulk stiffness of 50 lb/in.³. A total load of 10,000 lb over a central 1 ft² area was used,, and the results of the FE analysis were compared with the classical solution as modified by Losberg. Results are shown in Table 4-1. The Foster-Miller model and the closed form solution both agreed exactly, with a central vertical deflection of 0.023 in. The maximum flexural stress in the slab from our model was 265 psi compared to closed form solution of 285 psi, which is excellent agreement, given the coarse element size relative to the loaded area.

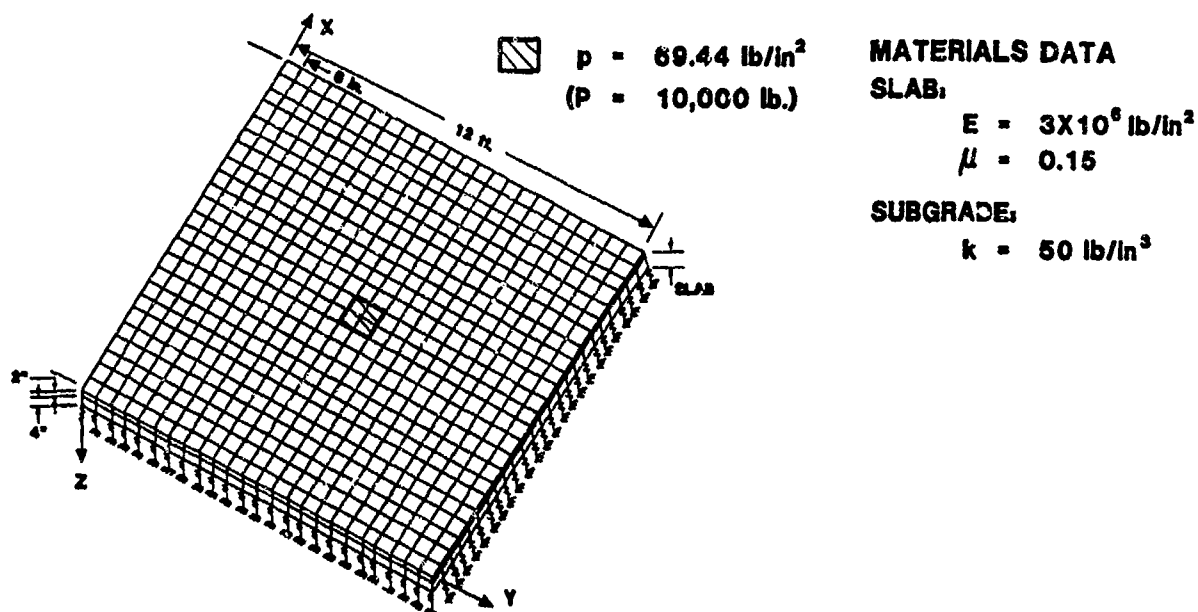


Figure 4-4. Westergaard Benchmark Model with Square Interior Pressure Load

Table 4-1. Comparison of Results for Westergaard Problem

	d_{\max} (in.)	s_{\max} (psi)
Foster-Miller NISA Model	0.023	265
Closed-form solution	0.023	285

In the FE model, the slab was modeled using a 12 ft x 12 ft area divided into a multilayer network of 3-D solid isoparametric "brick" elements. These consisted of 6 in. x 6 in. elements in plan view, two layers deep. For speed of modeling, no variation of element size away from the load was used in these early studies. The top layer of 2 in. and the bottom layer of 4 in. make up the 6-in. thick layer for the slab. Note that these are not plate bending elements, but 3-D solids.

Note also that no advantage was taken of the obvious bilateral symmetry. This could have easily reduced the model size by approximately a factor of four. Then the planes of symmetry would have used symmetry type boundary conditions with restrained edge moments, with vertical movements unrestrained. Because of the short solution time and the simple nature of the model, no real effort was extended to economize on the solution. However, in later cases we will see how we can take advantage of these principles.

4.4.2 3-D FE Analysis of Burmister Two-Layer Axisymmetric Problem

This 3-D FE solution was performed for a two-layer system, representing a classical Burmister [7] two-layer problem, with the bottom "layer" a semi-infinite elastic medium. As seen in Figure 4-5, a bilateral symmetric model was created resulting in one-quarter of the actual area being modeled, using two perpendicular planes of symmetry. In this example an 8-in. thick top layer with Young's modulus of 29,900 psi and Poisson's ratio of 0.49 was modeled with two layers of 4-in. deep 3-D isoparametric brick elements. These were arranged in a 6 ft x 6 ft. area, with individual element size in plan view being 6 in. x 6 in.

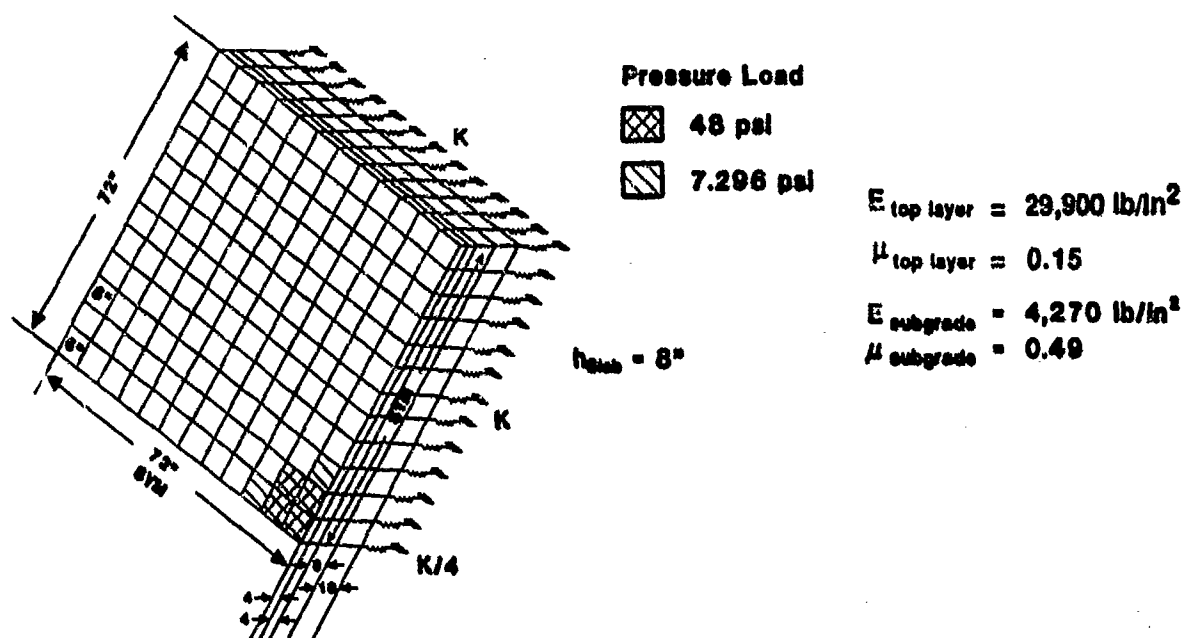


Figure 4-5. FE Approximation of Burmister Two-Layer Problem

The subgrade was assumed to be a softer material with a modulus of 4,270 psi, again with a Poisson's ratio of 0.49. Two layers of subgrade were modeled by 3-D brick elements, with the remainder below approximated by vertical spring elements. Note that when using symmetry (either in single- or double-axis form and using a spring representation for the continued depth of subgrade, care must be taken to allow for the "presence" of adjacent springs at all of the symmetric points so spring stiffnesses have to be adjusted along the lines and corners of symmetry.

The load here consisted of a 30-in. diameter circular area with vertical pressure of 48 psi, reflecting values used in early Burmister studies of the 1940s. These had originally been done by Burmister to evaluate the stiffening effect of a top base layer (compacted or stabilized) on the original subgrade, and proceeded to a general closed-form analysis of a two-layer system.

Comparison of the 3-D results, seen in Table 4-2 shows a reasonably good agreement for maximum deflection (the principal quantity used throughout the Burmister work). However, the use of springs to represent lower subgrade areas did not provide any meaningful savings, since the effort to properly model the continuum below was out of proportion to any execution time saved; total solution time was only a few minutes on a 386/25 PC. Also, there is no good equivalence of vertical springs to a 3-D elastic solid when differential vertical displacement occur. Future modeling of subgrades, therefore, was done using 3-D elements, without spring elements, terminating at much deeper levels (40 ft. range) using a progressively coarser mesh. This provided better replication of the actual physical conditions.

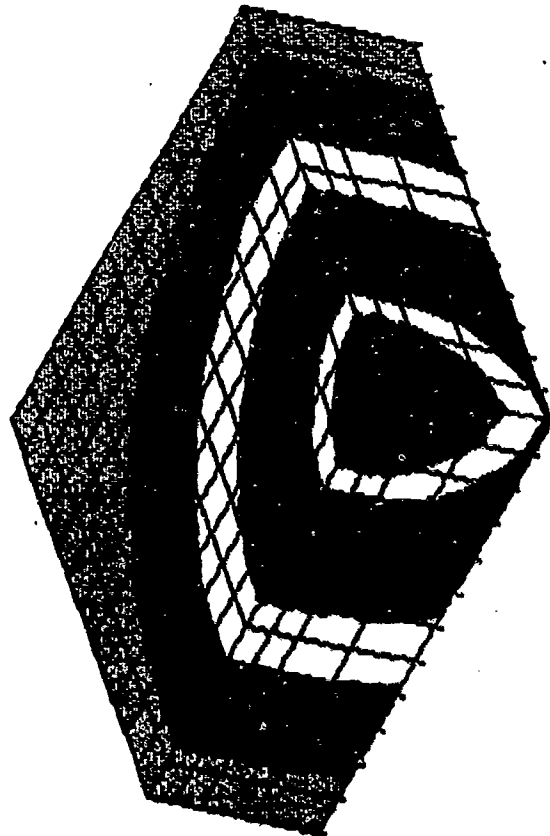
It should be noted that neither in this case nor in the previous case were any plate-type or flexural elements used. These elements are 3-D solid isoparametric elements, and therefore all equivalent shear and moment deflections are accounted for, with accuracy limited only by the numbers of elements used to represent the solid layers.

Table 4-2. Comparison of Results for Burmister Benchmark Problem

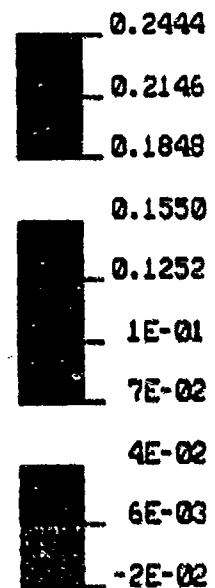
	d max	Remarks
Foster-Miller NISA	0.244 in.	Springs below 18 in. depth
Burmister Closed-Form	0.253 in.	Semi-∞ Elastic Solid

By inspection of the accompanying isometric color* plot (Figure 4-6) one can easily see the effects of variation of deflection as a function of distance away from the loaded area, serving as a valuable guide to the investigator so as to easily visualize the pavement area which has a meaningful response. For these purposes a detailed review of the printed output is not necessary, showing the value of advanced graphical post processors when evaluating 3-D results.

EMRC - DISPLAY II POST-PROCESSOR VER 90.0 Jan/15/91



DISPL. CONTOURS
Z - DISPLACEMENT
VIEW : -2.38E-02
RANGE: 2.44E-01



X
Y Z
RX= 160
RY= 60
RZ= -30

Figure 4-6. 3-D Burmister Benchmark Problem

* Color originals available at Foster-Miller.

4.4.3 3-D FE Model for Pavement Slab (Interior Load Case)

This 3-D FE demonstration case was undertaken to clarify our modeling and solution technique by comparison with earlier FE work for the USAF by Dr. A. Ioannides [1]. In the model, a relatively thin 8 in. concrete slab on a soft subgrade was deliberately chosen to enhance the magnitude of the results. In this particular case, a single wheel load of 30,000 lb representing that due to an F-15 aircraft, was applied to an unjointed slab, resulting in a so-called "interior" load case. A general depiction of the FE model is shown in Figure 4-7.

Extensive earlier work by Ioannides and others has shown that in order for the structural response to be properly evaluated, the slab area that needs to be modeled to obtain acceptable results may extend a relatively short distance away from the load. Naturally, this is a function of the interplay between the flexural rigidity of the slab, the characteristics of the subgrade, and especially the size of the loaded area. Dimensionless parameters containing the above [Ref 1] can be used to evaluate the slab area requirements for a given set of physical characteristics. The typical subgrade, however, should extend a substantial distance both laterally and vertically away from the loaded area, in order to properly evaluate the response of the system.

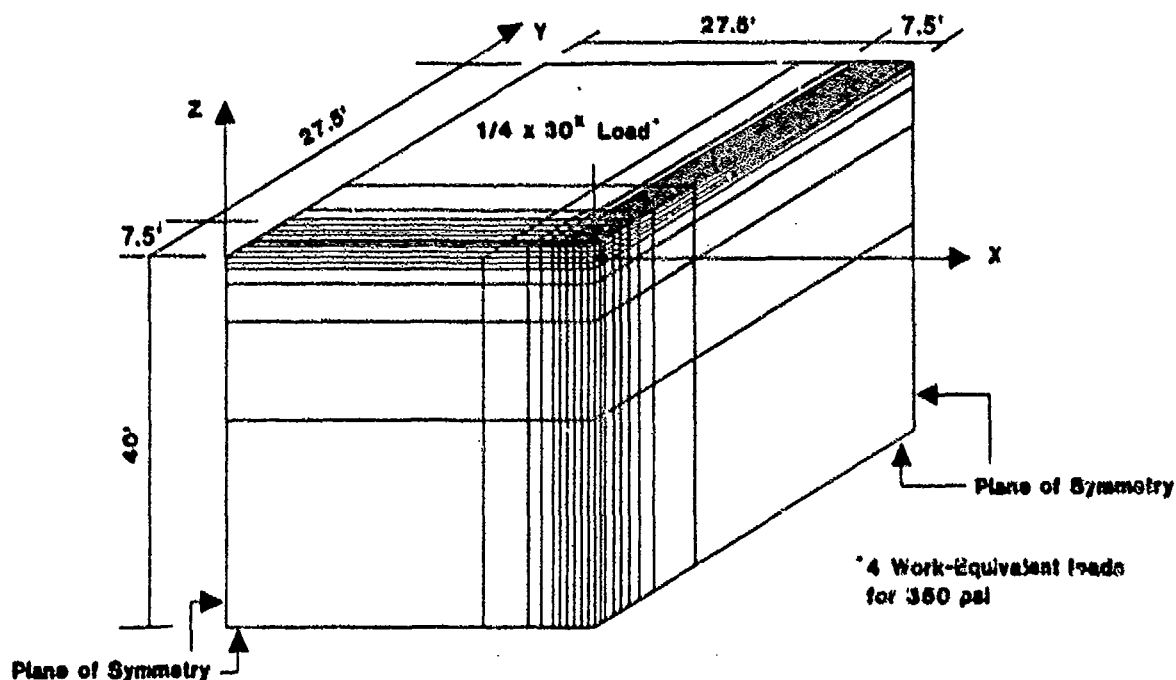


Figure 4-7. 3-D FEM for Interior Load Case - 8-Inch Slab with Single 30K Wheel Load

The size of the "interior" model can obviously be reduced by using double symmetry, i.e., symmetry about both xz and yz planes, thereby reducing the modeled volume to one-quarter of the original. Accordingly, in our case, the modeled area includes one-quarter of a 15 ft x 15-ft slab area, on a 35 ft x 35-ft subsoil or subgrade area, extending down to 40 ft below the surface. In this case, typical symmetry-type boundary conditions are applied to both planes of symmetry. In addition, the boundaries at the extremities of the model in both lateral and vertical directions are restrained by the appropriate "rollers" with zero transverse displacement permitted, which provides good representation of the true situation since the effects of the load have nearly been eliminated at this distance. Note also that in the model the size of the FE mesh progressively increases in all directions away from the loaded area. This reflects the normal practice in FE analysis to economize on the size of the model while sacrificing little of the accuracy for overall, or "global" response.

Figure 4-8 shows the center of the interior load model in detail. In this case we have divided the thickness of the slab into only two layers of 3-D isoparametric brick elements. The subgrade volume immediately below the slab has been divided into two 6-in. thick layers, with succeeding levels increasing rapidly in thickness proceeding vertically downward. In this figure the locations of interest for the pavement response are shown, in which vertical deflections are evaluated at the center surface of the pavement layer, in-plane flexural stresses are evaluated at the bottom of the slab and again in the center of the pavement area, and maximum subgrade pressure in the vertical direction is evaluated immediately below the slab in the subgrade layer. This FE model contained 584 elements and 2,532 degrees-of-freedom (DOF), including boundary restraints.

The execution time of this single static load case was performed with the NISA demonstration program in 18 minutes on an IBM 386/25 PC-type desktop system. This was later reduced to 6 minutes when run on a 486/33-type PC. In contrast, in an earlier FE analysis by Ioannides, using a similar model with the GEOSYS Program, the solution took 2.5 hours on a Harris 800 virtual memory computer. This shows the rapid decrease in solution times for 3-D models that we can expect with the advancing speed of PC workstations.

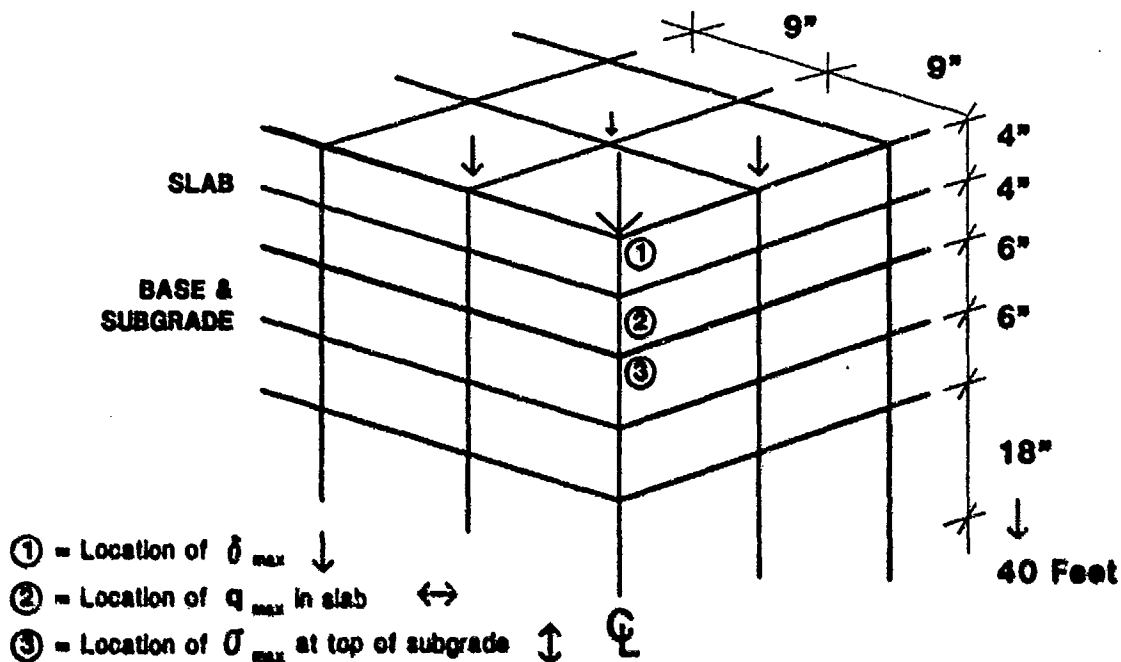


Figure 4-8. 3-D FEM - Detail at Center, Interior Load Case

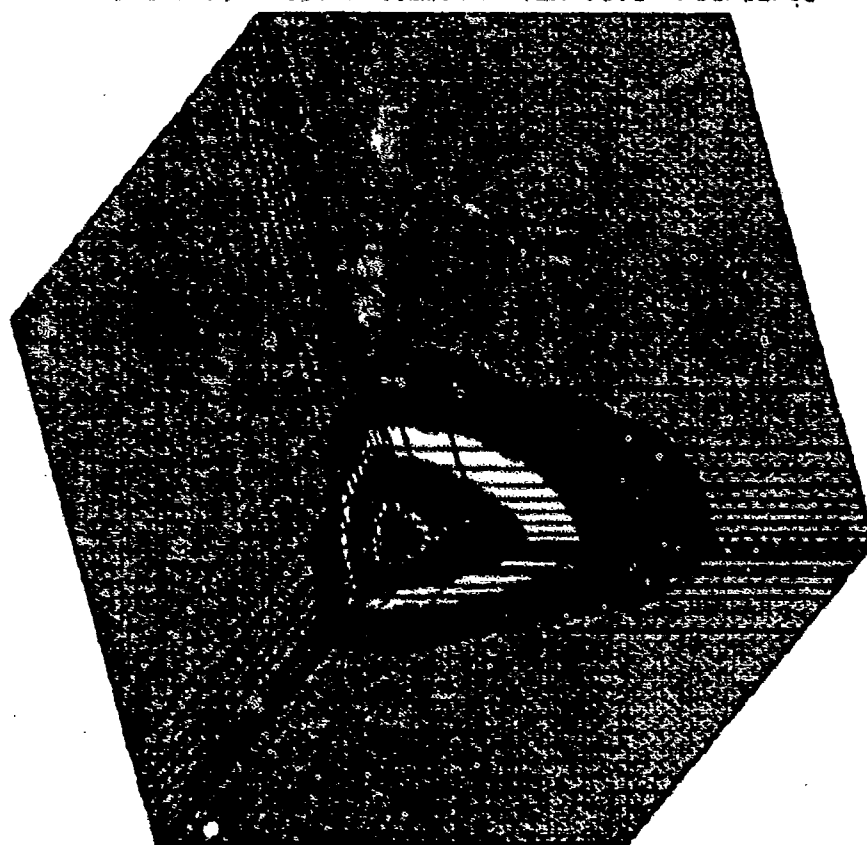
The results of this study are shown in Table 4-3, along with a comparison with earlier 2-D and closed-form analyses for the same problem. These included ILLI-SLAB, [8] used now by some designers for pavement studies, and the closed form Westergaard/Losberg solution. Exact agreement was obtained with the 3-D GEOSYS results, and good agreement with 2-D. (Later, we shall see that 3-D is especially useful for edge-loaded and similar situations which cannot be directly modeled by 2-D and type analysis).

The Foster-Miller results can again be effectively visualized by 3-D color graphics, produced with advanced post-processing techniques. In Figure 4-9 we see an isometric view of vertical deflections in 3-D contours. This confirms instantly how the "area of interest" for significant deflections includes a limited region (several feet away from the load for these particular pavement system characteristics). Max deflection is tabulated and others can be closely estimated throughout the system without searching through printed output, although these files furnish all "raw" data for any postprocessing operations that may be desired.

Table 4-3. Comparison of Results for Interior Load Case

	δ_{slab}/max (in.)	q_{subg}/max (psi)	s_{slab}/max (psi)
F-M NISA Model	0.031	5.02	608
GEOSYS (USAF) 3-D	0.031	5.03	609
ILLI-SLAB 2-D	0.037	5.10	697
Closed-Form (Losberg)	0.036	4.83	636

EMRC - DISPLAY II POST-PROCESSOR VER 90.0 Feb/12/91



DISPL. CONTOURS
Z - DISPLACEMENT
VIEW : -3.22E-02
RANGE: 1.54E-03

(Band * 1.0E-3)

1.536

-2.208

-5.952

-9.696

-13.44

-17.18

-20.93

-24.67

-28.42

-32.16

$\begin{matrix} y \\ \swarrow \\ x \end{matrix}$
 $\begin{matrix} z \\ \downarrow \end{matrix}$
 RX= 0
 RY= -60
 RZ= 30

Figure 4-9. 3-D Vertical Deflection, Interior Load Case

In Figure 4-10 we show an isometric color plot of vertical subgrade pressure in the vicinity of the load. Here, the slab has been removed for clarity. In later cases, we will also see how the model volume can easily be sliced or localized to produce clear graphical depiction of the pavement response wherever needed. Also, another type of graphical output that can be produced is a trajectory-type (vector arrows) map of displacements, which will also be familiar to FE analysts.

In these simplified 3-D Models, note the rather coarse mesh used under the vicinity of the load. In an actual application, a more refined mesh or a local model/substructure in the upper layers could be used to produce a finer resolution of stresses. However, the overall deflection (global response) of the model is not affected materially by this degree of model coarseness immediately under the load. In this case, the bending behavior of the slab was adequately represented by only two layers of isoparametric brick elements, showing that even with this absolute minimum number of elements, adequate slab behavior is obtained. But, for a more accurate rendition of slab stresses laterally and through the thickness under the load (especially if a complex tire pressure distribution is applied), a more finely divided mesh or local model can easily be used.

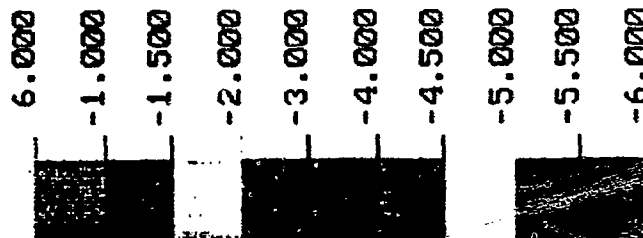
Comparing the earlier ILLI-SLAB 2-D and closed-form solutions, note that this double-symmetric configuration is not too dissimilar from the axisymmetric configuration represented by these approximate solutions. Therefore, here we could expect these latter to give a reasonable approximation of the true 3-D response. This doubly-symmetric example, although in practice rarely producing maximum stresses compared to an edge-loaded type configuration, nevertheless is valuable to verify the performance of the approach, and to compare against traditionally accepted axisymmetric and 2-D analysis tools.

4.4.4 3-D FE Study of Dual-Tandem Landing Gear Load for Wide-Body Aircraft

This is a more complex problem which extended the work of the previous example to a representative airport pavement situation. In this example, a single dual-tandem landing gear truck of the Boeing 747-200 aircraft, with takeoff gross weight (TOGW) of 775,000 lb was applied to the interior of a pavement slab area. An interior-type FE model was therefore constructed. As in the previous examples, advantage was taken of the dual planes of symmetry, so as to require modeling of only one quarter of the dual-tandem truck and the pavement system, using appropriate symmetry boundary conditions. There, individual wheel load was 46,000 lb, with a tire pressure of 200 psi, equivalent to that used in normal service. A three-layer PCC pavement system was

EMRC - DISPLAY II POST-PROCESSOR VER 90.0 Feb/13/91

STRESS CONTOURS
 SZZ - STRESSES
 VIEW : -5.62E+01
 RANGE: 2.22E+00



RX= 0
 RY= -60
 RZ= 30

Figure 4-10. 3-D Vertical Subgrade Stress, Interior Load Case (Detail)

used similar to that which would be designed today. A complete analysis for this four-wheel dual-tandem truck was performed in a single 3-D FE analysis run.

A plan view of the pavement system modeled area is shown in Figure 4-11.

As in the previous example, we initially modeled a 15 ft² slab area with the 747 dual-tandem landing gear truck, with the subbase and subgrade extending 40 ft away from the center of the gear in both lateral directions. In the elevation view, we depicted the cross section of this pavement system. The pavement layer consists of a 12-in. thick Portland cement concrete (PCC) slab with Young's modulus of 4,000,000 psi. This lies atop a 12-in. layer of compacted stabilized subbase, analogous to FAA specification P-304, with a modulus of 40,000 psi. This in turn is atop a "soft" subgrade with modulus of 7,700 psi. The depth of the modeled volume of 40 ft is sufficient to adequately represent a semi-infinite half space of subgrade material, according to previous USAF studies by Ioannides [1].

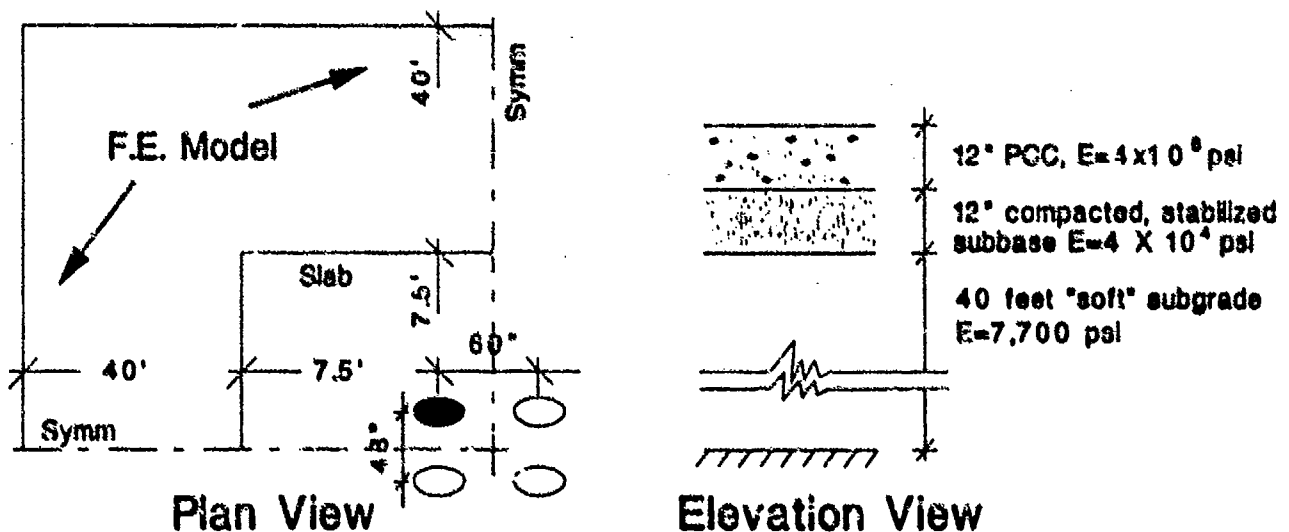


Figure 4-11. Dual-Tandem Widebody Gear Load on Three-Layer Pavement System

This three-layer airport pavement system complies with the requirements of the FAA AC150/5320 Airport Design Circular. This first phase demonstration problem used linear elastic analysis, but follow-on work could include the use of selected nonlinear representations for the subbase and subgrade, as will be seen in examples later in this report for edge-loaded slab configurations.

Again, one objective in this study will be to highlight the use of advanced post-processors which produce 3-D color contour plots for rapid visualization of deflections and stresses throughout the pavement system.

A close-up view of this finite element model in the vicinity of the tire load is shown in Figure 4-12. Here we can see that the 12-in. thick slab is modeled by only two layers of isoparametric brick elements. This was shown to be sufficient for representing the global response, although a finer 3-D mesh in the higher stress areas immediately beneath the tire would produce more accurate stresses. The 12-in. thick stabilized subbase layer is also modeled by two layers of these elements. The "soft" subgrade is modeled by deeper elements quickly increasing in size with depth down to 40 ft where the model is terminated. Likewise, the coarsening of the model as we proceed away from the center, or intersection of the axes of symmetry, can be seen in the figure. The aircraft tire load is modeled by six work equivalent loads in a rectangular pattern approximately representing the actual oval footprint. The total individual wheel load in this case is 46,000 lb, a typical wheel load for the Boeing 747-200. A depiction of the tire pressure distribution is shown in Figure 4-13.

In side view, the aircraft tire pressure distribution is approximately parabolic as shown with an average value of 200 psi. In the axial view, the tire sidewalls typically cause the pressure to be higher at the sides of the footprint, which is shown. This is approximated by the rectangular arrangements of the six equivalent loads shown previously. It should be noted that without a much more detailed FE representation of the area directly under the load, these minor differences in the tire pressure distribution have little effect on the overall structural behavior of the pavement system. However, for detailed local stress analysis, it would be appropriate to represent these details of the tire pressure distribution.

These tire pressure distributions could also be used to represent an aircraft of 50 percent higher weight, if the tire pressure for that aircraft were also increased by 50 percent. The behavior of this elastic model will be useful later via simple scaling at least to begin the study of the effects of higher widebody tire pressures.

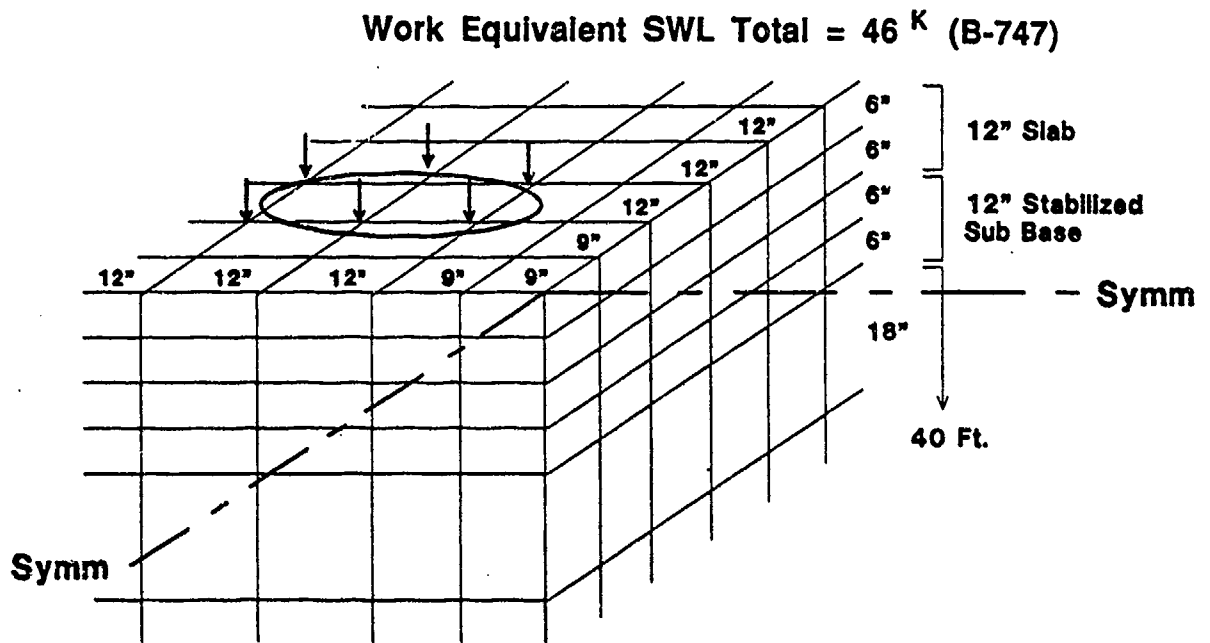


Figure 4-12. FE Model for 4-Wheel DT Landing Gear

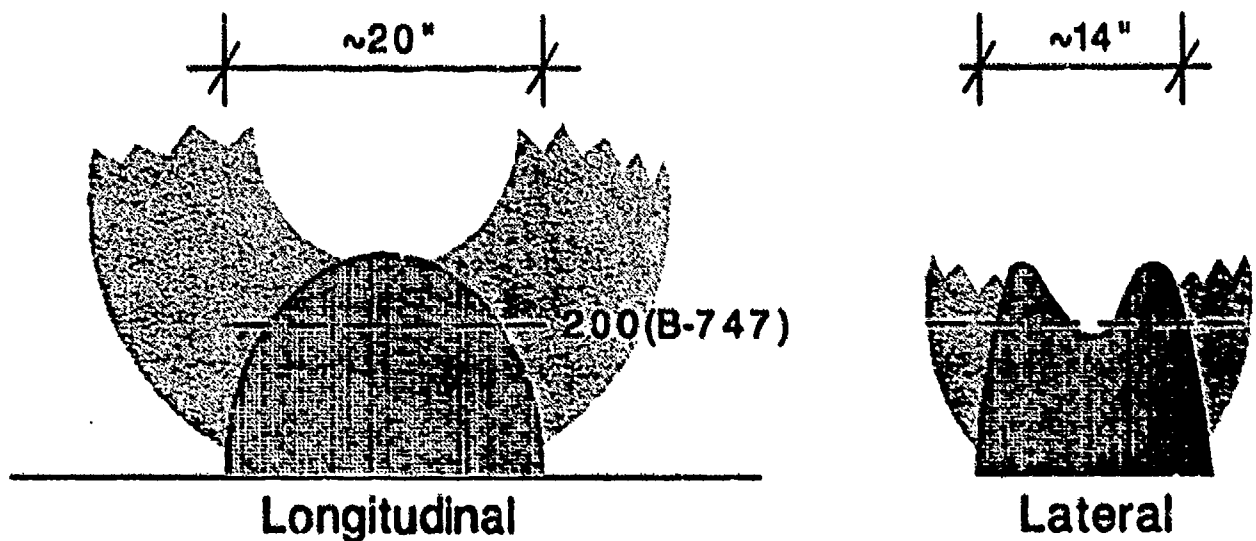


Figure 4-13. Tire Pressure Distribution

The flexural stresses at the bottom of the slab under the load in the longitudinal, or tire travel, direction are shown in Figure 4-14. Note that this model includes the behavior of all four tires simultaneously acting on the slab and pavement system. We can see from this figure that the flexural stresses in the pavement peak under the tire at slightly over 400 psi and that they decay to approximately 350 psi between the forward and aft tires before rising again in a symmetrical pattern. Forward of the tire footprint, the stresses can be seen to fall off rapidly.

Figure 4-15 shows the variation of the vertical compressive stresses in the pavement system under the center of the tire contact area. The stresses rapidly decrease proceeding down through the concrete slab, reaching a value of approximately 10 psi contact pressure at the base of the slab on top of the subbase layer. Stresses further reduce with depth as shown and at the interface of the subbase and the subgrade layers the contact pressure has reduced to approximately 6 psi.

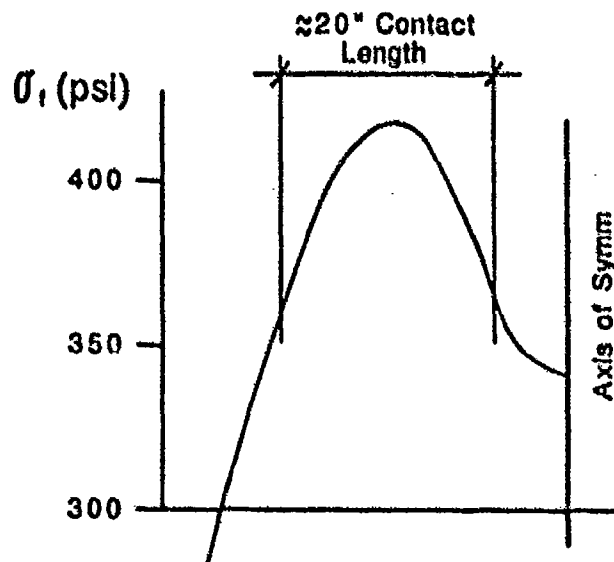


Figure 4-14. Flexural Stresses Under Load at Bottom of Slab-Longitudinal Direction

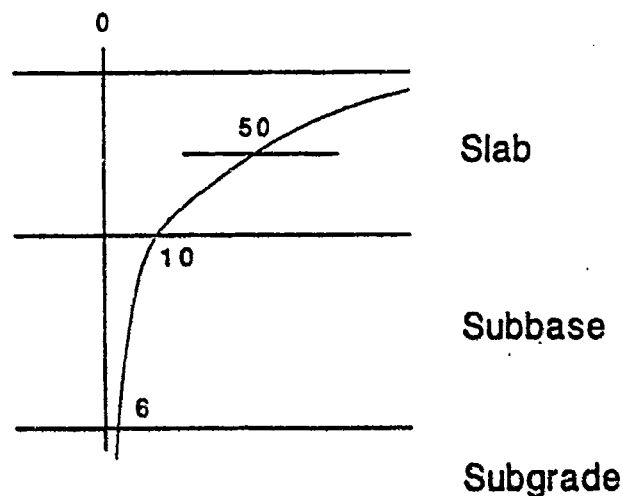


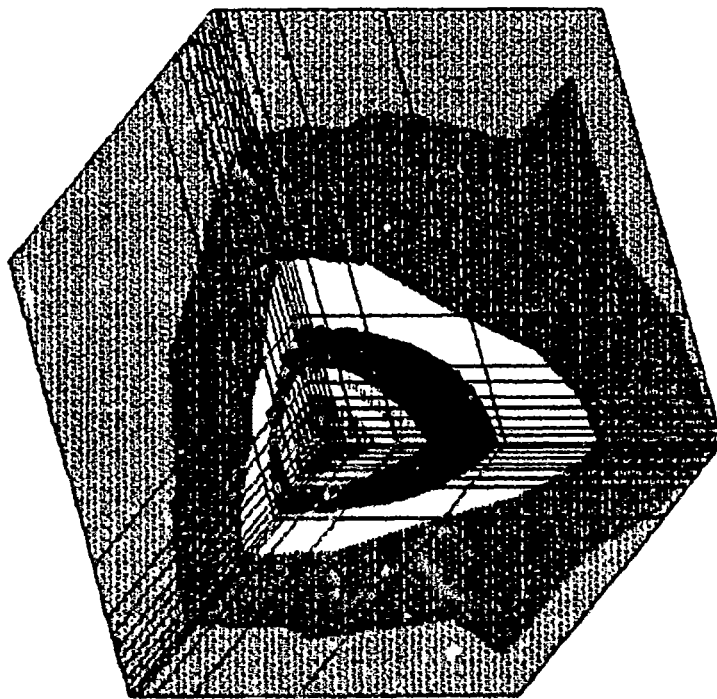
Figure 4-15. Vertical Compressive Stresses in Pavement Under Center of Contact Area

The overall response of the model can be quickly seen in the accompanying 3-D isometric color* contour plots shown in the following figures.

Figure 4-16 is a depiction of the vertical displacements in the total pavement system, shown in isometric view. The maximum value of 0.094 in. vertical deflection takes place at the center or intersection of the two planes of symmetry. The contour plot quickly shows the decrease of these vertical deflections as one proceeds away from the loaded area in all directions.

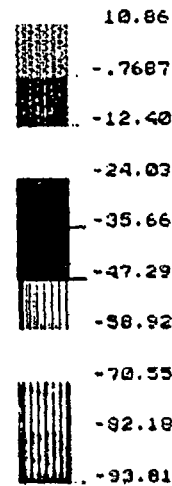
Figure 4-17 is a detail showing the principal in-plane stresses at the top of the slab, with only the slab stresses being shown. This gives a good idea of the distribution of flexural slab stresses, and it suggests that the modeled slab area might be insufficient for adequately representing the behavior of the pavement system. This will be treated in a later section.

* Original color plots available @ Foster-Miller.



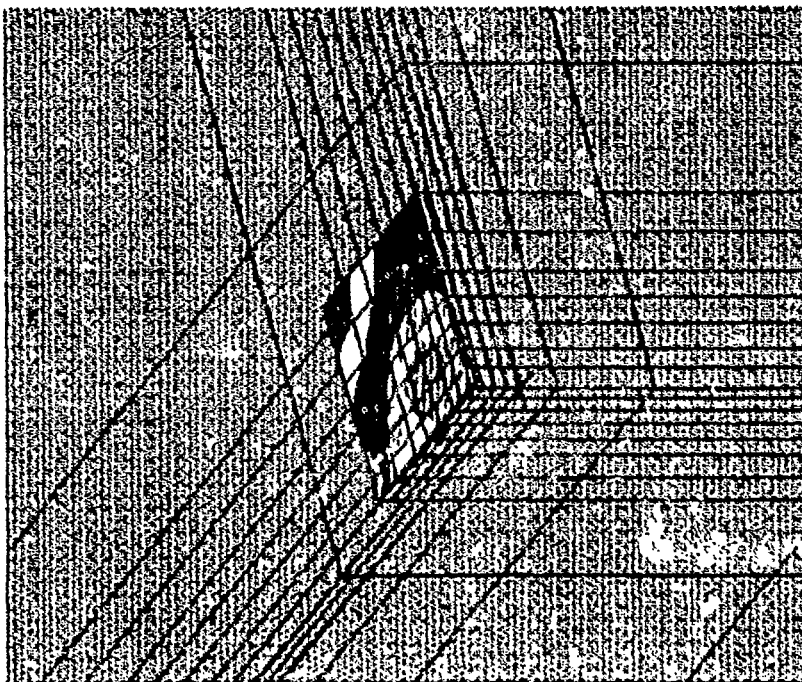
DISPL. CONTOURS
Z - DISPLACEMENT
VIEW : -9.38E-02
RANGE: 1.09E-02

(Band = 1.0E-02)

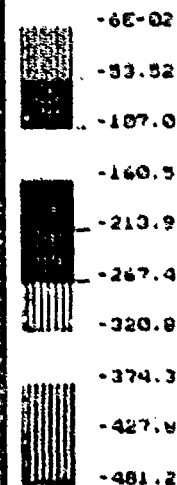


RX= 0
RY= -60
RZ= 30

Figure 4-16. 3-D Vertical Displacements - B-747 Dual-Tandem Gear



STRESS CONTOURS
S3 PRINCP STRES
VIEW : -4.81E-02
RANGE: -1.28E-01



RX= 0
RY= -60
RZ= 30

Figure 4-17. Top Slab Stresses, Y-Dir (15 x 15 ft Slab) - B-747 Dual-Tandem Gear

3-D graphical post-processing techniques can also be used to highlight a key area of the model. In Figure 4-18 the flexural stresses in the X direction are shown for the pavement system, sliced through the closest layer of nodes convenient to the loaded area, which is shown by a dashed elliptical line. The variation of flexural stresses with depth through the slab are clearly seen in this picture.

Also, certain areas of the pavement system can be removed for an unobstructed look at lower layers. This is seen in Figure 4-19 in which the vertical stress contours in the subbase and the subgrade layers is shown under the loaded area. This area was sliced in a manner similar to that in the previous figure. Here, we see how the vertical stress distribution decreases with distance away from the load.

Some numerical results for this dual-tandem gear loading example are summarized in Table 4-5. The maximum vertical deflection at the centerline of the gear truck, which was also the center of the model, was 0.094 in. as mentioned above. Under the center line of each tire, vertical deflection was slightly less, at 0.087 in., and decreased to approximately 0.050 in. 6 ft outward from the tire centerline. The peak slab flexural stresses of 430 psi under the slab were higher in the direction parallel to the direction of travel. This was in good agreement with an estimate using the closed form solution, after superposition of the four multiple loads. The maximum subbase pressure, at the interface of slab and subbase, was approximately 10 psi. This model did not allow for any potential slip at these interface planes, which can be corrected in further work by using sliding and gap type (nonlinear) elements.

ENRC - DISPLAY 11 POST-PROCESSOR UER 90.0 MAR/19/91

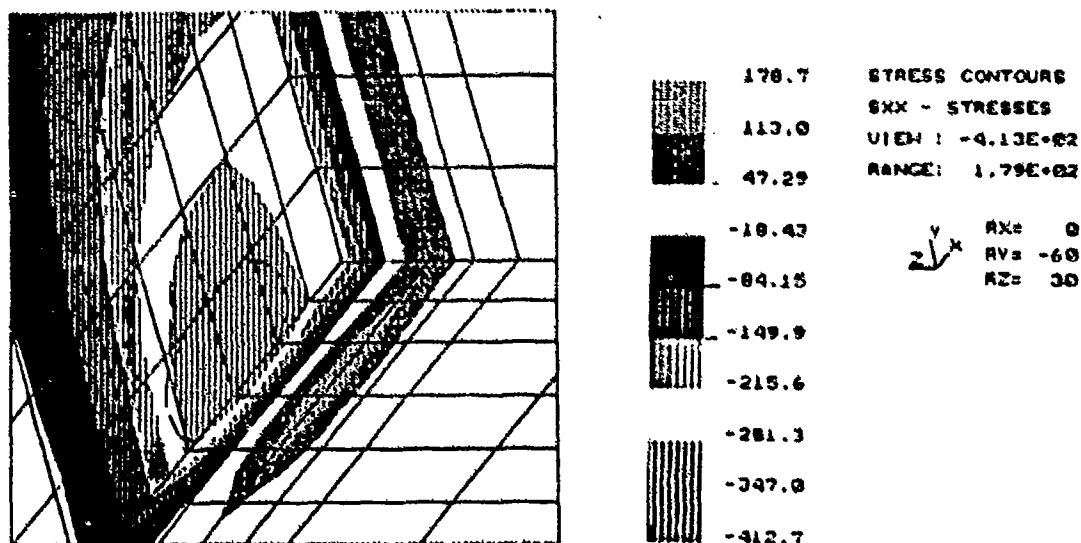
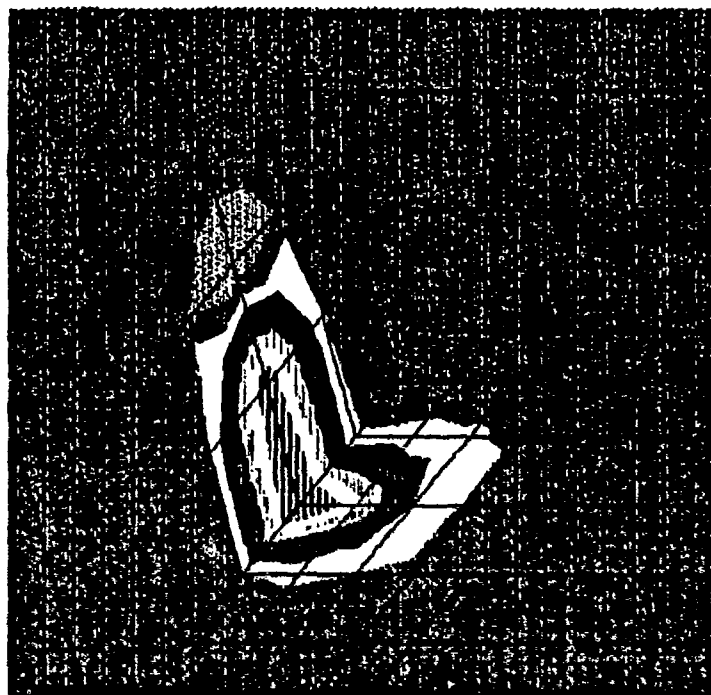
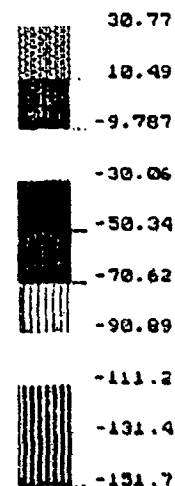


Figure 4-18. Top Slab Stresses, X-Dir - B-747 Dual-Tandem Gear



STRESS CONTOURS
 SZZ - STRESSES
 VIEW : -1.52E+02
 RANGE: 3.06E+01



RX= 0
 RY= -60
 RZ= 30

Figure 4-19. Vertical Stress - B-747 Dual-Tandem Gear

Table 4-4. Results for B-747 - 200 Dual-Tandem Gear - Elastic Analysis of Three-Layer System

Results		Remarks
Max Vertical Deflections at CL of truck at tire	0.094 in. 0.087 in.	0.050 in. 6 ft outward from tire CL
Slab Flexural Stress at bottom of slab under tire (max - along travel direction)	430 psi	Good agreement with Losberg (Westergaard) estimate after super-position of multiple loads
Max Pressure in Subbase (vertical component)	-10 psi	Further refinement of slab/base connectivity modeling desired

As was mentioned above, the distribution of slab flexural stresses and vertical deflections suggested that the 15 x 15 ft slab area included in the model was not sufficient to accurately represent the response of the pavement system, considering the large extent of the loaded area with

a wide body dual-tandem gear truck. Accordingly, a new analysis was made, in which the slab area included in the model was extended to the outward boundaries of the model volume, i.e., 40 ft in each of two lateral directions. This process is depicted in Figure 4-20.

Highlights of this model response are shown in Figure 4-21 in which the top slab stresses of the "extended" slab are shown in 3-D isometric color* plot.

Here the principal stresses on the top surface are somewhat reduced compared to the earlier corresponding plot. (Post processors could also display differential contours between cases.) The comparison of this case versus the original slab area is instructive and is shown in Table 4-6.

The maximum slab deflection at the centerline of the model was reduced to 0.83 in. Similarly, the slab tensile flexural stress was reduced 6 percent and the maximum subgrade pressure reduced approximately 10 percent. This latter percentage is only approximate since the pressure change was only 1 psi.

The conclusion that we can draw here is that the slab area for large dual-tandem gear trucks must be increased relative to that which would be sufficient for a single wheel loading. This is not unexpected. The actual area of the slab that needs to be modeled could easily be determined by further experimentation with this model, which is feasible at 6 minutes per run. Dimensionless parameters as proposed by Ioannides can also be used as an initial guide. It is likely that a slab area of 15 to 20 ft laterally from the extent of the loaded area would be adequate to represent the behavior of this particular pavement system.

* Original @ Foster-Miller.

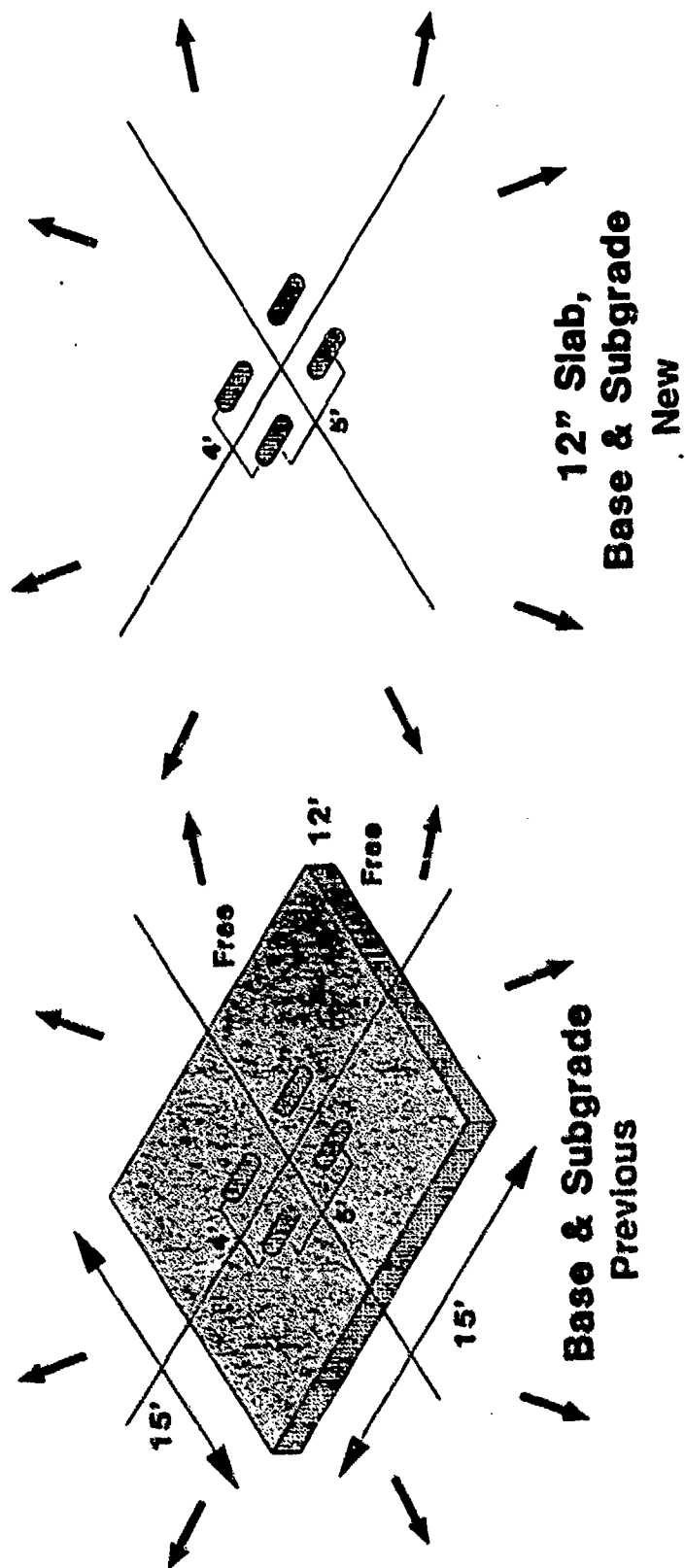


Figure 4-20. Effects of Slab Area Modeled

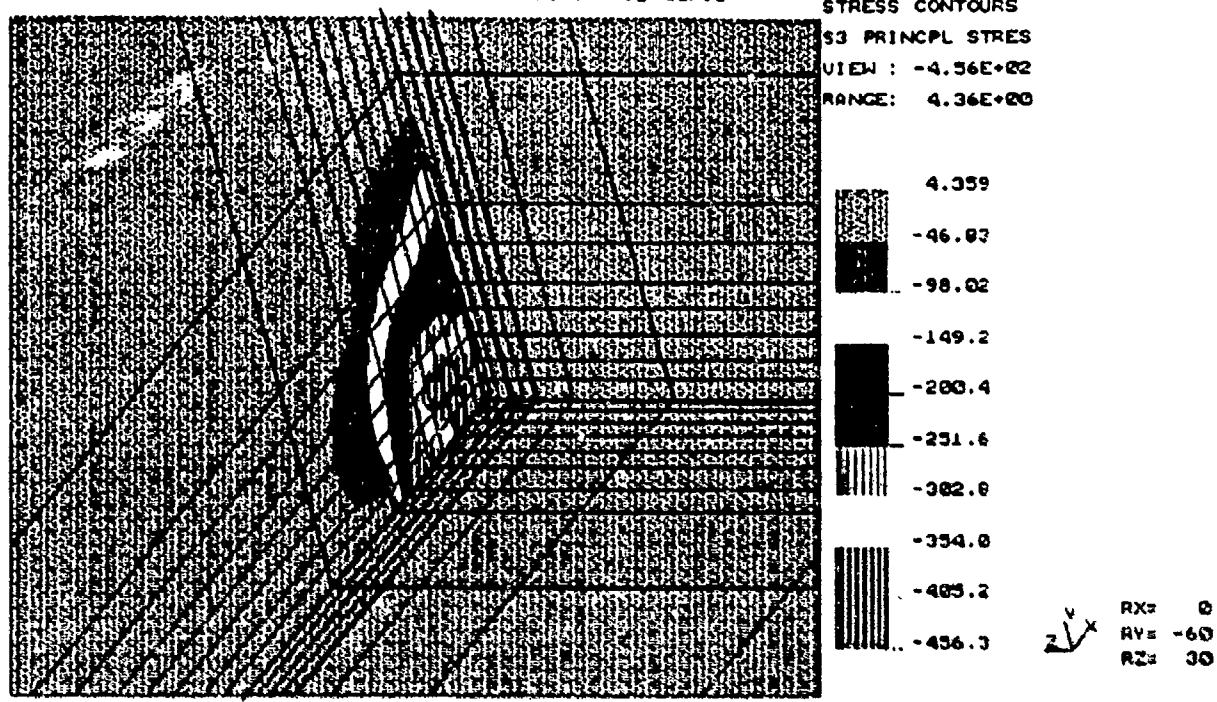


Figure 4-21. Top Slab Stresses ("Extended" Slab) - B-747 Dual-Tandem Gear

Table 4-5. Effects of Slab Area Modeled (Interior Case)

Response	Slab Area 15 x 15 ft	Slab Area Extended	Change Δ
Max slab deflection (at CL):	-0.094 in.	-0.083 in.	-12 percent
Max slab tensile flexure, s_y :	430 psi	405 psi	- 6 percent
Max base/slab pressure, s_z :	~ 10 psi	~ 9 psi	--10 percent

If we extrapolated the results of this study to gain some insight into the behavior of the same pavement system under projected super heavy aircraft loads, which for example, could be 50 percent greater than the existing 747, (assuming same gear geometry with a 50 percent tire pressure increase,) we can obtain a quick insight into the effects of such an aircraft on such a pavement system. As shown in Table 4-7, maximum slab deflections could increase to approximately 1/8 in. Maximum slab flexural tensions could exceed 600 psi, sufficient to cause concern for flexural cracking in 5,000 psi concrete (f'c). Subgrade pressures could increase to the 15 psi range. This result suggests that nonlinear representation of subbase and subgrade layers might be warranted, in particular with a typical stress softening subgrade. The slab stresses and deflections could further increase, with the possibility of permanent settlements. An analysis using a nonlinear representation of the subgrade would be required to confirm the effects of this 50 percent increase in gear load; however, using this economical example still gains valuable insight into the potential behavior of an existing airport pavement with new aircraft load. Similarly, it would be straightforward to investigate the effects of larger tire and gear dimensions for such an aircraft, in which the gear size and tire footprint are increased accordingly, with corresponding decrease in tire pressure. Boeing Aircraft is today considering the use of 200 psi, larger tires for its projected double-deck 747 in the weight range of 1.3 million lb or higher. One important consideration is the desire not to increase the rating of such an aircraft on existing airport pavements, using present day rating methods. However, using the 3-D FE approach, it is possible that a limited pressure increase, with corresponding reduction in gear size and weight, could be accommodated by existing airports.

Table 4-6. Extrapolation to 1,160,000 lb Aircraft Using Same Gear Configuration and 300 psi Tire Pressure on Existing Runway

	B-747-200	"Super-Heavy"
Max Slab Defl. (d)	0.083 in.	0.125
Max Slab Tension (y)	405 psi	608 psi*
Max Subgrade Pressure (z)	~10 psi	~15 psi
*Tensile failure in 5,000 lb concrete		

This FE model was executed in approximately the same time as the previous case: approximately 6 minutes for the 486/33 PC workstation. This shows that a practical response

model can be run in a very reasonable time, and can quickly and economically furnish useful results.

4.5 3-D Application to Edge-Loaded Pavements - Linear and Nonlinear Response

The 3-D FE method was also evaluated for application of edge-loaded cases, which would include jointed pavements. Our studies here included first another verification of the Foster-Miller 3-D FE representation with earlier USAF work by Ioannides [1], during the mid 1980s. As in previous examples, a relatively thin 8-in. PCC slab was modeled atop a "soft" subgrade, the latter with modulus of 7,700 psi. A 30,000 lb F-15 single wheel load was applied parallel to and adjacent to a free slab edge, typical of an idealized edge-type load case.

A plan view of this model area is shown in Figure 4-22.

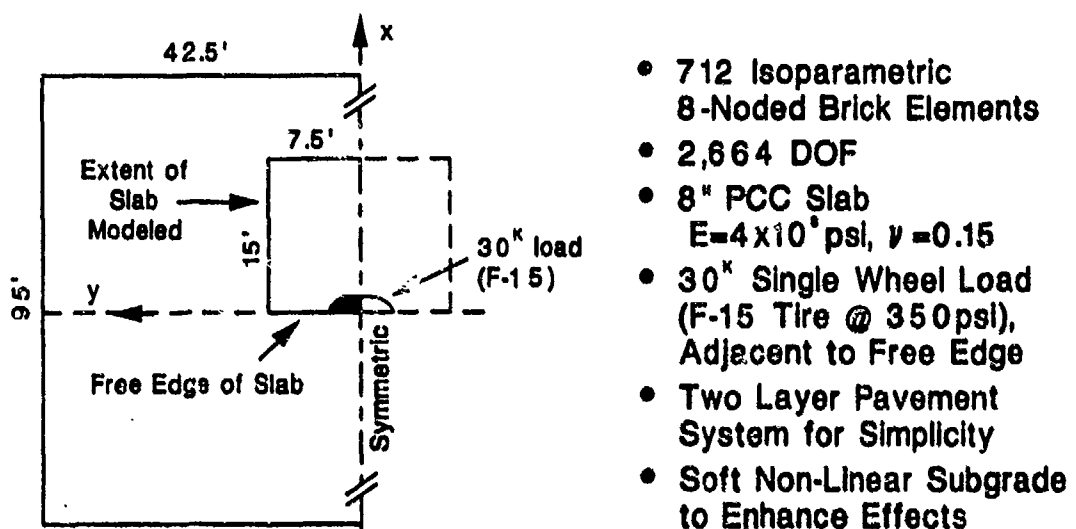


Figure 4-22. 3-D FE Model Area for Edge-Load Case

We can see that here, only one plane of symmetry can be used. The single wheel load of 30,000 lb is shown at the center of the model, which is the intersection of the free slab edge and the plane of symmetry.

An overall view of the FE model is shown in Figure 4-23.

Four work equivalent loads at corners of the element closest to the center are used for the 350 psi tire, totaling 15,000 lb for the model half.

A detailed view of the central area of the FE model is shown in Figure 4-24. Here the 8-in. thick slab is again modeled by only two layers of isoparametric 3-D brick elements. The base and subgrade are shown by a succession of layers increasing progressively in thickness, starting with two 6-in. layers followed by an 18-in. layer, etc. down to the 40-ft level, at which point the model is terminated. Again, the locations of interest are shown at the center of the model, including vertical deflection, slab flexural stress, and vertical subgrade pressure beneath the slab. Note that in this model, the mesh was elongated parallel to the direction of the tire travel, in an effort to assess the effect of "economizing" on the mesh in this direction.

This FE model included 712 isoparametric 3-D brick elements, with 2,664 DOF including boundary conditions. This single run using the demonstration NISA model took 18 minutes on a 386/25 desktop PC, and 6 minutes on a 486/33 desktop PC. The earlier USAF studies under USAF contract, using the GEOSYS FE program with the same mesh configuration, took 2.5 hours on the Harris 800 virtual memory computer, again indicating the rapid increase in processing speed available with improved desktop and workstation computers, and also with the use of advanced 3-D FE solution techniques.

The results of the Foster-Miller FE analysis are compared in Table 4-7 with earlier GEOSYS runs, as well as with the ILLI-SLAB 2-D and closed form solutions [3] that approximated this configuration. This shows excellent agreement with the earlier 3-D finite element work except that for slab stresses, the interpolation procedures needed to obtain stresses at the corners of the central element indicate that a finer mesh would be required to obtain better depiction of these local slab stresses directly under the load. The other 2-D and closed form applications are really quite approximate in terms of their stress and deflection because they are fundamentally axisymmetric type solutions adapted to the non-axisymmetric conditions of the edge-loaded case. However, the solution technique used here was sufficiently close to the earlier work that the verification of the method is considered satisfactory.

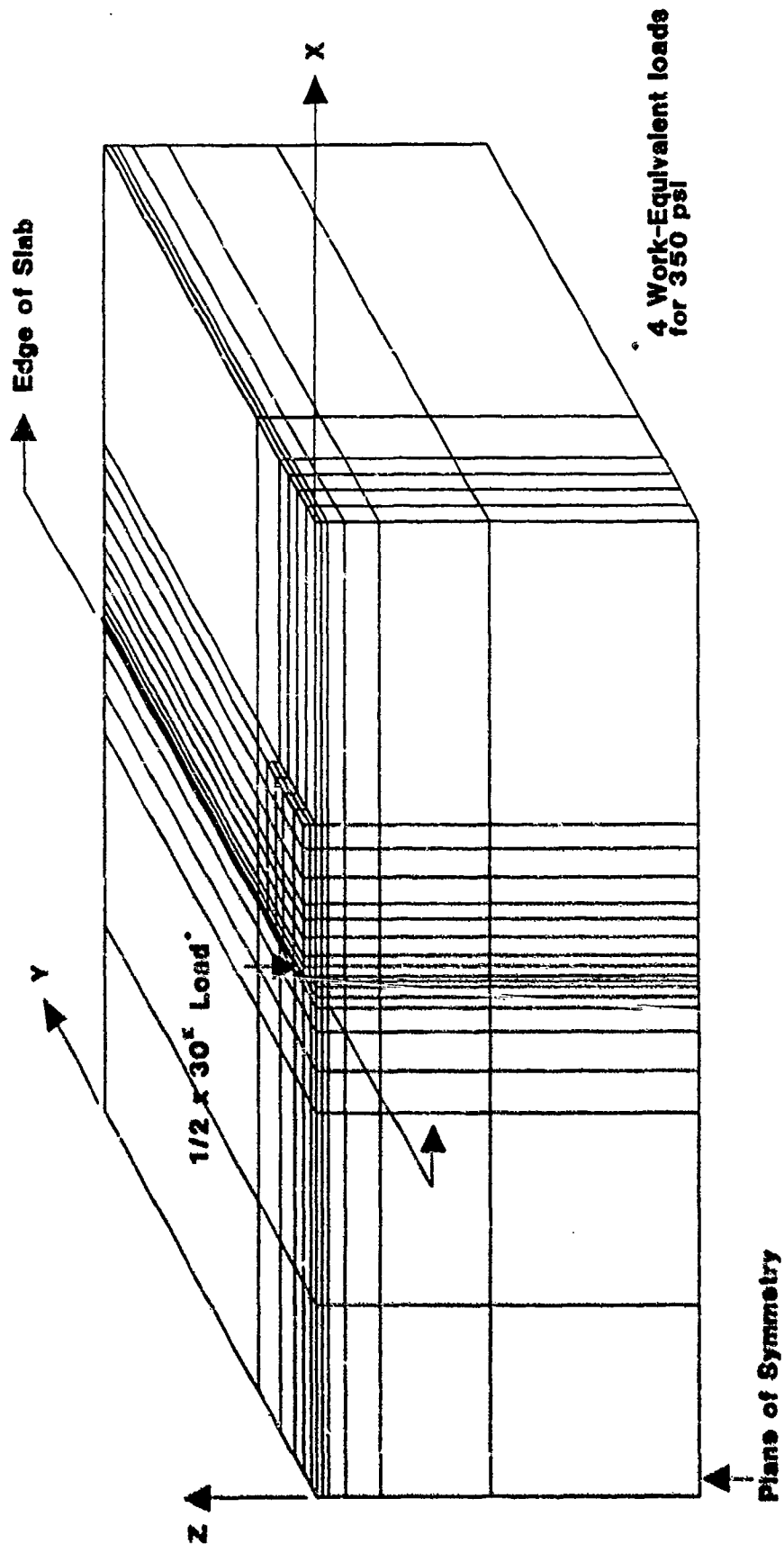


Figure 4-23. 3-D FEM for Edge-Load Case 8-inch Slab with Single 30K Wheel Load

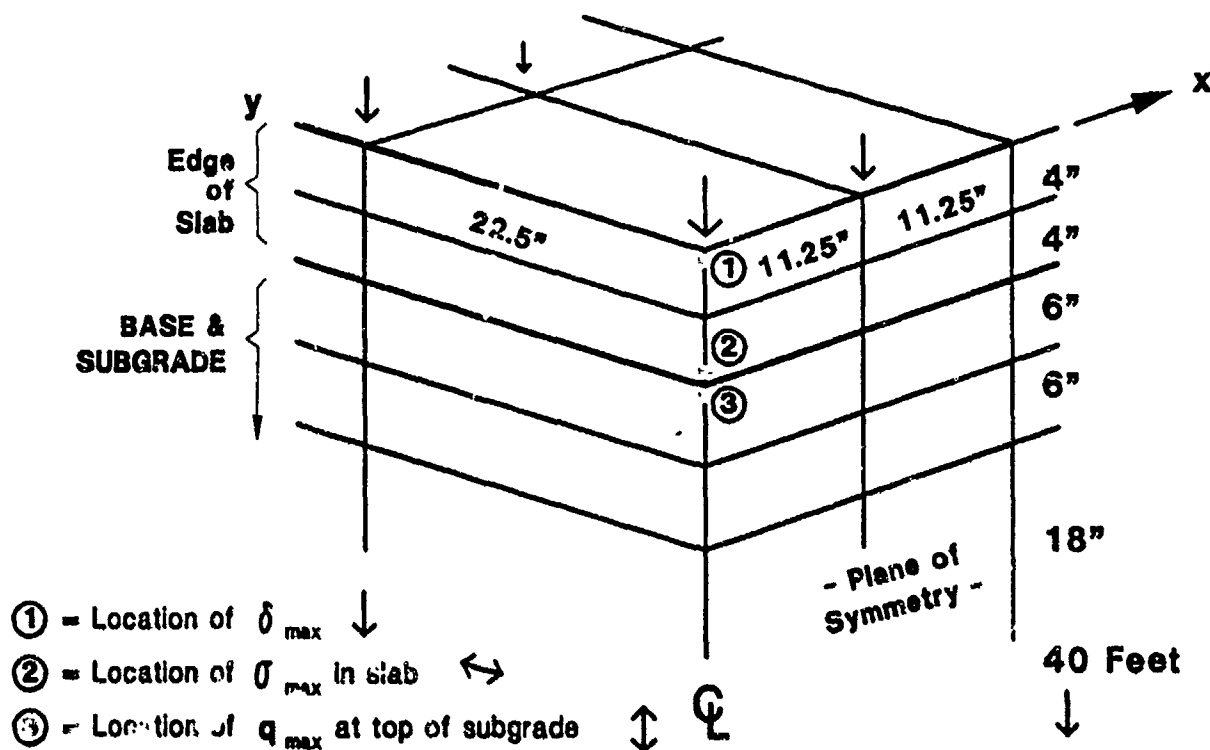


Figure 4-24. 3-D FE Model - Detail at Center (Edge-Load Case)

Table 4-7. Comparison of Results for Edge-Load Case

	d slab, max (in.)	q subgrade, max (psi)	z slab, max (psi)
Foster-Miller NISA Model	.063	24.7	769
GEOSYS (USAF) 3-D	.063	24.6	826
ILLI-SLAB 2-D	.066	58.8	1181
Closed Form Solution*	-	-	1056
*H51S using automated equivalent of Pickett & Ray			

In Figures 4-25 and 4-26 selected pavement system responses are shown using advanced graphical post processors with 3-D color* depiction of deflections and stresses. In Figure 4-25, an isometric view of the vertical displacement contours is shown. In Figure 4-26 the inplane slab flexural stresses are shown, in which the remainder of the model is removed for clarity. The stress distribution in the slab is clearly evident, and with a closer look the variation through the thickness could be highlighted.

In summary, this shows the value of the 3-D formulation for actual situations which are not well represented in 2-D. This type of global response model could also incorporate the restraining action of adjacent slab (using effective spring rates from a more detailed model of the joint/dowel area) to better represent the behavior of actual slab sections used in airport pavements.

4.6 3-D Finite Element Pavement Analysis for Nonlinear Subgrades

The Unified Pavement Analysis method must accommodate some form of nonlinear formulation especially for subbase and subgrade layers. In the following study, we have evaluated the 3-D FE method applied to examples of edge-loaded pavements, using two different simple nonlinear formulations presently available for subgrade modulus. In these demonstration examples, we have used internal iteration and convergence procedures in nonlinear static analysis to perform the response solution in a single run. (This can be compared to the earlier USAF/Ioannides work in which separate runs for each GEOSYS iteration were used.) In general deviator stress** is evaluated in each element at each step in the iteration. Then, the reformulated element stiffness matrix based on the updated modulus (as a function of deviator stress) is formed, transformed into a new global stiffness matrix, and then banded for solution, followed by the next iteration step.

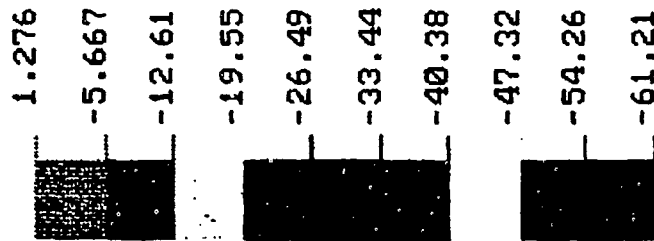
* Originals @ foster-Miller.

** Here, deviator stress is used as $\sqrt{3J_2D}$, in which J_2D is the second deviatoric stress invariant.

EMRC - DISPLAY II POST-PROCESSOR VER 90.0 Feb/12/91

DISPL. CONTOURS
Z - DISPLACEMENT
VIEW : -6.12E-02
RANGE: 1.28E-03

(Band * 1.0E-3)



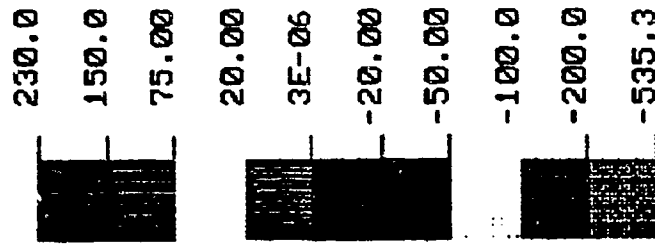
$\begin{matrix} Y \\ \swarrow \\ Z \end{matrix} X$
 RX= 0
 RY= -60
 RZ= 30



Figure 4-25. 3-D Vertical Displacement Contours (Linear Subgrade)

EMRC - DISPLAY II POST-PROCESSOR VER 90.0 Mar/ 1/91

STRESS CONTOURS
 SYY - STRESSES
 VIEW : -5.35E+02
 RANGE: 1.98E+02



RX= 0
 RY= 120
 RZ= 30

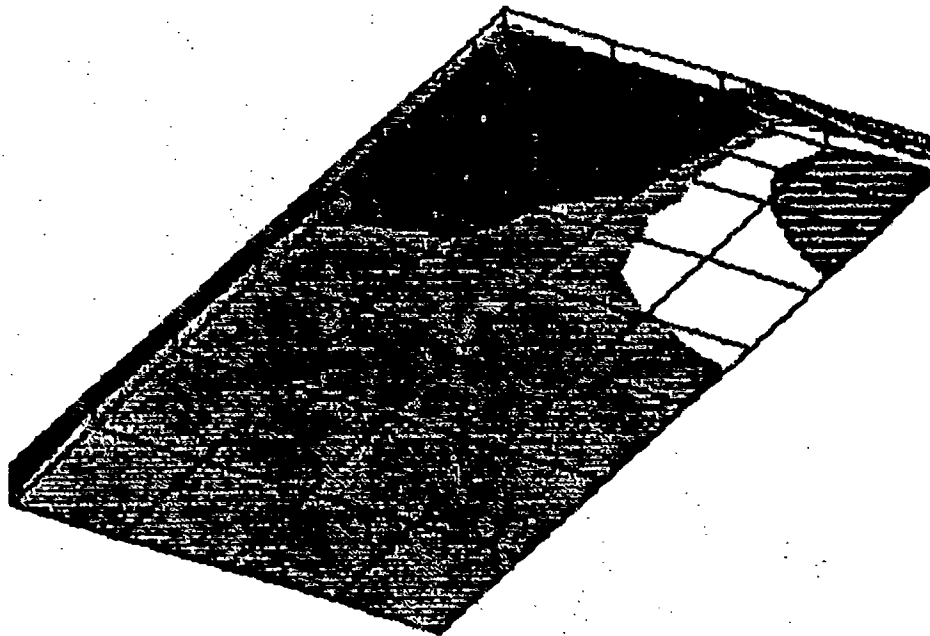


Figure 4-26. 3-D Flexural Slab Stresses (Parallel to Edge, Linear Subgrade)

In the Foster-Miller studies we obtained good agreement with the GEOSYS studies for vertical deflection, subgrade pressure beneath the slab, and slab flexural stresses by using, as a benchmark for the average of the second and third GEOSYS iterations. This was the procedure determined by Ioannides in the earlier studies to represent an accurate estimate of the final converged value. Note that in our studies, this procedure was not necessary, since iteration proceeded automatically to a converged solution.

A depiction of a simple resilient modulus type of stress dependent subgrade modulus is shown in Figure 4-27. Here, the maximum modulus value of 7,700 psi, used previously in the linear analysis examples, remained at values for deviator stress at or below 2 psi. The resilient modulus then decreased linearly with deviator stress, and remained at a minimum value of 3,000 psi for deviator stresses of 6.2 psi and above.

Solution of this problem took a total of 6 hours on a 386/25 PC desktop minicomputer, including all automatic iteration steps. This same run takes 2 hours on a 486/33 PC workstation, and we estimate that it would take 40 minutes on a RS6000 Unix-type workstation. By comparison, the earlier USAF studies using the GEOSYS FE program on the Harris 800 virtual memory computer, were performed in five iterations of 2.5 hours each for a total of 12.5 hours running time. This demonstrates the considerably greater speed and shorter running time possible with modern workstations, which trend is expected to continue.

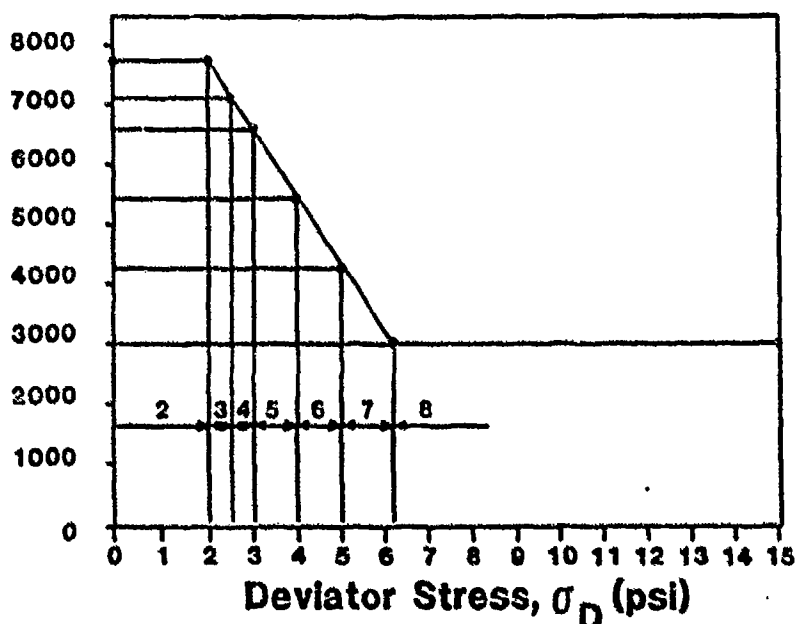


Figure 4-27. Simplified E_R versus S_D Relation for "Soft" Subgrade Used In FEM Analysis

The results of this nonlinear analysis can be compared to the previous linear analysis of the edge-load case in Table 4-8.

Here it can be seen that the stress softening behavior of the subgrade led to increases in the maximum slab deflection, and in maximum slab flexural stresses of approximately 7 to 8 percent compared to the case with non-softening linear subgrade. Subgrade maximum pressures under the load decreased over 20 percent, reflecting the expected greater load transfer to the slab with stress softening behavior.

Also, for purposes of verification of the Foster-Miller FE analysis, comparison was made of our results versus the GEOSYS nonlinear finite element analysis, and this is shown in Table 10. Good agreement was obtained within a few percent, for both slab deflection and slab flexural stresses. Agreement was not exact since in the present demo NISA code the resilient modulus behavior had to be represented by a variable deviator stress-versus-strain curve which is not rigorously equivalent.

Table 4-8. Comparison of Results Nonlinear versus Linear Subgrade (Edge-Loading)

	d slab, max (in.)	q subgrade, max (psi)	s slab, max (psi)
Linear Subgrade (Previous Example)	0.063 in.	24.7 psi	769 psi
Nonlinear Stress-softening Subgrade	0.068 in.	19.5 psi	815 psi
Change	+8%	-23%	+7%
Note: Max Nonlinear Modulus = Linear Modulus Value			

**Table 4-9. Comparison of Foster-Miller versus GEOSYS Results for
Nonlinear Subgrade**

	d slab, max (in.)	q subgrade, max (psi)	s slab, max (psi)
Foster-Miller NISA (single run)	.068	19.5	815
GEOSYS (multiple runs)	.066	19.0	890

A last comment on the greater running time required for nonlinear analysis, which is typical of the solution procedures and convergence checks required is that the Foster-Miller analysis times may be further reduced 30 to 50 percent through variable spacing of fewer pseudo time points. This would involve a gradual reduction in the intervals of the pseudo time load iteration steps as convergence was approached in the solution. In the present analysis, 10 equally-spaced intervals were chosen for simplicity.

The pavement system response can again be quickly and effectively visualized using 3-D color* available at Foster-Miller graphic post processors. In Figure 4-28 we see the isometric view of vertical displacements throughout the pavement system, highlighting the response of the loaded area. In addition, the flexural stress distribution in X and Y directions, (perpendicular and parallel to the free edge, respectively) is shown in color contour plots in Figure 4-29 and 4-30. Here the slab was again isolated from the remainder of the model for clarity.

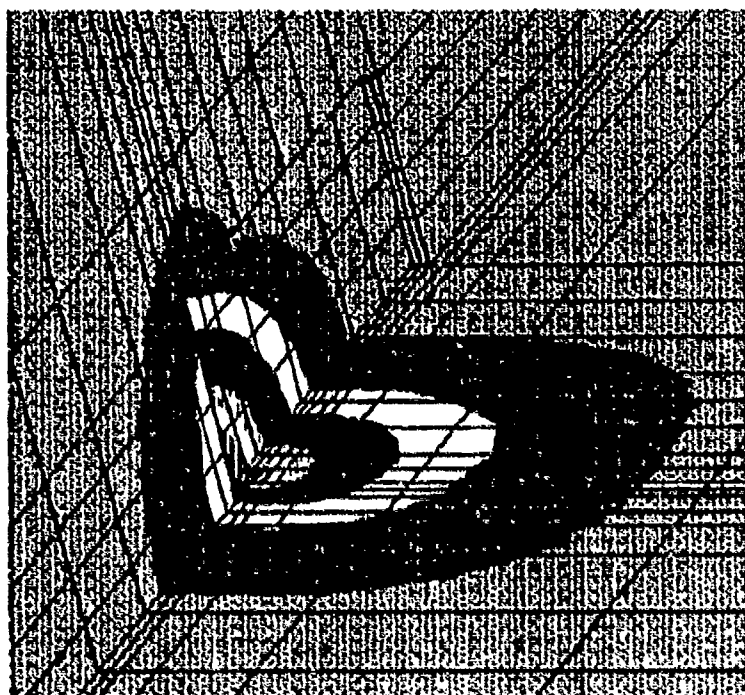
4.7 Alternative Nonlinear Subgrade Representation

We made an additional analytical study of the edge-loaded slab using a different representation of the soft nonlinear subgrade. In this analysis, we included a stress softening subgrade behavior as in the previous example, but we used a nonlinear deviator stress/strain curve representation in which a linear region transitioned gradually to a region of linear hardening, with the same general overall stiffness response as in the previous example. This provided a more realistic representation of continued stress softening with load since the previous case led to a deviator stress-strain curve that was not smoothly varying in the region of transition to the constant

* Available @ Foster-Miller.

minimum modulus value. This depiction is shown in Figure 4-31. There is a curved transition region from linear to linear hardening areas as shown, corresponding to the ramp in the resilient modulus curve in the previous case.

ENRC - DISPLAY II POST-PROCESSOR VER 90.0 May/21/91



DISPL. CONTOURS
Z - DISPLACEMENT
VIEW: -6.76E-02
RANGE: 1.29E-03

(BASE: 0.1000E+01)

1.286

-6.367

-14.02

-21.67

-29.33

-36.98

-44.63

-52.29

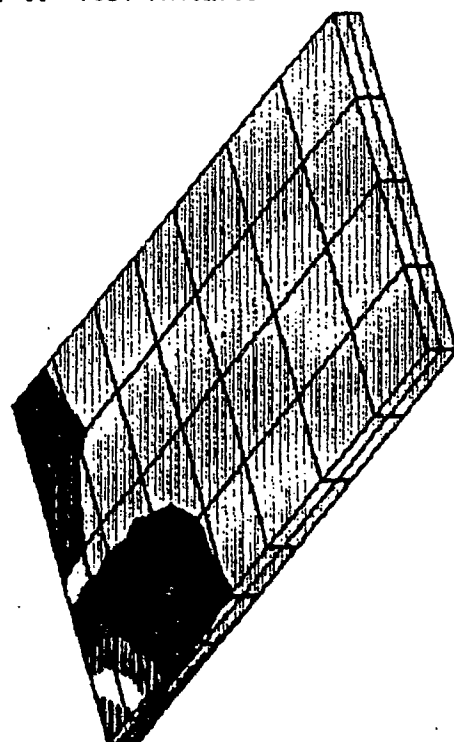
-59.94

-67.59

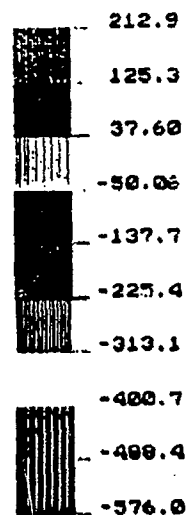
TIME: 0.10000E+01

RX= 0
RY= -60
RZ= 30

Figure 4-28. 3-D Vertical Displacement Contours: Edge-Loaded Slab with Nonlinear Subgrade



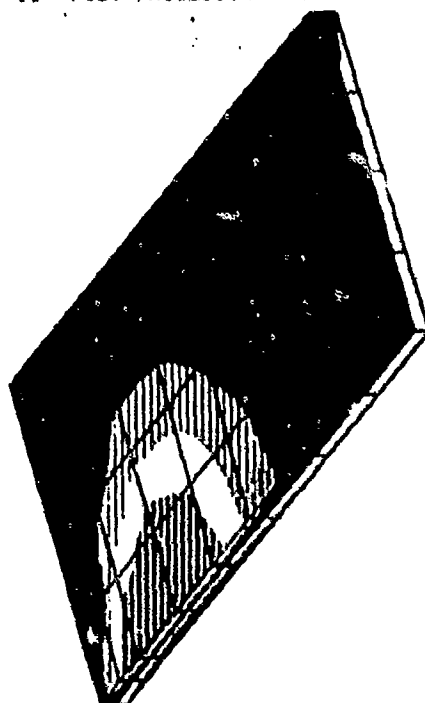
STRESS CONTOURS
SVY - STRESSES
VIEW : -5.76E+02
RANGE: 2.13E+02



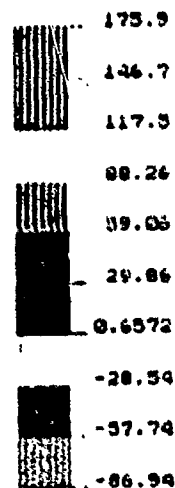
TIME: 0.10000E+01

RX= 0
RY= -60
RZ= 30

Figure 4-29. Distribution of Flexural Stresses Parallel to Edge - Nonlinear Model



STRESS CONTOURS
SXX - STRESSES
VIEW : -8.69E+01
RANGE: 1.74E+02



TIME: 0.10000E+01

RX= 0
RY= -60
RZ= 30

Figure 4-30. Distribution of Flexural Stresses Normal to Edge - Nonlinear Model

Also, an important new evaluation was made here of the effect of multiple loading and unloading cycles on the response model performance and computer running time. This is depicted in Figure 4-32 in which the five events are schematically indicated on the chart, showing successive loading and unloading cycles through three loading and two unloading events. Each of these events corresponded internally to a new nonlinear analysis, containing 10 load steps per event. (Although this is not a dynamic analysis, these load steps are referred to taking place sequentially in "pseudo time".) Also, in addition to contour graphics, we used the post-processing capability of the demo program system to follow certain deflections and stresses through the history of the load/unload cycling.

It should be noted that this entire five-event nonlinear analysis was accomplished in a *single run* without user intervention.

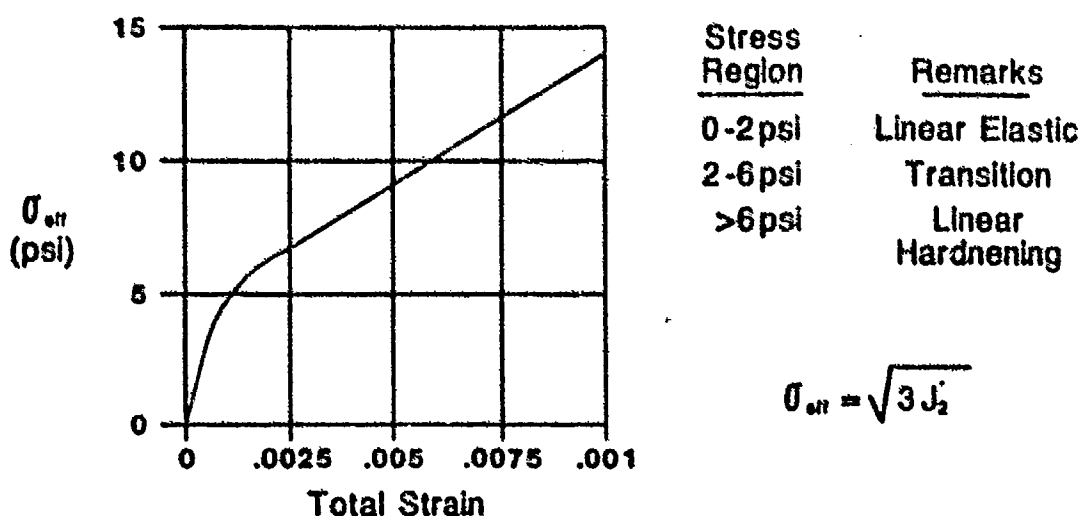


Figure 4-31. Elasto-Plastic Nonlinear Subgrade with Transition to Linear Hardening

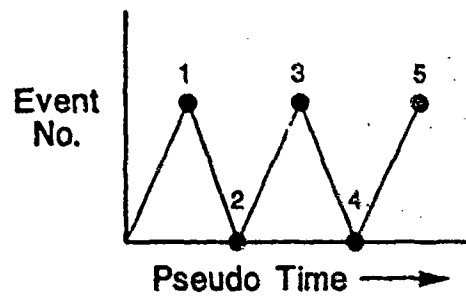


Figure 4-32. Elasto-Plastic Nonlinear Subgrade with Transition to Linear Hardening

This edge-loaded nonlinear pavement model, identical to that used in the previous case contained 2,644 DOF. Using the 486/33 PC desktop workstation, average time per load step was approximately 18 minutes, compared to 6 minutes for a purely elastic analysis. Each load step included 3 to 5 Newton-Raphson iterations, as determined automatically in the program by internal convergence criteria. As can be seen in Figure 4-33, the total solution time for all five events with 10 loads step per event was in the region of 15 to 16 hours. However, we believe that the number of load steps per event could be reduced by at least 30 to 50 percent by optimizing the load step spacing and number within each event, with solution times reduced proportionally.

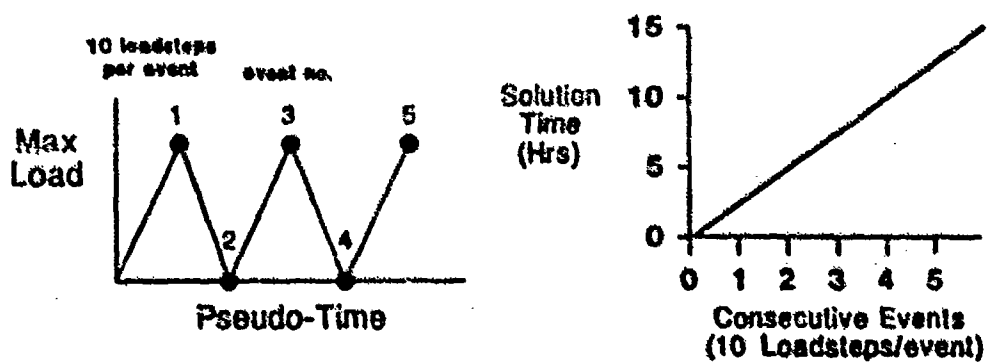


Figure 4-33. Solution Times on PC Workstations

Some results from this study are shown in Table 4-10. The maximum vertical deflections down through the pavement system are shown for the first load and the following unload cycle. The maximum vertical deflection in the slab at the first load (Event 1) was similar to that in the previous case. Here we have also monitored the vertical deflections proceeding down through the pavement system and it can be seen how these deflections decrease with depth. After Event 2, which was the first unload cycle, residual vertical deflections remained. These range from 0.006 in. near the top of the subgrade with corresponding smaller permanent settlements proceeding down through the pavement system. A 3-D isometric color plot* of the vertical deflections are shown in Figure 4-34. Here the slab area and the pavement system in the vicinity of the slab has been highlighted. Figures 4-35 and 4-36 show distribution of flexural stresses in the slab parallel to, and normal to the edge as one in the previous cases, and likewise these show that the flexural slab stresses in the edge-loaded slab would differ significantly from stresses calculated by any form of axisymmetric approaches, demonstrating the advantage and the utility of full 3-D modeling of these situations.

Table 4-10. Deflection Results - First Load/Unload Cycle

	Event 1 Max Load	Event 2 Unload
Max Vertical Deflection in Slab (at CL)	.068 in.	.006 in.
Vertical Deflection in Subgrade (at CL)		
6 in. depth	.055 in.	.004 in.
12 in. depth	.044 in.	.003 in.
30 in. depth	.030 in.	.002 in.

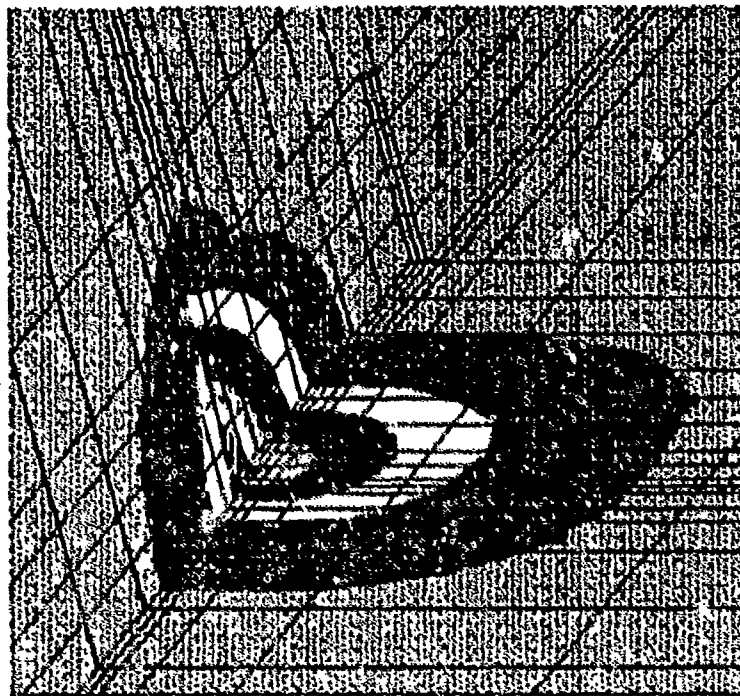
Another helpful way to visualize the results is to view the deflected shape of the pavement system via a deflected "wire frame" model. This is shown in Figure 4-37 in which the elevation view of the free edge of the slab and the subgrade region in that vicinity are shown both in their original and deflected positions. (This corresponds to the first load cycle). Note that the subgrade beneath the free edge is attempting to move laterally away from the edge when vertical wheel load is applied. This is consistent with previous experience for this type of pavement system. There is a potential incompatibility of the subgrade and the slab at the point where the free edge bears on the subgrade, since there is a mathematical singularity at this point. This shows that careful attention must be paid to the FE modeling and these interfaces in order to better represent the real physical situation. In an actual airport pavement system, two adjacent slabs might be joined by keyway or

* Available @ Foster-Miller.

dowel bar type (bridging) structural elements. This would reduce the relative deflection of one slab compared to its adjacent slab on the other side of the joint, possibly reducing the effect of this incompatibility. However, these observations suggest the need for proper boundary elements (linear or nonlinear) at the pavement/subbase interface which could require the incorporation of a frictional interface element.

Another informative look at the subgrade deflections can be made via a color history plot* using the pseudo time deflection response. In Figure 4-38, the horizontal deflections normal to the free edge proceeding downward through the pavement system from the slab are shown, following the load and unload cycles.

ENRC - DISPLAY II POST-PROCESSOR VER 90.0 May/21/91



DISPL. CONTOURS
Z - DISPLACEMENT
VIEW : -6.76E-02
RANGE: 1.29E-03

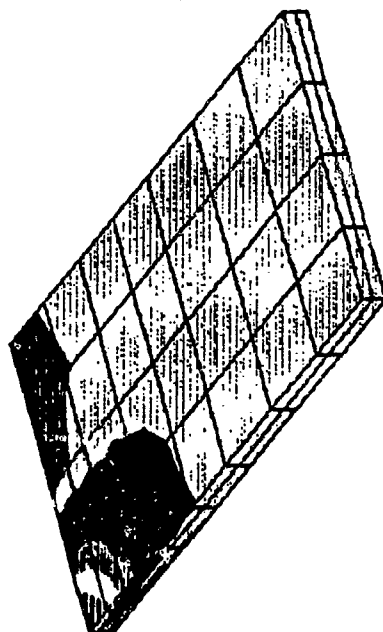
(Basis = 1.0E-1)

1.286
-6.367
-14.02
-21.67
-29.33
-36.98
-44.63
-52.29
-59.94
-67.59

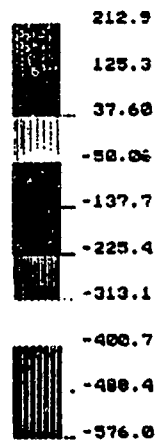
TIME: 0.10000E+01

$\begin{matrix} V \\ X \\ Z \end{matrix}$
 RXs 0
 RVs -60
 RZs 30

Figure 4-34. Vertical Displacement Contours for Edge-Loaded Slab with Nonlinear Subgrade No. 2



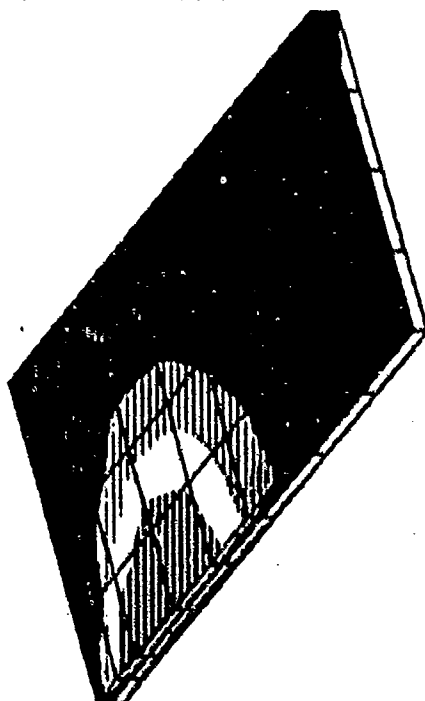
STRESS CONTOURS
SVY - STRESSES
VIEW : -5.76E+02
RANGE: 2.13E+02



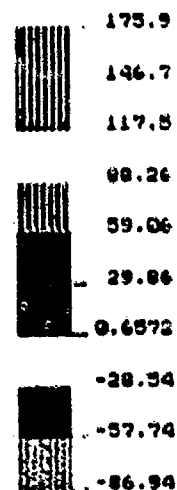
TIME: 0.10000E+01

RX= 0
RY= -60
RZ= 30

Figure 4-35. Distribution of Flexural Stresses Parallel to Edge - Nonlinear Model No. 2



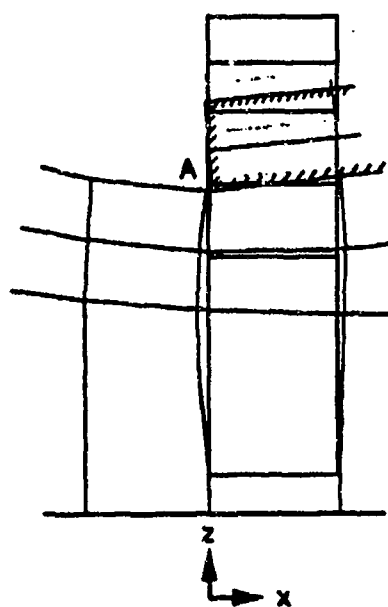
STRESS CONTOURS
SXX - STRESSES
VIEW : -8.69E+01
RANGE: 1.76E+02



TIME: 0.10000E+01

RX= 0
RY= -60
RZ= 30

Figure 4-36. Distribution of Flexural Stresses Normal to Edge - Nonlinear Model No. 2



- Lateral Expansion of Subgrade with Vertical Compression Under Slab Edge
- Potential Local Subgrade Incompatibility with Slab at Point "A"

Figure 4-37. View of Deflected Shape at Slab Edge

Vertical subgrade stresses can be followed in a similar manner, as can be seen in Figure 4-39. The nonlinear response in this particular case is confined mostly to the first load cycle, in which permanent sets in the horizontal direction are exhibited. Naturally, the magnitude of the deflections and the permanent sets decreased with depth.

When the subgrade vertical pressure directly beneath the slab through the first load and unload cycle was evaluated, it was found after the first unloading (at the conclusion of Event 2), a residual vertical "tension" of 4 psi remained at the interface between slab and subgrade. This was due to the simple modeling of the interface as being able to equally withstand compression or tension equally. However in a real situation, this showed that there would be a potential for separation of the slab and subgrade since lost cohesion would normally be expected at this interface. This suggests that eventually a void could form under the slab for this loading situation. Further development of the proper type of nonlinear interface elements would be required to give a better, more accurate representation of this behavior, but this relatively straightforward analysis quickly highlights potential problem areas in the pavement system. It would be also be productive to include the restraint of an adjacent slab, joined by the appropriate dowels or keyway and using nonlinear springs, to evaluate the pavement system response at this point. It would be anticipated that this would help reduce the potential settlement void.

This behavior can also be highlighted by a quick look at the vertical stress history plot down through the system directly beneath the load in Figure 4-39. At the level representing the vertical "tension" displayed. (Note that the stress convention used in the computer plots is the normal stress analysis convention in which tension is positive; however, in most conventional soil mechanics and geotechnical work, compression is normally assumed positive.)

4.8 Conclusions

These studies with nonlinear subgrade representations, although somewhat over-simplified at this point, from the point of view of constitutive modeling show how even an approximate representation of known nonlinear behavior can lead to a quick preliminary evaluation of the behavior of the pavement system. Coupled with the relatively clear three-dimensional color plots of deflection, stress, and strain, we can see how these early analyses can point the way towards the need for further work, for example in interface element modeling, and in improving the constitutive representations of the base subgrade, and flexible pavement layers.

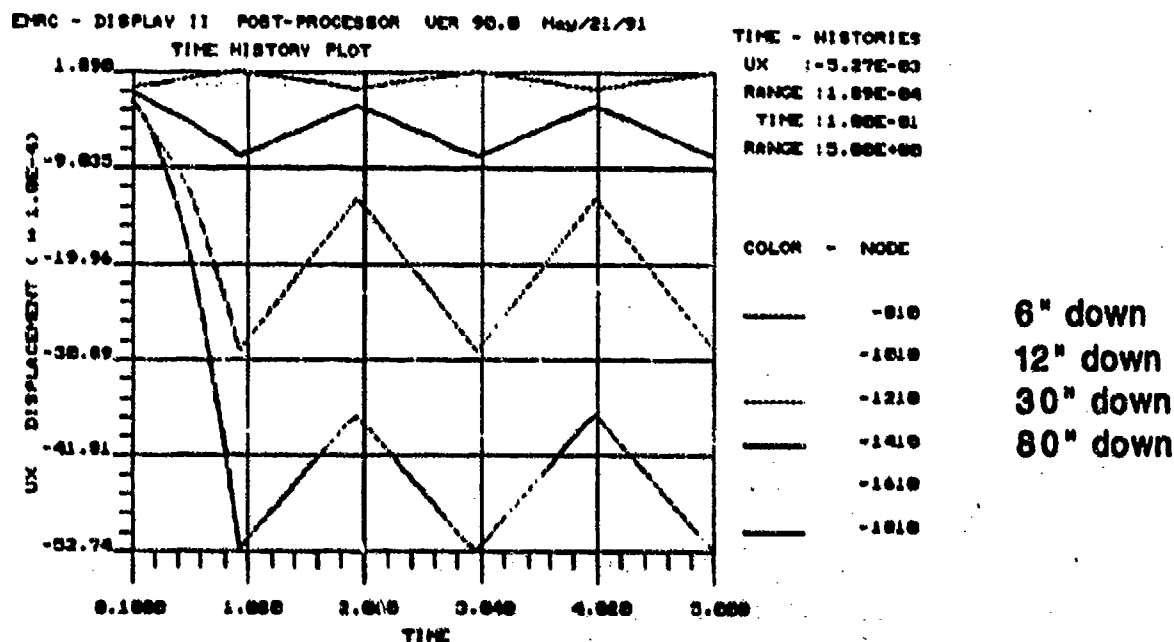
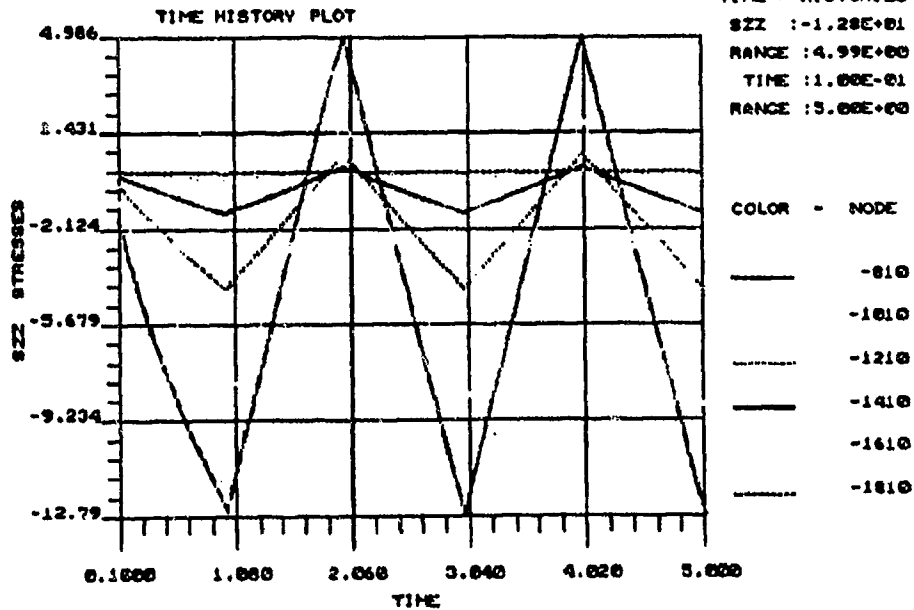


Figure 4-38. Horizontal Subgrade Deflections Normal to Edge - Nonlinear Case No. 2



Subgrade Depth
Below Slab

6" down
12" down
30" down
80" down

Figure 4-39. Schematic Vertical Stress History - Down Through System at CL (Nonlinear Case No. 2)

Also, although present solution times on desktop workstations do extend for several hours, the continued rapid increased in speed and further development of nonlinear solution procedures will afford significant gains for such analysis, even for larger, more complex models.

5. Overall Accomplishments of Foster-Miller 3-D Finite Element Studies

First, these FE studies have shown the validity of guidelines developed earlier using dimensionless parameters [1] which incorporate the relative stiffnesses of the pavement system elements. These guidelines can be used to develop a progressively coarser mesh sizes with depth and in the lateral directions to most economically represent the pavement system.

Secondly, the FE models described earlier are of a representative complexity which give usable results for real pavement systems, and have been shown to have reasonable solution times on modern desktop PCs and workstations. Further increases in computational speed, refinement of solution techniques, and available memory size, are anticipated as the state of the art continues to rapidly progress for this hardware. Also, a better understanding of the spacing of load steps in nonlinear analysis will yield further savings.

Thirdly, we have shown how to effectively utilize the 3-D FE approach with the ability to rapidly evaluate the pavement response via a specialized system of post-processors which furnish a graphical depiction of their response. The 3-D representations are particularly helpful for the pavement engineer. Note that in the previous studies, much of the insight as to the structural behavior was obtained via the use of these methods.

These studies showed that even with a simple starting point for material constitutive relationships, meaningful evaluation of pavement system behavior can be made. However, it is clear that much needs to be done to incorporate more accurate material representations. This is especially true for the behavior of typical base, subbase and subgrade materials. Along with these FE studies, the Foster-Miller program has incorporated some new work which will be discussed in the following sections. Although this work has not yet been incorporated into the FE method, we anticipate that in the next phase a coordinated effort will be made to progressively incorporate the appropriate stress-dependent constitutive relations into the FE solution method in such a way that the value of each new enhancement of the properties can be related to the previous stage of development.

5.1 Near-Term Follow-On Work for Demonstration Cases Above

The incorporation of nonlinear subgrade behavior can be extended to the multiwheel wide body landing gear case shown earlier. This could incorporate a Mohr-Coulomb failure law, plus a

linear hardening "cap" for the subgrade material. Similar representations for both the compacted, stabilized base and the subgrade can also be included.

To show the value of the 3-D FE analysis method for evaluation of new aircraft tire loadings on modern airport pavements, the studies above could be extended to include a super-heavy aircraft having conventional, larger 200 psi tires arranged in a larger dual-tandem footprint. These results could be compared with the case cited earlier in which only a scale-up of tire pressure was made to carry the 50 percent increased load. Here, the graphical representations of pavement response could be used to quickly visualize the difference in effect between these two landing gear configurations.

Also, work on the edge-loading configurations could be expanded to cases in which an adjacent slab is included next to the existing free edge, representing a joint. This joint could incorporate dowels or reinforcing bars using nonlinear springs, and this, in turn, could be used to evaluate the difference in pavement system response for various simple joint configurations. These results could be compared to the traditionally used design charts, in which an arbitrary percent of restraint of the adjacent slab is used. Again, the graphical output capability would be valuable in assessing the pavement response. These studies could include both linear subgrade and simplified nonlinear subgrade constitutive relations, as well as representative multiwheel gear trucks.

A final valuable area for near-term investigation could include a resolution of the slab/subgrade compatibility problem mentioned earlier. Interface elements incorporating a nonlinear frictional response at the interface of the paving and subbase or subgrade layers could be used to evaluate the degree of refinement that is meaningful to provide a reasonable depiction of actual response down through the pavement system. This study could be integrated with the joint studies cited above, to gain some insight into the actual behavior of the system beneath the joint. Although it can be argued that the constitutive relationships presently on hand for the base and subbase materials need substantial further development, nevertheless these FE techniques can be economically and efficiently used to begin a rational study of this important area of pavement system behavior.

5.2 Pavement System Response Model Development

While for the present studies, NISA 90.0 was used to demonstrate that 3-D analysis for typical airport pavement configurations is practical with careful use of FE techniques, the overall objective of the program will be to produce a specific pavement response model tailored for use by

government and industry. All of the essential elements of the FE solution procedure, however, are available in open literature and are familiar to the Foster-Miller team.

The important constituents of this response model will certainly include the use of "prepackaged" FE model mesh layouts suitable for various pavement configurations, appropriate selection of some material constitutive and failure models, essential static, quasistatic, and visco-elastic solution procedures, and vital post-processing and data display modules to produce the graphical 3-D output. It should be noted again that dependency on existing general purpose FE programs is not required. These general purpose programs have many features and capabilities which are not required for the pavement response model; conversely, the important constitutive relations for the various pavement system materials are not present in any known general purpose FE model and will be developed specifically for the pavement system requirements.

To summarize:

- a. Stiffness matrices for 3-D isoparametric elements are available today in explicit form.
- b. Efficient solution techniques have been widely developed and are under continuous refinement at Foster-Miller.
- c. Standard pre- and post-processors can be either obtained or developed, and will be integrated into the solution package.
- d. With an additional dedicated effort to incorporate constitutive and failure material representations, we can now develop a 3-D pavement analysis system for use by government and the design community.

6. References

1. Ioannides, A.M., M. R. Thompson, et.al. "Three-Dimensional Finite Element Analysis of a Slab of Stress Dependent Elastic Solid Foundation," prepared for USAFOSR/AFSC by the Transportation Research Laboratories, University of Illinois Department of Civil Engineering, Urbana, IL, October 1986.
2. Han, D.J., and W.F. Chen, "Strain Space Plasticity Formulation for Hardening-Softening Materials with Elasto-Plastic Coupling," *Ing. J. Solids and Structures*, Vol. 22, 1986.
3. Pickett, G. and K.G. Ray, "Influence Charts for Concrete Pavements," *Trans. ASCE*, Vol. 116, 1951.
4. Ioannides, A.M., J.P. Donnelly, M.R. Thompson, and E.J. Barenberg, "Three-Dimensional Finite Element Analysis of a Slab on Stress Dependent Elastic Solid Foundation," Report No. TR-86-0143, USAF, Bolling AFB, 1984.
5. Desai, C.S., *Lectures Notes for Advanced School Numerical Methods in Geomechanics including Constitutive Modelling*, Int. Center for Mechanical Sciences, Udine, Italy, 10-14 July 1989.
6. Westergaard, H.M., "Stresses in Concrete Pavements Computed by Theoretical Analysis," *Public Roads*, Vol. 7, 1926, "Stresses in Concrete Runways of Airports," *Proc. HRB*, Vol. 19, 1939. New Formulas for Stresses in Concrete Pavements of Airfields," *Proc. ASCE*, Vol. 113, 1947. "Analysis of Stresses in Concrete Pavements Due to Variation of Temperature," *Proc. HRB*, Vol. 6, 1926.
7. Burmister, D.M., "The Theory of Stresses and Displacements in Layered Systems and Application to the Design of Airport Runways," *HRB Proc.* 1943. Burmister, D.M., "The General Theory of Stresses and Displacements in Layered Soil System, I, II, III," *Journal of Applied Physics*, Vol. 16, No. 2, No. 3, No. 5, 1945.
8. Tabatabaie, A.M. and E.J. Barenberg, "ILLI-SLAB Finite Element Computer Program for Structural Analysis of Concrete Pavement Systems."

List of Symbols

p	=	pressure
P	=	load
E	=	Young's Modulus
μ	=	Poisson's Ratio
k	=	modulus of subgrade reaction
δ	=	deflection
σ	=	stress
q	=	subgrade pressure
σ_f	=	flexural stress
σ_n	=	deviator stress
σ_{eff}	=	effective stress
J_2	=	second invariant of deviatoric stress tensor

Federal Aviation Administration Pavement Modeling

T. Forte
K. Majzadeh
J. Kennedy
J. Hadden
T. White

Battelle

Acknowledgements

The authors gratefully acknowledge the assistance and encouragement of Mr. Andrew Sluz of VNTSC, who served as Contracting Officer's Technical Representative on this project. We also wish to thank Dr. Aston McLaughlin of FAA's Airport Systems and Technology Branch, who is primarily responsible for the creation of the UPDAP research program and provided us with valuable guidance during the project.

1. Introduction

The Federal Aviation Administration (FAA) of the U.S. Department of Transportation (DOT) has recognized the significant limitations of current pavement design and analysis techniques. As a result, the FAA has initiated a multi-year program to develop a model capable of predicting accurately the useful life of airport pavements. This model, a Unified Pavement Design and Analysis Program (UPDAP), will be capable of predicting stresses, deformations, and performance in any airport pavement system for nearly any pavement configuration, material and operating/environmental condition. It will be based on mechanistic principles, rather than on empirically derived relationships, and will provide pavement engineers with a comprehensive, flexible analytical tool for efficient design or evaluation of new and existing pavements. For existing pavements, the UPDAP will be capable of integrating inspection data to establish the current state of the pavement, and to assess proposed rehabilitation actions.

The benefits of the UPDAP will be substantial. A primary benefit to the FAA will be the improved ability to develop guidelines and standards that will assure (1) that federal funds are spent efficiently for the construction, rehabilitation and maintenance of airport pavements, and (2) that the pavements will provide safe and effective usage by aircraft and ground vehicles.

The work described in this paper was performed as the initial task of this program. The scope of this task was the development and justification of a concept for the UPDAP. A team comprised of Battelle, Resource International, Inc. (RII) and consultants performed the work for the Volpe National Transportation Systems Center (VNTSC) under Contract No. DTRS-57-89-D00006, Procurement Request No. VA 1023. The team combined the talents of experts in pavement technologies from RII with Battelle's experts in engineering mechanics. The result has been the development of innovative concepts and fresh perspectives of the issues associated with pavement modeling.

Subsequent sections of this paper describe our recommended concept for the UPDAP. An overview of the criteria and features of our concept is presented in Section 2. An in-depth presentation of our recommended methodology for pavement constitutive modeling is provided in Section 3. Our recommendations for pavement structural modeling are presented in Section 4. Damage modeling considerations are presented in Section 5. A discussion of the critical issues associated with field testing of pavement systems is presented in Section 6. Conclusions and recommendations for further study are provided in Section 7.

2. Recommended UPDAP Methodology

In this section we present an overview of our concept for a unified theory of pavement design and analysis.

2.1 General UPDAP Requirements

The basic requirement for UPDAP is similar to that for all comprehensive engineering design/analysis tools: it must predict accurately the response of the physical system (i.e., the pavement) under the range of expected environmental and operating conditions and for both existing and new system configurations. For the development of UPDAP, the following modeling criteria are implicit in this requirement:

2.1.1 Theoretical Soundness

The models (material, structural and damage) included in UPDAP must be derived from a solid theoretical mechanics foundation. This *mechanistic modeling* approach differs significantly from the *empirical modeling* approaches currently used for airport pavement design and analysis. Empirical models are derived directly from laboratory and field data; therefore, the range of validity generally is limited to the configuration and environmental/loading conditions associated with the specimens and/or site. Further, empirical models generally include terms (coefficients, functional relationships, etc.) which do not describe explicitly the influence of the pavement parameters on pavement response. In contrast, mechanistic models are based on proven mechanics principles and verified by critical laboratory experiments and field data. The range of validity of mechanistic models inherently is broader than that of empirical models, because the pavement system is described explicitly in the model. Thus, the influence of changes in the pavement configuration and environmental/operating conditions may be evaluated directly.

2.1.2 Comprehensiveness and Adaptability

UPDAP must be capable of design and analysis of the range of existing pavement configurations and loading conditions. Further, the methodology must be sufficiently flexible to accommodate new configurations and loadings.

2.1.3 Validation

The models which comprise UPDAP must be validated by comparing analytical predictions to observed and measured pavement performance over the range of expected pavement configurations, operating conditions and environmental conditions. This activity is essential to substantiate the modeling assumptions and to ensure the reliability of the predictions. Validation activities must be repeated as revisions are made to the models.

2.1.4 Computational Friendliness

UPDAP users primarily would be practicing engineers involved in the design and evaluation of airport pavements. The software must be reasonably easy to use, with maximum use of menus.

2.1.5 Knowledge-Based System (KBS)

A KBS should be incorporated into the UPDAP which invokes appropriate criteria for selecting the most appropriate combination of material, structural and damage models, as well as model interactions, for a given pavement scenario. The KBS will improve the accuracy of the analysis and decrease analysis time and cost.

2.2 Form of the UPDAP

In our approach, the UPDAP is comprised of three basic components: sets of the material models, structural model and damage models. The interactions between these elements, as well as the input/output requirements, are depicted in Figure 2-1. As implied in the figure, the performance of the UPDAP depends strongly on several factors, including

- a. the accuracy and validity of the material, structural and damage models,
- b. the accuracy and validity of the interactions between the models,
- c. the selection of the most appropriate models and model interactions,
- d. the accuracy of the model parameters, and
- e. the accuracy and validity of the inputs to the models (e.g., applied loads, environmental conditions).

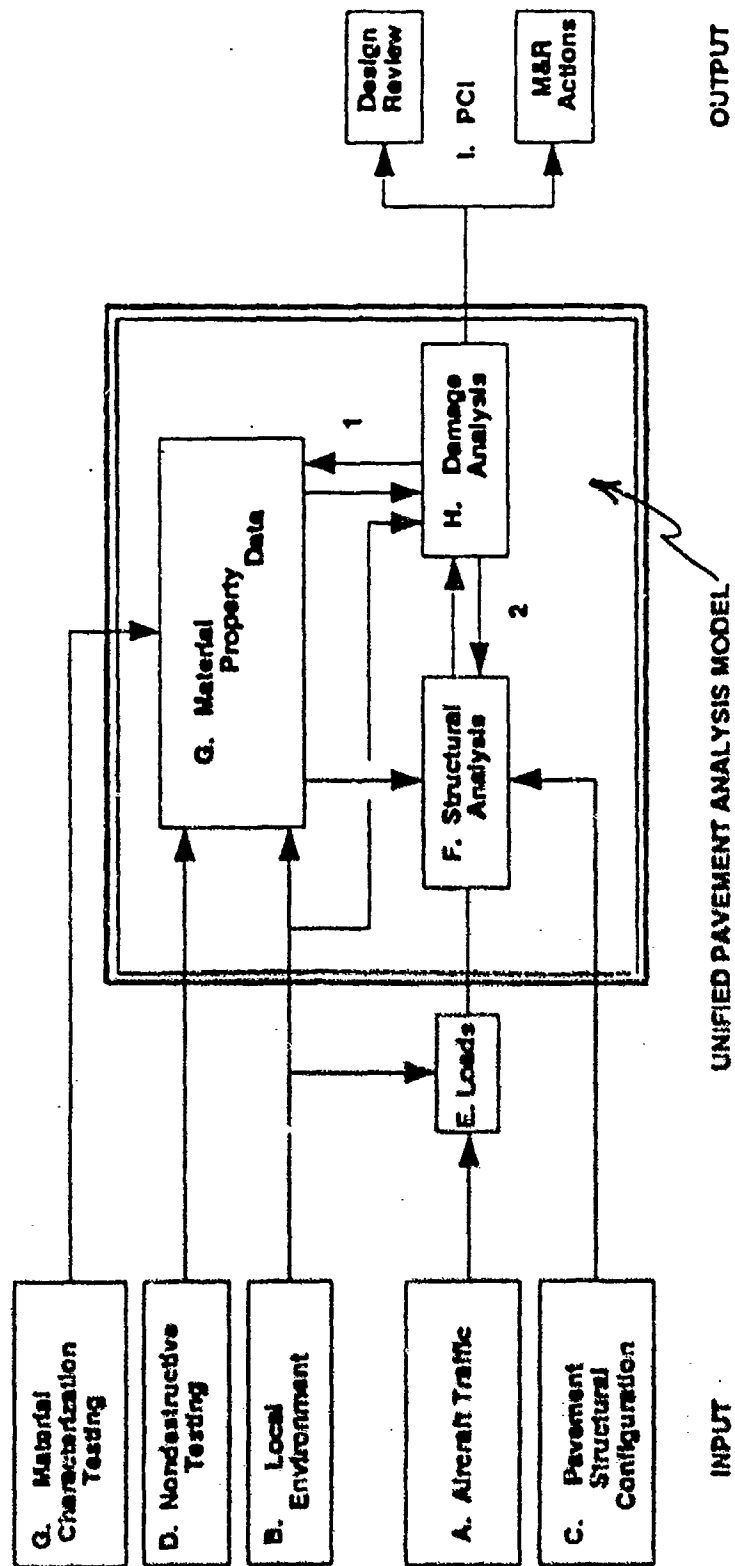


Figure 2-1. Overview of the Battelle/RII UPDAP Concept

The development of an effective UPDAP will require substantial laboratory and field testing to characterize material behavior, pavement damage mechanisms, environmental and mechanical (dynamic and static) loads. It is particularly important that correlations be established between material performance in the laboratory and field so that laboratory test data may be used with confidence to predict *in-situ* performance.

2.3 Features of UPDAP

The specific features of our UPDAP methodology are described for each model segment in subsequent sections of this paper. Our UPDAP concept includes the following significant features:

2.3.1 Structural Models

A three-dimensional finite-element model is recommended as the basic "platform" for the UPDAP. However, our preliminary work has indicated that in some cases a two-dimensional model will predict pavement performance with sufficient accuracy. Therefore, we recommend that criteria be established and used to select the simplest credible structural model for the design/analysis objective. This would be a function of the KBS.

2.3.2 Material Models

A hierarchy of material models should be developed for each material type. The selection of an appropriate model would be based on several factors, including load intensity, age, temperature, moisture, and pavement layer/thickness. Depending on these parameters, a sufficient material model may range anywhere from linear-elastic to nonlinear, viscoplastic.

Our preliminary work has focused partly on the influence of material model type on pavement response, from which we have begun to establish hierarchies of material models. Model selection would be aided by the KBS Damage Models and Model Interactions. Strong interactions exist between the structural response, material behavior and pavement damage/distress. The UPDAP should account for these interactions explicitly. Our preliminary work has indicated that such phenomena as the growth of voids under repeated loading are important considerations in predicting pavement performance.

2.3.3 Aircraft/Pavement Loading

The UPDAP should be based on aircraft-specific, deterministic loading. Once validated for this type of loading, probabilistic methods could be applied to the UPDAP to evaluate effects such as traffic mix and climatic variations. Although this was not a focus of our initial studies, we believe that it may be important to model aircraft loading to a level of detail that includes landing gear geometries and suspension dynamics. Contrary to current practice, wheel load equivalency factors should not form the basis for aircraft/pavement loading in the UPDAP.

2.3.4 Environmental Effects

Environmental factors such as temperature and moisture have a significant effect on pavement performance, and should be included in the material models. Our initial work has identified several important relationships between pavement material behavior and environmental condition.

2.4 Benefits of UPDAP

The benefits of the version of the UPDAP described above are significant. They include:

2.4.1 Reduced Construction Costs

The UPDAP will improve the accuracy of predictions of pavement performance over current techniques. Therefore, construction costs would be minimized because the risk of overdesigning the pavement system would be reduced.

2.4.2 Reduced Repair Costs

Because of the improved predictive capability of UPDAP, maintenance costs would be minimized, also, the risk of underdesigning the pavement system would be reduced.

2.4.3 Increased Pavement Life

By incorporating appropriate damage models and material/structural/damage interaction schemes into UPDAP, pavement distress can be predicted and an appropriate maintenance program implemented to maximize pavement life.

3. UPDAP Material Modeling

In this section, we present our recommended methodology for modeling pavement material behavior in the UPDAP. In Section 3.1, we describe a generalized constitutive model for pavement materials. In Section 3.2, we present our methodology for treating environmental effects in the material models.

3.1 A Generalized Constitutive Model for Pavement Materials

In the past, researchers and pavement technologists have addressed the constitutive modeling concerns of each pavement layer separately, and no attempt has been made to develop a unified material constitutive model for the pavement system. In this section, we present our concept for such a unified model.

3.1.1 Current State of the Art In Material Modeling

The wide variety of materials which currently are used for each pavement layer (e.g., subgrade, base/subbase, pavement, overlay) are presented in Table 3-1. The current state of the art in pavement material modeling is summarized in Table 3-2.

As shown in Table 3-2, the subgrade layer typically is represented as linear/nonlinear elastic (e.g., Programs RISC, OAF/OAR, ILLI-PAVE), linear viscoelastic (e.g., VESYS), or as a Winkler foundation (e.g., J-SLAB, ILLI-SLAB). Current state of the art models represent the granular base and subbase (unbound layers) as nonlinear (stress-dependent) elastic systems.

The constitutive models in ILLI-PAVE (FEM), OAF/OAR (closed form), RISC (closed form/FEM) are based on nonlinear elastic theory. The constitutive models for cement treated base (CTB), and Lime-Flyash (LCF) bound layers are best described as linear elastic. The state-of-the-art models for the asphalt-treated base (ATB) could be represented as either linear elastic, as used in ILLI-PAVE, OAF/OAR and RISC, or viscoelastic as used in VESYS. In ILLI-SLAB and J-SLAB, the base and subbase layers are represented by a Winkler foundation, the same as for subgrade layers.

Table 3-1. Pavement Component Selection Matrix

MATRIX TYPE	SUBGRADE (LAYER)	SUBBASE	BASE	STRUCTURE	SURFACE (LAYER)
JOINTED PLAIN CONCRETE			X	X	X
JOINTED REINFORCED CONCRETE			X	X	X
CONTINUOUS REINFORCED CONCRETE				X	X
PRESTRESSED CONCRETE				X	X
FIBER REINFORCED CONCRETE				X	X
POLYMER CONCRETE				X	X
HIGH STRENGTH CONCRETE ASPHALT CONCRETE				X	X
POLYMER MODIFIED ASPHALT CONCRETE				X	X
FIBER REINFORCED ASPHALT CONCRETE				X	X
LIME/CEMENT FLYASH		X	X		
GRANULAR BASE		X	X		
CEMENT TREATED BASE			X		
SAND ASPHALT BASE ASPHALT TREATED BASE			X		
LEAN CONCRETE		X	X		
COHESIVE SUBGRADE	X				
COHESIONLESS SUBGRADE	X				
STABILIZED SOIL	X				

Table 3-2. Capabilities of Existing Pavement Analyses Programs

LAYER	CONFIGURATIONS	RISC	ILLI-PAVE	ILLI-SLAB	J-SLAB	VESYS	OAF/OAR	CRCP
OVERLAY	• AC		✓			✓	✓	
	• JCP	✓		✓	✓			
	• JRCP	✓		✓	✓		✓	
	• CRCP	✓		✓	✓		✓	✓
	• Prestressed	✓			✓			
PAVEMENT	• AC		✓			✓	✓	
	• JCP	✓		✓	✓		✓	
	• JRCP	✓		✓	✓			
	• CRCP	✓		✓	✓		✓	✓
	• Prestressed	✓						
BASE/SUBBASE	• Bounded Layer			*	*		✓	
	• Asphalt ATB	✓	✓			✓	✓	
	• Cement CTB	✓	✓			✓	✓	
	• LCF Treated	✓	✓			✓	✓	
	• Unbounded, Granular	✓	✓			✓	✓	
SUBGRADE	• Compacted Soil	✓	✓	*	*	✓	✓	
	• Natural Soil	✓	✓			✓	✓	
	• Bedrock	✓	✓					
	• Reinforced Earth	✓	✓					
	• Other Geometries	✓	✓					
SPECIAL REQUIREMENTS	• Interface (Bonded & Unbonded)	✓		✓	✓			
	• Crack & Seal	✓		✓	✓			
	• Rubberized	✓		✓	✓			
	• Fabrics	✓		✓	✓			
	• Load Transfer	✓		✓	✓			
	• Voids	✓		✓	✓			
	• Warping/Curling	✓		✓	✓			
	• Multi-Slab	✓		✓	✓			

* = Winkler Foundation

AC = Asphalt Concrete

JCP = Jointed Plain Concrete Pavement

JRPC = Jointed Reinforced Concrete Pavement

CRCP = Continuously Reinforced Concrete Pavement

LCF = Lime-Cement-Flyash

The state-of-the-art constitutive models for the asphaltic concrete (AC) layer which is constructed as a structural layer for new pavements or as an overlay of rigid or flexible pavements are either linear elastic (temperature dependent moduli) such as ILLI-PAVE, OAF/OAR, and RISC, or linear viscoelastic as in the case of the VESYS program.

State-of-the-art material models currently used for rigid pavement systems are based on a linear elastic approach, such as those found in OAR, RISC, ILLI-SLAB and CRCP. The effect of geometrical nonlinearities such as cracks in CRCP pavements and joints in jointed concrete pavements are often reflected as transfer functions or adjustments to the moduli of the pavement layer.

3.1.2 Mechanistic Considerations

From a micromechanics point of view, the constitutive laws of pavement material response can be derived by combining the basic laws of chemistry and physics such as rate processes of kinetics of thermal activation.

While micromechanics principles have been used to model phenomena in penetration mechanics and high-speed flow problems the implementation of the phenomena into an analysis tool such as UPDAP must ultimately be formulated at the macro-level. Therefore from the practical standpoint of implementation into a code such as UPDAP, the micromechanics approach to this mechanistic formulation may have limited applicability.

From a macromechanics point of view, a generalized hierarchy of constitutive models is needed which could degenerate into special cases as appropriate for different systems. The generalized constitutive model should accommodate changing conditions of pavement throughout its service life, such as crack initiation, crack propagation and fracture, aging and accumulation of permanent deformation. The effect of environment, such as time, temperature, moisture, as well as the impact of dynamic loads, and geometrical nonlinearities also should be incorporated.

The constitutive model for the UPDAP must be a formalized model to incorporate all unique features of each pavement component materials and with consideration to various environmental and loading condition. In the formulation of a generalized constitutive model, one should recognize that material behavior is generally too complex to develop a single universal model for all environmental and loading conditions. However, considering the need for theoretical soundness and ease of numerical performance, we propose a hierarchy of constitutive models for

various pavement component layers. This would be used together with a KBS which would aid in selecting the most appropriate model for a given application.

A hierarchical approach permits the development of progressively more complex and higher order models from simple and basic constitutive models. Starting from the most basic, elastic viscoplastic model with isotropic hardening and associated FLOW, one could develop more complex models with inherent and induced anisotropy and non-associative flow behavior (Figure 3-1).

The basic assumptions are that:

- a. Deformations are small enough to disregard the nonlinear terms of the strain-displacement relationship. This should be a reasonable assumption for pavement systems.
- b. Elastic, plastic and viscoelastic deformation are uncoupled (Figure 3-1). This is, however, not a requirement. Phenomenological constitutive theories which do not distinguish between time-independent (plastic) and time-dependent (viscoelastic, viscoplastic, creep) could be considered later in the program.
- c. The distinction between the volumetric and deviatoric deformation is essential, once the linear threshold has been exceeded. The volumetric and deviatoric deformation, have, in turn, reversible and irreversible deformation components (Figure 3-2).

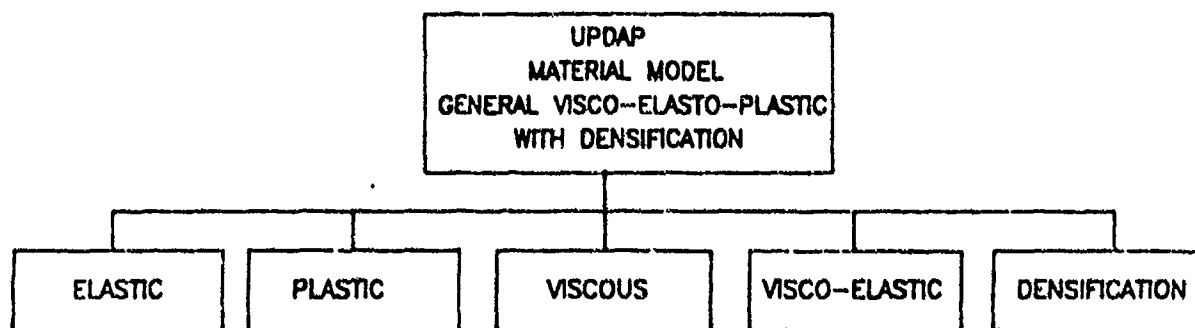


Figure 3-1. Elements of a Generalized Constitutive Model

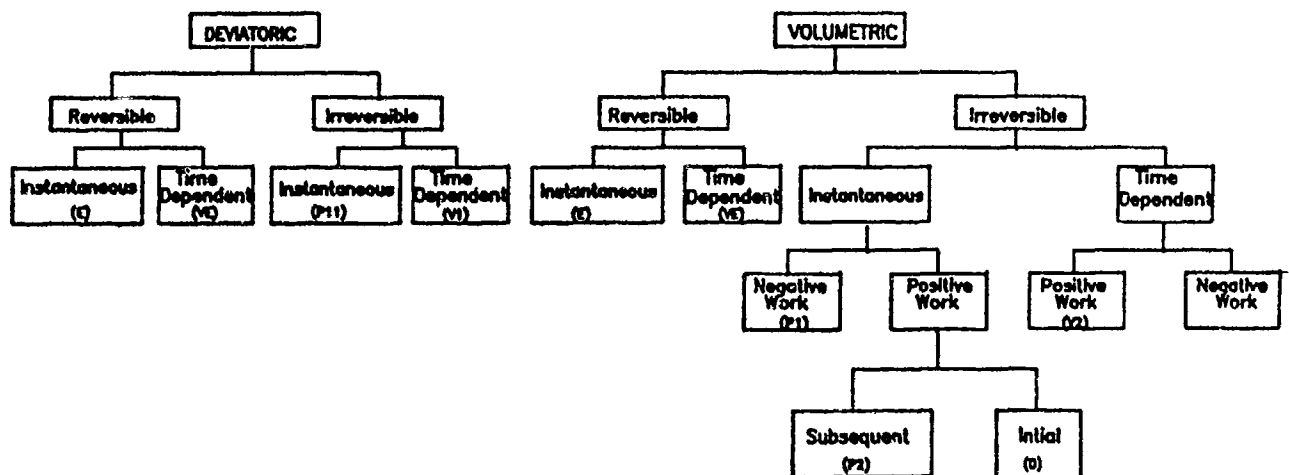


Figure 3-2. General Deformation Chart for Granular Multi-Phase Material

- d. The volumetric irreversible (both time dependent and instantaneous) deformation is induced not only by excessive volumetric stress (which performs *Positive Work* in this case) but also by excessive shearing. In the latter case volumetric stress performs *Negative Work* on volumetric strain. This phenomenon is termed *Dilation*. Physically, the shear distortion results in rearrangement of particles of aggregate, so that the total volume increases (Figure 3-3).

The volumetric irreversible deformation due to volumetric stress occurs not only for high stress but also initially. The virgin material contains air voids and the particles are not arranged in an optimal way. When subjected to low stresses the material exhibits *Densification* - an irreversible volumetric deformation. Figure 3-4 illustrates graphically the above discussion.

The volumetric irreversible time-dependent positive-work deformation has not been experimentally evidenced and is included in the chart only for theoretical completeness.

3.1.3 Plasticity

The pavement component materials, such as soils, aggregate matrix, concrete and asphalt, all exhibit the nonlinear, inelastic and rate independent response characteristics suited for plasticity theory. The elements describing the constitutive laws based on the theory of plasticity are:

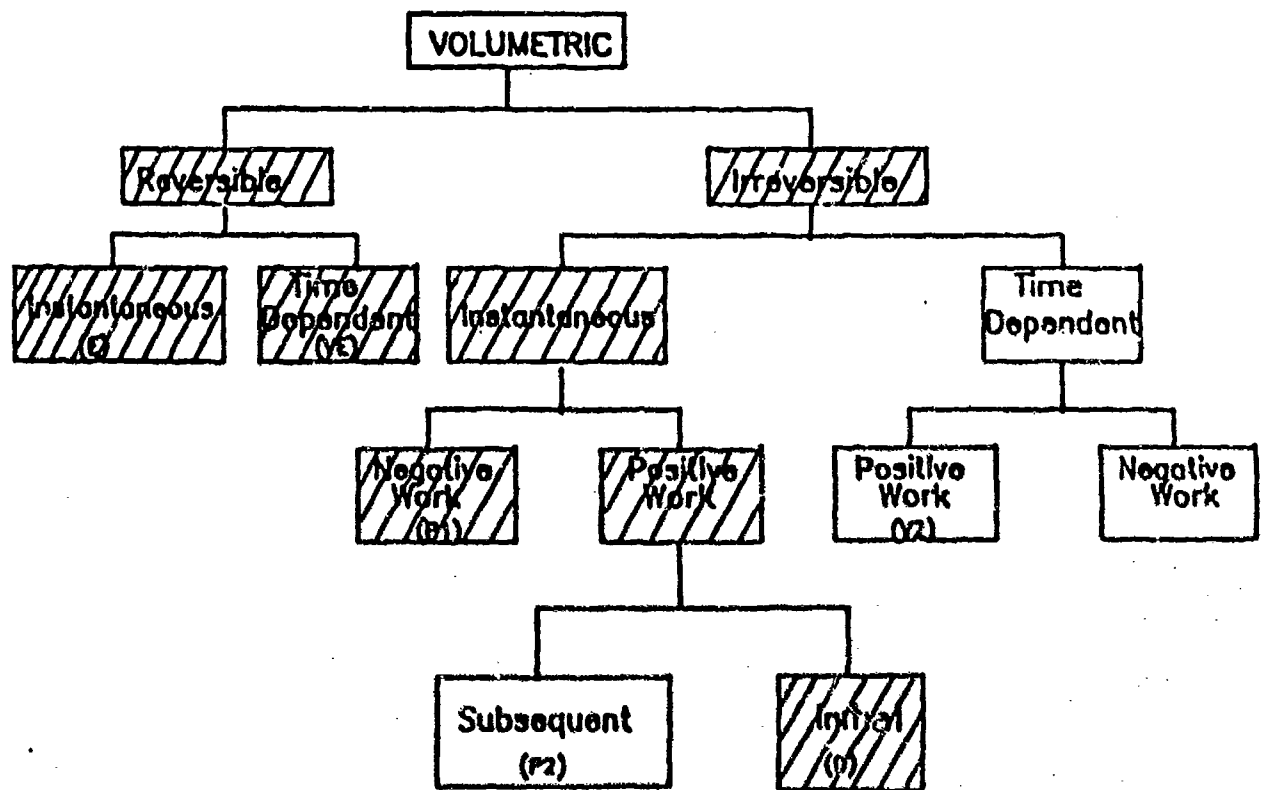
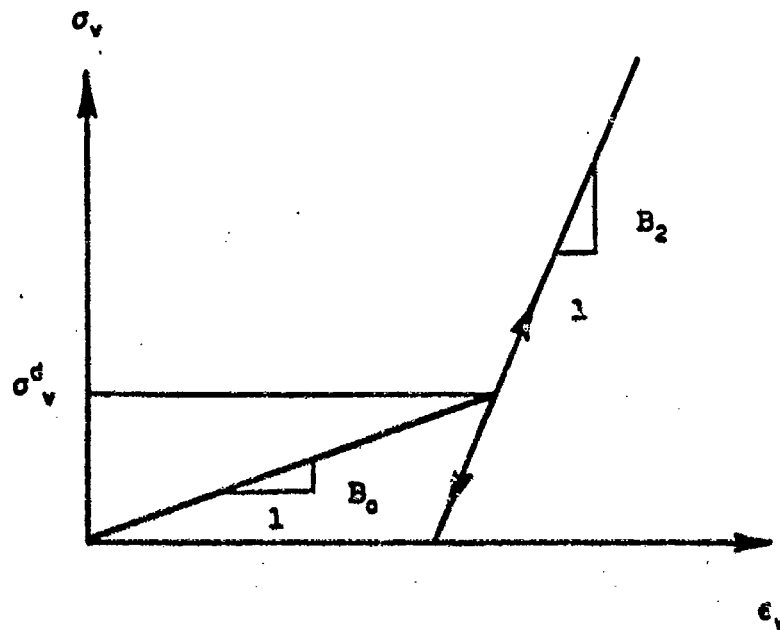


Figure 3-3. Deformation Chart for Granular Multi-Phase Material



Experiments with hydrostatic pressure show good agreement with the above model. However, two questions remain unresolved:

- i. Does the densification limit, as defined above, depend on the deviatoric stress?
- ii. Does the same limit depend on stress history?

Figure 3-4. Schematic Model of Densification

- a. yield condition
- b. flow rule
- c. hardening rule

The yield function F , defines the limit of elastic deformation expressed by the stress state. Under a three-dimensional stress state, the yield function, F , is very complex and not only dependent on the stress invariants but also on the joint or mixed invariants of stress and plastic strain tensors.

The hierarchical approach, as was indicated earlier, permits development of more complex functions, such as those presented by Desai [1].

The scalar function F , the yield criterion is given by:

$$F = F(J_i, I_k^P, K_j, A_m)$$

where

$$\begin{aligned} J_i (i = 1, 2, 3) &= \text{invariant of stress tensor} \\ I_k^P (i = 1, 2, 3, 4) &= \text{invariant of plastic strain tensor} \\ K_j (j = 1, 2, 3, 4) &= \text{joint or mixed invariant} \\ A_m &= \text{internal state variable.} \end{aligned}$$

Since the identification and determination of the yield function is a considerable task, it requires a series of different stress path tests. We recommend that the simple function form of a yield surface be assumed as the basic model. Since pavement materials are granular composites, which in general exhibit dependency on the volumetric stresses, the following Drucker-Prager yield function (an extended Von-Mises criteria) which considers all principal stresses, is recommended because of its simplicity and convenience for computer implementation (Figure 3-5):

$$F = J_{2D}^{1/2} - \alpha J_1 - k = 0$$

where

$$\begin{aligned} F &= \text{yield function} \\ J_{2D} &= 2^{\text{nd}} \text{ invariant of deviatoric stress tensor} \\ J_1 &= 1^{\text{st}} \text{ invariant of stress tensor} \\ \alpha, k &= \text{material constants} \end{aligned}$$

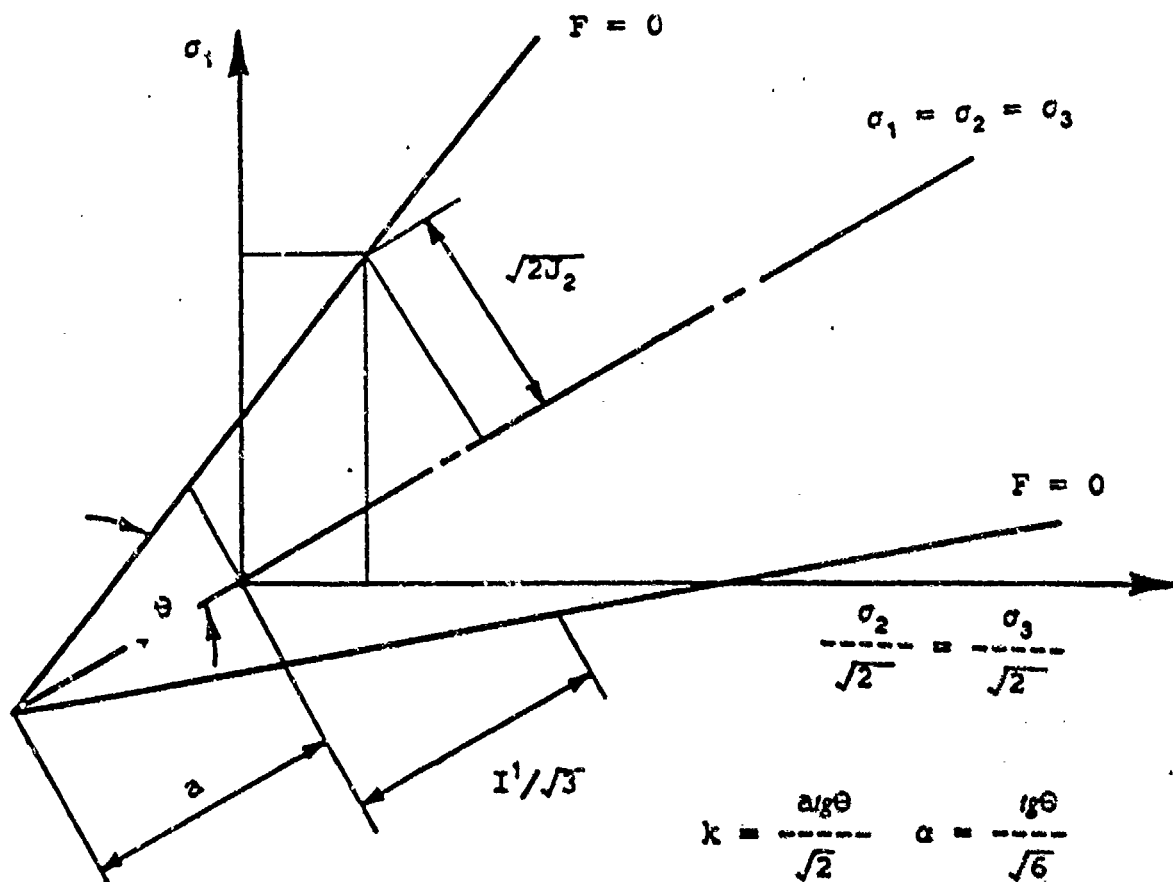


Figure 3-5. Intersection of Yield Surface with the Triaxial Plane

where

$$J_1 = \sigma_1 + \sigma_2 + \sigma_3 = 3\sigma_{oct}$$

$$J_{2D} = 1/6[(\sigma_1 - \sigma_2)^2 + (\sigma_2 - \sigma_3)^2 + (\sigma_3 - \sigma_1)^2]$$

α, k = material constants ($\alpha = 0$ for purely cohesive clay)

The Drucker-Prager function does not incorporate the third stress invariant J_3 , and has limitations for materials which exhibit strong stress path as well as confining pressure dependency.

3.1.4 Flow Rule

In the theory of plasticity, the strain increments $d\epsilon_{ij}$ due to the stress $d\sigma_{ij}$ are decomposed into elastic and plastic parts such as:

$$d\epsilon_{ij} = d\epsilon_{ij}^e + d\epsilon_{ij}^p$$

In the theory of plasticity, the incremental plastic strain $d\epsilon_{ij}^p$ is defined by a function g_1 , called plastic potential, which is a function of state of stress, σ_{ij} .

For some materials, the plastic potential, Q , and yield function, F , can be assumed to be the same. Such materials follow the so-called "associated flow" rules of plasticity. The associated flow rule assumes that the plastic strain increment is normal to the yield surface in the principal stresses space. It usually predicts significantly higher dilation than experiments suggest. On the other hand, the nonassociated flow rule that assumes only deviatoric flow would not predict any dilation. Experiments suggest that dilation in AC mixtures is much higher than in soils. The proper identification of the plastic potential function (the direction of flow in the strain space) is a task that requires sophisticated testing procedures and testing techniques.

As a first step toward the development of basic model (simplest credible model), we recommend the adoption of the associated flow rule. Obviously the hierarchical approach would later on lead to the development of the "nonassociated" flow rule if needed.

3.1.5 Hardening Rule

Experimental results on various pavement component materials have indicated that some strength gain or strain hardening is observed after the elastic limit. The hardening rule is intended to define the process of strength gain during monotonic or cyclic loading. Granular composites

such as soils, asphalt and concrete could exhibit, isotropic hardening, kinematic hardening or combination of isotropic and kinematic hardening.

For the most basic model, we recommend applying an isotropic hardening rule (see Figure 3-6).

3.1.6 Densification

Densification can be interpreted as a form of plastic behavior. However, it occurs initially at low stress levels, as opposed to yield surface plasticity, in which plastic deformation occurs after a threshold value of stress is reached. It is, therefore, modeled separately as an irreversible volume change proportional to the volumetric stress, up to a certain limiting stress level (see Figure 3-7). It is also assumed that no coupling occurs between plastic and viscous deformation. Viscous deformation occurs for any stress level while the plastic deformation occurs only when the threshold condition is satisfied. The one-dimensional representation using classical spring, dashpot and slider rheological models would have all major elements connected in series.

3.1.7 Viscous Behavior - Time-Dependent Irreversible Deformation

The pavement component materials, such as asphaltic concrete, asphalt treated base, clay, and lean concrete, exhibit time-dependent irreversible (viscous) deformation. For moderate stresses and strains, the linear viscous behavior usually is assumed, while for higher stresses and strains the nonlinearity becomes apparent. Various nonlinear viscous models have been presented in the literature for both shear-thinning and shear-thickening materials.

In the basic model, the linear model should be adopted until the experimental data has identified material and geometric nonlinearities. The volumetric viscous deformation (V2) is experimentally evidenced. However, its magnitude is seen to be small compared to other components. The modeling of this component would require a very complex viscous model. Herein, we recommend that only the deviatoric viscous deformation (V1) be modeled (Figure 3-2).

In addition, due to the time-dependent nature of deformation, for loads of long duration, the strains exceed the range of small strain assumption and geometric nonlinearities should be considered.

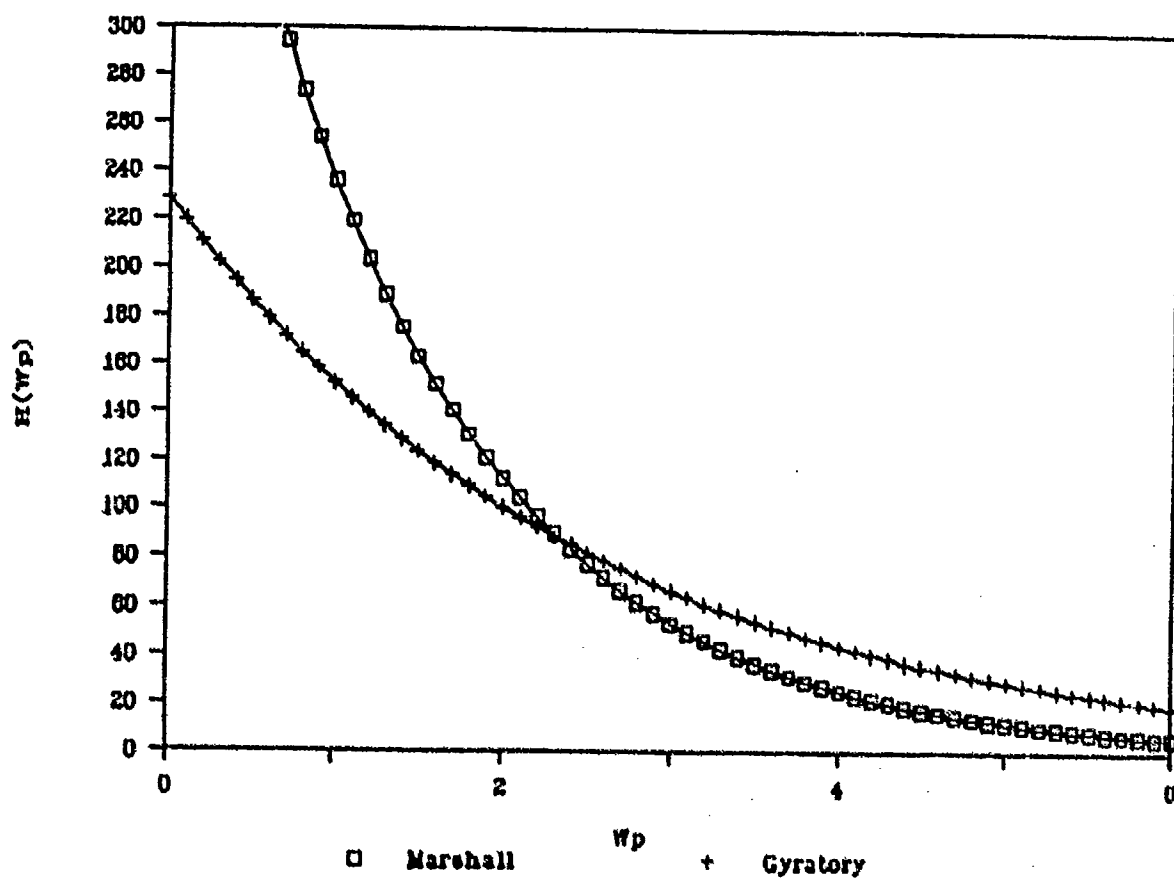


Figure 3-6. Models for Hardening Functions at 74°F

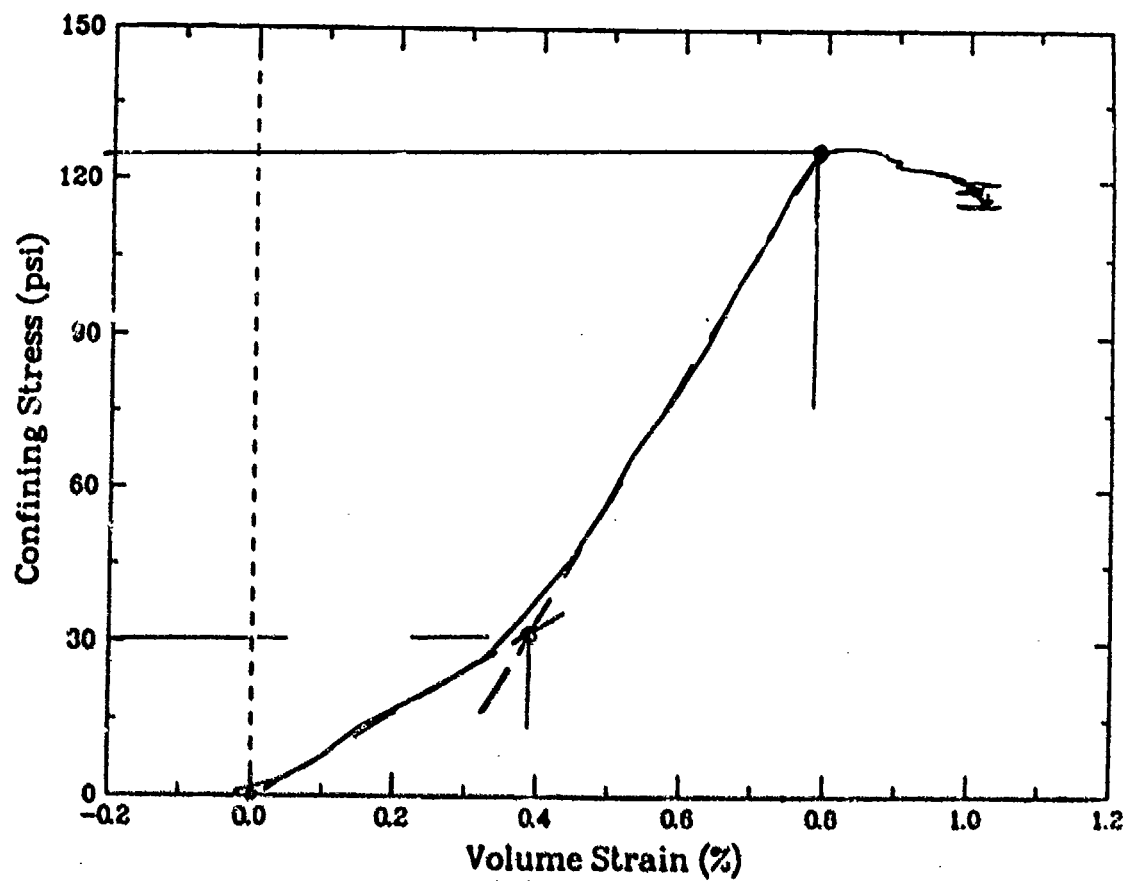


Figure 3-7. Hydrostatic Test on Marshall Mix at 120°F

3.1.8 Time-Dependent Reversible Viscoelastic Behavior

Experimental evidence indicates that most pavement component materials, such as asphaltic concrete, asphalt treated base, subgrade clay and portland cement concrete, exhibit some degrees of time-dependent reversible deformation. The generalized Kelvin model, GKM, with as many as 1 to 5 Kelvin units has been used to describe the "delayed elastic" response of various pavement component materials (Figure 3-8). In a basic and simple model, both elastic and viscous components are assumed to be linear; whereas in more complex models, presented for concrete and soils, the Newtonian linear viscous element has been replaced by nonlinear viscous elements governed by power law, Sinh law, and more complex equations.

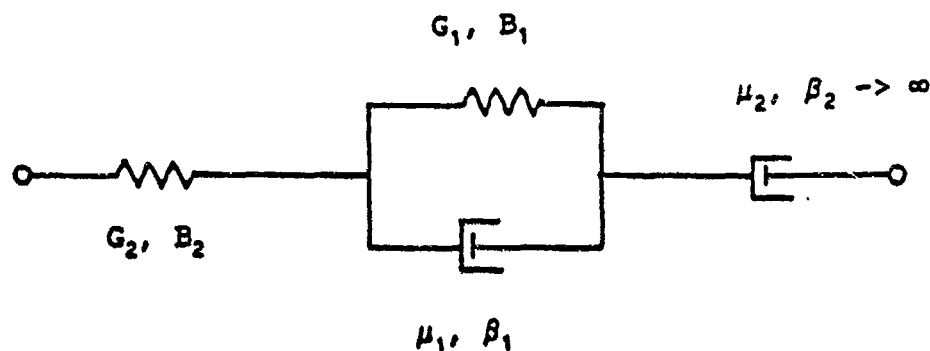


Figure 3-8. One-Dimensional Model of Asphaltic Concrete

3.1.9 A Hierarchical Concept: Toward a Complex Model

Although the application of a basic, simplest credible model as discussed previously may suffice for most conditions, more complex constitutive laws may be required for granular composite materials, such as asphalt concrete, portland cement concrete and aggregate base and lime/cement/aggregate materials subjected to complex stress states.

The more complex model should include the following features (after Desai [1]):

1. Yield function to be expressed in terms of J_1 , J_2 , J_3 , or J_{2D} and J_{3D}

2. Yield function to be a single yield surface, rather than two intersecting yield functions; such condition reduces the number of required parameters as compared to the multisurface models presented in literature.

As an example, one of many hierarchical models may have the general form of the yield function F as follows:

$$F = J_{2D} - (\alpha J_1^n + \delta J_1^2)(1 - \beta S_1)^m = 0$$

where

$$S_1 = J_3^2/J_2^3$$

$$m = 1/2$$

n, α, β, δ are constants

3. For materials having cohesion and tensile strength the stress terms in this equation are increased to include tensile strength, R .

$$\sigma_1^* = \sigma_1 + R$$

$$\sigma_2^* = \sigma_2 + R$$

$$\sigma_3^* = \sigma_3 + R$$

4. The model is expected to represent Portland cement concrete, asphaltic concrete, and aggregate base.
5. The model includes material constants which can simulate hardening and include the effects of stress path, volume change and coupling of shear and volumetric responses.

3.2 A Micro-Rheological Approach to the Development of Primary Response Environmental Models

The primary and ultimate response of pavement component materials are influenced by a wide range of environmental variables, such as temperature, moisture, oxidation and age hardening, curing, frost damage, expansion and contraction, etc. In this paper, only the influence of environment on the primary response of pavement component materials is discussed.

The effect of environment on the pavement performance shall include, but not be limited to moduli of elasticity, and creep compliance, relaxation modulus, dynamic and loss modulus, or viscoelastic modulus, rutting and cracking parameter, which describe the primary response of pavement structure. The effects of environment, such as temperature, moisture, age hardening,

curing and maturity, have been observed in all components of pavement structures such as soil-cement, soil-aggregate, asphaltic cement, portland cement concrete, lime cement flyash and others.

In this section we present a concept for a unified environmental model for all pavement component materials based on the principles of microrheology, in which the flow and deformation are controlled by the thermally activated processes. These processes in turn are dependent on temperature and activation energy, ΔE , which represent the energy barrier required for the deformation process. Depending on the complexity of the deformation phenomena and the number of micromechanisms involved, the activation energy may attain a wide range of values.

When two operating micromechanisms depend on each other, the process with the largest activation energy controls the deformation. On the other hand, the reverse is true when micromechanisms are independent of each other. Therefore in a complex body, it may not be possible to determine the activation energy ΔE_i for each process explicitly. Instead, an apparent activation energy can be determined to represent the deformation of the material body. In viscoelastic materials such as bituminous mixtures, it is often assumed that the material is a thermorheologically simple system. That is, it is considered that the deformation process is only governed by a single thermally activated process. This assumption simplifies the analysis of deformation and flow in rheological bodies.

In rheologically simple material such as asphaltic concrete, polymer/asphaltic, asphalt aggregate systems, the effect of environment is often represented by a temperature-dependent function, a_T , which is related to the activation energy and temperature. In soils, however, the energy of cohesion or binding energy which is also related to the activation energy and in turn to the moisture content and clay-fabric structure, reflect the influence of environment. The aging phenomena which are observed as age hardening in the asphaltic and polymeric pavement structure, and as maturity in cementitious material such as lime flyash, portland cement concrete are also dependent on the activation energy, temperature and time. In the following sections various primary response environmental models are discussed.

3.2.2 Moisture and Temperature Effects

Moisture and temperature effects will be accounted for in the following model through adjustment to the material modulus and describing an effective modulus that is dependent on time, temperature and moisture.

The principles of rate processes theory, activation energy and the energy barrier can be applied to temperature and moisture sensitive materials such as soils, soil-aggregate system and even biological systems which are both temperature and mixture dependent.

Assuming that a material is either a thermorheologically and/or hydorrheologically simple or both, as suggested by Hammerle and Mohsenin [2], the viscoelastic functions such as relaxation curves can be shifted to obtain a consolidated or "master" curve for the material. To demonstrate the meaning of shifting the curves let $E_M(t)$ be the relaxation function at some moisture, and let $E_{M_0}(t)$ be the relaxation function at some reference moisture, one can then write

$$E_M(t) = E_{M_0}(t)a_M(M) \quad (5)$$

where

$$a_M = \text{shift factor}$$

The quantity $a_M(M)$ is called the reduced time or pseudotime.

For materials which are both thermorheologically and hydorrheologically simple material, the relaxation master curve could be represented by a generalized equation:

$$E(t, M, T) = E_0 + E_1 \exp \left[\frac{\alpha_1 t}{a_T(T)a_M(M)} \right] + \dots + E_n \exp \left[\frac{\alpha_n t}{a_T(T)a_M(M)} \right] \quad (6)$$

in which

$$\begin{aligned} a_T(T) &= \text{temperature shift factor} \\ a_M(M) &= \text{moisture shift factor} \\ \alpha_j (j = 1, 2, \dots, n) &= \text{inverse of the characteristic time of the Maxwell element} \\ E_j (j = 1, 2, \dots, n) &= \text{a constant} \\ E_0 &= \text{a constant} \end{aligned}$$

This principle has been applied to determine the relaxation modulus of corn endosperm, as shown in Figure 3-9. The shift functions are as follows:

$$\begin{aligned} \log a_T &= 0.23 - 1.114 (T - 40^\circ) \\ \log a_M &= 0.136 - 0.278 (M - 14.4\%) \end{aligned}$$

so that the master curve is given by

$$E(t, M, T) = E_0 + \sum_{j=1}^5 E_j \exp(\alpha_j / a_T a_M) \quad (7)$$

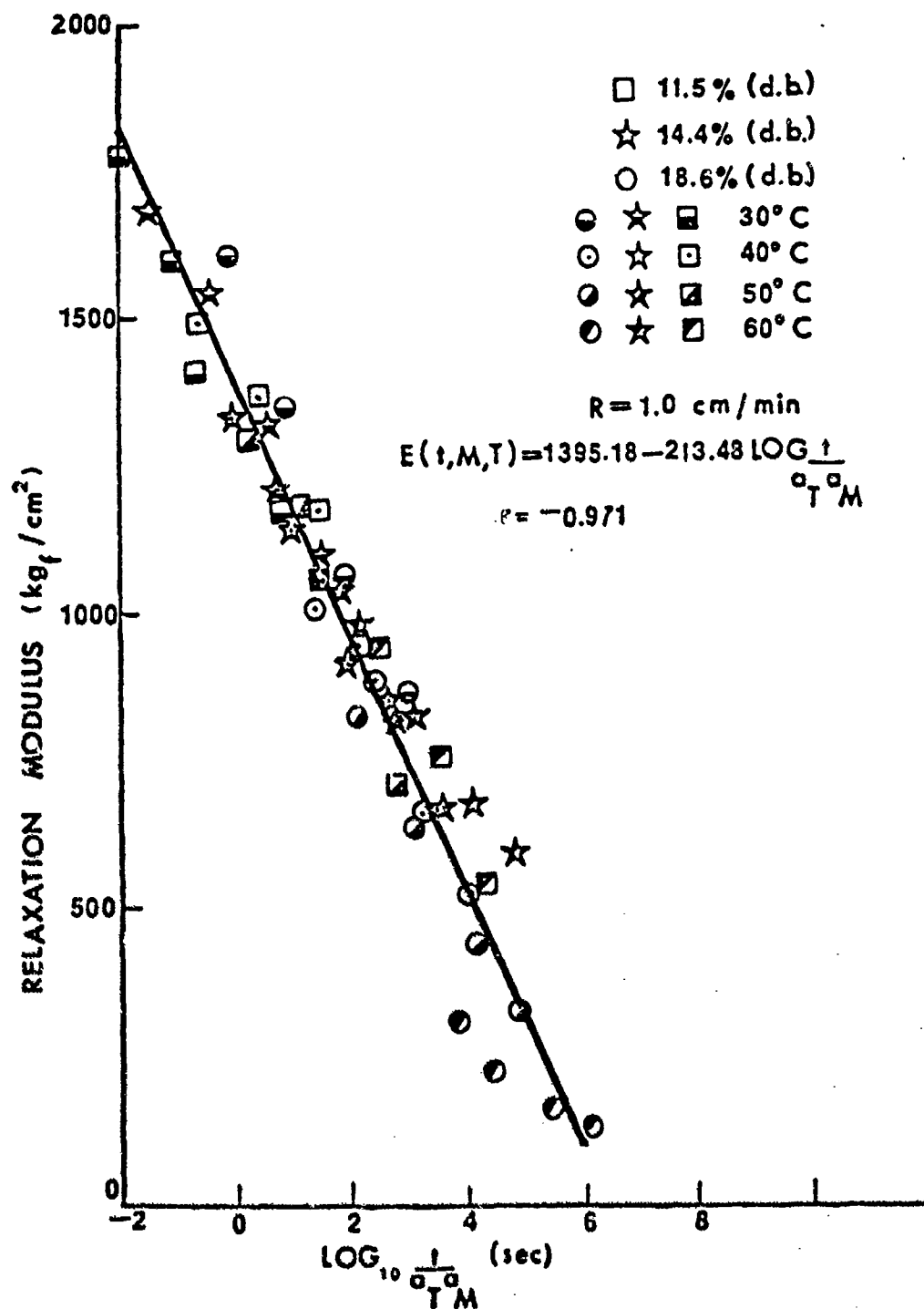


Figure 3-9. Relaxation Modulus Master Curve for the Corn Endosperm

Here the relaxation modulus is represented by a spring and 5 Maxwell elements in parallel.

Assuming that soils are hydromechanically simple materials, the principles of moisture dependent function a_M has also been applied to compacted silty clay soils. Majidzadeh et al.[3] have applied the concept of time-moisture superposition to compacted silty clays (where temperature effects are not considered) and developed moisture shift functions in the form of Figure 3-10.

$$a_M = e^{C(w-w_o)} \quad (8)$$

where

- w = moisture content
- W = optimum moisture content
- C = 1.07 for wet side of optimum
- C = -0.53 for dry side of optimum

Given these shift functions, the permanent deformation for moisture content on the wet and dry sides of optimum are given by Figures 3-11 and 3-12, respectively.

$$\epsilon_p/N = 0.00139 N^{-0.918} \exp (1.07(W-W_o) + B(\sigma_{app}/\sigma_{ult})) \quad (9)$$

and for the dry side of optimum

$$\epsilon_p/N = 0.000879 N^{-0.908} \exp (-0.53(W-W_o) + B(\sigma_{app}/\sigma_{ult})) \quad (10)$$

where

- ϵ_p = permanent deformation
- N = number of load application
- $\sigma_{app}, \sigma_{ult}$ = applied and ultimate stress and strength, respectively.

3.2.3 Aging and Maturity

Pavement component materials, such as asphaltic materials, soil-cement, lime-cement flyash and portland cement concrete exhibit time and temperature dependencies reflected by aging of the binder in the mixture, as well as maturity of cementitious component. Research results have shown that the degree of aging and hardening asphalt mixtures are related to the change in the energy of activation, given by:

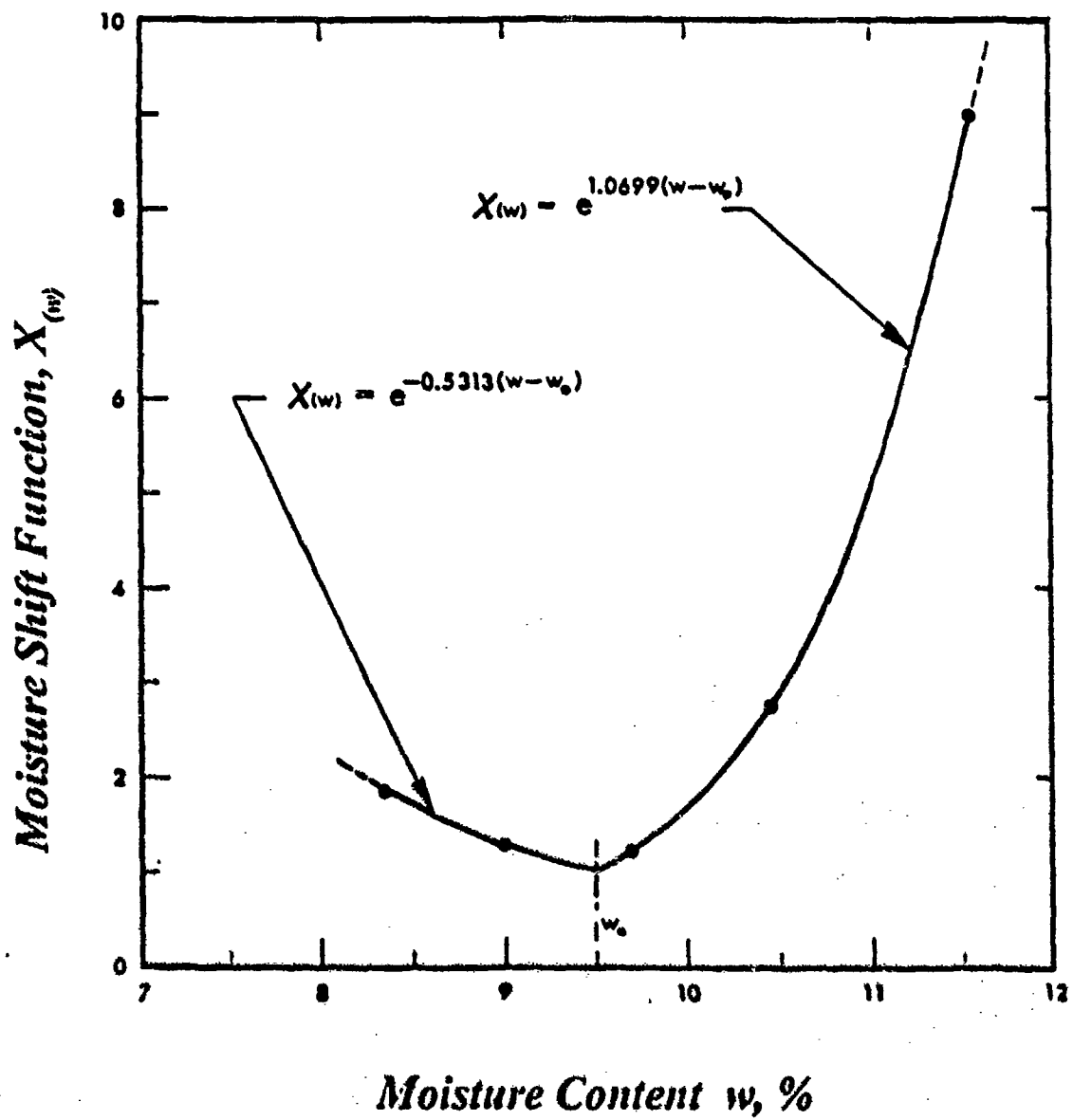


Figure 3-10. Moisture Shift Function for Silty Clay
 (Developed by Majidzadeh et. al. [3])

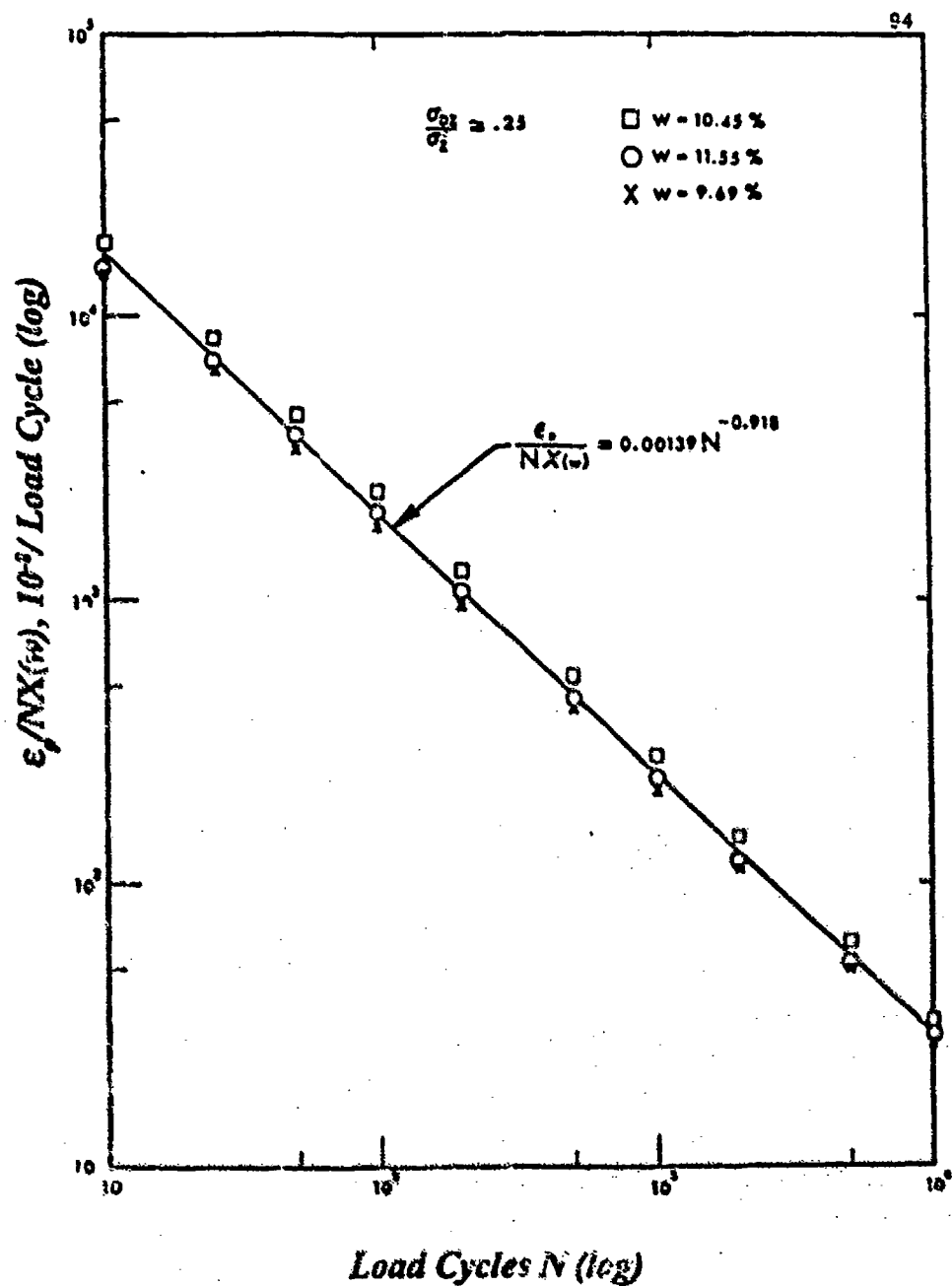


Figure 3-11. Master Curve for Rutting on Wet Side of Optimum

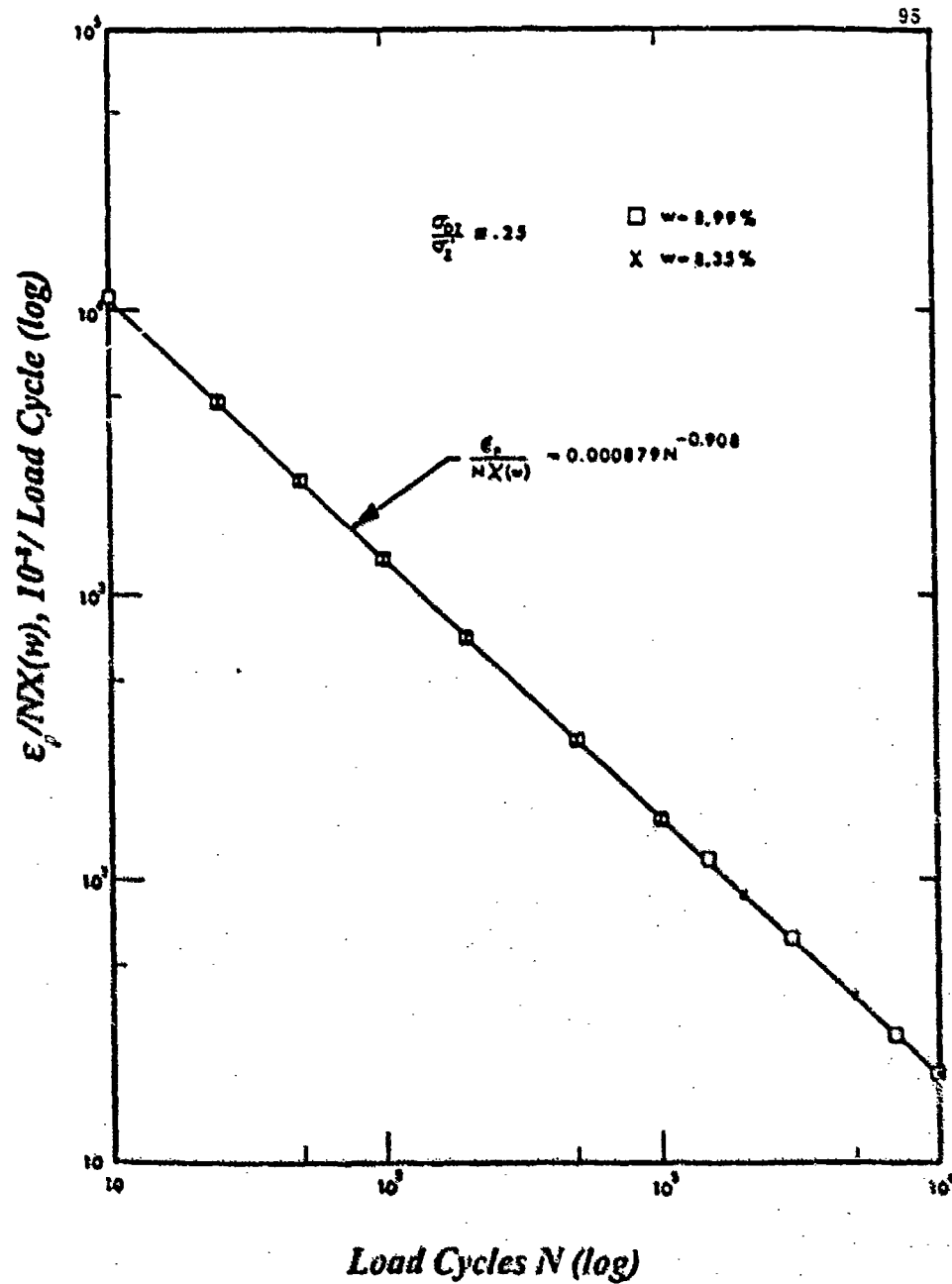


Figure 3-12. Master Curve for Rutting on Dry Side of Optimum

$$AI = \exp(\alpha_a/\alpha_u) \cdot \exp [(\Delta E_a - \Delta E_u)/RT] \quad (11)$$

where the subscripts a, u refer to aged and unaged asphaltic concrete, respectively.

Similar recent results have also shown that viscoelastic parameters, such as creep compliance $J(t)$ and the distribution function of reduced time as well as discrete model parameters λ_i , are influenced by the aging process as given by:

$$E_i \text{ or } \lambda_i \propto (AI)^n$$

or

$$a_A = f(AI) = f(\Delta E_a, \Delta E_u, T)$$

The effect of aging on creep compliance, $J(t)$ and retardation distribution function is shown in Figures 3-13 and 3-14.

3.2.4 The Environmental Function (a_E)

Based on the foregoing discussion one could postulate that there exists a fundamental environmental parameter, a_E which is a function of temperature, moisture, aging, and maturity, and the activation energy, i.e.,

$$a_E = a_E(a_M, a_T, a_A)$$

Therefore, a unique environmental shift function could be developed to encompass a broad range of environmental concerns.

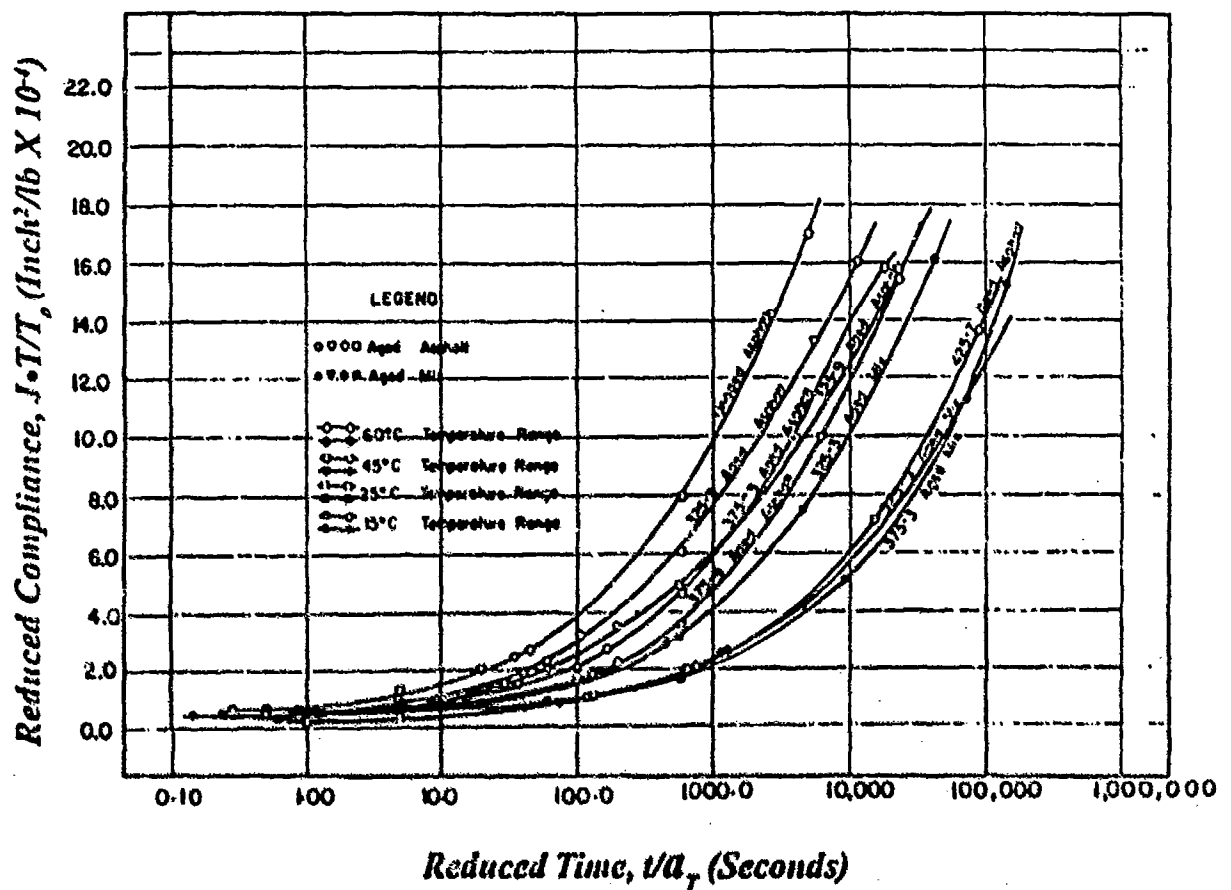


Figure 3-13. Master Creep Curve for Sand Asphalt

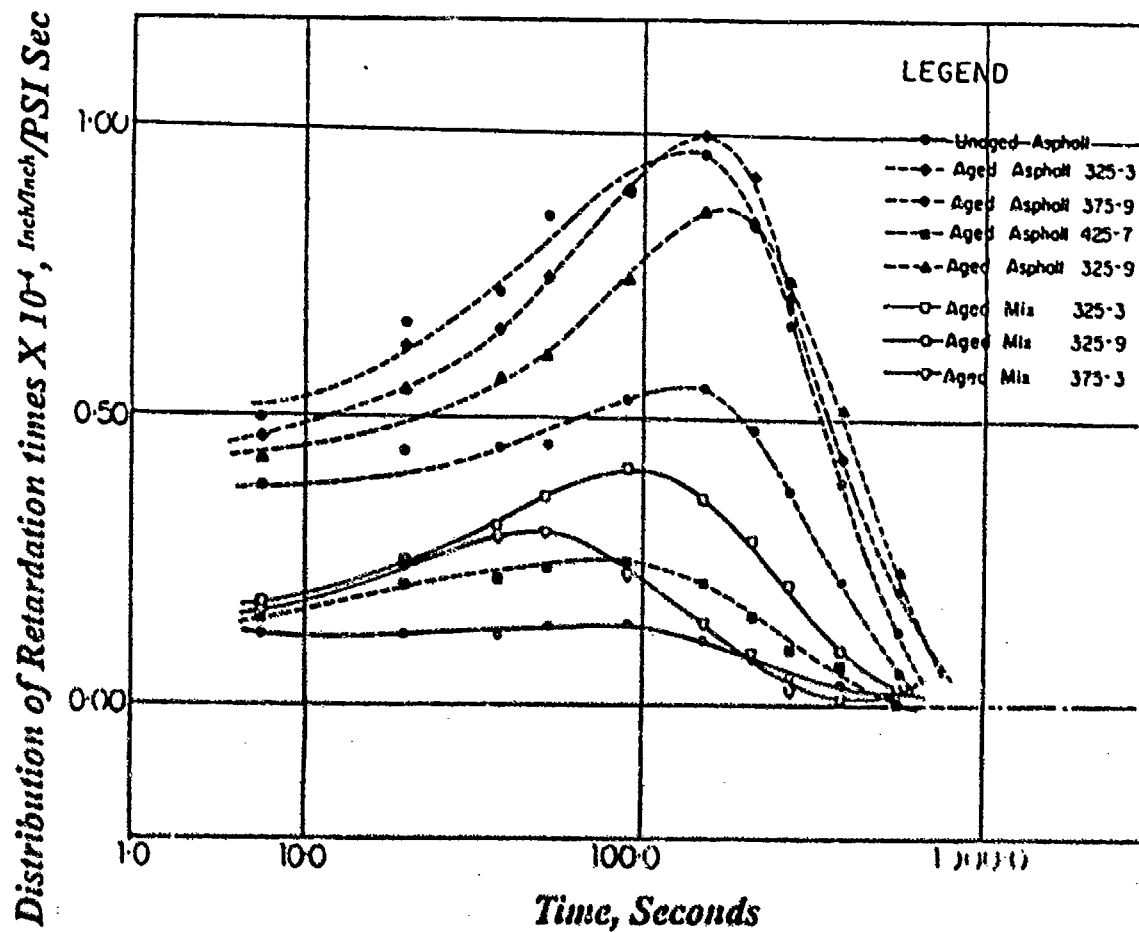


Figure 3-14. Distribution of Retardation Times for Sand Asphalt

4. UPDAP Structural Modeling

Our recommended UPDAP concept is based on the primary response model which includes the interactions of the structural, material and damage models. The importance of accounting for the interactions between these models cannot be overemphasized. In this section, we will discuss the role that the structural model plays in the UPDAP and the various factors that must be accommodated in this model.

4.1 Structural Modeling Considerations

There are a variety of modeling methods available for the analysis of structural systems. These essentially consist of closed-form solutions, various discretization schemes (e.g., finite difference and finite element analyses) and combinations of these methods (hybrid models). Depending on the objective of the analysis and the characteristics of the modeled system, one method may be more advantageous than the other methods. However, generally speaking, closed-form solutions commonly are employed in the case of linear systems and also are typically used for one- and two-dimensional analyses. The obvious appeal of the closed form approach lies in the computational speed associated with the solution and the straightforward approach to sensitivity studies.

However, closed-form solutions are difficult to employ when nonlinear phenomena are involved in the structural system. These nonlinear phenomena can result from inelastic material response characteristics, geometrical nonlinearities and the presence of pavement related anomalies such as voids, joints, boundary conditions between pavement layers (bonding to slippage), etc.

Over the past 25 years, discretization procedures have become increasingly employed in the solution of structural systems because of the enormous improvement in computational techniques, both in the software and the hardware aspects of the solution procedure. Large structural models involving many thousands of degrees-of-freedom are routinely exercised today, using a variety of general-purpose computer codes on a number of types of computer systems (mainframes, work stations and PCs). Probably the most popular technique in use today and for the foreseeable future represents the structure as discrete elements. Finite element representation possesses the ability to incorporate three-dimensional effects and anomalies (voids, cracks, joints, edges, etc.) explicitly into the simulation, although the calculations resulting from inclusion of such nonlinearities may increase execution times significantly.

The hybrid solution method combines closed-form solutions and the finite element method. Hybrid solutions will probably play an important role in the analysis of structural systems in the future because of the ease with which these methods can be joined and the added simplicity which may be accomplished with incorporation of the closed-form into the finite element representation when appropriate.

Based on these considerations, we believe that a three-dimensional finite element capability generally will be required to solve pavement design problems in future applications, and should be the primary structural modeling tool for the UPDAP.

It appears that the improvements in the use of the finite element method (FEM) are almost without bound for future use. The need to improve element types, numerical convergence, algorithm efficacy, solution accuracy and speed, and the desire for solution on smaller, faster computers are the objectives of the present research and development work. Thus, we believe that it is premature to select existing FEM computer codes for structural response modeling in UPDAP. We expect that advancements in structural modeling software and computer hardware will continue at a rapid rate, and the development of the UPDAP over the next few years should be tailored to incorporate these advancements.

We recommend the incorporation of a KBS into the UPDAP, with the capability for selecting the type and complexity of finite element representation needed to design and analyze any type of pavement system. The KBS also would select the appropriate representations of the environmental conditions, pavement material types, and structural anomalies and features. The essential point here is that in order to accommodate and account for all of these effects, a three-dimensional finite element representation will be necessary.

4.2 Current Methods of Analyses

Current methodologies employed in the structural analysis of pavement systems fall into one of two categories: rigid or flexible. If the pavement structure has characteristics which are not consistent with those associated with "flexible" or "rigid" pavements, neither methodology may be effective for predicting pavement response and performance. However, the current structural analysis codes can treat a multilayered (usually linear-elastic) pavement configuration and predict the stress and vertical displacement distributions throughout the layered system. These calculation schemes are limited by the number of layers and types of material constitutive characteristics that can be ascribed to each layer. These models are also limited by their inability to accommodate most

pavement anomalies in their calculation schemes. These limitations will be significant in the future when analysis of airport pavements must include the effects of the next generation of commercial transports that can have gross weights of over one million pounds.

For the large applied loads associated with such aircraft, the interaction of the damage, material and structural models is critical for the accurate prediction of pavement response and performance.

4.3 Structural Modeling Case Studies

It was stated in our earlier discussion that it would be inappropriate to focus on a single FEM computer code for use in the UPDAP. An important feature of our UPDAP concept is that it has a modular form, with "stand-alone" modules (e.g., the primary response model) which are appropriately linked. To achieve this form, the structural model should not only accommodate various structural pavement characteristics (e.g., joints, voids), but also should accommodate various material constitutive models and damage mechanisms. We performed studies to investigate the importance of these features in predicting pavement response.

Our initial studies included the development of pavement finite element models, which were exercised to investigate the influence of material models on predicted pavement response. The models were developed using ABAQUS, a commercially-available finite element code which is used widely in the engineering (and particularly the structures) community. ABAQUS was selected for our studies primarily because it contains a comprehensive library of advanced material models for pavement materials.

We evaluated two airport pavement configurations. One configuration consisted of an 18-inch-thick PCC layer on 12 inches of granular base and a 90-inch clay subbase. The other configuration consisted of an 18-inch thick-asphalt concrete layer on the same base and subbase (see Figure 4-1). For simplicity, the static landing gear was represented as a circular footprint with constant load (pressure) intensity. The axisymmetric nature of these examples required that the boundary conditions along the centerline of the applied load prevent horizontal (radial) motion and admit vertical displacements. The interface between the different layers was assumed to be fully bonded. This assumption was used for simplification purposes. The boundary at the far right side of the load provides for vertical displacements but no radial motion. The bottom of the subbase is considered to be simply supported.

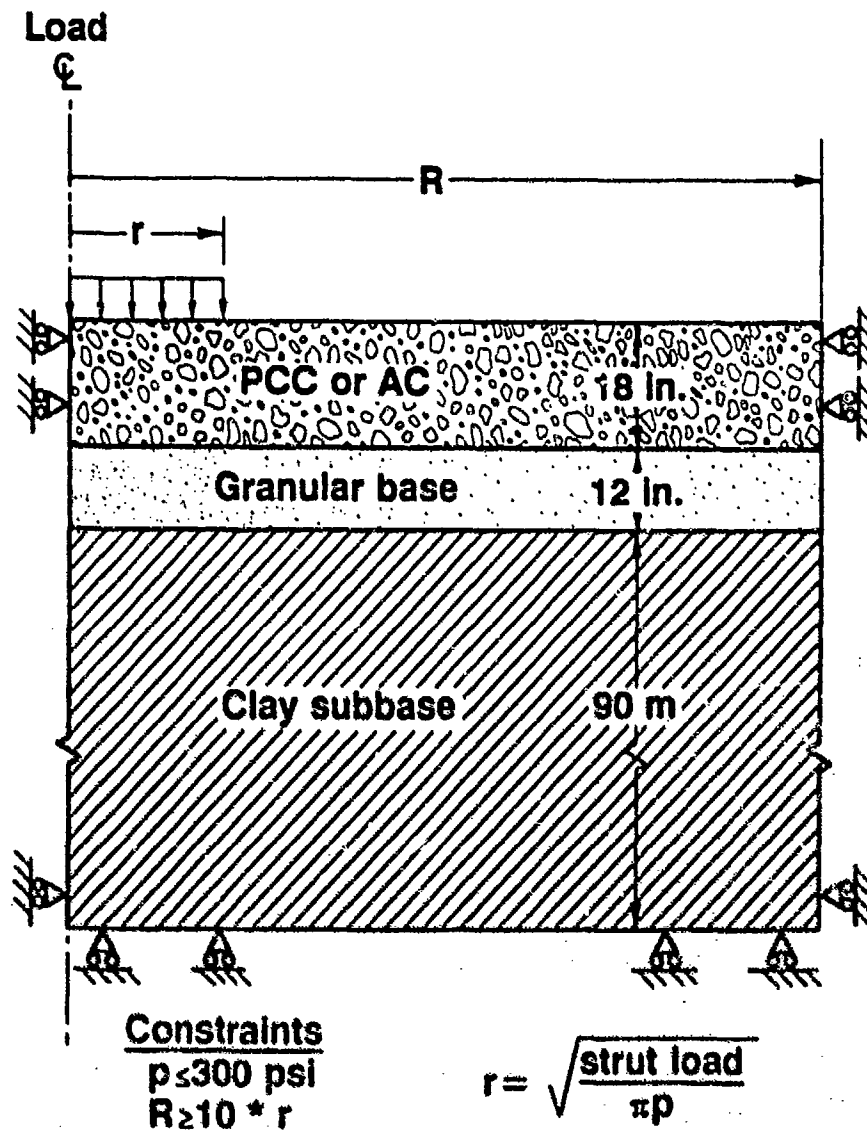


Figure 4-1. Idealized Airport Pavement Configuration

We have assumed that for future applications, tire pressures will be limited to 300 psig. Consequently, we generated a finite element mesh that is appropriate for loads up to the maximum weight expected for the next generation commercial transport (about 1.3 million gross pounds). Assuming a configuration for this aircraft of four main gear struts and four wheels per strut, we derived an effective load of 309,000 lbf applied over a circular footprint, with an effective load radius of about 18 inches. It has been established [4] that the extreme (right side) boundary in the structural representation (located at R in Figure 4-1) be positioned so that $R > 10r$. Based on this criteria, we chose $R=200$ inches.

The finite element mesh included 164 nodes, 520 elements, and 3282 degrees-of-freedom. The elements under and in the vicinity of the applied load are small (fine mesh) and those in the lower layers and radially removed from the vicinity of the applied load are less fine. (See Figure 4-2.)

4.3.1 FCC/Granular Base/Clay Subbase Pavement System

Linear and nonlinear solutions were compared for the configuration consisting of PCC, granular base and clay subbase. For the linear case, the three pavement layers were assumed to possess linear elastic material characteristics. For the nonlinear cases, all three layers were represented by appropriate inelastic characteristics

For the linear case, the following values were used:

Concrete: $E = 4.15 \times 10^6$ psi
 $\nu = 0.15$

Granular Base: $E = 30,000$ psi
 $\nu = 0.3$

Clay Subbase: $E = 8,000$ psi
 $\nu = 0.45$

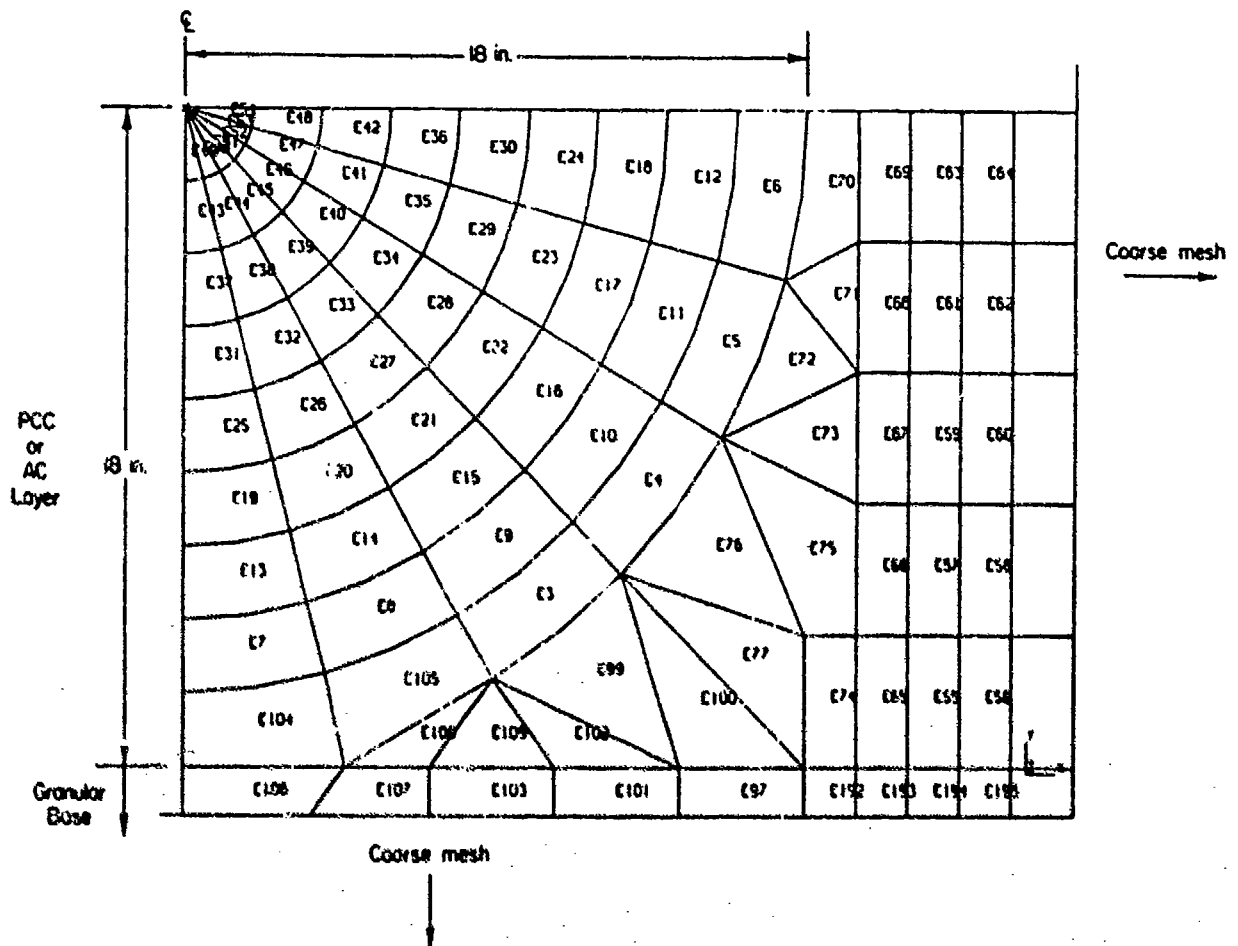


Figure 4-2. Finite Element Mesh in the Vicinity of the Applied Load

For the nonlinear (inelastic) case, the following parameters were used:

Concrete:	Yield Stress = 3000 psi Failure Stress = 550 psi Plastic Strain = 1.5×10^{-3} (at failure) Tension Stiffening Included
Granular Base: (Extended Drucker-Prager)	Friction angle, $\beta = 50$ degrees Associated Flow, $\Psi = B$ Third stress invariant Factor $K = 1.0$
Clay Subbase:	Initial response: Porous Elastic Log/Bulk Modulus = 0.0002 1; $G = 2758$ psi Plasticity: Critical State Ratio $M = 1.0$ Consolidation Parameter $a_0 = 103.56$ Third Stress Invariant Factor $K = 1.0$ Initial Void Ratio $e = 0.98$

The results of the linear case were compared to predictions from a typical multilayer analysis procedure, called Elastic Linear Half Space Analysis (ELHSA-5). The results compared well, and provided some level of verification of our model.

It has been observed that for a relatively thick rigid pavement that is supported on a sound base and subbase system, the major portion of the applied load will be reacted in the PCC layer. Consequently, the supporting layers - in our case the granular base and clay subbase - will experience very low levels of stress. The results of our inelastic analyses were consistent with these observations. Since the major portion of the applied load was reacted by the PCC layer, failure in the form of cracking occurred initially in the bottom fibers of the concrete slab.

The constitutive material model employs tension stiffening capability for the concrete layer elements. Thus, the cracked element can support some tensile load immediately after the onset of cracking. In order to accommodate this effect, a shear imbalance will occur in the cracked element. This shear imbalance will in turn be equilibrated by a tensile force acting in the vertical direction on the top of the cracked element. Thus, under the applied load at the bottom fibers of the rigid slab, the elements that are cracked can exhibit a vertical tensile stress.

The influence of applied (gear/wheel) load on pavement response was evaluated for this configuration. For simplicity, we held the pressure constant (300 psi) and varied the effective load radius over a range that represented various aircraft configurations (727, 747, HSCT, etc.). Since the load required to induce cracking in the concrete layer is not the same for all aircraft configurations, we performed a parameter study to determine the pressure required to initiate cracking as a function of the load radius associated with several aircraft configuration. The results of this study are presented in Figure 4-3 where the data are labeled with the aircraft model association with the indicated (strut) load radius. As indicated in the figure, for the HSCT configuration, tire pressures as low as 150 psi - corresponding to about 50 percent of its gross take-off weight - would initiate cracking in this pavement model. Similarly, the 747 configuration would cause cracking in this concrete pavement at gross take-off weights of over about 540,000 lbf.

The results of this limited study indicate the importance of applying aircraft-specific loading conditions - rather than equivalent loads which attempt to represent all of aircraft - to predict pavement performance with sufficient accuracy.

For the analyses performed with this pavement configuration, there was no inelastic response in either the granular base or clay subbase. This is attributed to the relatively low levels of stress in these layers. In all of our cases, the maximum vertical stress experienced in the base did not exceed 10 psi.

4.3.2 Asphalt Concrete (AC)/Granular Base/Clay Subbase

We performed parameter studies for the AC/Granular Base/Clay Subbase case using a linear representation of the AC layer and nonlinear representations of the base and subbase layers. For the AC layer, we used $E=500,000$ psi and $\mu = 0.4$, while for the base and subbase layers, we used the values indicated previously for the PCC configuration. The structural configuration assumed for this case was identical to that for the PCC case, which was shown in Figure 4-1.

The primary objective of our studies with this pavement configuration was to evaluate the influence of material inelastic behavior in the base and subbase on the overall pavement response for loading conditions representative of the HSCT type of aircraft. For these studies, we applied loads in a circular footprint of an 18-inch radius at pressures of from 25 psi to 300 psi in 25-psi increments.

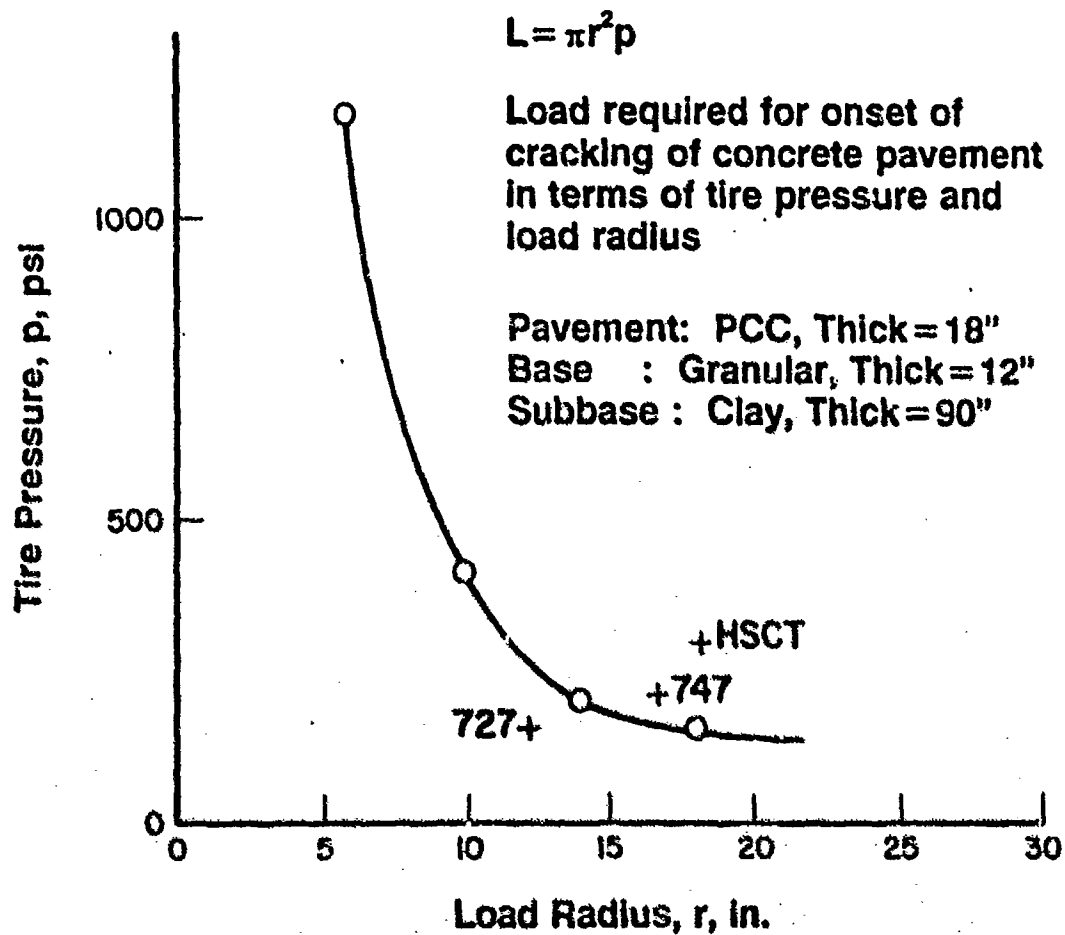


Figure 4-3. Pavement Cracking as a Function of Tire Pressure and Load Radius

The results indicate that plastic flow initiated in the bottom segment of the granular base at a pressure of about 75 psi. This response is shown graphically in Figure 4-4, which shows the plastic strain component in the radial direction as PE11. The highest positive values of PE11 are indicated by the red areas; as shown, this area is at the intersection of the base and subbase layers. The vertical component of the plastic strain, PE22, is shown in Figure 4-5 for an applied pressure of 75 psi. These plastic strains result in nonrecoverable deformation.

Figures 4-6 and 4-7 show radial and vertical plastic strain components for a pressure of 125 psi. Figures 4-8 and 4-9 show the same plastic strains at 225 psi. As indicated in these figures, the plastic region increases rapidly with increasing applied pressure.

The deformed state of the pavement structure at applied pressures of 75 psi and 225 psi are shown in Figures 4-10 and 4-11, respectively.

We investigated the influence of inelastic behavior on pavement surface deformations by permitting only linear elastic behavior in the base, while prescribing porous elastic behavior for the subbase. The porous elastic model used for the subbase basically involves hydrostatic behavior, which has a stiffening effect with increasing load. Results for this case are presented as the curve labelled "Porous Elastic" in Figure 4-12, which describes the surface displacement directly under the centerline of the applied load as a function of tire pressure. The other curve shown in the figure, which is labeled "Inelastic Base", represents the condition when both base and subbase are permitted to have inelastic behavior. As indicated in the figure, the inelastic material response in the base has a significant effect on the pavement response, and this effect is stronger with increasing load. Further, the pavement displacements are underestimated with the model using a linear representation of the base layer. This implies that a linear representation of the base layer is generally not conservative.

It is pointed out that complete bonding between layers was assumed in this analysis and this will support bonding in the layers which permits maximum deformation. It therefore is important to properly simulate the conditions at the layer interface. This is an important consideration in the UPDAP.

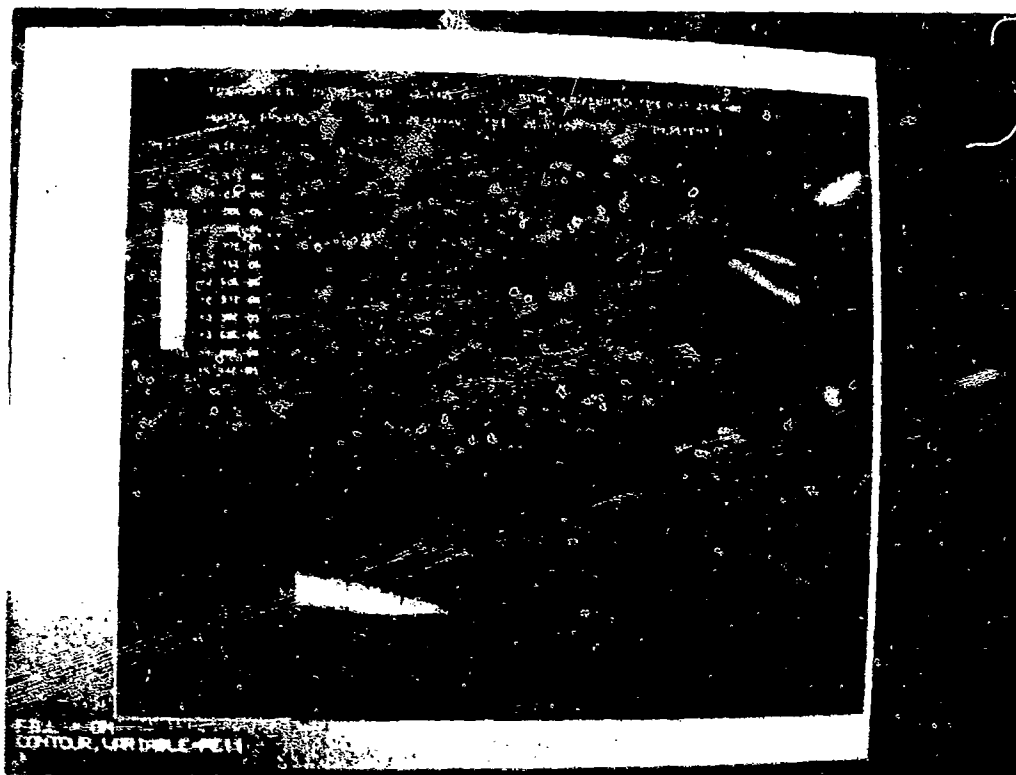


Figure 4-4. Radial Plastic Strain, PE11, @ $p = 75$ PSI

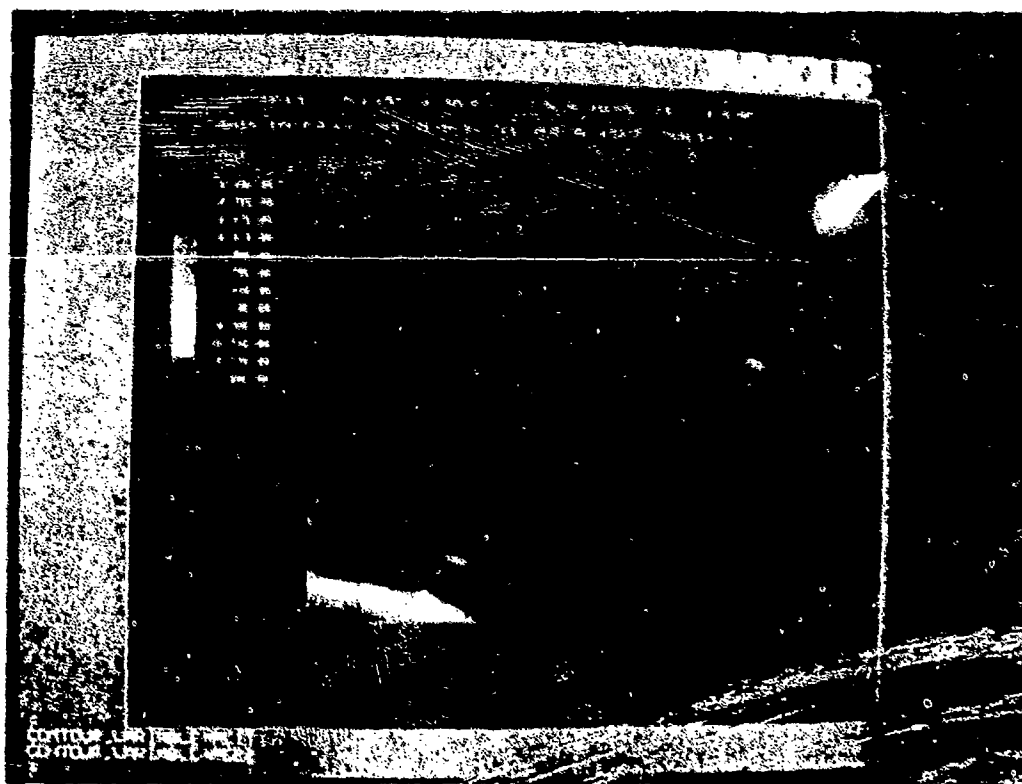


Figure 4-5. Vertical Plastic Strain, PE22, @ $p = 75$ PSI

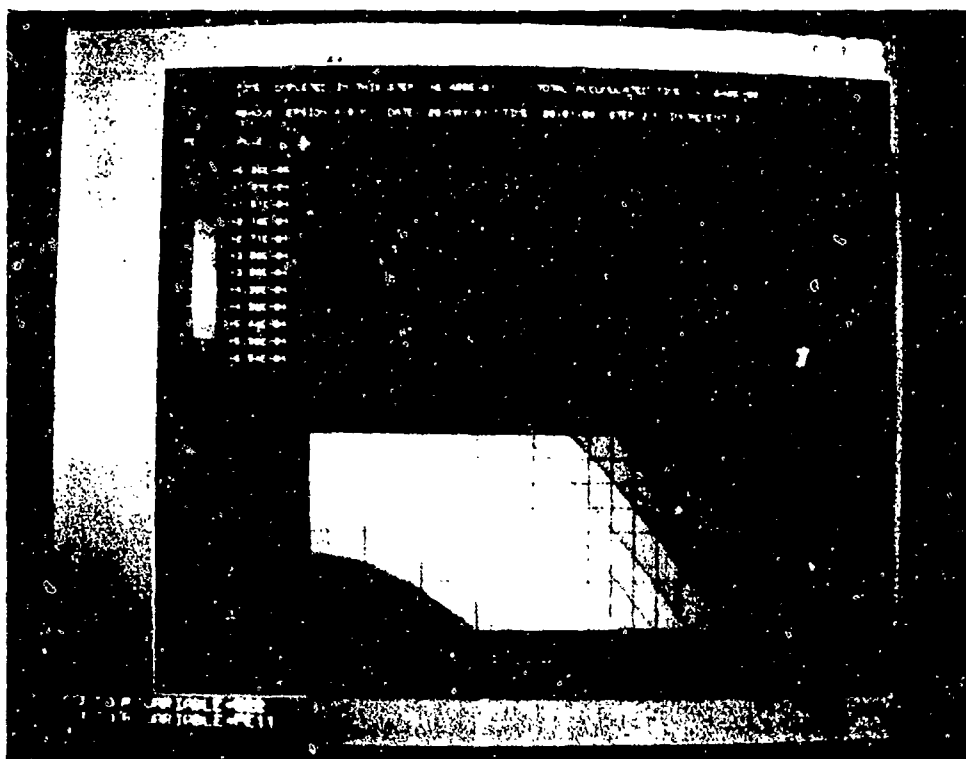


Figure 4-8. Radial Plastic Strain, PE11, @ $p = 225$ PSI

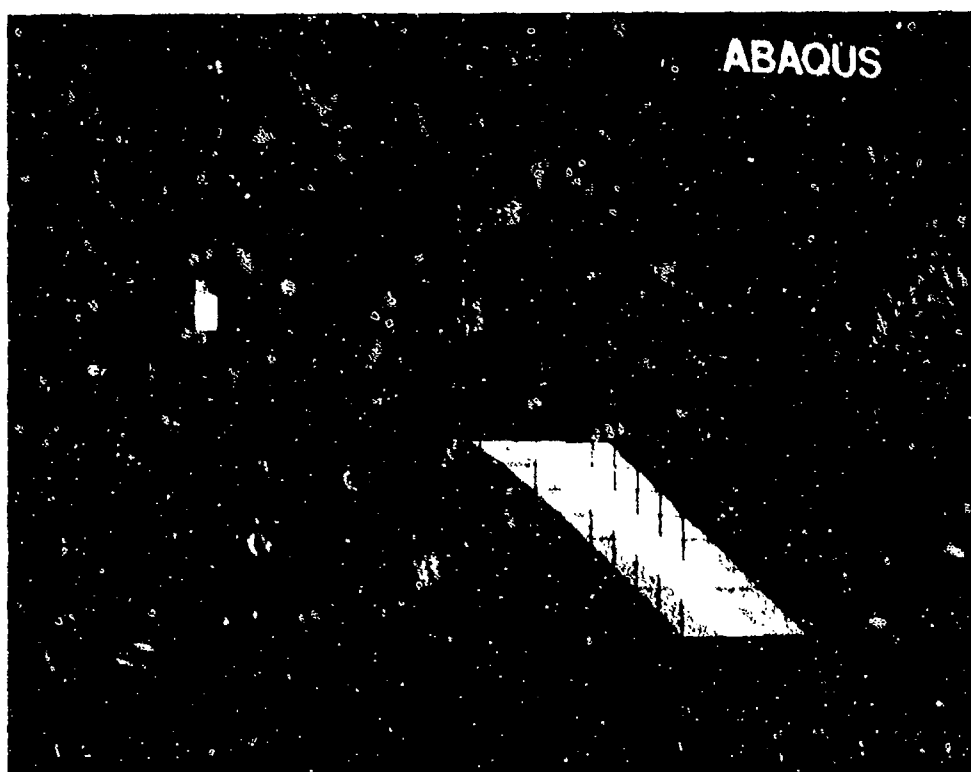


Figure 4-9. Vertical Plastic Strain, PE22, @ $p = 225$ PSI

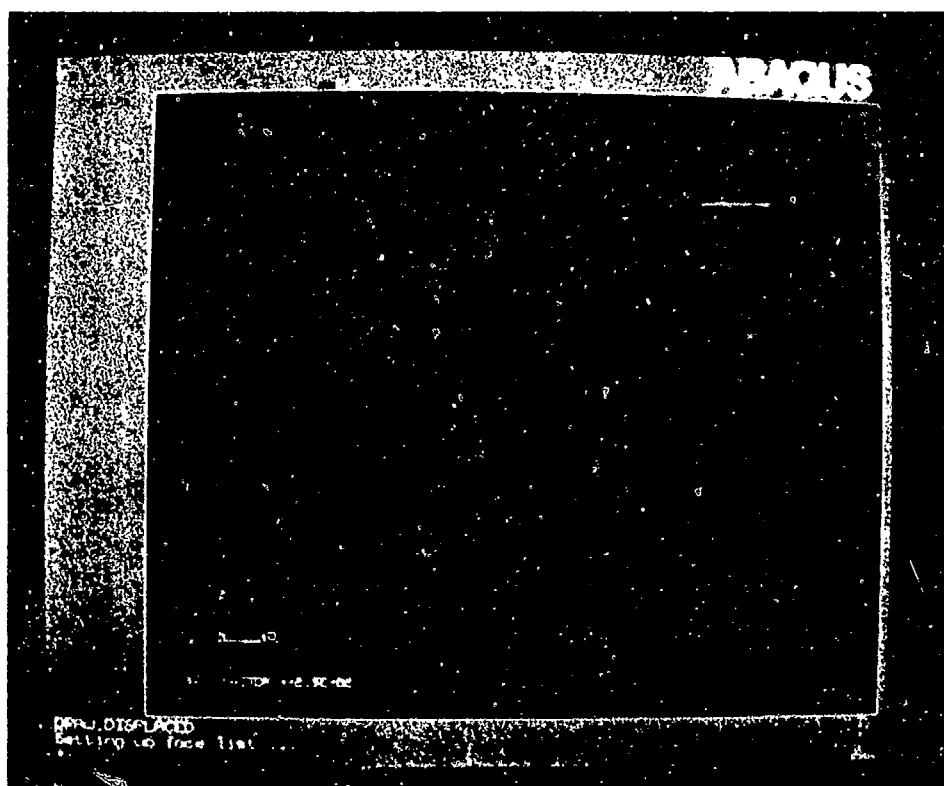


Figure 4-10. Displacement Contour When $p = 75$ PSI

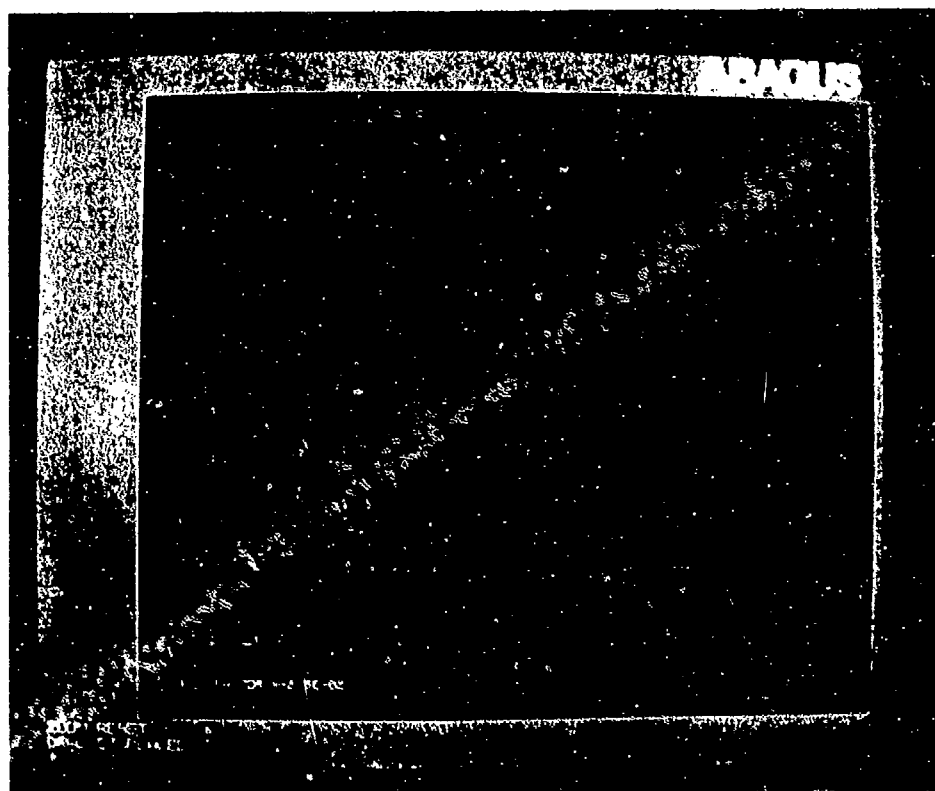


Figure 4-11. Displacement Contour When $p = 225$ PSI

ASPHALT/CONCRETE PAVEMENT SUPPORTED ON GRANULAR BASE AND CLAY SUBBASE

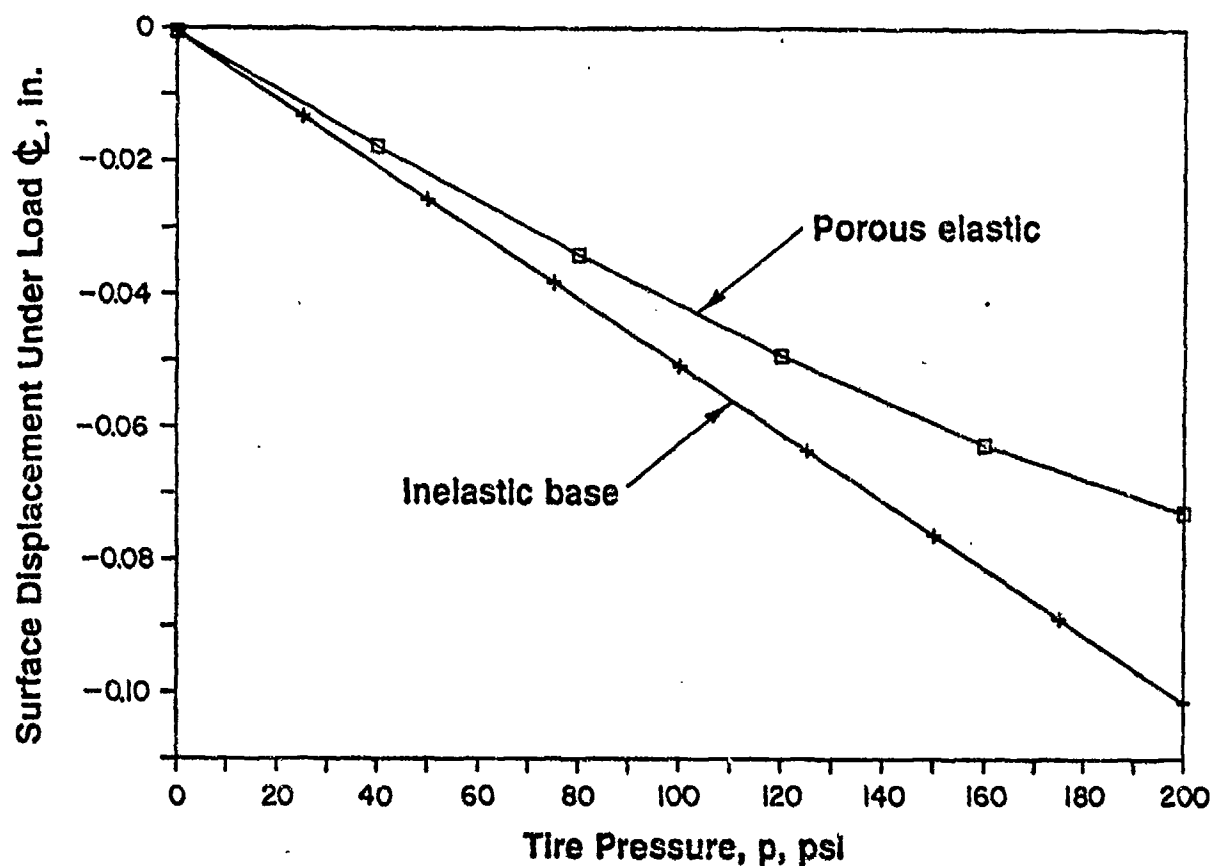


Figure 4-12. Displacement Under Load Centerline vs. Tire Pressure

5. Damage Modeling

Damage models are a critical part of the UPDAP because the ultimate purpose is to determine the performance of the pavement in service. Therefore, events that damage the pavement, reducing its serviceability, must be represented in the UPDAP.

5.1 Modeling Issues

Presently there are mechanistic damage models for only a fraction of the types of damage that can occur in airport pavements, see Table 5-1. There are empirical models for others. However, most have been developed for highway pavements. Because with airport pavements the layers are substantially thicker and the loads are substantially greater, the empirical highway models are of limited value.

Mechanistic models are required for all damage mechanisms that will be included in the UPDAP. As stated above, many of these models have to be developed and verified. In developing damage models several issues must be addressed. Significant issues include the definition of damage, and the relationship between damage and the mechanistic quantities available from the structural analysis model.

A clear definition of damage is needed for the development of damage models consistent with this, the damage models need to be integrated into the UPDAP. Using the finite element method, damage in pavements can be divided into two categories: structural damage, and material damage. Structural damage requires modification of the elements and nodes (the mesh) which define the structural configuration of the pavement for the analysis. In contrast, material damage can be accommodated with the material model. For example, microcracking of PCC can be incorporated into the analysis through the material model as a nonisotropic reduction in stiffness. Similarly, the healing of small cracks in AC can be accounted for with the material model. Accounting for structural damage to the pavement generally requires a change in the continuity or connectivity, within or between the layers. Structural damage of this type can not be adequately accounted for with the material models. The structural model (mesh) of the pavement must be changed to reflect the damaged state. This often requires the replacement of some elements with "gap-contact" elements or crack elements, and analysis techniques such as fracture mechanics.

Table 5-1. Distress Types and Availability of Mechanistic Models

Pavement Type	Distress Type	Mechanistic Model
Rigid	Cracking:	
	- Longitudinal	x
	- Transverse	x
	- Diagonal	x
	- Corner	x
	- "D" Cracking	
	Disintegration:	
	- Scaling	
	- Spalling	
	- Blowups	
	- Shattered Slabs	
	- Joint Seal Damage	
	Distortion:	
	- Pumping	x
Flexible	- Faulting	x
	- Settlement	
	Loss of Friction:	
	- Polished Aggregate	
	- Rubber Build-up	
	- Fuel Spillage	
	Cracking:	
	- Longitudinal	x
	- Transverse	x
	- Alligator	x
	- Block	x
	- Slippage	
	Disintegration:	
	- Ravelling	
	- Stripping	
	Distortion:	
	- Rutting	x
	- Corrugation	x
	- Depression	
	- Swelling	
	Loss of Friction:	
	- Bleeding	
	- Polished Aggregate	
	- Rubber Build-up	
	- Fuel Spillage	

Tests conducted to define the material response models and damage models must be defined in a manner that is consistent with the definition of damage that is used to construct the FEM model. Otherwise, there will be the potential for misinterpreting the analysis results. For example, there is a great deal of fatigue data available for PCC pavements. Tests conducted to derive these data generally include a supporting base and subbase. It is highly desirable to use this body of data to develop a comprehensive fatigue model for PCC. Typically, such a model is developed by defining the mechanical parameter(s) responsible for the damage. With fatigue of PCC pavements, this is typically the bending stress, or some quantity which embodies bending stress. For discussion purposes, the mechanistic quantity referred to as mechanical parameter responsible for the damage is simply the damage parameter. The comprehensive fatigue model is calibrated by fitting a mathematical expression through the damage parameter versus load cycles to failure data.

Issues that must be addressed in defining the comprehensive fatigue model are: (1) what is failure, and (2) what is the value of the damage parameter corresponding to the failure? The answers to these questions must be consistent with the definition of failure used in the development of the UPDAP finite element structural analysis model. For instance, as microcracks develop in the PCC due to repeated loading, its stiffness will change; it will become more flexible. This stiffness change will cause the stresses in the structure to be redistributed. Consequently, the value of the damage parameter will change during the test once the microcracks develop, and will continue to change as the microcracking propagates. This could make it difficult to calibrate the fatigue damage model for PCC using these data, and bending stress as the damage parameter.

In order to determine the stresses in the PCC responsible for fatigue cracking, an analysis is required. In addition, accurate material models are needed for the PCC, the base and the subbase. Because the stresses computed in the PCC are very sensitive to changes in these material models, it is essential that the PCC fatigue data be reduced using the same analysis procedure and material models that will eventually be used to analyze other PCC pavements. Consequently, it is important to define damage consistently, so that the analysis can reasonably model the pavement response. For these reasons, accurate structural and material models are needed in order to interpret PCC fatigue data from tests on actual pavement of multilayer test specimens.

Two other aspects of damage modeling need to be addressed. First, the damage models developed for the various mechanisms will require a scheme for damage accumulation. For fatigue the Miner linear damage accumulation approach is typically used to determine the damage done by variable amplitude loading. In other words, the damage parameter is not the same on every cycle.

Second, a definition is needed for a cycle that is consistent with the definition of damage as defined by the damage parameter for variable amplitude loading. Several schemes are available for counting fatigue cycles. These range in complexity from simple peak counting to the "rain-flow" method [5]. The "rain-flow" method is generally the best for metals because it properly accounts for the hysteresis and the memory of prior strain events exhibited by metals.

5.2 Interaction Issues

Damage mechanisms operative in airport pavements can interact. These interactions are symbolized in Figure 2-1 as feedback loops between the Damage Analysis and the Material Property Data (loop 1) and the Damage Analysis and the Structural Analysis (loop 2).

An example of the damage/material interaction (loop 1) has been given with regard to rutting of AC pavements. Rutting develops due to a combination of flow and densification. Furthermore, densification changes the response of the AC sufficiently to change the stresses in the AC layer. By accounting for this interaction, rutting damage model can be accurately predicted.

As an example of the damage/structural interaction (loop 2), consider the PCC pavement shown in Figures 5-1 and 5-2. This pavement has a void located beneath the corner of one slab, and is loaded by a single vertical force as shown in the figure. An analysis package called, RISC, has been developed by Resource International, Inc to determine the effect of voids on pavement performance [6]. The void beneath the PCC slab will alter the overall response of the pavement for this position of the applied load. More specifically, as voids develop and grow the following conditions will develop.

1. The damage mechanism most likely to result in failure can change. For example, as a corner void develops a greater portion of the load is transferred through the dowel bars to the adjacent slabs. This results in greater dowel bar bending stresses and greater bearing stresses in the PCC at these dowel bar locations. The elevated stresses may lead to premature failure of the pavement structure because the void compromises the load carrying capacity of the base.
2. The location of the maximum bending stress in the PCC slabs will change because the support condition for the slab changes with the development of the void. This means that the focal point for fatigue damage due to repeated application of the load will move across the slab as the void grows. Thus, fatigue damage produced by the application of

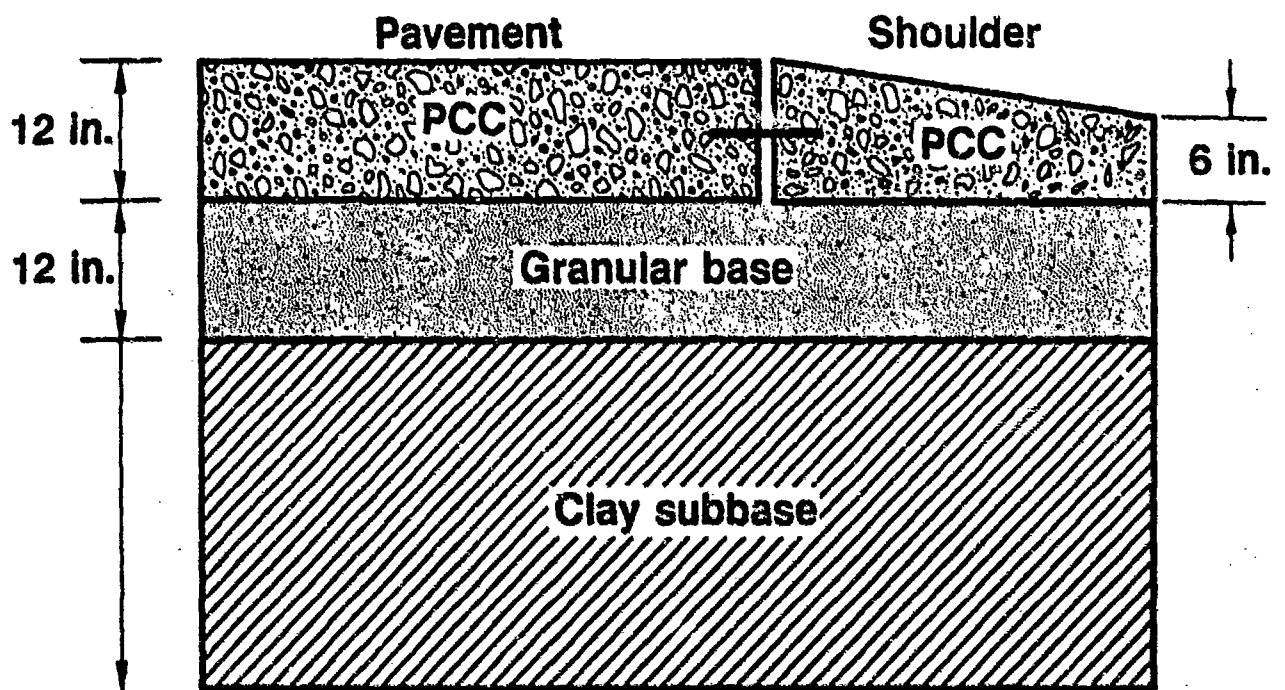


Figure 5-1. Pavement Configuration (Elevation View)

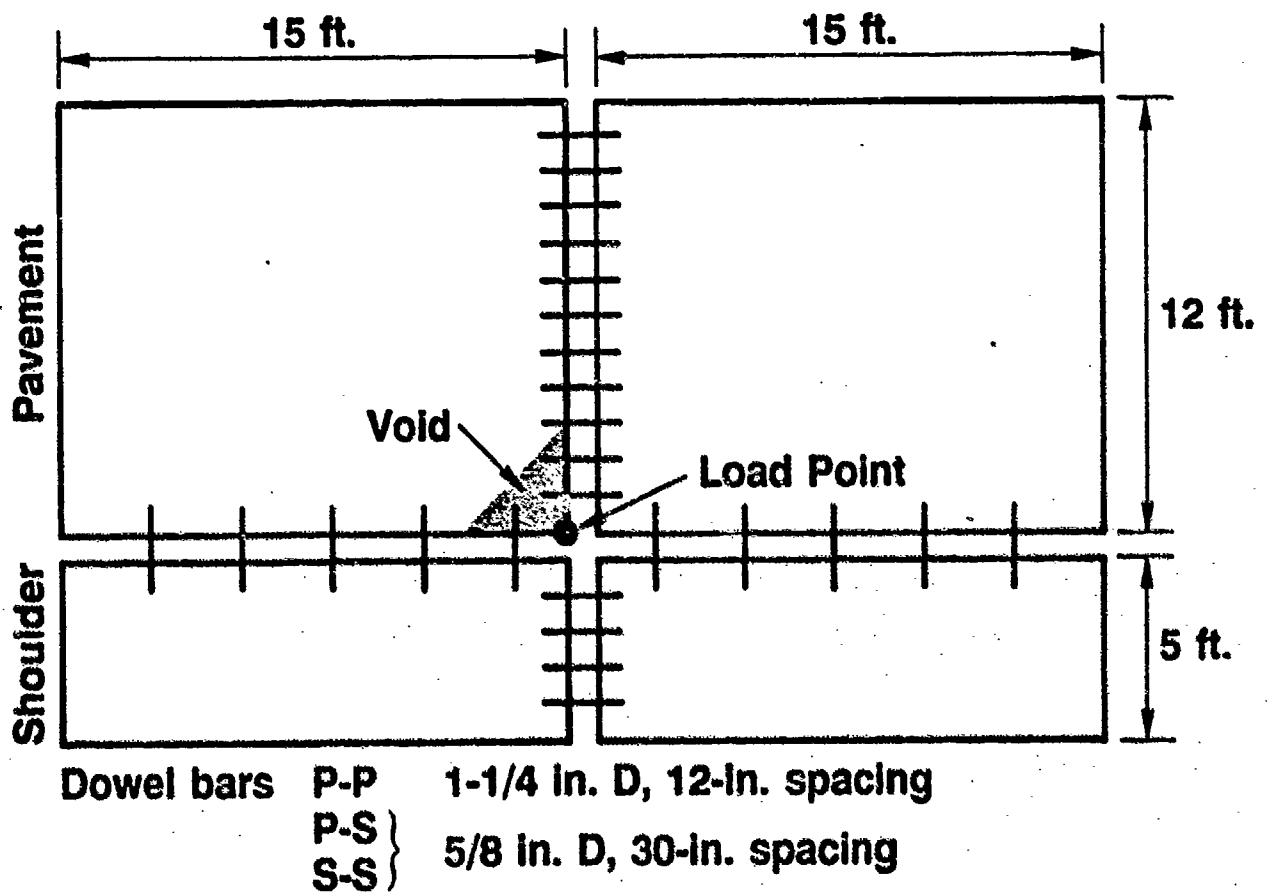


Figure 5-2. Pavement Configuration (Plan View)

the load shown in Figure 5-2, will not be concentrated at a single site. This could increase the fatigue life of the PCC slab in bending.

In order to model this type of behavior, the structural model must incorporate the following features:

- a. multiple PCC slabs,
- b. dowel bars for load transfer between the slabs,
- c. damage in the form of voids located beneath PCC slabs, and
- d. multiple layers to represent the base, subbase, etc.

While not essential for this discussion, the structural model should also include the weight of the slabs and through-thickness thermal gradients. These specialized features make RISC an ideal test bed for demonstrating the Damage/Structural interaction, as well as highlighting other important modeling issues.

RISC uses a hybrid FEM/closed form analysis procedure to account for the three-dimensional nature of pavement structures. The FEM solution is used to compute the stresses in the PCC slabs and the dowel bars. The closed-form elastic layer theory is used to determine the flexibility of the foundation beneath the slabs.

The damage analysis contained within RISC is presented in the form of a flowchart in Figure 5-3. Inputs for RISC are summarized on the left side of the flowchart. These include the load, the pavement parameters (number of slabs, number of layers, dimensions, material properties, etc.), and the void (size, shape and location). The outputs, shown at or on the right side of the flowchart, include the fatigue performance (number of load applications to failure) and faulting performance (fault size). The inputs are used by the structural model (Primary Response Model) to determine the bending stress in the PCC slabs, the bearing stress in PCC at the dowel bars, and the bending stress in the dowel bars. The fatigue model uses the bending stress in the PCC to determine the fatigue life, i.e., the number of cycles to failure, N_f , for the PCC slabs. At the same time, the faulting model uses the bearing stress in the PCC to determine the amount of faulting that will exist after N_f load cycles.

A schematic of the results from such an analysis are shown in Figure 5-4, in the form of a damage interaction diagram. The data points, and the dotted line, indicate the number of load cycles that will cause a bending fatigue failure in the PCC. The solid lines indicate the faulting that will develop with load cycles based on a model by Darter [7].

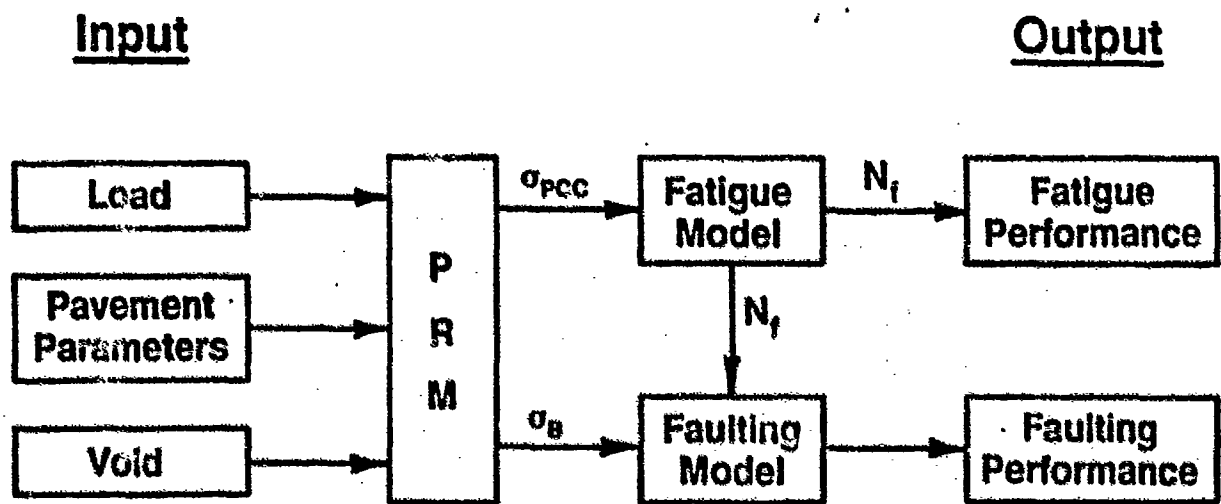


Figure 5-3. Analysis Procedure Used by RISC

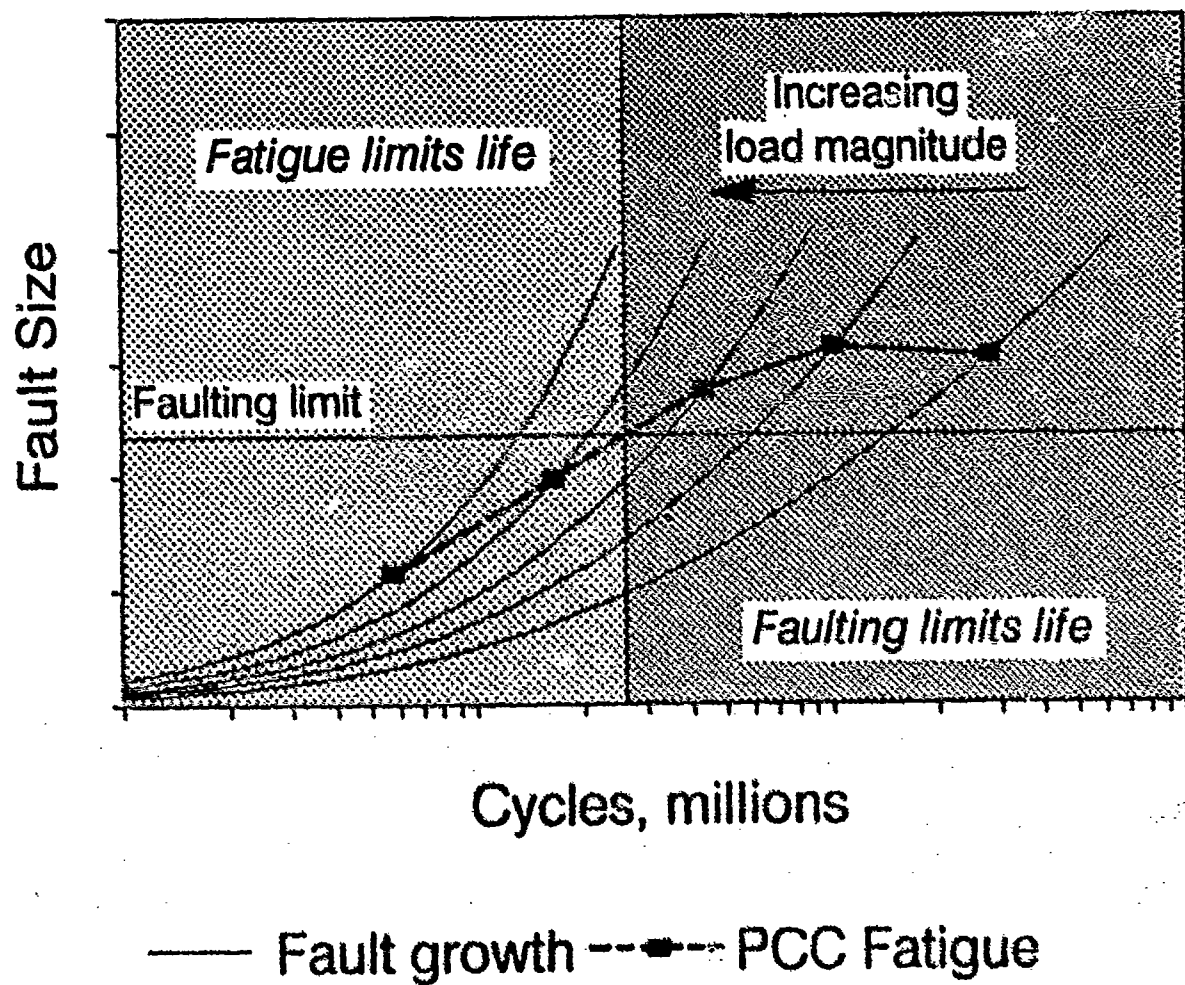


Figure 5-4. Fatigue-Faulting Damage Interaction Diagram

Naturally, there is a limit on the amount of faulting that can be permitted to develop in a pavement. A faulting limit is shown in a or the damage interaction diagram shown in Figure 5-4. The point where the faulting limit intersects the fatigue curve (the dotted line) divides the life of the pavement into regions, one where fatigue limits the life of the pavement and another where faulting limits the life of the pavement. Fatigue damage of the dowel bars could also be incorporated into the damage interaction diagram.

The growth of the void caused by the load cycles can either accelerate or retard the development of damage done in the pavement. The growth of the void increases the bending stresses in the dowel bars and the bearing stresses in the PCC at these dowel bars, thereby accelerating damage in these areas. At the same time, the effect of bending fatigue damage in the PCC is diffused over a wider area of the pavements increasing the total life of the slab. However, as the void grows the magnitude of the maximum bending stress increases, which would tend to reduce the life slab. As such, the damage mechanisms operating on the structure are in competition with one another. The mechanism which eventually causes the failure depends on the interaction between the various mechanisms and the structural analysis model.

Because more than one damage mechanism will be active, each must be tracked in the UPDAP. Furthermore, because fatigue damage, for example, can be distributed over the slab, the fatigue damage at each portion of the slab must also be tracked. This suggests a local damage approach is needed, wherein the effect of each damage mechanism is tracked throughout the model.

6. Pavement Testing and Instrumentation

A key to developing the UPDAP is an effective test program that will provide measured response and calibration of the analytic model.

There are several significant benefits to be accrued from airport pavement instrumentation and testing. Perhaps the most important is better understanding of the response phenomenon of pavement systems. Existing analytic procedures have proven to be beneficial in interpolating and in some cases extrapolating pavement response and materials properties for design and evaluation. However, there have been limited research efforts to combine theoretical studies with data collection from instrumented airport pavements. The limited results that can be referenced indicate that currently used analytic model predictions of pavement response do not agree with measured response. Figures 6-1 and 6-2 show predicted and measured surface deflection and deflection with depth, respectively, in instrumented pavement test sections.

Pavement physical response data from well-conceived instrumentation can be effective in calibrating various performance factors. In addition, the data can also be the basis for conceptualizing pavement mechanics or response phenomena. If more and better calibration of factors is desired then better understanding is needed of how pavement materials and layers react to a spectrum of loading. As an example, total deflection data from aircraft loading is shown in Figure 6-3. Deflection gages were anchored at different depths from the surface and deformation recorded in each gage, as shown in Figure 6-4. Subsequent rebound in each gage is shown in Figure 6-5. These data are from between the wheels of a 727 aircraft and reflect data from selected events showing where in the pavement system deflection and rebound are occurring. A wave emanating from and trailing away from the path of loading was observed in the same test data. In addition to this dynamic loading response, the pavement model and associated material characteristics need to have a capability to reflect changing conditions and performance. The performance may be associated with environment and traffic. Figure 6-6 shows the surface and in-depth profile deformations in a MWHGL test section. Figure 6-7 shows surface cracking in another MWHGL test section. The convention of assuming that asphalt pavement fatigue cracking initiates in the lowest asphalt layer is not substantiated in Figure 6-8. These types of phenomena underscore the need for response data. Such observations and data will be the basis for better and accurate models of pavement response and behavior.

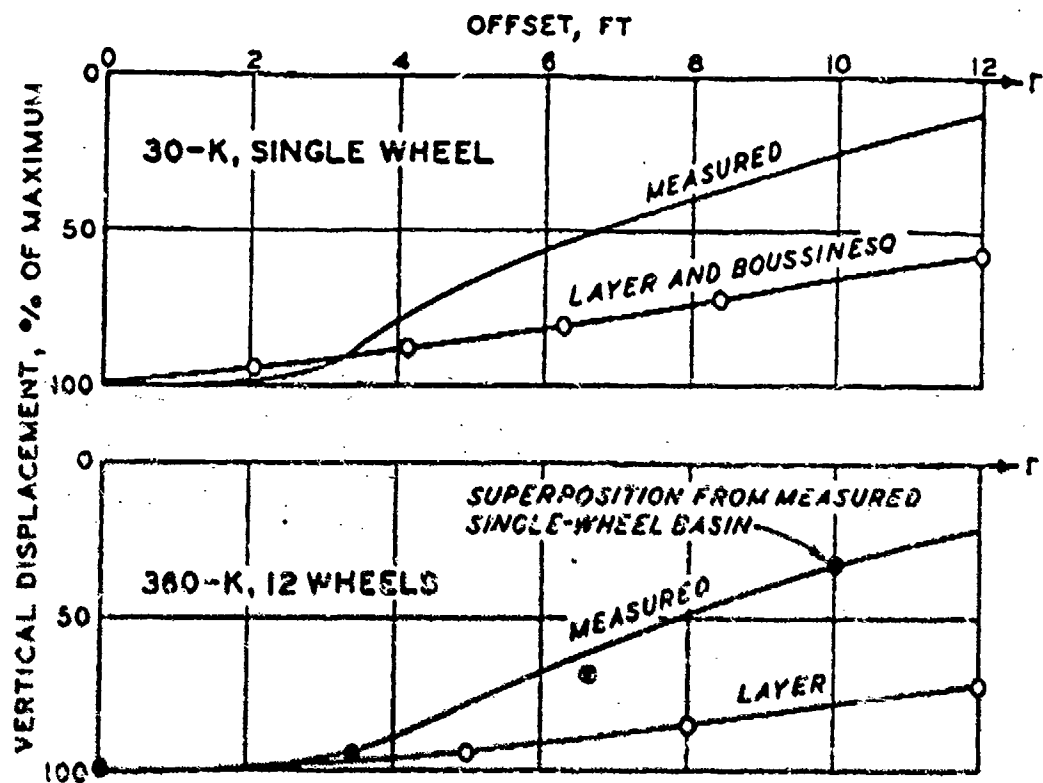


Figure 6-1. Computed and Measured Deflection Basins at 12-ft. Depth, Item 3, MWHGL Test Section, 30 KIP Static Load, Single- and 12-Wheel Assemblies (Note: Load Indicated In all Figure Captions Refers to the Load per Wheel)
(Chou and Ledbetter)

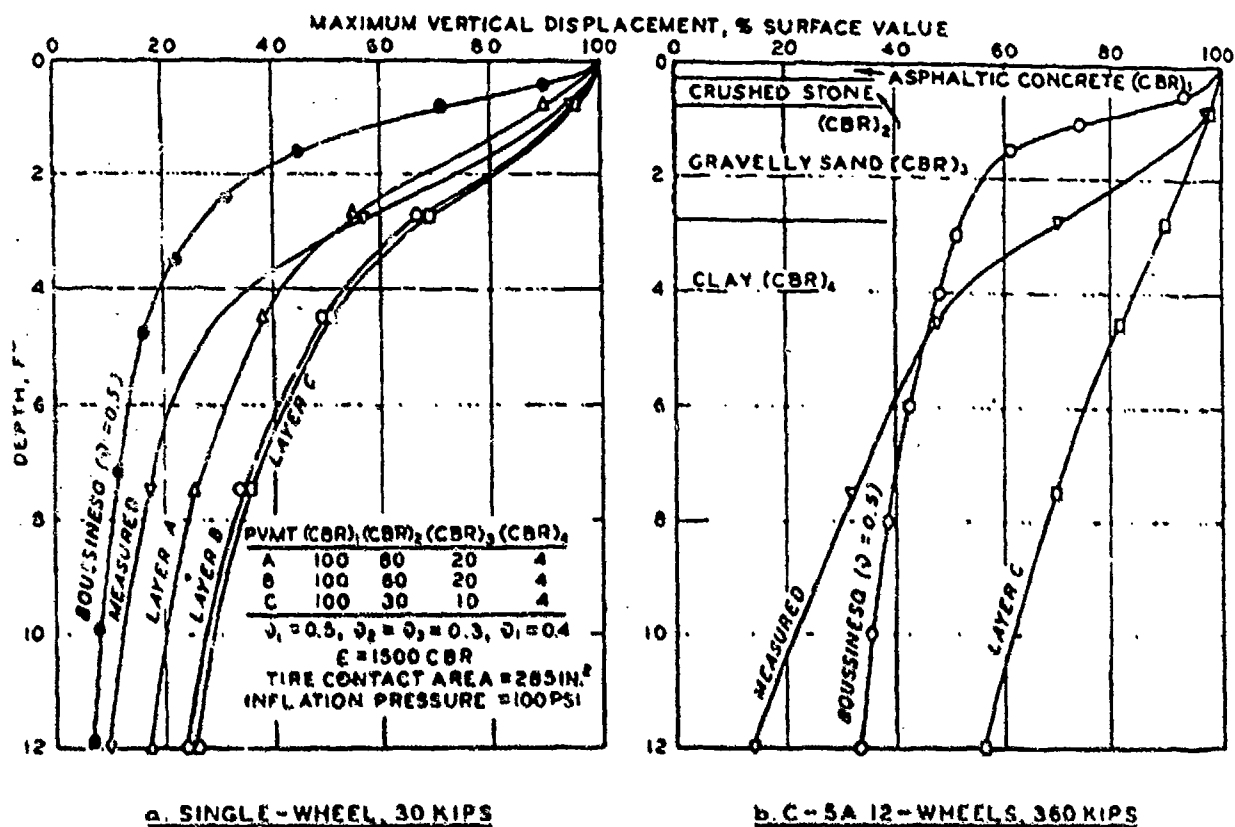
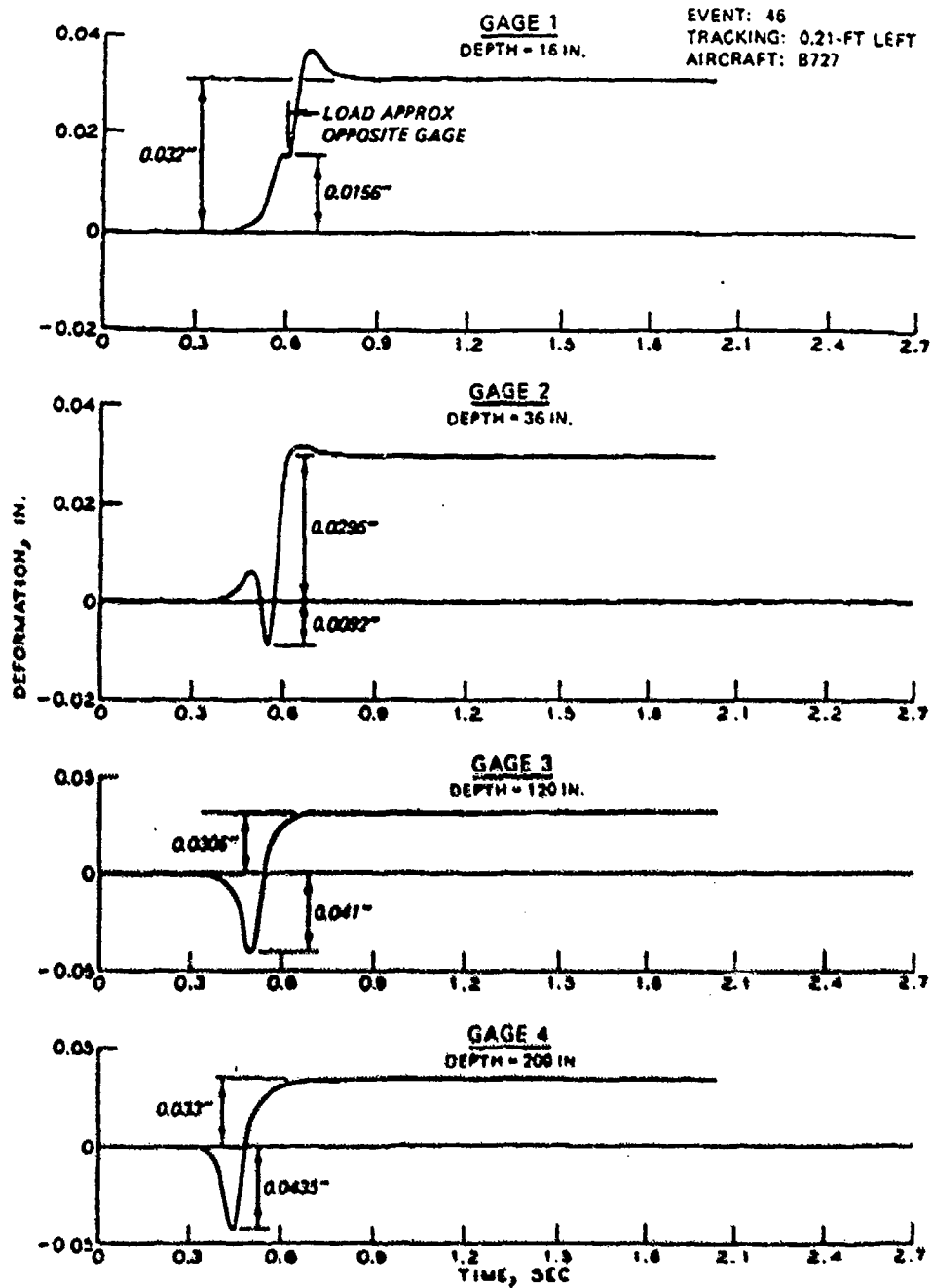


Figure 6-2. Computed and Measured Maximum Deflection Under Static Single- and 12-Wheel Loads, Item 3, MWHGL Test Section (Measured Data from Ahlvin, et al. [9])



**Figure 6-3. B-727 Pavement Response Between Wheels
(White [10])**

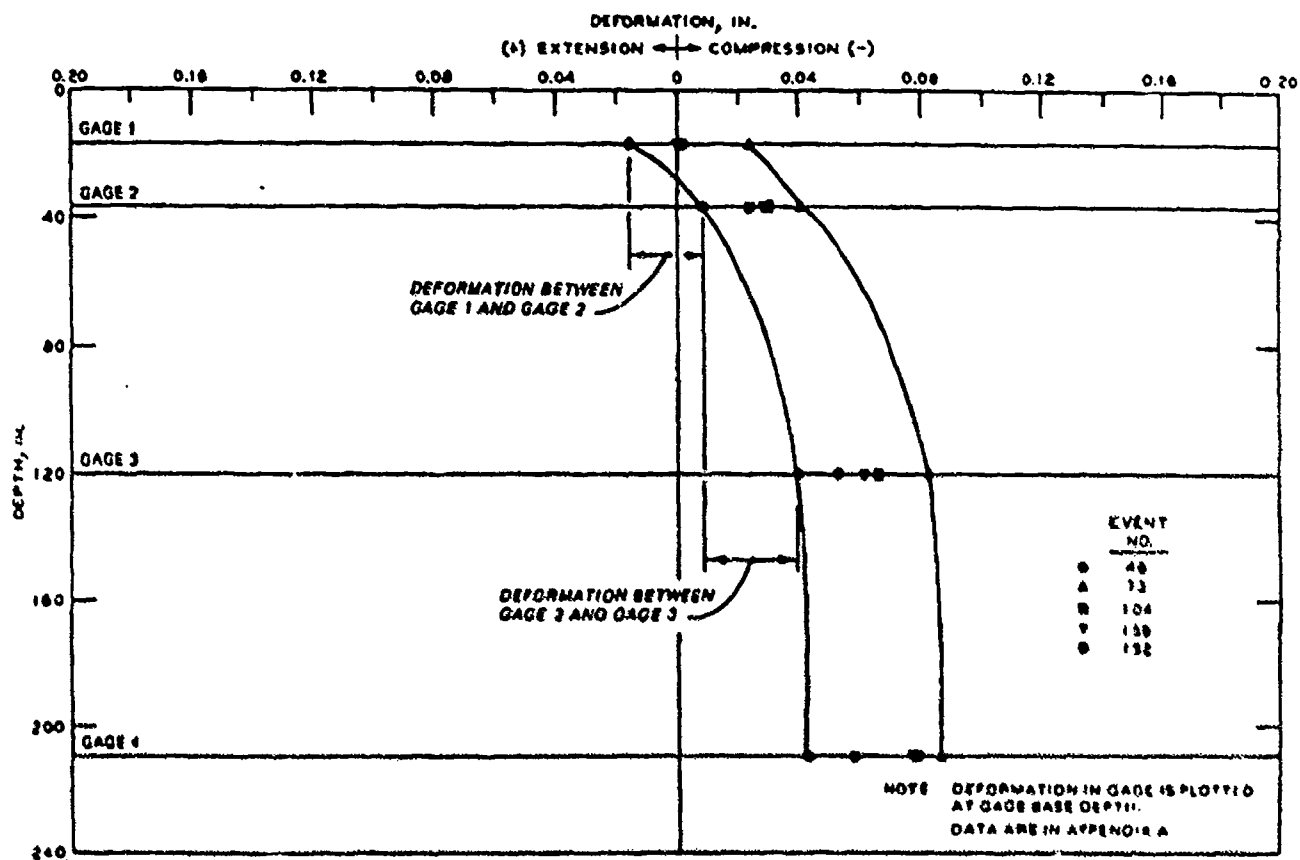
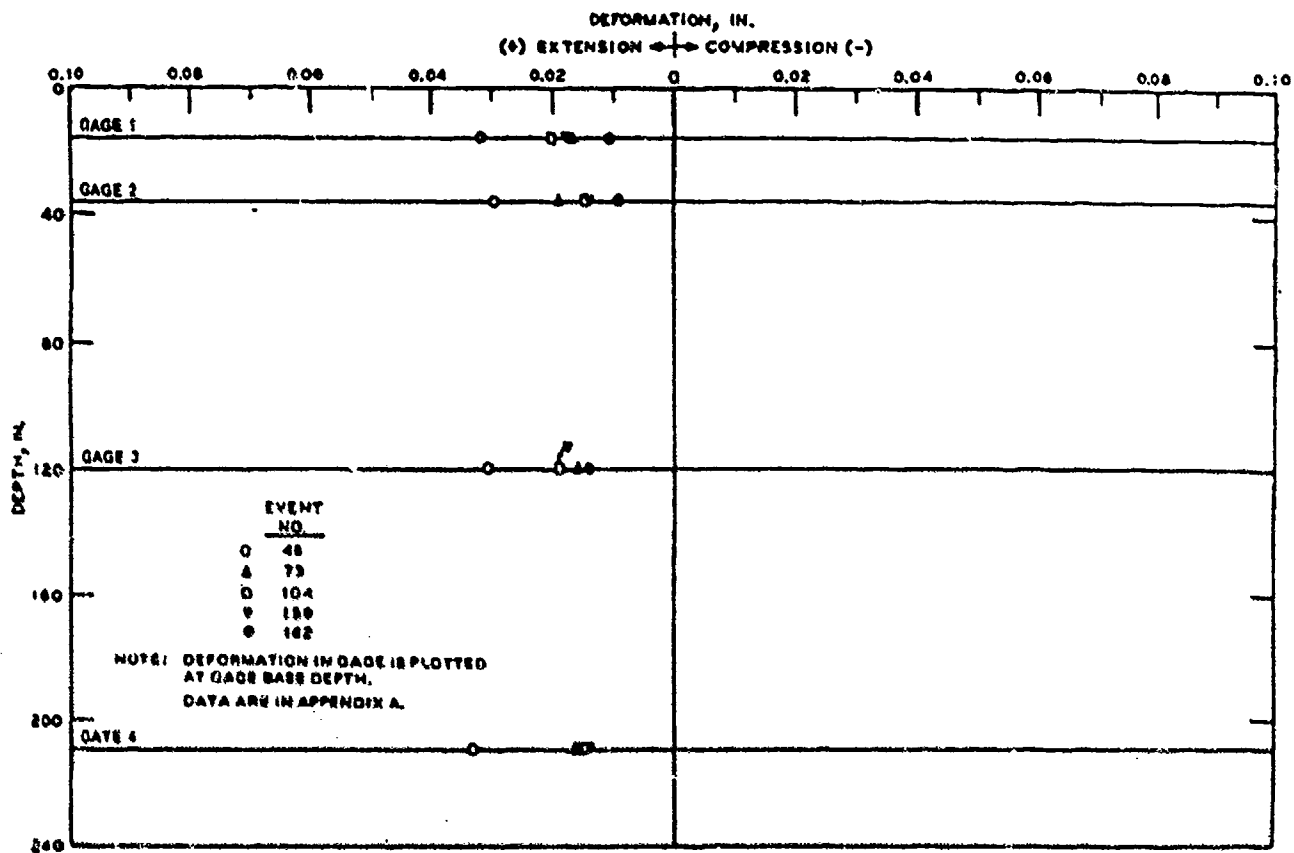
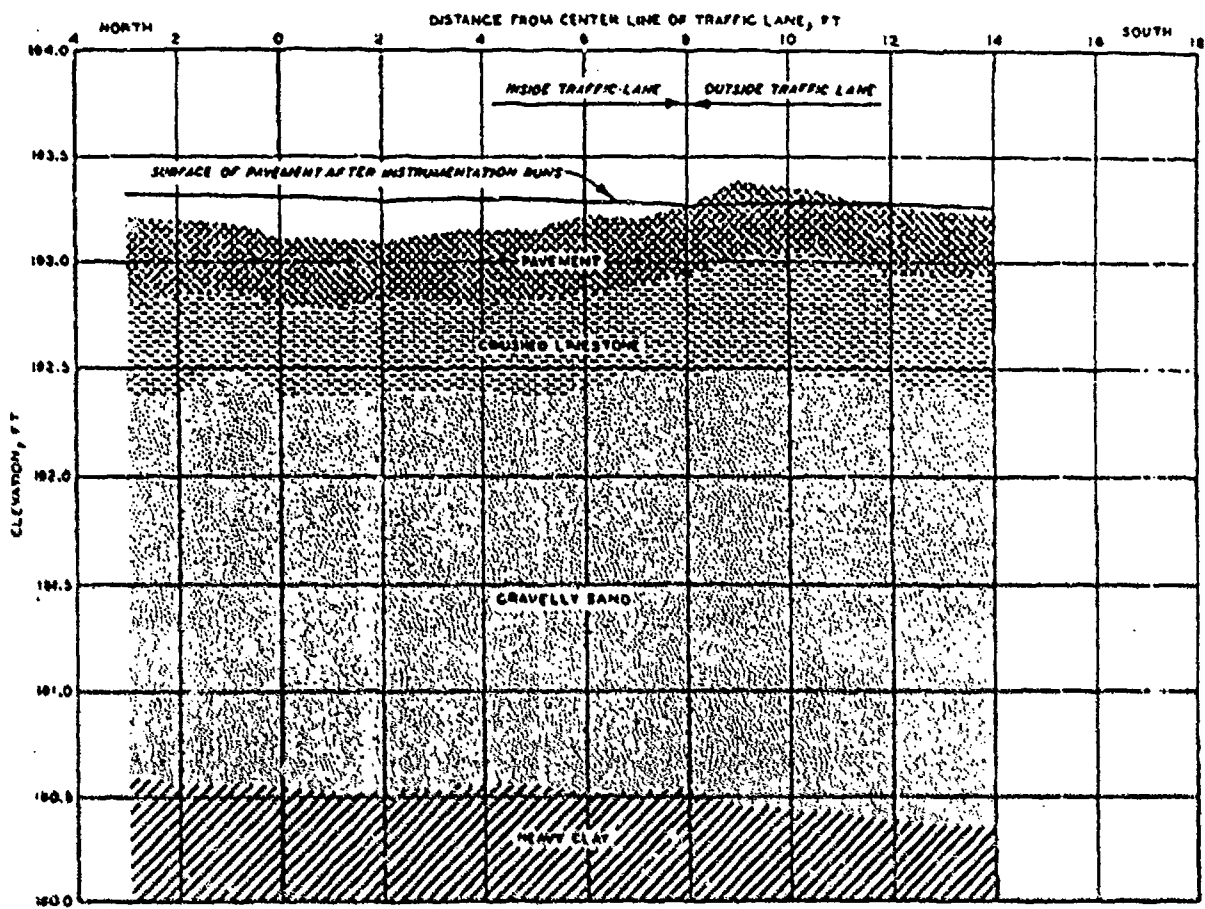


Figure 5-4. B-727 "Peak" Deformation in Each Gage, Between Wheels (0±0.85 ft.)



**Figure 6-5. B-727 Rebound In Each Gage, Between Wheels
(0±0.85 ft.)
(White [11])**



NOTE: ITEM 3 WAS CONSIDERED FAILED AT 180F COVERAGES.

**Figure 6-6. Test Pit Profile, Flexible Pavement Lane 1, Item 3, Sta. 2 + 30 After 2342 Coverages
(Ahivin, et al. [11])**

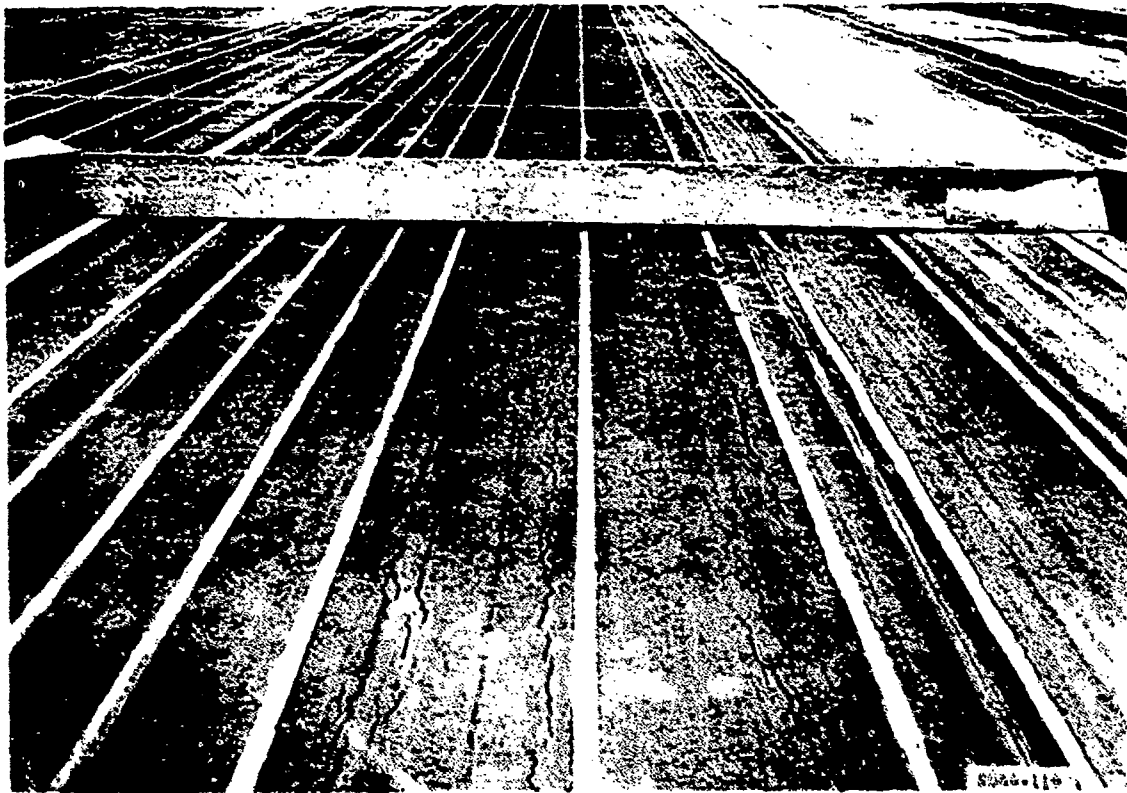


**Figure 6-7. Flexible Pavement Lane 1, Item 2, Permanent Deformation in the Lane After 200 Coverages
(Ahlin, et al. [9])**



**Figure 6-8. Sample Taken from Flexible Pavement Lane 2, Item 2 at Sta.
2 + 90 After 200 Coverages of Traffic
(Ahlin, et al. [9])**

6.1 Instrumentation

For the benefits of pavement instrumentation to be realized a comprehensive plan is needed. The plan should address loads as well as other effects. Potential effects include:

1. Load
 - a. Deflections and deformations
 - b. Strains
 - c. Pore pressures
2. Environmental
 - a. Temperature
 - b. Frost penetration
 - c. Moisture
3. Other
 - a. Density
 - b. Volume of water (subdrainage)

Supporting data includes weather-related data such as air temperature, precipitation and solar radiation.

Traffic information is important with respect to instrumentation and includes aircraft type, position, speed and weight. The current FAA design procedure allows for varying pavement thickness based on the pavement feature (i.e., runway, runway edge, taxiway, apron). Multiple instrumentation sites would be required to obtain pavement response associated with aircraft operating modes on these different features.

The type of pavement response that is important varies and depends on pavement type. Candidate rigid pavement features for instrumentation include:

1. Slabs
 - a. Edge
 - b. Corner
 - c. Center
 - d. Interaction (Joint-vertical, Horizontal)
2. Reinforcement
 - a. Dowels
 - b. Ties
 - c. Temperature Steel
 - d. Prestress Tendons

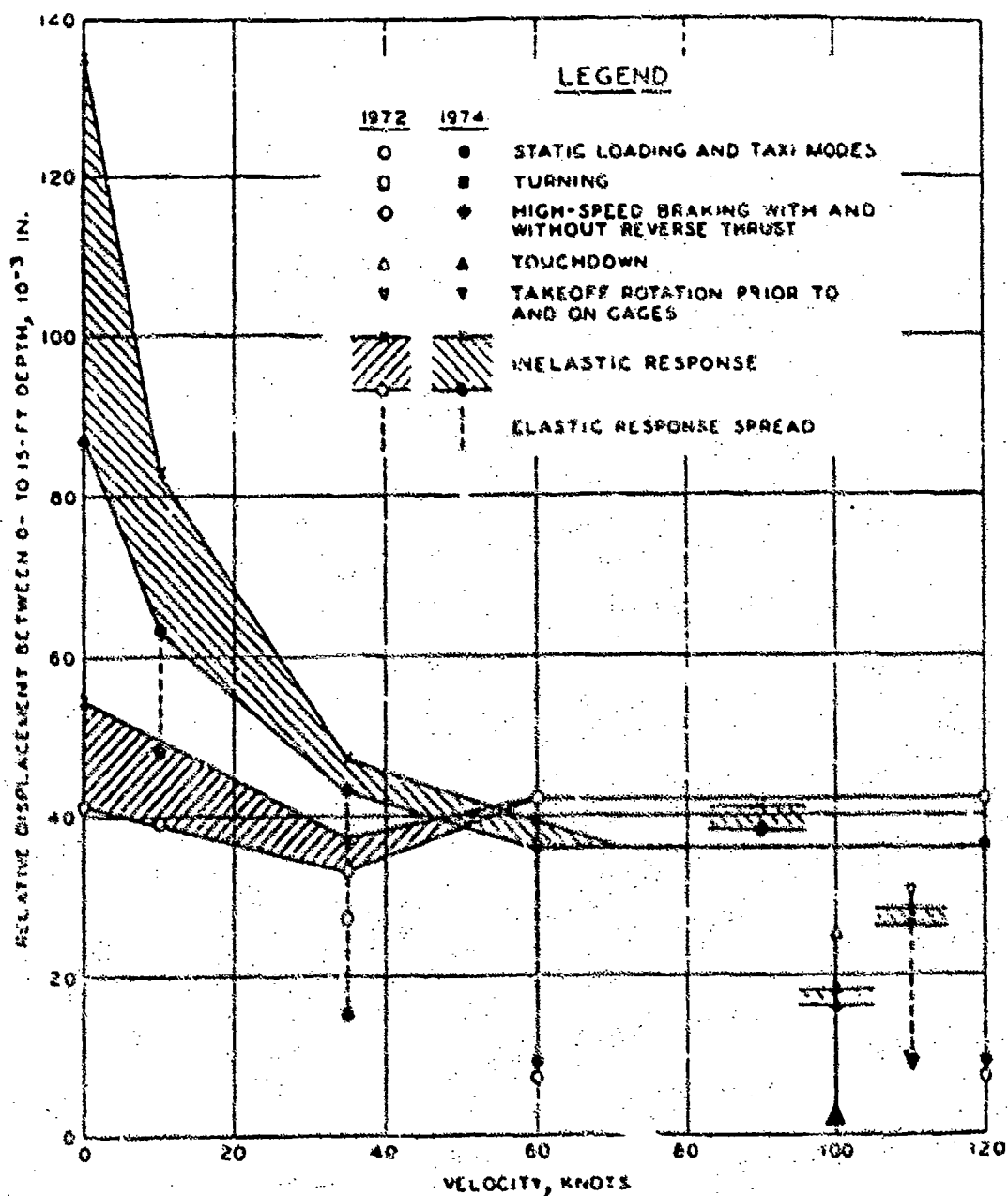


Figure 6-9. Maximum Vertical Relative Displacement vs. Velocity, Flexible, Row 1, 0 to 15 ft., B-727 (Ledbetter [12])

form and use. Also, because of the labor and time involved in manual data reduction, the majority of the data is filed without being utilized.

7. Summary and Recommendations

As a result of our work, we have developed a more clear understanding of the issues associated with the development of an effective UPDAP-Based on these issues, we recommend a concept with the following features:

1. A three-dimensional structural response model based on the finite element method.
2. A hierarchy of mechanics-based pavement material models from which the most effective set of models can be selected, based on environmental conditions, loading conditions, and the structural configuration of the pavement.
3. A selection of mechanics-based damage models that describe with sufficient accuracy the relevant mechanisms which lead to potential modes of pavement distress.
4. The development of effective interaction schemes between the material, damage and structural models that will ensure accurate predictions of pavement response.
5. The development of model selection criteria, implemented via a KBS, that is designed to establish the simplest credible models that meet the pavement design/analysis objectives.
6. Integration of the components listed above into a user-friendly code tailored for practicing pavement engineers, with sufficient flexibility to adapt to the rapid advancements in computer technology.

The FAA has planned a multiyear program that should provide sufficient time and resources to develop the UPDAP with the features described above. We recommend that this program include the following activities:

1. Extensive laboratory and in-situ testing of pavement materials to support the development of more generalized and mechanistically based material models.
2. Analytical and experimental studies of vehicle/pavement interactions, with emphasis on characterizing aircraft-specific dynamic loads both normal to and in the plane of the pavement.
3. Long-term controlled tests to characterize pavement damage mechanisms.
4. Continued and close interaction with the mechanics community to identify the applicability of advancements in material and damage modeling to pavement design/analysis.

5. The development of a KBS methodology and appropriate software architecture, which will provide a framework for the UPDAP.

8. References

1. Desai, C. S., et al, "Constitutive Laws for Engineering Materials", Proc. Third International Conference Tucson AZ, 1991; ASME Press, NY, 1991.
2. Hammerle, J. R., and Mohsenin, N. N., "Tensile Relaxation Modulus of Corn Horny Endosperm as a Function of Time, Temperature and Moisture Content," Transactions of the ASAE, 13(3):372-275, 1970.
3. Majidzadeh, K., et al, "Field Study of Subgrade Compaction," Final Report of EES 406, 1974.
4. Harichandran, R. S., and Yeh, M., "Flexible Boundary in Finite-Element Analysis of Pavements," Transportation Research Board Record 1207, January 1983.
5. Endo, T., Mitsunaga, K., Takahashi, K., Kobayashi, K., and Matsuishi, M., "Damage Evaluation of Metals for Random or Varied Loading," paper presented at 1974 Symposium on Mechanical Behavior of Materials, Kyoto, August 1974.
6. Concrete Pavements, edited by A. F. Stoke, Elsevier Applied Science, 1988.
7. Darter, M. I., "Design of Zero-Maintenance Plain Jointed Concrete Pavement," Vol 1: Development of Design Procedures, Federal Highway Administration, 1977, Report No. FHWA-RD-77-111.
8. Chou, Y. T., and Ledbetter, R. H., "The Behavior of Flexible Airfield Pavements Under Loads - Theory and Experiments," Miscellaneous Paper S-73-66, USAE Waterways Experiment Station, Vicksburg, MS, July 1973.
9. Ahlvin, R. G., et al, "Multiple-Wheel Heavy Gear Load Pavements Tests," Technical Report 5-17-17, Vol. I-IV, U.S. Army Engineer Waterways Experiment Station, CE, Vicksburg, MS, November 1971.
10. White, T. D., "Measured Pavement Response to Transient Aircraft Loadings," Ph.D. Thesis, Purdue University, May 1981.

11. White, T. D., "Pavement Instrumentation: Guide Instrumentation Plan for Flexible and Rigid Pavements," FHWA/EP-621-01, Federal Highway Administration, Washington, D.C., December 1965.
12. Ledbetter, R. H., "Pavement Response to Aircraft Dynamic Loads, Volume II, Presentation and Analysis of Data," Technical Report 5-75-11, USAE Waterways Experiment Station, Vicksburg, MS, September 1975.

9. List of Symbols

G_i, B_i, μ_i = spring and dashpot constants

R = tensile strength

ΔE_i = activation energy

σ = stress

$n, a, \beta S, m$ = material constants

$E_M(t)$ = relaxation function

$a_M(M)$ = reduced or pseudo time

t = time

State of the Art Review of Rutting and Cracking in Pavements

K. Majidzadeh

**The Ohio State University
Resource International, Inc.**

**C. L. Sarai
S. Mesarovic
G. J. Ives**

Resource International, Inc.

1. Introduction

Rutting prediction has been a subject of concern of pavement researchers and practitioners alike in recent years. Rutting directly affects pavement serviceability and it is often considered as one of the criteria to define pavement failure after it reaches a predetermined level above which ride quality and safety are seriously impaired.

Previous efforts have been directed at estimating rutting in flexible pavements as a result of permanent deformations occurring in the subgrade soil. However, in view of the need to rehabilitate pavements that have reached their useful life, more emphasis is needed in developing methods or adapting currently available methods to predict the amount of rutting in asphalt concrete pavement and overlays.

The following sections include reviews of several available computer methods and models to predict rutting. All these programs were originally developed for highway pavement distress prediction and/or analysis. Thus, some modifications will be needed considering the substantially higher tire pressures and wheel loads to be expected from aircraft. Careful consideration of the asphalt concrete rutting prediction models is necessary in view of the inherently high tire pressures (over 300 psi) (2 MPa) applied by some aircraft. It is estimated that plastic yield of asphalt concrete occurs at this high pressure which is well above the threshold pressure used for permanent deformation characterization of asphalt concrete mixtures for highway applications.

Rutting can be indirectly considered through the use of empirical or semi-empirical relationships between the amount of rutting and elastic response parameters obtained from the structural analysis of pavements such as deflections, stresses and strains. In most cases a threshold value of the vertical stress or strain on the subgrade surface is specified to limit rutting. This approach, however, implies that no rutting occurs within the pavement layers above the subgrade, contrary to experience.

1.1 Empirical Models

Several rutting models based on empirical relationships are discussed below. This discussion is not intended to be exhaustive but will serve the purpose of presenting some models that are worth mentioning.

1.1.1 Monismith and McLain Approach

Monismith and McLain conducted research on the permanent deformation properties of asphaltic pavements, using two theories [1]. The first theory was based upon a linear elastic approach in which an elastic layer program (CHEV5L) was used to analyze the data.

The equation for permanent deformation is given by:

$$\epsilon_{1p} = K(\sigma_d - \epsilon_e)^n \quad (1)$$

where

ϵ_{1p} = permanent strain at first load application

σ_d = $\sigma_1 - \sigma_3$ (stress difference is triaxial compression)

ϵ_e = elastic strain

K, n = experimentally determined constants

One major conclusion of their analysis was that the permanent deformation predicted using the elastic analysis method was much higher than the results calculated or predicted by the VESYS II procedure, which is based on the viscoelastic theory.

1.1.2 Simulative Statistical Based Approach

This approach was proposed by Morris et al. and is based on laboratory simulation conditions using triaxial testing [2]. A regression equation was developed for the laboratory test data relating the permanent deformation to testing variables. This equation was in the form:

$$\epsilon_p = f(\sigma_1, \sigma_3, T, N) \pm E \quad (2)$$

where

ϵ_p = vertical permanent strain

σ_1, σ_3 = vertical and lateral stresses

T = temperature

N = number of load applications

E = error of estimate

The total permanent deformation is calculated using the sublayers system.

$$p = \sum_{i=1}^n \epsilon_{p_i} h_i$$

where

p = total permanent deformation of the pavement system

ϵ_{p_i} = average permanent strain in the i th layer

h_i = thickness of the i th layer

n = number of layers in the pavement.

This method has the following shortcomings: (1) it introduces no basic constitutive law of material behavior for incorporation into a rational design scheme; (2) the method assumes no subgrade contribution to the total system permanent deformation, while it has been proven that the subgrade, in many instances, plays an important role in the effect of overall permanent deformation; (3) the method requires extensive testing programs for each material characterization, which makes it somewhat impractical; (4) the permanent deformation in the field was assumed to be zero between December and March, due to low temperatures; and (5) the method also assumes constant traffic over a given period of time.

In spite of all these assumptions, some of which appear questionable, the results of the above laboratory tests were in agreement with field measurements at the Brampton Test Road.

1.1.3 Saraf and Flinn Model

Saraf, Flinn et al. presented a regression model to obtain a correlation between the seasonal rutting rate and primary response for an 18 kip single axle load [3,4]. The model is of the form:

$$RR = f(\sigma_c, \epsilon, d, \text{ and } N_{18}) \quad (3)$$

where

RR = seasonal rate of rutting or permanent deformation per equivalent load application

σ_c = vertical compressive stress in component layer (psi)

ϵ = strain in component layer

d = surface deflection ($\times 10^{-3}$ in)

N_{18} = total equivalent 18 kip single axle loads up to and including the season for which the rate of rutting is to be calculated (10^5 repetitions)

Depending on this general form two different forms for predicting RR were suggested, depending on the pavement asphalt concrete layer thickness.

For pavements with a 6-inch (152 mm) or less thickness of asphalt concrete:

$$\text{Log RR} = -5.617 + 3.343 \log d - 0.167 \log N_{18} - 1.118 \log \sigma_c \quad (4)$$

For pavements with more than a 6-inch (152 mm) thickness of asphalt concrete:

$$\text{Log RR} = -1.173 + 0.717 \log d - 0.658 \log N_{18} + 0.666 \log \sigma_c \quad (5)$$

The subgrade contribution to total permanent deformation for the entire pavement system cannot be predicted using this model. In addition, this model cannot be used to predict rutting in granular materials. Therefore, it can be said that its applications are limited to asphalt pavements.

1.1.4 Barksdale and Romain Model

Barksdale and Romain developed a rutting model consisting of predicting rutting using permanent deformation characteristics determined from laboratory tests along with an analysis procedure for the pavement using linear elastic theory [5].

In this procedure each layer of the pavement is divided into several sublayers and the stresses calculated at the center of each sublayer, directly under the load center. The total rut depth (R) is given by

$$R \sum_{i=1}^n \epsilon_i z_i \quad (6)$$

where

R = total cut depth

ϵ_i = average plastic strain in the sublayer

Z_i = sublayer thickness

n = number of sublayers in the pavement system

The plastic strain can be determined from laboratory tests similar to those used in VESYS.

This method is known as the layer strain method and had been used in various forms by many researchers and is also the basis of the Shell design procedure.

1.1.5 Brown and Pell Model

Brown and Pell also developed a rutting model using the layer strain method but they used non-linear finite element theory to calculate layer stresses using the program DEFPAY. [5] The rutting is computed from

$$\epsilon_p = \left(\frac{q^b}{a}\right) (N) \quad (7)$$

where

ϵ_p = permanent shear strain

q = deviatoric stress

a, b = constants

N = number of load applications

The laboratory testing required is axial repeated load test.

Brown and Pell found that substantial errors in plastic strain develop if shear stresses are ignored in the determination of the state of stress, underestimating the plastic strain by as much as 40 percent.

1.1.6 Monismith, et al. Model

Monismith, et al. used elastic layer theory (ELSYM) to compute the rutting as

$$\epsilon_z = [\delta(T) N^a \sigma^{n-1} t] [\sigma_z - 1/2(\sigma_x + \sigma_y)] \quad (8)$$

where

ϵ_z = vertical permanent deformation

$\delta(T)$ = a function of temperature

s_z, s_x, s_y = stresses in x, y, z directions, respectively

a = coefficient

N = number of stress repetitions

σ^{n-1} = equivalent stress defined as a function of principal stresses is loading time

t = loading time

Repeated load triaxial compression tests provide input to the model.

Material properties as a function of temperature for each month in the year were developed using temperature distribution calculated from the method proposed by Barber [6]. The permanent deformation was then calculated for each month and summed to obtain the annual rutting.

Reasonable agreement was reported between computed and measured rut depth values.

1.1.7 Brown and Smith Approach

Brown and Snaith based their approach on laboratory simulation conditions, and presented data obtained from testing under different vertical stress levels (static or dynamic) relating the permanent deformation to testing variables, as expressed by the following equation [7]:

$$\epsilon_{tp} = a t^b \quad (9)$$

or

$$\log \epsilon_{tp} = \log a + b \log t \quad (10)$$

where

ϵ_{tp} = permanent strain at time, t

$\log a, b$ = constants estimated from laboratory test results which depend on temperature and applied stress

1.2 Linear Visco-Elastic VESYS System

One of the earliest attempts to predict the amount of rutting in pavement layers, including asphalt concrete layer, dates to 1974 with the introduction of the VESYS (Visco-elastic system) program.

The VESYS II M is a computer system that combines viscoelastic theory with laboratory-based permanent deformation accumulative damage law [8].

VESYS IV B is one of the latest editions of this system. It combines several versions of the program into a single computer program that models an n -layer flexible pavement structure using resilient moduli, creep compliance or a combination of these by specifying layer stiffnesses. Finally, there is VESYS-3H which is a modification of the VESYS III A program to provide the capability to back-calculate rutting parameters given a field rutting measurement [9].

The VESYS system uses creep compliance $J(t)$ and permanent deformation characteristics as measured from repeated incremental static loads to characterize rutting parameters ALPHA and GNU, with the ratio between permanent deformation and total strain at the N th cycle is given as:

$$F(N) = GNU \cdot ALPHA \quad (11)$$

where

$$ALPHA = 1 - S$$

$$GNU = IS/\epsilon_n$$

$$S = \text{slope of the total permanent strain vs } N \text{ curve where } \epsilon = IN^S$$

$$I = \text{intercept (at } N = 1) \text{ of the total permanent strain vs } N \text{ curve}$$

ϵ_n = total strain at the n^{th} cycle

The creep compliance is given by

$$J(t) = \sum A_i e^{-\alpha_i t} \quad (12)$$

where

A_i, α_i = constants determined from the creep curve

t = time

Three models make up the VESYS Program. These are:

- a. The Primary Response Model, which calculates the stress, strain and deformation in the pavement system at any time due to the static load applied at the surface. The static load response is then used to predict the related distress modes to this condition, or can be converted to responses that could occur under moving load situations, and, in turn, predicts its related mode of distress. The material is characterized following an elastic and/or linear viscoelastic constitutive law. VESYS uses the elastic-viscoelastic correspondence principle applied to a three layer closed-form elastic solution to obtain the corresponding viscoelastic solution.
- b. The Damage Model, which predicts rutting, cracking and roughness and is based on the cumulative damage law.
- c. The Performance Model, which indicates the pavement's ability to meet an acceptable serviceability level (measured by the Present Serviceability Index = PSI) and projected service life.

The permanent deformation properties ALPHA and GNU are derived from repetitive-loading creep compliance tests in compression to define the fraction of the predicted total strain that is permanent, as a function of load cycles. The permanent strain is plotted versus load repetitions on log-log paper, a straight line of best fit is drawn to approximately predict permanent strain over the range of loadings of interest. ALPHA is defined as one minus the slope (S) of this line, and represents the rate of change in the permanent strain. GNU is the product of the intercept value (I) of the permanent strain at one load repetition multiplied by the slope (S) divided by the average resilient strain (ϵ_r).

The VESYS model represents the first attempt to consider viscoelastic properties of pavement materials to calculate rutting. Pavement response calculations are performed using the elastic layer theory which in itself constitutes a limitation. A more rigorous pavement analysis using finite elements techniques will allow a more strict calculation of stresses and strains which will also lead to a more accurate prediction of the amount of rutting. Finally, the model has not been validated for high tire pressures and high wheel loads as those expected from aircraft.

1.3 Probabilistic Distress Models for Asphalt Pavement (PDMAP)

The PDMAP program was developed to enable highway personnel to predict distress conditions of given pavement sections [10]. The program uses fatigue cracking and permanent deformation (rut depth) due to traffic as the specific distress modes to determine pavement performance.

PDMAP uses probabilistic analysis to compute the expected amount of damage as well as damage with specified reliability factors at any time during the analysis period. The program uses elastic layer theory for the structural analysis of pavements. The probabilistic analysis of the total structural response due to a dual wheel load system and the probabilistic predictions of fatigue and rut depth are completely new and were specifically developed for the PDMAP program.

The rate of rutting (RR) is assumed to be related to the cumulative number of load applications, X_1 (in 10^5 units); surface displacement, X_2 (in 10^{-3} inches); and maximum compressive stress, X_3 (in psi), at the bottom of the AC under the center of a wheel load.

$$\log_{10}RR = B_0 + B_1\log_{10}X_1 + B_2\log_{10}X_2 + B_3\log_{10}X_3 + \delta \quad (13)$$

where δ = random error with mean = 0 and variance = σ^2

$$B_0 = -5.619, B_1 = -0.09467, B_2 = 4.4866,$$

$$B_3 = -1.2958, \sigma = 0.2832$$

The main disadvantages of the PDMAP program are related to the type of rut depth prediction and structural analysis models used, namely:

- a. Elastic-plastic techniques are preferred in the prediction of permanent deformation.

- b. The finite elements technique for pavement analysis is a more appropriate substitute. In addition, the PDMAF program is not capable of considering lateral discontinuities such as joints or cracks when modelling layer systems.

1.4. The O.S.U. Method

The formulation of the rutting phenomenon in this method is based on research work conducted at The Ohio State University over a period of more than eight years. [11-15] The rutting models developed are based on the observation that the amount of rutting can be given by the following equation: [12,13]

$$\frac{\epsilon_p}{N} = A N^{-m} \quad (14)$$

ϵ_p = Cumulative permanent strain at the N^{th} repetition

N = Number of load repetitions

A = Permanent strain after the first repetition ($N = 1$) calculated using linear regression of the $\log \epsilon_p/N$ versus $\log N$ relationship

m = Absolute value of the slope of the linear relationship between $\log \epsilon_p/N$ versus $\log N$

This relationship was initially observed to describe the rutting process in subgrade materials. The rate-process theory is used as a theoretical explanation for the micro-rheological response of compacted soils under repeated stress applications.

The theory of absolute reaction rates or rate process theory, proposed initially by Eyring et al. [16], and applicable to any process involving the motion of particles, has been used to extensively to describe and predict the creep and consolidation behavior of clays as well as other materials [17-26].

Glynn and Kirwan [27] applied the theory of rate processes to the study of clays subjected to repeated loading. The authors used Murayama and Shibata's concept [19] of a threshold stress, a stress intensity below which only purely elastic strains are produced, to derive an equation relating magnitude of permanent strain ϵ_p in terms of the applied stress and the number of load applications.

Majidzadeh, Guirguis and Joseph [28] used the theory of rate process to study the mechanism of the steady-state deformation of compacted silty clay and found out, for constant temperature, time of loading and structure, that the deformation rate is given by:

$$\frac{d\epsilon_p}{dN} = A e^{Bs} N^{-m} \quad (15)$$

where

- ϵ_p = permanent deformation
- N = number of load repetitions
- s = deviatoric stress
- A, B, m = constants

Which describes the deformation characteristics during work-hardening of silty clay soil under repeated loading.

Buranarom [29] added another term to the equation to describe the effect of water content. It is in the form of a shift function. The general equation is thus,

$$\frac{\epsilon_p}{N} = A e^{Bs} N^{-m} X(w) \quad (16)$$

where

- $X(w)$ = $\exp[c(w-w^0)]$ = moisture shift function
- w = the water content
- w^0 = the optimum water content
- c = constant

This equation is used as one of the bases of this study. The equation, though, needs to be simplified and converted to more practical terms to make its applicability a simple task.

The parameter A can be used to describe the stress and moisture effects. It would be stress dependent constant.

The same form of mechanistic relation can describe the permanent deformation of asphalt concrete, except that the parameter A would have different dependencies. The parameter would normally be stress, rate, and temperature dependent. The relation would then be:

$$\frac{\epsilon_p}{N} = A(\sigma, w, T) N^{-m} \quad (17)$$

The permanent deformation evaluation can be a much easier task because the same mechanistic law is applicable to all pavement components, i.e., asphalt, concrete and subgrade. The permanent deformation of the system is a result of the deformation of each of the pavement component layers. Each layer would contribute differently to the total deformation according to each road condition (Figure 1-1).

For the range of moisture contents on the wet side of the optimum (Figure 1-2):

$$\frac{\epsilon_p}{N} = 0.00139 N^{-0.918} \exp(1.0699(w-w_o) + B(\sigma_{\text{appl}}/\sigma_{\text{ult.}})) \quad (18)$$

For the range of moisture content on the dry side of the optimum (Figure 1-3):

$$\frac{\epsilon_p}{N} = 0.00879 N^{-0.918} \exp(-0.531599(w-w_o) + B(\sigma_{\text{appl}}/\sigma_{\text{ult.}})) \quad (19)$$

with the coefficient of multiple determination $R^2 = 0.9999$

In both expressions [18] and [19], the moisture content is expressed in percent and ϵ_p has the unit of length per length. The moisture shift function ($\exp C(w-w_o)$) is shown in Figure 1-4.

In a continuing series of studies by Majidzadeh et al., it was shown that this relationship is also valid for describing rutting progress in all pavement layers -- asphalt concrete surface layer, granular base course, subbase materials, and subgrade soils [14,15]. In fact, the variation in the applicability of this model to different materials is manifested in the variation of parameters A and m commonly known as rutting parameters.

The equation for subgrade rutting is

$$\epsilon_p = R E^{-0.4} \sigma_d N^{1-m} \quad (20)$$

where

R, S = material constants

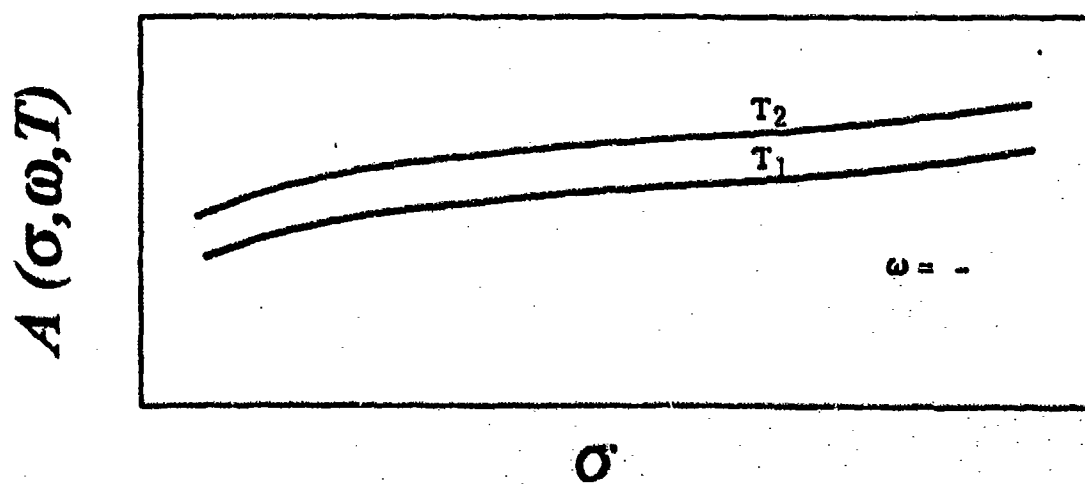
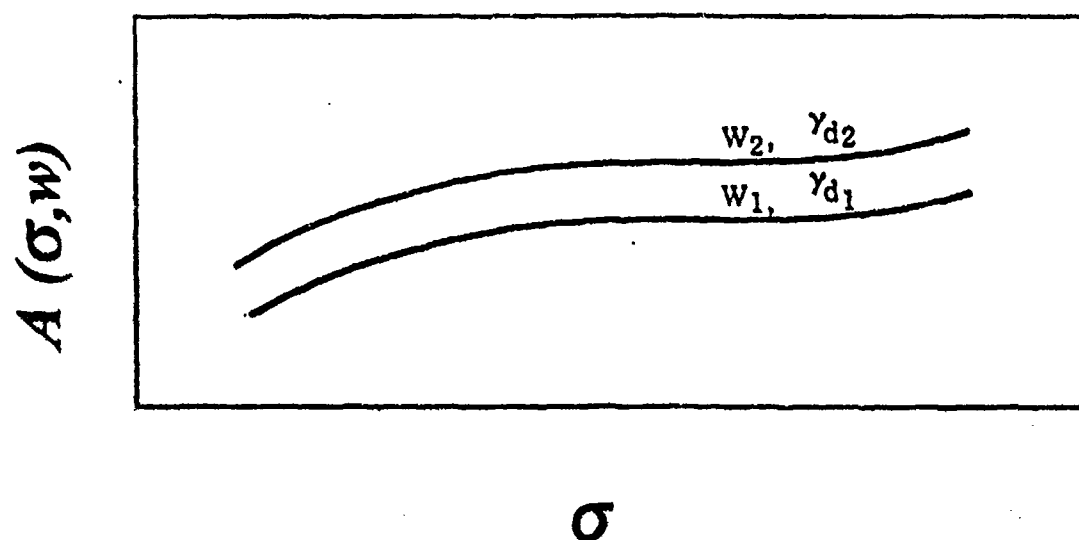
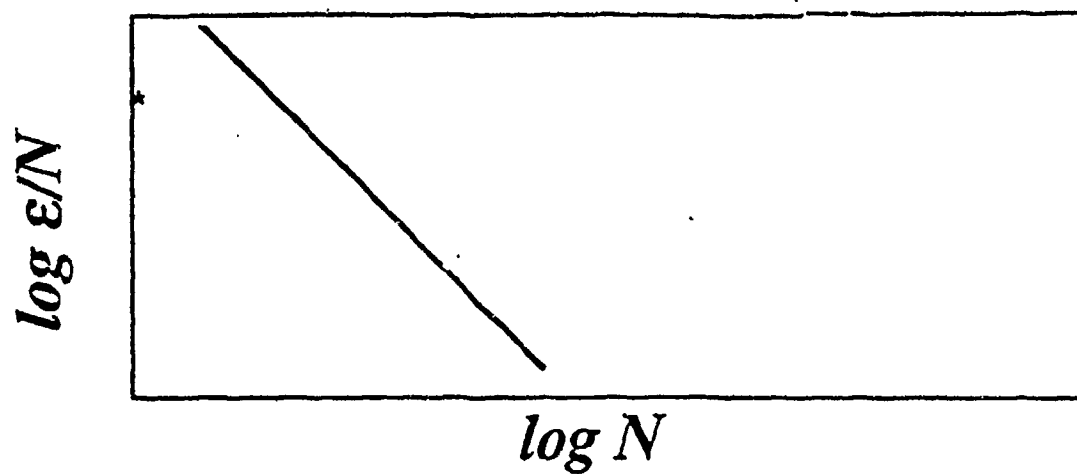


Figure 1-1. Deformation of Each of the Pavement Component Layers

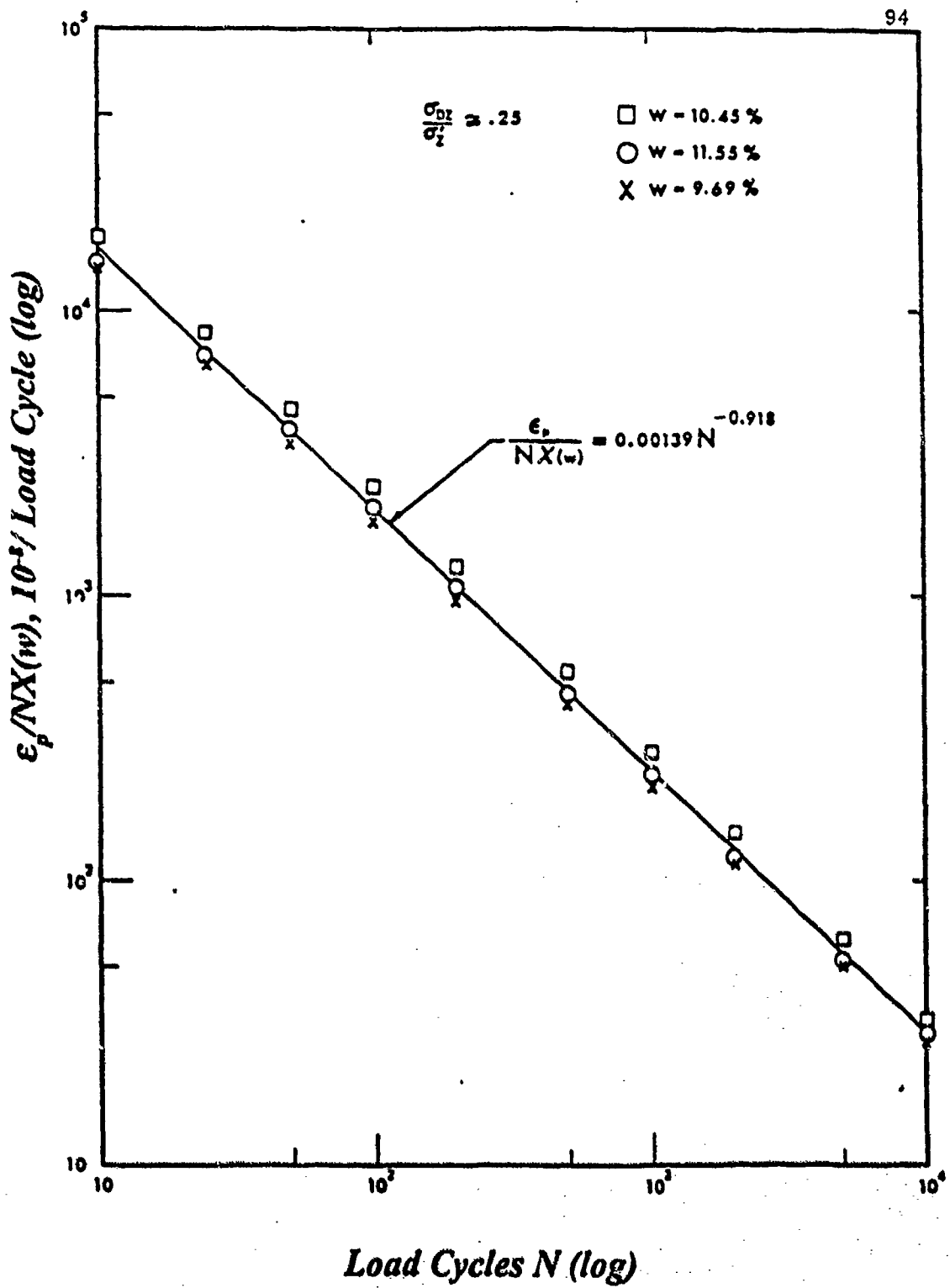


Figure 1-2. Master Curve for Rutting on Wet Side of Optimum

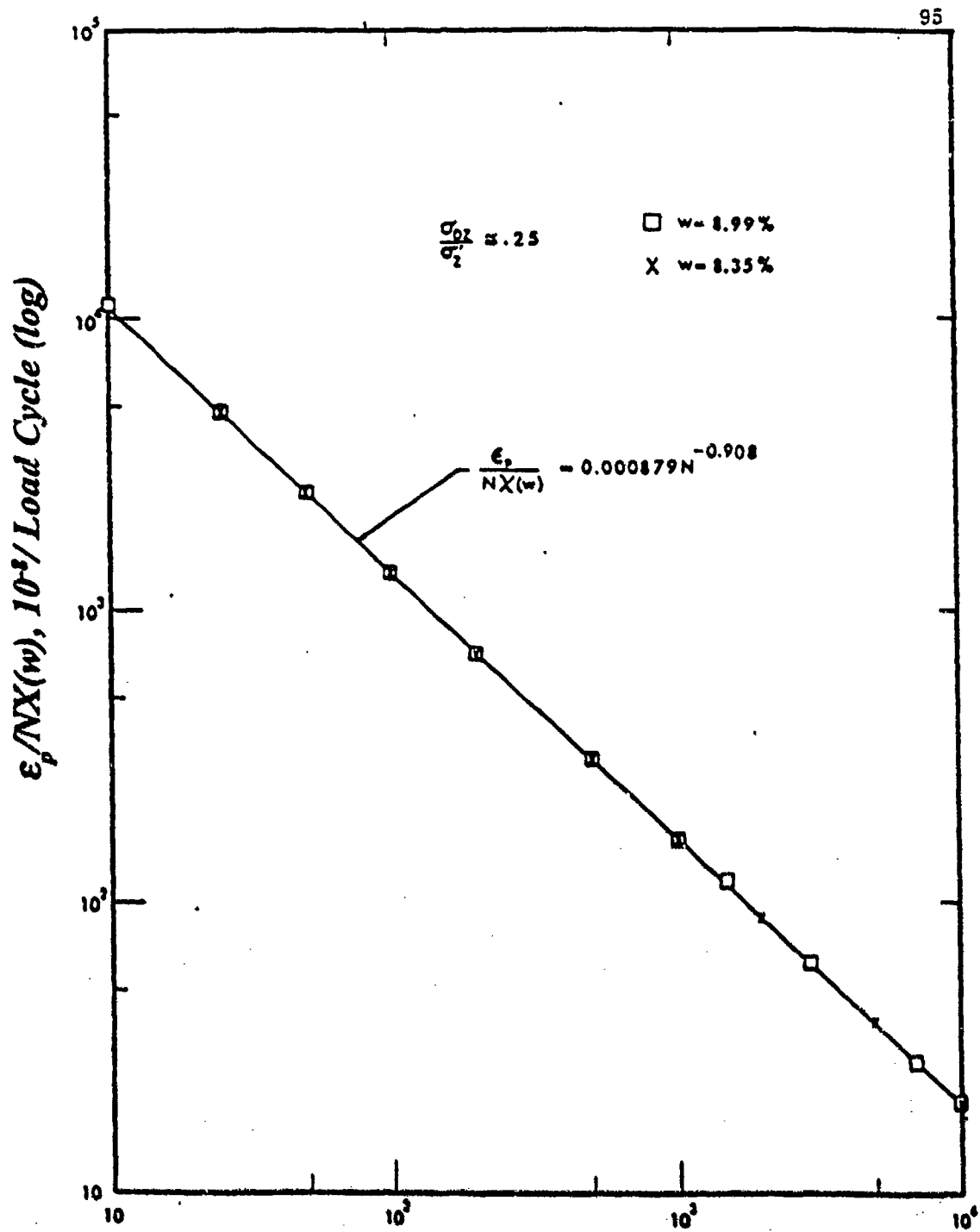


Figure 1-3. Master Curve for Rutting on Dry Side of Optimum

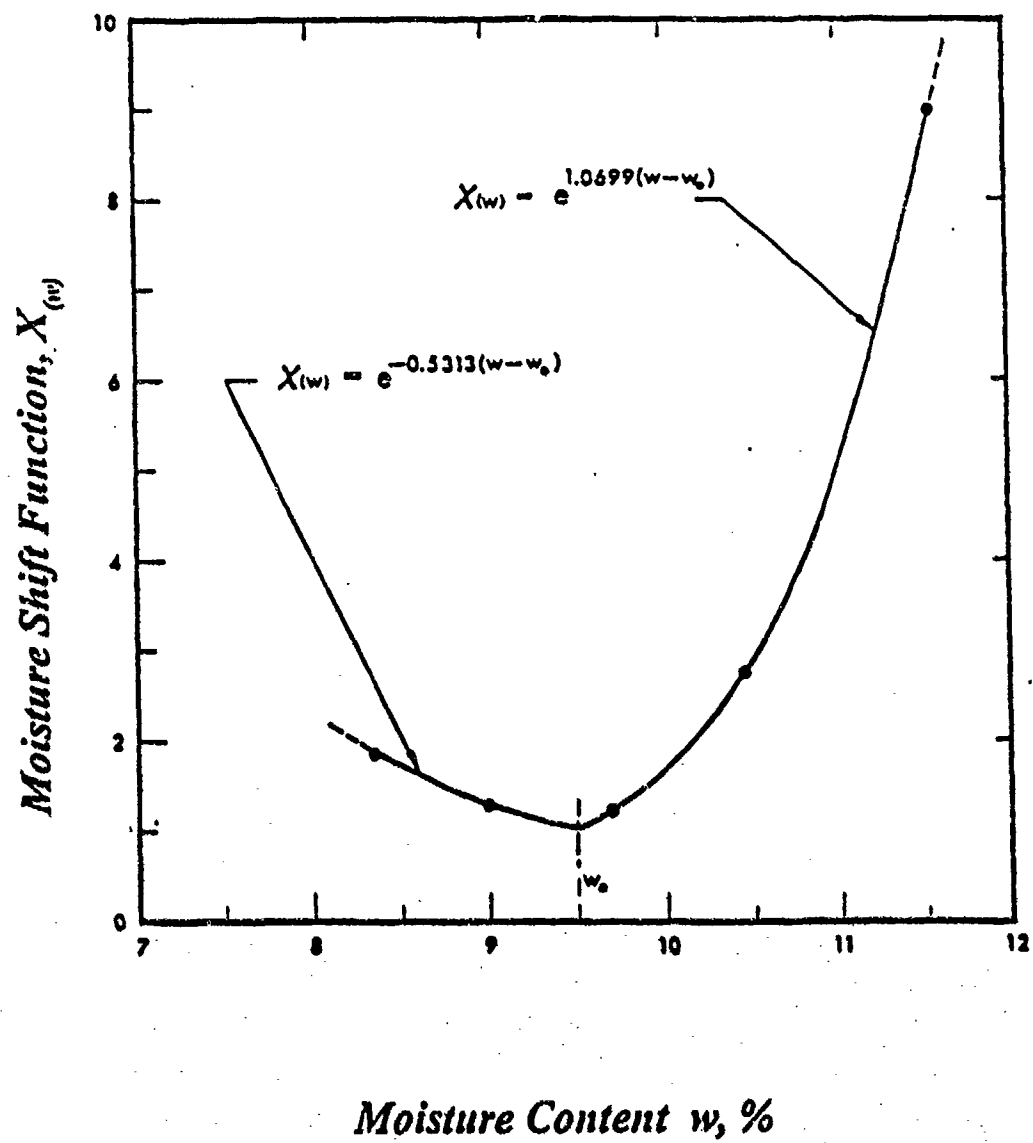


Figure 1-4. Moisture Shift Function for Silty-Clay

- E^* = dynamic modulus
 σ_d = deviatoric stress
 m = slope of subgrade layer
 N = number of repetition

The equation for granular base or subbase rutting is:

$$\epsilon_p = C_1 M^{c_2} E^{*c_3} N^{1-m} \quad (21)$$

where

$$M = \frac{\tau_o}{\sigma_o}$$

τ_o = octohedred shear stress

σ_o = octahedral normal stress

m = slope for granular material

c_1, c_2, c_3 = material constraints

The equation for asphalt concrete rutting is

$$\epsilon_p = J \frac{\sigma_1^S}{E^*} N^{1-m} \quad (22)$$

where

J, S = material constants

σ_1 = principal normal stress

m = slope for asphalt layer

The original O.S.U. rutting prediction method has been recently modified to include the consideration of material cross-anisotropy and bimodularity which are present in most naturally occurring materials and which would affect the pavement response to loading [11]. In addition a

finite element computer code has been developed for pavement analysis which includes the concept of material non-linearity and temperature dependency (when applicable).

1.5 Texas A&M Model

Crockford, et al. developed a rutting model for granular materials and subgrade where the modulus of the material is given as a nonlinear function [30]:

$$E = B_0 I_1^{B_1} (\tau_{oct})^{B_2} \delta^{B_3} W^{B_4} \quad (23)$$

where

I_1 = first stress invariant

τ_{oct} = octahedral shear stress

δ = density

W = moisture content

B_0, B_1, B_2, B_3, B_4 = regression constraints

Asphalt layer modulus is assumed to be a linear function. The finite element code TTIPAVE was used to calculate the stresses and strains in the granular layer using the moduli given by the above equation. This model was applied to an airfield pavement with very good agreement between measured and predicted rut depths.

1.6 The Elasto-Visco-Plastic (EVP) Model

Rutting occurs as a combination of densification (volume change) and shear deformation. It has been observed by a number of investigators [4,31,32] that the shear portion is more significant than the volumetric one. The major portion of permanent deformation occurs during initial loading. The initially soft material is being load-compacted and stiffens until the yield point is reached where additional plastic shearing accompanied by dilation (increase in volume due to the rearrangement of particles) occurs. The irreversible deformation is, during the entire process, strongly time dependent, primarily because the viscous nature of the bituminous binder.

The major factors influencing the rutting behavior are [1]:

- a. aggregate gradations, size, angularity and perhaps surface roughness
- b. mixture composition
- c. compaction procedure
- d. temperature
- e. load magnitude, distribution and frequency
- f. thickness of the asphalt concrete layer, etc.

For all granular materials (and for that matter, for most other materials), the distinction between **VOLUMETRIC** and **DEVIATORIC** deformation is essential, once the linear threshold has been exceeded. For some stress levels, both volumetric and deviatoric deformation have their **REVERSIBLE** and **IRREVERSIBLE** (permanent) portions. Each of these may or may not depend on the duration of the load and is modelled accordingly as either **TIME-DEPENDENT** or **INSTANTANEOUS**.

In addition, volumetric deformation can be such that volumetric stress performs **POSITIVE** or **NEGATIVE** work. The later one is termed **DILATION**. The volumetric irreversible deformation due to volumetric stress occurs not only for high stress but also initially which is referred to as **DENSIFICATION** - an irreversible initial volumetric deformation.

Figure 1-5 illustrates graphically the above discussion. The components of deformation shown can be modelled using classical plasticity and viscoelasticity theory with some modifications. Figure 1-6 demonstrates, on the actual test results, the existence of both instantaneous and time dependent irreversible deformation.

1.6.1 Elastic, Viscoelastic and Viscous Deformation

Elastic and viscoelastic behavior can be modelled in a simple manner: linear elastic - Kelvin viscoelastic material. For the modelling of rutting of asphalt concrete pavements, i.e., the accumulation of irreversible deformation - the reversible portions are of lesser importance. In addition, pure elastic behavior occurs for a relatively small stress range (if indeed it occurs at all).

Viscous behavior of asphalt concrete for moderate stresses and strains is usually modelled as linear, while for higher stresses and strains, nonlinearity becomes apparent [33].

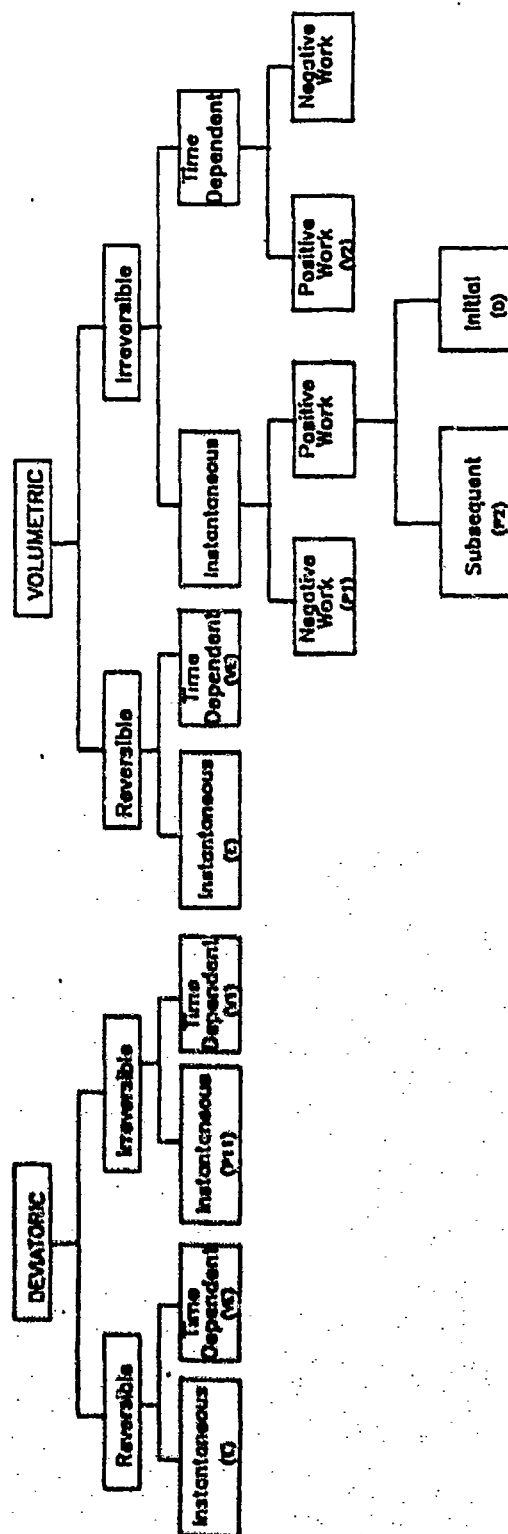


Figure 1-5. Deformation Chart

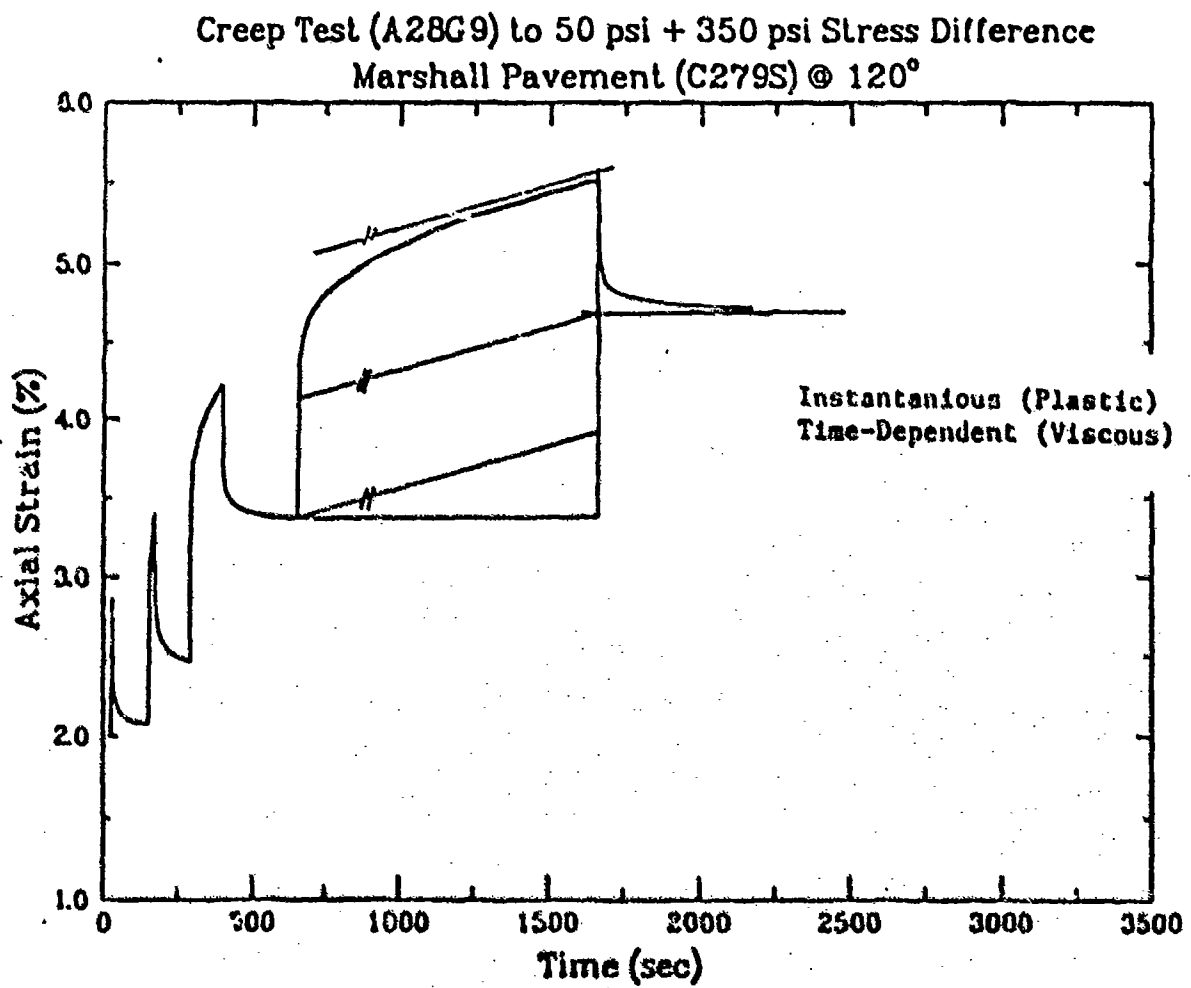


Figure 1-6. Creep Test - Series of Loading and Unloading

In addition, due to the time-dependent nature of deformation, for loads of long duration the strains exceed the range of small strain assumption and geometric nonlinearities should be considered.

1.6.2 Plastic Behavior

Within the framework of classical (yield surface) plasticity the following need to be identified and quantified:

- a. Yield Surface
- b. Flow Rule
- c. Hardening Rule

The accurate identification of the yield surface requires a series of different stress path tests. The triaxial test apparatus, with electronic control of both axial stress/strain and confining pressure, provides sufficient flexibility for such testing.

The associated flow rule assumes that the plastic strain increment is normal to the yield surface. When applied to soils, with the Drucker-Prager or Mohr-Coulomb yield condition, it usually predicts significantly higher dilation than experiments suggest [34,35].

Hardening rule can be specified as isotropic or anisotropic. The latter may contain kinematic and/or distortion components. Kinematic hardening accounts for the Bauschinger effect.

1.6.3 Densification

Densification can also be understood as a plastic behavior. However, it occurs initially, at low stress levels, as opposed to the yield surface plasticity, where the plastic deformation occurs after the threshold value of stress is reached. The following questions need to be answered:

- a. Does the densification limit, as defined above, depend on the deviatoric stress?
- b. Does the same limit depend on stress history?
- c. What is the shear stiffness in the densification region of the stress space?

To answer the first question one needs to perform essentially the same set of tests as for the proper definition of yield surface. The second question is similar to the hardening problem in the plastic model. Shear stiffness (linear or nonlinear) can be determined from a series of triaxial shear tests.

The components of the deformation are defined in the simplest possible manner:

- a. Linear elastic, viscoelastic and viscous behavior rheologically modelled as a Burger body with deviatoric viscous deformation only (Figure 1-7). The differential equations of such a model read:

$$\dot{S}_{ij} + \left\{ \frac{G_1 + G_2}{\mu_1} \right\} + \frac{G_2}{\mu_2} \dot{S}_{ij} + \frac{G_1 + G_2}{\mu_1 \mu_2} S_{ij} = 2G_2 \dot{e}_{ij} + \frac{G_1 + G_2}{\mu_1} e_{ij} \quad (24)$$

$$\dot{\sigma}_{ij} + \frac{B_1 + B_2}{\beta_1} \sigma_v = \dot{\epsilon}_{ij} + \frac{B_1 B_2}{\beta_1} \epsilon_v \quad (25)$$

where

S_{ij} = deviatoric component of the total stress

σ_{ij} = stress

σ_v = volumetric stress

e_{ij} = deviatoric component of the total strain

ϵ_{ij} = strain

ϵ_v = volumetric strain

$B_{1/2}, G_{1/2}, \beta_{1/2}, \mu_{1/2}$ = bulk and shear moduli of the corresponding strain components. The differential equation is readily solved for the constant stress/strain (rate) conditions.

- b. Drucker-Prager yield condition: $F(\sigma_{ij}) = I_1 + \sqrt{J_2} - k = 0$, with associated flow and isotropic hardening.
- c. Linear densification model with the limits: $0 < \sigma_v < \sigma_v^d$.
- d. Elastic, viscoelastic and densification Poisson ratios assumed equal.
- e. All components of deformation independent of each other.

In order to define model parameters, tests are performed at two standard mixes (Marshall and Gyratory) and two ambient temperatures. Elastic, viscoelastic and viscous parameters can be determined from uniaxial or triaxial creep test by simply fitting the creep compliance:

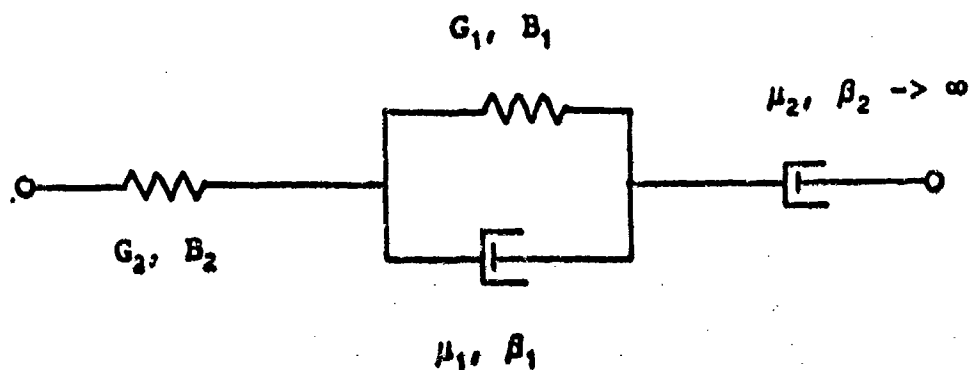


Figure 1-7. Elastic, Viscoelastic and Viscous Model of Asphalt Concrete

$$J(t) = \frac{1}{2G_2} + \frac{t}{2\mu_2} + \frac{1}{2G_1} (1 - \exp(-\frac{G_1}{\mu_1}t))$$

to the experimentally obtained curve.

Densification bulk modulus and densification limit can be obtained from hydrostatic test performed on virgin material. Figure 1-8 shows the volumetric stress-strain curve for Marshall mix at 120°F.

Plasticity parameters are somewhat more difficult to obtain. First parameters to be obtained are the yield function parameters, α and k . Yield surface is defined by two points in the stress space. It is therefore sufficient to recognize the initial yield points for any two different tests. The main difficulty is the recognition of yield point. Asphalt concrete always exhibits viscous and viscoelastic behavior so that nonlinear stress-strain behavior is always present. However, one distinct quality can be attributed to the plastic flow consistent with the model used - large dilation. Consequently, one can define yield as the beginning of large dilatation and recognize it from experimental data accordingly. Figure 1-9 shows typical volumetric behavior during constant strain rate triaxial test.

Having defined the yield surface, the next step is the definition of the hardening function. This is done by using the results of the constant strain rate triaxial test. Since all the other (non-plastic) components of deformation are defined, plastic strain can be determined at any time, as the difference between the observed and the predicted non-plastic strain. Figure 1-11 shows the deviatoric stress-strain curve for both theoretical non-plastic model and real behavior.

The accumulation of strain is modelled following the O. S. U. model [12]. The strain accumulated after N cycles, $\epsilon_{acc}(N)$, is given by:

$$\ln\left(\frac{\epsilon_{acc}(N)}{\epsilon_{acc}(1)}\right) = (1-m) \ln N \quad (26)$$

where

$\epsilon_{acc}(1)$ = one cycle permanent strain

m = constant determined experimentally from series of uniaxial cyclic loading tests

N = number of cycles

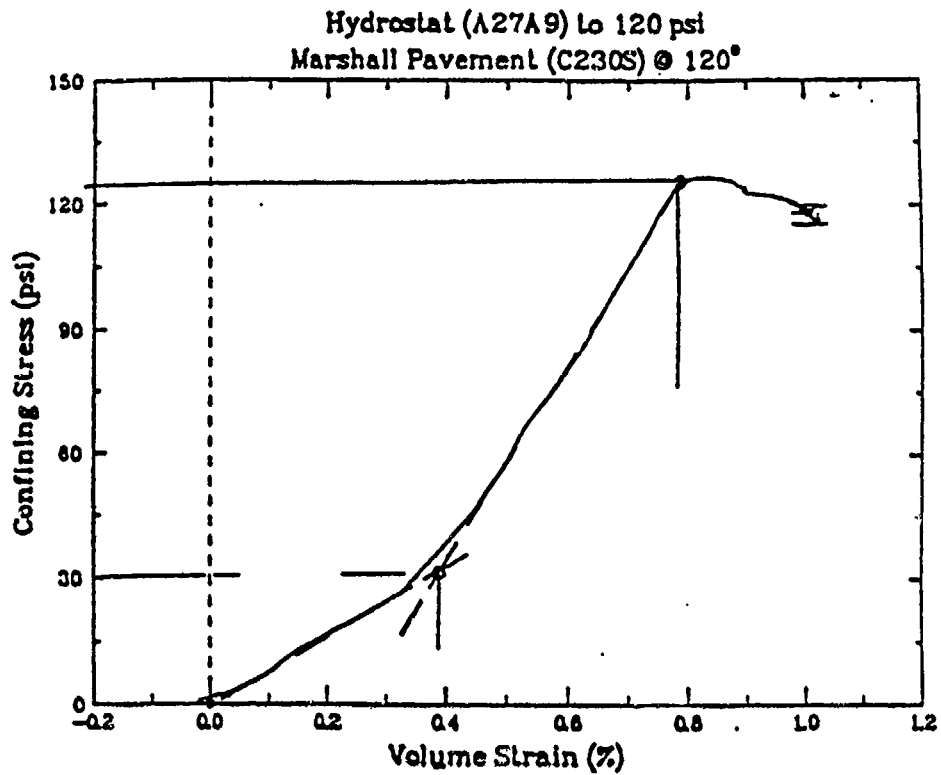


Figure 1-8. Hydrostatic Compression on Marshall Mix at 120° F

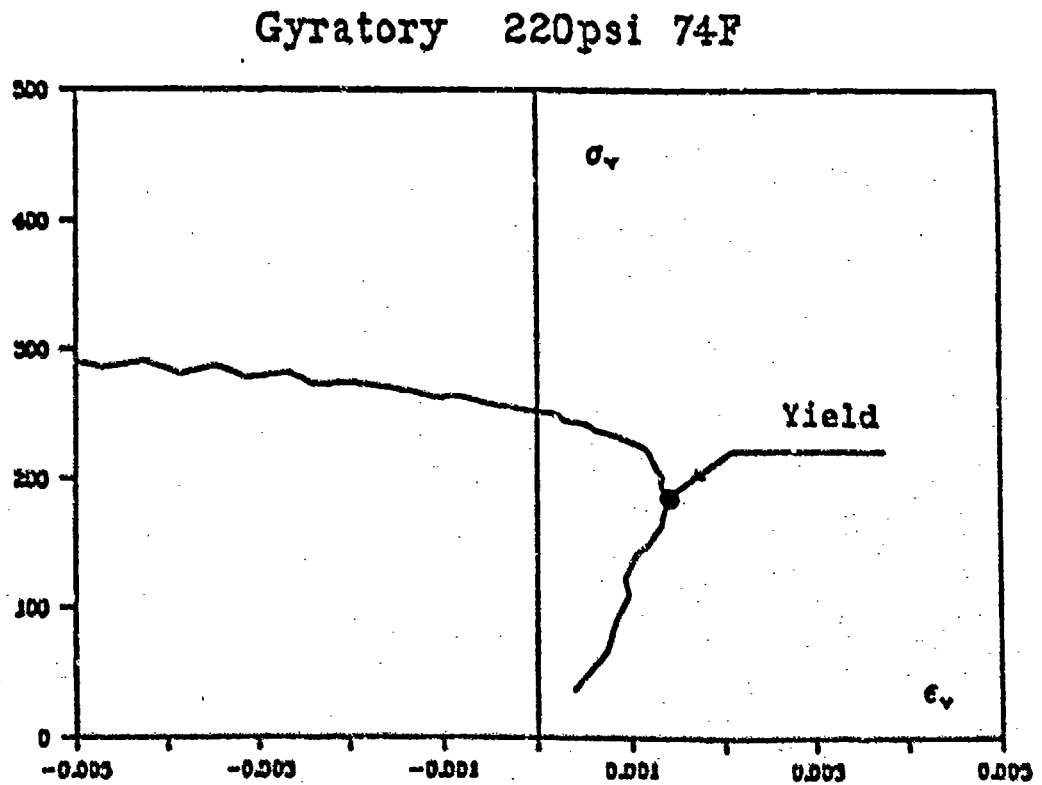


Figure 1-9. Volumetric Behavior During Constant Strain Rate Triaxial Test

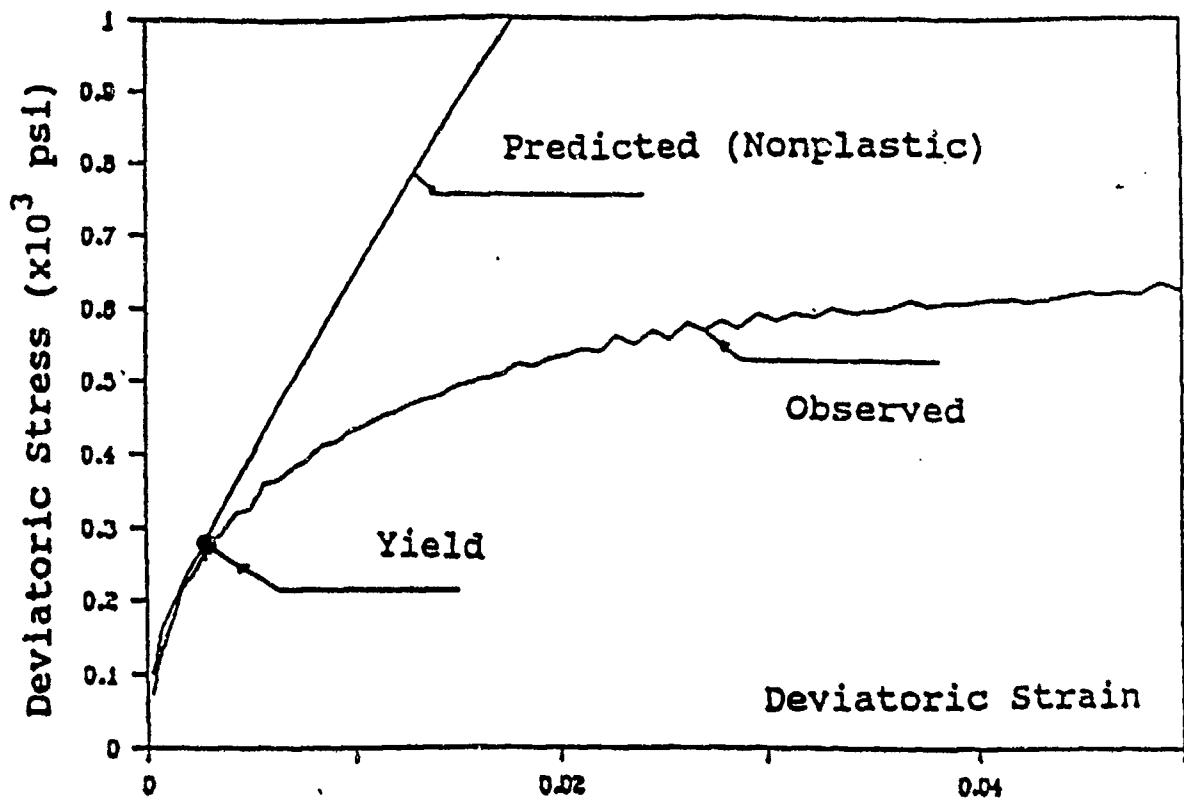


Figure 1-10. Deviatoric Behavior During Constant Strain Rate Triaxial Test

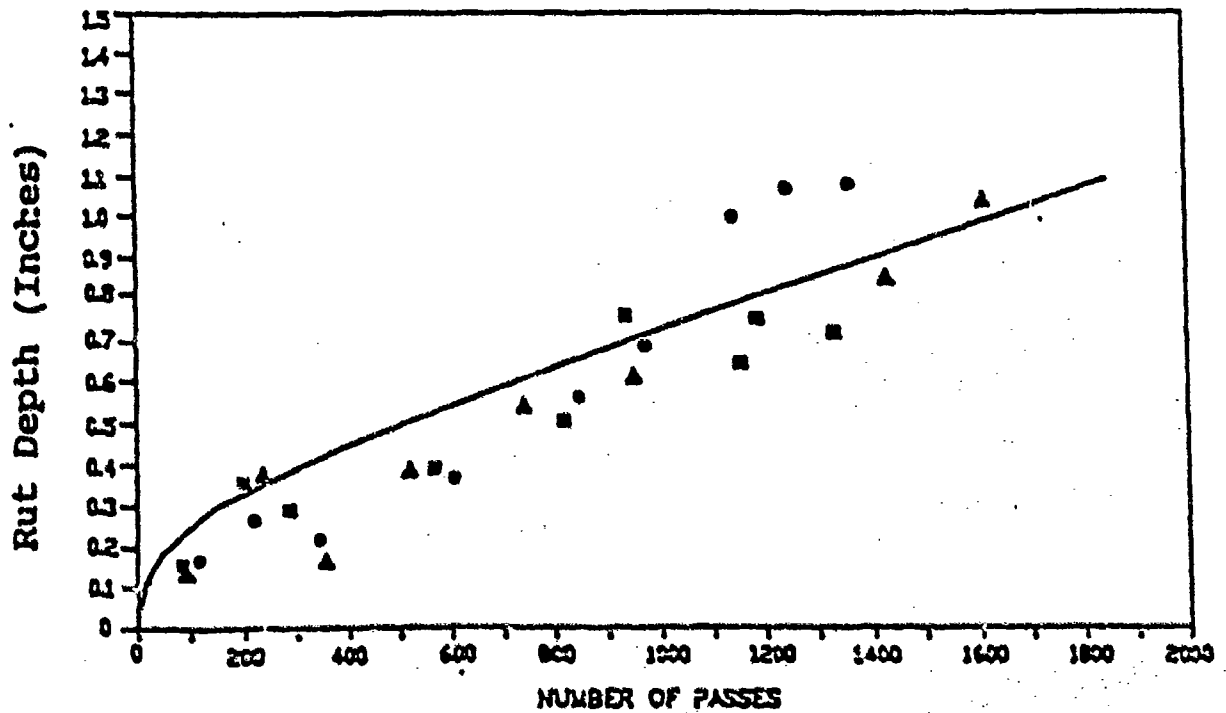


Figure 1-11. Experimental and Theoretical Rut Depth Accumulation for Marshall Pavement at 105° F

The above model is successfully implemented in the FE code. Figure 1-7 shows the comparison between predicted and field test rutting for the Marshall mix pavement.

The model has all the major components of deformation, at least qualitatively. The direction of future research are as follows:

- a. Components of the model, keeping the same general theoretical framework, will be defined in a way that conforms to reality.
- b. The theoretical framework will be expanded to include more complex phenomena, such as the viscous plastic interaction, history dependence, induced and inherent anisotropy. A variety of models is presently available for the modelling of these phenomena [36]. Recently developed hierarchical plasticity models [34-38] have the capability to model the history dependence of the material, viscoplastic responses, induced and inherent anisotropy. These models have been verified with respect to laboratory and field tests for a number of geologic materials which exhibit properties similar to those of asphalt concrete. This will be one avenue of the proposed theoretical research.
- c. Knowledge of the history dependence of the different components of the model will enhance the understanding of the accumulation process and allow the improvements of the accumulation model.

1.7 Hierarchical Concept: Toward a Complex Model

Although the application of a BASIC, simplest credible model as discussed previously may suffice most conditions, more complex constitutive laws are required for Granular Composites Materials, such as asphalt concrete, portland cement concrete and aggregate base and lime/cement/aggregate materials subjected to complex state of stresses. The more complex model should include [36]:

- a. Yield function to be expressed in terms of J_1 , J_2 , J_3 , or J_2D and J_3D , and mixed variant I_p .
- b. Yield function, shall be a single yield surface, rather than two intersection yield functions; such condition reduces the number of required parameters as compared to the multi-surface models presented in literature (Figure 1-12).

As example, one of many hierarchical models may have a general form of the yield function F is as follows:

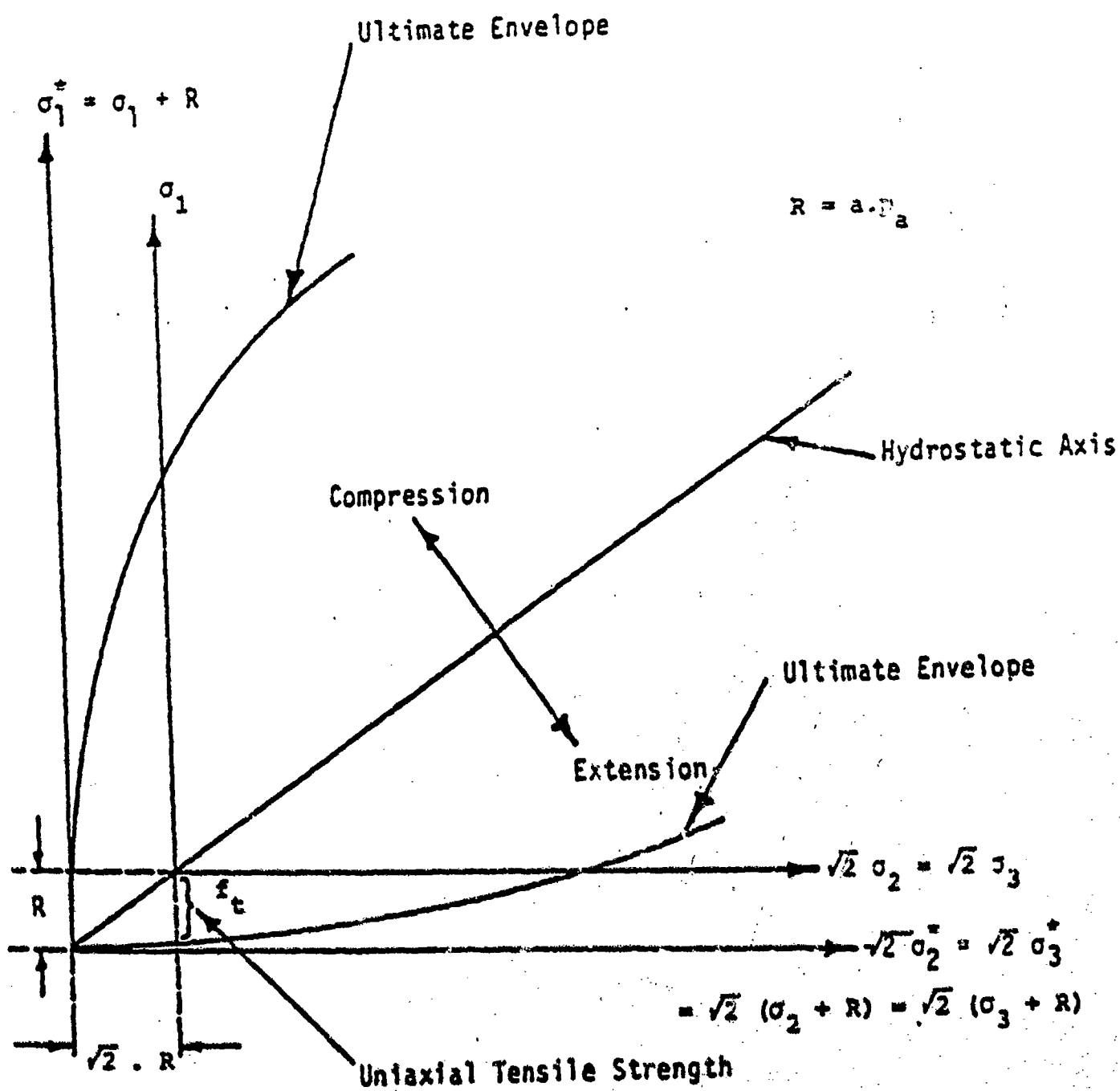


Figure 1-12. Single Yield Surface

$$F = J_{2D} - (\alpha J_1 + \delta J_1^2) (1 - \beta S_1)^m + 0 \quad (27)$$

where

$$S_1 = \frac{J_{3D}^{1/3}}{J_{2D}^{1/2}}$$

$$m = -1/2$$

$$\alpha, \beta, \delta = \text{constants}$$

For materials having cohesion and tensile strength the stress terms in this equation are increased to include tensile strength, R .

$$\begin{aligned} \sigma_1^* &= \sigma_1 + R \\ \sigma_2^* &= \sigma_2 + R_1 \\ \sigma_3^* &= \sigma_3 + R \end{aligned}$$

The model is expected to represent Portland Cement concrete, asphaltic concrete, and aggregate base.

It includes material constants which can simulate hardening and include the effects of stress path, volume change and coupling of shear and volumetric responses.

2. State-of-the-Art Review of Cracking Prediction Models Using Fracture Mechanics

2.1 Introduction

Fracture mechanics has been used in the past to analyze cracking in metals. However, due to the heterogeneous characteristics of pavement materials, the application of fracture mechanics to analyze cracking in pavements was not attempted until the Ohio State University. Researchers initiated a study in early seventies to investigate the feasibility of using fracture mechanics for this purpose. This research indicated that fracture mechanics analysis was suitable for analyzing cracking in pavements [39]. Subsequent research resulted in the development of methods and procedures which could be used to analyze the damages in pavements of different structural configuration and subjected to various traffic loading and environmental conditions. The objective of this paper is to briefly describe the advancements in this technology since early seventies. These advancements closely followed the developments in the analysis and application of fracture mechanics in metals and other materials.

Initially the technology was developed to apply linear fracture mechanics in the analysis of cracks in beam and slabs resting on elastic foundations. The main concern at that time was to estimate the stress-intensity factor of various types of loading configuration, crack patterns and geometry so that the rate of cracking relationship represented by the following formula can be developed:

$$dc/dN = A K^n \quad (28)$$

where

c = crack length

K = stress-intensity factor

A, n = regression constants determined from the analysis of data

N = number of repetitions

A method was developed at the O.S.U. in 1970 to estimate the stress-intensity factor, K for a beam on elastic foundation loaded at the center using the boundary collocation method [40]. The

stress-intensity factors for a slab with a semi-infinite crack and resting on an elastic foundation were obtained using the solution developed by Ang, et al. [41]. Ramsamooj [40] developed an analytical procedure to estimate K-values for moving loads also.

Subsequent improvements in the analytical and experimental techniques included the considerations for mix of mode crack propagation, specially when rigid pavements are overlaid with asphaltic mix layers. In these pavements, Mode I cracking (or tension cracking) can occur due to thermal stresses in the asphalt concrete layer. Also, due to traffic loads, the cracks at a joint may occur due to normal shear (Mode II). Thus reflection cracking in these pavements may occur due to a mix mode fracture of the asphaltic material.

For mixed mode fracture, the O.S.U. model utilized the crack growth law in terms of the strain-energy-density factor along the direction of fracture (S_{min}):

$$dc/dN = B(S_{min})^n \quad (29)$$

The fatigue life, or number of load applications to produce a crack through the overlay, is given by:

$$Nf = \int_{c_0}^{c_f} \frac{dc}{B(S_{min})^n} \quad (30)$$

where

c_0 = initial starter flaw length

c_f = crack length at which the overlay is considered failed (either its thickness or the length at which the critical $S_{min} = S_{cr}$, is reached, whichever is less) and S_{cr} , B , and n are material constants derived from fatigue tests on asphaltic concrete beams

Further developments in the analysis of stresses at or near the crack tip indicated that the assumptions of linear fracture mechanics may not be valid for ductile materials like asphaltic mixes because the size of plastic zone in this area may be large enough to cause significant deviations from the assumption of linear fracture mechanics. Therefore, the use of J-integral and C^* line integral in the analysis of cracking in pavements was investigated and procedures were developed to test the pavement materials in the laboratory for this purpose. It was noted that the use of these parameters could improve and extend the use of fracture mechanics analysis to materials depicting non-linear behavior.

The above is a very brief description of the developments related to the use of fracture mechanics in the prediction of cracking in pavements. Further details of some of these developments are briefly summarized in the subsequent sections of this paper. For this purpose, the discussions in the paper have been divided into the following topics:

- a. Application of fracture mechanics to pavement materials,
- b. Application of fracture mechanics to analyze pavements,
- c. Effect of mix variables on the fatigue parameters,
- d. Extension of cracking analysis to include non-linear behavior of materials, and
- e. Considerations for the statistical nature of the pavement system and its components.

2.2 Application of Fracture Mechanics to Pavement Materials

Due to the heterogeneous nature of common asphaltic mixes, relatively uniform mix of sand-asphalt was initially selected for testing samples in the laboratory. Three different systems, viz., simply supported beams, beams supported on elastic foundation, and slabs supported on elastic foundation were subjected to repeated loads of constant magnitude. The results obtained from these tests indicated that the rate of crack propagation, dc/dN , in each system could be represented by the general relationship known at that time [42,43] and represented by Equation (28).

Subsequent research included asphalt mixes containing aggregates which were used in the surface mixes by the Ohio Department of Transportation [44]. It was observed that the relationship represented by Equation (28) was still valid for these mixes. This was considered to be sufficient evidence of the hypothesis that the concepts of fracture mechanics were applicable to pavement materials. Therefore, the research was continued to determine the various items needed for the analysis of cracking in the pavements.

2.3 Application of Fracture Mechanics to Analyze Pavements

Once it was established that the concepts of fracture mechanics were applicable to the pavement materials, it was necessary to investigate the applicability of Equation (28) in the analysis of pavement damage. A pavement system is generally affected by several variables, among which the pavement support conditions, traffic loading, environmental conditions, and structural

geometry are important. Therefore, the research was conducted to determine the effect of these variables on the rate of cracking as represented by dc/dN in Equation (28). Since dc/dN is a function of parameters A , n , and K , the purpose of research in this connection was to determine the effect of various variables on any one or more of these parameters. The results of this research are briefly summarized in the following paragraphs. Sand-asphalt beams and slabs resting on elastic foundation were used in most of these investigations (except for tests to determine the effect of support conditions, in which simply supported beams were used). The beams were generally 3 inches wide x 2 inches deep x 24 inches long and slabs were 44 inches in diameter and 1.5 inches thick. Elastic foundation consisted of natural rubber. Different thicknesses were used for beams and slabs.

2.3.1 Effect of Support Conditions on the Rate of Cracking

Two different elastic supports as well as no support (beam supported at its ends only) were used in this experiment. The results of these experiments are shown in Figure 2-1. These results indicate that there is a significant effect of support conditions on the rate of cracking. Both parameters A and n of Equation (28) are affected by these conditions as shown in Figure 2-1.

2.3.2 Effect of Load Magnitude on the Rate of Cracking

Sand-asphalt beams (3 inches wide x 2 inches deep x 24 inches long) resting on elastic foundation were subjected to three levels of constant load amplitude (20,30 and 40 pounds). Figure 2-2 shows the crack growth in these beams for normalized fatigue life N_i/N_f . It is important to note that the load magnitudes of 20,30 and 40 pounds result in an identical $c - (N_i/N_f)$ relation. This implies that for monotonic loading of constant amplitude, the crack growth or "damage" accumulation is independent of stress levels [39]. Also, the rate of crack propagation was plotted against the stress intensity factor. This plot (see Figure 2-3) shows that the data follows the general trend represented by Equation (28) with n being equal to 4.0.

Tests were also conducted on sand asphalt slabs of 44 inches diameter and 1.5 inches thick. The results of these tests indicated that the rate of cracking (dc/dN) followed the same relationship as beams (see Equation 28) as shown in Figure 2-4.

2.3.3 Effect of Rest Period on the Rate of Cracking

The effect of rest period on the rate of cracking (dc/dN) was studied on beams as well as slab samples. For this purpose the load was applied for a duration of 0.1 second (half-sine form)

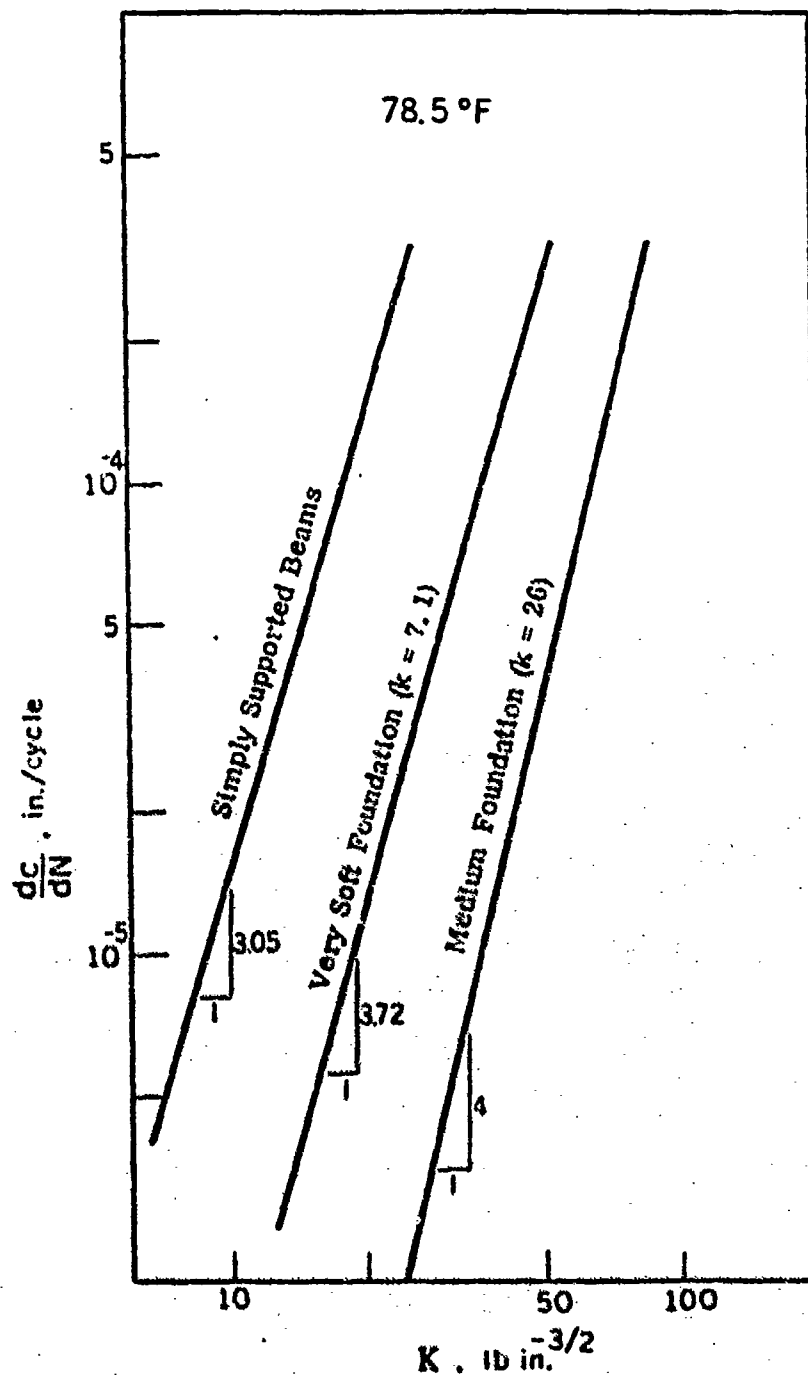


Figure 2-1. Comparison of Rates of Crack Propagation in Simply Supported Beams and Beams on Elastic Foundation

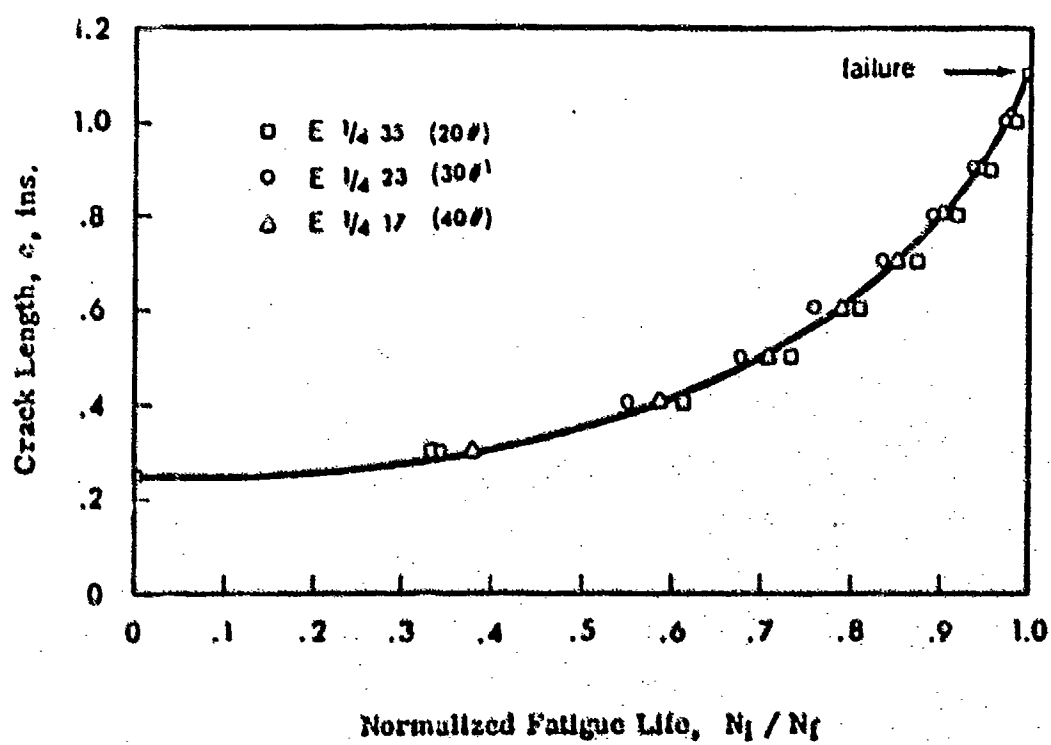


Figure 2-2. Crack Length - Normalized Fatigue Life for Monotonic Loading

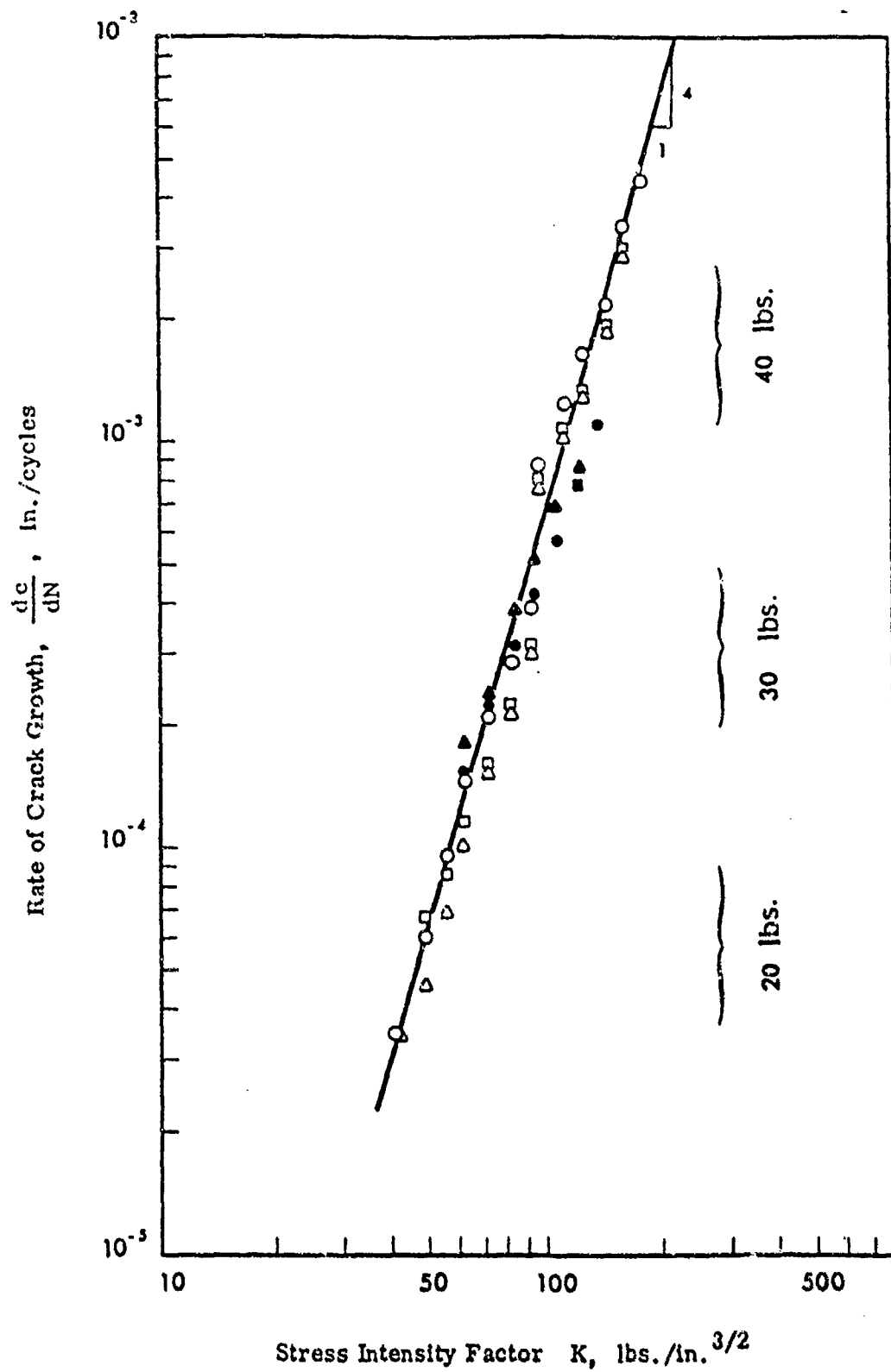


Figure 2-3. K versus dc/dN for Monotonic Loading with Different Amplitudes

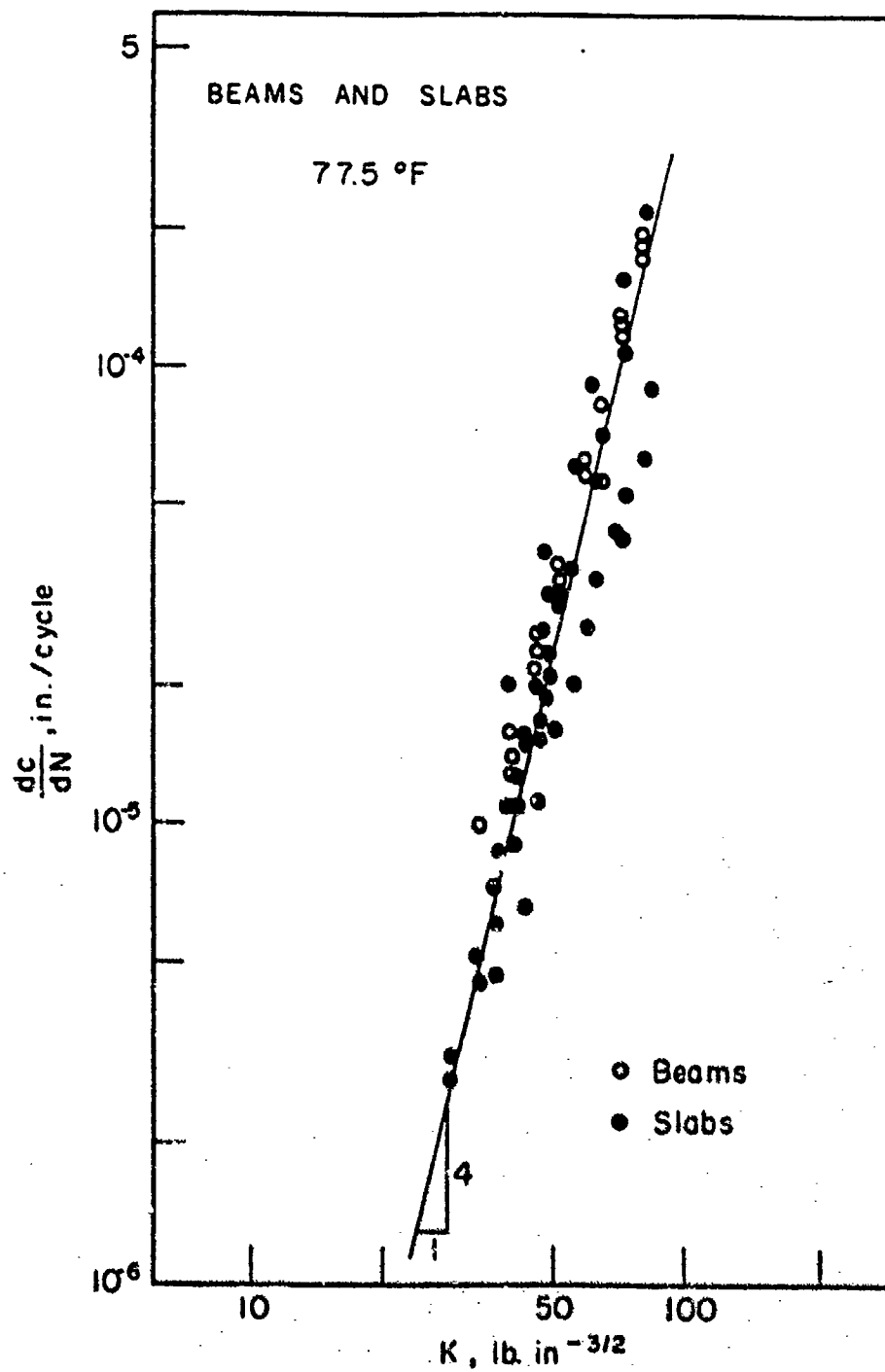


Figure 2-4. Comparison of the Crack Growth Rates for Beams on Elastic Solid and Slab Tests

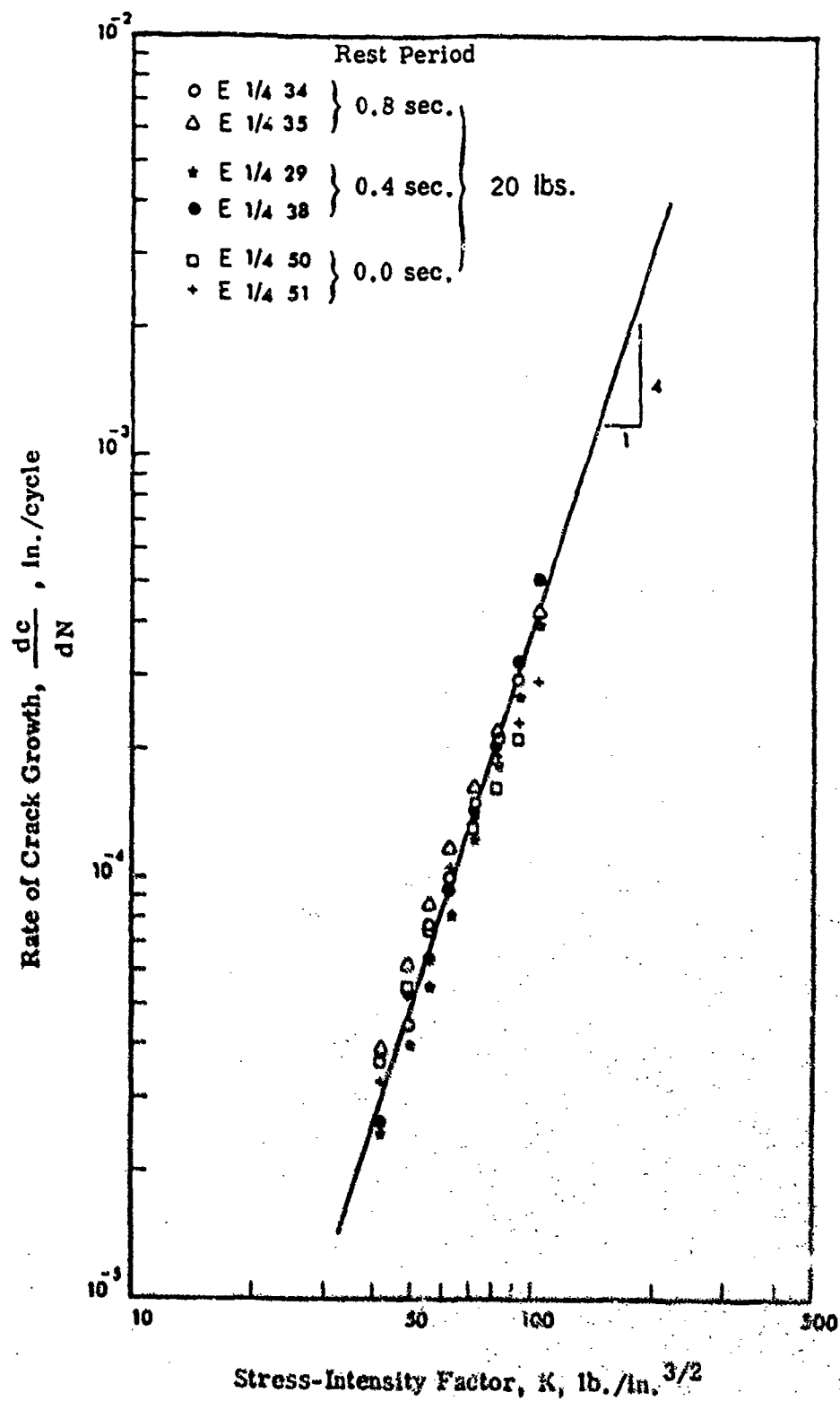


Figure 2-5. K versus dc/dN , for 20 lbs. Monotonic Loading with Different Frequencies

and was followed by a rest period of specified duration. In case of beam samples, the rest periods of 0, 0.4 and 0.8 second were selected. The results of these tests are shown in Figure 2-5. It is evident from this figure that the effect of rest period on the rate of cracking is insignificant and the same general Equation (28) applies to this case. Subsequent tests on slabs resting on elastic foundation indicated similar trends [39].

2.3.4 Effect of Load Sequence on the Rate of Cracking

The effect of load sequence on the rate of cracking (dc/dN) in beam samples is shown in Figure 2-6. This figure shows the results of tests using three different loading sequences. The members in each sequence represent the loads in pounds. For example, 20/30/40 represents the sequence of 20, 30, and 40 pound loads applied to the sample. It is evident from this figure that the load sequence affects the rate of cracking significantly [39]. Similar results were obtained from tests on slabs using two different loading sequences as shown in Figure 2-7. Both of the parameters A and n are to be adjusted to include the effect of loading sequence on the damage in pavements.

2.3.5 Effect of High Stress Levels on the Rate of Cracking

The Elastic Fracture mechanics studies of crack tip stresses and deformations are useful but limited as pointed out by Rice and Drucker [45,47]. The limitation is mainly due to the inherent assumption in elasticity, which disregards the geometrical singularity or material strength limit at the point where stresses are concentrated. Therefore, in order to verify the applicability of analysis based on these assumptions, the slabs were subjected to high levels of stresses. Loads of 500 and 600 pounds were used for this purpose. The results of these tests indicated that crack patterns in the slab were very similar to that obtained from loads of lesser magnitude. However, large amount of permanent deformations were observed under the loaded area. Figure 2-8 shows the accumulation of permanent deformation under the load. Except for the initial portion, where the plot is curved, it was noted that the rate of change in permanent deformation was approximately constant and can be represented by a relationship of the following form:

$$(dp/dN) = \text{Constant} \quad (31)$$

It was also observed that the permanent deformations under the load were not caused by the densification of the material. This fact was verified by the x-ray photographs of the area.

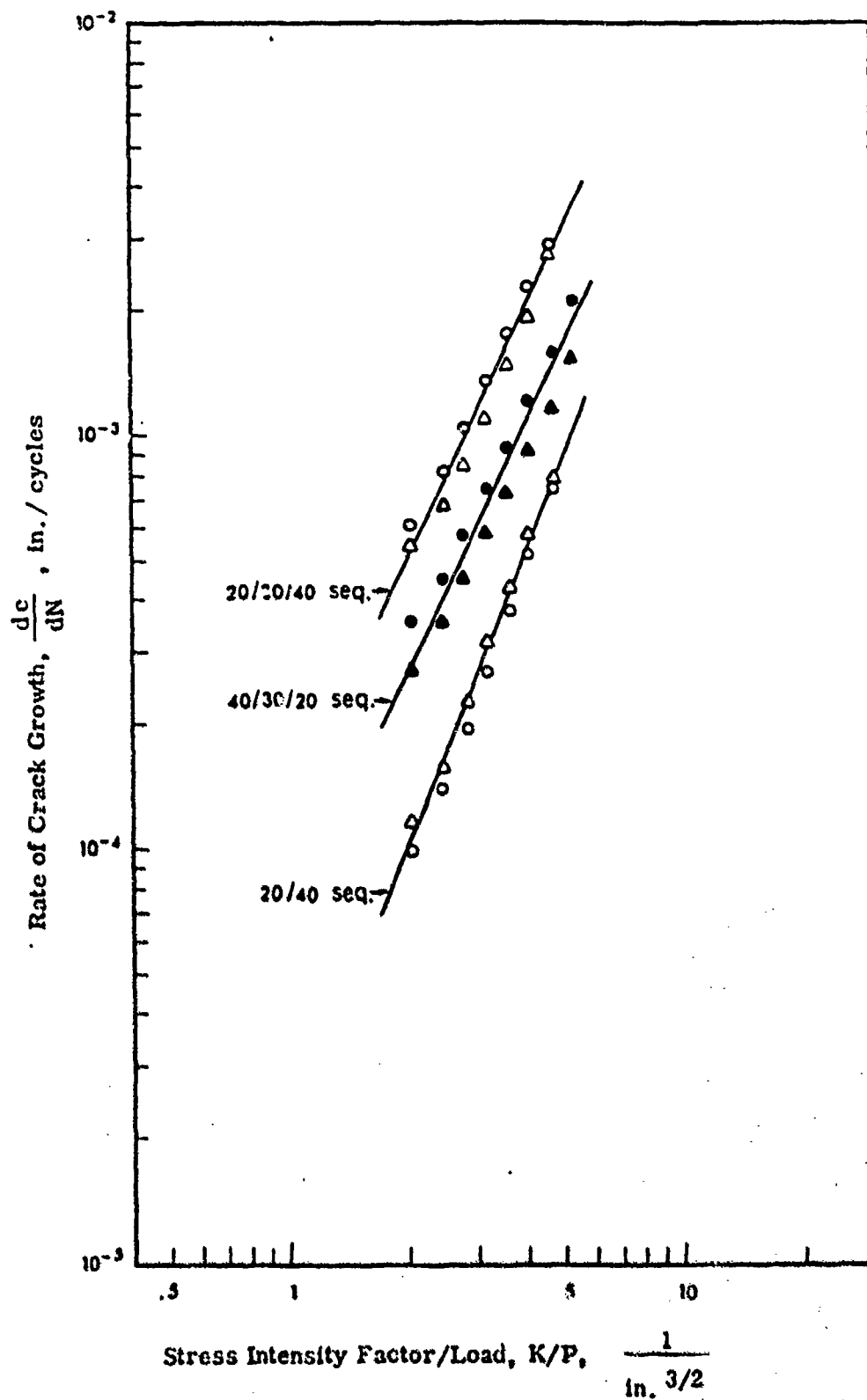


Figure 2-6. dc/dN versus K/P for Sequential Loads

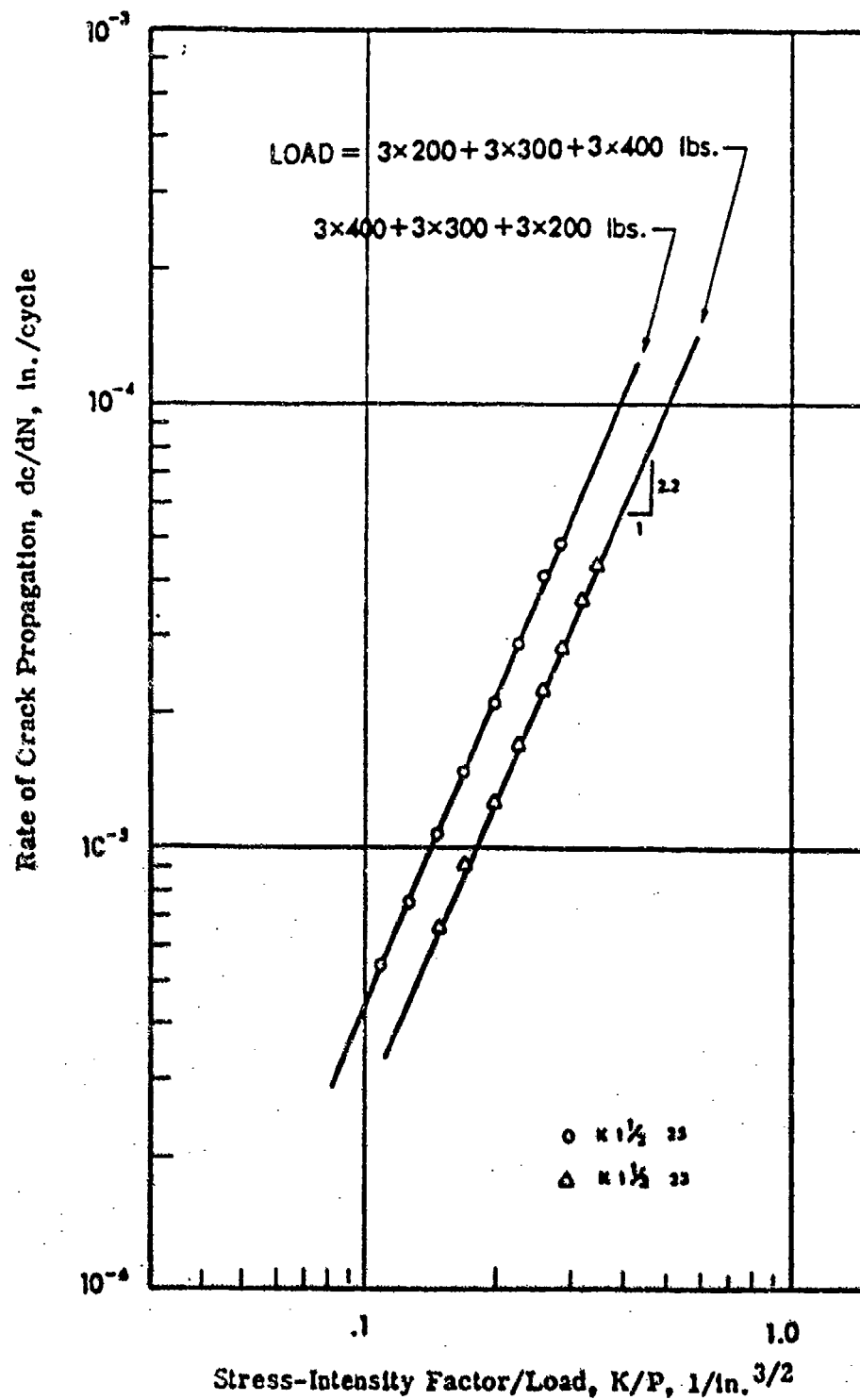


Figure 2-7. dc/dN - K/P Relationship for $3 \times 200 + 3 \times 300 + 3 \times 400$ lbs. and $3 \times 400 + 3 \times 300 + 3 \times 200$ lbs. Sequence

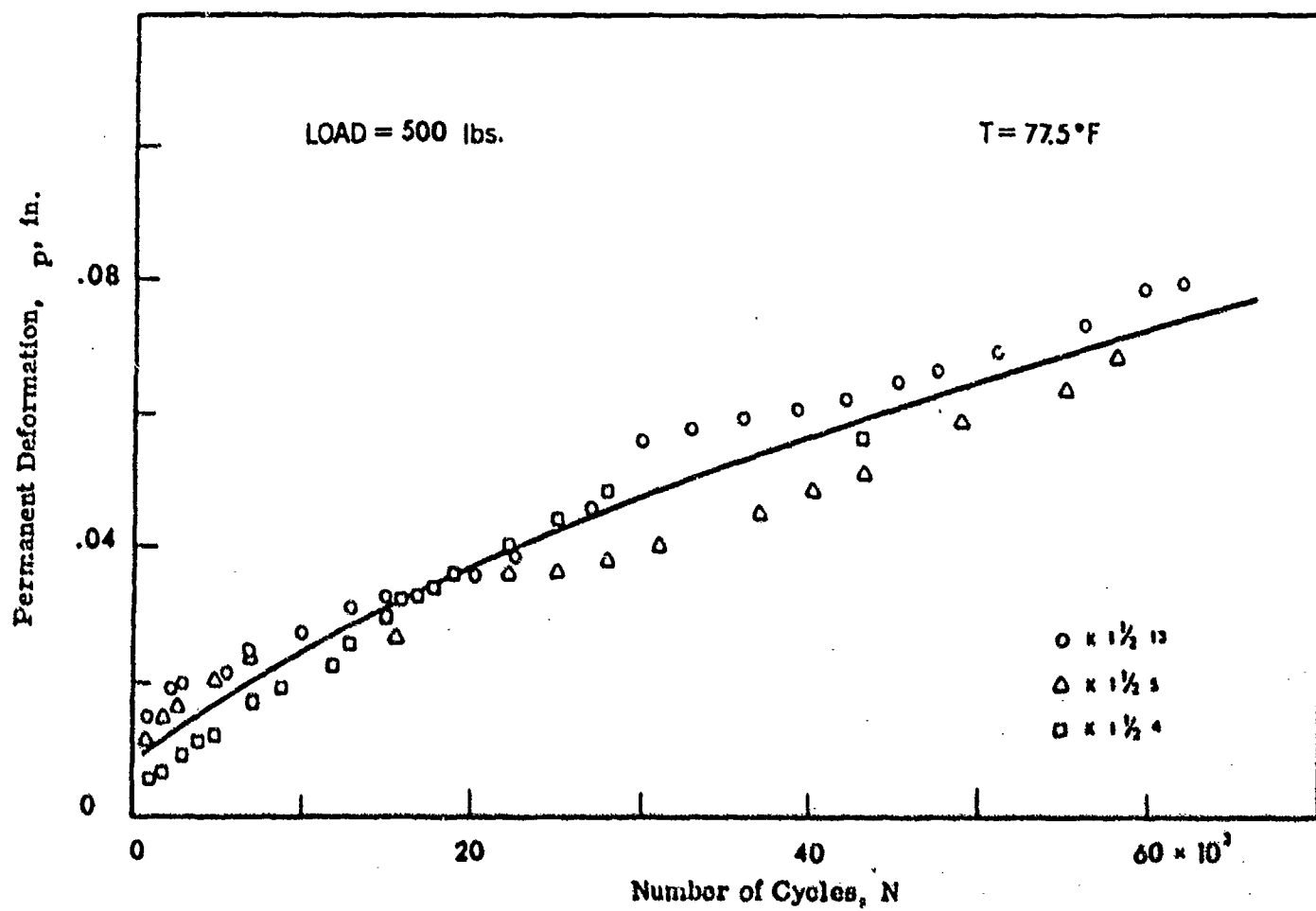


Figure 2-8. Variation of Permanent Deformation with Load Repetition for 500 lb. Load Series

Therefore, the flow of material under the loaded area was suspected to be the cause of permanent deformation recorded.

The rate of crack propagation for cracks outside the loaded area (until to the point of failure) were plotted and are shown in Figures 2-9 and 2-10. These plots show that the rate of cracking can still be represented by Equation (28) and is not affected by the amount of permanent deformation under the loaded area.

2.3.6 Effect of Temperature on the Rate of Cracking

Slabs resting on elastic foundation were tested at temperatures of approximately 41, 77, and 90°F to determine the effect of temperature on the rate of cracking. The results of these tests indicated that for the range of temperatures selected for this study, the crack growth rate represented by Equation (28) was still a valid relationship. However, at low temperatures, when the crack appeared on the top of slab, it propagated rapidly and catastrophic failure occurred. Thus the failure criteria in this case is represented by the critical stress-intensity factor, K_{Ic} as shown in Figure 2-11. These results were verified by applying two different levels of loads to the slabs.

Tests conducted at 90°F indicated that the crack growth rate relationship still applied to the cracks at the top of surface as shown in Figure 2-12.

2.3.7 Effect of Structural Geometry on the Rate of Cracking

Two-dimensional pavement models represented by a beam on elastic foundation as well as three-dimensional pavement models represented by a slab on elastic foundation were tested in the laboratory to compare the rate of cracking in each case. It was observed that the rate of cracking was unaffected by the geometry of model structure and parameters A and n obtained from both system were same. Thus, the stress-intensity factors estimated for each system accommodated the differences in the structural geometry of these two models as shown in Figure 2-4.

2.3.8 Effect of Moving Load on the Stress-Intensity Factors

The discussions so far related to the experiments conducted by loading the samples at a given point. However, it was considered important to study the effect of moving load on the pavement damage. Therefore, analytical procedures were developed to estimate the stress-intensity

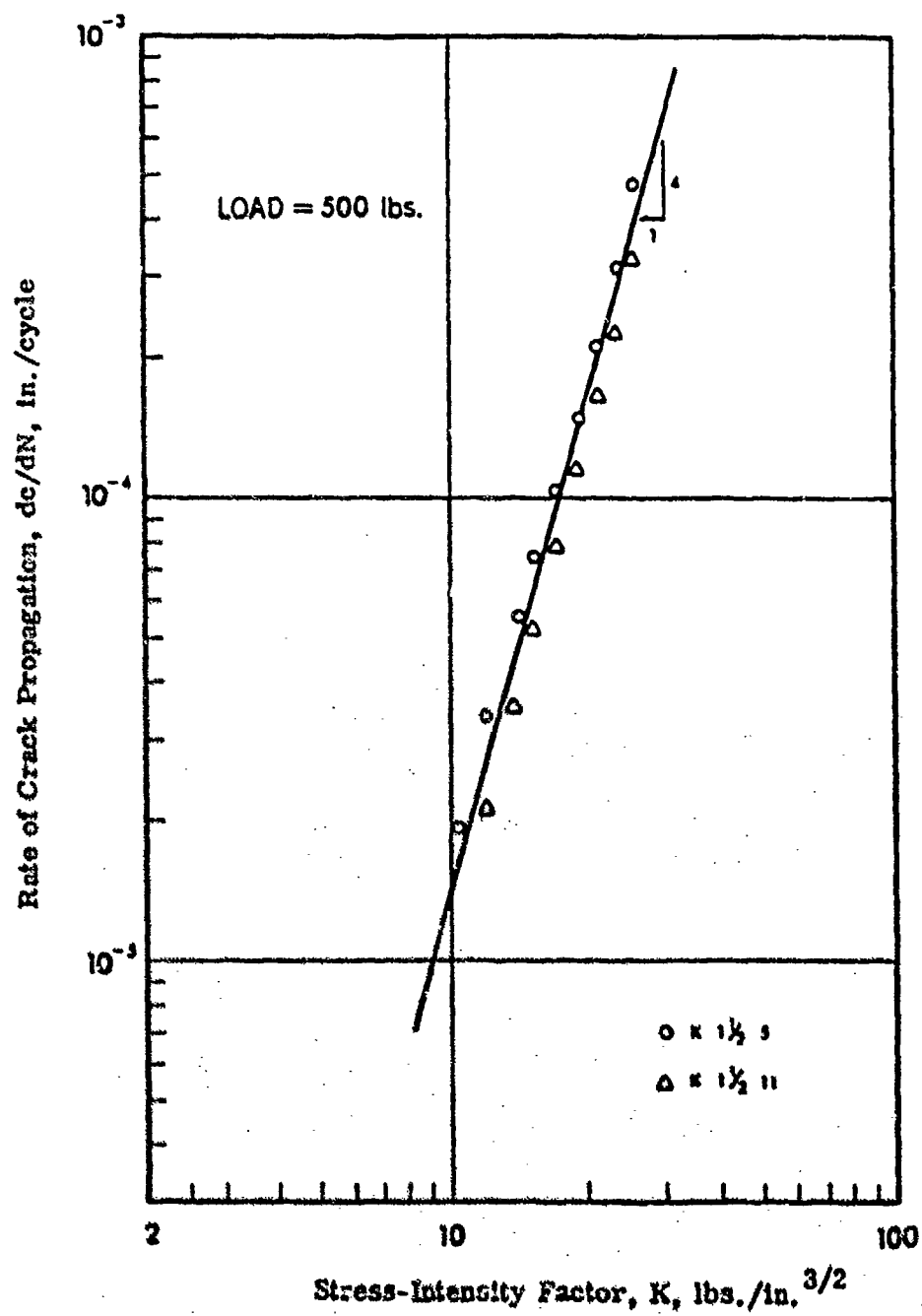


Figure 2-9. dc/dN - K Relation for a 500 lb. Load Series

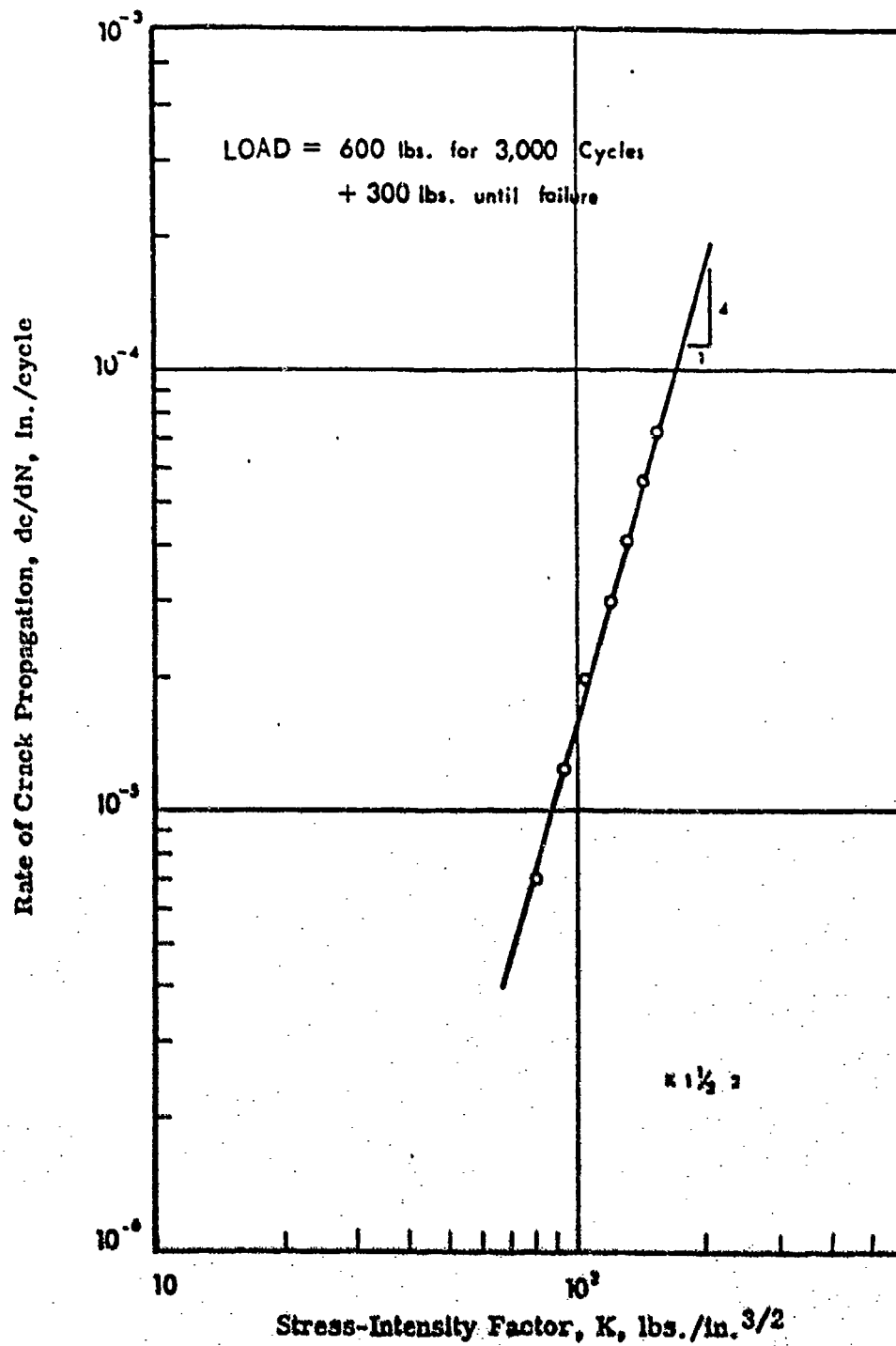


Figure 2-10. dc/dN - K Relation for a 600 lb. - 300 lb. Load Sequence

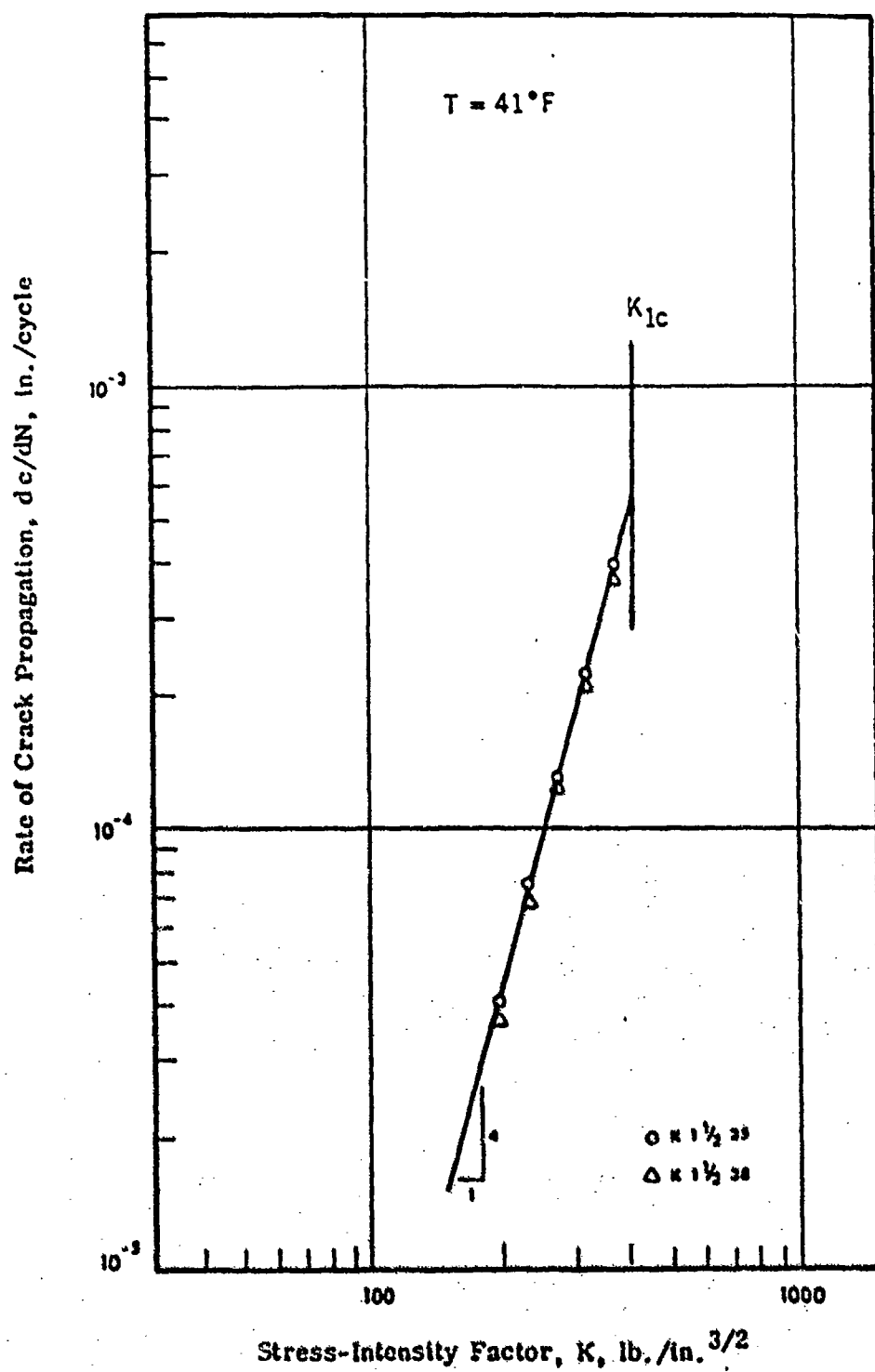


Figure 2-11. dc/dN - K Relation for Tests at 41°F

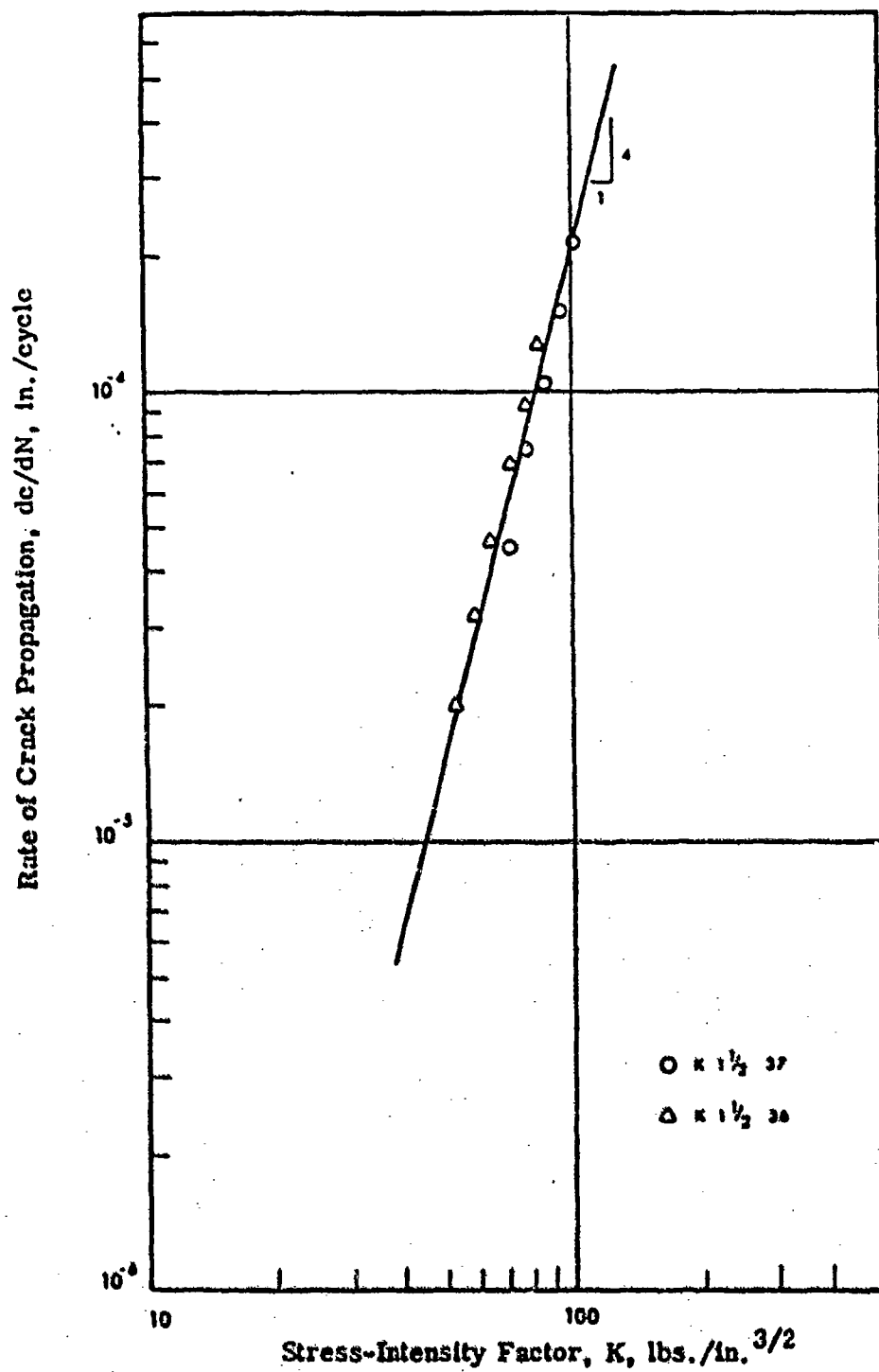


Figure 2-12. da/dN - K Relation for Tests at 90°F

factor for these cases. A typical plot of influence lines of the indicated loads is shown in Figure 2-13. Damage due to each moving load can be accumulated for each crack location and the position of load as shown in this figure.

2.3.9 Fatigue-Life of a Pavement

The results of various tests on beams and slabs, which were conducted in the laboratory to determine the applicability of rate of cracking Equation (28) to various load configurations and geometry of structure have been summarized in this section. These results indicated beyond doubt that Equation (28) was applicable to beams and slabs as well as wide range of loads and pavement temperatures. Therefore, it is feasible to use this approach in estimating the fatigue life of a pavement, provided the parameters A and n of the material and related support conditions have been determined from laboratory tests. For this purpose, Equation (28) can be rearranged and integrated as indicated below:

$$dc/dN = A K^n$$

or

$$dN = dc/(A K^n)$$

or

$$\int_{N_0}^{N_f} dN = \int_{c_0}^{c_f} [1/K^n] dc$$

or

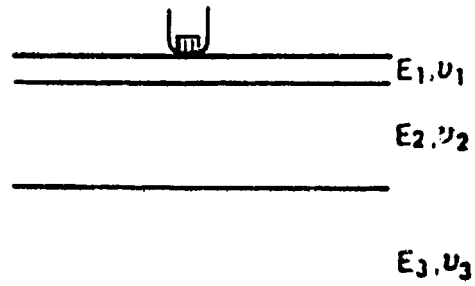
$$N_f = \frac{1}{A} \int_{c_0}^{c_f} (1/K_n) dc \quad (32)$$

where

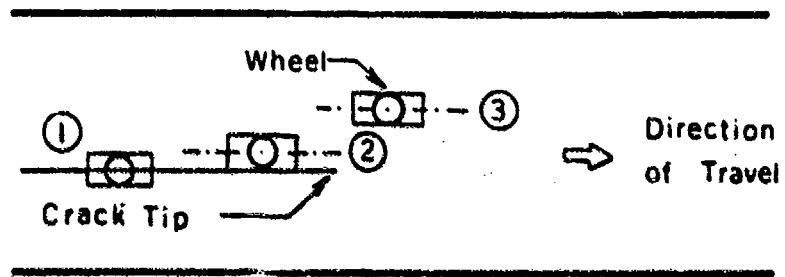
N_f = fatigue life in number of cycles applied

c_0 = initial flaw size in pavement at cycle = 0

c_f = final crack size at the end of N_f cycle or failure



Pavement Section



Pavement with a Long Crack

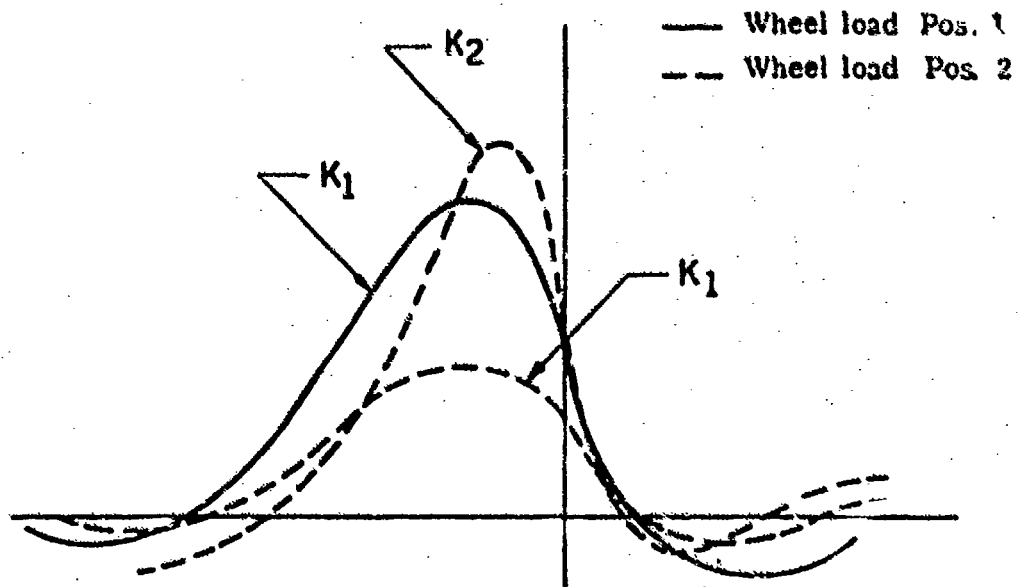


Figure 2-13. Typical Influence Lines for K_1 and K_2 for a Semi-Infinite Crack

K = stress-intensity factor,

A, n = material parameters determined from laboratory tests

The above equation indicates that the fatigue life can be estimated by integrating the plot of crack, c vs. $(1/K^n)$ between the boundaries of c_0 and c_f .

Experimental as well as analytical procedures have been developed to determine the stress-intensity factors for various crack lengths in beams and slabs. These methods utilize boundary collocation and finite element methods to estimate K for the given structural geometry [39]. Thus a c - K relationship or c - $(1/K^n)$ relationship can be developed for the given pavement which has been subjected to specified load. A normalized c - (K/P) relationship can also be developed if the given load P is expected to vary. The starter flaw size c_0 and final crack size c_f can be determined for the given pavement and A and n can be experimentally determined so that the fatigue life of the given pavement can be estimated. The details of procedure to obtain various parameters of Equation (30) are described in previous reports [39,47]. A brief discussion of the effect of mix variables on fatigue parameters is included in the subsequent paragraphs.

2.4 Effect of Mix Variables on the Fatigue Parameters

Important mix variables which affect the fatigue parameters (c_0 , A , n) are the aggregate gradation, mix density, asphalt content, void content of the mix, moisture content, and temperature of the mix. Studies were conducted to determine the effect of each one of these variables on any one or more fatigue parameters A , n and c_0 . The results of these studies are available in references [44,47] and other reports published in this connection. A brief summary of some important results of these studies is included in the following paragraphs:

2.4.1 Initial Flaw Size, c_0 :

Initial flaw size, c_0 is a property of pavement material and vary with the type of mix, gradation, etc. Although an average value as determined from laboratory tests can be used for deterministic analysis, the distribution of c_0 in a given mix can be successfully used in the stochastic analysis of fatigue failure in pavements. Results of previous studies indicate that flaw size, c_0 does not depend on the air voids in the mix, but the distribution of c_0 in a given mix depends on its air void content. More air voids in the mix tend to distribute c_0 more widely than the mixes with less air voids [44].

2.4.2 Parameters A and n:

The value of fatigue parameter A decreases as the dynamic modules of asphalt mix increases [44] for the mixes of same density. Also, as the temperature of mix increases, the value of parameter A increases as shown in Figure 2-14. These results can be used to adjust the value of parameter A for these mix variables.

The value of parameter n was found to remain constant for most of the mixes tested previously and vary only with the support conditions (see Figure 2-1).

2.5 Extension of Cracking Analysis to Include Nonlinear Behavior of Materials

Fatigue life generally passes through three distinct periods: initiation of crack, propagation of the crack to a critical size, and ultimate failure. Throughout this process plastic zones are created in the material even when it is subjected to the alternating low levels of stresses. These zones are created mainly due to the presence of crack. In addition, during each loading cycle the sharp aggregate corners transmit point loading conditions to the asphalt cement with a stress singularity. Hence, even before crack formation, a plastic zone exists at each contact point of sharp aggregate and asphalt cement, and energy is dissipated through cyclic plasticity. Once a crack is initiated, then at the tip of the crack, stresses assume an inverse, square root stress (and strain) singularity. Because the material can tolerate stresses up to its yield point, a plastic zone around the crack tip forms and blunts the crack advance. The size of this plastic zone is critical in the analysis of fatigue life. If the plastic zone thus formed is small compared to the crack size and the geometry of the continuum, linear elastic fracture mechanics can approximate conditions of failure favorably (small scale yielding). On the other hand, if the size of the plastic zone cannot be ignored (several orders of magnitude of the crack size), a nonlinear fracture mechanics approach is more appropriate. With this in mind, analysis based on J integral and C*-line integral was developed.

The path independent J integral was defined by Rice [48] as follows:

$$J = \int_{\Gamma} W dy - T \frac{\delta u}{\delta x} ds \quad (33)$$

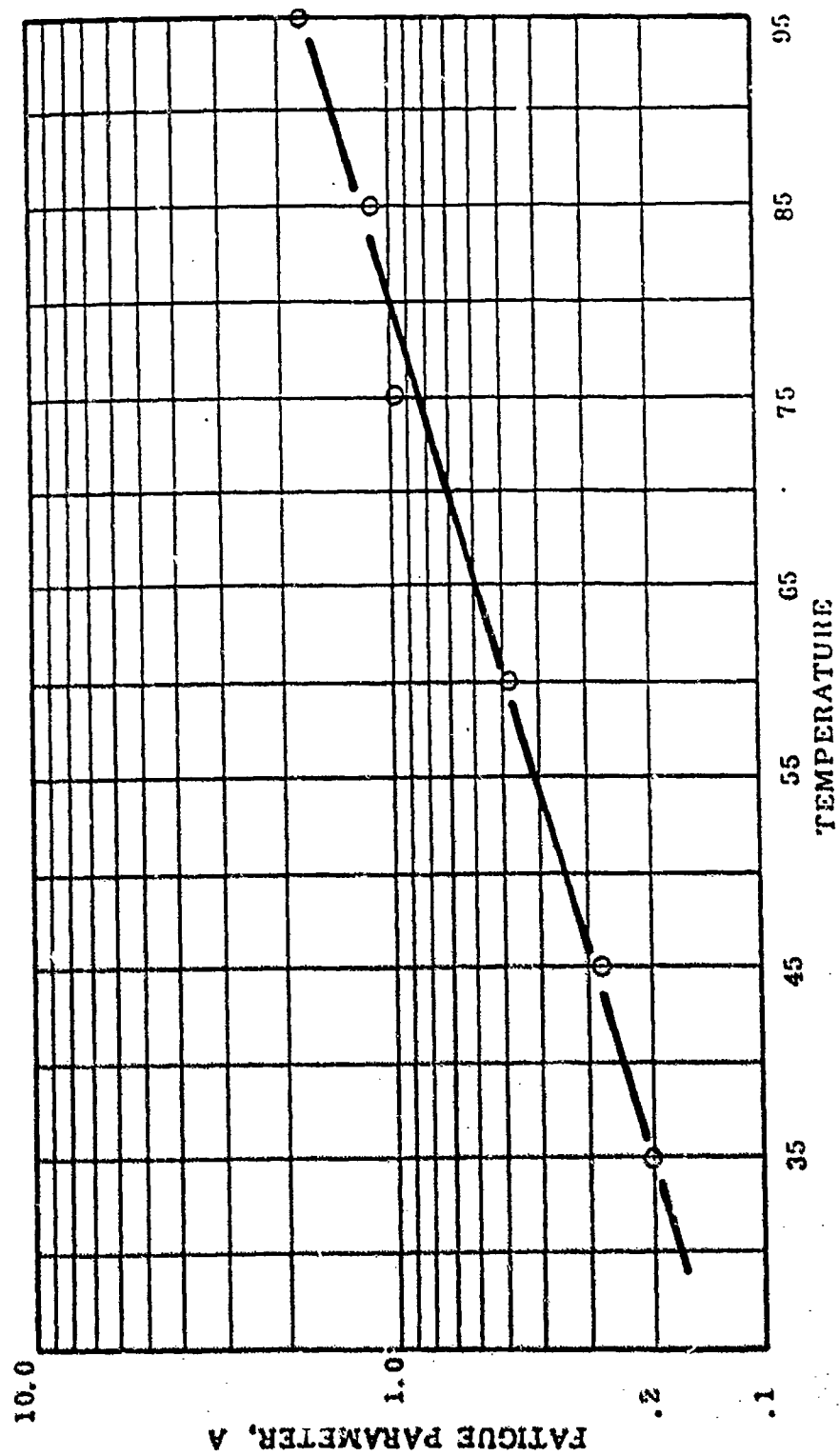


Figure 2-14. Variation of Fatigue Parameter A with Temperature

where

- Γ = contour surrounding the tip of the crack extending in the x direction
- W = strain energy density function
- T = traction vector defined by the outward normal n along Γ : $T_i = \delta_{ij}N_j$
- u = displacement vector
- s = arc length along Γ

Rice has also proven the path independence of this integral. Since the only point surrounded by the all possible paths is the crack tip, it follows that the J integral is the description of the crack tip field. For the linear case (or small scale yielding), the the J description is equivalent to the stress intensity and energy release rate (crack driving force) descriptions:

$$J = \frac{K_I^2}{E'} = G_I \quad (34)$$

In case of large scale nonlinearities, the interpretation of J as a crack driving force is lost, however the J integral still represents the energy difference between two similar, identically loaded bodies with different crack lengths l and $l + dl$:

$$J = \frac{dU}{dl} \quad (35)$$

where U is the potential energy [49]; Begley and Landes [49] discuss the application of the J integral as a fracture criterion. The basis for the application to the large scale nonlinearities is provided by Hutchinson [50] and Rice and Rosengreen [51] who analyzed the crack tip fields within the framework of deformation plasticity. The J integral turns out to be a valid description of the crack tip field in this case. The limitation is obviously that the unloading is not allowed, which limits this application to crack initiation and small subcritical growth.

Abdulshafi and Majidzadeh [52] applied the J integral concept to the fracture and fatigue of asphalt pavements. They used the notched disc specimens loaded within the notch with various thicknesses c_0 and initial crack lengths c . Table 2-1 shows the comparison of K_{IC} and J_{IC} failure criteria. The J_{IC} does not show any variation with c_0 and can be accepted as a material property with more certainty. The same authors attempted to establish the fatigue crack growth relation, analogous to the Paris equation but in terms of J , rather than K as follows:

$$\frac{dc}{dN} = f(J)$$

(36)

Figure 2-15 shows the results of this study. The relation appears to be bilinear but more experiments are needed to establish this relation.

Table 2-1. Comparison of K_{Ic} and J_{Ic}

C_o	Thickness t (Inches)	P_{fall} (lb)	K_{Ic} (psi)	J_{Ic} (lb.in. x 10^{-2})	(psi)
0.25	2.6	1,287.5	496.9		
0.5	2.60	1,225	531	1,900	169.2×10^2
0.75	2.55	987.5	540	1,900	174.9×10^2

2.6 Consideration for the Statistical Nature of the Pavement System and Its Components

The stochastic nature of the fracturing process has been realized for a long time. The fundamental Weibull's weakest link theory [53] has been used extensively. According to this theory, the failure probability, P_f , in volume V is given by:

$$P_f \approx 1 - \exp\left\{-\int_V dv \int_0^\infty g(s) ds\right\}$$

where

$$g(s) = \text{number of defects per unit volume with "strength" between } s \text{ and } s + ds$$

Although useful in many cases, this theory has significant drawbacks, as pointed out by Bazant et al. [54]. Besides its statistical (rather than physical) basis [55], weakest link theory completely ignores the cooperative nature of the fracture process. As a matter of fact, it does not look upon fracture as a process at all. Moreover, it has originally been derived for the uniaxial

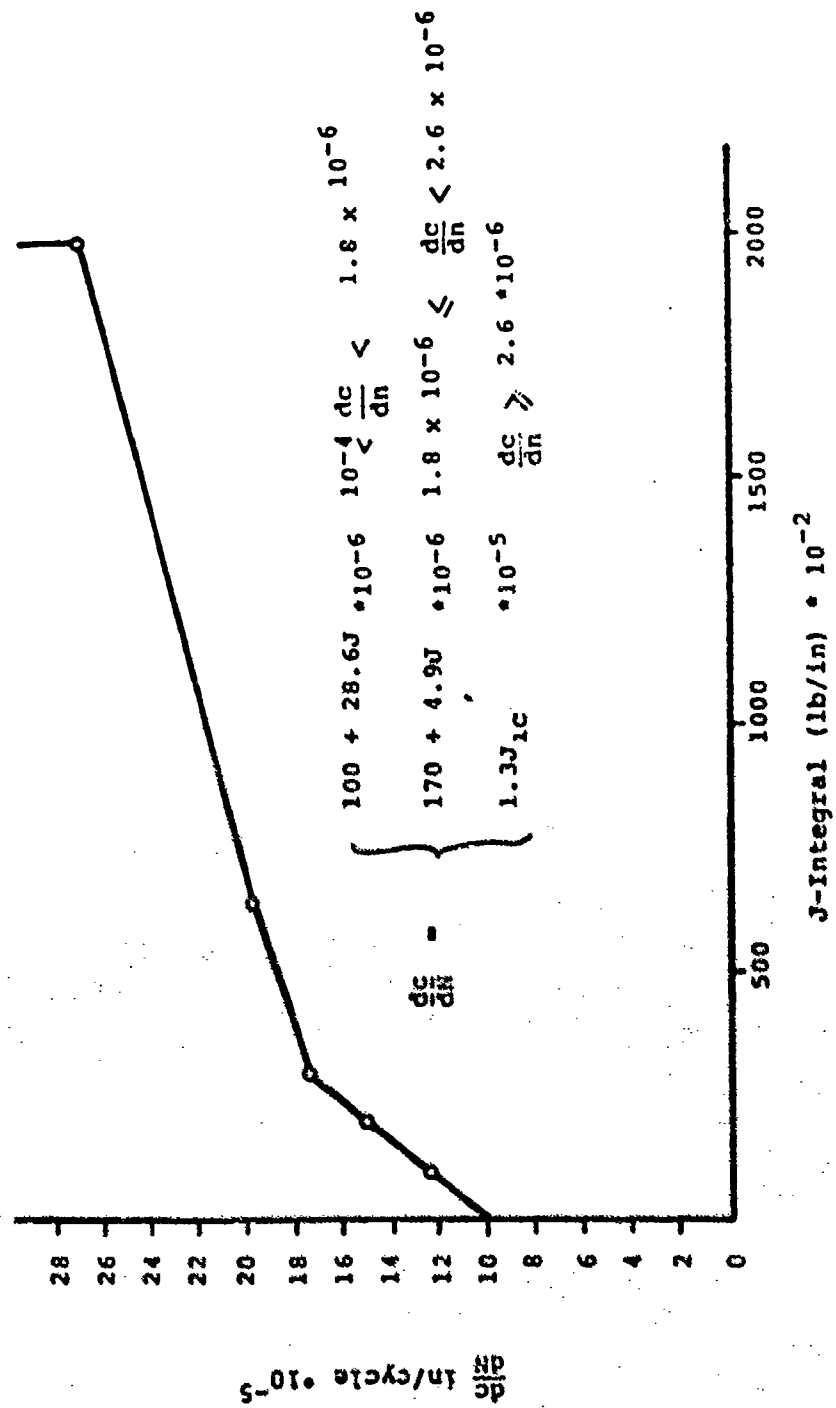


Figure 2-15. dc/dN versus J Integral Relationship

stress state and despite many attempts to generalize it [e.g., 56,57], its application to a multidimensional stress state remains questionable [54].

In a complex material, like the granular material with a binder, randomness of the fracturing process is a consequence of the random nature of the following:

- a. microstructure (fabric)
- b. defect types and distribution
- c. environmental effect including loads, temperature, moisture, chemical processes

Various researchers have studied some of these effects Lamon and Evans [56], Batdorf and Heinisch [57], Mesarovic et al. [58], and others analyzed the crack size and orientation distributions effect in a perfectly brittle material with no crack interaction. While the crack size distribution is either determined experimentally or assumed, the orientation distribution can be derived rationally. Consider a penny crack whose normal forms angle θ with the principal stress direction (Figure 2-16). Since the normal can intersect the unit sphere anywhere with equal probabilities the distribution function is the ratio of the shaded and the total area of the sphere: $F_\theta(\theta) = 1 - \cos\theta$. Figure 2-17 shows the probability of crack growth in a Poisson field (density λ) of penny cracks in the volume V , under the uniaxial tension with the assumed size distribution:

$$f_a(a) = \frac{1}{\eta} \left(\frac{a}{\eta}\right)^{\eta-1} \exp\left(-\frac{a}{\eta}\right) (\Gamma(\eta))^{-1}$$

The abscissa is proportional to the expected value of \sqrt{a} which is a direct consequence of the fracture criterion based on the maximum directional mode I stress intensity factor.

Cooperative nature of the fracturing process presents very complex problem. Researchers have addressed this problem in several ways using different techniques and philosophies.

Work of Kachanov [59] provides a solid mechanics basis for the study of the crack interaction by solving for the approximate stress field in the vicinity of two interacting cracks with the various relative positions. He has used a superposition technique for two-dimensional and three-dimensional crack arrays of arbitrary geometry. The procedure yields approximate analytical solutions for stress intensity factors up to close distance between cracks and microcracks. Of special interest to us is the solution developed for the interaction of a crack in the brittle material, such as concrete with a "damage field" created near the crack tip. Depending on the geometry of microcrack array, both stress amplification or shielding of the stress intensity factor can occur. The superposition principle, for a semi-infinite crack and a microcrack array, yields:

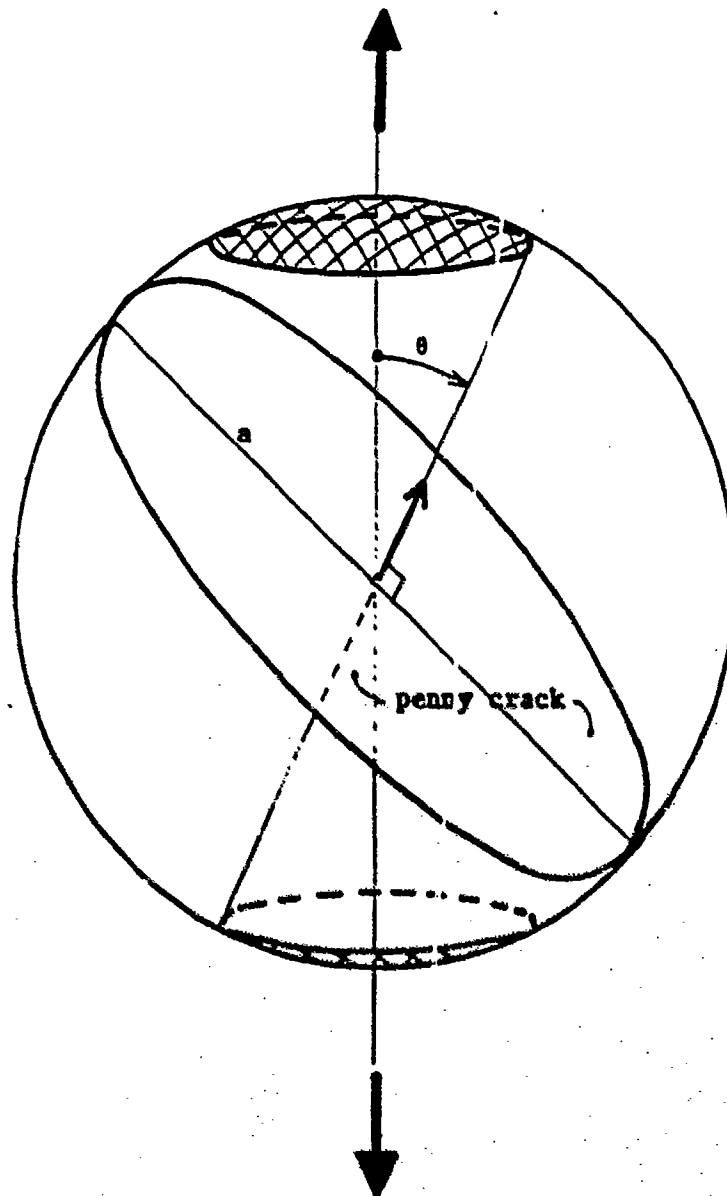
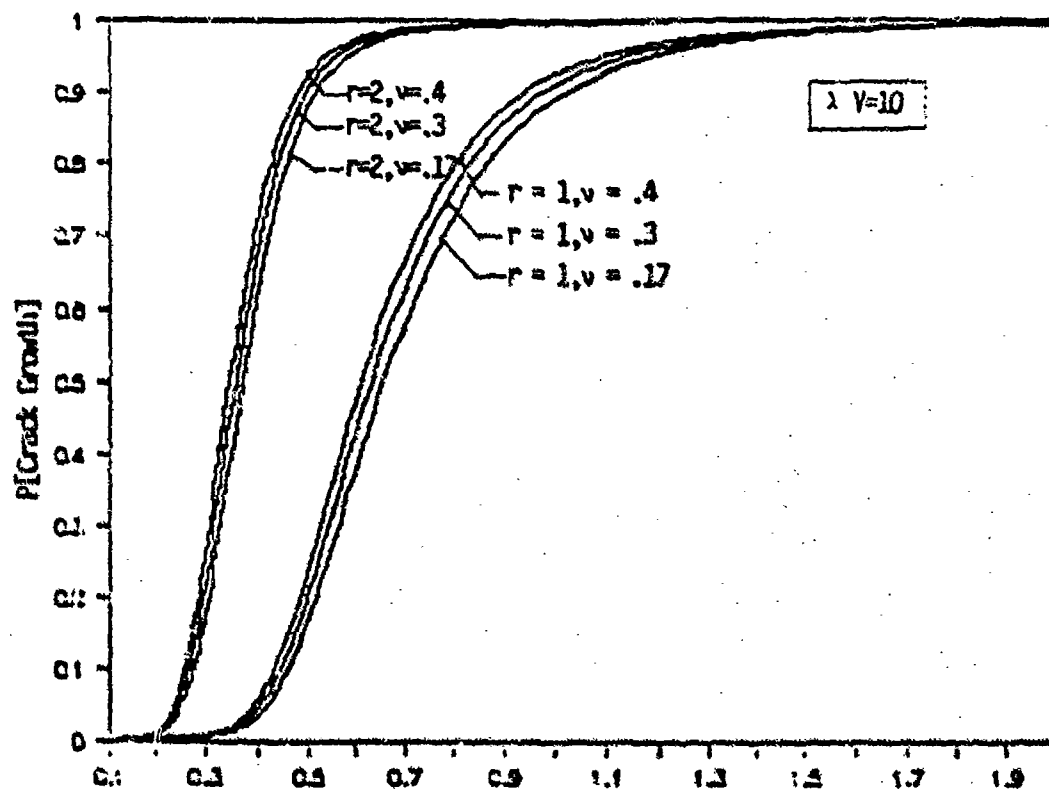


Figure 2-16. Orientation of the Penny Crack [58]



$$E[K_I^2(0=0)]/K_{IC} = 2\sigma E[\epsilon] / K_{IC} \sqrt{a}$$

Figure 2-17. Probability of Crack Growth [58]

$$\sigma(x) = K_I \sigma_I(x) + K_{II} \sigma_{II}(x) + \sum \sigma_i(x)$$

where

N = number of microcracks

$$\sigma_I = f_I(\theta)/\sqrt{2\pi r}; \sigma_{II} = f_{II}(\theta)/\sqrt{2\pi r}$$

denote the mode I and II crack tip stress fields, and $\sigma_i(x)$ is the i -th microcrack generated stress-field. Figure 2-18 shows two characteristic cases of interaction.

However, crack coalescence and growth process are much more complex than the simple static interaction. Therefore, the idea of following the exact continuum solution for the stress and strain fields near defects has not been pursued much further.

Another approach, used by Srolowitz and Beale [55], Duxbury and Kim [60] and others is based on the lattice network model, computer simulation of random defects and the fracturing process. A step further in this direction has been made by Bazant et al. [61] who used the aggregate size distribution to define an equivalent, nonhomogeneous spring network (Figure 2-19). Softening springs with the fixed fracture energy model the normal component of the interparticle forces. Figure 2-20 shows the actual cross-section of the asphaltic concrete section. The model shows a qualitatively similar behavior to the observed one; after the initial phase where defects are randomly scattered, the clustering and coalescence occurs and the macroscopic stress and strain symmetry is broken. Macroscopic Poisson effect, however, cannot be modeled without frictional component of the particle interaction.

The continuum nonlocal stress-strain relation has been analyzed within the framework of Damage Mechanics [62,63]. The most general relation in this context [64] is:

$$\sigma = [M(D) C^0] \epsilon^e$$

where

σ = homogenized stress vector

C^0 = virgin elastic constitutive tensor

ϵ^e = elastic strain vector

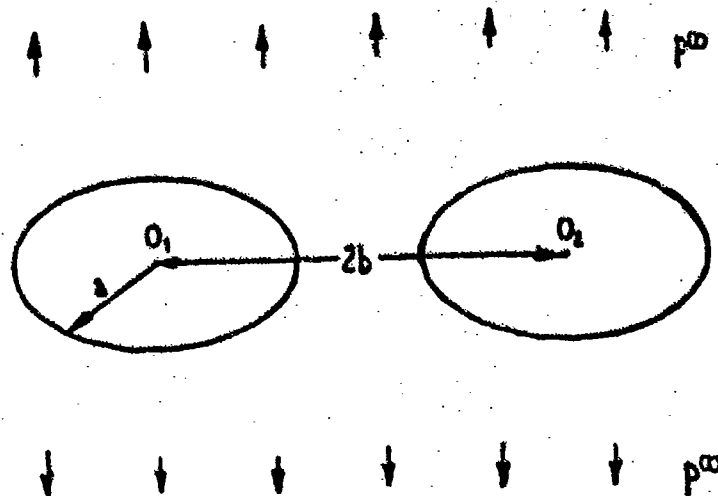
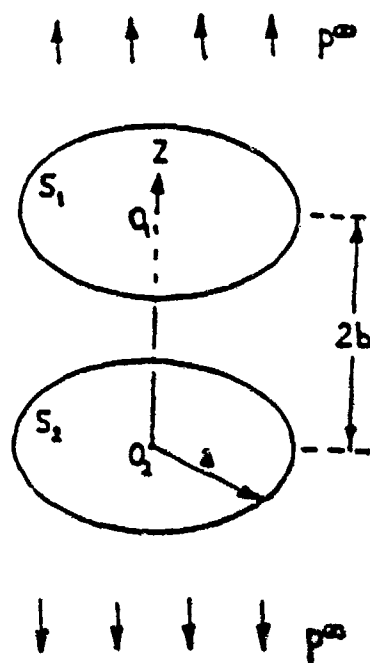


Figure 2-18. Two Cases of interaction [59]

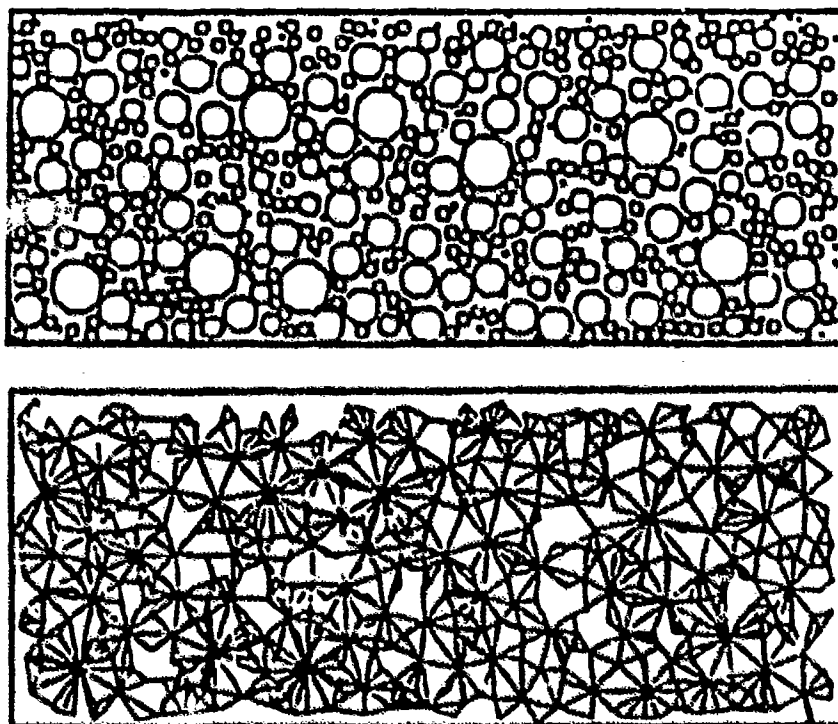


Figure 2-19. A Typical Randomly Generated Specimen and its Corresponding Mesh of Truss Elements



Figure 2-20. A Cross Section View of Asphaltic Concrete Core Specimen

$M(D)$ = fourth order tensorial function of the damage tensor D

In the simplest case of scalar damage, it reduces to:

$$\sigma = (1-d) C^0 \epsilon^e$$

where

d = scalar damage parameters

Number of theoretical and practical problems exist for defining the damage variable (tensor), some of which were addressed on the recent conference [65].

A very general approach to the stochastic fracturing process is used by Krausz and Krausz [66]. The process is described mathematically through the Markov chain concept or the Fokker-Planck transport equation. The formulation includes the random fluctuations in loads and other environmental effects through the random fluctuations in the available energy and the energy required for the crack growth (Figure 2-21), which result in the probabilities of crack growth (bond breaking) and crack closing (bond healing). Figure 2-22 illustrates the energy barrier crossing during the slow crack growth process. The rate of bond breaking is:

$$k_b = \frac{kT}{h} \exp \left(- \frac{\Delta G_b - W_b}{kT} \right)$$

and the rate of bond healing is:

$$k_h = \frac{kT}{h} \exp \left(- \frac{\Delta G_h - W_h}{kT} \right)$$

where

ΔG_b = change in Gibbs free energy for bond breaking

ΔG_h = change in Gibbs free energy for bond healing

k and h = Boltzmann and Planck constant respectively

T = absolute temperature

W = function of the crack driving force such K , J integral, etc.

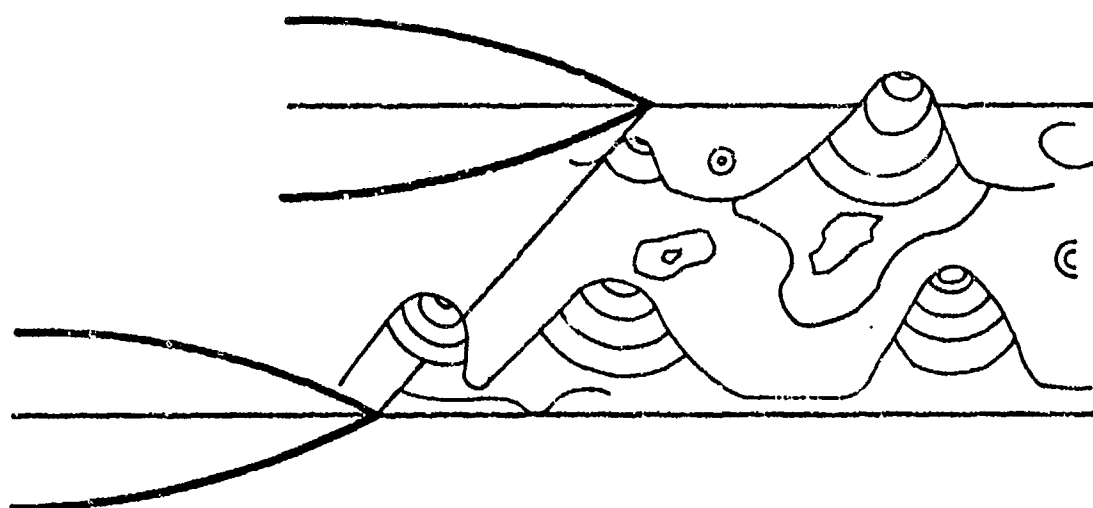


Figure 2-21. Random Variations of Thermal Energy in the Plane of the Crack

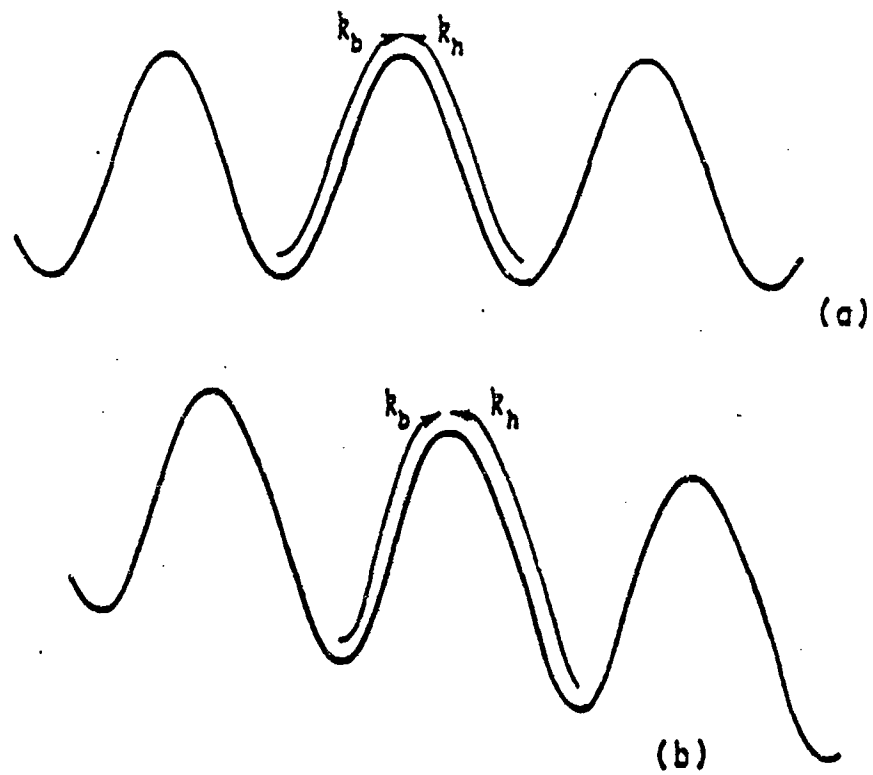


Figure 2-22. Energy Barrier Crossing During the Slow Crack Growth Process

One of the conclusions is that "many of the cracks that appear in structures over the service life are not caused by defective production, testing, or the Weibull effect, but are inevitable consequence of the stochastic character of the physical process itself."

The idea of the Markov chain model for the progressive cracking was also used by Bazant and Xi [67]. The simplified form of the stationary unit-jump random walk (Figure 2-23), independent of both loading and state variables (stage of the process), is used. The state variable is the position of crack tip or state of damage. The process is obviously nondecreasing. The above assumptions lead to the simple one-parameter transition probability matrix. Markov chain description seems suitable for the fracturing process, particularly for the nonhomogeneous materials like asphalt concrete and portland cement concrete. The assumptions of independence of load and state variables, as well as the unit-jump model require further analysis.

The implementation of the Markov chain description may be easier for the asphalt concrete than to portland cement concrete. In the former case the crack is expected to grow either through the binder (asphalt) or through the asphalt-aggregate interface; growth through the aggregate is unlikely.

In order to implement the Markov chain model several issues need to be addressed: (1) while the crack growth through the binder is expected to show more or less ductile properties (depending on the temperature and load duration, the behavior of the asphalt -aggregate interface is not well understood; and (2) the randomness of the aggregate size and relative positions needs to be mathematically defined and related to the transition probabilities of the Markov chain. The body of work by Cowin [e.g., 68], Oda et al. [69], and others, provides a very promising background. The mathematical definition of the fabric of the granular material is introduced through the concept of fabric tensor, defining the distribution of interparticle contact planes orientations (Figure 2-24). Although the existing work is concerned more with relations between the continuum stress and strain tensors with the fabric tensor, it seems inevitable that the fabric tensor have a role in the fracturing process, primarily in defining the randomness of the crack growth direction.

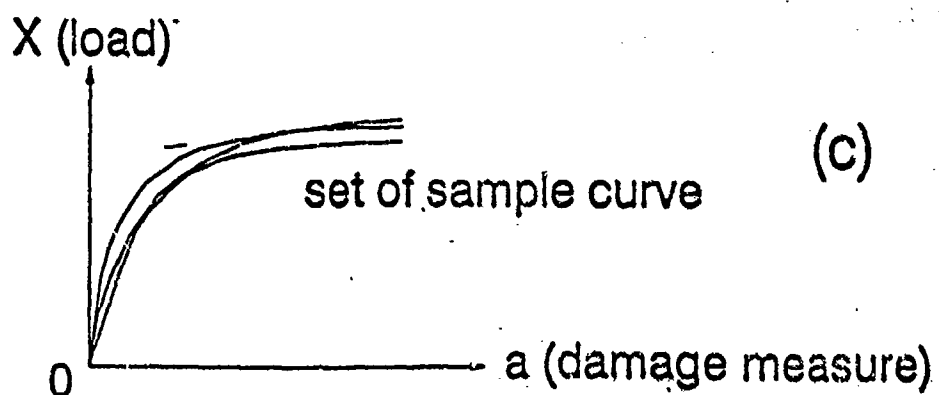
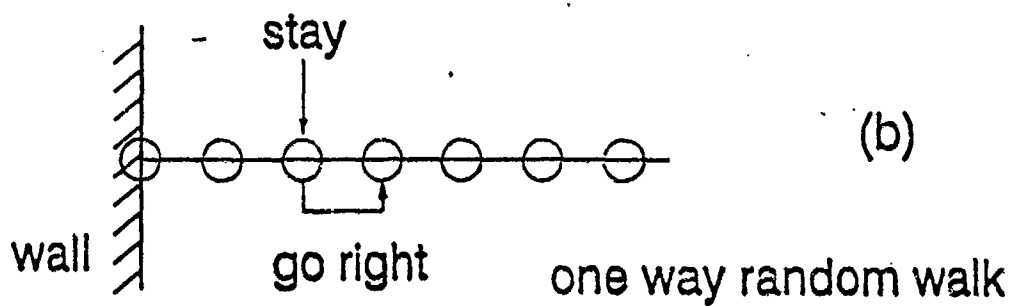
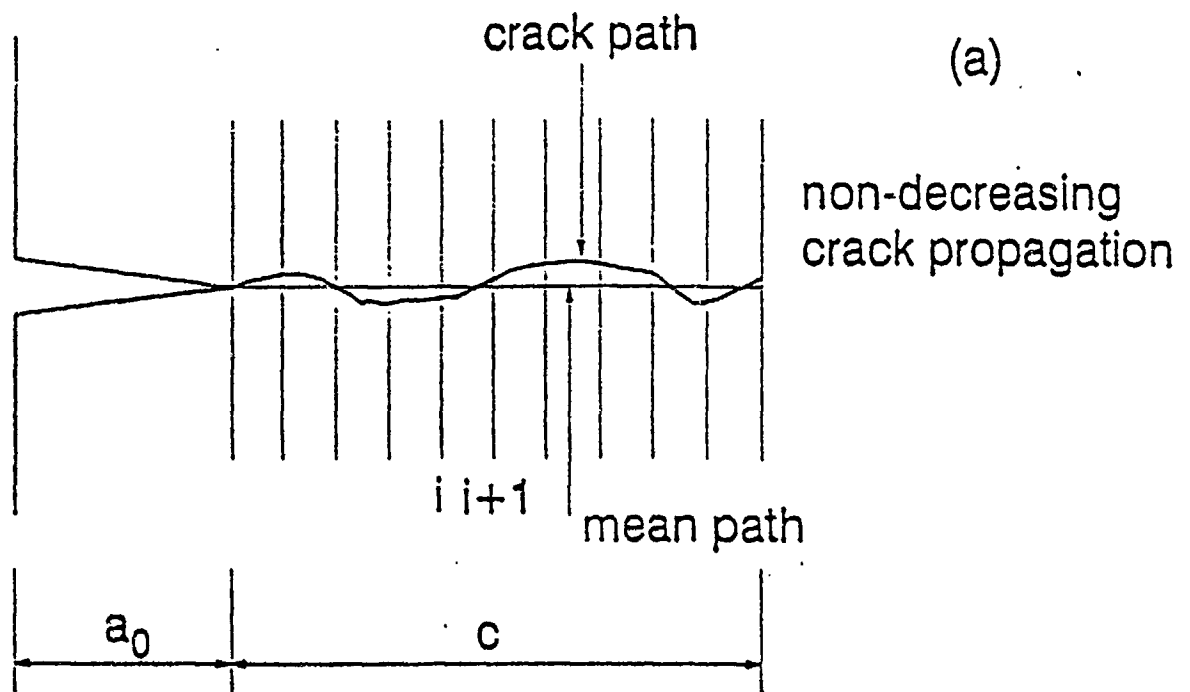


Figure 2-23. Crack Propagation as a Random Walk [67]

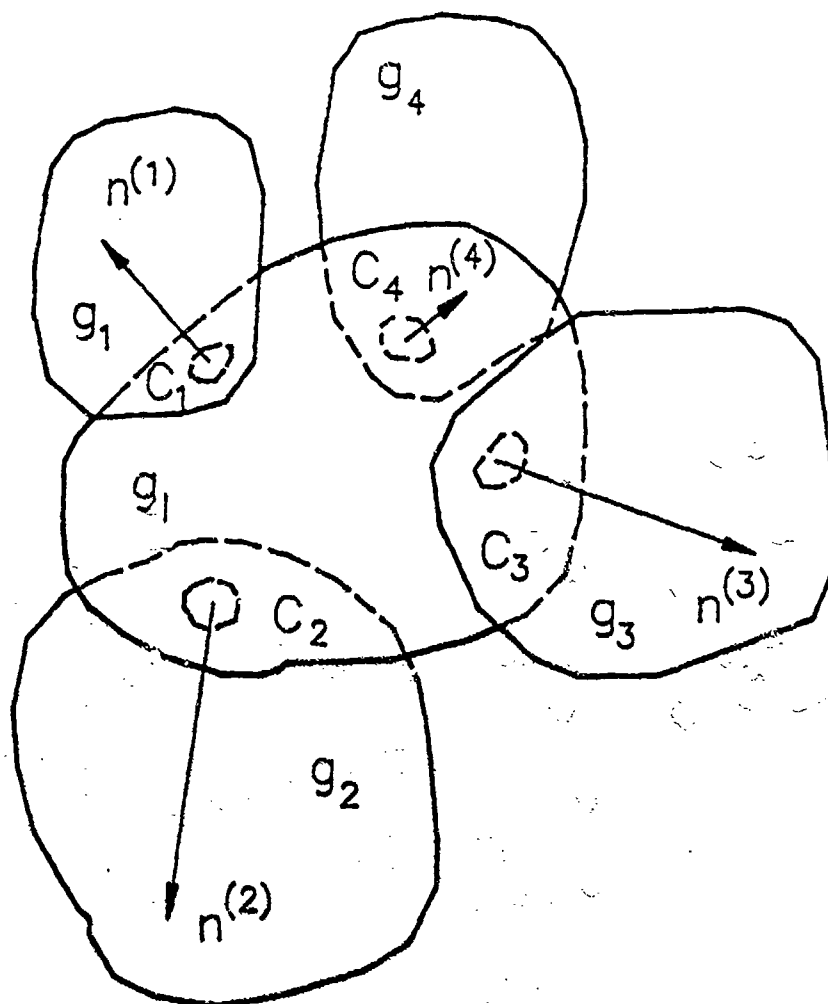


Figure 2-24. Granular Structure (Fabric)

References

1. McLain, D.B. and Monismith, C.L., "Estimation of Permanent Deformation in Asphalt Concrete Layers Due to Repeated Traffic Loading," TRB Bulletin, No. 510, 195.
2. Morris, J., Hass, R.C.G., Reilly, P. and Highnell, E.T., "Permanent Deformation in Asphalt Pavements can be Predicted," Proceedings Association of Asphalt Paving Technologists, Vol. 43, 1974.
3. Saraf, C.L., Smith, W.S. and Finn, F.N., "Rut Depth Prediction," Transportation Research Board, TRB Record, No. 616, 1976.
4. Finn, F., Saraf, C.L., Kulkarni, R., Nair, K., Smith, W. and Abdullah, A., "The Use of Distress Prediction Subsystems for the Design of Pavement Structures," Proceedings, Fourth International Conference on Structural Design of Asphalt Pavements, 1977.
5. Bousa, J.B., Craus, J. and Monismith, C.L., "Summary Report on Permanent Deformation in Asphalt Concrete," SHRP Report No. SHRP-A/IR-91-104, 1991.
6. Barber, E.S., "Calculation of Maximum Pavement Temperatures from Weather Reports," HRB 168, Highway Research Board, 1957.
7. Brown, S.F. and Snaith, M.S., "The Permanent Deformation Characteristics of Dense Bitumen Macadam Subjected to Repeated Loading," Proceedings, AAPT, Vol. 43, 1974.
8. Kenis, W.J., "Predictive Design Procedure, VESYS Users Manual - An Interim Design Method for Flexible Pavements Using the VESYS Structural Subsystem," Report No. FHWA-RD-77-154, Washington, D.C., January 1978.
9. Beckedahl, H., Gerlach, A., Lucke, H., and Schwaderer, W., "On Improvements of the Existing VESYS Concepts," Sixth International Conference, Structural Design of Asphalt Pavements, 1987.
10. Finn, F., et al., "Development of Pavement Structural Subsystems," Final Report, Project 1-10B, Volumes 1 and 2 prepared for the Transportation Research Board by Woodward-Clyde Consultants, San Francisco, California, February 1977.
11. El-Mitiny, M.R., "Material Characterization for Studying Flexible Pavement Behavior in Fatigue and Permanent Deformation," Ph.D. Dissertation, The Ohio State University, 1980.

12. Majidzadeh, K., Bayomy, F. and Khedr, S., "Rutting Evaluation of Subgrade Soils in Ohio," Transportation Research Record, No. 671, 1978.
13. Guirguis, H.R., "Subgrade Compaction and its Performance Under Traffic Loads," M.S. Thesis, The Ohio State University, 1970.
14. Khedr, S.A., "Residual Characterization of Untreated Granular Base Course and Subgrade Soils," Ph.D. Dissertation, The Ohio State University, 1979.
15. Majidzadeh, K., Aly, M.G., Bayomy, F.M. and El-Lathy, A.M., "Implementation of Pavement Design System, Volumes 1 and 2," Final Report, EES 578, The Ohio State University Engineering Experiment Station, June 1980.
16. Glasstone, S., Laidler, K. and Eyring, H., "The Theory of Rate Process," McGraw-Hill Co., New York, 1941.
17. Abdel-Hady, M. and Herrin, M., "Characteristics of Soil-Asphalt as a Rate Process," Journal of the Highway Division, ASCE, Vol. 92, No. HY1, March 1966.
18. Christensen, R.W. and Wu, T.H., "Analysis of Clay Deformation as a Rate Process," Journal of the Soil Mechanics and Foundation Division, ASCE, Vol. 90, No. SM6, November 1964.
19. Murayama, S. and Shibata, T., "Rheological Properties of Clays," Proceedings, Fifth International Conference on Soil Mechanics and Foundation Engineering, Paris, France, 1961.
20. Singh, A. and Mitchell, J.K., "General Stress-Strain-Time Function for Soils," Journal of the Soil Mechanics and Foundation Division, ASCE, Vol. 94, No. SM1, January 1968.
21. Wu, T.H., Resendiz, D. and Neukirchner, R.J., "Analysis of Consolidation by Rate Process Theory," Journal of the Soils Mechanics and Foundations Division, ASCE, Vol. 92, No. SM6, November 1966.
22. Andersland, O.B. and Akili, W., "Stress Effect on Creep Rates of a Frozen Clay Soil," Geotechnique, Vol. 17, London, England, March 1967.
23. Herrin, M. and Jones, G., "The Behavior of Bituminous Materials from the Viewpoint Paving Technologists," Vol. 32, February 1963.

24. Herrin, M., Marek, C.R. and Strauss, R., "The Applicability of the Absolute Rate Theory in Explaining the Behavior of Bituminous Materials," Proceeding, Association of Asphalt Paving Technologists, Vol. 35, February 1966.
25. Mitchell, J.K., Campanella, R. and Singh, A., "Soil Creep as a Rate Process," Journal of the Soil Mechanics Division, ASCE, Vol. 94, No. SM1, January 1968.
26. Mitchell, J.K., "Shearing Resistance of Soils as a Rate Process," Journal of the Soil Mechanics Division, ASCE, Vol. 90, No. SM1, January 1964.
27. Glynn, T.E. and Kirwan, R.W., "A Stress-Strain Relationship for Clays Subjected to Repeated Loading," Proceedings, Seventh International Conference on Soil Mechanics and Foundation Engineering, Mexico, 1969.
28. Majidzadeh, K., Guirguis, H.R. and Joseph, G., "Fundamentals of Soil Compaction," Final Report, EES 248, The Ohio State University Engineering Experiment Station to the Federal Highway Administration and The Ohio Department of Transportation, 1971.
29. Buranarom, C., "A Laboratory Investigation of the Dynamic Behavior of a Compacted Silty Clay," M.S. Thesis, The Ohio State University, Columbus, Ohio, 1973.
30. Crockford, W.W., et al., "Modeling Stress and Strain States in Pavement Structures Incorporating Thick Granular Layers," Final Report of Contract F08635-87-C-0039, April 1990.
31. Hofstra, A., and Kloppe, A.J.G., "Permanent Deformation of Flexible Pavements Under Simulated Road Traffic Conditions," Proceedings, Third International Conference on the Structural Design of Asphalt Pavements, Vol. I., London, England, 1972.
32. Eisenmann, J., Hilmer, A., "Influence of Wheel Load and Inflation Pressure on the Rutting Effect of Asphalt Pavements - Experiments and Theoretical Investigation," Proceedings, Sixth International Conference on the Structural Design of Asphalt Pavements, Vol. I., Ann Arbor, Michigan, 1987.
33. Abdulshafi, A. and Majidzadeh, K., "Combiviscoelastic/Plastic Modelling and Rutting of Asphaltic Mixtures," TRB No. 968, Washington D.C., 1984.
34. Somasundaram, S. and Desai, C.S., "Modelling and Testing of Anisotropic Behavior of Soils," ASCE J. Eng. Mech., Vol. 114, No. 9, September 1988.

35. Desai, C. S., "Notes for Advanced School Numerical Methods in Geomechanics Including Constitutive Modelling," International Center for Mechanical Sciences, Udine, Italy, May 1989.
36. Desai, C. S., Krempl, E., Frantziskonis, G. and Saadatmanesh, H., "Constitutive Laws for Engineering Materials," Proceedings, Third International Conference, Tuscon, Arizona, 1991, ASME Press, New York, 1991.
37. Desai, C.S., Somasundaram, S. and Frantziskonis, G., "A Hierarchical Approach for Modelling Geologic Materials", *Integral J Number Analytical Methods in Geomechanics*, Vol. 11, No.3, 1986.
38. Desai, C.S. and Zhang, D., "Viscoplastic Model with Generalized Yield Function," *Integral J Number Analytical Methods in Geomechanics*, Vol. II, 1987.
39. Majidzadeh, K., Kauffmann, E.M. and Chang, C.W., "Verification of Fracture Mechanics Concepts to Predict Cracking of Flexible Pavements," Final Report No. FHWA-RD-73-91, Federal Highway Administration, Washington, D.C., June 1973.
40. Ramsamooj, D.V., "The Design and Analysis of the Flexibility of Pavements," Ph.D. Dissertation, The Ohio State University, 1970.
41. Ang, D.D., Folias, E.S. and Williams, M.L., "The Bending Stress in a Cracked Plate on an Elastic Foundation," *Journal of Applied Mechanics*, June 1963.
42. Paris, C.P., "The Growth of Cracks due to Variation in Load," Ph.D. Dissertation, Lehigh University, September 1962.
43. Paris, C.P., "The Fracture Mechanics Approach to Fatigue," *Fatigue: An Interdisciplinary Approach*, Syracuse University Press, 1964.
44. Saraf, C.L., "Effect of Mix Variables on the Fatigue Response of Asphaltic Mixes," Ph.D. Dissertation, The Ohio State University, Columbus, Ohio, 1973.
45. Rice, J.R., "Mechanics of Crack Tip Deformation and Extension by Fatigue," *Fatigue Crack Propagation*, ASTM, pp. 247, 1967.
46. Drucker, D.C. and Rice, J.R., "Plastic Deformations in Brittle and Ductile Fracture," *Eng. Fract. Mech.*, Vol. 1, pp. 577-602, 1970.

47. Majidzadeh, K., Dat, M. and Makdisi-Ilyas, F., "Applicaton of Fracture Mechanics for Improved Design of Bituminous Concrete," FHWA, Final Report No. FHWA-RD-76-92, Vol. 2, June 1976.
48. Rice, J.R., Journal of Applied Mechanics, Transactions of the American Society of Mechanical Engineers, pp. 379-386, June 1968.
49. Begley, J. A. and Landes, J.D., "The J Integral as a Fracture Criterion," Fracture Toughness Proceedings of the 1971 National Symposium on Fracture Mechanics, Part I, ASTM STP 514, American Society for Testing and Materials, pp. 1-20, 1972.
50. Hutchinson, J.W., Journal of the Mechanics and Physics of Solids, Vol. 16, pp.13-31, 1968.
51. Rice, J.R. and Rosengren, G.F., Journal of the Mechanics and Physics of Solids, Vol.16, pp. 1-12, 1968.
52. Abdulshafi, A.A. and Majidzadeh, K., "J Intergral and Cyclic Plasticity Approach to Fatigue and Fracture of Asphalt Mixes," TRR 1034, 1985.
53. Weibull, W. "Statistical Theory of the Strength of Materials," Ingenioers Vetenskaps Akademien Handlingar, Vol. 151, p. 45, 1939.
54. Bazant, Z.P. and Ki, Y., "Statistical Size Effect in Quasibrittle Structures Part I. Is Weibull Theory Applicable?" Submitted to ASCE Journal of Engineering Mechanics.
55. Srolowitz, D.J. and Beale, P.D., "Computer Simulation of Failure in an Elastic Model with Randomly Distributed Defects," J. Am. Ceram. Soc., 71 [5], 1988.
56. Lamon, J. and Evans, E.G., "Statistical Analysis of Bending Strength for Brittle Solids: A Multiaxial Fracture Problem," J. Am. Ceram. Soc., 66 [3], 1982.
57. Batdorf, S.B. and Heinisch, H.L., "Weakest Link Theory Reformulated for Arbitrary Fracture Criterion," J. Am. Ceram. Soc., 61 [7-8], 1978.
58. Mesarovic, S., Gasparini, D., Muju, S. and McNelis, M., "Probability of Crack Growth in a Poisson Field of Penny Cracks of Random Size and Orientation," Submitted to ASCE J. Eng. Mech.

59. Kachanov, M., "Elastic Solids with Many Cracks: A Simple Method of Analysis," *Integral J Solids Structures*, Vol. 23, No. 1, 1987.
60. Duxbury, P. M. and Kim, S.G., "Scaling Theory and Simulations of Fracture in Disordered Media," *Damage Mechanics in Engineering Materials, Proceedings, Winter Annual Meeting ASME*, 1990.
61. Bazant, Z.P., Tabbara, M.R., Kazemi, M.T. and Pijardier-Cabot, G., "Random Particle Simulation of Damage and Fracture in Particulate or Fiber-Reinforced Composites," *Damage Mechanics in Engineering Materials, Proceedings, Winter Annual Meeting ASME*, 1990.
62. Krajcinovic, D., "Damage Mechanics," *Mech. Materials*, Vol. 8, 1989.
63. Kachanov, L.M., "Introduction to Continuum Damage Mechanics," *Martinus Nijhoff Publishers, Dordrecht, Netherlands*.
64. Ju, J.W., "On Isotropic and Anisotropic Damage Variables in Continuum Damage Mechanics", *Proceedings, ASCE Mechanics, Computing 1990s and Beyond*, Vol.1, 1991.
65. Adeli, H., Sierakowski, R.L., editors, "Mechanics, Computing 1990s and Beyond," *Proceedings, ASCE*, Vol. 1, 1991.
66. Krausz, A.S. and Krausz, K., "The Conceptual Physical Framework of Stochastic Fracture Kinetics", *Integer J Fracture*, 39, 1989.
67. Bazant, Z.P. and Xi, Y., "Probabilistic Modeling of Progressive Cracking," *NSF Center for Science and Technology of Advanced Cement Based Materials, Northwestern University, Report No. 90-6*, pp. 616, 1990.
68. Cowin, C.C., "The Relationship Between the Elasticity Tensor and the Fabric Tensor," *Mech of Materials*, 1985.
69. Oda, M., Konishi, J. and Nemat-Nasser, S., "Some Experimentally Based Fundamental Results on the Mechanical Behavior of Granular Materials," *Geotechnique*, 30, No.4, 1980.

List of Symbols

J_1	=	first invariant of stress tensor
J_2	=	second invariant of deviatoric stress tensor
J_3	=	third invariant of deviatoric stress tensor
α, k	=	yield function flow rule parameters
x_1	=	cumulative number of load applications, in 10^5 units
x_2	=	surface displacement, in 10^{-3} inches
x_3	=	maximum compressive stress, in psi
k_I	=	stress intensity factor, mode I
E'	=	energy release rate
U	=	potential energy
c, l	=	crack length
P_f	=	failure probability
σ_i	=	i^{th} microcrack generated stress field
k_b	=	rate of bond breaking
k_h	=	rate of bond healing

Development of a Unified Airport Pavement Analysis and Design System

E. Owusu-Antwi

M. G. Sharma

R. H. Dodds

P. D. Hilton

M. I. Darter

H. T. Yu

Abstract

Aircraft weight and number of operations at our nation's airports are expected to continue to increase into the foreseeable future. This will place a heavy burden on the pavement facilities at U.S. airports, which if not adequately designed, will result in significant deterioration. To insure that airport pavement facilities will be capable of carrying these increased traffic levels, the Federal Aviation Administration (FAA), through the Volpe National Transportation Systems Center (TSC), is sponsoring research on the development of a unified pavement model for the analysis and design of airport pavements. The goal of this program is to make the technological leap that will allow a more reliable analysis and design of all types of airport pavements, since current design procedures have many serious deficiencies.

This paper describes the concepts proposed for the development of such a unified airport pavement analysis and design system. The central component of the system is a 3-dimensional finite element analysis (FEA) based primary response model, applicable to the nonlinear analysis of all types of airport pavements. A unique solution procedure is proposed that will allow the realistic solution of complex airport problems on desktop computers. This procedure is expected to reduce memory requirements and increase processing speed by a factor of between 5 and 10, in comparison to currently available 3-dimensional codes, and thus reduce computation costs.

Another major portion of the proposed system is the material constitutive models proposed for incorporation in the primary response model. Incremental constitutive models for the major classes of airport pavement materials, that will allow a stepwise addition of "memory" variables or parameters to basic constitutive models to accurately describe the physical behavior of increasing complex materials, will be incorporated into the primary response model. A database of the outputs of nodal displacements, stresses, strains and local damage measures generated by the primary response model will be used in a damage analysis, the results of which can be used to predict key distress types. This will provide for greater design reliability and cost-effective pavement design.

1. ERES Consultant, Inc.
2. Pennsylvania State University
3. University of Illinois at Urbana-Champaign
4. Arthur D. Little, Inc.

1. Introduction

The enormous demands on airport facilities in the country continues to be a topic of major concern. Although, most projections point towards substantial increases in the volume of air travel through the next century, it is doubtful whether such increases will be accompanied by corresponding increases in the number of airports or the pavement facilities at existing airports. In anticipation of such increases, aircraft manufacturers and the airline industry are moving towards the use of wide-bodied aircrafts with increased capacities in terms of maximum takeoff weights by the turn of the century. Therefore, it is becoming increasingly necessary for pavement engineers to provide airport pavements that are capable of meeting the needs of such demands over time.

Typically, empirical procedures based on the observation of pavement performance over the years are still relied upon to design airport pavements. In a few instances, a select number of consultants have used mechanistic-empirical procedures, which combine pavement responses from analytical methods and performance data from pavement research and observation, for the analysis and design of airport pavements. These procedures are not adequate for analyzing new designs and materials which go beyond the existing experience regime.

Thus, providing airport pavements capable of carrying the loads imposed by the future generation of aircrafts, for the wide range of environmental conditions and pavement materials, is one of the most challenging aspects of airport pavement design and analysis facing pavement engineers. Realizing the need for a more reliable approach to the analysis and design of airport pavements, with a realistic consideration of all the inputs and conditions over time, the Federal Aviation Administration (FAA) of the U.S. Department of Transportation is sponsoring a project, under the direction of the Volpe National Transportation Systems Center (VNTSC), to develop a unified pavement modeling program for such applications.

This report describes a unified concept developed by the team of Arthur D. Little, Inc. (ADL) of Cambridge, MA; ERES Consultants, Inc. of Savoy, IL; and the Pennsylvania Transportation Institute of the Pennsylvania State University (PSU), for the design and analysis of all types of airport pavements, using the most advanced technology.

This conceptual formulation of the unified theory is to form the basis for future work to develop the concept into a unified airport pavement design and analysis program for all types of pavements. A laboratory validation and field verification of the program, and the implementation of the system into an applicable product for use by pavement engineers, researchers, the airline

industry and others, in all aspects of airport pavement design, is the ultimate goal of this program initiated by the FAA.

2. Objectives and Scope

The primary objective of this program is to develop a unified model for the analysis and design of all types of airport pavements. The specific requirements of this unified pavement model include the following:

- a. A primary response model applicable to the realistic solution of airport pavement problems involving the realistic modeling of complex three-dimensional (3-D) loading and boundary conditions;
- b. Proper constitutive relations for new and existing airport pavement materials that take into account the time and deformation dependent characteristics of the materials; and
- c. Proper models for assessing the nonlinear accumulation of damage in airport pavements due to the effects of aircraft and environmental loading over time.

This unified pavement model must be applicable to the analysis and design of new airport pavements, the strengthening of existing pavements, and the accurate interpretation of nondestructive test results. This report addresses the concepts proposed by the ADL/ERES/PSU team in the development of a unified airport pavement analysis and design system with these specific features.

After a brief discussion of the technical issues faced in the development of such a system, the report addresses the framework for the unified analysis and design system envisaged as the final product of this project. Emphasis is then placed on the concepts proposed for the development of the primary response model applicable to the 3-D airport pavement problems often encountered. The primary response model is considered the central element around which the entire system is built and is the main focus of this report. However, since the incorporation of the appropriate constitutive models into the PRM and the proper interpretation of the engineering significance of the results obtained from the PRM are paramount to the successful application of the unified airport pavement analysis and design system envisaged, the concepts proposed for their treatment are also addressed. A discussion of the advantages of the proposed unified analysis and design system, and the recommendations for its development are then presented.

3. Technical Issues

Many significant technical issues exist in adequately designing an airport pavement that will provide satisfactory service throughout its intended service life. These issues range from obtaining the proper design inputs; to the use of a realistic primary response model to determine the stresses, strains, displacements, and local damage measures that result from multiple load applications under varying environmental conditions; and, finally, to the adequate assessment of the resulting cumulative damage that leads to the different types of distress that eventually occur.

Until now, airport pavements have been designed as either "flexible" or "rigid" pavements using methods that are mostly empirical and based on engineering experience. Although no one method is predominately used, most of the design procedures for flexible pavements, including the method recommended by the FAA [1], are based on the CBR method of design. In certain instances, design methods such as the Shell [2], Asphalt Institute [3] and other methods of pavement design used by pavement consultants, which are based on mechanistic principles and include many empirical assumptions, have also been used. For example, ERES Consultants Inc. has utilized 2-D mechanistic-empirical design procedures for the past 10 years in airport pavement design and overlay design.

Most of the current airport rigid pavements design methods are based on idealized analytical methods such as the Westergaard analysis of a free edge or interior loaded slab resting on a Winkler foundation. Examples are the FAA [1] and Portland Cement Association (PCA) [4] design methods for rigid airport pavements. However, these methods also require empirical modifications, such as the modification made in the FAA pavement design method to accommodate the load transfer that occurs at joints, wherein edge stresses are reduced by 25 percent where load transfer is provided. Another major limitation is that these procedures can only consider two layers, whereas actual pavements have several layers.

It is clear that, despite the many advances in pavement research, current procedures for the design of airport pavements lag behind the available technology. In fact, no specific design procedures are available for the pavement types which fall between flexible and rigid pavements (e.g., AC over PCC, multiple overlays, unbonded overlays). For such pavements, structural design becomes a matter of designing the pavement using the principles of one of the two major types of pavements, and somehow compensating for the model assumptions.

Some attempts have been made in recent years to develop better procedures for the analysis and design of airport pavements. For example, the Corps of Engineers has developed new flexible

[5] and rigid [6] pavement design procedures which rely on linear elastic theory. While the flexible pavement design procedure is an advancement over the CBR procedure, it is not able to account for the nonlinear and time-dependent material influences on pavement behavior. The procedure for rigid pavement design does not adequately consider the effect of thermal gradients or the different joint designs that provide varying amounts of load transfer. Additional severe limitations are also associated with overlay design. Nondestructive testing of pavement layer properties, reflective cracking and the assessment of past damage are a few of the items that are inadequately addressed.

With such limitations, there have been numerous examples of pavements failing earlier than anticipated. The empirical and mechanistic-empirical methods mentioned above are limited with respect to the proper characterization of materials, aircraft loading conditions and, especially, the environment. They are also limited in their ability to treat nonlinear or deformation dependent, time dependent material/soil changes, geometric conditions such as joints, and layer interface conditions; and they do not directly treat all of the key types of pavement failures that may occur, in a realistic assessment of damage. These limitations preclude a practical prediction of pavement performance for the various operating conditions experienced, and do not allow the design engineer to have an effective control over the design and analysis process.

4. Framework of Unified Pavement Analysis and Design System

It is against the background of such technical issues that a framework for a unified airport pavement model was developed. In formulating this framework, consideration was given to address the need to utilize the most recent advances in several areas of engineering, and at the same time address the practical needs of airport pavement analysis and design. The requirements of a realistic primary response model, which is central to the unified pavement analysis and design system, drove the development of the framework.

A major requirement of the framework is that it permits the realistic solution of complex airport pavement problems, by specifically allowing a realistic representation of the time and deformation dependent or nonlinear behavior of pavement materials and a better representation of the 3-D loading and boundary conditions of airport pavements. Since pavement material properties change with time, often accompanied by changing loading and boundary conditions, a framework is developed that will also address this issue. Provisions are made in the framework to permit the determination of outputs that will allow the assessment of damage to a pavement structure as a result of these changing conditions.

Figure 4-1 is a simplified illustration of the framework developed. The unified airport pavement model proposed is comprised of a core primary response model for the structural analysis required for pavement design. This primary response model is the central processing unit for the structural analysis to determine the responses required to ultimately predict the performance of a design. For a particular set of inputs, and for a specific geometric and material design, the primary response model is used in an analysis to determine the stresses, strains, displacements, and damage measures from which the structural integrity of the design is determined. The history of the primary response model outputs over time under changing conditions are used in a damage assessment to determine the adequacy of a design. A design determined to be unacceptable is revised and the analysis process repeated until an acceptable design is obtained. The general features of the major components of this framework are discussed next.

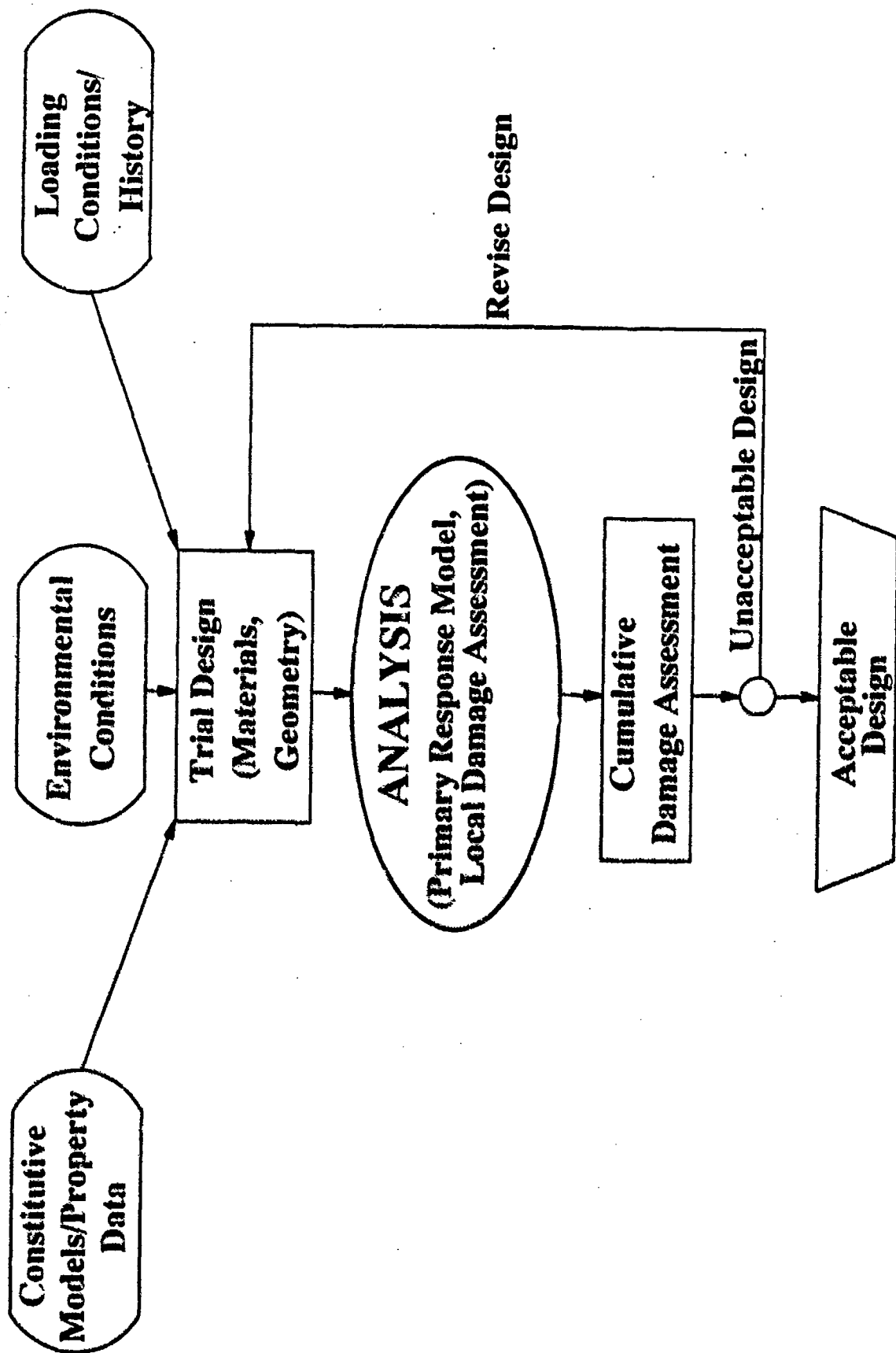


Figure 4-1. Framework for the Analysis and Design of Airport Pavements.

4.1 Role of Primary Response Model

The primary response model is the nucleus of the proposed unified airport pavement analysis and design system. For a particular pavement problem, the primary response model is used in a structural analysis to determine the structural responses over time. In current state-of-the-art mechanistic practice, linear elastic layered analysis and 2-D finite element analysis (FEA) are the mainstay of airport pavement structural analysis, with consideration only given to static loads and simplified geometric and boundary conditions. Given the complex nature of the airport pavement problem as discussed above, this is not adequate since elastic layered analysis and 2-D FEA do not allow a realistic simulation of the pavement behavior. The three-dimensional effects that result from joints and cracks, corners, and multiple wheel load configurations cannot be accurately modeled in elastic layered analysis and 2-D FEA; and material, geometric, and boundary nonlinearities cannot be adequately considered. In addition, the use of these structural models do not permit the use of a unified approach for the design of portland cement concrete and asphalt concrete pavements.

The primary response model for the framework proposed for the unified airport pavement analysis and design system is based on 3-D FEA. With more accurate inputs on loading conditions, traffic history, environmental conditions, material properties, geometry, and boundary and initial conditions, such a primary response model can be used to generate a database of displacements, strains, stresses, and local damage measures over time for an airport pavement problem. It will also allow the unified modeling of all types of airport pavements. It is necessary to ensure that the proper material models and property data are entered into the primary response model, and that there is an accurate representation of the loads and boundary conditions for any particular problem. The accurate interpretation and use of the outputs obtained from the primary response model is also essential. The rest of this section is devoted to discussions of these aspects of the framework.

4.2 Inputs

As shown in Figure 4-1, the major inputs to the proposed primary response model can be grouped under 1) the constitutive models and property data for the materials used in airport pavements; 2) loading conditions; 3) environmental conditions; and 4) other design inputs. Much of the success of the unified airport pavement model will depend on how well the required inputs to the primary response model are defined and are reliably obtained.

4.2.1 Constitutive Models and Property Data

The constitutive models and property data for the pavement materials used are a major input to the unified pavement model. These materials fall into the categories of asphalt concrete, portland cement concrete, granular materials (aggregates), subgrade soils and other materials or new materials such as composites and fiber reinforced materials. In current pavement analysis and design approaches, these materials are idealized as materials with deformation independent constitutive relations, i.e., linear elastic, and are characterized by fundamental parameters and property data such as Young's modulus E , shear modulus G , Poisson's ratio μ , and the modulus of subgrade reaction k .

Since such models do not realistically represent the actual behavior of the materials in airport pavements, constitutive models that are able to do so and account for nonlinear material behavior are proposed for the primary response model. The distinguishing characteristics identified as requiring particular attention in the development of the constitutive models for the airport pavement materials are the time dependency of asphalt concrete, the brittle fracture of cement concrete, and the yield surfaces of granular materials and subgrade soils that include a consideration of volumetric sensitivity. More details are subsequently provided on the concepts for the development of the constitutive models required for the unified airport pavement analysis and design system.

4.2.2 Loading Conditions

Airport pavements experience a wide range of load magnitudes applied through many different gear types with different wheel bases and threads. In addition, the manner of application of the loads vary depending on the location of a pavement section, with the loading condition on an apron for example being very different than that on a runway. A problem faced by the airport pavement engineer is how to characterize this loading over the service life of a pavement for analysis and design. To be able to do this, one must take into account current and future aircraft traffic distribution patterns, current and future aircraft loading characteristics, and future aircraft growth rates. The distribution patterns include such factors as aircraft traffic mix, the time distribution of traffic, and the lateral and longitudinal distribution of traffic. The loading characteristics include such factors as the gear type, the maximum takeoff weight, the number of coverages, the tire pressure and contact area stress distribution, and the speed and dynamic effects.

The current procedures used, such as the equivalent single wheel load concept, the FAA procedure based the equivalent annual departures of a design aircraft [1], and the Aircraft

Classification Number (ACN) [7] do not take all these factors into account. Although a load characterization system is not required for this phase of the model development, a mechanistic-based procedure will eventually be needed to convert the mixed aircraft traffic into a realistic representation of loading on airport pavements for use in the unified pavement analysis and design system.

4.2.3 Environmental Conditions

Temperature and moisture are the two most important environmental variables that must be taken into account in the analysis and design of airport pavements. Daily temperature and moisture variations can lead to expansion and contraction of pavements; thermal and moisture gradients which result in curling and warping stresses in portland cement concrete pavements; and changes in material properties such as asphalt concrete stiffness. In the long term, temperature and moisture variations can also lead to low temperature cracking of asphalt concrete pavements; freeze-thaw damage effects; soil swelling and frost heave; and subgrade softening due to saturation.

In current conventional methods of analysis and design, however, emphasis is placed on the construction procedures that minimize environmental effects. Thus, for example, in most instances the effects of curling and warping stresses are only considered empirically through the limiting of joint spacing in rigid pavement analysis and design; and the changes in the stiffness of asphalt concrete with temperature variation are only considered in flexible pavement analysis and design through the selection of the viscosity grade of the asphalt.

Although the full treatment of the effects of the environment are to be treated in subsequent phases of this project following the development of the primary response model, the framework is developed with these factors in mind. The successful application of a unified pavement model will be possible only if such factors are taken into consideration in a realistic portrayal of the airport pavement operating environment.

4.2.4 Design Inputs

As shown in Figure 4-1, another aspect of airport pavement analysis and design is the selection of the initial trial design for analysis. This involves the selection of the pavement geometry, materials, boundary and initial conditions, and other features to characterize the pavement in a representative manner for analysis. Currently there are no rational procedures for dealing directly with design parameters such as load transfer, joint spacing, reinforcement, and

layer interface conditions. In the unified pavement model it is envisaged that mechanistic based principles will be used to represent such factors in the primary response model. Consequently, although the actual concepts for doing this are not elaborated here, the framework developed has appropriate provisions.

4.3 Assessing Cumulative Damage

Postprocessing of the outputs from a primary response model to permit a useful interpretation of the results obtained is a stage of structural analysis which is often not given the attention it requires by engineers. In most instances postprocessing has been limited to the graphical presentation of the results obtained, for example, in the form of principal stress, shear stress, displacement and failure criteria contour plots. It must be noted, however, that in airport pavement design and analysis, in addition to such graphical representation of results, the accurate interpretation of the engineering significance of the results is essential to the determination of the structural integrity of a design. This is because in most instances in airport pavements, failure is due to the repeated action of loads and not the long-term application of a single major load. Optimization of design, therefore, often involves several design and analysis iterations to determine whether the particular design is appropriate for the repeated occurrence of numerous sets of conditions (at the least cost).

Postprocessing of the outputs of the primary response model of the unified analysis and design system, as a result, will involve assessing the damage to the design due to the repeated application of the various kinds of loads it is subjected to and to predicting the performance of the given design. One can then determine whether a design will be adequate for the given conditions over time. If the design is not adequate, the materials and/or geometry of the design must be changed and the entire process of analysis repeated. The interpretation of the outputs in this manner will be useful to obtaining an improved airport pavement system.

In current practice, such interpretation of the engineering significance of structural analysis results of airport pavements has been conducted using simple damage assessment concepts in the fashion of Miner's cumulative damage theory. A limitation of this approach is the assumption that the sequence of loading and history of damage do not influence the accumulation of damage. Studies show this not to be the case [8]. Consequently, the assessment of airport pavement damage within the context of mechanistic analysis, which takes into account such factors, is proposed as a useful and integral part of the unified airport pavement analysis and design system.

Such a concept will allow a realistic assessment of damage resulting from the repeated application of aircraft and environmental loading.

5. Primary Response Model

The primary response model proposed by the ADL/ERES/PSU team combines the most advanced technology currently available in FEA and the practical requirements of pavement analysis and design to give a system that is well suited for the airport problems often encountered. The details of this primary response model are given in this section. As the central component of the unified airport pavement analysis and design system, a primary response model with dynamic, nonlinear, large deformation, and time-dependent capabilities is proposed. The primary response model proposed will be comprised of a 3-D nonlinear FEA kernel with constitutive models for nonlinear material behavior incorporated in it. A model that also incorporates local damage models in the FEA kernel to account for the effect of damage accumulation is proposed.

5.1 Analytical Capabilities

Modern FEA has advanced to the degree where there can be close simulation of the behavior of most designs under the actual conditions they are to be subjected, to give results that can be used to determine structural integrity and to optimize design. The analytical capabilities envisioned for the primary response model proposed for the design and analysis of all types of airport pavements are discussed in this section. These include the generation of the finite element model for any particular design, representation of loading and boundary conditions, material modeling capabilities, the solution algorithms used in the FEA procedure, and the graphical interface used to display the results of an analysis.

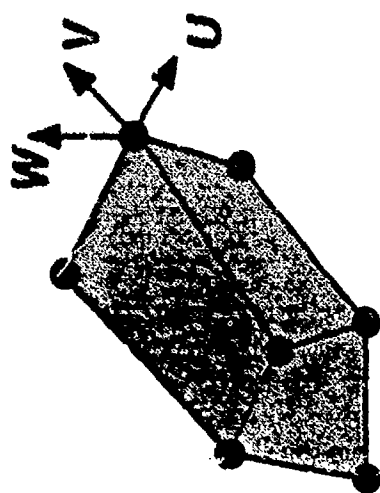
5.1.1 Preprocessing Capabilities

The preprocessing envisioned for the primary response model will involve model development, the application of load and boundary conditions, and the specification of the material properties for the design of an airport pavement to be analyzed. A graphical processor with capabilities for the automatic isoparametric generation of the finite element mesh for a design based on a library of structural elements for airport pavements is envisioned. The library of stress elements to be developed as part of the primary response model will comprise of 2-D and 3-D element types that will enable the physical representation of all aspects of airport pavements.

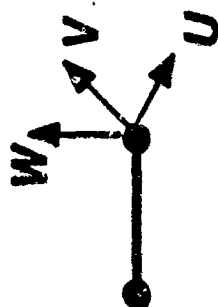
Figure 5-1 shows examples of the types of elements that may be used in the primary response model. The 8-node brick (or solid) elements with one point quadrature and hourglass control will be provided to model the majority of the pavement layers. Solid beam elements such as the 2-node bar element shown in the figure will be provided to model dowel bars at joints; and discrete springs of the type shown may be used as first-order interface elements to represent the conditions at "soft" joints or cracks. Slideline elements will be furnished to allow modeling of the interface and contact conditions between the different pavement layers. To decrease memory requirements and increase computation speed, infinite domain elements of the kind shown in Figure 5-1 will be provided for representation of the infinite effect of most, if not all, of the subgrade soil. An effort will also be made to provide the capability for the addition of reinforcement to elements for composite modeling of materials like reinforced concrete and fiber reinforced asphalt concrete, and to give the mesh generator the ability to use any combination of the elements in the library with different material models in the same model. A graphic processor which will allow the mesh generation to interface with other software such as Autocad is proposed.

The ability to represent the wide range of loading and boundary conditions that occur on airport pavements is also essential. The loading conditions that will be represented include the usual mechanical loads of point loads, distributed loads and edge or axial loads. The preprocessor must also have the ability to represent the effect of loads due to environmental variations. Specifically, techniques will be provided for depicting the effect of temperature and moisture loading such as, for example, the use of a specified displacement to represent the displacement due to curling and/or warping. Ways to represent initial stresses and plastic strains that might be present in some cases, such as in asphalt concrete, will also be provided.

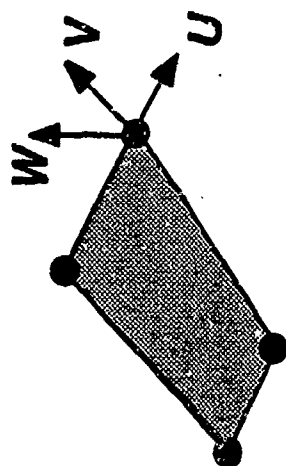
The preprocessor will have the ability to apply the various boundary conditions such as foundation conditions, and constraints such as at joints, to the model. In most instances the loads on airport pavements are applied repeatedly and the boundary conditions may change over time. The preprocessor proposed will provide the capabilities to characterize the repeated nature of the loads applied and any changes in boundary conditions. The other capabilities of the preprocessor envisaged include mesh editing; geometric transformations including reflection, rotation, translation, scaling and mirror imaging; and automatic mesh rezoning.



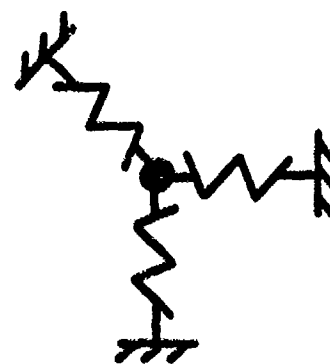
8-Node Solid
(1 Pt. Quadrature,
Hourglass Control)



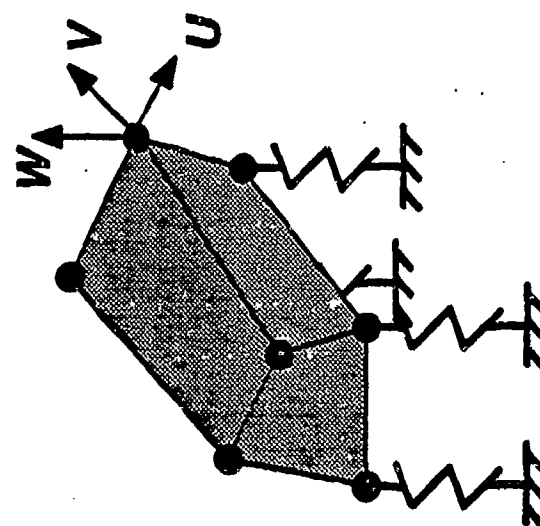
2-Node Bar



**Contact/Interface
(Slidelines)**



Discrete Springs



Infinite Domain

Figure 5-1. 3-D Finite Elements

5.1.2 Material Modeling

Various material models will initially be provided for portland cement concrete, asphalt concrete, granular materials, fine-grained subgrade soils and some of the composite materials currently used in airport pavement design. However, the option will also be provided to allow the incorporation of user defined material models for futuristic airport pavement materials. The intent in this area of the development of the response model is to provide material models that closely model the multidimensional response of pavement materials.

A library of material models is proposed which will comprise of a hierarchy of models for the major classes of pavement materials. The models will be able to represent isotropic, orthotropic, anisotropic, and time-dependent material properties. The generalized models required include those for materials that display linear elastic, nonlinear elastic, viscoelastic, viscoplastic, elastic-plastic, and elastic-viscoplastic responses. All these models will be provided with the ability to take into account the effects of fracture, fatigue, and damage on material properties over time. Yield surfaces that include volumetric sensitivity will also be provided for granular materials and soils.

5.1.3 Solution Procedure

The solution procedure used in the primary response model, to a large extent, will determine the success or failure of the development of the unified airport pavement analysis and design system. Realistic modeling of the 3-D response of pavements requires a large number of nodes (about 10,000 to 20,000) and corresponding large number of equations (about 750,000). In addition, iterative analysis methods are required to resolve the nonlinear response of pavement materials. This greatly increases the computer time required for solution.

Consequently, instead of the traditional approach of a direct solution of a linearized system of equations within a nonlinear iterative algorithm such as the modified Newton-Raphson, we propose to use an alternate FEA approach for the unified airport pavement analysis and design model. This unique approach employs the preconditioned conjugate gradient technique as an iterative linear solver or a replacement for the traditional Newton-Raphson iterative algorithm. This proposed approach reduces memory requirements for complex nonlinear airport problems by a factor of 10-100, making it possible to solve large and realistic problems on smaller computers and with greatly reduced computation costs/times.

Other features proposed include automatic load/time stepping and recovery from divergent solutions. Such features will ensure convergent solutions at a minimum cost. Restart files which allow the segmented solution of problems and give protection against unexpected aborts are also proposed. The capability to use the data from the restart files for postprocessing at any stage of a run will also be provided. We have initial experience which demonstrate the effectiveness of this approach.

5.1.4 Postprocessing Capabilities

The primary response model envisioned will generate a database that will include the history of stresses, strains, displacements, and failure criteria for a given problem. The efficient postprocessing of the data in this database will be paramount to the proper interpretation and application of the results obtained. A major aspect of this will be the graphical postprocessing of the results. The special graphical postprocessing features proposed for the unified airport pavement analysis and design system include the following:

- a. Displaying the deformed and undeformed geometry of the model to show static deformations. Provisions will be made to allow the superposition of the deformed shape on the undeformed shape.
- b. Color contour/fringe plots for any of the scalar outputs obtained to permit the determination of damage measures and the critical areas (permanent deformation, fracture areas, etc.) of the model. Continuous contour lines or color shadings will be provided for showing the surface contours of the displacements, stresses, strains, velocities and accelerations on the various elements or on full mesh plots. Additional features include automatic or user definition of the intervals and range for the contours, and the capability to obtain a contour plot during a run or by postprocessing of the results from an output file.
- c. X-Y plots of variables as a function of location, load, time (history plots), or other variables.
- d. Vector plots which show either by color or length the value of scalar outputs at the nodes of a model.
- e. Selective scanning and reformatting of the output obtained for further postprocessing. The further postprocessing could include the use of the output as input to other postprocessors, for damage assessment, and for printing of outputs in user specified tabular forms.

5.2 Software Structure

The solution procedure proposed for the primary response model will be based on the preconditioned conjugate gradient framework as an iterative linear solver or replacement for the nonlinear iterative algorithm in the finite element model. This unique solution procedure has many advantages which include reduced memory requirements and computation costs, making it applicable to the solution of large and complex airport pavement problems on smaller computers. The structure and developmental path of the 3-D-based FEA software proposed, based on this solution procedure, are discussed here.

A stepwise developmental process is envisaged. The initial goal will be to develop a finite element code with the capability for linear static/dynamic analysis. This basic code will incorporate linear elastic material constitutive models. This initial code will be adequate for the structural analysis of models with static or quasi-static and long-time dynamic loads, and linear boundary conditions.

The next developmental stage will concentrate on the incorporation of features to permit the solution of nonlinear problems involving both material and geometric nonlinearities. The code will progressively be improved to take into account realistic material properties, by implementing constitutive models with parameters for isotropic, orthotropic, anisotropic, and temperature-dependent material properties. It is expected that this process will take a considerable calendar time, as it will be dependent on the speed with which the appropriate constitutive models which account for material nonlinearities can be developed in a parallel effort. Additionally, there will be the incorporation of features in the software to allow transient analysis for cases where there are impact responses typically of less than 50×10^{-6} seconds duration.

The final product of this developmental process will be a unique public-domain code with capabilities for 3-D simulations and particularly suitable for linear and nonlinear analysis of airport pavements. An advantage of this stepwise developmental process is that a version of the software will be available for use by the FAA at the end of each of the stages of development identified. At each of these stages the program can be demonstrated and validated without the "ultimate" constitutive models.

A 3-D finite element-based unified airport pavement analysis and design system that will run on a PC (1995) is the ultimate goal of this program. It is expected that, in the initial stages, the primary response model proposed will be run on currently available workstations with run-times in the tens of hours for full nonlinear analysis of pavement systems. However, with major advances

likely in the computing power of workstations and PCs in the next few years, it is expected that run-times will be reduced to hours and minutes. In addition, efficient memory management techniques (virtual memory) will be employed to ensure the solution of large complex problems on the next generation of computers.

6. Material Constitutive Models

The material constitutive models that will be incorporated into the primary response model are paramount to the applicability of the unified analysis and design system to be developed to the solution of the complex airport pavement problems we are constantly faced with. The proper constitutive models must be able to realistically account for the time and deformation dependent properties of the materials. The details of the concepts proposed for the development of the appropriate constitutive models for the unified pavement model are discussed here.

Airport pavements are layered systems with each layer displaying varied mechanical behavior. Therefore, constitutive relations which represent the generalized stress-strain behavior are different according to what material is used for each layer of the pavement system. Asphalt and portland cement concretes are generally used for the top structural layers in airport pavements, which are then placed on a base and/or subbase layer(s) often made of granular materials (aggregates). In some instances a stabilized material is used as the base layer, with cement and asphalt as the most often used stabilizing materials.

These layers described so far, which make up the pavement structure, are placed on a prepared subgrade, the foundation soil. Constitutive models are needed for each of the materials used for the layers described as well as for other materials such as the composite materials and any futuristic materials that are expected to be used for airports in the coming decades.

6.1 Generalized Constitutive Relations

A library of material models comprised of a hierarchy of models able to represent the isotropic, orthotropic, anisotropic, and time-dependent material properties are needed for the unified airport pavement analysis and design system. The generalized models required include those for materials that display linear elastic, nonlinear elastic, viscoelastic, viscoplastic, elastic-plastic, and elastic-viscoplastic responses. All these models must have the ability to take into account the effects of fracture, fatigue, and damage on material properties over time. Yield surfaces that include volumetric sensitivity for the granular materials and subgrade soils are also needed. Following is a discussion on the generalized models that are representative of the major classes of airport pavement materials.

6.1.1 Asphalt Cement Concrete

Asphalt concretes are rheological in nature. Their mechanical behavior depends to a considerable extent on loading rate and temperature. In order to characterize such materials it is necessary to determine the master creep compliance (relaxation modulus) curve and the shift factor. Typical master creep compliance curves and the shift factor are given in Figures 6-1 and 6-2 [11] and generalized constitutive relations for asphalt concretes are given by [9]:

$$\epsilon_{ij} = \frac{1}{3} \delta_{ij}$$

∇

$$\int_0^{\zeta} \left[\frac{1}{3K} - \frac{J(\zeta - \zeta')}{2} \right]$$

$$\frac{d\sigma_{kk}}{d\zeta'} d\zeta' + \frac{1}{2} \int_0^{\zeta} J(\zeta - \zeta')$$

$$\frac{d\sigma_{ij}}{d\zeta'} d\zeta' \quad (1)$$

where

$\sigma_{ij}, \epsilon_{ij}$ = stress and strain tensors

ζ = reduced time and $\zeta = t/a_T$ where a_T is the shift factor which is a function of temperature only

$J(t)$ = creep compliance in shear

δ_{ij} = kronecker delta

K = bulk modulus

Another type of constitutive relations, that is suitable for evaluation of rutting in asphalt concrete pavements is the elastic-viscoplastic constitutive relations is given by:

$$\varepsilon_{ij} = \frac{\dot{s}_{ij}}{2G} + \frac{\dot{\sigma}_{kk}}{3K} \delta_{ij} + \lambda < \Phi(F) > \frac{\partial f}{\partial \sigma_{ij}}$$

where

$\dot{\varepsilon}_{ij}$ = strain rate tensor

γ_{ij} = stress tensor

G = shear modulus

K = bulk modulus

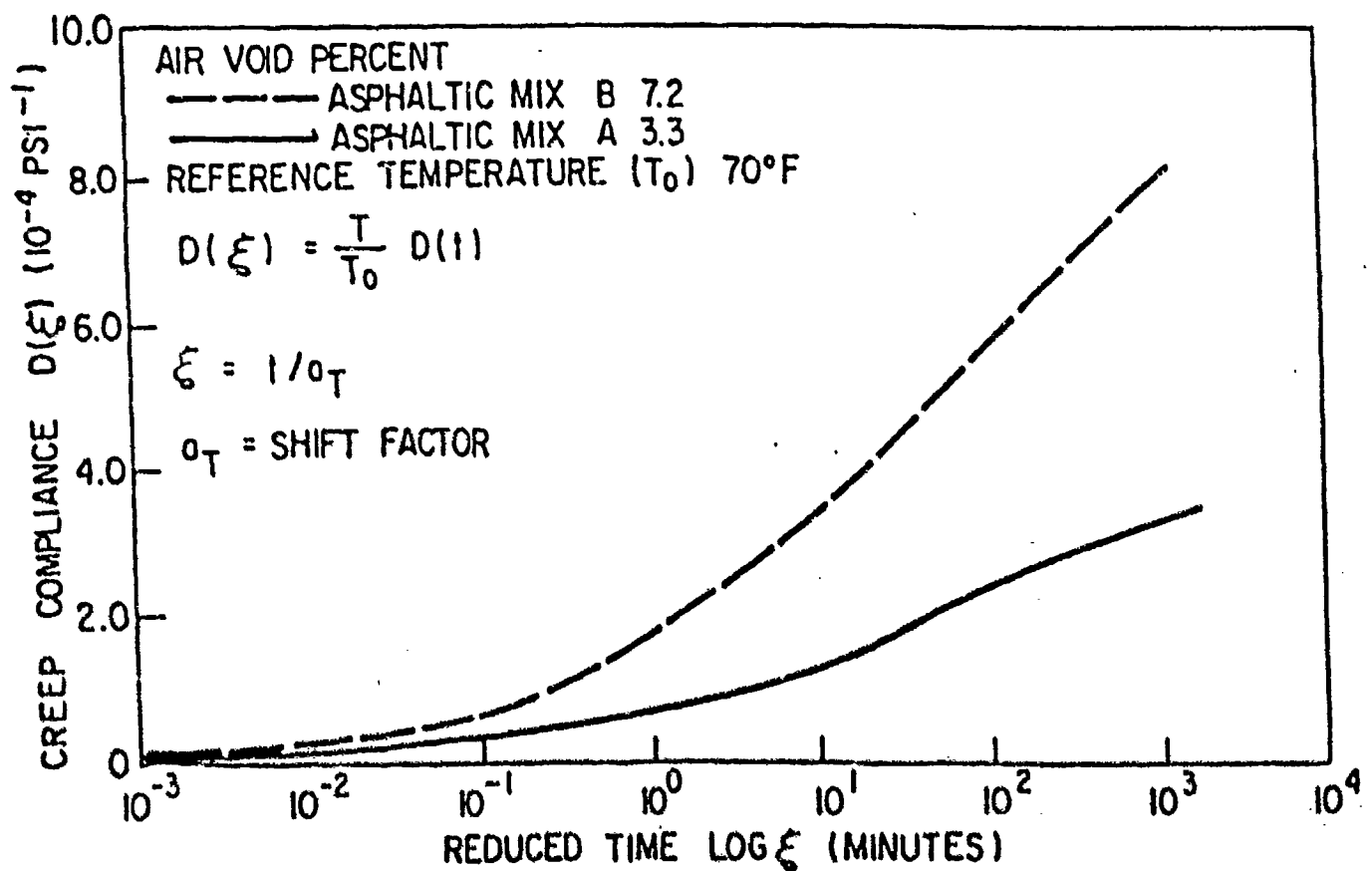


Figure 6-1. Master Compliance Curves under Linear Viscoelastic Behavior

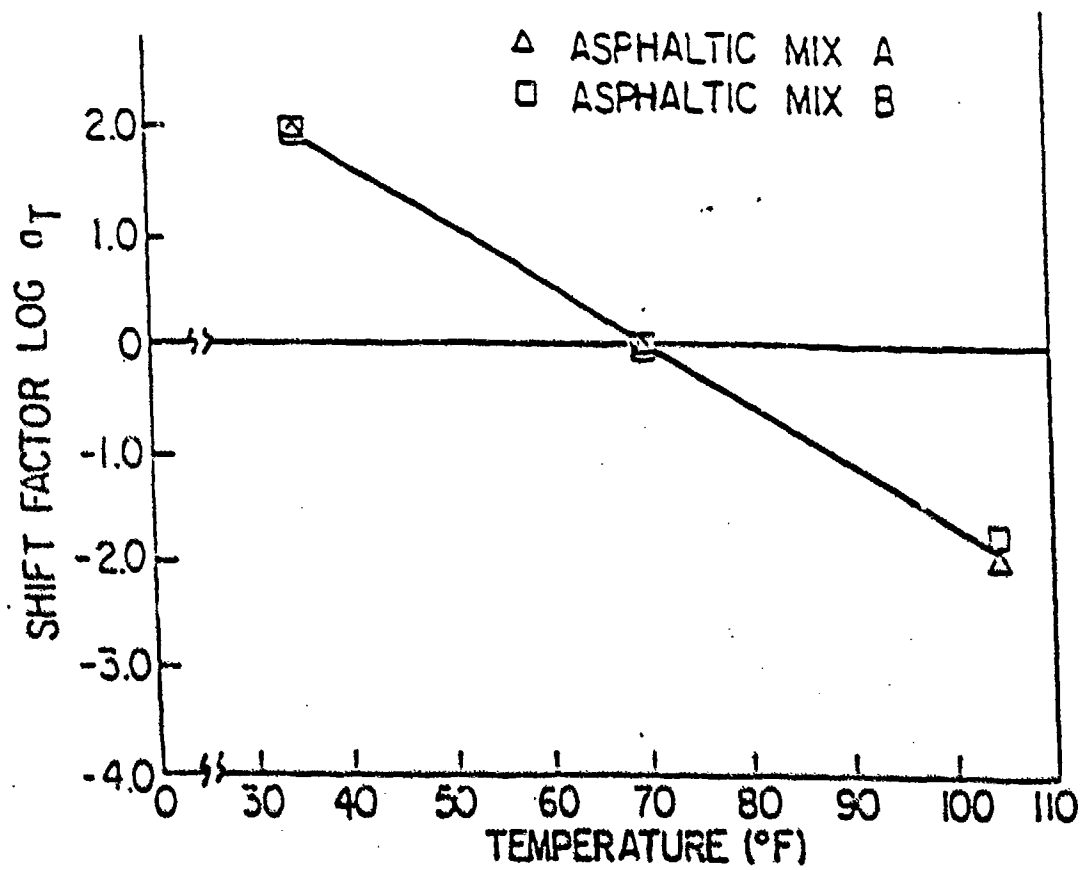


Figure 6-2. Shift Factor as a Function of Temperature

- F = yield function
- f = yield criterion
- γ = plastic viscosity coefficient

Typical permanent deformation versus number of cycles of loading for an asphalt mix is given in Figure 6-3 [12].

6.1.2 Portland Cement Concrete

Since portland cement concrete behaves in an elastic or elastic-plastic manner, the constitutive relations proposed are to be of the Cauchy type or the Green (hyperelastic) type or the incremental (hypoelastic) type. The incremental type constitutive relations require the knowledge of tangent and secant moduli for the material. A particular type of hypoelastic constitutive relations is given by

$$\dot{\sigma}_{ij} = 2 \left[\left(\frac{K_t}{2} - \frac{G_s}{3} \right) \delta_{ij} \delta_{kl} + G_s \delta_{ik} \delta_{jl} + \eta e_{ij} e_{kl} \right] \dot{\epsilon}_{kl} \quad (3)$$

where

$$\eta = 4(G_t - G_s)/3\gamma^2_{oc}$$

K_t, G_s = tangents and secant moduli respectively

δ_{ij} = kronecker delta

$\dot{\sigma}_{ij}$ = stress rate tensor

$\dot{\epsilon}_{ij}$ = strain rate tensor

Figure 6-4 shows the typical stress-strain curves for cement concrete in compression [12].

Base Course Material

Temp. = 75°F. (23.75°C.)

$\sigma_c = 30 \text{ psi (206.85 kN/m}^2\text{)}$

σ_c (psi)	0	15	30
Repeated Load Test Data	⊙	△	□
Incremental Creep Test Data	⊕	⊗	⊞

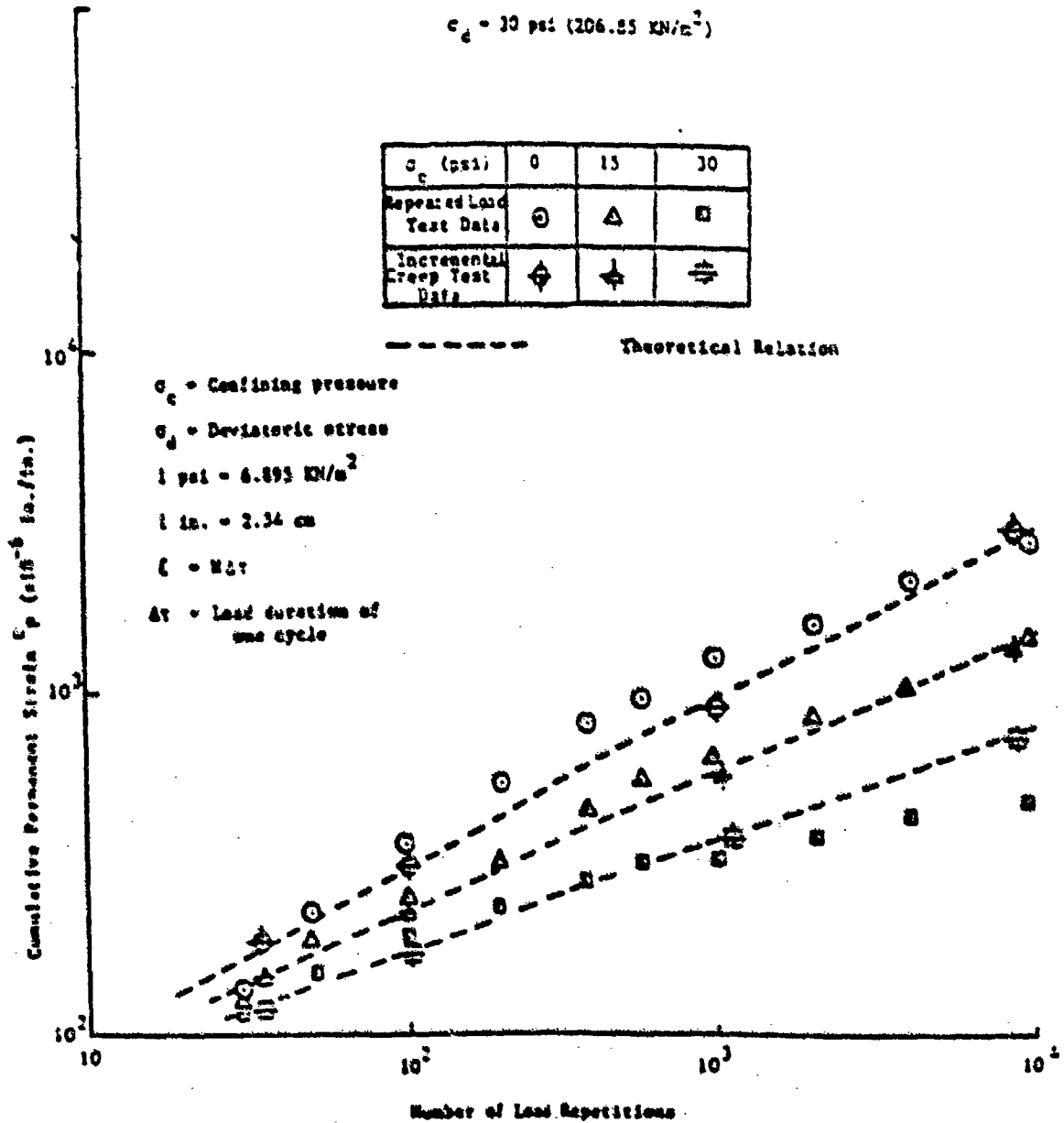


Figure 6-3. Permanent Strain Curves for Bituminous Concrete

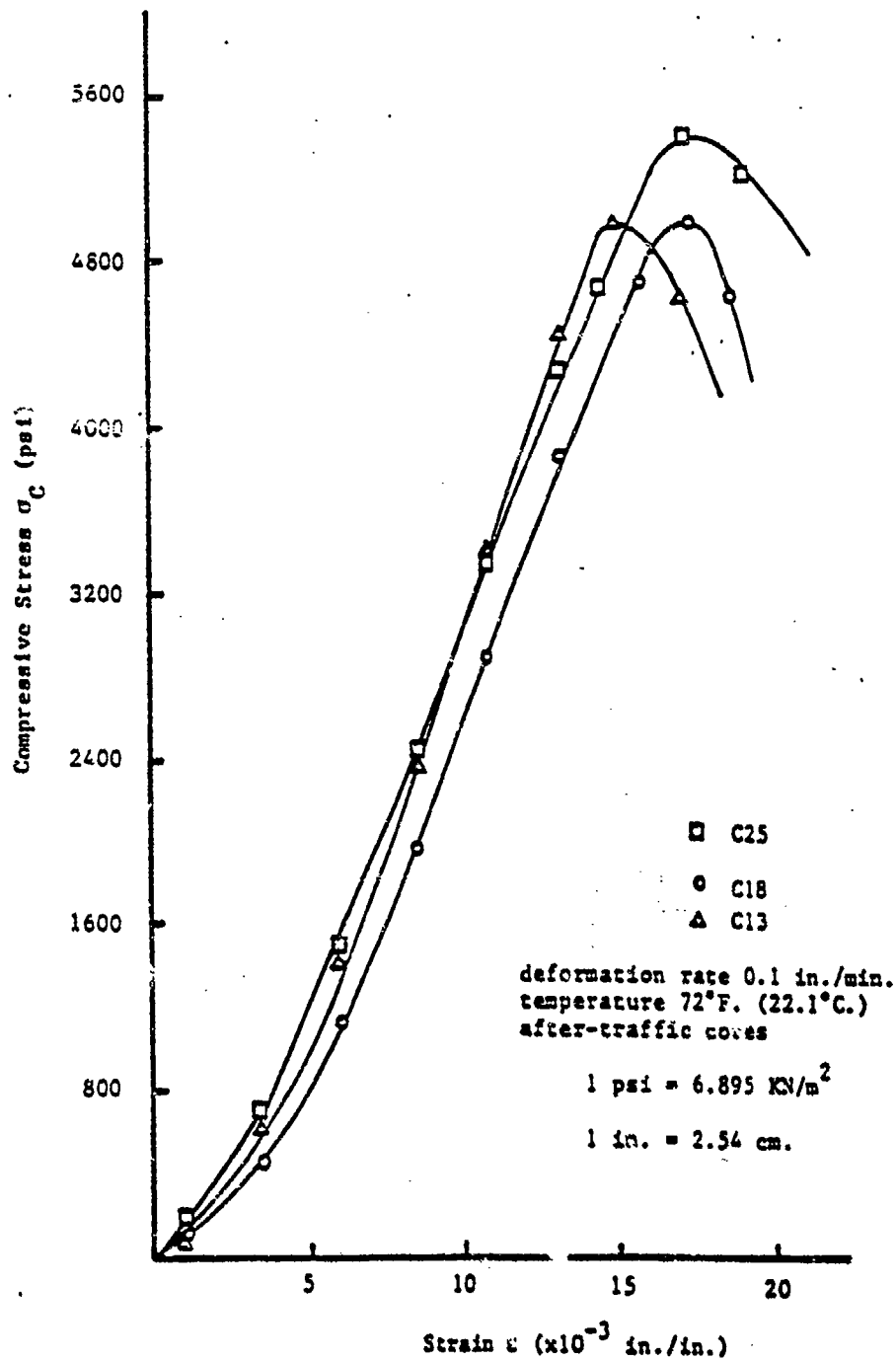


Figure 6-4. Compressive Stress-Strain Curves for Cement Concrete

6.1.3 Granular Materials

The base and subbase layers are granular in nature, and the base may consist of crushed stone. Consequently, the constitutive relations for the base and subbase material are generally different from those for the subgrade material. The base and subbase materials display elastic-plastic or elastic-viscoplastic responses. Since the base and/or subbase layers experience high rate of loading in practice, the appropriate constitutive relations for these granular materials are [10]:

$$\dot{\epsilon}_{ij} = \frac{\dot{s}_{ij}}{2G} + \gamma < \Phi \left[\frac{f(J_2 J_3)}{c} - 1 \right] > \frac{\partial f}{\partial \sigma_{ij}} \quad (4)$$

$$\dot{\epsilon}_{ii} = \frac{\dot{\sigma}_{kk}}{3K} \quad (5)$$

where

J_2, J_3 = 2nd and 3rd invariants of the deviatoric stress tensor

The above constitutive relations involve elastic constants G and K and plastic viscosity coefficient γ and the dynamic yield criterion F . Typical resilient modulus versus confining pressure, and the permanent deformation versus cycles of loading curves are shown in Figures 6-5 and 6-6 [12]. Using the data of the type shown in Figures 6-5 and 6-6, the elastic properties and dynamic yield function can be established.

6.1.4 Subgrade Soils

For subgrade soils, in the selection of constitutive relations there are three alternatives. For moderate loading rates, the soils behave linear or nonlinear viscoelastic. For this case it is necessary to obtain viscoelastic constitutive relations as given by:

$$\sigma_{ij} = \delta_{ij} \int_0^t \left[K(t-t') \frac{2}{3} G(t-t') \right] \frac{d\epsilon_{kk}}{dt'} dt' + 2 \int_0^t G(t-t') \frac{d\epsilon_{ij}}{dt'} dt' \quad (6)$$

where $K(t)$ and $G(t)$ are the relaxation moduli in dilatation and shear, respectively. Typical creep and creep recovery data on subgrade soil obtained from incremental creep tests is shown in

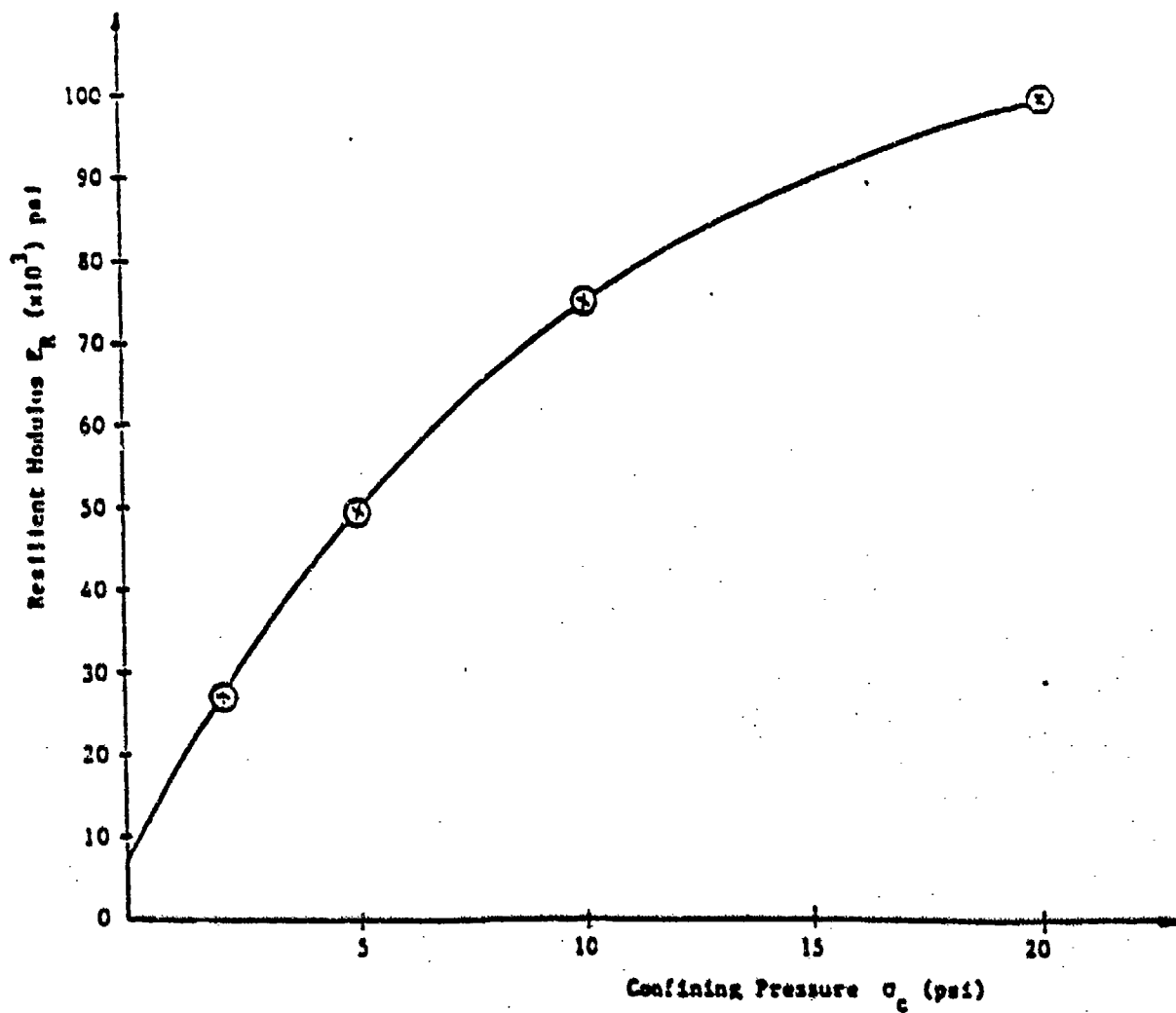


Figure 6-5. Resilient Modulus Variation with Confining Pressure for the Subbase Material

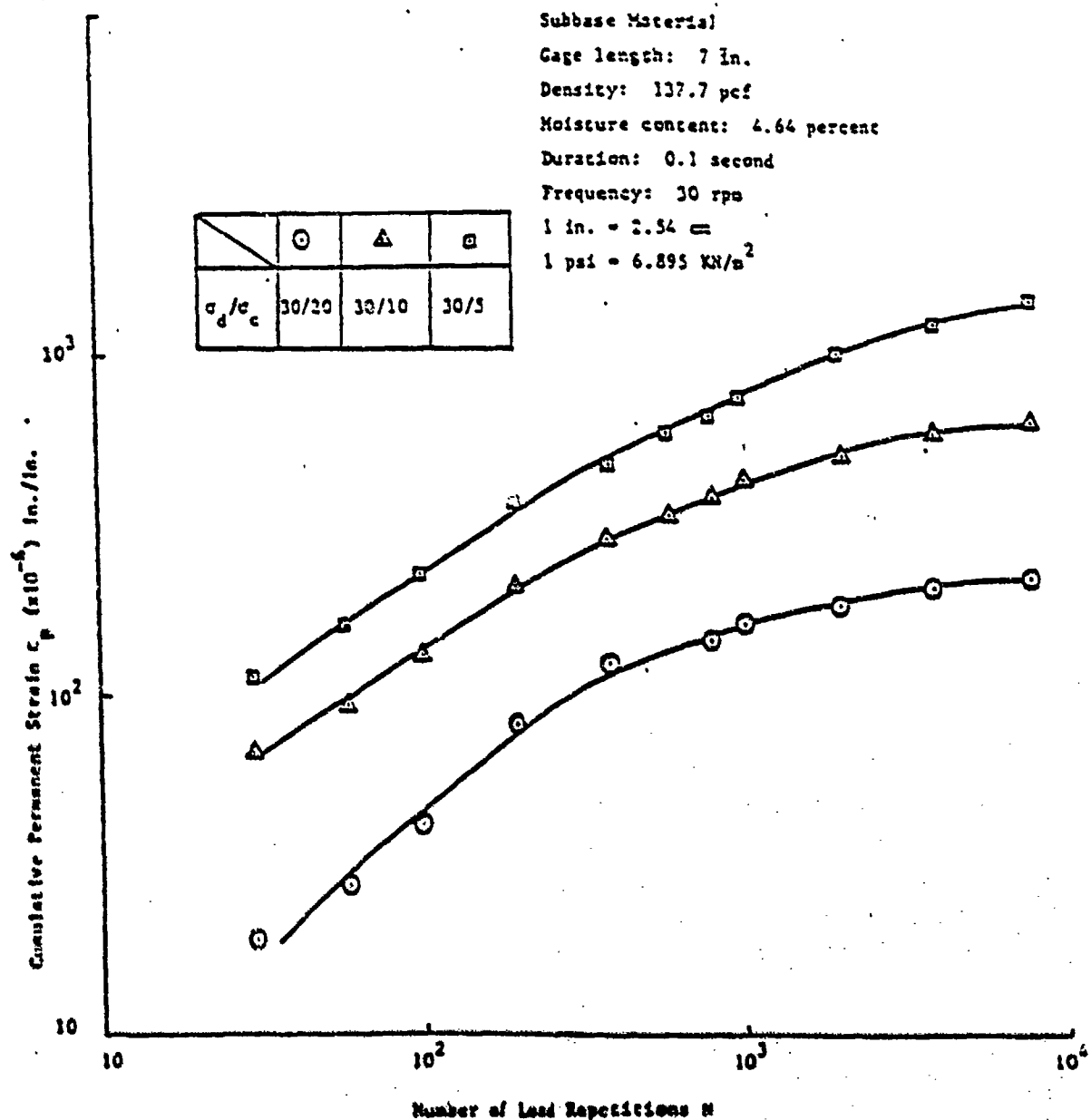


Figure 6-6. Permanent Strain Variation with Number of Cycles of Load Repetitions for Typical Subbase Material

Figure 6-7 [12]. From the data given in Figure 6-7 it is possible to evaluate the creep compliance function or the relaxation modulus function.

The second alternative is to use elastic-plastic constitutive relations which imply the existence of a yield function that takes into account the dilatancy effects. In the literature, various types of yield criteria which use associative and nonassociative flow rules have been developed. Some use isotropic hardening and some others use kinematic hardening. The model by Lade splits the strain in three components - the elastic strain, plastic collapse strain, and the plastic expansive strain. Plastic collapse strains are determined from spherical yield surface and associated flow rule. The plastic expansive strains are evaluated from a conical yield surface and nonassociated flow rule. Figure 6-8 shows dilatancy observed during a triaxial test and Figure 6-9 shows the conical and spherical yield surface [13].

The soil model by Prevost is an elastoplastic anisotropic hardening model for characterizing a wide range of stress-strain-strength responses for cohesive and cohesionless soils and is the third alternative. The model takes into account mechanical property change brought about by arbitrary changes in direction of loading unloading and reversal of loading. Figure 6-10 shows the yield surface used in Prevost model [13]. Sharma has also developed elastic-viscoplastic constitutive relations for clay which takes into account dilatancy. These constitutive relations are given by [14]:

$$\dot{\epsilon}_{ij} = \frac{\dot{s}_{ij}}{2G} + \frac{\dot{\sigma}_{kk}}{3K} \delta_{ij} + \gamma < \Phi(F) > \alpha \delta_{ij} + \frac{S_{ij}}{2\sqrt{J_2}} \quad (7)$$

where

$$< \Phi(F) = 0 \text{ for } \epsilon_p \geq 0.002$$

$$< \Phi(F) = F + (1 - e^{-30F}) \text{ for } \epsilon_p \geq 0.002$$

$$F = \frac{\alpha J'_1 + \sqrt{J_2}}{k(\epsilon_p)} - 1$$

$$\alpha = 0.856 \epsilon_p^{0.156}$$

$$k = 73.5 \epsilon_p^{0.115}$$

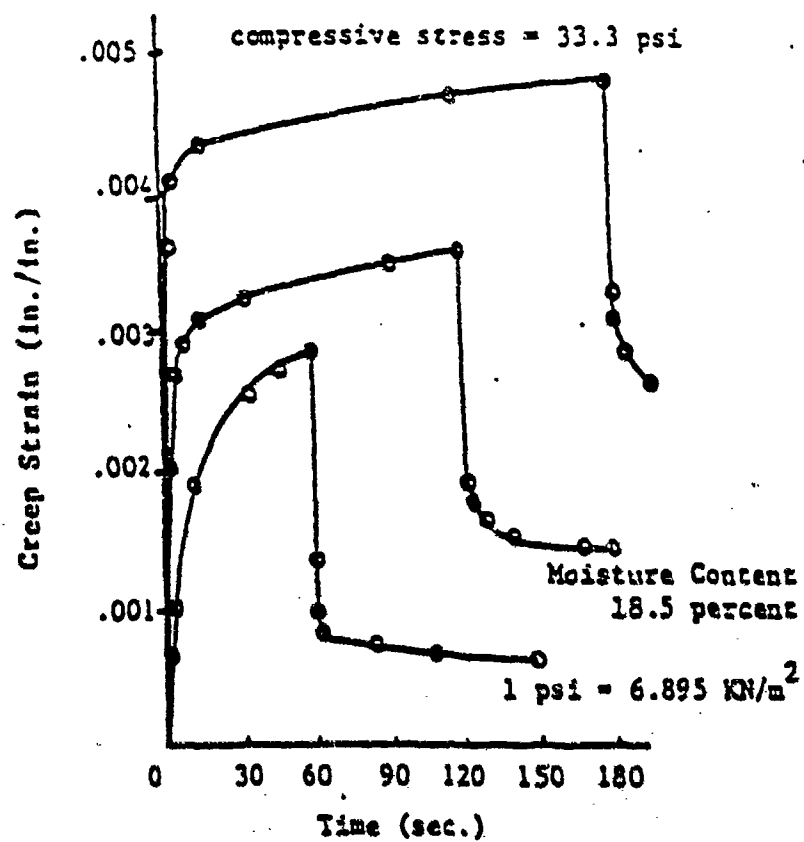
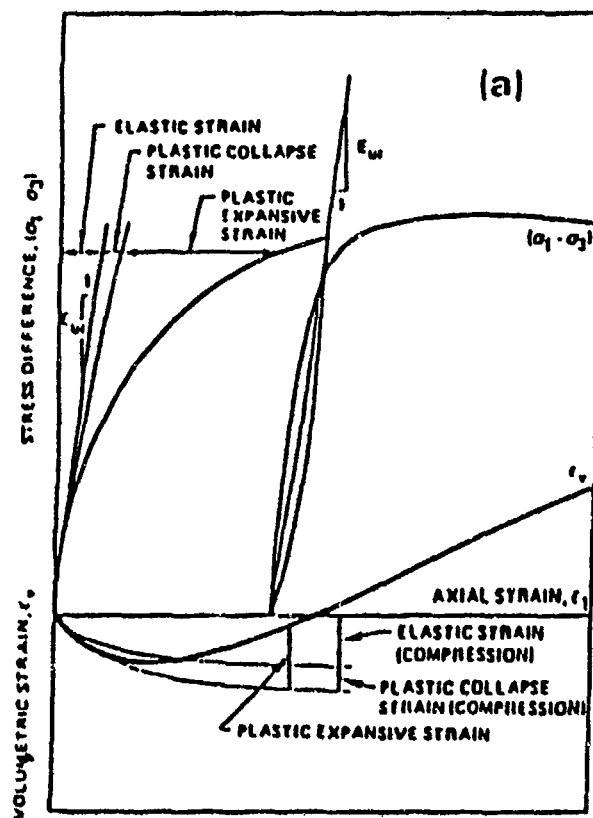


Figure 6-7. Creep and Creep Recovery Curves for the Subgrade Material



$$\dot{\epsilon}_v = \dot{\epsilon}_v^e + \dot{\epsilon}_v^c + \dot{\epsilon}_v^p$$

Figure 6-8. Typical Stress-Strain Curve for Soils

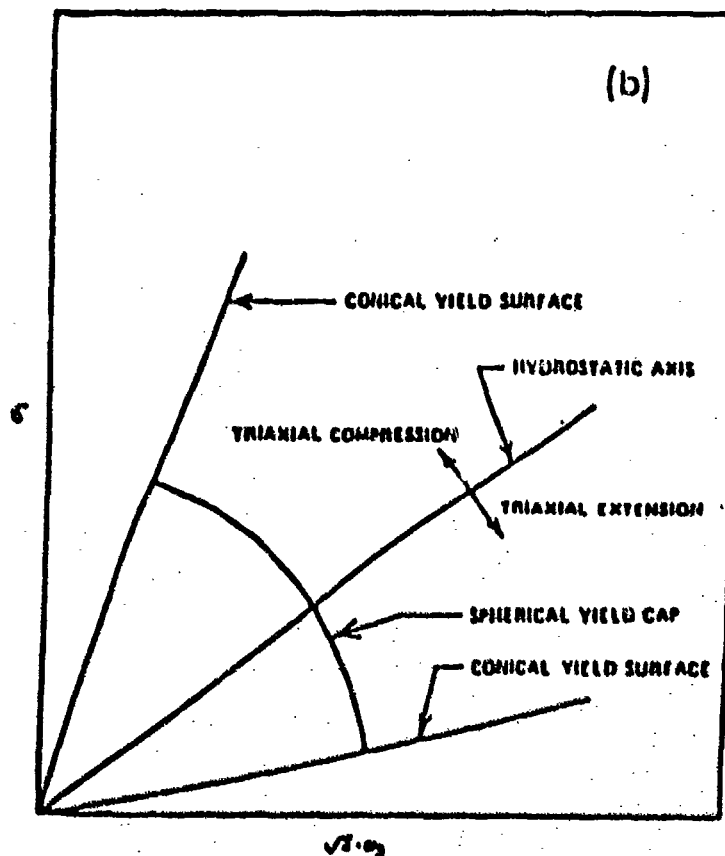


Figure 6-9. Yield Surface Representation Based on Theory by Lade

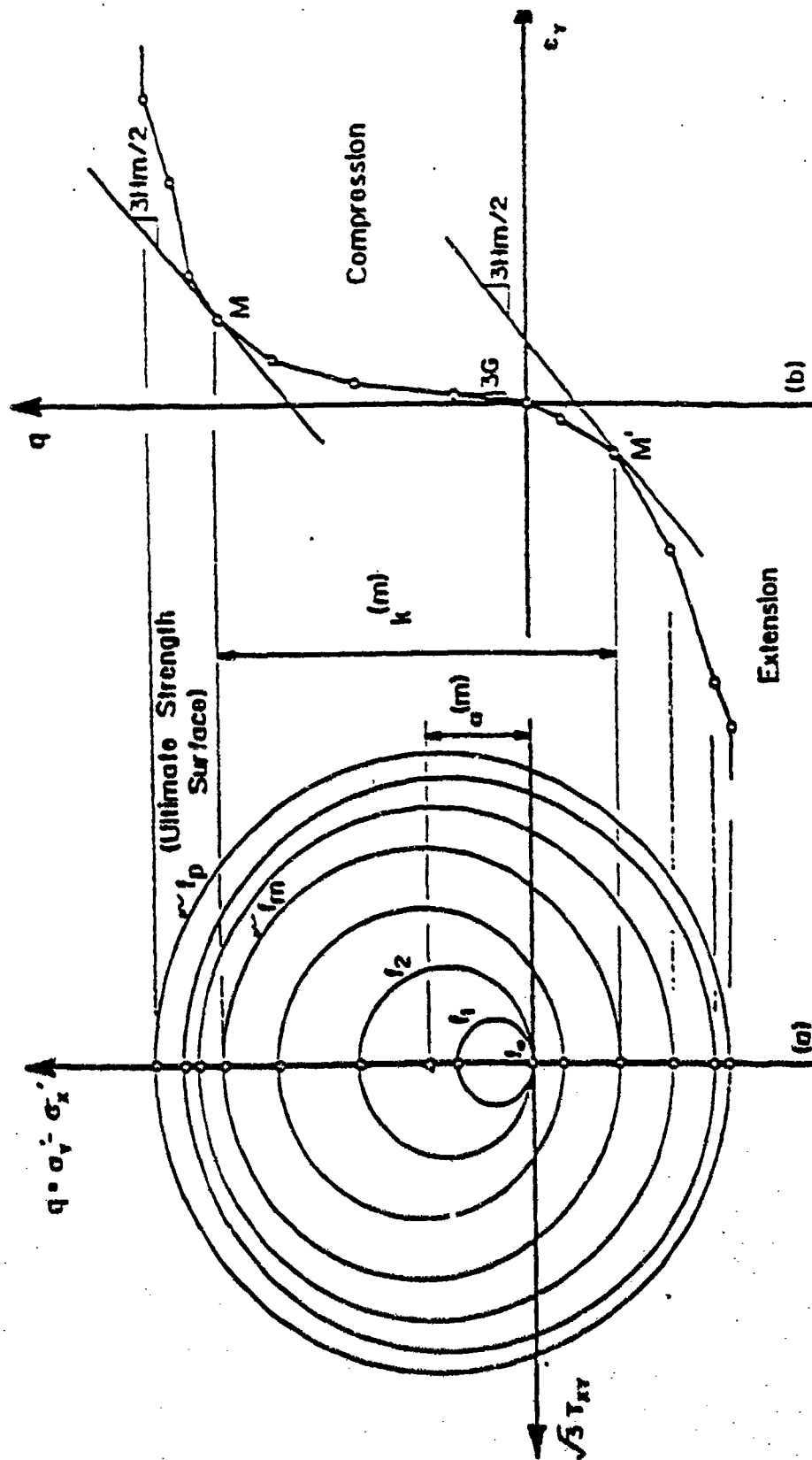


Figure 6-10. Nesting Surfaces in Prevost's Model Obtained from Triaxial Testing

$$G = 1.21 \times 10^5 \text{ psi}$$

$$E = 3.35 \times 10^5 \text{ psi}$$

$$K = 3.58 \times 10^{-6} \text{ psi}$$

$$\gamma = 186 \text{ psi sec}$$

The dynamic yield function (Eq. 8) was obtained by plotting the data as shown in Figure 6-11. Figure 6-12 shows the variation of dilatancy coefficient α with uniaxial plastic strain.

6.2 Incremental Constitutive Models

The materials used in airport pavements are constantly undergoing changes. For example, there is progressive micro-cracking in portland cement concrete, and plastic or irreversible strain accumulation in asphalt concrete which eventually lead to rutting, immediately upon the opening of an airport pavement to traffic. Also, the analysis of airport pavements inherently involve many sources of non-linearities which make it necessary to solve problems in increments tied to the load/time stepping.

Consequently, more often than not, the global and idealized constitutive models described above for airport pavement materials, which may be representative of the initial conditions of the materials, are not adequate for characterizing the physical behavior of the materials over time. They are not able to take into account the effects of factors such as aging, micro-cracking, plastic or irreversible strains, and other forms of damage.

For the 3-D finite element model of the proposed primary response model, therefore, incremental constitutive models [15 and 16] are proposed. These models are also sometimes called hierarchical single surface constitutive models [17 and 12]. Work on such models has been conducted in the last two decades with the advent of numerical methods such as the finite element method, which involve incremental analysis to take account of the various sources of non-linearities and are able to also take into account the effects of aging, micro-cracking, plastic or irreversible strains, and the other forms of damage.

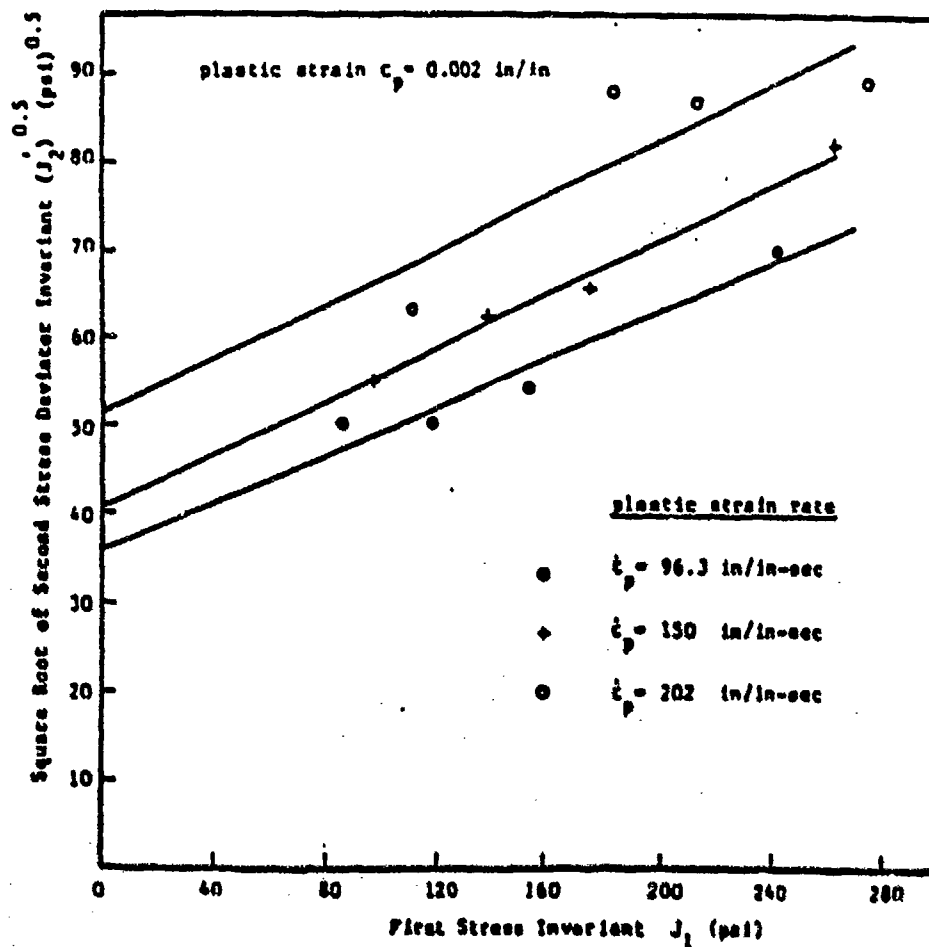


Figure 6-11. Square Root of Second Stress Deviator Invariant versus First Stress Invariant for 0.002 in/in Plastic Axial Strain and Different Plastic Strain Rates

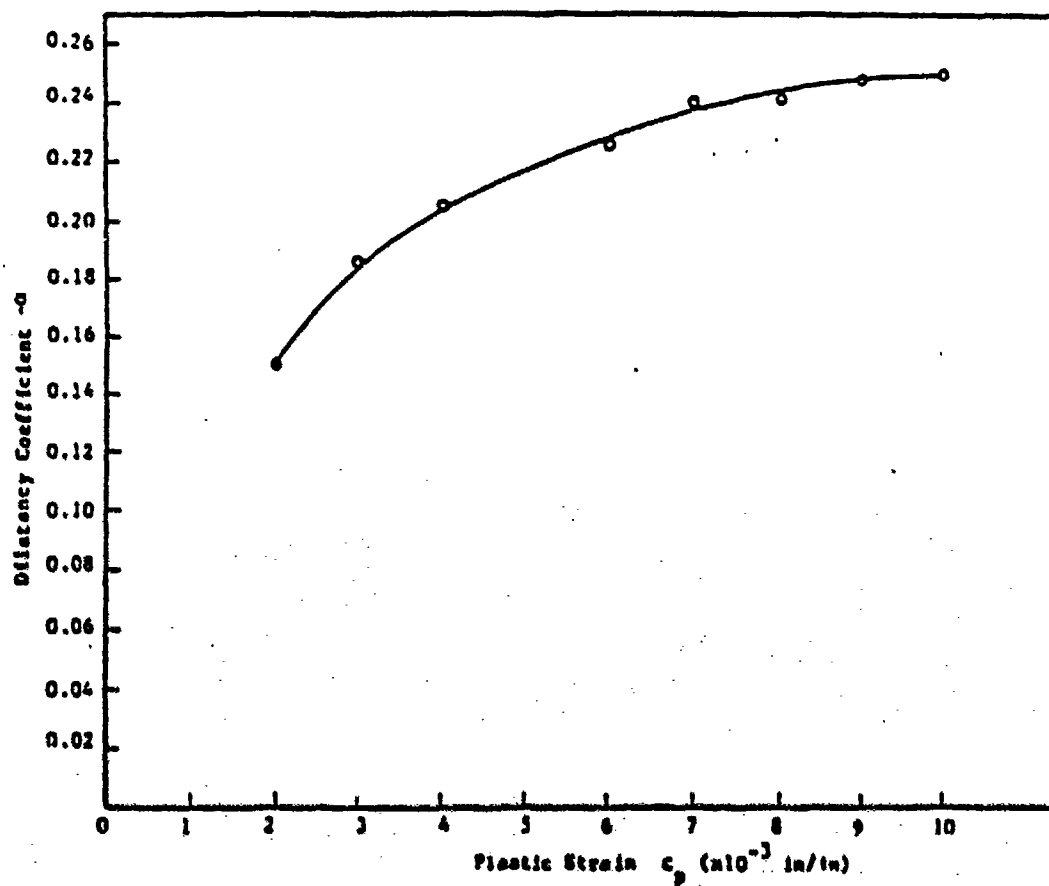


Figure 6-12. Variation of the Dilatancy Coefficient with Plastic Axial Strain

The incremental models proposed will be classes of constitutive models to which parameters that characterize the previous stress-strain history of materials can be added to describe the increasingly complex response of the materials. The parameters, to a large extent, are able to describe the deformed state of materials at any particular time. Consequently, the effect of any progressive local damage on the properties of the materials and on the subsequent behavior of the materials can be accounted for in the constitutive models.

In conjunction with the library of classes of constitutive models to be developed, a database of constitutive parameters for the variety of airport pavement materials will be developed as input for the primary response model. Generally, these parameters are functions of environmental variables such as temperature and moisture, and also change with factors such as aging, load history, and the other forms of damage. An important part of the development of the unified pavement model proposed, therefore, will be a comprehensive laboratory testing program to determine constitutive parameters that will make up this database. These parameters are given several names including "hardening parameters," "internal variables," and "memory variables" [16].

7. Cumulative Damage Assessment

The primary goal of the design of an airport pavement is to develop a structural design that will withstand the repeated application of aircraft loading and the effect of environmental variations over time. A particular pavement structure with defined materials and design parameters when subjected to a combination of aircraft traffic and environmental loading will over time experience damage. For a selected failure mechanism, damage analysis can be used to determine when these repeated loading cycles and the resulting accumulated damage will reach a limit that will cause the pavement to fail according to a pre-determined criteria.

A particularly important aspect of analysis and design using the unified pavement model, therefore, is the interpretation of the output obtained from the primary response model in an assessment of the cumulative damage that will be sustained by an airport pavement. This will involve postprocessing of the database of nodal displacements, strains, stresses, and damage measures (e.g., equivalent plastic strain) generated per load/time step from the primary response model, to obtain some measure of the cumulative damage experienced by the pavement over time.

This is perhaps one of the most important aspects on the design of any structure, including pavement design, since it is the only way an engineer can determine whether a particular product will meet the requirements for which it is provided. Thus, although the development of a cumulative damage assessment procedure is not explicitly stated as a goal of the development of the primary response model, it is important to give some consideration to its role in the provision of an adequate product.

7.1 Assessing Overall Pavement Damage

Traditionally, simple damage assessment procedures in the fashion of Miner's theory have been used in assessment of cumulative damage. These procedures assume damage is history independent and that the magnitude and sequence of loading have no effect on the accumulation of damage. For the unified airport pavement analysis and design system to be useful, a more realistic assessment of damage is required.

The table below shows the major forms of damage that occur in airport pavements and the causes and consequences of these forms of damage. The damage assessment procedure developed will concentrate on the determination of the overall damage to pavements based on these major damage forms. The response of a pavement system to a particular load is influenced by its history

vis-a-vis prior cracking, prior permanent deformation and material aging, and by the current environmental (temperature and moisture) conditions. In addition, several of the failure modes interact with each other, which increases the complexity of the problem. The damage accumulation procedure must account for these factors and interactions.

Table 7-1. Major Forms of Damage and Causes and Consequences that Occur in Airport Pavements

Form of Damage	Cause	Consequences
Cracking	Localized stress (thermal and mechanical)	Stress redistribution in pavement structure
Permanent deformation	Stress	Stress redistribution, rutting
Aging	Environment	Altered constitutive behavior, increased susceptibility to damage
Fatigue	Cyclic loading	Cracking

7.2 Damage Accumulation Procedure

Equation 9 depicts the concept proposed for the assessment of cumulative damage in airport pavements over time. The stress, strain, displacement and local damage in the brackets represent the nodal outputs obtained from the primary response model per load step:

$$\sum \left\{ \begin{array}{l} \text{Finite} \\ \text{Element} \\ \text{Analysis} \end{array} + \begin{array}{l} \text{Constitutive} \\ \text{Models} \end{array} = \begin{array}{l} \text{Stress} \\ \text{Strain} \\ \text{Displacement} \\ \text{Local Damage} \end{array} \right\} \Rightarrow \text{Cumulative Damage} \quad (9)$$

Load
Temperature
Moisture
Time
etc.

For the typical 20-year analysis period for an airport pavement, this translates into thousands of cycles or finite element analyses which have to be evaluated, if the effect of factors such as the repeated traffic loading, temperature and moisture changes, material aging and other local damage are to be modeled accurately. There is also the non-deterministic aspect of determining the load and environmental condition for each particular load step. A major objective in the development of the unified airport pavement model will be to determine how best this summation can be carried out to realistically assess cumulative damage within the limitations of computer capabilities.

At the extreme one can theoretically simulate the actual condition of a design and accumulate the damage generated per load step for the entire analysis period. This is the ultimate approach for a realistic assessment of damage but requires an unrealistic amount of computer time to simulate the typical 20-year analysis period for airport pavements. More practically, the analysis period can be broken up into a small number of increments, with the conditions (material properties, temperature, moisture, etc.) within each increment assumed to remain constant. The average damage for each increment (e.g., hourly increment) can then be determined with some degree of accuracy, and the damages for the increments accumulated to give the total damage over the analysis period. A procedure for determining the damage in pavement systems based on this practical approach will be developed for the proposed unified airport pavement analysis and design system. The procedure will provide for a sufficient number of iterations to approximate reality.

8. Summary and Recommendations

The concept development described above comprise the first step in a multi-phase program towards the development of a unified airport pavement analysis and design system. The subsequent phases of the program will concentrate on the actual development of the analysis system, the laboratory and field testing of the system for verification, and, finally, the implementation of the system. In this initial step, the framework of the unified pavement model has been outlined. The main features of the unified pavement model proposed are:

- a. A central primary response model based on 3-D FEA for the realistic structural analysis of all types of airport pavement under varying aircraft traffic, environmental and material conditions. A 3-D FEA model is proposed to permit the solution of the complex airport pavement problems in which many non-linearities exist in terms of materials, geometry, and boundary conditions.

Advanced preprocessing capabilities are proposed that will allow the automatic mesh generation for a design using 3-D element types. Other preprocessing capabilities include realistic representation of a wide range of load and boundary conditions. Users will be able to represent mechanical loads as point, distributed, or axial loads, and techniques such as the use of a specified displacement to represent the effect of environmental loading will be provided.

A powerful solution procedure that will result in reduced memory requirements and allow the solution of the complex, non-linear airport problems on smaller computer is proposed for implementation. The solution procedure will result in an increase in computation speeds by a factor of between 5 and 10 in comparison to the traditional solution procedures.

Graphical postprocessing capabilities to allow the efficient interpretation and reporting of the results obtained from the primary response model include the ability to plot deformed and undeformed shape of a model, color contour plots, and X-Y plots of all the scalar variables obtained as a function of location, load, time (history plots) or other variables.

- b. A library of incremental constitutive models for the major classes of airport pavements. For each of these classes of materials, the constitutive models can be progressively modified by the addition of parameters which will better describe the physical behavior of the materials as they become more complex.

- c. A procedure for assessing the cumulative damage experienced by a design as a result of the repeated application of aircraft traffic loads under different environmental conditions, and changing material and structural conditions, over the life of the design. This procedure will require the incremental summation of damage over the analysis period.

There is agreement throughout the airport pavement community on the need to move to mechanistic procedures that will allow a more realistic analysis and design of airport pavement to meet the enormous demands of the future. The development of the unified airport pavement analysis and design system proposed herein will provide us with such an opportunity.

The development of a powerful, 3-D finite element framework with fast static/dynamic solution algorithms and associated library of elements is emphasized. A stepwise incorporation of constitutive models to take account of increasingly complex material properties will enable a progressive development of the unified airport pavement analysis and design system, that will increase its capabilities as time goes on. A unified pavement model for new pavement design, which is capable of handling existing pavement evaluation and the design of strengthening overlays, involving the use of nondestructive testing to obtain insitu material properties, is envisaged.

It must be noted that the primary response model will only be as accurate as the quality of the model generated for a design; the constitutive models used; the realistic representation of the loads and boundary conditions; and the solution algorithms implemented in the 3-D FEA program. Demonstration and validation of the program at regular intervals, even without the ultimate constitutive models implemented, is recommended. This will permit improvements to take care of shortcomings encountered and, at the same time, provide a program for preliminary work.

9. References

1. Federal Aviation Administration, Airport Pavement Design and Evaluation, Advisory Circular AC 150/5320-6D, Washington, D.C., 1978.
2. Edwards, J. M. and C. P. Valkering, "Structural Design of Asphalt Pavements for Heavy Aircraft," Shell International Petroleum Company Limited, London, England, 1970.
3. Asphalt Institute, Thickness Design - Asphalt Pavements for Air Carrier Airports, Manual Series 11, 3rd Ed., College Park, Maryland, 1987.
4. Packard, R. G., Design of Airport Concrete Pavement, Engineering Bulletin, Portland Cement Association, Skokie, Ill., 1973.
5. Joint Departments of the Army and Air Force, "Flexible Pavement Design Method for Airfields, Elastic Layer Method," Technical Manual 5-825-2-11, AFM 88-6, 1989.
6. Department of the Army, "Rigid Pavement Design for Airfields, Elastic Layered Method," Technical Manual 5-825-3-1, Washington, D. C., 1988.
7. International Civil Aviation Organization, Aerodrome Design Manual, Part 3: Pavements, 1st ed., ICAO, Montreal, Que., Canada, Doc. 9157-AN/901, 1980.
8. Oh, B. H., "Cumulative Damage Theory of Concrete Under Variable-Amplitude Fatigue Loadings," ACI Materials Journal, Vol. 88, No. 1, January-February, 1991.
9. Sharma, M. G., Viscoelasticity Theory and Application, Book under preparation for publication.
10. Perzyna, P. "The Constitutive Relations for Rate Sensitive Plastic Materials," Quarterly of Applied Mathematics, Vol. 20, No. 4, 1963, pp. 321-332.
11. Sharma, M. G. and Kim, K. S., "Nonlinear Viscoelastic Properties of Bituminous Concrete," Journal of Testing and Evaluation, Vol. 3, No. 3, 1975, pp. 182-190.
12. Sharma, M. G., Formero, G., and Lim, E. I., Mechanical Characterization of Pavement Materials, Final Report, Project 75-2, Pennsylvania Department of Transportation, April 1979.
13. Constitutive Equations for Granular and Non-Cohesive Soils, Ed. A. Saade and G. Bianchini, A.A. Balkema, 1989.

14. Sharma, M. G., "Constitutive Relations for Granular Materials Under High Strain Rates," Journal De Physique, Colloque C 3, Supplement au n^o 9, Tome 49, September 1988.
15. Drave, F., Une Formulation Incrémentale Des Lois Rhéologiques: Application Aux Sols, Thèse d'Etat, Grenoble, 1978.
16. Darve, F., "Rheological Laws and the Main Classes of Constitutive Equations, " Geomaterials. Constitutive Equations and Modeling, Ed. Felix Darve, Elsevier Applied Science, 1990.
17. Desai, C.S., Somasundaram, S. and Frantziskonis, G., "A Hierarchical Approach for Constitutive Modeling of Geologic Materials," Int. J. Num. Anal. Meth. Geomech., Vol 10, No. 3, 1986.
18. Desai, C. S., Numerical Methods in Geomechanics Including Constitutive Modelling, Unpublished Notes for Advanced School, Udine, Italy, July 1989.

10. List of Symbols

$\sigma_{ij}, \epsilon_{ij}$	= stress and strain tensors
ζ	= reduced time and $\zeta = t/a_T$
a_T	= shift factor which is a function of temperature only
$J(t)$	= creep compliance in shear
δ_{ij}	= kronecker delta
K	= bulk modulus
γ_{ij}	= stress tensor
G	= shear modulus
K	= bulk modulus
F	= yield function
f	= yield criterion
γ	= plastic viscosity coefficient
η	= $4(G_t - G_s)/3\gamma_{oct}^2$
K_t, G_s	= tangents and secant moduli respectively
$\dot{\sigma}_{ij}$	= stress rate tensor
$\dot{\epsilon}_{ij}$	= strain rate tensor
J_2, J_3	= 2 nd and 3 rd invariants of the deviatoric stress tensor

Unified Airport Pavement Design Procedure

L. Seaman
J. W. Simons
D. A. Shockey

Poulter Laboratory

R. F. Carmichael, III
B. F. McCullough

ARE, Inc.

Summary

We have taken initial steps toward developing a mechanistic approach to the design of airport pavement structures and carried through sufficiently to provide proof of concept. At the start of this project, the major elements that were unavailable were determined to be a method for lifetime prediction and material models to describe fatigue cracking and rutting. During this project, we have developed initial versions of all three of these elements. We have developed a method for predicting pavement lifetimes using three-dimensional finite element codes and the material models. This prediction procedure led us to requirements on the nature and accuracy of the material models.

The material model for fatigue cracking is a micromechanical extension of an available fatigue model used for metals and other materials. This mechanistic model is based on the presence of flaws in the material that are grown during periods of tensile stress. With sufficient growth, these flaws become the large cracks that represent destruction of both Portland cement and asphalt concrete pavement. The fatigue model was incorporated into an SRI multiple-plane plasticity model to be able to represent the serious anisotropy that develops during cracking. This combined model, in a computer subroutine, was included with the three-dimensional finite element code DYNA3D, and simulations were made for an aircraft wheel gear rolling over a pavement. Then a lifetime prediction was made based on fatigue cracking in the base of the pavement.

The rutting model was developed based on an examination of the observed (and unusual) viscoelastic, dilatant, and viscoplastic behavior of asphalt concrete pavement. The model has components that represent each of these aspects, although rutting probably depends primarily on the permanent deformation caused by the viscoplastic behavior. The model appears to reproduce laboratory data satisfactorily. We have not completed implementation of the model into a computer subroutine appropriate for combining with DYNA3D, so we could not perform simulations of wheel loading tests.

Through this project we have developed a lifetime prediction procedure, a material model for fatigue damage, and a model for rutting. We have shown that each appears to represent field and/or laboratory conditions, although we do not have complete quantitative verifications. However, we feel that we have shown that each of these major new aspects of the pavement design procedure is feasible. Because the concept of a unified pavement theory has been proved in this initial project, we recommend continuation of the effort to develop a mechanistic design procedure for pavements.

1. Introduction

The Federal Aviation Agency has recognized the need for an advanced airport pavement design procedure because of the rapid decay of existing pavements, increasing wheel loads and tire pressures, and the opportunity to incorporate new materials. One example of the new materials is fiber-reinforced concrete, being developed by the NSF-funded Center for Cement-Based Materials at Northwestern under Prof. Shah [1]. Current activities in pavement by the Strategic Highway Research Program and by European agencies and contractors, according to Prendergast [2], follow a trend toward providing performance requirements rather than specifying materials, mixtures, and procedures. All these new developments encourage us to develop a more mechanistic approach toward pavement design so that we can account for new types of materials and loadings in rational ways. We believe that it is now possible to take a more mechanistic approach to design so that we can minimize the need for extensive field tests for each pavement configuration, wheel load, and paving material and yet produce longer lasting pavements.

We envision the following components in a unified pavement design procedure:

- a. A material constitutive model for high-cyclic loading. This model is almost linearly elastic, but includes fatigue cracking and rutting, and provides a way to account for other factors such as moisture, temperature, and sunlight degradation.
- b. A finite element computational code, which contains the material constitutive model, to calculate the stress and strain distributions and distress for specific loading situations and pavement configurations.
- c. An expert system program for interfacing between the finite element simulations of the pavement loading/distress response and the pavement design engineer to aid him/her in reaching a design or evaluation.

1.1 Objectives

The project is an initial exploratory step into a much larger program for the development of a new design procedure. The objectives of the current project are to:

1. Develop a physically based mechanistic approach to modeling pavements made of Portland cement concrete, asphalt concrete, and other materials.
2. Demonstrate the suitability and feasibility of the approach by applying it to selected pavement distress scenarios.

The proposed pavement design concept is intended to provide:

1. An ability to predict stress and deformation as a function of rate of loading, tire footprint, magnitude of loading, material properties, temperature, density, and other factors.
2. A theoretical foundation for the prediction of pavement displacement and deflection basin profiles under various types of aircraft tire loading and nondestructive test devices. This new concept should provide an analysis method for determining pavement properties from nondestructive testing data.
3. A means for computing the conditions at joints in rigid pavements, including the strains, stresses, and displacements under various loadings.
4. A method for predicting levels of stress at which pavement materials will rupture under loading or thermal effects. This method must be compatible with crack propagation theory.
5. An analysis for determining the maximum thermal stresses as a function of temperature, temperature gradient in depth, and distance from the free surface
6. A means for relating the results of nondestructive tests on existing pavements to the strength of the pavement to withstand aircraft tire loadings.
7. A method for analyzing and accounting for the presence or absence of bond between pavement layers.

During this initial project, the emphasis is on fatigue and rutting distress for the pavement. Later stages of the program will account for the effects of moisture, temperature, and other factors.

1.2 Approach: Vision of the Design Procedure

We envision a PC-based expert system to guide the pavement designer and decision-maker. When initial decisions are made on the pavement type and thicknesses, these are tested by the code for adequacy. The tests consist of finite element simulations of pavements to predict the lifetimes under representative loadings, temperatures, wetting cycles, and other conditions.

Current computations require several hours for three-dimensional simulations of a wheel loading on a pavement. We expect improvements in computational times of about 5-fold each year so that simulations will take minutes when the project is completed. Hence, we believe that the

pavement loading simulations can be performed on a workstation in short enough time that they can be integrated into the expert system for overall decision making.

The finite element code should be three-dimensional because the problems to be treated are almost all clearly three-dimensional. The code should also be a public-domain code so that it can be readily distributed by the FAA to prospective users. It must be equipped with a powerful preprocessing system to automatically lay out wheels or to provide the stress footprint under wheels for minimal input from the user. The user should specify only the aircraft type and possibly the weight to obtain the loading required. There should be a similar simple description of the pavement. The post-processor should mainly display an indication of under- or over-design and guide the selection of the next pavement design. Figures of loading damage contours should be available on request, but are not the primary information required by the designer.

In our view the critical elements for the program and their availability at the beginning of the project were as follows:

1. Response model or finite element code: largely available
2. Material model for rutting in pavements: unavailable
3. Material model for fatigue damage in pavements: unavailable
4. Lifetime prediction on a mechanistic basis: unavailable
5. Expert system: not available, but can be developed when the preceding items are available.

To show the feasibility of our approach, we concentrated our efforts on items (2), (3), and (4) because these were largely unavailable. The following sections describe our efforts in these areas. We begin with the life prediction because it focused our attention on the most critical aspects of the material models, which are discussed later.

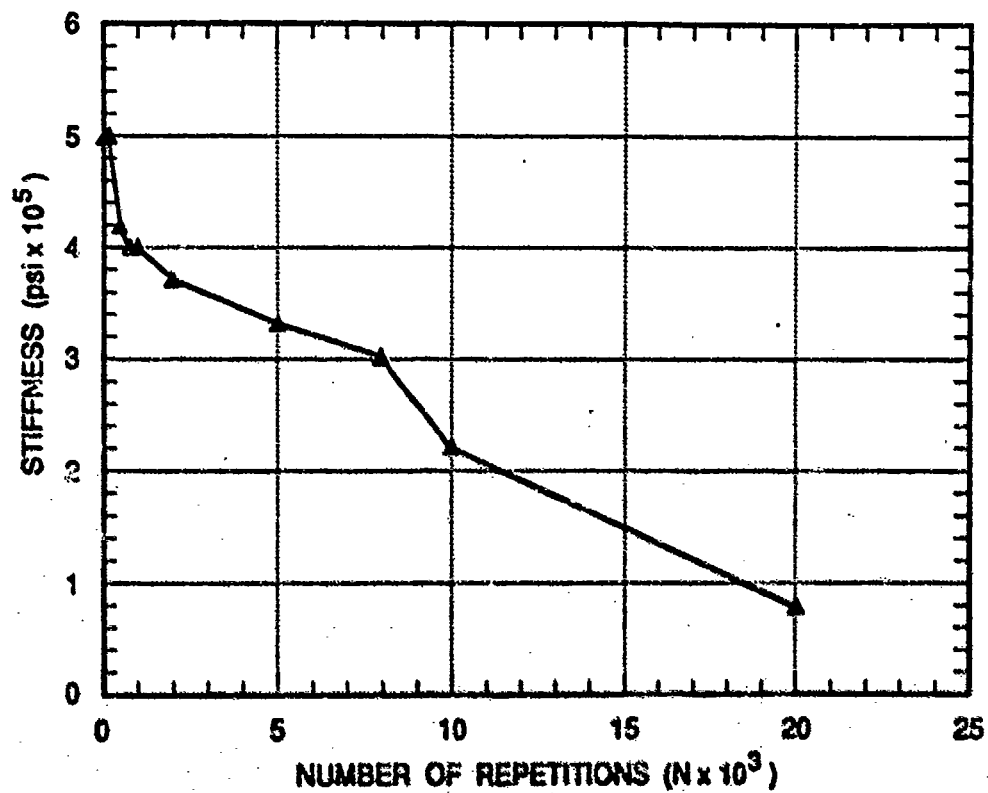
2. Lifetime Prediction

The suitability of a pavement design is based largely on the lifetime predicted for the pavement, and the lifetime is determined by the gradual development of damage to the point at which the pavement is judged unsatisfactory. We concentrate here on just two types of damage: fatigue cracking and rutting. Other types of damage should be dealt with in later phases of the contract. First, we illustrate with experimental data some aspects of the lifetime prediction and then describe our approach to the prediction.

Fatigue damage, in our view, occurs through the gradual growth of initial flaws in the pavement. Eventually, after many loadings, these flaws grow to be large, readily visible cracks. Figure 2-1 shows the variation of the stiffness of small asphalt concrete samples in laboratory fatigue testing. The plot shows that the stiffness is seriously decreasing throughout the life of the pavement. This stiffness variation reflects the growing presence of the cracks, we believe. To represent this gradual growth of damage, the fatigue material model must be able to describe very small growth (micrometers and smaller) of the cracks during each loading cycle.

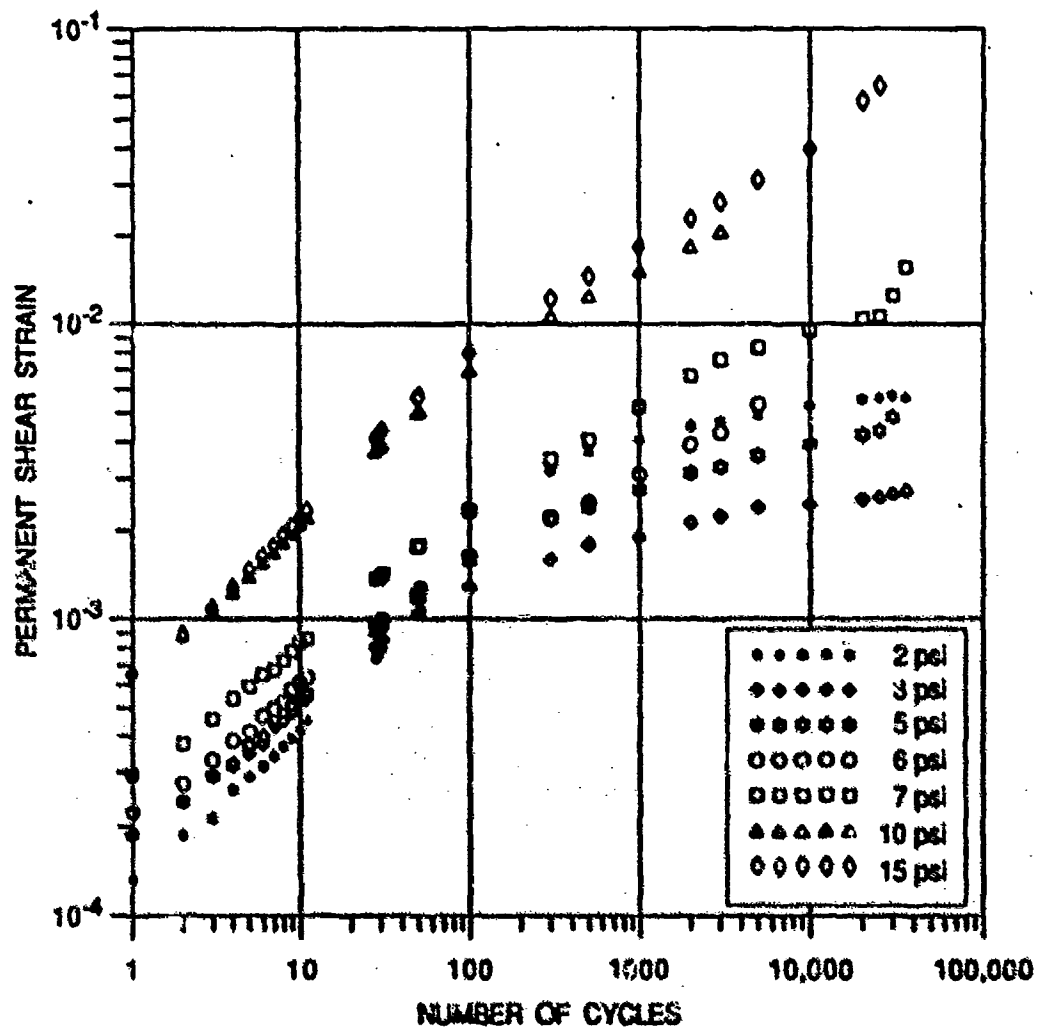
A similar plot of permanent deformation (the major cause of rutting) under cyclic shearing loading is shown in Figure 2-2. Here there is a gradual development of deformation during the entire lifetime. On each loading cycle, the strains are very small (tens to hundreds of microstrain), but they lead to significant rutting after many thousands of cycles. Therefore, the material model for rutting must be able to represent accurately the gradual buildup of very small permanent deformations during each loading. The prediction of the lifetime depends critically on an accurate representation of the rate of development of this deformation.

To develop a predictive capability for the lifetime of a given pavement structure, we expect to take the following steps. We presume that we begin with a fully defined pavement and subgrade, mix of wheel loads, temperature and moisture conditions, and other considerations. Then we perform a representative set of finite element simulations of the loadings on the structure. This set will include the range of wheel loads and other conditions such that it represents the loadings over a month or a year. From this set of simulations, we obtain the amount of damage present in the structure and the rate of increase of that damage. Thus we have the first point on a lifetime prediction plot like Figure 2-3. Here we are showing only a generic damage that could be fatigue cracking, rutting, or some other kind of damage.



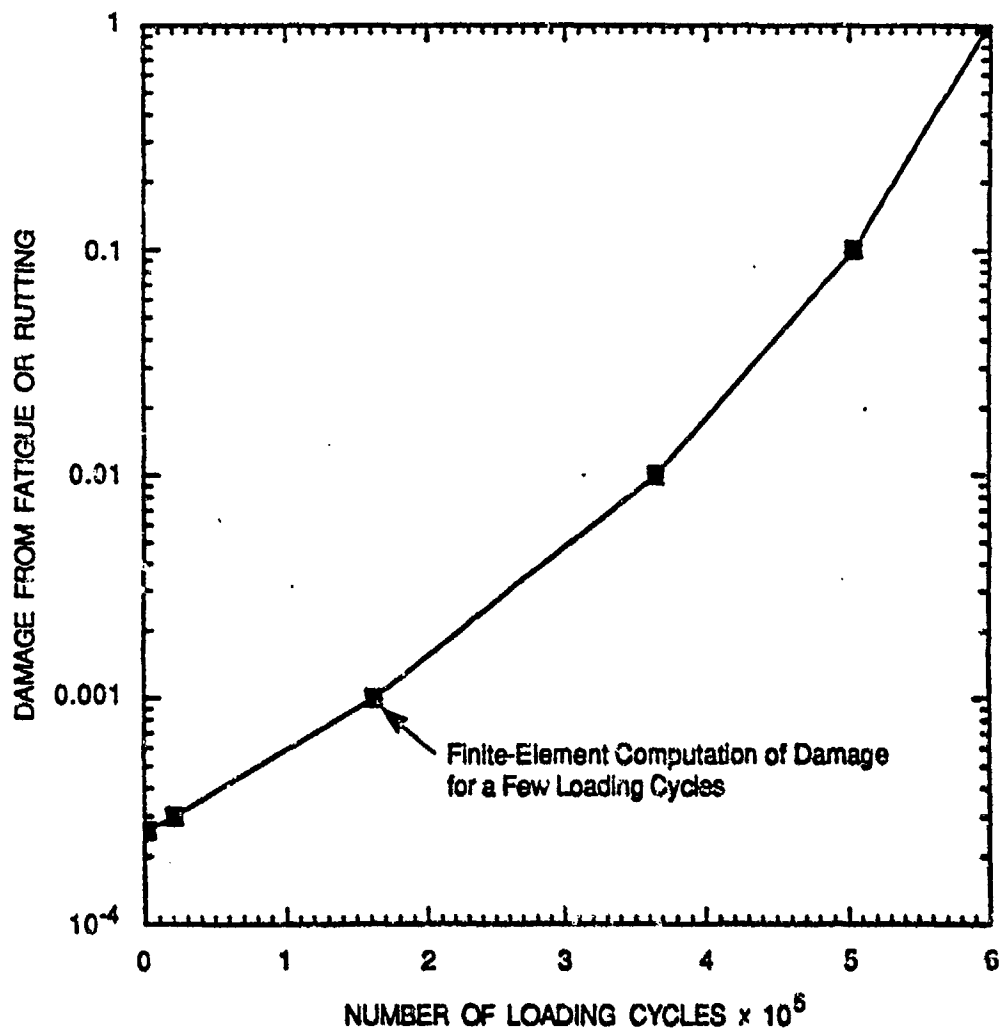
CM-1830-1

Figure 2-1. Change in Stiffness with Number of Loading Cycles (from page 19 of Monismith et al, Ref. 3)



CAH-1480-2

Figure 2-2. Accumulation of Permanent Deformation as a Function of Loading Cycle Under Repetitive Shear Stresses (from page 51 of Monismith et al., Ref. 3)



CAM-1889-3

Figure 2-3. Planned Prediction Procedure for Lifetimes Based on Finite Element Calculations at Intervals During the Life

From the computed damage point on the prediction curve of Figure 2-3, we extrapolate to some future time, using the computed rate of damage per loading cycle. A similar extrapolation procedure is used to update the amount of damage stored in the finite elements of the computer simulation. Then a set of finite element simulations are made at this future time, providing new damage and rate-of-damage values. This procedure of extrapolating to a new time and performing a set of finite element simulations is then repeated until the pavement has reached the level of damage that is considered to be critical.

We note several problems connected with this lifetime procedure. First, it requires extrapolation, and extrapolation always introduces uncertainties. Because of the inherent uncertainty of extrapolation, we want very good precision in its bases. Therefore, we make the following requirements on the material model and the finite element calculations:

- High accuracy in the calculation of small increments of damage so that the rate of damage is given with good precision.
- Analytical and mechanistic prediction for the variation of damage with loading cycles.

As noted in later sections, we have developed material models that appear to fulfill the first requirement. The second requirement is met by the fatigue model because we have a mechanistic model for the rate of development of crack damage with loading cycle. Such a mechanistic and analytical prediction is not yet available for rutting.

In the procedure described above, we have performed the lifetime prediction using small increments of damage or life, rather than predicting the entire life from an initial point. We feel this incremental approach is essential to minimize the errors of extrapolation and to provide appropriately for the interaction between the various forms of damage. For example, we expect that rutting damage will change the geometry enough to lead to cracking damage in some cases. This change in geometry can be handled only by an incremental approach.

In the next sections we discuss the finite element code and the material models with the foregoing lifetime prediction requirements in mind. We will return to the consideration of lifetime prediction for both model types. Only for the fatigue model have we been able to proceed to a full prediction of the lifetime. However, when the rutting model is fully implemented in the finite element code, we believe that we can perform such a lifetime prediction for this model also.

3. Finite Element Code for Structural Simulations

As our basic response model or computational tool, we have chosen to use a three-dimensional finite element code with dynamic capabilities. Such a code permits a detailed representation of the loading and geometry of the problem and provides an accurate solution for the stresses, strains, and displacements under all the conditions we expect to encounter. With this approach we can account for all the factors thought to be important: sunlight degradation, temperature, moisture, variation of properties with depth, as well as inelastic and nonlinear elastic processes. We can also perform both static and dynamic analyses as required for the conditions of interest. Therefore, we have chosen the finite element model over closed form analytical or empirical approaches.

The response model or finite element code contains several material models as subroutines that can be used to represent specific types of materials. Usually more material models can be added as required. We recognize that finite element codes will not have available an appropriate constitutive model or damage model for pavement and that this model must be added to the code. As described in Sections 4 and 5, standard constitutive models, including elastic, elastic-plastic, viscoelastic, and viscoplastic, are inadequate to describe the fatigue and rutting behavior of pavement. Hence, we must expect to add appropriate material models to any finite element code selected.

3.1 Selection Criteria for a Finite Element Code

The selection criteria that we considered in choosing a code are as follows:

1. The code must handle dynamic behavior. We are expecting loadings (such as those produced by aircraft landings and falling-weight devices) in which the critical loading times will be several milliseconds. Such loading rates are readily treated by standard finite element codes with dynamic equations of motion.
2. The code must handle sophisticated loading such as moving loads, temperature loads, contact load, and impact loads, and it must handle interfaces between layers.
3. The code must be able to model complex geometries, including layering, joints, and gaps and interfaces between materials.

4. Nonlinear material behavior must be treated. For example, if any standard plasticity models are handled in the code, the code has sufficient nonlinear capability for our purposes.
5. The code must accept material models of general, anisotropic type. For a material with developing damage, the response becomes highly anisotropic. Also, the code must permit the storage of many history variables per element (say, 50). These extra variables are needed to store the information related to the accumulation of fatigue cracking damage and of rutting damage.
6. There should be a suitable preprocessor to lay out the finite element grid and a postprocessor to exhibit the results. During later phases of the work, as the code is integrated into the expert system software, these two processors will need to be further automated.
7. The source code for the analysis and pre- and postprocessing programs must be in the public domain and be sufficiently well-documented to allow modifications. In the long run, the analysis program (response model) must be readily available and usable by designers who will typically not be experts in running finite element codes.

Although several codes are available from commercial vendors that meet requirements 1-6, as far as we know, the only codes in the public domain that satisfy all the requirements listed are the DYNA3D [4] and NIKE3D [5] finite element codes developed at Lawrence Livermore National Laboratories (LLNL) by John Hallquist. These codes are sophisticated three-dimensional finite element codes that have been used extensively to analyze the static and dynamic response of structures over a wide range of geometries, materials, and loading conditions. At SRI, we have used these codes for analyzing the response of space structures [6], underground tunnels [7], solder joints [8], welded structures [9], as well as ice/pavement interaction [10] and soil/structure interaction [11]. In doing so, we have become familiar enough with the source codes to have made significant modifications to them. These codes have very advanced capabilities suitable for the computations we expect to perform and for displaying the results.

Within this family of codes, there are two options depending on the solution procedure. DYNA3D is an explicit code in which the dynamic equilibrium equations and constitutive relations are integrated as a function of time directly, using a time increment that is governed by the wave speed through the materials. This code is well suited to the analysis of highly dynamic problems with large nonlinearities and short loading times (impact problems, for example).

NIKE3D is an implicit code in which the relevant equations are solved simultaneously through inversion of a structure stiffness matrix. The time steps can be selected to fit the nature of the problem and are typically one to several orders of magnitude larger than for an explicit code. This method is well-suited to quasi-linear problems with minor dynamic effects.

The choice of code depends typically on the relative calculation times. Although implicit codes take fewer time steps, each step takes considerably more calculation time than for explicit codes, especially for three-dimensional configurations. Because NIKE3D and DYNA3D share similar architecture, we would implement the pavement model into both codes. The only significant difference in the two models is that the model for NIKE3D requires an element stiffness matrix.

3.2 Pre- and Postprocessors

DYNA3D and NIKE3D share a common preprocessor, INGRID, and postprocessor, TAURUS. An example of the sophisticated types of analysis possible with these codes is shown in Figure 3-1. We have modeled a tandem landing gear traveling at 100 mph over a layer of Portland cement concrete (PCC) pavement. Calculations of the resulting stresses, strains, and damage in the pavement are described in Section 4 in connection with the fatigue model.

3.3 Interaction of the Finite Element Code and the Material Constitutive Model

We considered the possibility of performing strictly elastic computations with the finite element code and then using the stress or strain states to determine the development of damage (fatigue cracking or rutting) as separate analyses based on the stress or strain states. In our experience, there is a large interaction between damage and stress, so the interaction becomes an important aspect of the problem. It is well established that the development of cracks (orientation as well as amount of growth) depends on this interaction. In rutting, the later stages especially depend on the change in geometry and properties that have built up over time. This change in geometry caused by rutting can lead to cracking in the top of the pavement. Hence, the interaction between the stress and strain states and the distress is too important to be neglected. Therefore, we have chosen to make our material model represent all the damage processes and interact with the finite element code so that the distress will be directly exhibited from the finite element computations.

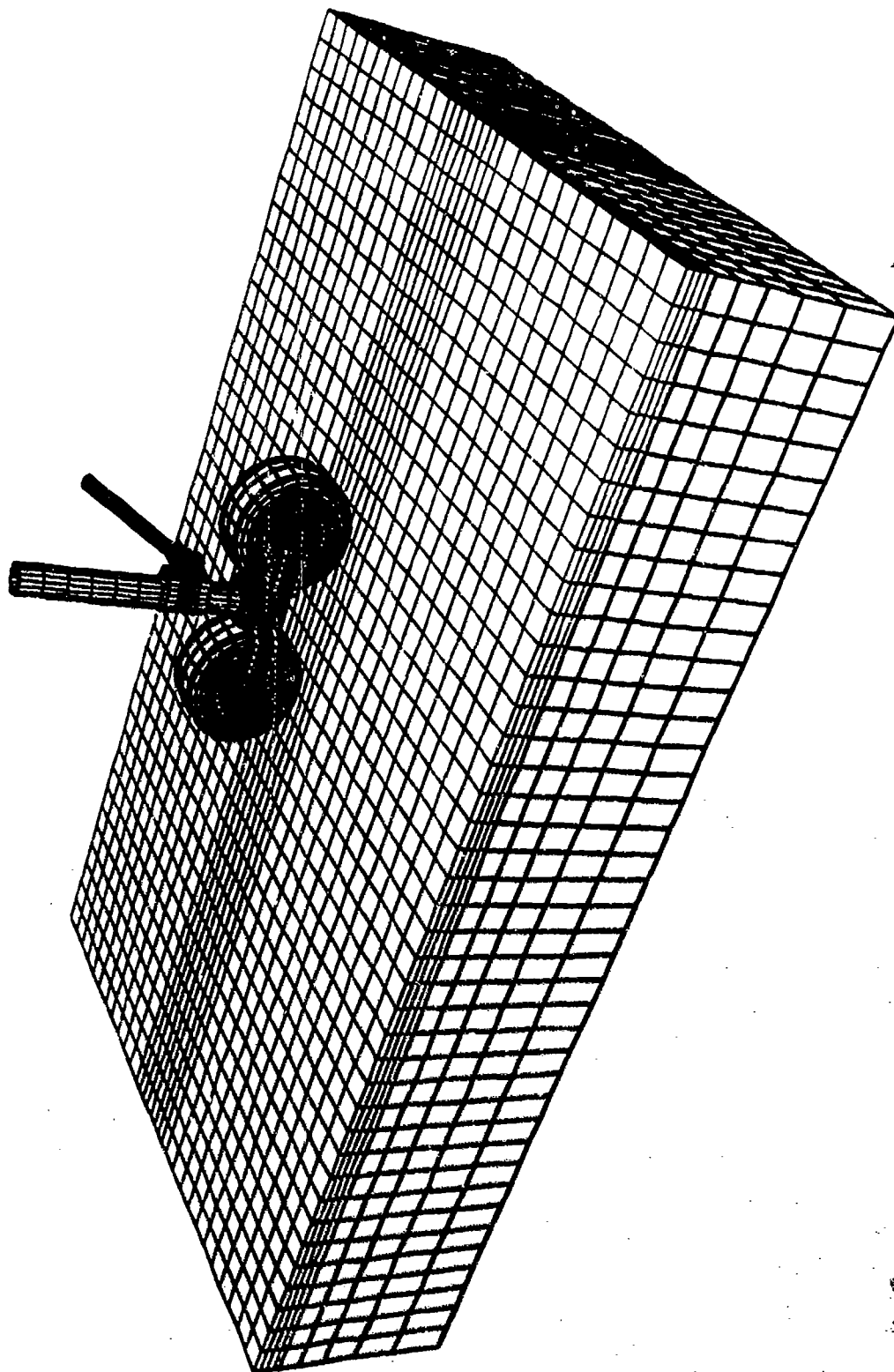


Figure 3-1. Finite Element Layout of an Aircraft Landing Gear on a 12-Inch-thick Portland Cement Concrete Pavement, Provided by the Preprocessor with DYNA3D

4. Fatigue Model

Both Portland cement concrete and asphalt concrete can undergo cracking under repeated loading. We expect similar cracking behavior for any other paving material with intermediate behavior and properties. This fatigue damage has been observed to occur in a variety of ways in pavement:

- a. Cracking at the base of a slab by tensile bending stresses
- b. Delamination between pavement layers (reflection cracking)
- c. Cracking along the surface at the edge of ruts in asphalt concrete
- d. Cracking around dowels, corners, and joints in Portland cement concrete.

Here we focus on only the first of these problems for simplicity because this cracking is closely related to the continuum stresses. Later we expect to be able to adapt the fatigue model to treat other types of cracking.

In the following paragraphs, we describe first our view of the fundamental processes that occur in fatigue cracking and some data obtained from field and laboratory fatigue tests. Then we discuss available fracture models and assess their applicability to the pavement problem. Finally, we outline the fatigue model we have developed and present some initial results with the model.

When fatigue cracking occurs, we expect that it begins by initiating small flaws in the cement matrix or in the aggregate or at the interface between the aggregate and the cement. These small flaws have sizes on the order of the sizes of the aggregates. At each loading cycle, these cracks grow by a small amount. After a thousand or a hundred thousand loading cycles, the cracks have become so large that they are noticeable and require repair. This gradualness of the development of fatigue cracks is supported by the laboratory fatigue testing of Monismith and co-workers [3, 12]. In their tests on small asphalt concrete beams, they observed a gradual reduction in stiffness with increasing numbers of loading cycles. This decreasing stiffness is probably caused by the opening of the small, but growing cracks. An expression for the apparent modulus of a material containing cracks is given in Appendix A, Eq. (9), showing how the presence of cracks reduces the apparent stiffness. During the fatigue tests, the stress is always a small fraction of the critical tensile stress for fracture.

4.1 Review of Available Models for Cracking

To develop or adapt a model to represent the foregoing perception of the fatigue cracking processes in pavement, we began by examining a few commonly used fracture models. The standard approach to fracture uses linear elastic fracture mechanics (LEFM). In this approach a flaw of radius a and the fracture toughness of the material K_{Ic} are introduced. The critical tensile stress for which a penny-shaped crack will grow is

$$\sigma_{cr} = \sqrt{\frac{\pi}{4a}} K_{Ic} \quad (1)$$

When a tensile stress greater than σ_{cr} is applied to the object containing the flaw with a radius a , the crack grows until the stress drops below the critical value (the critical value decreases as the crack grows). Thus, generally, we have either

$\sigma < \sigma_{cr}$: no growth, or

$\sigma > \sigma_{cr}$: catastrophic growth.

Because we expect thousands of cycles of essentially the same stress level before the cracks become noticeable, this LEFM model is not an appropriate description of pavement behavior.

Since the late 1960s LEFM has been amplified to treat more gradual cracking of ductile materials. This theory is called elastic-plastic fracture mechanics (EPFM). In EPFM initial cracking occurs when the stress exceeds a critical value related to J_{Ic} (similar to K_{Ic}), but here the crack may grow stably for some time. If the crack opening relieves some of the stress, the crack may cease growing. This model behavior is similar to some aspects of fatigue cracking seen in pavement, but there are also important features that conflict with observations:

1. The crack growth rates from EPFM are too large when the stresses are above the critical level.
2. The critical stress is nearly equal to the tensile strength of the material when only intrinsic flaws are considered.
3. A small increase in stress causes unstable crack growth.
4. No growth occurs if the stress is below the critical level.

Hence, EPFM is also inappropriate for pavement.

Another fracture model is the standard fatigue model, which was proposed by Paris [13, 14] in the early 1960s. This model gives the rate of crack growth per loading cycle as a function of the applied stress normal to the crack face.

$$\frac{da}{dN} = B \left(\frac{\Delta K_I}{K_{Ic}} \right)^n \quad (2)$$

Here B and n are constants ΔK_I is the change in the stress intensity factor according to linear elastic fracture mechanics, and K_{Ic} is the fracture toughness. Then K_I is related to the stress on a penny-shaped crack by

$$K_I = 2\sigma \sqrt{\frac{a}{\pi}} \quad (3)$$

The form for crack growth in Eq. (2) appears to represent fatigue data in many metals and other materials. As shown in Appendix A, Eq. (2) can also be integrated to obtain the pavement damage model:

$$N = A \left(\frac{f}{\sigma} \right)^n \quad (4)$$

where N is the number of cycles to damage, σ is the peak tensile stress at the base of the slab during a loading cycle, and A , f , and n are constants. The fatigue model appears to represent well several aspects of pavement damage. The model provides for small amounts of damage under a range of stresses and does not require that a critical level of stress be reached before any damage occurs. The stress levels of interest are all below the critical level from LEFM. But the model does require the presence of a single crack, measures the response to a single stress level, and is tied to the definition of a loading cycle.

4.2 SRI Fatigue Model

We began our development of a fatigue model with the model described by Eq. (2). We made extensions to account for the fact that a single crack does not control pavement degradation, but rather a large number of microcracks with a variety of orientations and sizes. We also must use our model in a finite element code to represent wheel loading so that the stresses will vary in direction and magnitude in nontrivial ways during the loading. Based on these considerations we propose the following constitutive fatigue model for the development of crack damage τ_f :

$$\Delta\tau_F = g\Delta\epsilon_c \sqrt{\frac{a_0}{a}} \left(\frac{\sigma}{\sigma_{cr}}\right)^{n-1} \quad (5)$$

where g and n are dimensionless constants and σ_{cr} is obtained from Eq. (3) by taking K_I as K_{Ic} and σ as σ_{cr} . The factor $\Delta\epsilon_c$ is the crack opening strain under the imposed stress. The $\sqrt{a_0/a}$ term was added to aid in matching this equation to Eq. (4). By our definition, τ_F ranges from zero at no damage to 1 at full damage and is proportional to the number of cracks per unit volume and the crack radius cubed. Equation (5), which is from Appendix A, has allowed us to match both the dR/dN expression (2) and the pavement damage model (4).

As noted in Appendix B, we have implemented our pavement fatigue model, Eq. (5), into a constitutive relation for pavement and connected it to the finite element code DYNA3D for routine simulations of pavement loadings. (Later we also expect to connect the rutting model with DYNA3D.) Critical tests of the model are determination of the damage from a loading and unloading process in a one-element calculation and the representation of damage from a rolling wheel in a full three-dimensional calculation. These results are presented in the following figures.

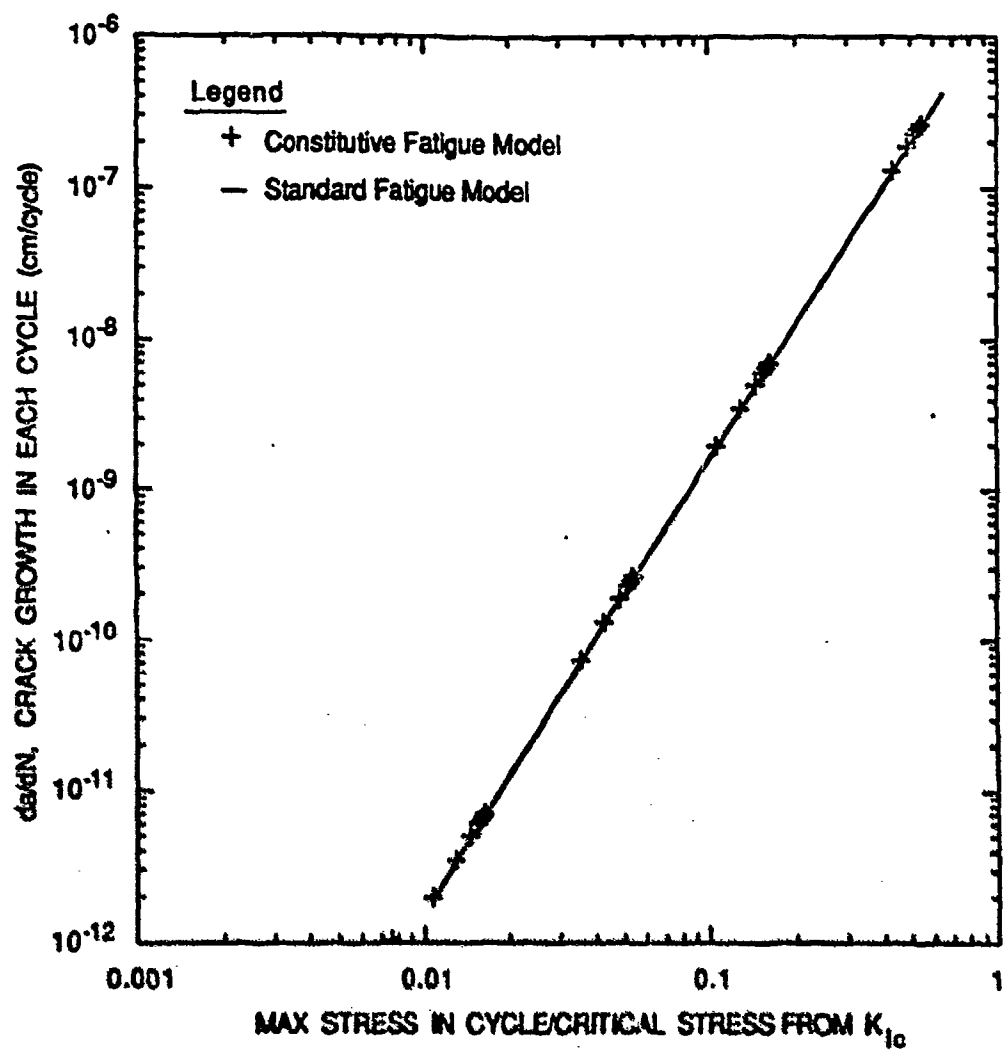
For the one-element computation, we used the fatigue parameters from Table A-1 in the Appendix A and loaded the element with a haversine stress function:

$$\sigma = \frac{1}{2} \sigma_{max} (1 - \cos 2\pi t/T) \quad (6)$$

where σ_{max} is the maximum imposed stress, t is time, and T is the period of the loading. Computations were made for increasing values of the initial radius, from 0.4 cm to 1.3 cm, for four stress levels from 0.03 to 1 MPa. After each loading cycle, the total growth of the radius according to the constitutive fatigue model, Eq. (5), was determined and plotted with a + sign as shown in Figure 4-1. Also Eq. (2) was evaluated and the line in the figure was plotted. Clearly, our constitutive fatigue model accurately represents the standard fatigue model.

4.2.1 Demonstration of the Fatigue Model in DYNA3D

Next we developed a full constitutive relation for DYNA3D by combining a standard thermodynamic Mie-Grüneisen relation for pressure, a multiple-plane plasticity model for deviator stresses, and the constitutive fatigue model. The new model is called SRI-PAVEMENT. The



CAM-1889-4

Figure 4-1. Comparison of Computed Crack Growth from Constitutive Fatigue Model with Standard da/dN Fatigue Model

multiple-plane feature was used so that fatigue crack growth could occur on each of the nine planes used in the model. The arrangement of the planes is such as to provide for a nearly uniform orientation distribution of planes. As the damage develops on some of the planes, the behavior becomes distinctly anisotropic because the stiffness reduces in directions normal to the crack faces.

Following insertion of this new constitutive relation into DYNA3D, we tested the combined model to verify that it could also reproduce the points in Figure 4-1.

We then simulated the rolling of a pair of wheels configured as a 727 landing gear over a concrete pavement as shown in Figure 3-1. The problem was laid out with the wheels on the right side of the pavement slab and moving toward the left at a speed of 100 mph. In the initial configuration, the wheels were off the right edge of the pavement. The calculation was performed to a time of 0.15 s, at which time the landing gear had traveled 22 feet. Although our calculational model allows the load to be applied via pressurized tires, for these calculations the load was applied by specifying a load footprint for each tire that moves along the pavement surface at the speed of the landing gear. The loading footprint for each wheel was a uniform pressure of 200 psi over a rectangular area 16 inches long by 12 inches wide. At the leading and trailing edges of the wheel, the pressure was linearly decreased to zero over a 2-inch length for a total load of 86 kips for the two wheels. By assuming a vertical plane of symmetry through the center of the landing gear, we analyzed half of the configuration shown in Figure 3-1.

The runway was modeled as a single slab of concrete pavement over subgrade. The dimensions of the slab are 25 x 45 feet with a thickness of 12 inches. The material constants for the pavement are an elastic modulus of 4.4×10^6 psi, a Poisson's ratio of 0.15, an unconfined compressive strength of 2.9 ksi, and a tensile strength of 290 psi. The subgrade was modeled as an elastic layer 6 feet thick with an elastic modulus of 4.4×10^5 psi and a Poisson's ratio of 0.15. We assumed that the midplane of the pavement was pinned in the vertical direction and that the vertical surfaces of the subgrade were transmitting boundaries. The interface between the pavement and subgrade was allowed to slip without friction.

Figures 4-2(a) and (b) shows contour plots of the vertical stress in the elements on the upper surface of the pavement and on the cut vertical surface at two times, $t = 0.075$ and 0.15 s. The view in these figures is through the vertical plane of symmetry, so we see into the half-wheels and landing gear. As expected, the loads are greatest beneath the tires. The loads in the subgrade are all less than 40 psi. From the similarity of Figure 4-2 a and b, we see that there is little boundary effect on these vertical stresses.

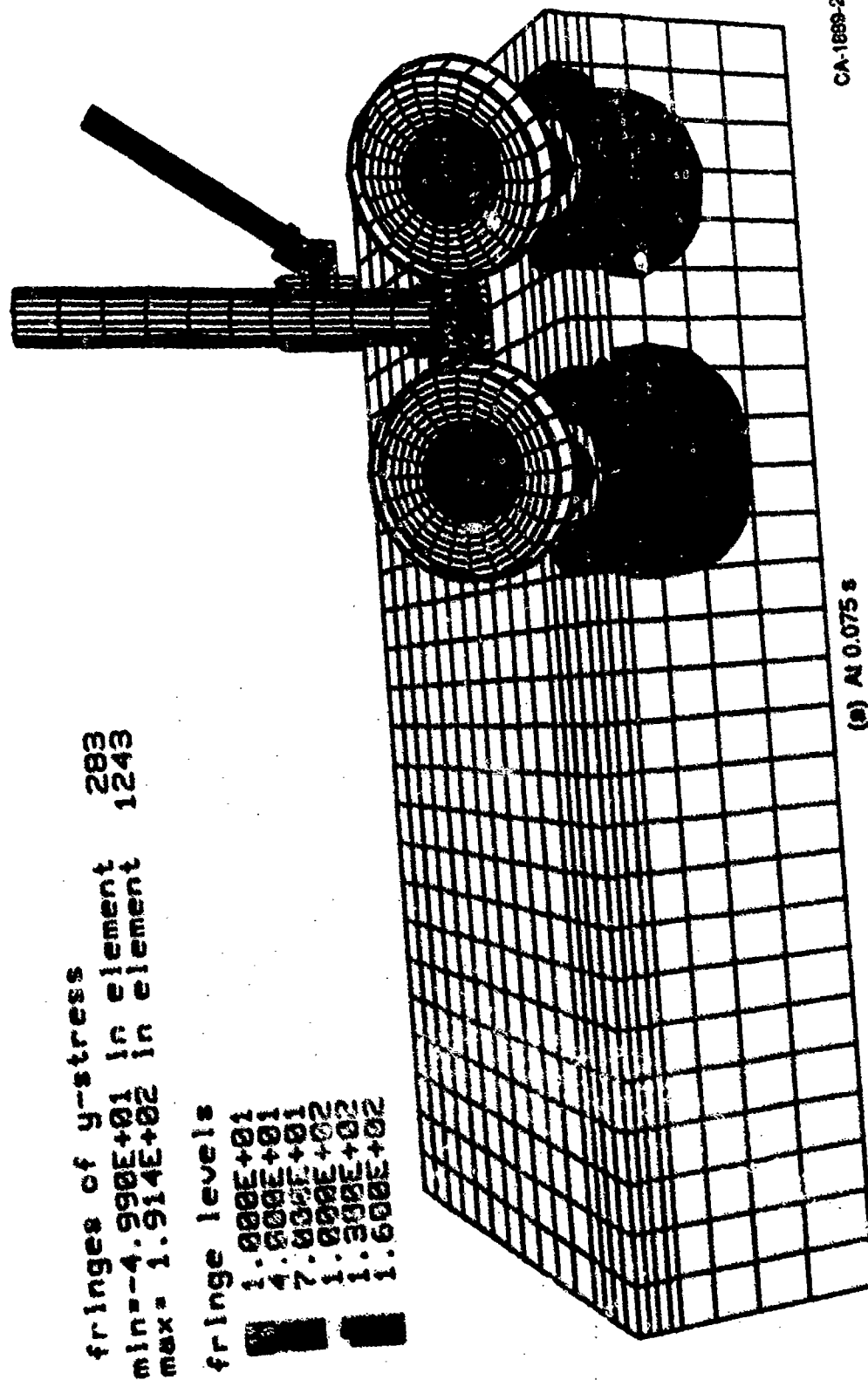


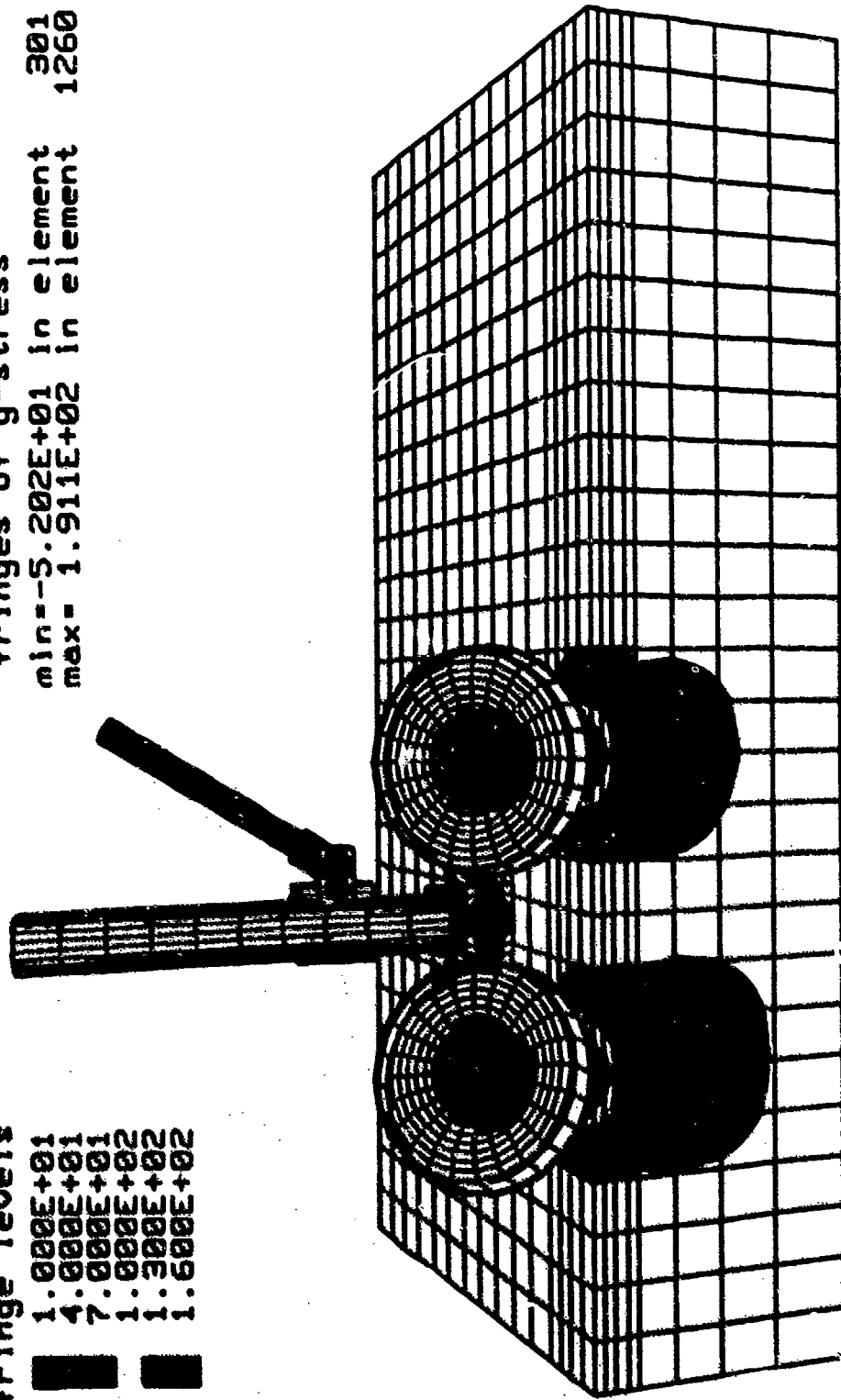
Figure 4-2a. Vertical Stress Contours under the Landing Gear

fringe levels

■	1.000E+01
■	4.000E+01
■	7.000E+01
■	1.000E+02
■	1.300E+02
■	1.600E+02

fringes of y-stress

min=-5.202E+01	in element	301
max= 1.911E+02	in element	1260



(b) At 0.15 s

CA-1889-1

Figure 4-2b. Vertical Stress Contours under the Landing Gear
(continued)

Figure 4-3 shows contours of tensile x-stresses (horizontal in the direction of travel, caused by bending in the pavement) at $t = 0.15$ s. The maximum x-stresses are about 180 psi located on the lower surface of the pavement directly under the wheels. These stresses are high enough to produce some cracking damage on the vertical planes. Higher tensile stresses were computed in the z-direction (horizontal, normal to the direction of travel), so the crack growth is larger at the base of the slab on vertical planes along the direction of motion.

The contour plot in Figure 4-4 shows the accumulation of cracking damage τ_F at time $t = 0.15$ s. This damage parameter represents the sum of damage on all planes. The view in Figure 4-4 is looking up at the lower surface of the pavement where the damage is the greatest. The passage of the first wheel causes an increment of damage of about 3×10^{-7} and the passage of the second wheel increases the damage to about 6×10^{-7} .

4.2.2 Estimate of Fatigue Life from Single Cycle Calculation

Using the value of 6×10^{-7} for $d\tau_F/dN$ obtained from the finite element calculation, we can make an estimate of fatigue life, that is, the number of loadings required to cause complete fracture of some portion of the pavement. Using the other parameters in Table A-1 of Appendix A, we can determine $da/dN = dR/dN = 3.12 \times 10^{-5}$ cm/cycle and predict a lifetime of 14,700 loadings from Eq. (32) of Appendix A.

4.2.3 Calculation Time

Our model contained about 8000 elements and took 13,100 time steps. The calculation required about 16 hours CPU on a SUN SPARC station 2 with 18 Mbytes of memory. SUN representatives claim that the 1992 SPARC station will perform about 6 times faster than the current model (about 160 MIPS compared to 26 MIPS) and expect that future improvements will increase speed by a factor of about 5 to 6 every year for the foreseeable future. This calculation may have been faster using the implicit code NIKE3D, but we have not yet implemented the pavement routine in that code.

4.2.4 Summary of Demonstration Calculation

The preceding development verifies that our approach to fatigue life prediction can be implemented and yields realistic values for pavement lifetimes. Many aspects of the model and its use are still in the early stage of development, yet the complete path from determination of

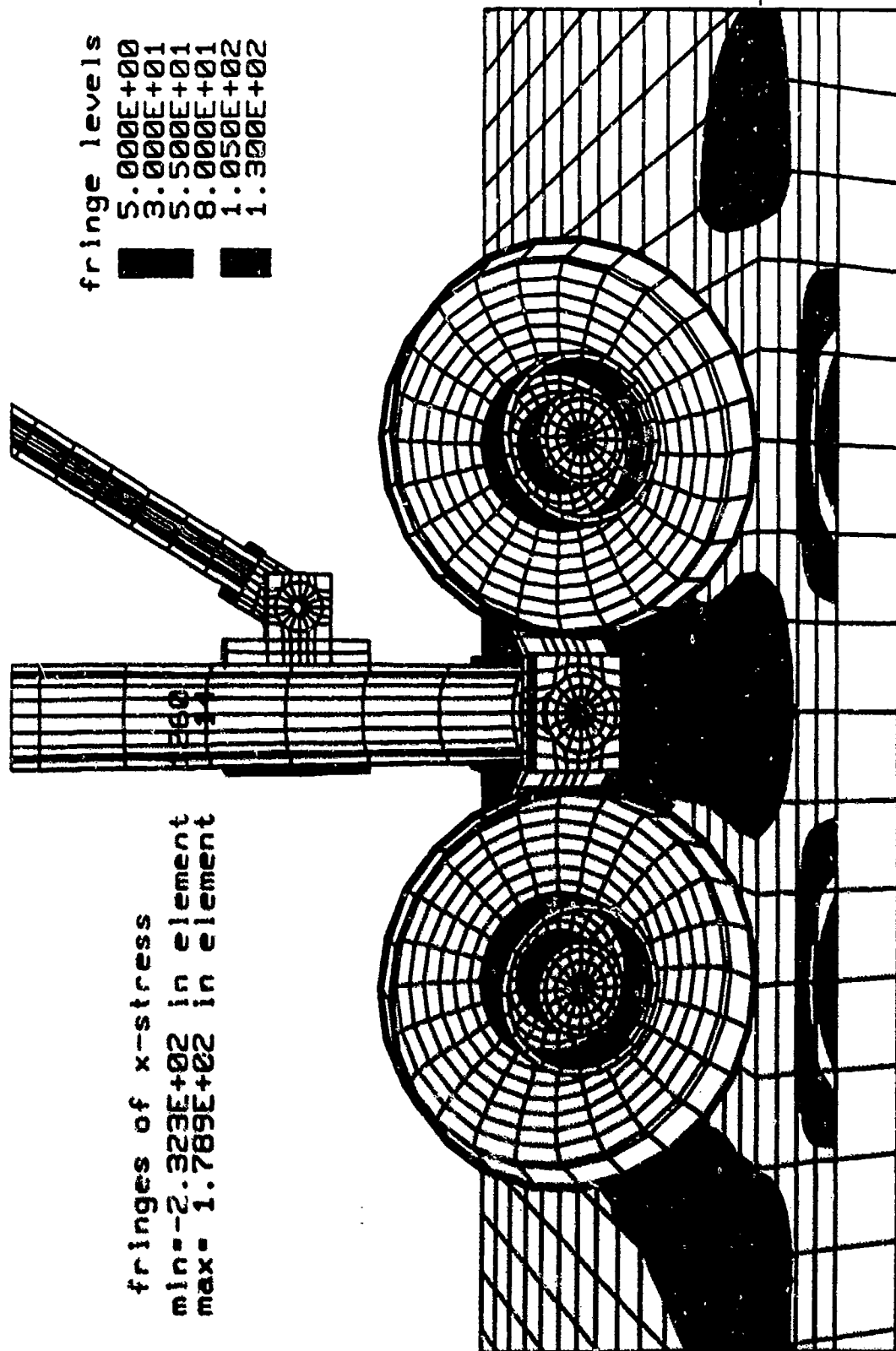
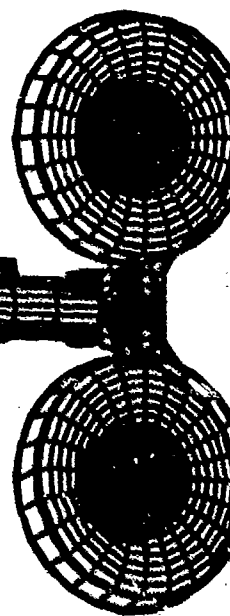


Figure 4-3. Horizontal Tensile Stress Contours under the Landing Gear at 0.15 s.

fringes of damage
 min= 0.000E+00 in ele
 max= 8.329E-07 in ele

7976
 12

fringe levels
 1.000E-09
 1.458E-07
 2.906E-07
 4.354E-07
 5.802E-07
 7.250E-07



CA-1889-23

Figure 4-4. Contours of Fatigue Damage on the Cut Vertical Section and Bottom Surface of the Concrete Slab as seen from under the Slab at 0.15

s.

properties to prediction of lifetime has been made. The constitutive fatigue model appears to represent laboratory and field data acceptably and is based on the known mechanisms of cracking. The model has been incorporated into a three-dimensional finite element code, and simulations of aircraft loading have been made. A method was developed to take the damage from a single loading (or several loadings) and to predict the lifetime of the pavement.

5. Rutting Model

Rutting refers to the permanent deformation that gradually develops in asphalt concrete pavements through the repeated passage of tires over the surface. Many factors are associated with the ruts, including the combination of loading, thermal effects, fatigue cracking, and moisture in the pavement. The ruts probably occur through the gradual massaging of the aggregate particles into different configurations. Rutting deformation is probably contributed to by the surface, base, and/or *in situ* soil layers. Very small deformations (microstrains) during each tire passage causes significant deformation after thousands or hundreds of thousands of loading cycles. Our purpose here was to develop a constitutive model representing the material behavior that leads to rutting. The model is written as a subroutine for use in finite element simulations so that we can account in detail for the loading as well as for thermal, fatigue, and moisture effects.

To develop the material model, we began by examining a variety of laboratory data and then constructed a model based on these data. Here we first review some of these data, emphasizing those aspects of the material behavior that lead to permanent deformation. Then we review the available types of material models that can represent these behaviors. Finally, we propose a model that matches well the measured behavior.

5.1 Data on Deformation of Asphalt Concrete

There is a wealth of data on asphalt concrete. Here we wish to present only a brief sample to indicate the nature of the stress-strain relations for asphalt concrete, especially those aspects that may contribute to rutting. Temperature and moisture effects are important for determining the response of asphalt concrete, but we have omitted these effects here for simplicity. In later work, we will account for these effects by using temperature- and moisture-dependent material properties.

Under standard triaxial compression testing, asphalt concrete shows a strain-rate-dependent stiffness. A similar rate dependence occurs under shear loading. This rate-dependent deformation is mainly recoverable, that is, elastic. Over the range of strain rates from 0.0002/s to 0.02/s, there is a five-fold increase in stiffness.

When the material is sheared, it expands, or if the sample is confined axially, the axial stress rises. This dilatant effect is also strongly rate dependent: there is a five-fold increase in the

axial stress amplitude for a 100-fold increase in the shear strain rate. Because of these five-fold changes, the time dependence cannot be neglected without sacrificing accuracy. These data are more fully presented in Appendix C.

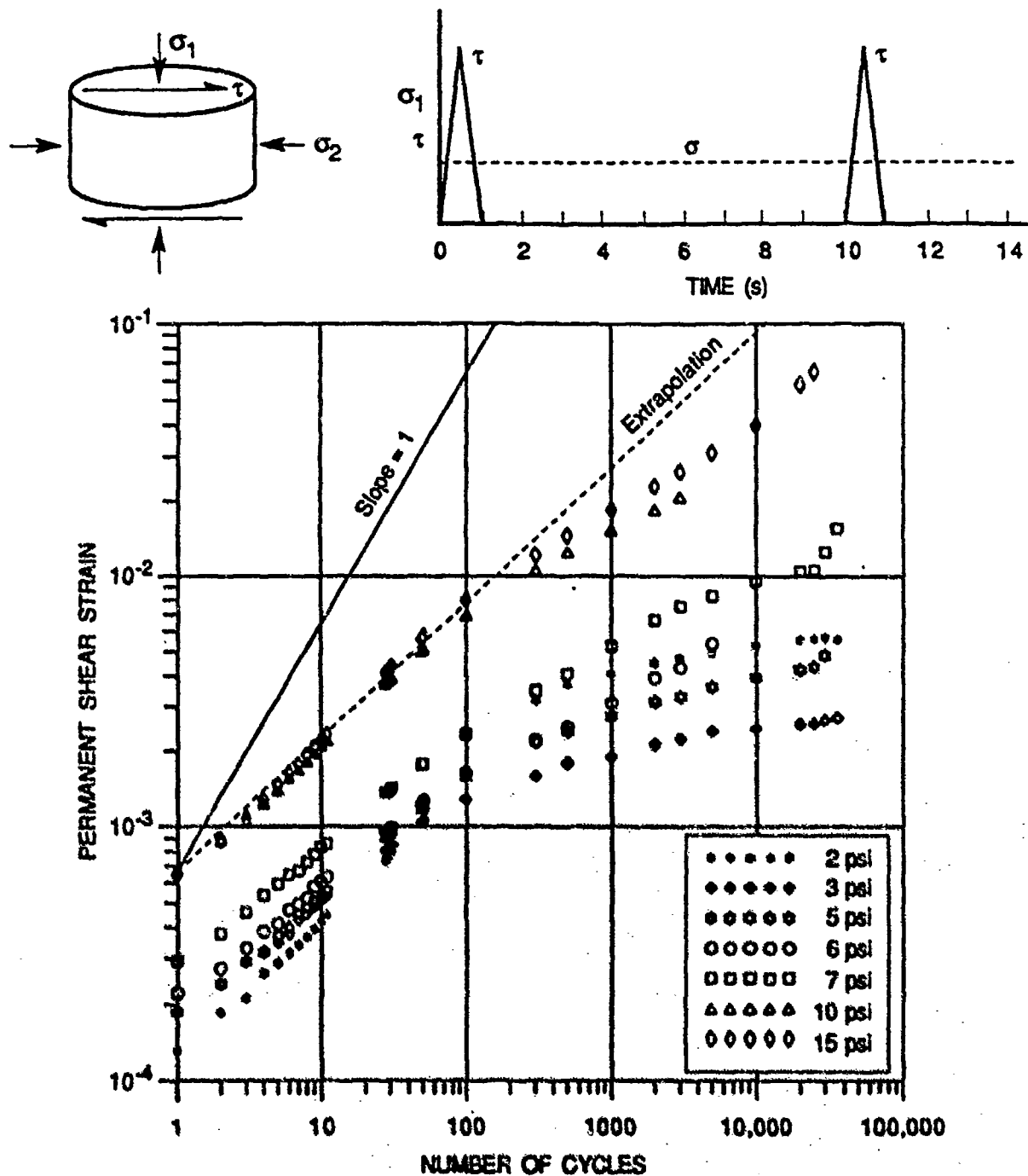
In addition to these viscoelastic deformations are permanent deformations that develop gradually during cyclic loading. The experimental data in Figure 5-1 show how permanent deformation varies with loading cycle for several stress levels. The inset shows the general test setup with a constant axial load and a time-varying shear load. Note that the initial loading cycles lead to larger increments of permanent deformation than later ones, yet there is never a cessation of permanent deformation. If each cycle contributed the same amount, then the curves would all have a slope of 1 in the log-log plots. The amount of deformation depends on the stress level, but not linearly so (this fact is not obvious from the graph). From our reviews, it appears that permanent deformation depends on stress to the first or second power.

We believe that the permanent deformation observed in this shear test is directly related to the rutting deformation obtained under wheel loads. Hence, we could see the ordinate in Figure 9 as rut depth versus an abscissa of wheel load applications. When we see it this way, we can relate a serious rut depth to some amount of permanent deformation, say 10 percent. Then we note that the curve for 15 psi would strike the 10 percent permanent deformation level at about 100,000 cycles. If we had merely extrapolated from the initial slope of the curve, we would have reached 15,000 cycles, a very poor estimate. If we had assumed that the deformation is the same on each loading cycle, we would have followed the line with a slope of 1 and predicted 200 cycles. Hence, we see that the prediction of the number of loading cycles to reach a critical rut depth is very sensitive to the shape of the curve of permanent deformation versus loading cycles.

We realize that the pressure and shear stress levels used in the foregoing studies are not representative of the levels of interest in aircraft pavement; however, we feel that the general character of the asphalt response is similar at the higher stress levels.

5.2 Review of Possible Models for Rutting in Asphalt Concrete

The foregoing review of the data in asphalt concrete shows that asphalt exhibits important viscoelastic, dilatant, and permanent deformation behavior. Of these three aspects, the permanent deformation is probably most closely associated with rutting. Here we examine the range of usual models for materials to determine their applicability for use on the present problem.



GAM-1889-5

Figure 5-1. Accumulation of Permanent Deformation as a Function of Loading Cycle under Repetitive Shear Stresses (Axial Stress is 5 psi)

The *rate-dependent properties in shear* (from axial and shear loadings) appear to fit the behavior of viscoelastic models. The standard linear viscoelastic model does not have sufficient flexibility to fit the data, but a multiple-variable version does, as outlined in Appendix D.

The *dilatant properties* probably arise from the relative motion of aggregates in the asphalt concrete. The data show that axial stresses arise for applied shear stresses in either direction. The behavior is unusual for three reasons:

1. Normal stress arises from shear stress for stress levels in which the strains are essentially fully recoverable; that is, this is not plastic behavior.
2. The relationship between normal and shear stress is strongly viscoelastic.
3. The normal stress depends on the magnitude of the shear stress, but not on its direction or sign.

This combination of behavior is very difficult to approximate with any of the usual models. Here we mention some models that may be applicable to some aspects of the asphalt response. Linear viscoelastic models, such as the multiple-variable linear viscoelastic model of Appendix D, describe the correct rate dependence. The dilatant behavior can be represented by a modification of the reference density for thermoelastic surfaces, a standard feature of SRI's porous material models. The relation of pressure to the absolute value of shear presents a dilemma: axial stress is proportional to $|t|$ according to the data, not to τ^2 as required by nonlinear isotropic models. Also in such isotropic models, pressure must also lead to shear stress according to reciprocity, but we do not feel that such a shear stress arises from axial loading. The dilemma is solved in Appendix C by proposing that the shear-axial stress relation be exercised only on a selected set of planes in the material. So the behavior is treated with a multiple-plane plasticity model, but operates in the elastic range. The current magnitude and orientation of the shear stress is stored to account for the special relation between axial stress and shear stress. This procedure appears to provide an accurate mechanism for representing dilatancy in asphalt concrete.

The most important feature of the behavior of asphalt concrete for rutting is its *permanent deformation under shear stress*. Here we review the response of available models to explore what model types could be used. Features of especial importance here are the stress dependence and the tendency to build up permanent deformation under each loading cycle, but at a decreasing rate.

Standard Mises, Mohr-Coulomb, Tresca, and cap models are rate-independent; hence, yielding occurs at a predetermined stress condition. These models have the result that there is no

plastic flow until a critical stress is reached; then for larger stresses, the permanent deformation is very large. Hence this model type cannot represent the stress-dependence observed.

When work hardening is added to these models, we obtain permanent deformation that can depend in an arbitrary way on the stress level. However, these models accumulate permanent deformation only on the first cycle: thereafter, no further yielding occurs because the yield curve is no longer exceeded. These models would lead to a horizontal line (not shown) in Figure 5-1 at the level of the permanent deformation reached on the first cycle.

Viscoelastic models may be able to represent some features of the permanent deformation. If we choose, for example, a model with one or more Maxwell elements (a spring and dashpot in series) in parallel (as in Figure D-1 of Appendix D, but without the G_0 spring), then permanent deformation occurs on each cycle. For such a model, the deformation is proportional to the stress level: the proportionality is not like that observed, but at least there is a stress dependence. The same amount of deformation occurs on each loading cycle, so the predicted response is that shown in Figure 5-2. Clearly, we can choose model parameters to fit fairly well for the first few loading cycles, but the correspondence deteriorates for later loading. This type of model, while attractive for representing the permanent deformation, has no static modulus and therefore must be severely limited in its ability to represent a full range of loading rates on the asphalt concrete. Therefore, we have not considered this type of viscoelastic model further.

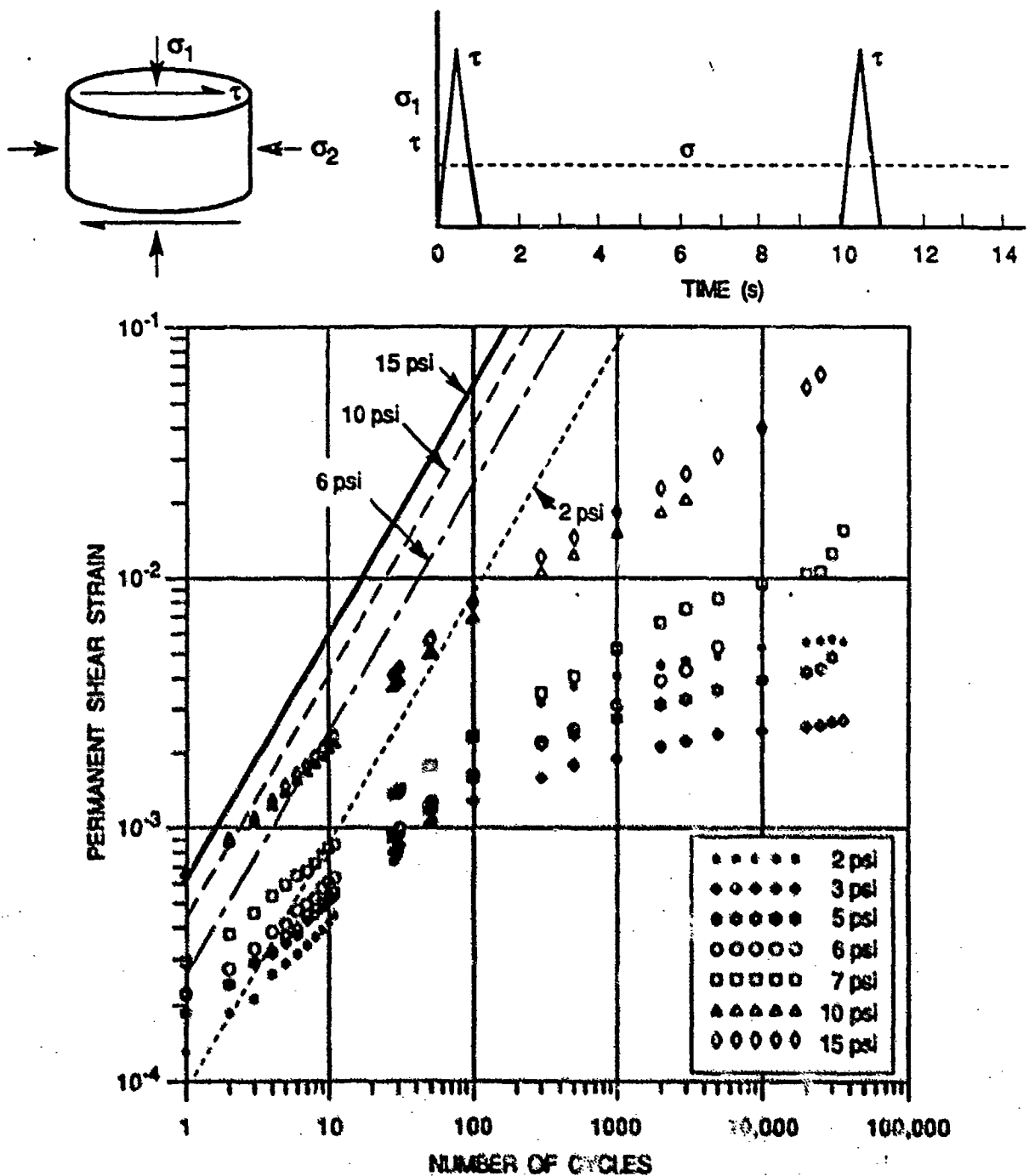
Viscoelastic models such as the multiple-variable model in Appendix C have a minimum modulus even at low loading rates. Therefore, they do not build up any permanent deformation and cannot be used to represent this aspect of the behavior of asphalt concrete.

Creep and viscoplastic models represent another possible approach. The basic differential equation for the unified creep-plasticity model developed by Krieg [15] is

$$\frac{d\sigma}{dt} = 3G \frac{d\epsilon}{dt} - 3G \left(\frac{\sigma}{k} \right)^n \quad (7)$$

in which the plastic strain rate is given by

$$\frac{d\epsilon^p}{dt} = \left(\frac{\sigma}{k} \right)^n \quad (8)$$



CAU-1888-6

Figure 5-2. Cumulative Permanent Deformation as a Function of Loading Cycle under Repetitive Shear Stresses and Comparisons with Predictions of Viscoelastic Models

The quantities σ and ϵ are the equivalent stress and strain, t is time, G is the shear modulus, ϵ^P is the plastic or permanent strain, and k and n are material constants. This type of model represents both creep and rate-dependent yield behavior in metals and other materials. A typical set of response curves is shown in Figure 5-3. The apparent yield level is

$$\sigma_{ss} = k \left(\frac{d\epsilon^P}{dt} \right)^{1/n} \quad (9)$$

where σ_{ss} is the steady-state value, which clearly depends on the strain rate. At stresses well below yielding, the curve appears as a work-hardening curve that is strongly stress dependent. The location of the curve depends on the loading rate. By adjusting n in Equation (7), we can control the stress dependence of the permanent deformation. Hence, many features of this model fit the observed data. However, in this model, each loading to a given stress provides the same increment of permanent deformation. Hence, again we obtain the kind of results seen in Figure 5-2.

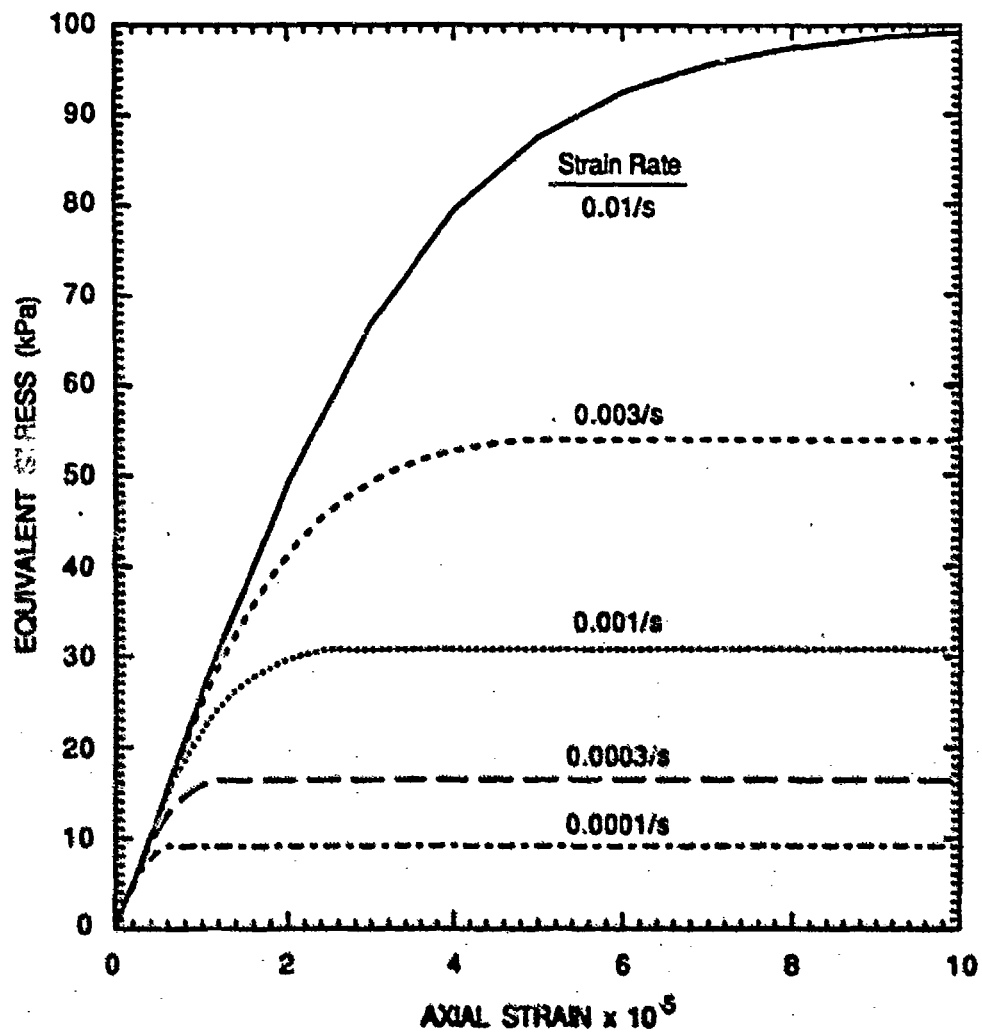
5.3 SRI Rutting Model

To build a model that can represent the observed permanent deformation behavior of asphalt concrete, we started with the creep-plasticity model above. We recognized that, to match the data, the apparent value of k must increase gradually with repeated loading. We selected residual deformation as our indicator to gradually alter the material's acceptance of further permanent deformation. We incorporated this change in behavior through a change in k in the model:

$$k = k_0 + k_1 \epsilon^P \quad (10)$$

where k_0 and k_1 are new material constants with the units of stress \times (time)^{1/n}. With this form, and the values of 0.47 and 100 MPa \sqrt{s} and $n = 2$, we generated the curves for 2 and 15 psi shown in Figure 5-4. Clearly we are only approximating the measured rate of permanent deformation, but the match is fairly good.

The foregoing discussion of models shows the general nature of the model required to represent the viscoelastic, dilatant, and permanent deformation characteristics of asphalt concrete. Further information on the model we have developed is given in Appendix C.

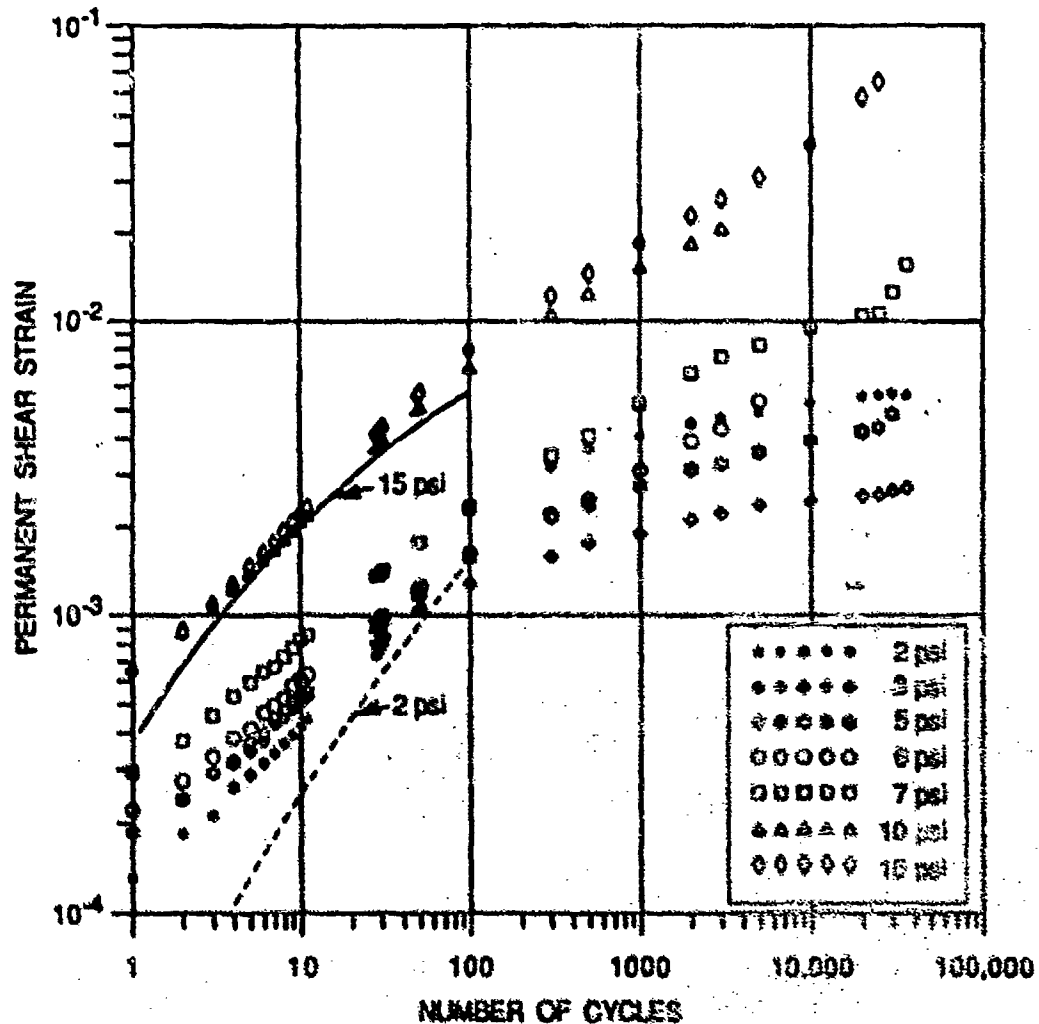


CAM-1880-7

Figure 5-3. Stresses from Constant-Strain-Rate Loadings for the Unified Creep-Plasticity Model

Unified Creep-Viscoplastic Model

$$\frac{d\bar{\epsilon}^P}{dt} = \left(\frac{\bar{\sigma}}{K} \right)^n \text{ with } k = k_0 + k_1 \bar{\epsilon}^P$$



CM-1989-8

Figure 5-4. Cumulative Permanent Deformation as a Function of Loading Cycle under Repetitive Shear Stresses and Comparisons with Predictions of the SRI Creep-Viscoplastic Model

6. Recommendations

Because of the feasibility shown in this initial project, we are recommending continuation of the effort to develop a mechanistic design procedure for pavements. In addition to the topics dealt with in this report are two other concerns: we need a model to treat the response of the granular subgrade materials, and we need to examine the nature of the distress experienced in the field. Below we describe these two concerns and then present detailed recommendations for improvements in each aspect of the work.

6.1 Subgrade Model

The porous granular materials that form the subgrade and underlying soils are not well represented by the elastic model or other models currently available. Yet much of the distress observed may be traceable to the behavior of these granular materials. As with the pavement materials, we expect that the response is mainly elastic, but with some small component of slipping between particles and particle rearrangement. Such behavior is not treated by standard plasticity models, which are representing gross flow of the material, as in the failure of an embankment. Here in the subgrade, there must be very small inelastic strains on each loading, which gradually allow for excessive settlement. Such behavior must be treated in our computational approach.

6.2 Field Observation of Distress

So far we have emphasized fatigue cracking and rutting as the primary distress factors, and these are probably among the dominant factors and certainly the factors that must be treated. However, the designer must handle a great list of distress factors, and only some of them appear to be associated with cracking and rutting. Some of these observed distress types result from combinations of cracking, rutting, and settlement of the subgrade. For example, for what is termed rutting (inelastic deformation in the pavement), the settlement of the subgrade may initiate formation of a groove in the pavement layer. The change in geometry of the pavement leads to cracking at the base of the pavement. This loss of stiffness due to cracking in the pavement leads to inelastic deformation in the pavement layer. Hence, all three of these factors contribute to the observed distress. Therefore, to make certain that we are indeed treating the appropriate distress modes, we should have a small parallel effort to examine field distress conditions. At this stage the examination can be qualitative, to evaluate the sequence of events and the nature of the causes of

distress. The effort could consist of taking a few cores of distressed areas of pavements and making a few tests of the cored materials in the laboratory.

In addition to the two concerns described above, we recommend tasks on the following topics.

6.3 Lifetime Prediction

A method should be developed for predicting the lifetime of pavement materials, considering rutting and fatigue distress, and the method should be verified through comparisons with laboratory data. The method described in this report, combining finite element simulations with analytical extrapolations, can serve as a starting point. Where possible, the extrapolations should be based on analytical treatments of the underlying mechanisms.

6.4 Fatigue Model

The present constitutive fatigue model has been developed to the point of showing how to combine finite element computations with a detailed representation of damage. The next step should be to make the model more quantitative by determining model parameters for representative pavements. These determinations can be made with both field and laboratory data. These initial parameters can be the first elements of a data base of fatigue data for regular use with the finite element calculations in routine design operations.

6.5 Rutting Model

A full three-dimensional computer subroutine should be constructed to combine the deformation features of asphalt concrete that affect rutting: viscoelastic, dilatant, and viscoplastic. This model should be incorporated into a finite element code such as DYNA3D and simulations made of rutting experiments under actual wheel loads. These steps will constitute a full verification of our modeling approach and our selection of the shear test data as representing the essential material behavior that controls rutting. Following these steps are a series of combined experimental and computational steps to:

- a. Determine the appropriate stress states for use in the laboratory tests (those that most closely approximate critical field conditions).
- b. Measure asphalt properties over the appropriate loading rate ranges.
- c. Fit the rutting model parameters to the data.
- d. Test and fit to a variety of data to establish a data base of fitted model parameters and to facilitate later determination of model parameters for a new asphalt concrete.

6.6 Model for Granular Subgrade

A material constitutive model for granular subgrade materials should be developed to represent settlement and other inelastic deformation that can lead to pavement distress. The model should emphasize the very small inelastic processes that occur in the material at stresses well below yield stress levels. This model should then be incorporated into a finite element code, and finite element simulations should be performed to verify the model by comparison with laboratory test data.

6.7 Finite Element Code

The pre- and post-processors now connected with DYNA3D and NIKE3D are very satisfactory for our research work. However, we should add routines to further simplify the designer's task. For example, the pre-processor should permit the full layout of the landing gear from very little input (aircraft type and loading, for example). Similarly, the post-processor should be amplified to provide the summary information required by the designer as well as contour plots, such as in Figures 3-1, 4-2 (a) and (b), 4-3, and 4-4, with very little instruction from the user. This task includes the determination of appropriate boundary conditions and element sizes for static and rolling loads.

6.8 Field Studies

A small field effort should be undertaken to examine field distress conditions to determine the sequence and importance of the cracking, inelastic deformation, and other factors that

contribute to the damage. These results will aid in determining the emphasis of the theoretical modeling and the laboratory work.

7. References

1. C. Ouyang, B. Mobasher, and S. P. Shah, "Fracture Response of Cement Matrices Reinforced with High Volume Fiber Fraction," presented at ASCE conference, Mechanics Computing in 1990s and Beyond, Columbus, Ohio, May 20-22, 1991, pages 1066-1070.
2. John Prendergast, "Anatomy of Asphalt," Civil Engineering, Vol. 61, Number 7, July 1991, published by American Society of Civil Engineers, New York, pages 56-59.
3. C. L. Monismith, R. G. Hicks, and F. N. Finn, "Performance Related Testing and Measuring of Asphalt-Aggregate Interactions and Mixtures," Quarterly Report on SHRP Project A-003A, January 1 to March 31, 1991 (April 1991).
4. J. O. Hallquist and R. G. Whirley, "DYNA3D User's Manual (Nonlinear DYnamic Analysis of Structures in Three Dimensions)," University of California, Lawrence Livermore National Laboratory, Report UCID-19592 (1989).
5. J. O. Hallquist, "NIKE3D: An Implicit, Finite Deformation, Finite Element Code for Analyzing the Static and Dynamic Response of Three-Dimensional Solids," University of California, Lawrence Livermore National Laboratory, Report UCID-18822 (1984).
6. B. S. Holmes, S. W. Kirkpatrick, and J. K. Gran, "Structural Response of Solid-Fueled Booster Motor and Interstage Structures," SRI Final Report PYU-5659, Contract DNA 001-88-C-0047 (June 1990).
7. J. W. Simons, J. D. Colton, and A. L. Florence, "Laboratory Testing of Scale-Model Intersections," Proceedings of the First International Workshop on Scale Effects in Rock Masses, Loen, Norway (June 1990).
8. C. G. Schmidt, J. W. Simons, S. W. Kirkpatrick, and D. C. Erlich, "Solder Joint Integrity Multiclient Program," Second Semiannual Report, SRI Project 7908 (November 1990).
9. J. H. Giovanola, R. W. Klopp, J. W. Simons, and A. H. Marchand, "Investigation of the Fracture Behavior of Scaled HT-130 Steel Weldments," SRI Final Report PYU-2612, Naval Surface Warfare Center, Contract No. N60921-86-C-0253 (June 1990).
10. C. G. Schmidt, "A Study of the Effects of Ice on Asphalt Pavements," in preparation (July 1991).

11. P. R. Gefken and J. W. Simons, "Using the RESCUE Technique to Investigate the Soil-Structure Interaction for a Nuclear Reactor," Trans. of the 10th International Conference on Structural Mechanics in Reactor Technology, August 1989, Anaheim, California.
12. S.C.S. Rao Tangella, J. Craus, J. A. Deacon, and C. L. Monismith, "Summary Report on Fatigue Response of Asphalt Mixtures," Final Report TM-UCB-A-003A-89-3 by the Institute of Transportation Studies of the University of California at Berkeley, for Strategic Highway Research Program (February 1990).
13. P. C. Paris, "The Growth of Fatigue Cracks due to Variations in Load," Ph.D. Thesis, Lehigh University (1962).
14. P. C. Paris, M. P. Gomez, and W. E. Anderson, "A Rational Analytic Theory of Fatigue," *The Trend in Engineering*, Vol. 13, pages 9-14, 1961.
15. R. D. Krieg, "Numerical Integration of Some New Unified Plasticity-Creep Formulations," Transactions of the 4th International Conference on Structural Mechanics in Reactor Technology, Volume M, T. A. Jaeger and B. A. Boley, Eds. (August 1977).

8. List of Symbols

μ	=	Poisson's ratio
E	=	Young's Modulus
σ	=	stress
σ_{cr}	=	critical stress used in linear elastic fracture mechanics
a	=	radius of flaw; crack length
K_{IC}	=	critical fracture toughness for mode I cracking
J_{IC}	=	critical J-integral value for mode I cracking
N	=	number of cycles
A, B, n, f	=	constants
τ_F	=	crack damage due to fatigue
ϵ_c	=	crack opening strain
g, n, β	=	dimensionless constants
a_0	=	initial flaw size, initial crack length
t	=	time
T	=	period of loading in Haversine stress function
R	=	radius of crack
ϵ^p	=	plastic strain
G	=	shear modulus
k, n	=	material constants
ϵ	=	equivalent strain
σ	=	equivalent stress
σ_{ss}	=	steady state value of stress
k_0, k_1	=	material constants

Constants in Appendices

ϕ_k	=	orientation of crack
J_k	=	density of crack per unit volume
R_k	=	radius of crack
T_f	=	constant
δ	=	half crack opening

V_{1c}	= crack volume
$\Delta\epsilon$	= imposed change in strain
$\Delta\epsilon_s$	= change in solid strain
L	= longitudinal modulus
K	= bulk modulus
G	= shear modulus
L_{app}	= apparent secant modulus
B, m	= constants
P	= Pressure
L, D, S	= constants defining hydrostatic pressure-volume curve
M	= volumetric strain
ρ	= density
ρ_o	= initial density
Γ	= Grüneisen ratio
E	= internal energy
D_{js}	= dilatant moduli
G_n, μ_n	= spring and dashpot factors for nth Maxwell element
ρ_{so}	= initial density
ρ_{oi}	= density representing current porosity
ϵ_d	= dilatant strain
S	= deviator stress tensor

9. Appendix A

Theoretical Development of a Model for Fatigue

A model for fatigue has been developed to represent the observed damage to pavement. The new fatigue model is constructed for use in finite element codes as part of the general constitutive relation for pavement materials. Thus it is an adjunct to the usual determination of the stress from the strain at each increment of loading. It differs markedly from earlier fatigue models, which were designed to represent damage over a complete loading cycle. Here, because of the nonlinearities of the loading and response, several loading increments may occur during each loading cycle. Therefore, the new model was written to treat the damage that can occur during any increment of loading.

Here we present the usual forms for pavement damage results and a proposed form for the finite element model. Then we derive a relation between them such that the finite element model parameters can be obtained from the pavement damage data.

A.1 Pavement Damage Observations

The pavement damage observations are made by passing a number of aircraft or trucks over the pavement section and observing the development of cracking. Thus the "damage" here refers to some level of cracking, probably the presence of large cracks that have grown from the bottom of the pavement slab to the top. Observations of this type are then collected for a range of slab thicknesses (different thicknesses provide different stress levels under a given wheel load) and represented by an equation of the form:

$$N = A \left(\frac{f}{\sigma} \right)^n \quad (\text{A-1})$$

where N is the number of cycles to damage, σ is the peak tensile stress at the base of the slab during a loading cycle, and A , f , and n are constants. This equation, which will be called the *pavement damage model*, defines a curve corresponding to some (undefined) damage level. We could expect that lines corresponding to lesser damage would be parallel and below this line; hence, they would correspond with smaller A values.

A.2 Growth of Fatigue Damage in the Finite Element Calculations

The fatigue damage is presumed to exist in the material in the form of microcracks distributed with a range of sizes, locations, and orientations. In each orientation ϕ_k we will have a density of cracks J_k per unit volume. For simplicity, we will consider only one crack size with radius R_k , rather than a distribution of sizes; that is, we expect that only the largest sizes will grow and become important. In the following derivation, we consider only one orientation at a time so we drop the subscript k .

The level of damage at any time will be represented by the quantity τ defined as

$$\tau_F = T_F J R^3 \quad (\text{A-2})$$

where T_F is a constant on the order of 1, J is the number of cracks per unit volume, and R is the crack radius. In other works on fracture,¹ we have found that, with this definition, τ is proportional to the fragmented fraction of the solid. Thus we define T_F such that $\tau = 1$ means full fragmentation. On this scale, $\tau = 0.001$ is barely observable damage and $\tau = 0.1$ is serious damage.

When a tensile loading is applied, the cracks open in proportion to the stress normal to their plane. The opening displacement and volume are

$$\delta = \frac{4(1 - \nu^2)}{\pi E} R \sigma \quad (\text{half crack opening}) \quad (\text{A-3})$$

$$V_{1c} = \frac{16(1 - \nu^2)}{3E} R^3 \sigma \quad (\text{crack volume}) \quad (\text{A-4})$$

where E and ν are Young's modulus and Poisson's ratio, R is the crack radius, and σ is the stress normal to the plane of the crack. The crack opening strain is defined as the sum of the crack volumes for all the cracks:

$$\epsilon_c = \frac{16(1 - \nu^2)}{3E} J R^3 \sigma = \frac{T_c}{E} \tau \sigma \quad (\text{A-5})$$

where

¹D. R. Curran, L. Seaman, and D. A. Shockey, "Dynamic Failure of Solids," *Physics Reports* 147, 253-388 (March 1987).

$$\tau = J R^3 \text{ and } T_c = \frac{16(1-\nu^2)}{3} \quad (\text{A-6})$$

If the applied tensile stress exceeds the critical stress corresponding to K_{Ic} , the crack grows to a new equilibrium size. This critical stress for a penny-shaped crack is

$$\sigma_{cr} = \frac{K_{Ic}}{2} \sqrt{\frac{\pi}{R}} \quad (\text{A-7})$$

where K_{Ic} is the fracture toughness from linear elastic fracture mechanics. Then the crack grows to the point at which the imposed $\Delta\epsilon$ is fully taken by the change in solid strain $\Delta\epsilon_s$ and the change in crack opening strain $\Delta\epsilon_c$. That is,

$$\Delta\epsilon = \Delta\epsilon_s + \Delta\epsilon_c \quad (\text{A-8})$$

The change in solid strain is determined by the longitudinal modulus $L = K + 4G/3$ (K and G are the bulk and shear moduli):

$$\Delta\epsilon_s = \frac{\Delta\sigma}{L} = \frac{\sigma_2 - \sigma_1}{L} \quad (\text{A-9})$$

where $\Delta\sigma$ is the change in the normal stress from the previous state (A-1) to the current state (A-2). The crack opening strain for J cracks per unit volume is derived using the volume of a single crack in Eq. (A-4).

$$\Delta\epsilon_c = \frac{16(1-\nu^2) J}{3E} (R_2^3 \sigma_2 - R_1^3 \sigma_1) \quad (\text{A-10})$$

The combination of Eqs. (A-7) through (A-10) provides the means for determining the new stress σ_2 and the new crack size R_2 .

The apparent secant modulus L_{app} is obtained from the ratio σ_2/ϵ_2 .

$$L_{app} = \frac{\sigma_2}{\epsilon_2} = \frac{\sigma_2}{\epsilon_{2s} + \epsilon_{2c}} = \frac{\sigma_2}{\frac{\sigma_2}{L} + \frac{T_c \epsilon_2 \sigma_2}{E}} = \frac{L}{1 + \frac{L}{E} T_c \epsilon} \quad (\text{A-11})$$

The preceding relations all represent standard procedures.

Now we present a relation for the fatigue growth process. The cracks grow while the normal stress is tensile yet below the critical stress level for rapid growth. We assume that inelastic strains are occurring at the crack tip at all stress levels. During repeated loadings, these inelastic strains lead to gradual growth of the crack during each loading cycle. A general discussion of such mechanisms in metals and ceramics has been given by Ritchie.² The growth expression must be appropriate for the finite element situation in which the strain (or stress) is being imposed in small increments so that even a single loading cycle might be imposed in ten or more steps. Hence, the expression should contain a term related to the strain increment size $\Delta\epsilon$ or $\Delta\epsilon_c$. The growth also increases in relation to the stress level σ . In addition, we want an expression that will be integrable later. Therefore, we propose the following form for the increase in crack damage τ_F in the *constitutive fatigue model*:

$$\Delta\tau_F = g\Delta\epsilon_c \sqrt{\frac{R_0}{R}} \left(\frac{\sigma}{\sigma_{cr}}\right)^\beta \quad (A-12)$$

where g and β are dimensionless constants and σ_{cr} is from Eq. (A-7). The $\sqrt{R_0/R}$ term was added to aid in matching this equation to Eq. (A-1) later. By using Eq. (A-2), we can relate the growth of damage τ_F to the increase in the crack radius R :

$$dR = \frac{d\tau_F}{3\tau_F JR^2} \quad \text{or} \quad \frac{dR}{R} = \frac{d\tau_F}{3\tau_F}$$

Therefore,

$$\Delta R = \frac{g\Delta\epsilon_c}{3\tau_F JR^2} \sqrt{\frac{R_0}{R}} \left(\frac{\sigma}{\sigma_{cr}}\right)^\beta \quad (A-13)$$

Expression (A-13) is suitable for incorporation into a constitutive model for use in a finite element code. Then at each cycle, the cracks in tensile orientations are grown by a small amount proportional to the loading increment.

The next step is to relate the parameters in Eq. (A-13) to those in Eq. (A-1) representing the observations of pavement damage.

²R. O. Ritchie, "Mechanisms of Fatigue Crack Propagation in Metals, Ceramics, and Composites: Role of Crack Tip Shielding," *Materials Science and Engineering A* 103, 15-28 (1988).

A.3 Relating the Fatigue Model to Observed Damage

To relate the fatigue crack growth process to the observed pavement damage, we introduce an alternative and commonly used fatigue damage equation. This equation is intermediate between the pavement damage and constitutive models in its level of detail about the fracture process. Therefore, we can relate this *standard fatigue model* to both the pavement relation and to the constitutive model.

$$\frac{dR}{dN} = B \left(\frac{K_I}{K_{Ic}} \right)^m \quad (A-14)$$

Here B and m are constants, K_{Ic} is the fracture toughness, and K_I is the stress intensity factor according to linear elastic fracture mechanics. Then K_I is related to the stress on a penny-shaped crack by

$$K_I = 2\sigma \sqrt{\frac{R}{\pi}} \quad (A-15)$$

Equation (A-14) gives much more detailed information than Eq. (A-1) about the fatigue process because it relates the crack growth during a single cycle to the peak stress intensity during that loading cycle.

Our next step is to relate Eq. (A-14) to the pavement damage equation, (A-1). To do this, we replace K_I in (A-14) with its expression from Eq. (A-15). Then

$$\frac{dR}{dN} = \frac{B}{K_{Ic}^m} \left(\frac{2}{\sqrt{\pi}} \right)^m \sigma^m R^{m/2} \quad (A-16)$$

or

$$\frac{dR}{R^{m/2}} = \frac{B}{K_{Ic}^m} \left(\frac{2}{\sqrt{\pi}} \right)^m \sigma^m dN \quad (A-17)$$

We wish to integrate Eq. (A-17) from $N = 1$ to the cycle at which the cracks grow catastrophically. This limit occurs when the crack radius reaches R_m , which is given either by $K_I = K_{Ic}$ (Eq. A-7)

$$R_m = \frac{\pi}{4} \left(\frac{K_{Ic}}{\sigma} \right)^2 \quad (A-18)$$

or when τ_f reaches 1 in Eq. (A-2):

$$R_{m2} = \frac{1}{\sqrt[3]{T_F J}} \quad (A-19)$$

Then we integrate Eq. (A-17) from the initial crack size R_0 to R_m and obtain

$$N = \left(\frac{\sqrt{\pi}}{2} \right)^m \frac{K_{Ic}^m}{B \sigma^{m(1-m/2)}} \left[R_m^{1-m/2} - R_0^{1-m/2} \right] \quad (A-20)$$

By comparing Eq. (A-20) with Eq. (A-1), we see that

$$m = n$$

$$\text{and} \quad A = \left(\frac{\sqrt{\pi}}{2} \right)^m \frac{K_{Ic}^m}{B(1-m/2)^m} \left[R_m^{1-m/2} - R_0^{1-m/2} \right] \quad (A-21)$$

Thus, when we know K_{Ic} and J , we can determine m and B in Eq. (A-14) from the pavement damage relation, Eq. (A-1).

To relate the constitutive fatigue equation (A-12) to Eq. (A-14), we replace $\Delta \epsilon_c$ by an expression in τ , using Eq. (A-2) and an approximation to Eq. (A-10).

$$\Delta \epsilon_c = \frac{16(1-\nu^2)}{3E} J R^3 \Delta \sigma = \frac{T_c \tau_F \Delta \sigma}{T_F E} \quad (A-22)$$

Combining this expression with Eq. (A-12), we obtain

$$\frac{d\tau_F}{\tau_F} = g \frac{T_c}{T_F E} \sqrt{\frac{R_0}{R}} \left(\frac{\sigma}{\sigma_{cr}} \right)^\beta d\sigma = \frac{3}{R} dR \quad (A-23)$$

Let us now integrate Eq. (A-23) over half a loading cycle from a stress of zero to σ_m . We obtain

$$2(\sqrt{R} - \sqrt{R_0}) = \frac{g T_c \sqrt{R_0} \sigma_{cr}}{3 T_F E (\beta + 1)} \left(\frac{\sigma}{\sigma_{cr}} \right)^{\beta+1} \quad (A-24)$$

To understand this equation, we rewrite σ_{cr} using Eq. (A-7) and change the left-hand term as follows:

$$2(\sqrt{R} - \sqrt{R_0}) = 2 \frac{R - R_0}{\sqrt{R} + \sqrt{R_0}} = \frac{\Delta R}{\sqrt{R}} \quad (A-25)$$

We also double the result to account for the rest of the loading cycle from the peak stress σ_m down to zero. Then Eq. (A-24) takes the form:

$$\Delta R = \frac{g T_c \sqrt{\pi R_0} K_{Ic}}{3 T_F E (\beta + 1)} \left(\frac{\sigma}{\sigma_\alpha} \right)^{\beta+1} = \frac{dR}{dN} \quad (A-26)$$

Because of the similarity of Eqs. (A-7) and (A-15), we can equate the stress and K factors

$$\frac{\sigma}{\sigma_\alpha} = \frac{K_I}{K_{Ic}} \quad (A-27)$$

Therefore, we can now compare the fatigue equation (A-14) with Eq. (A-26) and determine the controlling factors. Evidently, $m = n = \beta + 1$, and

$$B = \frac{g T_c \sqrt{\pi R_0} K_{Ic}}{3 T_F E (\beta + 1)} \quad (A-28)$$

The final step is to relate the factors in the constitutive model to those in the pavement damage relation. We can form this relation using Eqs. (A-21) and (A-28).

$$g = \left(\frac{\sqrt{\pi}}{2} \right)^n \frac{3 n E T_F K_E^{n-1}}{A T_c \sqrt{\pi R_0} (1 - n/2)} \left[R_m^{1-n/2} - R_o^{1-n/2} \right] \quad (A-29)$$

Thus it appears that we can form a direct relationship between the parameters of the constitutive fatigue relation and the pavement damage relation. In developing this relation, we presume that we can obtain values for K_{Ic} , J , E , ν , T_F , and R_o .

We may recast the lifetime prediction equation to a form that is convenient when we know dR/dN . Both laboratory tests and finite element calculations could naturally lead to values of dR/dN . For this derivation we start with Eq. (A-16) a modified form of the standard fatigue model. We rearrange it as follows, using $m = n$:

$$\frac{dR}{R^{n/2}} = B \left(\frac{2\sigma}{K_{Ic} \sqrt{\pi}} \right)^n dN \quad (A-30)$$

Only R and N vary here because B , K_{Ic} , and n are material constants and σ is the peak stress during the loading cycle. We integrate Eq. (A-30) to obtain

$$N_2 = N_1 + \frac{1}{B} \left(\frac{K_{Ic} \sqrt{\pi}}{2\sigma} \right)^n \frac{1}{1 - n/2} \left[R_2^{1-n/2} - R_1^{1-n/2} \right] \quad (A-31)$$

Next we replace B by its value from Eq. (A-16), using the quantities at the beginning of the interval:

$$\begin{aligned} N_2 &= N_1 + \frac{R_1^{n/2}}{(dR/dN)_1} \frac{1}{1 - n/2} [R_2^{1-n/2} - R_1^{1-n/2}] \\ &= N_1 + \frac{1}{(1 - n/2)(dR/dN)_1} \left[R_2 \left(\frac{R_1}{R_2} \right)^{n/2} - R_1 \right] \end{aligned} \quad (A-32)$$

With this equation we can predict the number of loading cycles N_2 required to reach a crack radius of R_2 . The only information required is the material parameters n , the crack radius R_1 , and the rate $(dR/dN)_1$.

A.4 Testing and Demonstrations of the Model

To test and verify the proposed constitutive model, we wrote a small code to exhibit Eq. (A-13) and wrote a full constitutive model and inserted it into a finite element code. Our calculations then showed that the same results were obtained by the constitutive fatigue model, the standard fatigue model, and the pavement fatigue model.

As a first step, the small code (FATIG1) was written to contain the constitutive model and perform simulations over a few loading cycles. For these tests it was necessary to assume a set of parameters for all the models: these are listed in Table A-1. These parameter values were taken from a mixture of sources. The A , n , and f factors are a report by the Center for Transportation Research of the University of Texas.³ K_{Ic} , J , R_0 , and T_F are from a recent paper by Gran et al. on high rate fracture.⁴ Many of the parameters used for the constitutive fatigue model are not required for the other models, as noted in the table. Most of these constitutive fatigue parameters can be determined from pavement fatigue data.

³A. Taute, B. F. McCullough, and W. R. Hudson, "Improvements to the Materials Characterization and Fatigue Life Prediction Methods of the Texas Rigid Pavement Overlay Design Procedure," Chapter 5 of Report 249-1, Center for Transportation Research, University of Texas (March 1981).

⁴J. K. Gran, L. Seamon, and Y. M. Gupta, "Experimental and Analytical Investigation of Tensile Failure in Concrete by Spallation," submitted to *J. Eng. Mech.*, ASCE (1991).

Table A-1. Parameters for the Concrete Fatigue Models

Symbol	Name of Parameter	Value	Source
-- Pavement Model --			
A	Pavement fatigue coefficient	46000	Pavement data
f	Stress factor	4.8 MPa	Pavement data
n	Stress exponent	3	Pavement data
-- Standard Model --			
B	Fatigue coefficient	Derived, cm	Lab data
m	Stress intensity exponent	= n	Lab data
-- Constitutive Model --			
K _{lc}	Fracture toughness	2.0 MPa√cm	Lab data
T _F	Fragmentation factor	4	Fit to pavement data
R ₀	Initial crack radius	0.4 cm	Aggregate size
g	Growth coefficient	0.017	Fit to pavement data
J	Crack density	0.01 No./cm ³	Fit to pavement data
b	Stress exponent for growth	= n - 1	Pavement data

FATIG1 acts like a constitutive relation for a finite element code in that it accepts strain increments and provides stresses and damage. The loading was applied as a sinusoid in time, with strain increments intended to provide stresses ranging from zero to σ_{\max} . Each loading cycle was discretized into 10 strain increments. After several loading cycles, an average value of dR/dN was obtained for a cycle. Computations were made for several stress levels to represent a range of loadings. To perform simulations that would represent the fatigue process at later times, we started some test series with the cracks at an initial radius of 0.6, 0.8, 1.0 cm, etc. (but the R_0 value was always 0.4 cm). In this way we established dR/dN values for a range of radii and also for different σ/σ_{cr} values. The results of these computations are shown in Figure A-1. Besides the dR/dN values from the constitutive model, there are results from Eq. A-14, the standard fatigue model. The comparison is essentially exact. Thus it appears that we have developed a constitutive model for fatigue and that it can run in a finite element code. Also the fatigue damage calculations are in a form that can be readily extended to predict lifetimes.

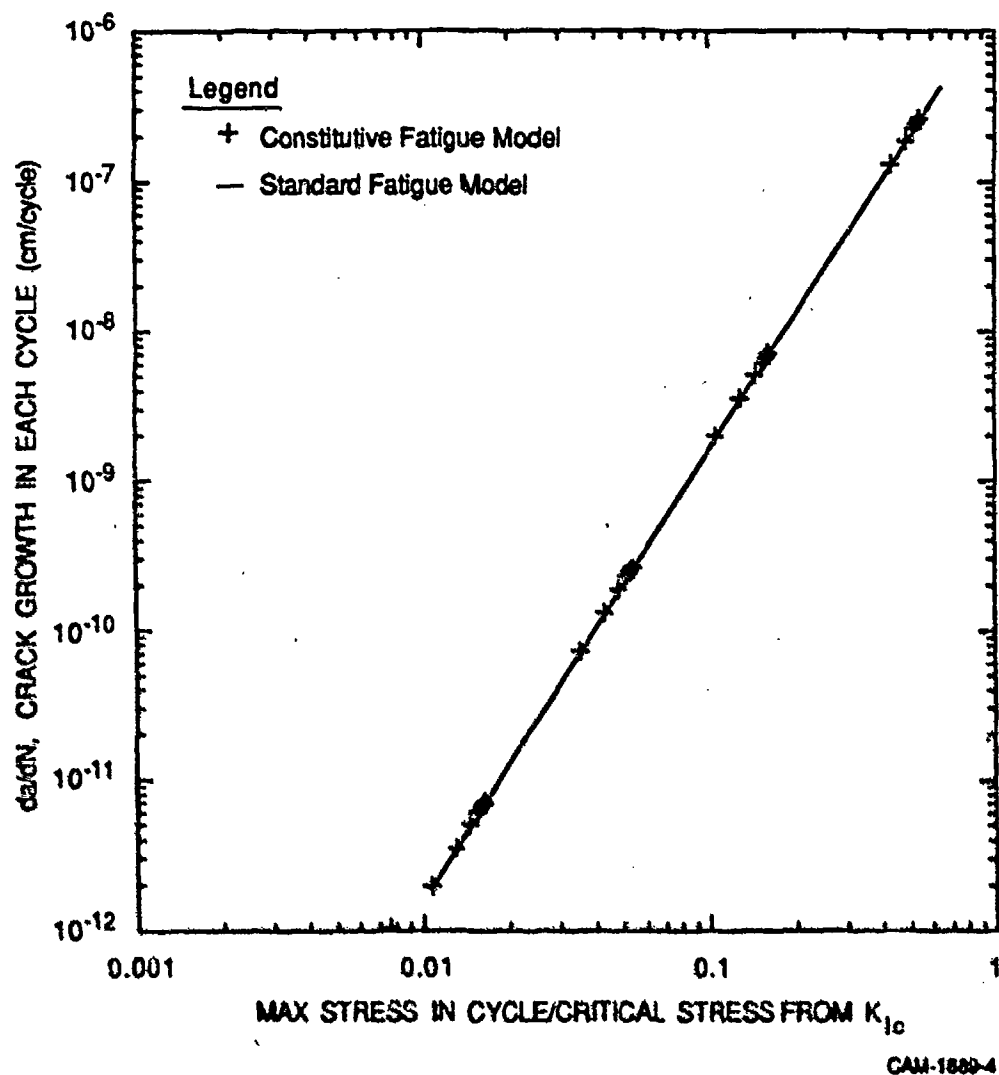


Figure A-1. Comparison of Computed Crack Growth from Constitutive Fatigue Model with Standard da/dN Fatigue Model

10. Appendix B

Implementation of the Fatigue Model in a Computational Subroutine

The complete constitutive relation combines the fatigue cracking processes of Appendix A with a standard stress-strain relation for the undamaged material between the cracks. Thus, the material appears as a two-phase composite: the intact, isotropic material plus the cracks, which have the fatigue equations governing their appearance and growth. The current model, termed SRI-PAVEMENT, was constructed by adding the cracking processes onto the planes of a multiple-plane plasticity model called SHEAR3D. Below we first describe general requirements for any computer subroutine that contains a material model; these requirements provide the framework within which we generate our pavement model. Then we proceed with the specific formulation of SRI-PAVEMENT by outlining the stress-strain relations for the matrix material and describing the special procedures required to account for the anisotropy associated with both plastic flow and cracking.

The subroutine containing the pavement model performs certain well-prescribed functions during a finite element simulation. For each time step during the calculation and for each element, the material model is called by the main program (DYNA3D here). DYNA3D provides the material model with a strain increment tensor, the old stress tensor from the previous time step, internal energy, and a complete description of the prior state of the material (such quantities as the amount of crack damage, orientations of the damage). The material model updates the damage and other state quantities and provides the new stress tensor for DYNA3D. Below we outline the processes that must occur on each computational time step for each element.

B.1 Pressure-Volume Relation

The intact material is assumed to be isotropic; hence, its pressure-volume and deviatoric stress relations can be treated separately. The pressure-volume (thermodynamic) equation used here is the Mie-Grüneisen equation:

$$P = (C\mu + D\mu^2 + S\mu^3)\left(1 - \frac{1}{2}\Gamma\mu\right) + \rho\Gamma E \quad (B-1)$$

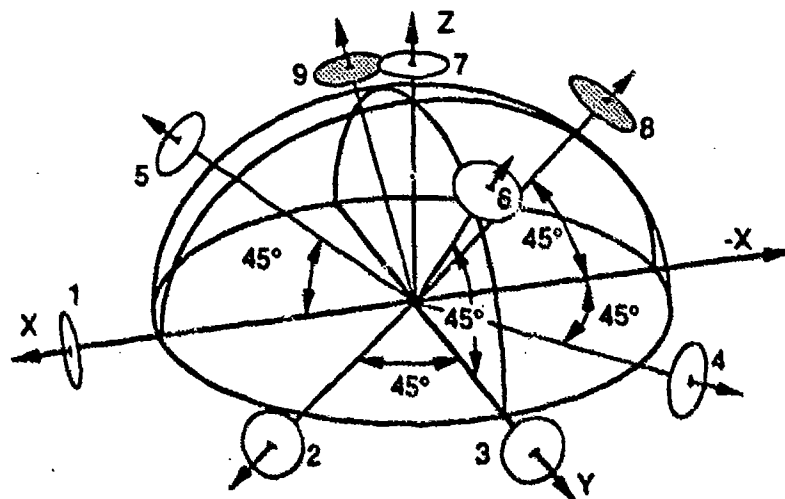
where P is the pressure; C , D , and S are constants defining the hydrostatic pressure-volume curve; $\mu = \rho/\rho_0$ is the volumetric strain; ρ and ρ_0 are the density at the present time and the initial density; Γ is the Grüneisen ratio (a dimensionless constant with values of about 2); and E is the internal energy referenced to zero at the initial state. With this formulation, the pressure changes both for changes in the specific volume (volumetric strain) and for changes in the internal energy (or temperature).

B.2 Multiple-plane Procedure for Deviator Stresses

The deviatoric stress tensor is computed from an elastic relation with a Tresca plasticity process. The plastic flow is treated on the discrete planes of the multiple-plane model. These planes are illustrated in Figure B-1 in their usual orientation. There are nine planes oriented to give an approximately isotropic behavior. Three planes are normal to the three coordinate directions and six are at 45 degrees between these directions. The planes have orientations, but no specific locations within a computational element, so there is no direct geometric interaction between the planes. All plastic flow is assumed to occur on these planes, not homogeneously throughout the material as in a Mises plasticity model, for example.

During the stress computation process for an element, we undertake the following steps:

- a. From the imposed strain increments $[\Delta\epsilon]$ and the old stress state $[\sigma_0]$, we compute the new stress state $[\sigma^N]$, treating the strain increments as elastic. Hence, this is a standard linear elastic procedure.
- b. We transform the new stresses to normal (σ_n) and shear stresses (τ_1 and τ_2) on each of the nine planes.
- c. The current yield strength is determined on each of the planes. A nonlinear, tabular work-hardening and thermal softening process is provided.
- d. We compute the plastic shear strains on each of the planes, using a stress-relaxation algorithm.
- e. From the known plastic strains on each plane, we compute the plastic strain increment tensor $[\Delta\epsilon^P]$.
- f. We recompute the stress tensor $[\sigma]$, taking the elastic strain increments as the imposed strain increments minus the plastic strain increments $[\Delta\epsilon] - [\Delta\epsilon^P]$.



MM-7893-3B

Figure B-1. Relative Locations of the Initial Orientations of the Fatigue Damage Planes with Respect to the Coordinate Directions

The foregoing procedure would be a complete solution in the standard isotropic treatment of stress relaxation. However, in the current context there are many planes that may absorb plastic strain independently. These multiple planes interact such that they may absorb too much plastic strain (so the elastic strain is misrepresented) or absorb too little. To provide for this interaction of the planes, we proceed through the foregoing steps many times and allow for only a small amount of stress relaxation on any step. The iteration and convergence procedure used is designed to provide for high fidelity to the intended stress-strain relations and also to provide relatively rapid solution even for large strain increments.

After the computation of the new stress state, we update the orientations of the planes. The orientation of each plane is given by θ , the angle from the X-direction in the X-Y plane, and ϕ , the angle from the Z-direction toward the X-Y plane. Rigid body rotation and shearing cause changes in these angles.

B.3 Incorporation of the Fatigue Cracking Process

Fatigue cracks and the fatigue cracking processes occur on all the planes of the model. During initialization of the material model, each plane is given its orientation and initial size distribution of flaws. The main program provides for about 65 extra variables for each element to store the special information required on the cracking processes.

At each time step normal and shearing stresses are computed for each of the planes (as noted in the second step above). When the normal stress is tensile on a plane, crack opening and shearing computations are made according to Eq. (A-5) of Appendix A. These crack strains are accounted for in determining the stress state. Then crack growth computations are made for each plane, following Eq. (A-13) of Appendix A.

B.4 Plan of the SRI-PAVEMENT Subroutine and the Connection to DYNA3D

SRI-PAVEMENT was designed as a standard material model for use in DYNA3D; however, it imposed some special requirements. DYNA3D stores all its variables in large COMMON arrays and SRI-PAVEMENT passes all variables through the CALL statement and has no COMMON. To account for this difference in basic storage strategy, a special DYNA3D

routine, F3DM60, was written to call SRI-PAVEMENT and make the storage transfers. The normal amount of element variable storage was extended to permit the large amount of special variables used with SRI-PAVEMENT. The connection to DYNA3D was made in such a way that all the variables are available for plotting by the post-processor. No attempt was made to vectorize SRI-PAVEMENT and we have not yet attempted to provide for restarting, but we have planned for that possibility.

SRI-PAVEMENT consists of one main subroutine and an auxiliary subroutine RESOLV. RESOLV is called at several points in SRI-PAVEMENT to transform the stress tensor to determine the normal and shearing stresses on each plane and to construct the plastic strain tensor from the plastic deformations on each plane.

Because of the complexity of the multiple-plane plasticity model, a large testing program was undertaken to verify its operations. First, we performed one-element computations. We imposed shears or rotations and monitored the rotations of the planes as computed by the model. These tests were imposed in several orientations and verified that appropriate symmetry in the X-, Y-, and Z-directions resulted. Then we applied uniaxial loading and unloading and verified that the computed normals and shears were correct on each plane and that the overall stress tensor was correct. We performed calculations with the model to match simulations that had previously been made with a two-dimensional version of the model and these agreed satisfactorily.

Following verification of the model in a one-element mode, we inserted SRI-PAVEMENT into DYNA3D. A new debugging procedure was inserted into all the subroutines so that we can monitor desired variables during a normal computation. We transformed to single precision (32-bit, to match the DYNA format), which required a special effort because some of the processes in SRI-PAVEMENT are very sensitive to the precision employed. Finally, we tested SRI-PAVEMENT in DYNA3D by simulating a fatigue test computation and comparing the result with an evaluation using the standard dR/dN fatigue model.

In all these tests the pavement fatigue model performed accurately, so it appears to be ready for pavement simulations.

11. Appendix C

A Model for Rutting of Airport Pavements

A preliminary model for the rutting process in airport pavements has been developed based primarily on the data of Monismith et al.¹ and Sousa² on selected asphalt concretes. Here we outline the data available, the requirements that they make for a model, and the nature of the model proposed. Then we begin to exercise the model to exhibit its characteristics and indicate to what extent the model matches the asphalt data.

C.1 Data on Rutting

Asphalt concrete appears to have a very complex response to loading so that even the development of a first-order model is difficult. Because of the complexity of the material, traditional tests are often not sufficient to delineate the important response characteristics. New types of tests are being developed at the Institute of Transportation Studies in Berkeley under the general direction of C. L. Monismith. The results of these tests are making it possible to generate a model that can describe much of the special behavior of asphalt concrete.

Some of the special features of the data provided by Monismith et al.¹ and Sousa² are:

- a. **Axial Loading** (unconfined compression tests). Triaxial tests with stresses to about 85 psi (0.6 MPa) were conducted at loading rates of 0.02/s, 0.002/s, and 0.0002/s. These data are given in Figure 66, page 117 of Ref. 1. Here in Figure C-1 they are replotted as axial stress versus axial strain for our convenience in understanding the data. The resulting Young's moduli were 263, 105, and 48 MPa and the shear moduli ($G = E/3$) were 88, 35, and 16 MPa. These results indicate a viscoelastic type of behavior.

¹ C. L. Monismith, R. G. Hicks, and F. N. Finn, "Performance Related Testing and Measuring of Asphalt-Aggregate Interactions and Mixtures," Quarterly Report QR-UCB-A-003A-91-1 of the Institute of Transportation Studies, Asphalt Research Program, University of California at Berkeley, Richmond, California 94804 (April 1991).

² Jorge Sousa, U. C. Berkeley, private communication to L. Seaman at SRI, April 1991.

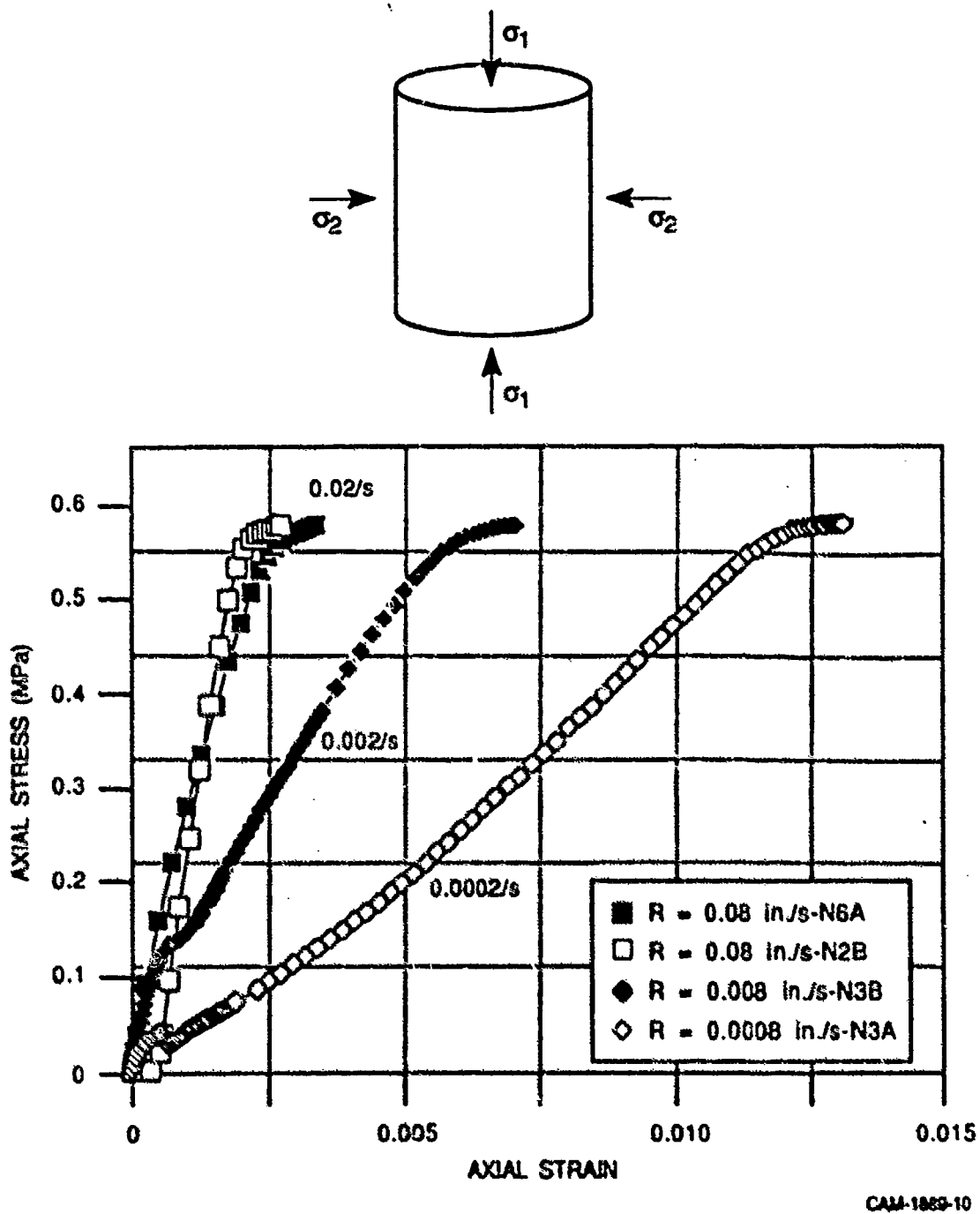


Figure C-1. Axial Stress-Strain Curves from Triaxial Tests at Three Loading Rates on Asphalt Pavement. From Monismith et al., page 117.

- b. **Axial stress developed under shear strain.** Shear strain was imposed on cylindrical specimens with a constrained height for strain rates of 0.02/s, 0.002/s, and 0.0002/s. We have replotted this graph from the data in Figure C-2, page 117 of Ref. 1, using axial stress in MPa and shear strain (instead of strain squared) to assist our intuition in understanding the phenomena (Figure C-2). The resulting dilatant moduli (D_{js}) were 69.0 MPa, 23.0 MPa, and 11.0 MPa. The plot of axial stress versus shear stress (page 62 of Ref. 1, and Figure C-3 here) shows a very large hysteresis loop, indicating rate-dependent processes in the shearing behavior, in dilatancy, or in both.
- c. **Permanent deformation as a function of time or cycles.** The permanent axial strain appears to grow as the square root of the number of cycles, with a strong dependence on the mix and the void content. (page 51 of Ref. 1, and Figure C-4 here). This measurement of permanent deformation may be the most significant for rutting because it, like rutting, refers to a permanent change in the material state, not a transient one.
- d. **Creep Modulus.** The creep modulus (σ/ϵ) as a function of time appears to decrease as the square root of time. The rates depend on the mix and void content (page 55 of Ref. 1).

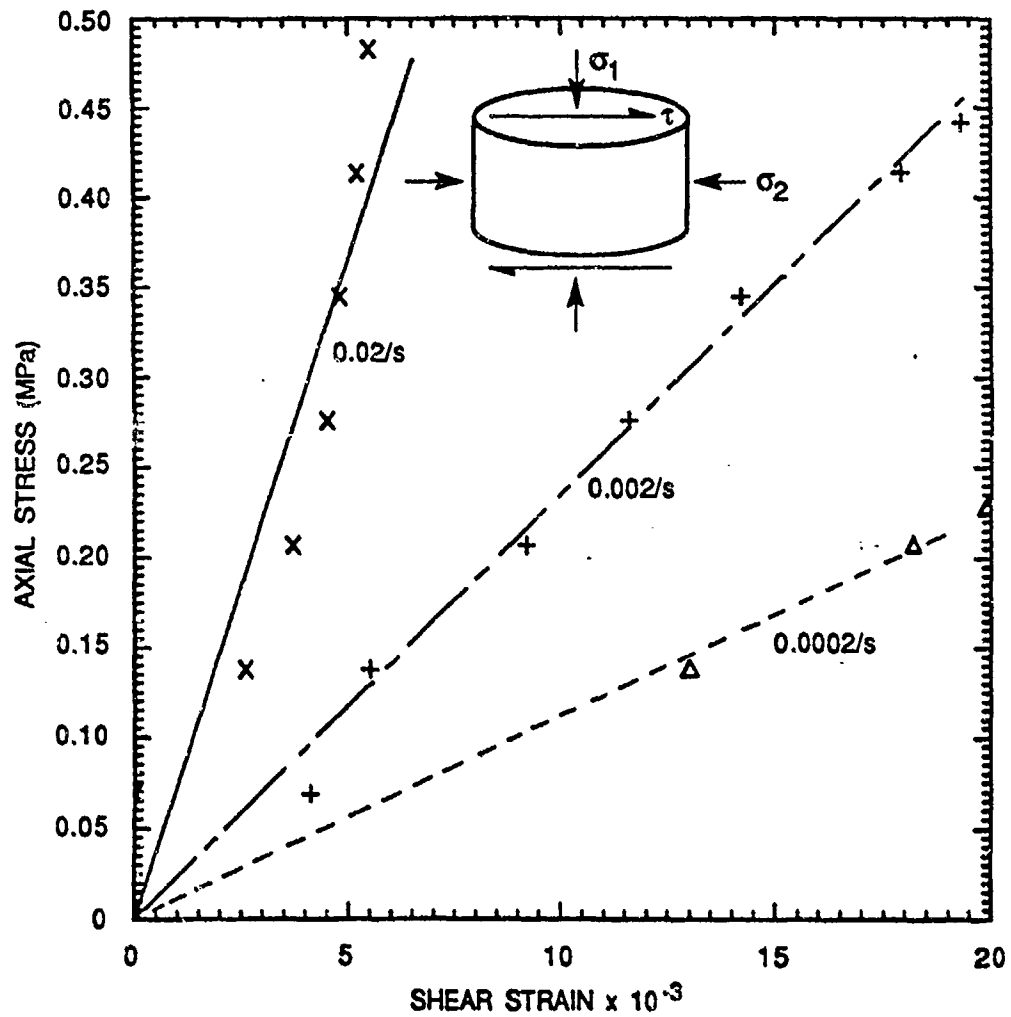
We can summarize these requirements under three headings:

- 1. **Viscoplasticity, or time-dependent permanent deformation.** This aspect especially leads to the observed rutting.
- 2. **Viscoelasticity, or time-dependent stiffness.** The variation of stiffness with loading rate is very significant and must be included in the modeling.
- 3. **Dilatancy, or increase in pressure with shearing strain.** The stresses associated with dilatancy are comparable to those from other sources.

All three aspects of the data are represented in the proposed model.

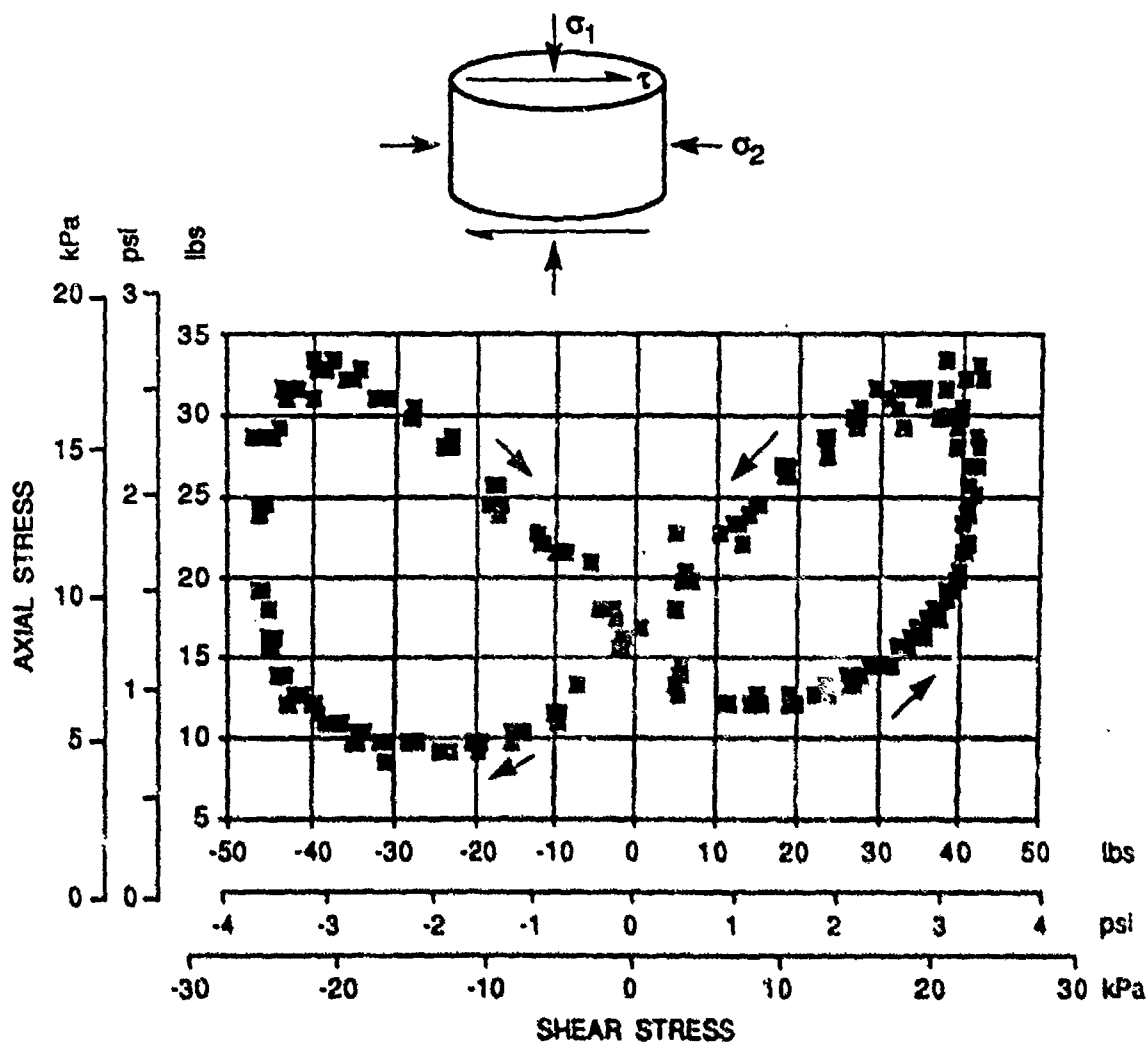
C.2 Model Development

We propose an isotropic model for the asphalt concrete, which would separate the deviatoric and volumetric responses of the material. The deviatoric stresses in the model are affected by both viscoelastic and viscoplastic behavior, and the pressure is provided by dilatant and viscoelastic behavior.



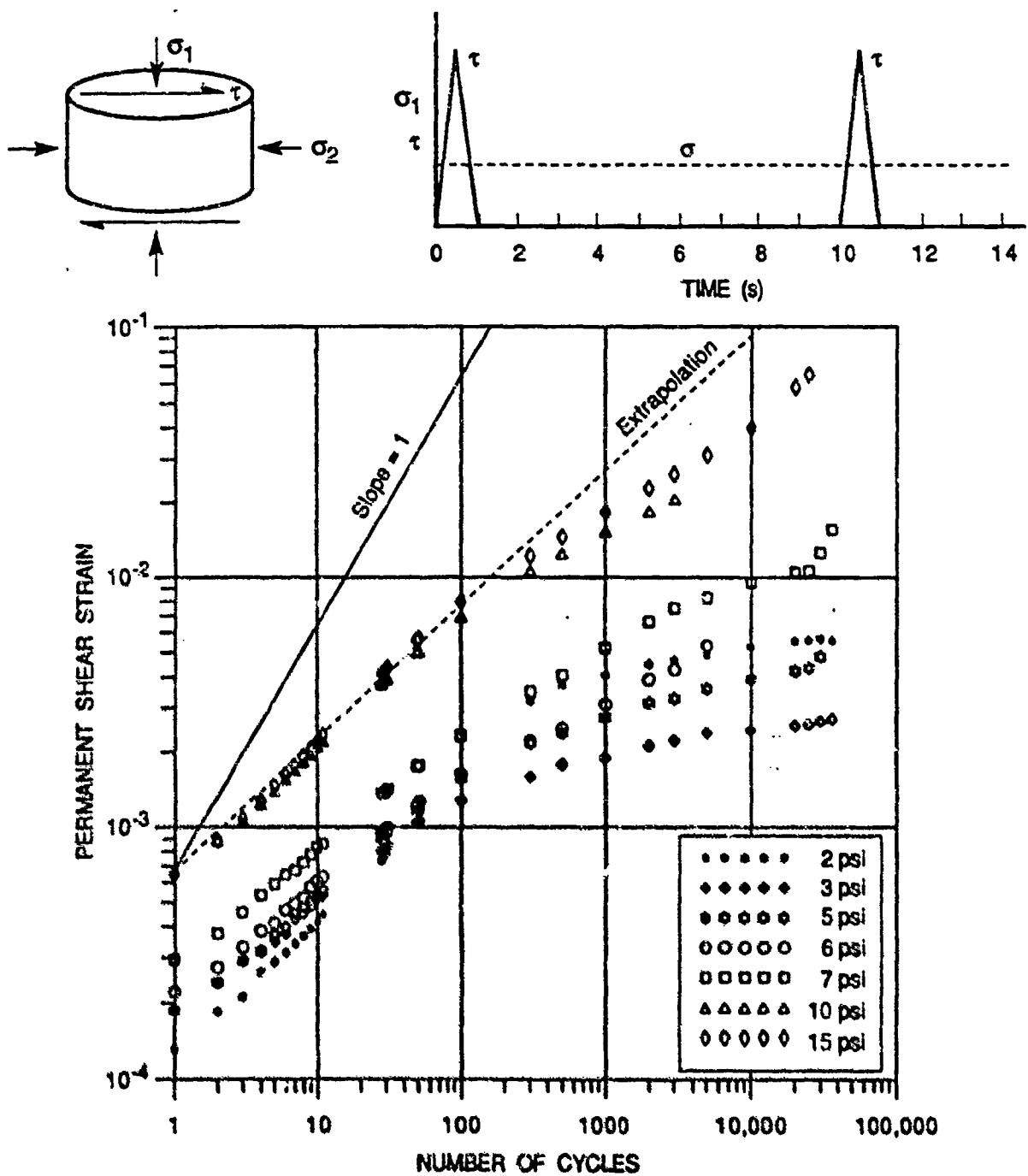
CAM-1889-11

Figure C-2. Development of Axial Stress During Shear Tests on Axially Confined Shear Samples of Asphalt Pavement. From Monismith et al., page 117.



CAM-1889-12

Figure C-3. Variation of the Axial Stress with Shear Stress for an Asphalt Concrete Mixture under Cyclic Shear Load with Axial Confinement. From Monismith et al., page 62.



CAM-1883-5

Figure C-4. Accumulation of Permanent Deformation as a Function of Loading Cycle under Repetitive Shear Stresses (Axial Stress is 5 psi)

C.2.1 Deviator Stress Model

For the computation of the deviator stresses, we propose the following standard relation:

$$\frac{d\sigma}{dt} = 3G(t) \left[\frac{d\epsilon}{dt} - \frac{d\epsilon^P}{dt} \right] + H(t) \quad (C-1)$$

where G and H are time-varying functions derived from viscoelasticity, $d\epsilon/dt$ is the imposed strain rate, and $d\epsilon^P/dt$ is the plastic strain rate. Here we are using σ and ϵ as the equivalent stress and strain. We plan to use the multiple-variable linear viscoelastic model described in Appendix D to represent the viscoelastic behavior. In this case we derive Eq. (C-1) by differentiating Eq. (D-30) of Appendix D with respect to time and recognize that the strain rate in that appendix is the elastic strain rate, $d\epsilon^E/dt = d\epsilon/dt - d\epsilon^P/dt$. Then the G and H functions are

$$G(t) = G_0 + \sum_{m=1}^I G_m e^{-G_m \Delta t / \mu_m} \quad (C-2)$$

and

$$H(t) = - \sum_{m=1}^I \sigma_{m0} \frac{G_m}{\mu_m} e^{-G_m \Delta t / \mu_m} \quad (C-3)$$

where G_m and μ_m are the spring and dashpot factors for the m^{th} Maxwell element in the multiple-variable viscoelastic model. The σ_{m0} values must be updated at each step using Eq. (C-29). The plastic strain rate is given by Eq. (8) in the main text:

$$\frac{d\epsilon^P}{dt} = \left(\frac{\sigma}{k} \right)^n \quad (C-4)$$

Here n is a material constant (between 1 and 2) and k is a function of plastic strain. From our initial review of the data from Sousa,² it appears that $n \approx 2$ and that k should be a linear function of the plastic strain (i. e., not a constant):

$$k = k_0 + k_1 \epsilon^P \quad (C-5)$$

where k_0 and k_1 are constants with dimensions like $\text{MPa} \sqrt[n]{\text{s}}$.

C.2.2 Pressure Model

The pressure model is formulated as a simplified Mie-Grüneisen model:

$$P = K\mu + \Gamma\rho_{so}E \quad (C-6)$$

where $\mu = \rho/\rho_{oi} - 1$, the compressive strain. K is the bulk modulus, Γ is the Grüneisen ratio, E is the internal energy, and ρ_{so} is the initial density. ρ is the current density and ρ_{oi} is a density representing the current porosity. We propose that, as shearing occurs, the aggregates roll over each other, causing dilation and changes in porosity and ρ_{oi} . The following relation may fit the data

$$\Delta\epsilon_d = -\frac{\Delta\rho_{oi}}{\rho_{oi}} = D \Delta\bar{\epsilon} \quad (C-7)$$

where ϵ_d is a newly defined strain quantity associated with the dilatation, D is a dilatant modulus, and $\Delta\bar{\epsilon}$ is a change in the total shear strain vector on a plane in the material. We are visualizing that $\bar{\epsilon}$ is a vector representing (on any plane) how far the material has been distorted from its zero-distortion position. As the shearing strain is applied, this vector is modified to account for the current amount of distortion. The length of the vector is proportional to the amount of stress that is generated normal to this plane by dilatancy. If the shearing strain reverses direction, then the vector may return to zero and the normal stress will also reduce to zero. This general description of the normal stress that arises with the imposition of shear strain appears to agree qualitatively with the data from confined shearing tests. However, those data also show significant time-dependent and dissipative effects. Therefore, we propose using a viscoelastic model as an extension of Eq. (C-7). The expressions are then

$$\epsilon_d = \epsilon_{d0} + D(t)\Delta\bar{\epsilon} - F(t) \quad (C-8)$$

where $D(t)$ and $F(t)$ have definitions similar to those for $G(t)$ and $H(t)$ in Eqs. (C-2) and (C-3). The strain vector quantity $\Delta\bar{\epsilon}$ will be computed on each plane of the multiple-plane plasticity model. Finally, the plastic strains are assigned to the planes on which they occur so that we will know the orientation of the permanent deformation as well as the magnitude.

The foregoing expressions for the deviatoric and pressure response to strain loadings completely define the model behavior.

C.3 Construction of the Material Model Subroutine for Rutting

A preliminary form of the preceding model was written into a computational subroutine. In most cases the viscoplastic and viscoelastic portions were run separately. The viscoelastic behavior was treated by the standard linear viscoelastic model, not the multiple-variable viscoelastic model.

We intend to incorporate the viscoelastic, dilatant, and viscoplastic processes into the multiple-plane plasticity model used for the fatigue modeling. The multiple-plane treatment is necessary to represent the dilatant modeling approach outlined above. Eventually we will integrate the rutting and fatigue processes into a single model.

C.4 Response of the Rutting Model to Loadings

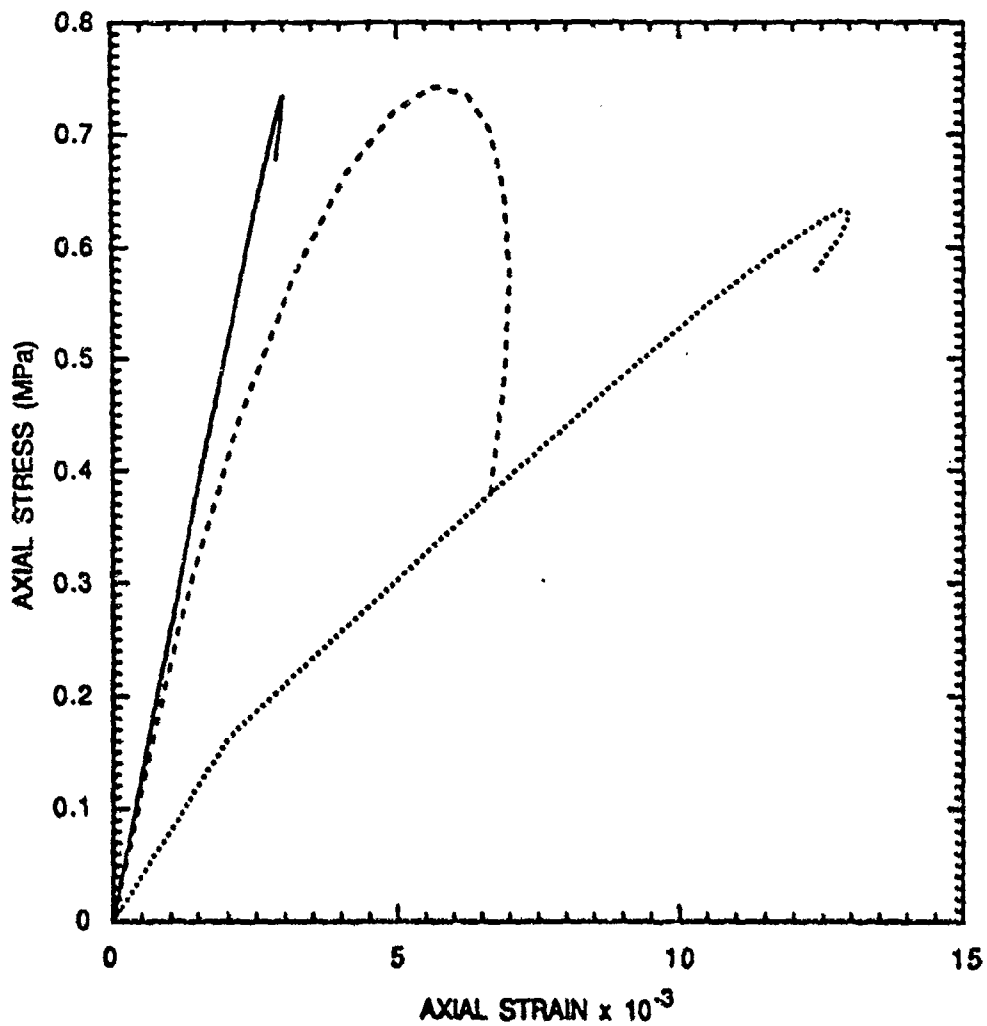
The following simulations are intended to illustrate the expected model behavior qualitatively, but not quantitatively. Truly quantitative comparisons must await construction of the fully three-dimensional subroutine with all model features combined.

In examining the response of the model, we want to illustrate the functioning of each aspect of the model. The first comparisons are for the axial stress as a function of axial strain in triaxial experiments (Figure C-1 above). Figure C-5 shows the computed results for the three testing rates shown. The computed results have approximately the correct slopes for the high and low rates, but not for the intermediate rate. This result suggests that we need to adjust the viscosity in the dashpot element. There is clearly a break in the low rate loading curve around 0.16 MPa, which this is caused by the step size we used in these computations. To make a more complete fit to the axial loading data, we need to have stress-strain data for a full loading cycle: then we can better represent the hysteresis loop (hence, the dissipation) that is occurring.

The dilatant behavior shown in Figure C-2 is one of the most interesting aspects of the pavement response. The axial stress rises as shear loading is applied to specimens, and the dilatant response is very rate-dependent. Figure C-6 shows the results of short simulations of shearing in the model at the three loading rates. The high and low rate simulations match fairly well, but not the one at the middle rate. This response can be adjusted somewhat by altering the viscosity of the dashpot in the model, but mainly the model does not have the flexibility to represent the correct amount of damping as well as the great range of stiffnesses seen in Figure C-2.

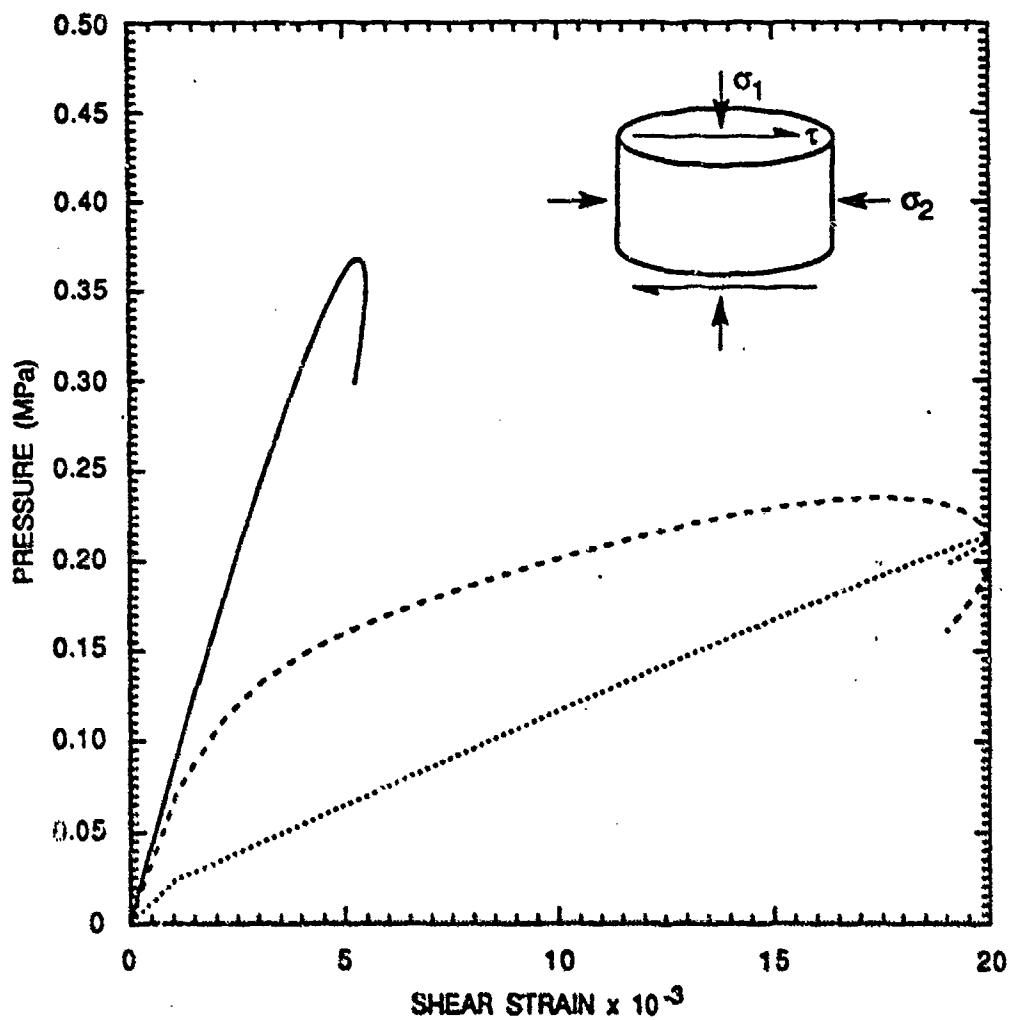
Full cycles of dilatancy caused by shearing are shown in Figure C-3 (Figure 40 on page 62 of Ref. 1). According to Sousa,² loading takes the lower curve of the Figure 4-4 shape in each case. We were able to match this data fairly well using the viscoelastic shearing parameters required for Figure C-5, but we made the dilatancy essentially elastic. The resulting figure (starting the plot after the first third of the first loading cycle) is shown in Figure C-7. Clearly this curve has about the right amplitudes and directions and the hysteresis loop is about right. Hence, this unusual hysteretic behavior can be represented by the combination of dilatant and viscoelastic behaviors.

The viscoplastic behavior of the model is compared with the data in Figure 5-4 of the main text. Again the correspondence is satisfactory.



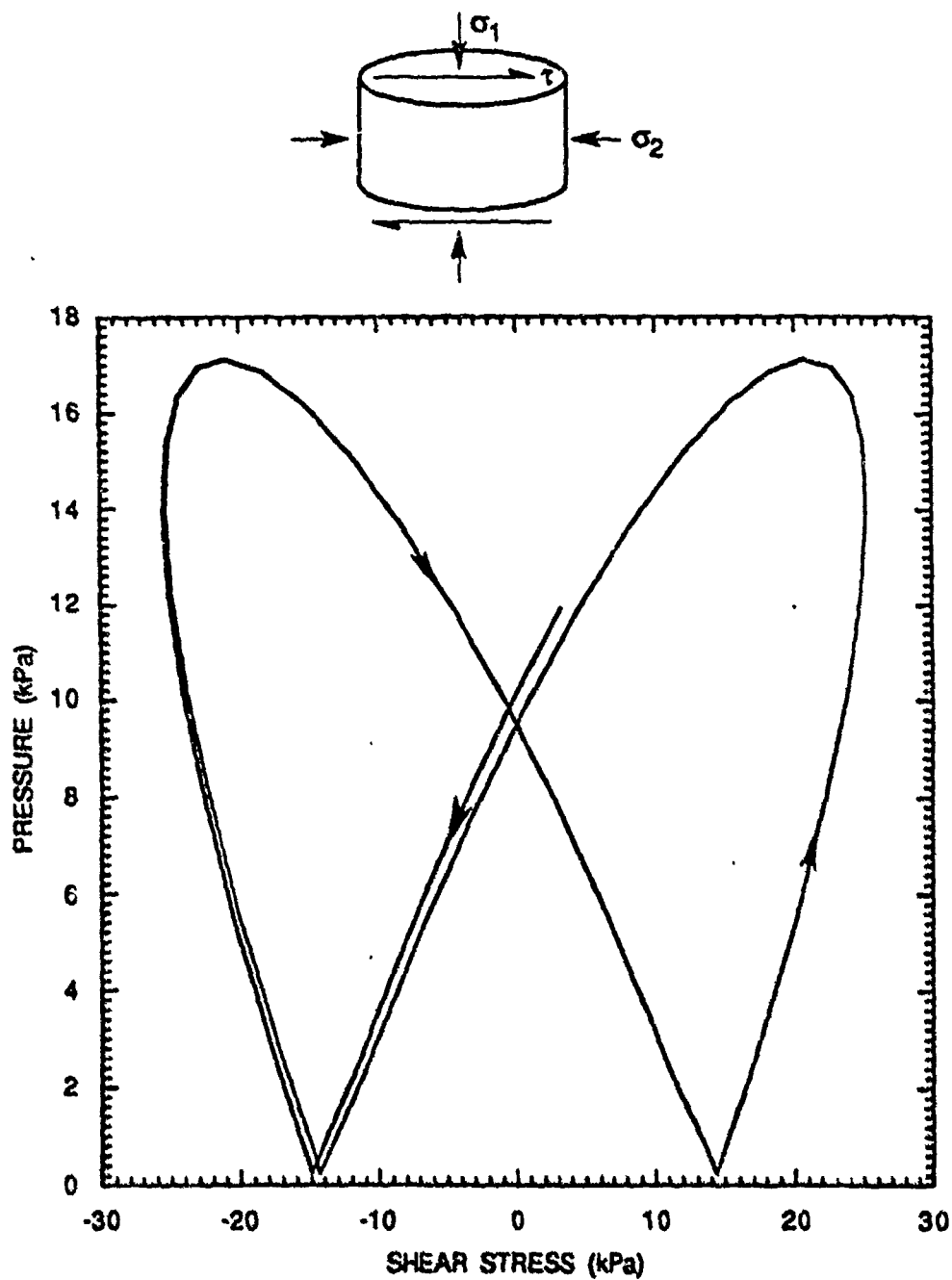
CAM-1885-14

Figure C-5. Simulation of the Axial Stress Tests in Figure C-1 with a Standard Linear Viscoelastic Model



CAM-1889-15

Figure C-6. Simulation of the Shear Tests in Figure C-2 with a Standard Linear Viscoelastic Model



CAM-1889-16

Figure C-7. Simulation of the Pressure Generated During Cyclic Shear Loading Corresponding to Figure C-3

12. Appendix D

Analysis and Implementation of the Multiple-Variable Linear Viscoelastic Model

D.1 Introduction

In the following discussion we derive general solutions for a multiple-variable linear viscoelastic model. We begin with a standard linear viscoelastic model (one spring in parallel with a Maxwell element – the Maxwell element has a spring and dashpot in series). Then we add more Maxwell elements in parallel to obtain the general behavior required to fit material data. The nature of the model and the model parameters are shown in Figure D-1. The G 's are the spring stiffnesses (representing shear moduli) and the μ 's are the dashpot response factor.

The stress analyses for the viscoelastic model must be performed on the full stress and strain tensors. Hence, we are establishing the shear modulus G that must be used in the relationship

$$\sigma_{ij} = 2G\epsilon_{ij} \quad (D-1)$$

However, in the derivation below, we will use only the invariants $\bar{\sigma}$ and $\bar{\epsilon}$ and not the full tensors.

$$\bar{\sigma}^2 = 1/2 \sigma_{ij} \sigma_{ij} \quad \text{and} \quad \bar{\epsilon}^2 = 2/3 \epsilon_{ij} \epsilon_{ij} \quad (D-2)$$

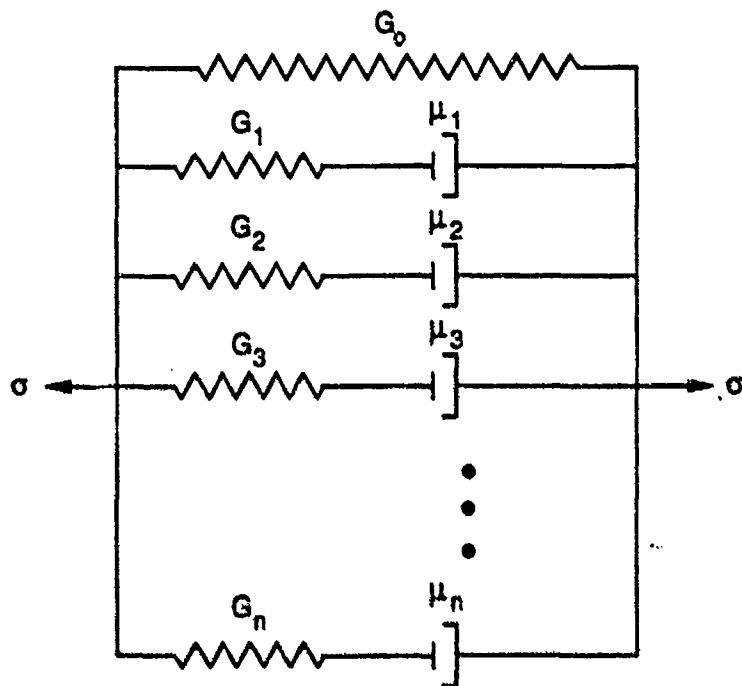
Because the numerical coefficients differ in these two definitions, the barred quantities are related as

$$\bar{\sigma} = 3G\bar{\epsilon} \quad (1)$$

instead of as in Eq. (D-1). In the following derivation we use these invariants only and drop the bars on the stress and strains.

During loading, a strain is imposed across the element from left to right and this total strain is felt by all the elements. Within each Maxwell element, the strain is separated into spring and dashpot components, such that the sum equals the total imposed strain:

$$\epsilon = \epsilon_{gm} + \epsilon_{\mu m} \quad (D-4)$$



CM-1889-17

Figure D-1. Spring and Dashpot Representation of the Multiple-Variable Linear Viscoelastic Model

where this relation refers to the m^{th} Maxwell element. The stress on the spring elements are given by $\sigma_m = 3G_m \epsilon_{gm}$ and on the dashpot elements by

$$\sigma_m = 3\mu_m \frac{d\epsilon_{\mu m}}{dt} \quad (\text{D-5})$$

For equilibrium, the stresses on the spring and dashpot of each element must be equal. The stress σ on the total model is simply the sum of the component stresses.

D.2 Response to Sinusoidal Loading

Insight can be gained into the behavior of the model by subjecting it to sinusoidal loading. Here we impose strains in the form of a sine function and compute the stresses. From these we obtain the apparent stiffness and phase lag as a function of the loading frequency.

The loading is given by

$$\epsilon = \epsilon_0 \sin \omega t$$

and we require that each component of the strains be also sinusoidal:

$$\epsilon_{gm} = B_{gm} \sin \omega t + C_{gm} \cos \omega t \quad (\text{D-7})$$

$$\epsilon_{\mu m} = B_{\mu m} \sin \omega t + C_{\mu m} \cos \omega t \quad (\text{D-8})$$

The overall strain is then

$$\epsilon = \epsilon_{gm} + \epsilon_{\mu m} = (B_{gm} + B_{\mu m}) \sin \omega t + (C_{gm} + C_{\mu m}) \cos \omega t \quad (\text{D-9})$$

Comparing Eq. (D-9) with Eq. (D-6), we see that

$$B_{gm} + B_{\mu m} = \epsilon_0 \quad (\text{D-10a})$$

and

$$C_{gm} + C_{\mu m} = 0 \quad (\text{D-10b})$$

Next we differentiate $\epsilon_{\mu m}$ with respect time to compute the stress on the dashpot

$$\frac{d\epsilon_{\mu m}}{dt} = \omega B_{\mu m} \cos \omega t - \omega C_{\mu m} \sin \omega t \quad (D-11)$$

and use the equality of the stress on the spring and dashpot to obtain the following relations:

$$G_m B_{gm} = -\mu_m \omega C_{\mu m} \quad (D-12a)$$

and

$$G_m C_{gm} = \mu_m \omega B_{\mu m} \quad (D-12b)$$

Combining Eqs. (D-12a) and (D-10b), we find that

$$B_{gm} = \frac{\mu_m \omega}{G_m} C_{gm} \quad (D-13)$$

When we use Eqs. (D-10a) and (D-12b) with this result, we obtain:

$$B_{gm} = \frac{\eta_m^2 \epsilon_0}{1 + \eta_m^2} \quad (D-14)$$

where

$$\eta_m = \frac{\mu_m \omega}{G_m} \quad (D-15)$$

With B_{gm} known in terms of ϵ_0 and η_m , we can now determine the other strain coefficients:

$$C_{gm} = \frac{\eta_m \epsilon_0}{1 + \eta_m^2}, \quad B_{\mu m} = \frac{\epsilon_0}{1 + \eta_m^2}, \quad \text{and} \quad C_{\mu m} = -\frac{\eta_m \epsilon_0}{1 + \eta_m^2} \quad (D-16)$$

The strains in the springs and dashpots are

$$\epsilon_{gm} = \frac{\epsilon_0}{1 + \eta_m^2} \left[\eta_m^2 \sin \omega t + \eta_m \cos \omega t \right] \quad (D-17)$$

$$\epsilon_{\mu m} = \frac{\epsilon_0}{1 + \eta_m^2} \left[\sin \omega t - \eta_m \cos \omega t \right] \quad (D-18)$$

$$\frac{d\epsilon_{\mu m}}{dt} = \frac{\omega \epsilon_0}{1 + \eta_m^2} \left[\eta_m \sin \omega t + \cos \omega t \right] \quad (D-19)$$

From the strains we can compute the stresses on each Maxwell element and hence the stress on the entire assemblage:

$$\sigma = 3G_0 \epsilon_0 \sin \omega t + \epsilon_0 \sin \omega t \sum_{m=1}^I \frac{3G_m \eta_m^2}{1 + \eta_m^2} + \epsilon_0 \cos \omega t \sum_{m=1}^I \frac{3G_m \eta_m}{1 + \eta_m^2} \quad (D-20)$$

This sinusoidal stress is the basic solution to the problem of sinusoidal loading on a multiple-variable linear viscoelastic model.

With the stress solution available, we can now determine the apparent stiffness and phase lag as a function of the loading frequency. The apparent stiffness on the stress-strain path is given by

$$3G = \frac{d\sigma}{d\epsilon} = \frac{d\sigma/dt}{d\epsilon/dt} = 3G_0 + \sum_{m=1}^I \frac{3G_m \eta_m^2}{1 + \eta_m^2} - \tan \omega t \sum_{m=1}^I \frac{3G_m \eta_m}{1 + \eta_m^2} \quad (D-21)$$

This stiffness goes through a local maximum at $\omega t = 0$, providing us with the required apparent stiffness:

$$G_{\max} = G_0 + \sum_{m=1}^I \frac{G_m \eta_m^2}{1 + \eta_m^2} \quad (D-22)$$

Our next step is to determine the apparent phase lag. We begin this analysis by writing the stress in the following form:

$$\sigma = \sigma_0 \sin(\omega t + \theta) = \sigma_0 \cos \theta (\sin \omega t + \tan \theta \cos \omega t) \quad (D-23)$$

When we compare this equation with Eq. (D-20), we can evaluate $\tan \theta$.

$$\tan \theta = \frac{\sum_{m=1}^I \frac{G_m \eta_m}{1 + \eta_m^2}}{G_0 + \sum_{m=1}^I \frac{G_m \eta_m^2}{1 + \eta_m^2}} \quad (D-24)$$

From Eq. (D-22) it appears that the stiffness variation with frequency is a direct superposition of the stiffnesses from the G_0 spring and the Maxwell elements. The phase lag given by Eq. (D-24) is not simply related to the μ and G values.

D.3 Exact Incremental Solution

The stress resulting from the application of a linearly varying strain can be obtained exactly for the multiple-variable linear viscoelastic model. This solution is the basis for the stress-relaxation and creep solutions that are presented later in this discussion and for the general implementation of the model into computer programs.

To obtain the solution for the stress in the model, we can concentrate on the stress in any of the Maxwell elements because they each operate separately. The two basic equations governing each element are

$$\sigma_m = 3G_m \epsilon_{gm} = 3\mu_m \frac{d\epsilon_{\mu m}}{dt} \quad (D-25)$$

and

$$\epsilon = \epsilon_{gm} + \epsilon_{\mu m} \quad (D-26)$$

For the computation, let the strain change linearly in time:

$$\epsilon = \epsilon_0 + at \quad (D-27)$$

Then the basic differential equation is obtained by combining the preceding three equations and eliminating ϵ_{gm} .

$$\frac{d\epsilon_{\mu m}}{dt} + \frac{G_m}{\mu_m} \epsilon_{\mu m} = \frac{G_m}{\mu_m} \epsilon_0 + \frac{G_m}{\mu_m} at \quad (D-28)$$

To solve the preceding differential equation, we multiply by $\exp(G_m t / \mu_m)$ and then integrate. The resulting strain at the end of the time interval is

$$\epsilon_{\mu m} = \epsilon_{\mu m 0} \exp\left(-\frac{G_m \Delta t}{\mu_m}\right) + \epsilon_0 \left[1 - \exp\left(-\frac{G_m \Delta t}{\mu_m}\right)\right] - \frac{\mu_m}{G_m} \frac{\Delta \epsilon}{\Delta t} \left[1 - \exp\left(-\frac{G_m \Delta t}{\mu_m}\right)\right]$$

We have replaced a with $\Delta \epsilon / \Delta t$ from Eq. (D-27), noting that $\Delta \epsilon$ is a change in the equivalent strain and not obtainable directly from the components. We derive $\Delta \epsilon$ later from the stress relationship. Next, we use Eq. (D-26) to obtain the elastic component of strain, ϵ_{gm} . Multiplying this strain by $3G_m$ gives the resulting stress at the end of the time interval.

$$\sigma_m = \sigma_{m 0} \exp\left(-\frac{G_m \Delta t}{\mu_m}\right) + 3\mu_m \frac{\Delta \epsilon}{\Delta t} \left[1 - \exp\left(-\frac{G_m \Delta t}{\mu_m}\right)\right] \quad (D-29)$$

We can now expand this result to obtain the solution for the total stress on the assemblage of elements:

$$\sigma = \sigma_{00} + \sum_{m=1}^I \sigma_{m 0} X_m + 3G_0 \Delta \epsilon + 3\frac{\Delta \epsilon}{\Delta t} \sum_{m=1}^I \mu_m (1 - X_m) \quad (D-30)$$

where σ_{00} is the stress in the G_0 spring at the beginning of the interval, and

$$X_m = \exp\left(-\frac{G_m \Delta t}{\mu_m}\right) \quad (D-31)$$

and the $\sigma_{m 0}$ values are updated at each time step using Eq. (D-29).

D.4 Stress Relaxation Solution

When a strain is applied and then held without a change in the subsequent deformation, we have a stress-relaxation problem. A useful case to consider is one in which the strain is applied instantaneously and then held. For the instantaneous application of pressure, the stress reached in each spring is simply

$$\sigma_{m 0} = 3G_m \epsilon_0 \quad m = 0 \text{ to } I$$

and the total stress is

$$\sigma_0 = 3\varepsilon_0 \sum_{m=0}^I G_m \quad (D-32)$$

Then the stress-relaxation solution can be obtained from Eq. (D-30).

$$\sigma = \sigma_0 + \sum_{m=1}^I \sigma_{m0} X_m \quad (D-33a)$$

When we nondimensionalize this result using σ_0 , we obtain

$$\frac{\sigma}{\sigma_0} = \frac{G_0 + \sum_{m=1}^I G_m X_m}{\sum_{m=0}^I G_m} \quad (D-33b)$$

D.5 Creep and Defined Stress Cases

The creep solution is obtained by requiring that the stresses remain constant and allowing the strain to change. For the defined stress case, the stress changes by a prescribed amount, so σ is known. To proceed we rewrite Eq. (D-30) in the following way:

$$\sigma = \sigma_0 - \sum_{m=1}^I \sigma_{m0} (1 - X_m) + 3G_0 \Delta\varepsilon + 3\frac{\Delta\varepsilon}{\Delta t} \sum_{m=1}^I \mu_m (1 - X_m) \quad (D-34)$$

where we may let $\sigma = \sigma_0$ for the creep case, or give σ the new value. When we choose the time step Δt , the only remaining unknown is $\Delta\varepsilon$. Hence, we can use Eq. (D-34) to solve for $\Delta\varepsilon$.

$$\Delta\varepsilon = \frac{\sigma - \sigma_0 + \sum_{m=1}^I \sigma_{m0} (1 - X_m)}{3G_0 + \frac{3}{\Delta t} \sum_{m=1}^I \mu_m (1 - X_m)} \quad (D-35)$$

The initial values of the σ_{m0} are given by the equation preceding (D-32), and these must be updated after each time interval using Eq. (D-29). With Eq. (D-35) we can construct a creep relaxation curve for appropriate time intervals for this model. We can also determine the stresses for a case in which the stress history is defined.

D.6 Extension to Three Dimensions

To extend into three dimensions, we can consider either that Eq. (D-30) pertains to the equivalent quantities or to the individual stress and strain components. Let us consider first the Maxwell model for the individual stress components.

$$S_{ij} = S_{ij00} + 2G_0 \Delta \epsilon'_{ij} + \quad (m = 0)$$

$$+ \sum_{m=1}^I S_{ijm0} X_m + 2 \frac{\Delta \epsilon'_{ij}}{\Delta t} \sum_{m=1}^I \mu_m (1 - X_m) \quad (m = 1 \text{ to } I) \quad (D-36)$$

where S is a deviator stress. Here S_{ijm0} is a stored quantity. For example, for a three-dimensional situation and four Maxwell models, 24 stored quantities would be required for each material element. To minimize the amount of storage, let us consider the possibility of not storing S_{ijm0} , but only σ_{m0} , and presume that all these S_{ijm0} components are proportional both to σ_{m0} and to S_{ij0} as follows:

$$S_{ijm0} = \frac{\sigma_{m0}}{\sigma_0} S_{ij0} \quad (D-37)$$

Here we develop both the approximate procedure using the assumption in Eq. (D-37) and the exact form based on Eq. (D-36). Then later we include some comparison computations that indicate the level of error expected based on using Eq. (D-37). In the approximate form we have available the equivalent stresses for each Maxwell model (σ_{m0}) and the old deviator stress tensor (S_{ij0}). Now we undertake a few steps to eliminate S_{ij00} and S_{ijm0} from the expression for S_{ij} . We note that

$$S_{ij0} = S_{ij00} + \sum_{m=1}^I S_{ijm0} \quad (D-38)$$

and then we can rewrite Eq. (D-36) as

$$S_{ij} = S_{ij0} - \sum_{m=1}^I S_{ijm0} + 2G_0 \Delta \epsilon'_{ij} +$$

$$+ \sum_{m=1}^I S_{ijm0} X_m + 2 \frac{\Delta \epsilon'_{ij}}{\Delta t} \sum_{m=1}^I \mu_m (1 - X_m)$$

or, using Eq. (D-37),

$$S_{ij} = S_{ij0} \left[1 - \frac{1}{\sigma_0} \sum_{m=1}^I \sigma_{m0} (1 - X_m) \right] + 2G_0 \Delta \epsilon'_{ij} + 2 \frac{\Delta \epsilon'_{ij}}{\Delta t} \sum_{m=1}^I \mu_m (1 - X_m)$$

or, defining some new scalar quantities for the nontensor terms,

$$S_{ij} = B S_{ij0} + \frac{2}{3} A \Delta \epsilon'_{ij} \quad (D-39)$$

where

$$A = 3G_0 + \frac{3}{\Delta t} \sum_{m=1}^I \mu_m (1 - X_m) \quad (D-40a)$$

and

$$B = 1 - \frac{1}{\sigma_0} \sum_{m=1}^I \sigma_{m0} (1 - X_m) \quad (D-40b)$$

In Eq. (D-39) we have a complete definition for the deviator stress tensor based on the properties of the Maxwell models, the old deviator stress tensor, the deviator strain increment tensor, and the stored Maxwell equivalent stresses. These Maxwell equivalent stresses are updated at each loading increment using Eq. (D-29).

With the foregoing definitions, the equivalent stress computation becomes

$$\sigma = B \sigma_0 + A \Delta \epsilon \quad (D-41)$$

With this method we can compute the individual stress components while fully accounting for the individual strain components. The steps include (1) determination of the A and B quantities, (2) computation of S_{ij} from Eq. (D-39), and formation of the equivalent quantities σ from Eq. (D-2) and $\Delta \epsilon$ from

$$\Delta \epsilon = \frac{\sigma - B \sigma_0}{A} \quad (D-42)$$

In addition, we use Eq. (D-29) to solve for the individual equivalent stresses on the Maxwell components.

The final step is to examine the error made based on the assumption in Eq. (D-37). For this examination we constructed two computer subroutines: the first contained the analyses based

on the equivalent stress approach in Eqs. (D-40) through (D-42) and using the assumption in Eq. (D-37), and the second used Eq. (D-36) and stored all the necessary Maxwell stress quantities. Two computations were made with each subroutine: a simple compressive load and unload case, and a loading in compression, shearing load, and unloading from compression. The loading rate was in the midst of the range used by Sousa (0.002 per second) and therefore also in the region of maximum dissipation of the fitted viscoelastic model.

The results for the load-unload case were identical, showing that any proportional loading situation is treated exactly with the assumption in Eq. (D-37). The axial stresses and shear stresses for the second computation are shown as a function of time in Figure D-2. The differences are only slightly discernible toward the end of the shearing period and become more important during the subsequent unloading.

On the basis of the foregoing computational exercise, we decided to use the equivalent stress approximation in Eq. (D-37) for all subsequent computations.

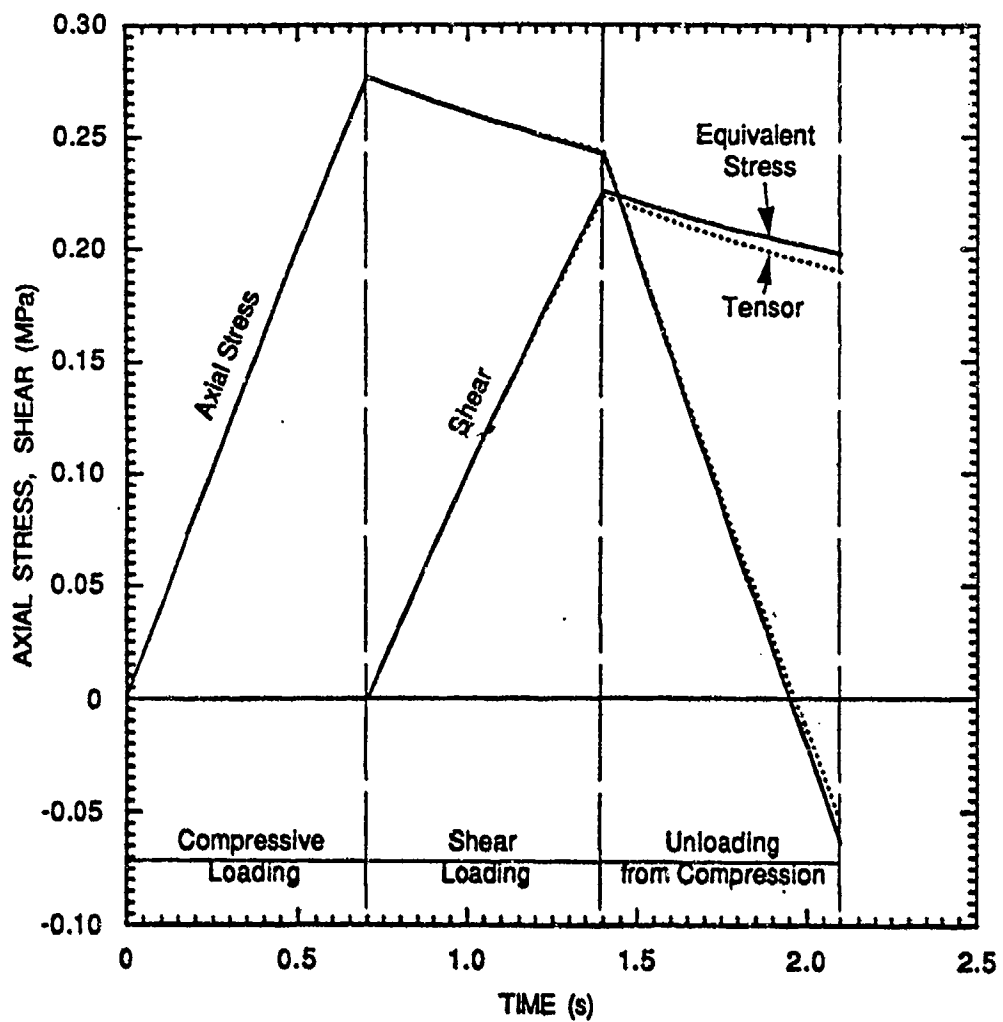
D.7 Fitting the Model Parameters to Data

The required data for the model are the curve of stiffness versus circular frequency and a similar curve of tangent versus frequency. With these data available, we can proceed with the following steps to determine the G_m and μ_m values for the model.

1. Draw the intended stiffness curve versus the circular frequency.
2. Cut the curve into small segments, using smaller segments at the low frequency end. Each segment corresponds to a Maxwell element. We expect that the loss tangent is proportional to the G_m of the individual Maxwell elements, so the foregoing procedure provides for a low loss tangent throughout.
3. Determine the G values from the differences between the stiffnesses at the right and left ends of the segments along the G curve. For example, at the low frequency end, $G = G_0$, the first stiffness parameter. For the m^{th} interval,

$$G_m = \Delta G = G_{m,\text{high}} - G_{m,\text{low}}$$

4. Determine the mid-height point of the m^{th} interval of the curve: this is the central frequency for the m^{th} Maxwell model. Here $\eta_m = 1$, so $\mu_m = G_m/\omega$.



CAM-1889-9

Figure D-2. Comparison of the Axial and Shear Stress Histories Produced by the Tensor Solution Procedure and the Approximate Equivalent-Stress Procedure for the Multiple-Variable Linear Viscoelastic Model

This procedure provides a good first estimate of all the model parameters. Next, the G and $\tan\theta$ values from Eqs. (D-22) and (D-24) should be evaluated over the range of frequencies of interest to verify the expected stiffness and lag variations.

Three-Dimensional Stress Analysis of Multilayered Airport Pavements: Integral Transform Approach

G. Samavedam

Foster-Miller, Inc.

1. Introduction

1.1 Background

With the increased traffic of current aircraft and larger and heavier aircraft likely to be introduced in the near future, the performance demands on existing airport pavements will be significantly higher than those envisioned a few decades ago. The maintenance and repair of the existing pavements and potential new designs in future must take full advantage of advanced theories on the subject. At present, several advanced concepts are available in the general field of structural mechanics which are not fully exploited for the pavement analysis. There are several reasons for the current state of art in the pavement being not on a par with modern developments in structural mechanics. One of the reasons is that the airport pavement structures were there long before the advanced computer models/concepts emerged. A large amount of work had already been expended in testing and empirical correlations of the test data. A primary reason, however, is due to the fact that no systematic investigations have been carried out on the validity and applicability of the advanced structural mechanics concepts to the pavement structure. Such investigations form a major part of the research being initiated by VNTSC/FAA, with the ultimate aim of synthesizing into *an advanced unified treatment* of all types of pavements. This report presents ideal characteristics of the structural and material modelling for pavement and deals specifically in an approach for three-dimensional stress analysis of the pavement structure.

2. Ideal Requirements of Advanced Unified Treatment for FAA Pavements

The requirements for an advanced unified treatment of FAA pavement can be arranged into three groups: general, structural modelling, and material modelling.

2.1 General

- a. All types of pavements (rigid, flexible, semi-rigid, etc.) should be handleable under the single unified approach.
- b. The approach should be usable as an expert system by practicing and other engineers in the pavement industry.
- c. The numerical results should be meaningful for application into practical situations and must result in improved predictions and cost benefits.
- d. The approach should be usable for analytic predictions of pavement repairs performance and for new designs with alternate materials. The approach should handle multiple and increased wheel loads of future.

2.2 Structural Modelling Requirements

- a. The structural model should unify and "cover" Westergaard [1], Burmister [2], Pickett and Ray [3], and other models.
- b. The structural model should reproduce the three-dimensional state of stress and strain in the pavement. The three-dimensional stress analysis will be required because the pavement structure seldom behaves as a simple beam or plate. The model should be capable of predicting both *global* and *local* behavior. The local behavior of interest is at joints, cracks, etc.
- c. The model should be capable of taking into account the property variations due to layering of different materials in the pavement and in the supporting soil. Hence, the material property variations in the cross section (transverse and depth wise) are important in the analytic model. Regarding the longitudinal direction, it *may* be reasonable to assume material properties to be constant for reasons presented later.

- d. The structural model should be capable of representing stress *singularities* and should lead to a computationally efficient nonlinear analysis. Singularities exist at the bottom edges of the pavement in contact with soil. Nonlinearity is in the material *constitutive relationships*. Geometric nonlinearity is not severe and can be neglected.

2.3 Material Modelling Requirements

- a. The material model should be based on advanced constitutive laws relevant to pavement and geotechnical materials. The model should account for "moduli" variations on three-dimensional state of stress, observed in tests. The constitutive laws should be applicable for cyclic loading and unloading.
- b. The model should identify failure or yield criteria for the pavement materials. These criteria must be capable of predicting pavement damage and failure modes commonly observed in pavements (rutting, fatigue cracking, thermal cracking, spalling, stripping, weathering and ravelling, corrugations and pumping, shrinkage and debonding, etc.).
- c. Ideally, the material model should integrate constitutive relationships and failures into a single set of equations or laws. This may facilitate unification of many failure mechanisms referred to above, into a single damage assessment model.

3. Review

A large number of structural models exist for the analysis of pavement systems. A brief review of the literature is presented here. The literature can be classified into the following groups:

1. Rigid Slab Systems
2. Layered Systems
3. Discrete Models
4. Finite Element Models
5. Mixed Models.

3.1 Rigid Slab Systems

The classical work by Westergaard [1] idealizes the slab as a plate on Winkler foundation. For rectangular slabs with constant thickness, this yields closed-form solutions for central, edge and corner loads. Pickett and Ray [2] extended this work for the preparation of influence charts and treated the subgrade as an elastic half space.

- a. Due to the fact that σ_z condition at the top surface is not satisfied (although equilibrium in the z-direction is satisfied in the plate model), the plate idealization will not yield correct stress distribution in the vicinity of the loaded zone.
- b. Variations of properties with depth in pavement slab and subgrade layers are not accounted for in the rigid slab systems.
- c. Voids, partial contact and joint discontinuities cannot be included in the rigid slab model.

3.2 Layered Systems

Burmister [3] presented solutions for axisymmetric multilayered elastic body. Each layer extends to infinity in the horizontal plane, and the bottom layer is a half space. Chevron research company developed a code for five layers. Other codes such as ELSYM5 and VESYS extended the work to multiloading and viscoelastic layers. BISAR is another code written in Holland for a layered system.

- a. Lack of finite boundaries is a fundamental drawback of the layered system approach. These solutions are not applicable for loads near slab edges and joints.
- b. Same as in step 1c applied here in regard to voids, etc.

3.3 Discrete Models

Newmark [4] and later Hudson and Mattock idealized the slab as made up of deformable hinges, springs and some rigid links. The subgrade is idealized as a Winkler foundation. Later models [5-6] considered the subgrade as a half space. It is not easy to estimate the parameters such as the spring stiffness in these models. It is not based on rigorous three-dimensional principles of continuum mechanics.

3.4 Finite Element Models

A number of FE models have appeared in literature. Some of them have recast rigid slab systems described above into standard FE routines, using standard plate elements. Likewise, axisymmetric layered systems have been treated by FE routines. Plane strain and prismatic type elements have also been used. A three-dimensional FE solution has also been attempted using a standard element.

Among the FE works Tabatabaie's and Barenberg's ILLI-SLAB code [7] deserves discussion. In this, the slab is treated as a two-layered plate with rectangular elements, supported on Winkler's foundation. Dowel joints are represented by beam elements and keyed joints by vertical springs. This permits determination of load transfer characteristics and overcomes parts of the shortcoming referred to in step 1c. Unfortunately, the model is not adequate for voids or partial contact due to Winkler foundation idealization.

The shortcomings in the ILLI-SLAB are overcome in another FE solution by Huang and Wang [8] to some extent by including the effects of curling and voids but sacrificing accuracy in the slab modelling. As a result, the solution cannot model cracks and joints in the slab adequately.

Prismatic models which retain constant two-dimensional shape are possible but are not adequate for representing joints and transverse cracks. They also do not adequately satisfy the σ_z condition at the top surface.

A direct three-dimensional FE analysis was attempted by Wilson [9] as long ago as 1969. Due to lack of efficient computers and computational algorithms, and the enormous amount of labor involved in those days, no useful results were obtained from his model.

Direct FE analysis using the displacement approach can be carried out by several existing general purpose commercial codes such as NISA, NASTRAN, MARC, ANSYS, ADINA and ABACUS and others. Some of the codes such as NISA have the advantage of being available on a PC and have excellent color graphics for post processing the data. However, to date only one commercial code (NISA) has been applied to the pavement problem, and excellent results have been obtained by Steve Kokkins [10]. The disadvantage of the commercial codes is that the source code tends to be proprietary, and manipulation of the program for specific requirements (change of solution algorithms) requires cooperation and permission of the code originator.

3.5 Mixed Models

In recent times, some authors attempted to combine different models previously referred to (steps 1 to 4) into a single code with the objective of removing deficiencies in individual models. Discrete model with multilayer model and even two different FE codes have been combined for the pavement system. For example, Saxena [11] used a mixed approach with discrete element model for the slab and Boussinesq's classical solution for the subgrade. Voids, partial contact and curling are not accounted for in the mixed model. Likewise, Huang [12] combined his previous FE slab model [Huang [12] and Wang [8] with Boussinesq's subgrade. As before, the mixed model is still inadequate for joints in the slab.

Majidzadeh [13] combined the ILLI-SLAB model with Huang's model [12] and attempted to develop a design oriented general purpose code. A deficiency in Majidzadeh's approach is lack of explicit formulations, since his method relied heavily on previously developed codes by other authors.

Numerical methods such as the boundary element method, or integral equation technique seem to provide alternate approaches for the three-dimensional stress analysis, but no direct applications to pavement systems have been made to date.

4. Proposed Structural Model

4.1 Local Analysis

The proposed structural model for local analysis is the three-dimensional brick element for pavement, beam elements for bars in doweled joints, vertical springs for keyed joints, etc. The three-dimensional solid brick is the standard eight-corner noded element [14] with linear displacement field (Figure 4-1).

$$\begin{aligned} U &= \sum_{i=1}^8 u_i \psi_i \\ V &= \sum_{i=1}^8 v_i \psi_i \\ W &= \sum_{i=1}^8 w_i \psi_i \end{aligned} \quad (1)$$

where, $\{u_i\}$, $\{v_i\}$, $\{w_i\}$ are nodal displacements and ψ_i is the shape function defined by

$$\psi_1 = (1 - x/a)(1 - y/b)(1 - z/c) \quad (1.1)$$

and companion expressions for ψ_2 to ψ_8 .

The resulting stiffness matrix is 24 x 24 in size. For the linear elastic case, the stiffness matrix can be explicitly derived by minimizing the strain energy expression with respect to the nodal variables. The strain energy expression is

$$\Omega_1 = \int_0^c \int_0^b \int_0^a \left\{ \frac{\lambda}{2} e^2 + \mu (e_x^2 + e_y^2 + e_z^2) + \frac{\mu}{2} (\gamma_{xy}^2 + \gamma_{yz}^2 + \gamma_{xz}^2) \right\} dx dy dz \quad (2)$$

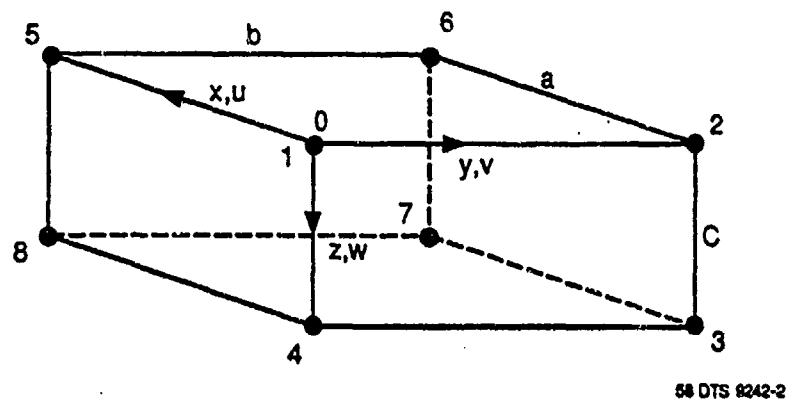


Figure 4-1. Eight-Noded Solid Brick Element

Here

$$\begin{aligned}
 \lambda, \mu &= \text{Lame's constants} \\
 e &= \text{volumetric strain} = \text{sum of extensional strains} = e_x + e_y + e_z \\
 e_x &= \partial U / \partial x \\
 e_y &= \partial V / \partial y \\
 e_z &= \partial W / \partial z
 \end{aligned} \tag{2.1}$$

The shear strain components are given by

$$\begin{aligned}
 \gamma_{xy} &= \partial U / \partial y + \partial V / \partial x \\
 \gamma_{yz} &= \partial V / \partial z + \partial W / \partial y \\
 \gamma_{xz} &= \partial U / \partial z + \partial W / \partial x
 \end{aligned} \tag{2.2}$$

Substitution of expression (1) into (2.1) and (2.2) and finally in Equation (2) gives:

$$\Omega_1 = \frac{1}{2} \{\delta\}^T [K] \{\delta\}$$

where $\{\delta\}^T = \{u_1, v_1, w_1, \dots, u_8, v_8, w_8\}$ and $[K]$ is the stiffness matrix. The integrations involved in the evaluation of $[K]$ have been performed exactly, and $[K]$ can be evaluated explicitly in terms of the element dimensions a, b, c and material constants λ and μ .

The three-dimensional solid brick element together with other standard structural elements such as beam or bar, is sufficient to give detailed stress distribution in joints (Figure 4-2), etc. Nonlinearities in constitutive equations due to stress dependent moduli can also be accounted through an iteration. Elastoplastic analysis can be performed using special algorithms, as discussed by Zienkiewicz [14]

4.2 Global Analysis

The overall response of pavement under multiple loads can of course be obtained using the three-dimensional solid element presented in the previous sections. In fact, this is the approach followed by Ioannides and coworkers [15], and also Kokkins [10], who employed the NTSA commercial code. A disadvantage of such an approach is the large number of degrees-of-freedom involved, and the resulting computer time. In view of the anticipated developments in high speed high capacity workstations and PCs in the next decade, the computer time may not be a serious

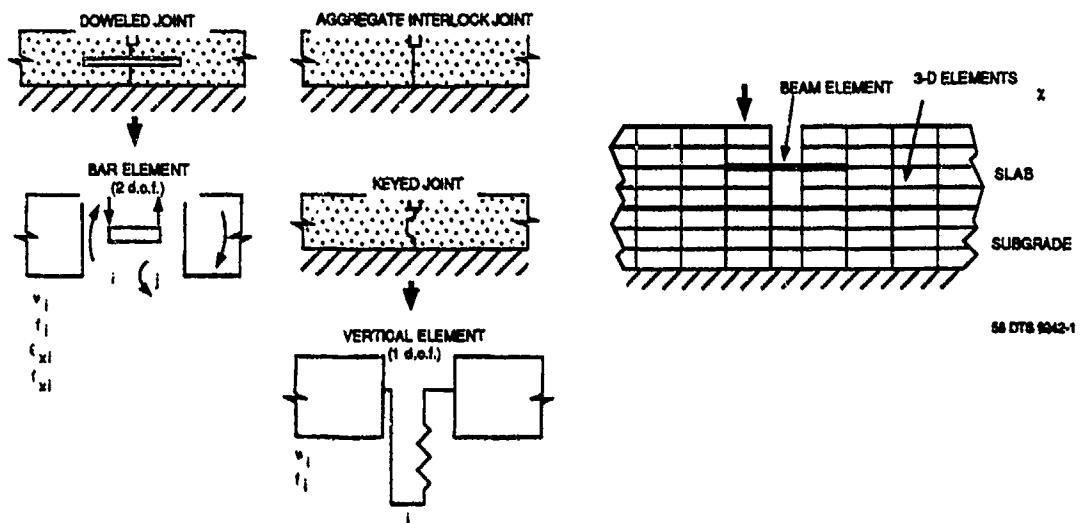


Figure 4-2. Example of Local Analysis

consideration in future. Still, a large number of parametric trade studies will be required in the development of advanced unified treatment of pavements. Therefore, it appears desirable to develop an alternate fast converging solution methodology for the global response of pavements.

The method proposed here is intended for this purpose. It will also form a check on the solutions developed by the standard three-dimensional solid brick element.

4.2.1 Integral Transform Approach

Figure 4-3 shows the cross section and the coordinate axes for the multilayer pavement structure. The proposed approach consists of the following steps:

1. Start with three-dimensional equations of elasticity in displacements.
2. Take Fourier integral transform in x-direction for all the displacement components and applied loads.
3. Derive the three differential equations for the *transformed* displacement components from step 1, which will be in two dimensions (y, z).
4. Construct a variational formulation for solution of differential equations in the two dimensions.
5. Minimize the integral using two-dimensional FE approach.
6. Perform numerical integration of the Fourier integrals.

Theoretical Equations

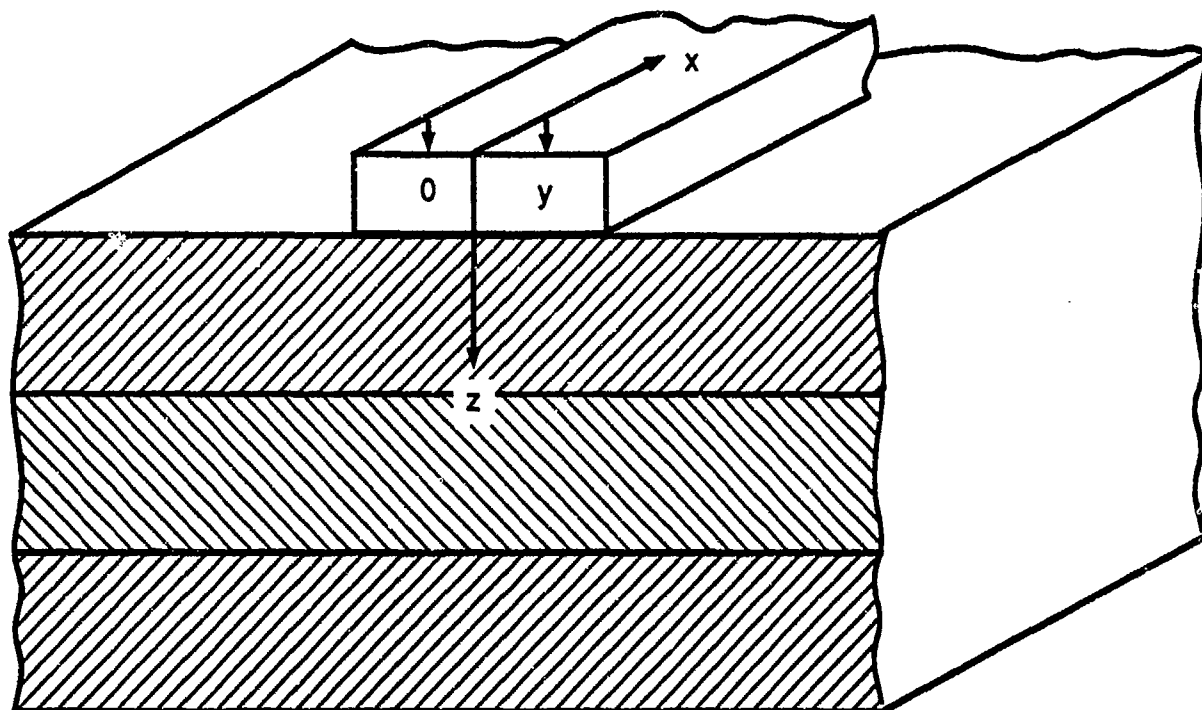
The equilibrium equations are:

$$(\lambda + \mu) \frac{\partial e}{\partial x} + \mu \nabla^2 U = 0$$

$$(\lambda + \mu) \frac{\partial e}{\partial y} + \mu \nabla^2 V = 0$$

$$(\lambda + \mu) \frac{\partial e}{\partial z} + \mu \nabla^2 W = 0$$

(3)



58-DTS-9242-2

Figure 4-3. Coordinate System for Multilayer Pavement Structure

U, V, W : displacement components along x, y and z
 λ, μ : Lamé's constants
 e = hydrostatic strain
 ∇^2 = Laplace operator
 $\equiv \partial^2/\partial x^2 + \partial^2/\partial y^2 + \partial^2/\partial z^2$

Following Tranter [16], the Fourier integral transforms are defined by,

$$\begin{aligned}
 U &= \frac{1}{\sqrt{2\pi}} \int_0^\infty u \sin \xi x \, d\xi \\
 V &= \frac{1}{\sqrt{2\pi}} \int_0^\infty v \cos \xi x \, d\xi \\
 W &= \frac{1}{\sqrt{2\pi}} \int_0^\infty w \cos \xi x \, d\xi
 \end{aligned} \tag{4}$$

Here, u, v, w are *transformed displacements* which are functions of y, z (cross-sectional coordinates) and the transform variable ξ .

Noting that,

$$\Im(\nabla^2 U) = \frac{1}{\sqrt{2\pi}} \int_0^\infty \left(-\xi^2 u + \frac{\partial^2 u}{\partial y^2} + \frac{\partial^2 u}{\partial z^2} \right) \sin \xi x \, d\xi$$

The differential equations for transformed displacements are

$$\begin{aligned}
 (\lambda + \mu) \left(-\xi^2 u + \xi v' + \xi \dot{w} \right) + \mu \left(-\xi^2 u + u'' + \ddot{u} \right) &= 0 \\
 (\lambda + \mu) \left(\xi u' + v'' + \dot{w}' \right) + \mu \left[-\xi^2 v + v'' + \ddot{v} \right] &= 0 \\
 (\lambda + \mu) \left(\xi \dot{u} + v'^* + \ddot{w} \right) + \mu \left[-\xi^2 w + w'' + \ddot{w} \right] &= 0
 \end{aligned} \tag{5}$$

The variational formulation for the foregoing differential equations can be shown to be

$$\begin{aligned}
\Omega = & \iint \left\{ \frac{\lambda}{2} (\dot{v} + \dot{w} + \xi u) + \mu \left[\xi^2 u^2 + v^2 + \dot{w}^2 \right] \right. \\
& + \frac{\mu}{2} \left[(\dot{v} + \dot{w})^2 + (u' - \xi v)^2 + (\dot{u} - \xi w)^2 \right] \left. \right\} dx dy \\
& - \int q(\xi, y) w(y, z_0) dy
\end{aligned} \tag{6}$$

Here, q is the intensity of load on the pavement surface.

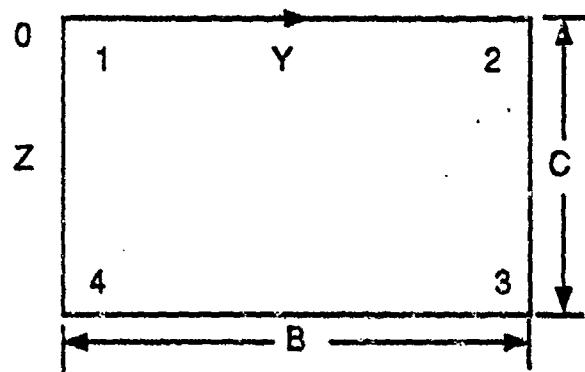
According to the calculus of variations, minimization of Ω with respect to u, v, w which satisfy the geometry boundary conditions gives the solutions of the transformed displacements. To prove this, one can apply Euler's equations, or take the variation with respect to virtual displacements (see Sokolnikoff [17]). The details of proof will be omitted in this paper.

The application of Fourier integral to the solution of half space problems has been done by a number of authors in classical mechanics. In fact, double and triple integral transforms have been used successfully by Fryba [18], and inversions of the transforms have been performed numerically, when it is difficult to obtain solutions in closed forms [16].

To facilitate solutions for any layered pavement structure, we divide the cross section into a number of "two-dimensional" FE and construct the stiffness matrix using expression (6). The two-dimensional stiffness matrix can be assembled and solved using standard procedures for each assumed value of the "harmonic," ξ .

For the rectangular element shown in Figure 4-4, the shape functions are

$$\begin{aligned}
\psi_1 &= (1 - y/b)(1 - z/c) \\
\psi_2 &= (y/b)(1 - z/c) \\
\psi_3 &= (y/b)(z/c) \\
\psi_4 &= (1 - y/b)(z/c)
\end{aligned} \tag{10}$$



$$U = U_1 \psi_1 + U_2 \psi_2 + U_3 \psi_3 + U_4 \psi_4$$

$$V = V_1 \psi_1 + V_2 \psi_2 + V_3 \psi_3 + V_4 \psi_4$$

$$W = W_1 \psi_1 + W_2 \psi_2 + W_3 \psi_3 + W_4 \psi_4$$

Figure 4-4. Rectangular Element with Corner Nodes

The stiffness matrix can be derived explicitly in terms of the element size b , c and element material properties λ and μ . A computer program is being developed with routines for data input (nodal coordinates and material properties), assembly, boundary condition application, solver and processing output data. The boundaries in the soil are terminated at sufficiently large depth and width, which are determined from a previous work [15]. Displacements normal to these boundaries are constrained as in Figure 4-5.

4.2.2 Numerical Results

Numerical results are obtained for a few benchmark problems to prove the validity of the proposed method. The problems studied are Westergaard pavement on elastic springs, and slab on half space. Figure 4-6 shows the Westergaard problem. Figure 4-7 gives the FE idealization used for the numerical work. Figure 4-8 shows the results for displacements, which are in reasonable agreement with the published values. In this problem, ξ is varied at 0.01 intervals for about the first 100 values.

In the second problem, the concrete slab ($E = 4 \times 10^6$ psi, $\nu = 0.15$) of size 15 ft x 8 in. is resting on the half space of soft soil ($E = 76\ 82$ psi, $\nu = 0.45$). A symmetric interior load of 30 Kips is applied over an area of 12 x 12 in. The FE model for a symmetric half of the cross section is shown in Figure 4-9. The maximum deflection is found to be about 0.03 in., which is in reasonable agreement with the published value. The deflection variation of the slab top surface in the transverse direction is shown in Figure 4-10. The vertical stress distribution is shown in Figure 4-11. These results are in reasonable agreement with published results.

The method can be applied for simultaneous inclusion of multiple wheel loads. Figure 4-12 shows the deflection results for a four-tire loading configuration.

4.2.3 Advantages and Comparison with Other Methods

The Fourier integral transform together with the two-dimensional FE offers certain advantages in the solution for global response of the multilayered pavement response. When applied in conjunction with the local analysis using the three-dimensional solid-brick element, the method has the potential to handle material nonlinearities and structural discontinuities as well. However, this has not been demonstrated as yet in the work reported here.

Tables 4-1 and 4-2 present a comparative summary of the characteristics of the present method, the BISAR code and the conventional FE.

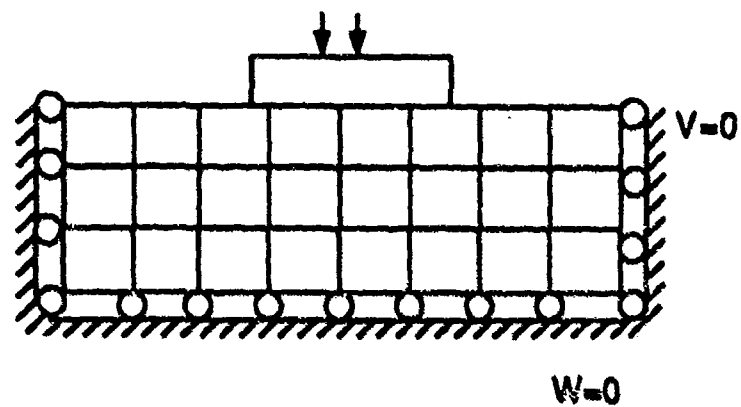
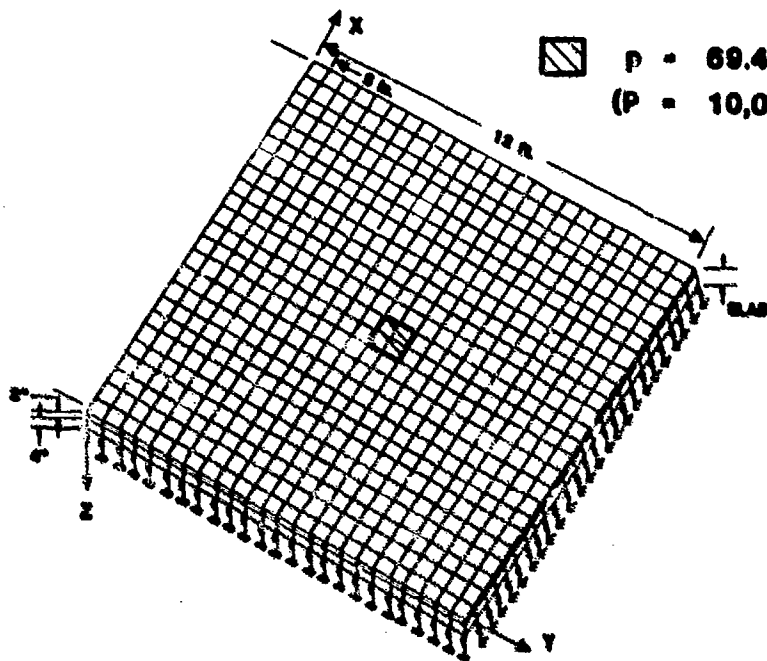


Figure 4-5. Assumed Boundary Conditions



MATERIALS DATA

SLAB:

$$E = 3 \times 10^6 \text{ lb/in}^2$$

$$\mu = 0.15$$

SUBGRADE:

$$k = 50 \text{ lb/in}^3$$

Figure 4-6. Westergaard Benchmark Model with Square-Interior Pressure Load

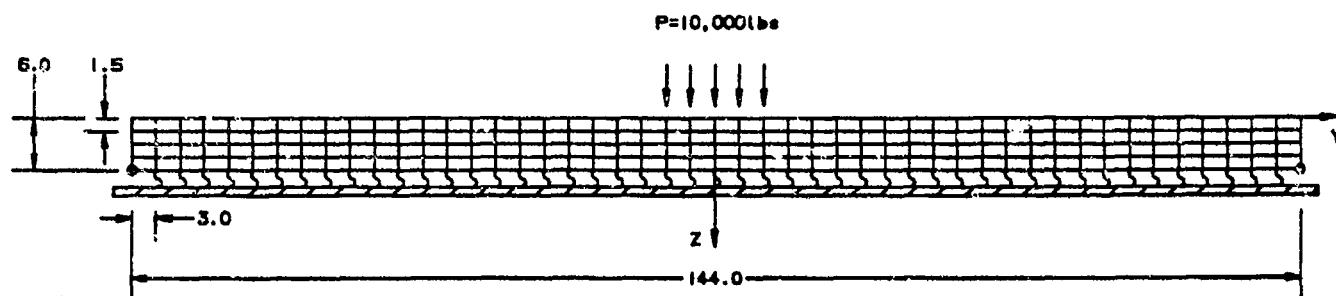


Figure 4-7. FE Idealization of Westergaard Slab

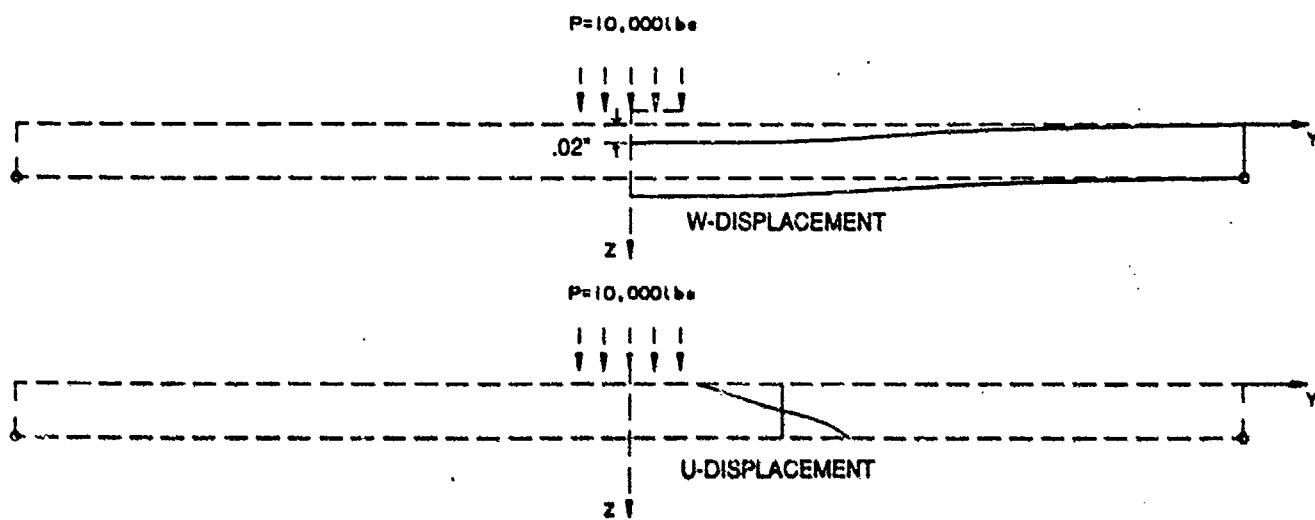


Figure 4-8. Displacement Results

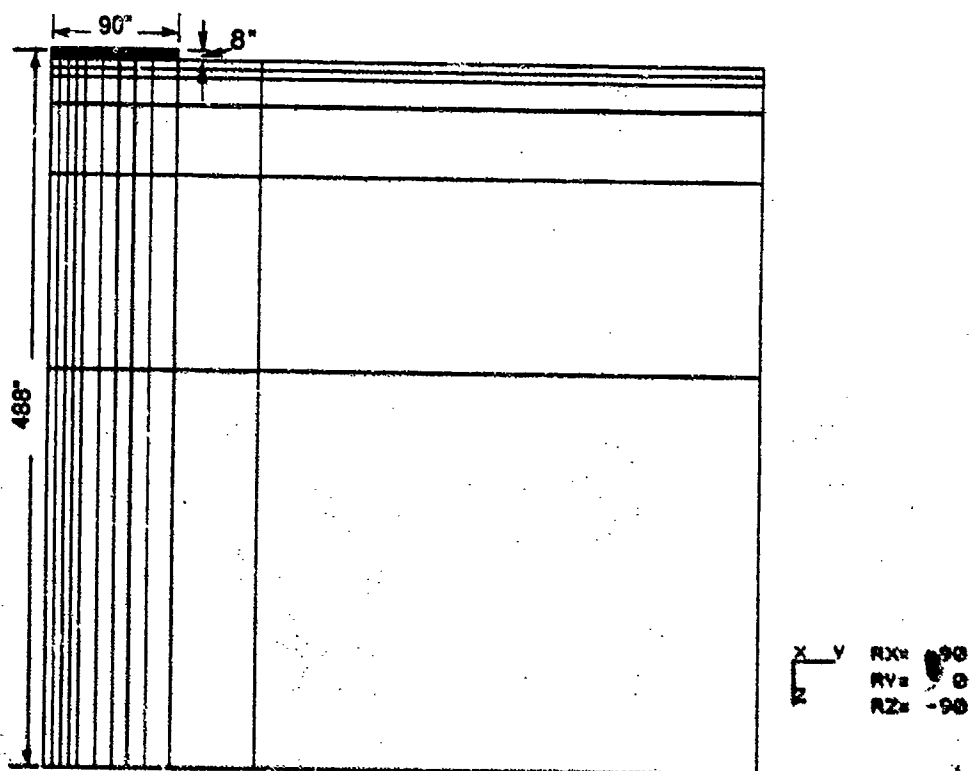


Figure 4-9. FE Idealization of Slab on Half Space

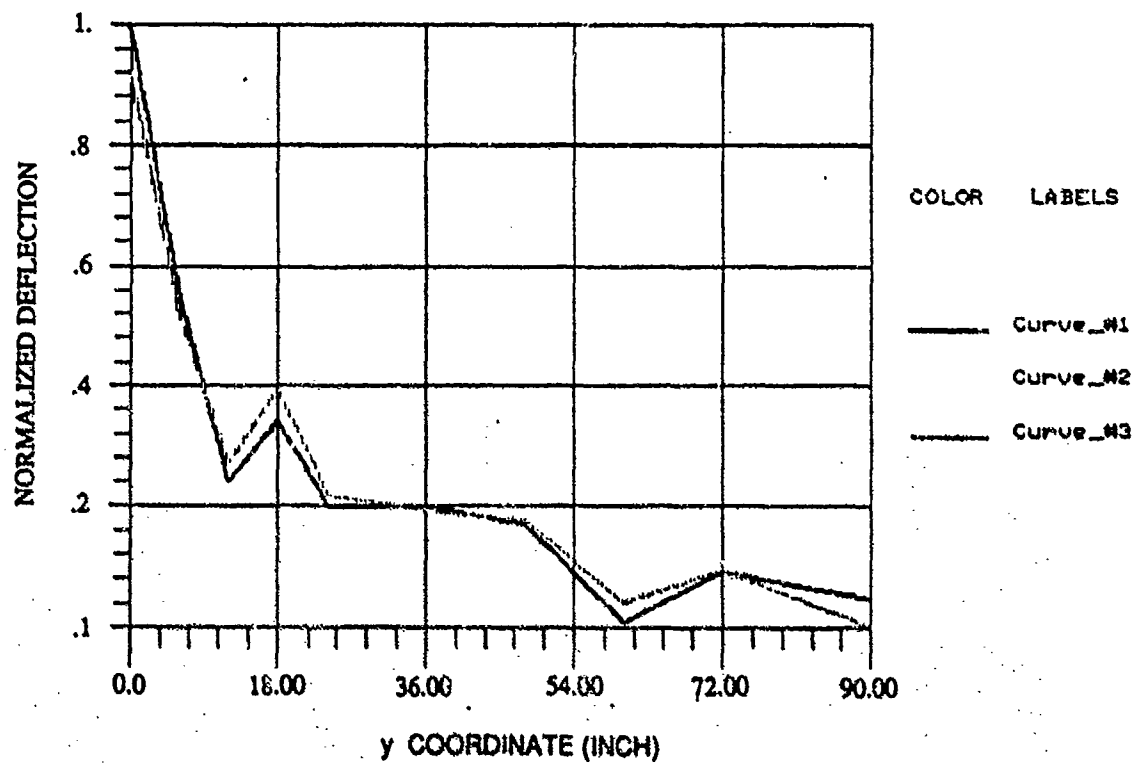


Figure 4-10. Deflection Variation with Distance

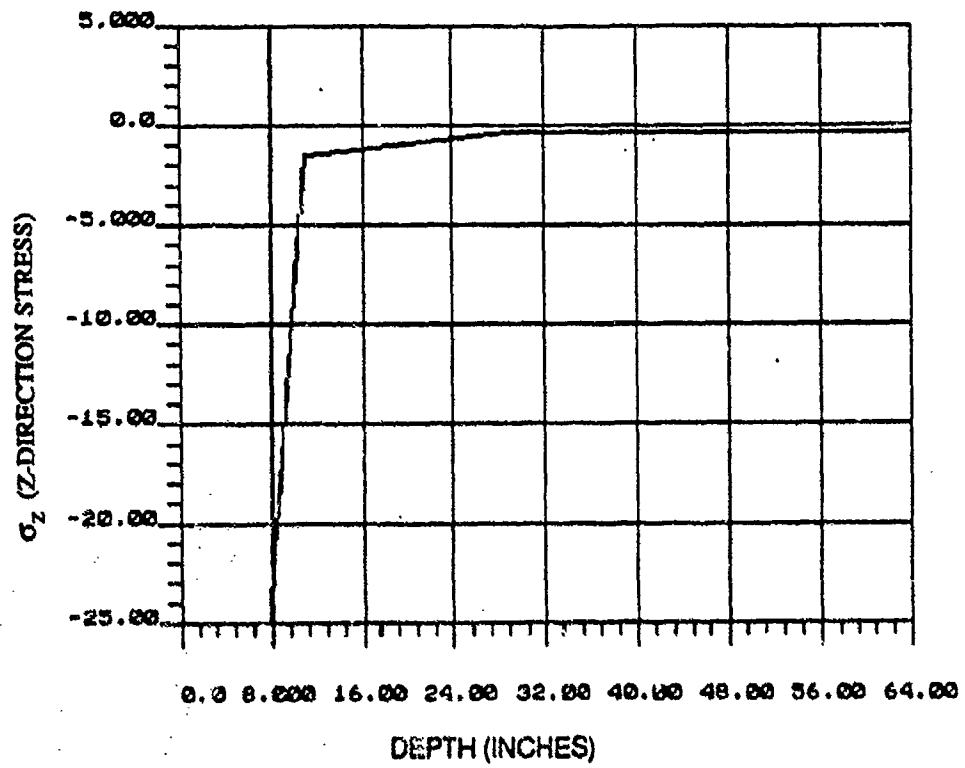


Figure 4-11. Vertical Stress Distribution

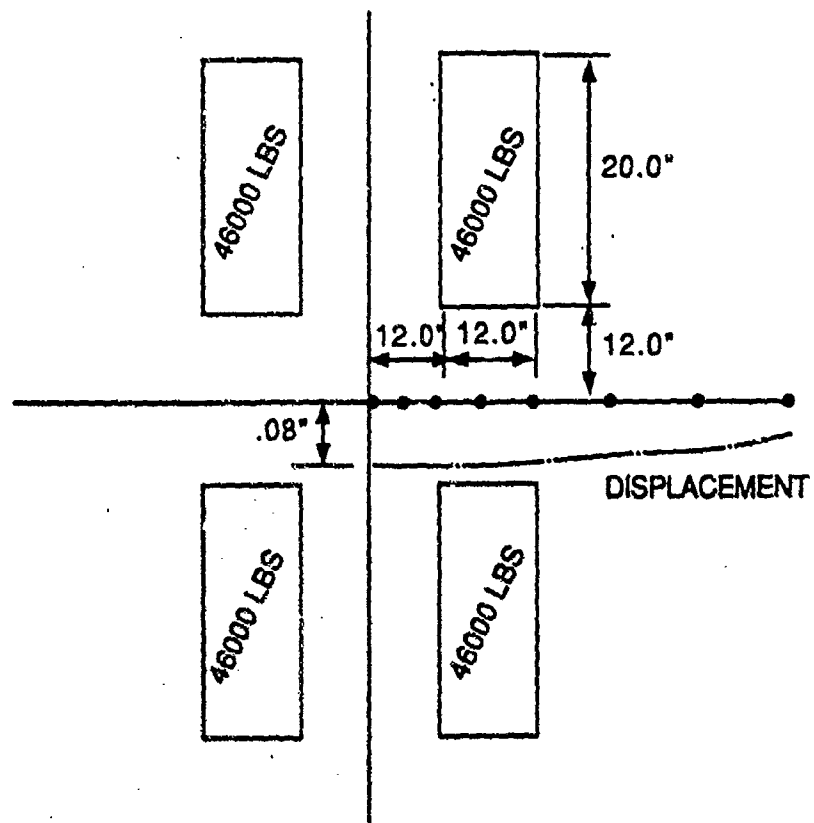


Figure 4-12. Multiple Load Case

Table 4-1. BISAR versus Present Method

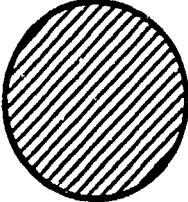
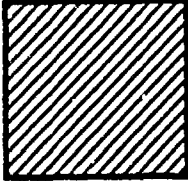
BISAR	Present Method
<ul style="list-style-type: none"> • Circular loading  <ul style="list-style-type: none"> • Two-dimensional axisymmetric theory • Plane strain solution not represented • Not ideal for finite width pavements 	<ul style="list-style-type: none"> • Rectangular loading/multiple loads  <ul style="list-style-type: none"> • Three-dimensional theory • Plane strain solution included • Well suited for finite size pavements

Table 4-2. Three-Dimensional Conventional versus Present Method

Conventional FE Method	Present Method
<ul style="list-style-type: none"> • Large DOF, labor intensive • Finite boundaries at $x = \pm l$ • No explicit plane strain solution 	<ul style="list-style-type: none"> • Easy mesh generation • No finite boundary in the x-direction. Asymptotic estimate for large x can be made • Explicit plane strain solution included

6. References

1. Westergaard, H.M., "Stresses in Concrete Pavements Computed by Theoretical Analysis," Public Roads, Vol. 7, 1926, "Stresses in Concrete Runways of Airports," Proc. HRB, Vol. 19, 1939. New Formulas for Stresses in Concrete Pavements of Airfields," Proc. ASCE, Vol. 113, 1947. "Analysis of Stresses in Concrete Pavements Due to Variation of Temperature," Proc. HRB, Vol. 6, 1926.
2. Burmister, D.M., "The Theory of Stresses and Displacements in Layered Systems and Application to the Design of Airport Runways," HRB Proc. 1943. Burmister, D.M., "The General Theory of Stresses and Displacements in Layered Soil System, I, II, III," Journal of Applied Physics, Vol. 16, No. 2, No. 3, No. 5, 1945.
3. Pickett, G. and K.G. Ray, "Influence Charts for Concrete Pavements," Trans. ASCE, Vol. 116, 1951.
4. Newmark, N.M., "Numerical Methods of Analysis of Bars, Plates and Elastic Bodies," in L.E. Grinter (ed.), Numerical Methods of Analysis in Engineering, the MacMillian Co., New York, 1949.
5. Vesic, A.S. and S.K. Saxena, "Analysis of Structural Behavior and AASHO Road Test Rigid Pavements," NCHRP Report 97, 1970.
6. Saxena, S.K., "Pavement Slabs Resting on Elastic Foundation," HRR No. 466, 1973.
7. Tabatabaie, A.M. and E.J. Barenberg, "ILLI-SLAB Finite Element Computer Program for Structural Analysis of Concrete Pavement Systems."
8. Huang, Y.H. and S.T. Wang, "Finite Element Analysis of Concrete Slabs and Its Implications for Rigid Pavement Design," HRR 466, 1973, "Finite Element Analysis of Rigid Pavements with Partial Subgrade Contact," HRR 485, 1974.
9. Wilson, E.L., Solid SAP, "A Static Analysis Program for Three-Dimensional Solid Structures," SESM 71-19, Structural Engineering Laboratory, Univ. of Calif., Berkeley, CA, 1969.

10. Kokkins, J.S., paper presented at "FAA Unified Pavement Design and Analysis," July 16-17, 1991, held at VNTSC, Cambridge, MA.
11. Saxena, S.K., "Foundation Mats and Pavement Slabs Resting on an Elastic Foundation-Analysis Through a Physical Model," Doctoral Dissertation, Department of Civil Engineering, Duke University, Durham, NC, 1971.
12. Huang, Y.H., "Finite Element Analysis of Slabs on Elastic Solids," *Transportation Eng. Journal of ASCE*, Vol. 100, TE2, May 1974.
13. Majidzadeh, K., G.J. Lives, and R. McComb (1981), "Mechanistic Design of Rigid Pavements," Proceedings: 2nd Int. Conf. Concrete Pavement Design, pp. 87-96, Purdue University also (1985), "RISC - A Mechanistic Method of Rigid Pavement Design," Proceedings: 3rd Int. Conf. Concrete Pavement Design & Rehabilitation, pp. 325-339, Purdue University.
14. Zienkiewicz, O.C., "The Finite Element Method," McGraw Hill, 1982.
15. Ioannides, A.M., J.P. Donnelly, M.R. Thompson, and E.J. Barenberg, "Three-Dimensional Finite Element Analysis of a Slab on Stress Dependent Elastic Solid Foundation," Report No. TR-86-0143, USAF, Bolling AFB, 1984.
16. Tranter, C.J., "Integral Transforms in Mathematical Physics," John Wiley & Sons, 1962.
17. Sokolnikoff, I.S., "Mathematical Theory of Elasticity," McGraw Hill Second Edition, 1956.
18. Fryba, L., "Vibration of Solids and Structures Under Moving Loads," Noordhoff International Publishing.